Mapping of signalling pathways using a FACS-based forward genetic approach



Erica De Zan

Trinity College

University of Oxford

A thesis submitted for the degree of

Doctor of Philosophy

Hilary 2020

Abstract

Since its inception, the central goal of functional genomics has been to gain a mechanistic understanding of how genes operate and interact with each other to regulate cellular and organismal phenotypes. To this end, screening approaches have been designed to systematically perturb the activity of every genetic element in the genome and identify mutants affecting defined phenotypic traits. Only recently, screenable phenotypes in mammalian cell systems moved past "fitness" and onto detection of molecular markers' gradients at single cell resolution. This thesis describes the interrogation of regulatory gene networks behind key intracellular signalling pathways using a Fluorescence Activated Cell Sorting (FACS)-based approach coupled to haploid genetic screening.

After establishing the technology's robustness and reproducibility in the first result Chapter, a set of iterative screens is performed in the presence of pharmacological and genetic perturbations to dissect mammalian target of rapamycin complex 1 (mTORC1) activation and tumour necrosis factor α (TNFα) pro-inflammatory signalling.

Data presented in the second result Chapter demonstrate that, contrary to previous assumptions, Ragulator subunit LAMTOR4 is not strictly required for in mTORC1 activation under steady-state conditions. Furthermore, LAMTOR4 is part of a "synthetic-sick" interaction with tumour suppressor gene FLCN, resulting in inhibition of cell proliferation which could be therapeutically relevant.

The third result Chapter describes a novel regulatory mechanism of TNFα-dependent pro-inflammatory signalling through transcriptional modulation of its receptor TNFR1. The

effect is mediated by the largely uncharacterised proteins QRICH1, SEPHS1 and ZNF652, the first two of which functionally, and possibly also physically, interact.

Together, this thesis details how genetic screening for modulation of molecular makers can advance understanding of functional cellular signalling network.

Declaration

I hereby declare that this dissertation is entirely my own work with the exception of:

- Delta MI (ΔMI) calculation, insertion location visualisation and relative method **Section 2.7**, which were developed by R. van Stipenhout, and
- p-RPS6 screen performed in T. Brummelkamp's lab (p-RPS6 NKI), which was conducted with the help of V. Blomen and B. Gapp.

In the text I have acknowledged the work performed by others. The data presented in **Chapter 4** and **Figure 3.8** have been published in article format as De Zan, E., et al., *Quantitative genetic screening reveals a Ragulator-FLCN feedback loop that regulates the mTORC1 pathway.* Sci Signal, 2020. **13**(649). The data presented in **Section 3.2.10** are part of a manuscript in preparation. **Chapter 5** presents unpublished results and figures.

Word count: 44.008

Acknowledgments

It takes a village to raise a child.

African proverb

The first thank goes to my parents Paolo and Milena, for always believing in me and giving me the freedom and the means to choose my path in life, even when it led me far away from home.

I want to acknowledge my supervisor Sebastian, for four years of trust, support, guidance and stimulating conversations. This DPhil has been a great learning opportunity and a true rollercoaster, with tough times and some successes, and I owe it to you have had the freedom to shape my DPhil and my project. A special thanks goes to my second supervisors Mads and Paul for their encouragement and support. I am especially grateful to Mads, for welcoming me in his group, for his advice and guidance when I moved the first steps in the innate immunity field.

I count myself fortunate to have belonged and be part, officially and non-officially, of different research groups during my DPhil, and have learned from each and every member of them. The support I received from members and staff of both the Ludwig Cancer Research Institute and the Target Discovery Institute went far beyond the lab and I am immensely grateful to all of them.

A warm thanks goes to all past members of the Nijman's lab. To Barbara, my lab mom, for taking me under her wing when I first arrived and still looking out for me, four years later and 4.000 km apart. To Roby, the molecular biology guru, for her support inside and outside the lab. To Ruud, the best coffee and lunch partner, for his insight and willingness to help with R scripts. To Bianca, for her incredible moral and practical

support in the first months of my DPhil. To Tomasz, for his much-needed help navigating computational issues. And then Ferran, Lu, Cathrine, Max, Shiv, Chandan, Stefania and Vineeth because, as it sometimes happens when working together, colleagues can become good friends. A special thanks goes also to Norma Masson, who become my scientific sounding board for the last year of my DPhil. I was lucky to work with smart and dedicated collaborators during my DPhil. A particular thanks goes to Thijn and the components of the Brummelkamp lab, for sharing the protocol of the FACS-based screening and providing continuous support and feedback ever since. It was a pleasure to work with Corinna, the late Vincenzo Cerundolo, Sumeet Pandey and Holm Uhlig.

My life in Oxford would not have been the same without a mixed and varied group of friends: Olivia, Anna, Luise, Angelo, Munadi, Carlos, Carol, Lu, Kristijan, Roberta, Kasper, Paulina, Jackie, Andra, Bedour, Yure and Nora. Thank you for all the dinners, pub visits, nights out, outings and trips. For all the laughter and good times, for sharing the “ups” and helping me go through the “downs”. Thanks to my flatmates, Marta, Mar, Isobel, and Mayra, for sharing my successes and frustrations and for putting up with me even in very stressful times.

Thanks to all my other friends, who at some point had listen to my DPhil-related chatter and bravely stood the test. To my childhood friends Micheal, Lucia, Brunilde, Serena and Silvia for all the years we have walked together and for many years more. To “il rombo”: my friends Bale, Bebe and Polly. For their “expert” insight into research life, our laughter and continuous support. To my friends Niklas, Sandra, Olga, David, and Camilla because the friends you make when living abroad for the first time are special. Finally, to Dean, for his unwavering and loving support, especially during the writing of this thesis.

Table of Contents

ABSTRACT I

DECLARATION III

ACKNOWLEDGMENTS IV

TABLE OF CONTENTS VI

LIST OF TABLES XII

LIST OF FIGURES XIV

LIST OF ABBREVIATIONS XVII

SYMBOLS AND UNITS XXIV

CHAPTER 1: INTRODUCTION 1

1.1 PHENOTYPE-TO-GENOTYPE RELATIONSHIP 1

1.2 GENETIC SCREENS TO MAP GENOTYPE-TO-PHENOTYPE RELATIONSHIP 2

1.3 GENERATION OF LIBRARIES OF PERTURBED GENOTYPES 3

1.3.1 Untargeted approaches 3

1.3.2 Targeted approaches 6

1.4 *IN VITRO* GENETIC SCREEN FORMATS 9

1.4.1 Viability screens 10

1.4.1.1 Genetic interactions 12

1.4.2 High-content genetic screens 15

1.4.3 Enrichment selection screens 16

1.4.4 FACS-based forward genetic screens 17

1.5 THESIS AIMS 20

CHAPTER 2:MATERIALS AND METHODS 22

2.1 ANTIBODIES, PLASMIDS AND REAGENTS 22

2.2 CELL LINES 31

2.3 GENERATION OF MUTAGENIZED HAP1 (MUT-HAP1) CELLS 31

2.4 FACS-BASED FORWARD GENETIC SCREEN 33

2.5 INSERTION SITES RECOVERY AND MAPPING 34

2.6 Mutation mapping and analysis 39
2.7 Delta MI (ΔMI) calculation and insertion location visualisation 40
2.8 pLentiCRISPR v2- sgRNA cloning strategy 41
2.9 Knockout cell generation via transient transfection 43
2.10 Knockout cell generation via lentiviral infection 44
2.11 HAP1 knockout clone generation and characterisation 45
2.12 Immunoblotting 47
2.13 Flow Cytometry 48
2.14 RNA isolation and quantitative Real Time PCR (qRT-PCR) 49
2.15 RNA sequencing and analysis 51
2.16 Immunofluorescence microscopy 52
2.17 Cell Fractionation 52
2.18 Immunoprecipitation 53
2.19 Amino acid starvation 54
2.20 Colony formation assay 54
2.21 Protein stability and half-life measurement 54
2.22 mRNA stability measurement 55
2.23 TIDE analysis 55
2.24 Data plotting 56
2.25 Statistical Analysis 56

CHAPTER 3: FACS-BASED FORWARD GENETIC SCREENING TECHNOLOGY 57

3.1 Introduction 57
3.1.1 Mutagenesis: gene-trapping on haploid cell line 58
3.1.2 Identification of phenotype of interest: Fluorescence Activated Cell Sorting (FACS) 60
3.1.3 Detection of causative mutation: sequencing and mapping 61
3.2 Results 63
3.2.1 Selection and validation of a reporter system 63
3.2.2 Generation of mutagenized HAP1 (mut-HAP1) cells 65
3.2.3 mut-HAP1 cells expansion 67

3.2.4 mut-HAP1 cells screen harvest and staining *68*
3.2.5 mut-HAP1 cells sorting *70*
3.2.6 Recovery of insertion sites and bioinformatic analysis *74*
3.2.7 Screen reproducibility *77*
3.2.8 Screen hits prioritisation *80*
3.2.8.1 Degree of connection with the phenotype ("guilt by association") 80
3.2.8.2 Effect size 81
3.2.8.3 Pattern of insertions within the gene body 81
3.2.8.4 Promiscuity across multiple screens 81
3.2.9 Screen example #1: HIF-1α regulation *83*
3.2.10 Screen example #2: MR1 surface presentation *86*
3.3 DISCUSSION 90
3.3.1 Choice of screen reporter system *91*
3.3.2 Choice of cell system and mutagenesis approach *92*
3.3.3 Gene-trapping versus CRISPR/Cas9 mutagenesis for FACS-based forward genetic screening *94*
3.3.4 Hit prioritisation for validation *95*
3.3.5 Future perspectives *96*
3.3.5.1 Technology advances 96
3.3.5.2 Building a genetic interaction map from FACS-based genetic screens 98

CHAPTER 4: A RAGULATOR-FLCN COMPENSATORY MECHANISM REGULATES MTORC1 ACTIVATION 100

4.1 INTRODUCTION 100
4.1.1 Mammalian target of rapamycin complex 1 (mTORC1) *101*
4.1.2 mTORC1 regulation *102*
4.1.2.1 The nutrient-sensing arm 102
4.1.2.2 The amino acid (AA) sensing arm 103
4.1.3 mTORC1 effectors *107*
4.1.4 mTORC1 in cancer *109*
4.3 RESULTS 111

4.3.1 Haploid genetic screen for mTORC1 activation *111*
4.3.2 Pharmacological modifier screen: mTORC1 activation in presence of rapamycin *115*
4.3.3 LAMTOR4 hit validation *119*
4.3.4 Genetic modifier screen: mTORC1 activation in ΔLAMTOR4 background *124*
4.3.5 ΔLAMTOR4 cells require FLCN to maintain mTORC1 activation *128*
4.3.6 LAMTOR4/FLCN synthetic sick interaction *130*
4.3.7 LAMTOR4/FLCN compensatory mechanism *131*
4.4 DISCUSSION 134
4.4.1 Comparative genetic screening *134*
4.4.2 Pharmacologically perturbed p-RPS6 screen *135*
4.4.3 Genetically perturbed p-RPS6 screen *137*
4.4.4 Future perspectives *138*

CHAPTER 5: QRICH1 AND SEPHS1 WORK TOGETHER TO REGULATE TNFR1 LEVEL IN HAP1 CELLS 141

5.1 INTRODUCTION 141
5.1.1 Tumour Necrosis Factor α (TNFα) *142*
5.1.2 TNFα-dependent NF-κB pro-inflammatory signalling *142*
5.1.3 TNFR1 regulation *145*
5.1.4 Anti-TNFR1 therapy *146*
5.1.5 Glutamine rich protein 1 (QRICH1) *147*
5.1.6 Selenophosphate synthetase 1 (SEPHS1) *149*
5.1.7 Zinc Finger Protein 652 (ZNF652) *150*
5.2 RESULTS 152
5.2.1 HAP1 cells as a model for TNFR1 surface level and TNFα-dependent NF-κB activation *152*
5.2.2 Haploid genetic screen for TNFR1 surface levels *155*
5.2.3 Haploid genetic screen for TNFα-dependent NF-κB activation *157*
5.2.4 Identification of hits' overlap between TNFR1 surface level and TNFα-dependent NF-κB activation screens *162*

5.2.5 QRICH1, SEPHS1 and ZNF652 hit validation 165
5.2.6 QRICH1, SEPHS1 and ZNF652 regulation of TNFR1 167
5.2.7 Haploid genetic screens for TNFα-dependent NF-κB activation and TNFR1 surface level in ΔQRICH1 background 169
5.2.8 Data mining for QRICH1, SEPHS1 and ZNF652 interactions 172
5.2.9 Subcellular localisation of QRICH1 173
5.2.10 Co-immunoprecipitation of QRICH1 and SEPHS1 176
5.2.11 Transcriptional signature in ΔQRICH1 and ΔSEPHS1 background ... 177
5.2.12 TNFα-dependent transcriptional response in ΔQRICH1 and ΔSEPHS1 background 183
5.2.13 Validation of ΔQRICH1 phenotype in other human cell lines 185
5.2.14 QRICH1 reconstitution 186
5.3 DISCUSSION 191
5.3.1 QRICH1, SEPHS1 and ZNF652 191
5.3.2 Other regulatory mechanisms 195
5.3.3 Future perspectives 197

CHAPTER 6: FINAL DISCUSSION: THE FUTURE OF GENETIC SCREENING TECHNOLOGIES 200

6.1 TOWARDS COMPLEX PHENOTYPES 200
6.2 HIGH-THROUGHPUT GENETIC SCREENING FOR MULTI-MODAL PHENOTYPES 203
6.2.1 Single cell transcriptomics 203
6.2.2 High-content imaging in pooled screening format 205

CHAPTER 7: BIBLIOGRAPHY 208

CHAPTER 8: APPENDICES 235

8.1 QRICH1 CDNA INSERTS IN PLENTI GFP 235
8.1.1 Relevant genetic elements 235
8.1.2 QRICH1 cDNA sequences 235
8.2 LIST OF GENE HITS (FDR < 0.05) FOR FACS-GENETIC SCREENS 239
8.2.1 p-RPS6 (NKI) screen 239
8.2.2 p-RPS6 (OX) 1% screen 245

8.2.3 p-RPS6 3% screen 248
8.2.4 HIF-1α screen 251
8.2.5 HIF-1α +DFOM screen 253
8.2.6 MR1 screen 256
8.2.7 p-RPS6$_{combined}$ screen 258
8.2.8 p-RPS6$_{rapamycin}$ screen 261
8.2.9 ΔMI p-RPS6$_{combined}$ - p-RPS6$_{rapamycin}$ 265
8.2.10 p-RPS6$_{ΔLAMTOR4}$ screen 266
8.2.11 TNFR1 screen 270
8.2.12 TNFα-dependent NF-κB activation screen 273
8.2.13 TNFR1$_{ΔQRICH1}$ screen 276
8.2.14 (TNFα-dependent NF-κB activation $_{ΔQRICH1}$) screen 278
8.2.15 ΔMI TNFR1 – TNFR1$_{ΔQRICH1}$ 280
8.2.16 ΔMI TNFα-dependent NF-κB activation – (TNFα-dependent NF-κB activation) $_{ΔQRICH1}$ 281

List of Tables

Table 1.1 List of untargeted mutagenesis approaches.....4

Table 1.2 List of FACS-based forward genetic screens presented in this study 21

Table 2.1 List of primary antibodies used in this study......23

Table 2.2 List of secondary antibodies used in this study.....23

Table 2.3 List of plasmids used in this study.....24

Table 2.4 List of reagents used in this study.....28

Table 2.5 List of buffers and solutions used in this study 29

Table 2.6 List of commercial kits used in this study 30

Table 2.7 Gene-trap retrovirus generation.....32

Table 2.8 List of primers used in recovery of gene-trap insertions 35

Table 2.9 LAM PCR reaction set-up for N = 1.....37

Table 2.10 Set-up for 1X 20 µl ssDNA ligation reaction.....38

Table 2.11 Master mix for 1 standard Illumina adaptors PCR reaction.....38

Table 2.12 List of sgRNAs used in this study.....42

Table 2.13 Cas9-sgRNA lentivirus generation.....45

Table 2.14 List of primers for validation of knockout genotype used in this study.....46

Table 2.15 Genomic PCR set-up for knockout clones genotyping 47

Table 2.16 cDNA synthesis reaction set-up.....49

Table 2.17 qRT PCR set-up.....50

Table 2.18 List of qRT PCR primers used in this study.....51

Table 3.1 Summary table of mutagenesis experiments.....67

Table 3.2 Harvesting and staining workflow for intracellular and surface markers 69

Table 4.1 List of molecular and phenotypic characteristics related to Ragulator components 105

Table 4.2 Genotype information for LAMTOR4 and LAMTOR5 knockout clones employed in the study 121

Table 4.3 Genotype information for FLCN and LAMTOR4-FLCN knockout clones generated in the study.....128

Table 5.1 Classification of human CARD-containing proteins by function and signalling complex 148

Table 5.2 Summary of reported QRICH1 pathogenic mutations in humans 149

Table 5.3 TNFα/TNFR expression and protein level in HAP1 cells.....153

Table 5.4 List of genes concomitantly affecting TNF receptor 1 surface levels and TNFα-dependent NF-κB activation.....163

Table 5.5 Genotype information for QRICH1, SEPHS1 and ZNF652 knockout clones used in the study 165

Table 5.6 List of 54 differentially expressed genes shared in the four independent ΔQRICH1 and ΔSEPHS1 clones.....181

List of Figures

Figure 1.1 Schematic representation of pooled fitness screens in a mammalian mutant cell pool 10

Figure 1.2 Principle of epistasis 13

Figure 1.3 Graphical representation of quantitative genetic interactions (GI) 14

Figure 1.4 Schematic representation of experimental Florescence Activated Cell Sorting (FACS)-based forward genetic screen workflow 19

Figure 2.1 Schematic overview of recovery of gene-trap insertion sites workflow 36

Figure 3.1 Fluorescence Activated Cell Sorting principle 60

Figure 3.2 Antibody testing for FC 64

Figure 3.3 Gene-trap mutagenesis on HAP1 cells 66

Figure 3.4 Primary antibody titration 70

Figure 3.5 FACS sorting workflow 71

Figure 3.6 Sorting parameters optimisation 73

Figure 3.7 Recovery of insertion sites and bioinformatic analysis workflow 75

Figure 3.8 Screen reproducibility 78

Figure 3.9 Regulation of HIF-1α stability in normoxia and hypoxia 83

Figure 3.10 Regulator maps for total levels of HIF-1α 85

Figure 3.11 Regulatory map for MR1 surface levels 87

Figure 4.1 mTORC1 activation requires both nutrient and AA sufficiency cues 102

Figure 4.2 FACS-based forward genetic screens on mTORC1 activation 113

Figure 4.3 Mitochondrial gene enrichment among mTORC1 positive regulators 114

Figure 4.4 Rapamycin dose finding 116

Figure 4.5 Pharmacological modifier screen identifies rapamycin-dependent effects involving FKBP1A and LAMTOR4 119

Figure 4.6 LAMTOR4 regulates mTORC1 activation only in presence of rapamycin .. 120

Figure 4.7 Functional effect of LAMTOR4 inactivation 122

Figure 4.8 Functional consequences of LAMTOR4 loss 124

Figure 4.9 FACS-based genetic screen in LAMTOR4-null background identifies additional layers of mTORC1 regulation 127

Figure 4.10 ΔLAMTOR4 HAP1 cells depend on FLCN to maintain mTORC1 signalling 129

Figure 4.11 FLCN upregulation in Ragulator-null background 131

Figure 4.12 Transcriptional upregulation of FLCN in Ragulator-null cells 133

Figure 5.1 Schematic representation of the TNFα/TNFR1/NF-κB signalling axis 144

Figure 5.2 DNA sequence 500 bp upstream of the TNFRSF1A start codon 146

Figure 5.3 Validation of HAP1 cells as a model for investigating TNFR1 expression and TNFα-mediated NF-κB activation 154

Figure 5.4 Forward genetic screen for TNFR1 surface level 156

Figure 5.5 Forward genetic screen for TNFα-dependent NF-κB activation 158

Figure 5.6 MI comparison for selected gene in TNFR1 and TNFα-dependent NF-κB pathway activation 161

Figure 5.7 Location of independent sense gene-trap insertions in TNFRSF1A, QRICH1, SEPHS1 and ZNF652 164

Figure 5.8 QRICH1, SEPHS1 and ZNF652 hit validation 166

Figure 5.9 QRICH1, SEPHS1 and ZNF652 regulate TNFR1 at transcriptional level 168

Figure 5.10 Haploid genetic screens for TNFα-dependent NF-κB activation and TNFR1 surface level in wild type and ΔQRICH1 cells 170

Figure 5.11 Unbiased genome-wide analysis of ΔMI in TNFα-dependent NF-κB activation and TNFR1 screen pairs 171

Figure 5.12 Correlation of dependency scores for QRICH1, SEPHS1 and ZNF652 (DepMap) 172

Figure 5.13 QRICH1 localises in the nucleoplasm 175

Figure 5.14 QRICH1- SEPHS1 co-immunoprecipitation 177

Figure 5.15 RNA sequencing workflow for ΔQRICH1 and ΔSEPHS1 clones 178

Figure 5.16 Differentially regulated genes in unstimulated ΔQRICH1 and ΔSEPHS1 background 182

Figure 5.17 Differentially Regulated Genes in TNFα-stimulated ΔQRICH1 and ΔSEPHS1 background 184

Figure 5.18 QRICH1-dependent TNFR1 downregulation in other cell lines 186

Figure 5.19 QRICH1 full length and mutant reconstitution in ΔQRICH1 HAP1 cells .. 187

Figure 5.20 Analysis of TNFR1 expression and NF-κB activation in reconstituted ΔQRICH1 cells 189

Figure 5.21 Schematic representation of two possible mechanisms of QRICH1-SEPHS1- and ZNF652-dependent TNFRSF1A transcriptional control 191

List of Abbreviations

4E-BP1	EIF4E-binding protein 1
AA	Amino acid
Ac-6-FP	Acetyl-6-formylpterin
ActD	Actinomycin D
ADAM17	ADAM metallopeptidase domain 17
ADP	Adenosine diphosphate
AKT	Protein kinase B
Ala	Alanine
AMPK	5' AMP-activated protein kinase
ANOVA	Analysis of variance
AP-3	Adaptor protein 3
Arg	Arginine
ATP	Adenosine triphosphate
B2M	β-2-microglobulin
BFP	Blue fluorescent protein
BHD	Birt-Hogg-Dubé
BLOC-1	Biogenesis of lysosome-related organelles 1
BSA	Bovine serum albumin
C/EBP	CCAAT-enhancer-binding protein
CARD	Caspase recruitment domain
CARNMT1	Carnosine methyltransferase
Cas	CRISPR associated protein
CBFA2T3	CBFA2 partner transcriptional co-repressor 3
cDNA	Complementary DNA
CEB	Cytoplasmic extraction buffer
CGAS/MB21D1	Cyclic GMP-AMP synthase
ChIP	Chromatin immunoprecipitation
CHMP3	Charged multivesicular body protein 3
CHMP5	Charged multivesicular body protein 5

CHX	Cycloheximide
cIAP1/BIRC2	Cellular inhibitor of apoptosis 1
cIAP2/BIRC3	Cellular inhibitor of apoptosis 2
CO_2	Carbon dioxide
COL10A1	Collagen type X α 1 chain
COL11A1	Collagen type XI α 1 chain
CRISPR	Clustered regularly interspaced short palindromic repeats
CRISPRa	CRISPR activation
CRISPRi	CRISPR interference
Ct	Cycle threshold value
Cys	Cysteine
DD	Death domain
DE	Differential expression
DEG	Differentially expressed genes
DEPDC5	DEP domain containing 5
DEPTOR	DEP domain-containing MTOR interacting protein
DFEB	Digitonin Ficoll extraction buffer
DFOM	Deferoxamine
dKO	Double knockout
DMSO	Dimethyl sulfoxide
DNA	Deoxyribonucleic acid
DUF3504	Domain of unknown function 3504
EDTA	Ethylenediaminetetraacetic acid
EEFSEC	Sec-specific elongation factor
eIF4E/EIF4E	Eukaryotic translation initiation factor 4E2
eIF4E2/EIF4E2	Eukaryotic translation initiation factor 4E
eIF4F/EIF4F	Eukaryotic translation initiation factor 4F
EMS	Ethyl methane sulphonate
ENU	N-ethyl-N-nitrosourea
eps	Events per second

ER	Endoplasmic reticulum
ERAP1	Endoplasmic reticulum aminopeptidase
FACS	Fluorescence activated cell sorting
FDR	False discovery rate
FKBP12	FK506-binding protein 12
FLCN	Folliculin
FNIP2	Folliculin interacting protein 2
GAP	GTPase-activating proteins
GAPDH	Glyceraldehyde 3-phosphate dehydrogenase
GATOR1	GAP activity toward the Rag GTPases 1
GATOR2	GAP activity toward the Rag GTPases 2
gDNA	Genomic DNA
GDP	Guanosine diphosphate
GEF	Guanosine exchange factor
GFP	Green fluorescent protein
GI	Genetic interaction
GIGYF2	GRB10-interacting GYF protein 2
Gln	Glutamine
GPI	Glycophosphatidylinositol
GPX4	Glutathione peroxidase 4
GTP	Guanosine triphosphate
haESC	Haploid embryonic stem cells
HAP1	Haploid human cell line
HAPLN3	Hyaluronan and proteoglycan link protein 3
HIF1α/HIF1A	Hypoxia-inducible factor 1-α
His	Histidine
HLA-A	Human leukocyte antigen A
HOIL-1/RBCK1	Heme-oxidised IRP2 Ub ligase 1
HOIP/RNF31	HOIL-1 interacting protein
HOPS	Homotypic fusion and vacuole protein sorting
IFN-γ	Interferon γ

IgG	Immunoglobulin
IKKα/CHUK	Inhibitor of κB Kinase α
IKKβ/IKBKB	Inhibitor of κB Kinase β
INDEL	Insertion–deletion mutations
ITFG2	Integrin α FG-GAP repeat containing 2
IκBα/NFKBIA	NF-κB inhibitor α
KBM7	Near-haploid human cell line
KCNC1	Potassium voltage-gated channel subfamily C member 1
KICSTOR	KPTN, ITFG2, c12orf66 and SZT2-containing regulator of mTORC1
KPTN	Kaptin
LAM-PCR	Linear amplification PCR
LAMTOR1	Late endosomal/lysosomal adaptor, MAPK and MTOR activator 1
LAMTOR2	Late endosomal/lysosomal adaptor, MAPK and MTOR activator 2
LAMTOR3	Late endosomal/lysosomal adaptor, MAPK and MTOR activator 3
LAMTOR4	Late endosomal/lysosomal adaptor, MAPK and MTOR activator 4
LAMTOR5	Late endosomal/lysosomal adaptor, MAPK and MTOR activator 5
LC3A/B	Light chain 3 A/B
lincRNA	Long intergenic non-coding RNA
LTR	Long terminal repeat
LUBAC	Linear ubiquitin chain assembly complex
MAP1A	Microtubule associated protein 1A
MEK1/2	Mitogen-activated protein kinase
MFI	Median fluorescence intensity
MHC	Major histocompatibility complex
MI	Mutational index
MIOS	Meiosis regulator for oocyte development
ML	Machine learning
mLST8	Mammalian lethal with Sec13 protein 8
MLV	Murine leukaemia virus
MR1	Major histocompatibility complex, class I-related protein
mRNA	Messenger RNA

mTOR/MTOR	Mammalian target of rapamycin
mTORC1	Mammalian target of rapamycin complex 1
mut-HAP1	Mutagenized HAP1
NEMO/IKBKG	NF-κB essential modulator
NFKB1	NF-κB subunit 1
NF-κB	Nuclear factor kappa-light-chain-enhancer of activated B cells
NKI	Netherlands Cancer Institute
NLS	Nuclear localization sequence
NMD	Nonsense mediated decay
NPRL2	NPR2 like 2
NPRL3	NPR2 like 3
O/N	Overnight
OX	Oxford
P/S-Glut	Penicillin streptomycin glutamine
PBS	Phosphate buffer saline
PCR	Polymerase chain reaction
PHD1/EGLN2	Prolyl hydroxylase domain 1
PHD2/EGLN1	Prolyl hydroxylase domain 2
PHD3/EGLN3	Prolyl hydroxylase domain 3
PI	Propidium iodide
PI3K	Phosphoinositide 3-kinase
PO_4^{3-}	Phosphate
PolyA	Polyadenylation tail
PRAS40	Proline-rich AKT substrate of 40 kDa
PSTK	Phosphoseryl-tRNA kinase
Q	QRICH1
Q_{CARD}	ΔCARD-QRICH1-FLAG
QFLAG	QRICH1-FLAG
Q_{NLS}	QRICH1-ΔNLS-FLAG
QRICH1	Glutamine rich protein
qRT-PCR	Quantitative reverse transcription PCR

Rag A/RRAGA	Ras related GTP binding A
Rag B/RRAGB	Ras related GTP binding B
Rag C/RRAGC	Ras related GTP binding C
Rag D/RRAGD	Ras related GTP binding D
RAPTOR/RPTOR	Regulatory-associated protein of MTOR
RELB	RELB proto-oncogene, NF-κB subunit
RHEB	Ras homologue enriched in brain
RIPK1	Receptor interacting protein kinase 1
RNA	Ribonucleic acid
RNAi	RNA interference
RNAse A	Ribonuclease A
RNA-seq	RNA sequencing
RPS27A	Ribosomal protein 27A
RPS6	Ribosomal protein S6
RPS6K1	Ribosomal protein S6 kinase 1
RT	Room temperature
SARS2	Seryl-tRNA synthetase 2
Sec	Selenocysteine
SECISBP2	Sec insertion sequence-binding protein 2
SEHIL	SEH1 like nucleoporin
SelD	Selenide, water dikinase
SEM	Standard error of the mean
SEPHS1	Selenophosphate synthetase 1
SEPHS2	Selenophosphate synthetase 2
SEPSECS	O-phosphoseryl-tRNA^{sec} selenium transferase
Ser	Serine
sgRNA	Single guide RNA
SHARPIN	SHANK-associated RH domain interactor
shRNA	Small hairpin RNA
SLC38A9	Solute carrier family 38, member 9
SPTLC1	Serine palmitoyltransferase long chain base subunit 1

SZT2	Seizure threshold 2 protein homolog
TAA	Tumour-associated antigen
TAB1	TAK1 binding protein 1
TAB2	TAK1 binding protein 2
TAB3	TAK1 binding protein 3
TABP	TAP binding protein
TAK1/MAP3K7	TGF activated kinase 1
TALEN	Transcription activator-like effector nuclease
TAP1	Transporter associated with antigen processing 1
TAP2	Transporter associated with antigen processing 2
TBC1D7	Tre2-Bub2-Cdc16-1 domain family member 7
TFE3	Transcription factor binding to IGHM enhancer 3
Thr	Threonine
TIDE	Tracking of Indels Decomposition
TNFAIP3	TNFα induced protein 3
TNFR1/TNFRSF1A	TNFα receptor 1
TNFR2/TNFRSF1B	TNFα receptor 2
TNFα/TNF	Tumour necrosis factor α
TOP	5’ terminal oligopyrimidine
TRADD	TNFRSF1A-associated via death domain
TRAF2	TNFR associated factor 2
TRAF5	TNFR associated factor 5
TRAPS	TNFR-associated periodic syndrome
tRNA	Transfer ribonucleic acid
TSC1	Tuberous sclerosis complex 1
TSC2	Tuberous sclerosis complex 2
TSS	Transcription start site
Ub	Ubiquitin
UBA52	Ubiquitin A52
UBB	Ubiquitin B
UBC	Ubiquitin C

UTR	Untranslated region
v-ATPase	Vacuolar ATPase
VHL	Von Hippel-Lindau syndrome
WDR24	WD repeat domain 24
WDR59	WD repeat domain 59
WIMM	Weatherall Institute of Molecular Medicine
WNT	Wingless and int-1
WT	Wild type
ZNF598	Zinc-finger protein 598
ZNF652	Zinc-finger protein 652

Symbols and Units

| |	Absolute value
°C	Degree centigrade
µ	Micro (10^{-6})
A	Adenine
bp	Base Pair
C	Cytosine
ds	Double-stranded
e.g.	Exempli gratia
E	x 10^
EPM	Expression per kilobase million
et al.	Et alia
Fe^{2+}	Iron
FPKM	Fragments per kilobase million
g	Gram
G	Guanine
h	Hour
i.e.	Id est
kb	Kilobase

kDa	Kilodalton
L	Litre
M	Molar
m	Milli (10^{-3})
Mg^{2+}	Magnesium
p	Pico (10^{-9})
p-	Phosphorylated
rcf	Relative centrifugal force
sc	Single cell
ss	Single-stranded
T	Thymine
Δ	Deleted

Chapter 1: **Introduction**

1.1 Phenotype-to-genotype relationship

In biology, the word "phenotype" (from the Greek *phainein* "to show," and *typos*, "type") is used to describe an organism's observable and measurable traits, such as its physiological and biochemical properties. In contrast, the word "genotype" refers to the organism's genetic makeup. According to genetics' traditional view, genes and observable traits are linked, and consequently, a genetic variation can affect the function of its encoded protein (or RNA) and may cause measurable changes in a phenotypic trait [1]. It follows logically that the study of phenotype variation(s) occurring in an organism characterised by a specific trait can be used to infer phenotype-to-genotype relationships and thus, gene function.

Initially, a "one-to-one" paradigm was proposed, according to which one trait was controlled by a single gene, however the theory was abandoned after 2001, when the full human genome was completed and was found to contain much fewer genes that would be required to explain human complexity under the "one gene-one phenotype" paradigm. In fact, sequencing efforts between 1990 and 2000 had shed light on the genetic makeup of model organisms and found a correlation between the number of genes and the molecular complexity of studied organisms [2]. The unicellular eukaryote *Saccharomyces cerevisiae* (budding yeast) carried 6.000 genes [3], while 13.600 and 19.000 genes were identified, respectively, in increasingly complex multi-cellular model organisms *Drosophila melanogaster* (fruit fly) and *Caenorhabditis elegans* (nematode worm) [4, 5].

To equate human complexity, the Human Genome Sequencing project initially estimated the existence of 100.000 protein-coding genes [6]. Surprisingly, the final figure was closer to approximately 24.000 genes, including both *bona-fide* protein-coding genes and genes transcribed into a functional RNA molecule [7-9]. To explain how a relatively low number of genes could orchestrate a suite of complex processes in humans, it was hypothesized that the various genetic elements acted in a concerted manner to yield a phenotype [2]. The "one-to-one" paradigm was thus replaced by a "many-to-many" hypothesis, according to which the majority of traits are affected by multiple genes and most genes impinge on multiple traits. Since then, the quest for mapping the function of each human gene (*i.e.* functional genomics) became closely interwoven with studying and understanding functional interdependencies between distinct genetic elements and how these operational blocks regulate complex cellular processes. These functional modules collectively driving the response to afferent endocrine and paracrine signals are termed signalling pathways [10].

1.2 Genetic screens to map genotype-to-phenotype relationship

The term "forward genetics" is used to describe the molecular approach for determining the genetic basis of an observable trait. In contrast to "reverse genetics", where phenotype is studied following the disruption of a known gene, forward genetics proceeds from a measurable trait to its causative gene. Thanks to its unbiased nature, forward genetics proved to be one of the most powerful tools for expanding the collective understanding of biological events [11]. As this approach relies on identification of mutants which could be informative of the phenotype of interest, the success of forward genetics

relies on efficient procedures to 1.) source mutants, 2.) select for the trait of interest and 3.) map the phenotypic variation back to the underlying genetic perturbation(s).

Initial examples of forward genetics analysed observable phenotypic variations that occurred spontaneously in animals, plants and yeast and linked them with specific genetic mutation(s) (reviewed in [12]). The process, albeit successful for a limited number of traits, was cumbersome and inefficient due to two main drawbacks: 1.) the low estimated frequency of naturally occurring variants (~ 5 x 10^{-6} per locus) and 2.) the difficulty to genetically map the causative mutation [13]. In order to overcome these limitations, systematic approaches to generate collections of mutants with relatively well-defined molecular lesions were developed (**Table 1.1**).

1.3 Generation of libraries of perturbed genotypes

1.3.1 *Untargeted approaches*

Studies performed in the late 1920s demonstrated that exposure to high-energy radiations caused large deletions and rearrangements in the fruit fly's genome at frequencies 20-100 times higher than would be expected to occur naturally [14]. The discovery, recognised with the 1946 Nobel Prize, found an application in generating vast collections of mutants in diverse model organisms [15, 16] and was instrumental to Lewis's seminal work of mapping the genetic basis of *Drosophila melanogaster's* body plan development, marking the first attempt to characterise all the mutations affecting a given process [17]. However, the extensive chromosomal rearrangements caused by irradiation, while being useful as a marker for mutation mapping, were difficult to control and often

impeded the identification of the underlining genetic basis as often aberrations affect large genome regions.

Mutagenesis strategy	Type of mutation	Primary advantage	Primary disadvantage
Spontaneous	Various	Visible phenotypes	Very low frequency of detection
Radiation	Spectrum of chromosomal rearrangements	Rearrangements as molecular marker for mapping	Multiple genes affected
Chemical (EMS/ENU)	Primarily point mutations	Single-gene mutation, high-throughput possible	Absence of molecular marker for mapping
Transgene/retroviral	Disruption of endogenous coding sequence	Ease of mapping	Laborious, not applicable in high-throughput
Gene-trapping	Disruption of endogenous coding sequence	Ease of mapping, expression of reporter gene for selection	Possible hypomorphic phenotypes

Table 1.1 List of untargeted mutagenesis approaches. Table adapted from [13].

An alternative, more precise mutagenesis protocol used chemicals, such as ethyl methane sulphonate (EMS) and N-ethyl-N-nitrosourea (ENU), that alkylated DNA bases and thereby induced single nucleotide changes [18, 19]. The chemicals were easily administered (either through diet or injection) and resulted in a mutational frequency of approximately 10^{-3} per locus in spermatogonial stem cells [20]. Furthermore, when applied to eukaryotic organisms with relative fast reproductive cycles such as fruit fly, nematode worm, and mouse (*Mus musculus*), chemical mutagenesis approaches enabled males to sire mutant offspring for a prolonged period of time. Chemical mutagenesis thus became widely popular with geneticists, leading to landmark studies on embryonic patterning in fruit fly [21], neuronal fate regulation in nematode worm [22] and enabling the first large-scale genetic screen in mouse [23]. While single-base mutations unambiguously linked a genetic locus to a phenotype, the absence of molecular cloning markers, *i.e.* DNA sequences

which can be used to recover information about genomic location, rendered mapping of point mutations a laborious and lengthy process [20].

Another untargeted mutagenesis method relied on introduction of exogenous DNA into near-random locations in the genome using transgenes or retroviruses. In general, this method harnessed the intrinsic capacity of retroviral DNA [24] and transposons to integrate into the genome [25, 26] and provided defined molecular markers that simplify insertion locations mapping. Despite its low mutagenesis efficiency (approximately 10% of the chemical approaches) and some intrinsic insertional biases, transposon-based mutagenesis was widely adopted in model organisms [27-29].

A further advance in insertional mutagenesis techniques came with gene-trap vectors, engineered viral vectors that integrated into endogenous genes and hijacked the host transcriptional apparatus to express an engineered marker (usually conferring resistance to an antibiotic) [30, 31]. In this case, expression of selectable marker was ensured by the presence of a splice acceptor sequence on the viral vector. The resulting fusion product between the upstream coding sequence and the reporter gene not only disrupted the genomic locus, but also simultaneously informed over the expression pattern of the trapped genomic element and enabled selection of "gene-trapped" cells [13]. Gene-trap approaches were used to generate collections of mutagenized model organisms and of mouse embryonic stem (ES) cells [32-34].

It is important to note that all mutagenesis approaches described so far, due to their random nature, typically only affected one allele, resulting in very low probabilities of bi-allelic inactivation. As a consequence, in disomic cells, only disruption of dominant alleles and haploinsufficient loci could generate an observable phenotype, while studying recessive alleles required laborious crosses of heterozygous individuals [35]. With the

exception of near-haploid and haploid mammalian cells, reviewed in depth in **Chapter 3**, generation of homozygous mutants in cell culture systems using untargeted mutagenesis was mostly unfeasible. This drawback, united to discovery of new methods of genetic manipulations, led to the surge of targeted approaches over random mutagenesis.

1.3.2 *Targeted approaches*

Early approaches to introduce mutations in pre-determined DNA locations relied on homologous recombination, a physiological process whereby nucleotide sequences are exchanged between highly similar DNA strands. This mechanism was co-opted to introduce parts of engineered plasmids into an endogenous locus. Such vectors were designed to contain a selectable marker flanked by two short sequences matching regions at either side of the endogenous target locus [36]. Recombination between the homologous sequences resulted in genome-edited cells which could be easily isolated thanks to the inserted selectable marker cassette. This approach was successfully applied to *Saccharomyces cerevisiae* and, due to yeast's high efficiency of homologous recombination and its ability to exist in a haploid state, led to the generation of the first genome-wide collection of deletion mutants [37]. Homologous recombination was also extensively used in mouse embryonic stem cells (ESCs) and fruit fly to introduce molecular tools for spatial and temporal control of gene expression [38, 39]. To this end, genetic regions containing recognition sequences (loxP and FRT) for site-specific recombinases (Cre and Flp, respectively) were initially inserted through homology recombination [40]. In an edited organism, expression of recombinases either in specific tissues or in response to exogenous stimuli, led to controlled target locus inactivation through excision of the loxP- or FRT- flanked region. Methods coupling homologous

recombination with spatial and temporal control of gene inactivation led to the generation of a vast collection of mouse mutant strains [39, 41] and additionally contributed to elucidate *Drosophila melanogaster* development program [42]. Gene editing via homologous recombination was however impractical in mammalian somatic cells, where homologous recombination is very infrequent and target DNA integrates almost exclusively in non-homologous fashion resulting in random insertion locations [43].

The first genetic manipulation tool readily applicable to mammalian somatic cells did not induce hereditable genetic mutations but, instead, led to degradation of specific mRNAs and therefore a down-regulation of the gene of interest at transcriptional level ("knockdown"). First described in *Caenorhabditis elegans*, the system, named RNA interference (RNAi), relies on an endogenous, conserved mechanism which leads to degradation of double-stranded RNA (dsRNA) molecules [44]. The mechanism was readily adapted for targeted gene silencing by employing synthetic RNA molecules complementary to the target mRNA [45]. Introduced into cells as dsRNA or short hairpin RNA (shRNA), functional ribonucleotide molecules were cleaved by cellular enzymes to 21-23 nucleotides RNA duplexes [46]. Through the action of the RNA-induced silencing complex (RISC), a single strand of the RNA duplex was released and paired with the endogenous target mRNA, inducing its degradation. The unprecedented ease of the technology and the compatibility with many different biological systems resulted in widespread application of RNAi to generate knockdown libraries for screening at both organismal and cell level (reviewed in [47, 48]). In particular, a number of landmark RNAi studies in eukaryotic cells uncovered genetic regulators of *Listeria monocytogenes* bacterial infection [49], the metabolism of anticoagulant drug warfarin [50], and nuclear factor kappa-light-chain-enhancer of activated B cells (NF-κB) intracellular pathway activation

[51]. Despite its transformative role in molecular biology and in particular for screening applications, later studies reported several pitfalls of RNA interference technology, mainly related to its off-target effects and incomplete target gene knockdown [52].

To overcome these limitations, the genetic screening field required new molecular biology tools capable of scalable and precise genome editing to generate large mutant collections of mammalian cells. In this context, engineered fusion proteins comprising of a DNA-binding and a DNA-cleavage domain were developed (reviewed in [53, 54]). These systems, of which zinc-finger nucleases (ZFNs) and transcription activator-like effector nucleases (TALENs) constitute the most notable examples, allowed precise genome editing in a number of higher organisms with minimal off-target effects. Notwithstanding, the considerable cloning effort required to generate mutant nucleases libraries for genome-wide applications significantly hampered the adoption of engineered nucleases beyond low throughput applications. In fact, to date, only a handful of pilot screens using ZFN or TALEN system have been performed [55].

A final, potent addition to the genome editing toolbox unexpectedly arose from an RNA-based bacterial defence mechanism. First described in *Streptococcus thermophilus,* the system works by recognition and cleavage of foreign DNA based on similarity with bacteriophage-derived sequences that had been priorly integrated in the prokaryotic genome after exposure to the pathogen [56]. The transcript derived from these integrated sequences, known as clustered regularly interspaced short palindromic repeats (CRISPR), is processed, paired to foreign DNA, and cleaved by a CRISPR associated protein (Cas). This system was successfully repurposed for facile genome editing by introduction of Cas nuclease 9 (Cas9) together with an RNA molecule complementary to the genomic target site (single guide RNA, sgRNA) [57, 58]. The discovery of the

CRISPR/Cas9 system had a profound, transformative effect on the genetic screening field [59, 60]: CRISPR/Cas9 genome editing was since used in mammalian somatic cells to unveil tumour cells' genetic dependencies [61, 62], investigate resistance genes to environmental stressors [63] and viral infection [64], to name just a few of the exponentially growing number of applications.

In addition, the discovery of a facile targeted genome engineering systems allowed, for the first time, scalable endogenous DNA manipulation beyond gene inactivation. Leveraging the system's modularity, inactivated genome targeting module ("dead" Cas9) was coupled to various transcriptional activator or repressor domains [65]. Transduction in conjunction with appropriate sgRNAs thus paved the way to genome-wide transcriptional activation (CRISPRa) and repression (CRISPRi) screens [66], exemplifying the versatility of the ever-expanding "CRISPR toolbox".

1.4 *In vitro* genetic screen formats

For decades, systematic identification of genotype-to-phenotype relationships was limited to model organisms such as yeast and fruit fly. These models, albeit enabling the detailed investigation of many hitherto unknown biological mechanisms, cannot efficiently recapitulate the human genetic architecture. In fact, a vast number of human genes do not possess orthologues in lower organisms and, as such, phenotypic outcomes of selected mutations can widely differ between model systems [67]. The availability of molecular tools to efficiently mutagenize mammalian somatic cells led to the widespread adoption of genetic screening systems using human cell cultures. While these set-ups allowed efficient genetic manipulation, large number of parallel experiments, and extensive control of culturing conditions, the nature of the interrogable phenotypes

changed profoundly, from whole organism traits to changes that could be detected at cellular and molecular level. This led to the added challenge of defining robust subcellular markers of phenotype of interest.

1.4.1 *Viability screens*

The most straightforward phenotype to interrogate by far is cellular fitness. Mutants exhibiting proliferation defects or undergoing cell death at a rate different than wild type cells can be easily identified by comparing how many instances of a specific mutation are present in the mutant pool at the start of the experiment versus a later time point. Measurement of mutant fitness can be performed in a "pooled" format, where collections of mutants are investigated simultaneously for differential proliferation. Compared to a format where individual mutants' phenotypes are separately measured ("arrayed"), isolation of cells carrying the desirable trait in pooled screens is inexpensive, easily scalable, and straightforward [68].

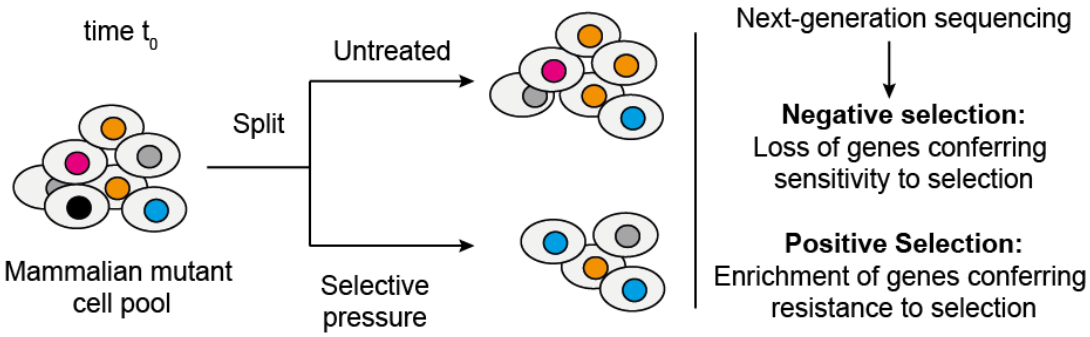


Figure 1.1 Schematic representation of pooled fitness screens in a mammalian mutant cell pool. Depending on the screen set-up, negative or positive selection screens can be performed. Image adapted from [65].

Pooled fitness screens can be broadly divided in two categories: positive and negative selection screens (**Figure 1.1**). In positive selection screens, a mutant pool is

subjected to a strong selective pressure, by treatment with a drug, a toxin, or a pathogen. In this case, surviving cells carry mutations in genes conferring susceptibility to the added agent. This approach was widely used to find genetic determinants of viral and bacterial susceptibility [69-71] and to dissect the mechanism of action of toxic drugs [72, 73]. In the case of anti-cancer drugs, a positive selection screen was able to identify mutants which rendered tumour cells resistant to pharmacological treatment and constituted potential targets for combination therapy [60, 74].

Conversely, a negative selection screen identifies genetic perturbations impinging on cell proliferation or survival, resulting in mutant depletion over time [75]. This type of screen played a pivotal role in identifying genes critical for cell survival (also defined as "essential") in model organisms and different cancer cell lines [60, 76-78]. Contrary to their "positive" counterpart, negative selection screens are more technically challenging, requiring greater sensitivity to detect changes in pool composition and advanced computational methods to detect false positives [79]. Depending on the type and efficiency of the mutagenesis technology used, non-perturbed cells can persist in the final pool, making screen results "noisy" and hard to interpret [80]. Hence, reliable mutagenesis methods such as CRISPR/Cas9 knockout and insertional mutagenesis in haploid cells were shown to outperform RNAi and CRISPRi approaches in identifying essential genes [81].

Despite their successful role in uncovering new biology, pooled genetic screens have limited applicability when it comes to dissecting intracellular pathways beyond viability. In fact, a readout based on cell fitness overshadows the mechanism underpinning the interaction and, as multiple processes can lead to cell death and/or proliferation inhibition, it is difficult to disentangle the mechanism of action of the screen

hits. While generating *de novo* signalling maps from a single fitness screen is unfeasible, data from a large number of fitness screens can be interpreted collectively to map interactions between two genetic components [82].

1.4.1.1 Genetic interactions

In broad terms, the term "epistasis" characterises the discrepancy between the expected and observed phenotype of two independent genetic mutations [83]. In a landmark study, Bateson described the phenomenon of epistasis in the colour of sweet pea flowers: when crossing two colourless flowers each bearing one mutation, purple flowers were obtained in non-Mendelian ratios (**Figure 1.2**) [84]. This suggested the two disrupted genes worked in concert in the anthocyanin synthesis pathway and mutation of either of them affected the resulting phenotype. In general, when a phenotype depends on the combination of multiple genetic loci, these genes are assumed to be in an epistatic relation with each other (*i.e.* to functionally interact). Thus, systematic screening of single and double mutants for a given phenotype, such as fitness, extends beyond identifying the role of a single gene and, by identifying epistatic relationships at genome level, can inform about cellular genetic architecture [83].

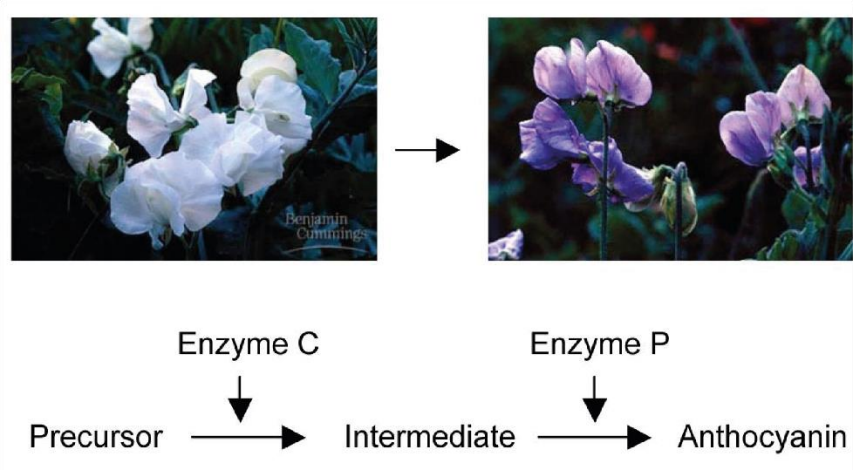


Figure 1.2 Principle of epistasis. Combination of two independent mutations (in "Enzyme C" and "Enzyme P") defines flower colour in sweet peas by impinges on the anthocyanin pathway. Image adapted from [83].

However, the execution of such experiments presented consistent challenges. The systematic study of pairwise interactions among n genetic loci amounts to n(n-1)/2 (assuming reciprocity) hypothesis to test, which, for human cells containing approximately 24.000 genes, would translate to investigating more than 2.8 x 10^8 interactions. Global genetic networks maps were nevertheless obtained for the model organism *Saccharomyces cerevisiae*, leveraging yeast's haploid/diploid life cycle and relatively simpler genome [85-87]. Genetic interactions (GIs) were inferred by measuring viability of single and double mutant phenotypes and calculating the deviation from the expected combined effect of two individual mutants (calculated as the product of the two single mutant phenotypes) (**Figure 1.3**) [82]. Thus, GIs were defined by double mutants having a more severe defect than predicted by the multiplicative model. In its extreme case, this interaction can result in synthetic lethality where the simultaneous perturbations of two genes leads to cell death, while single perturbations in either gene do not affect fitness.

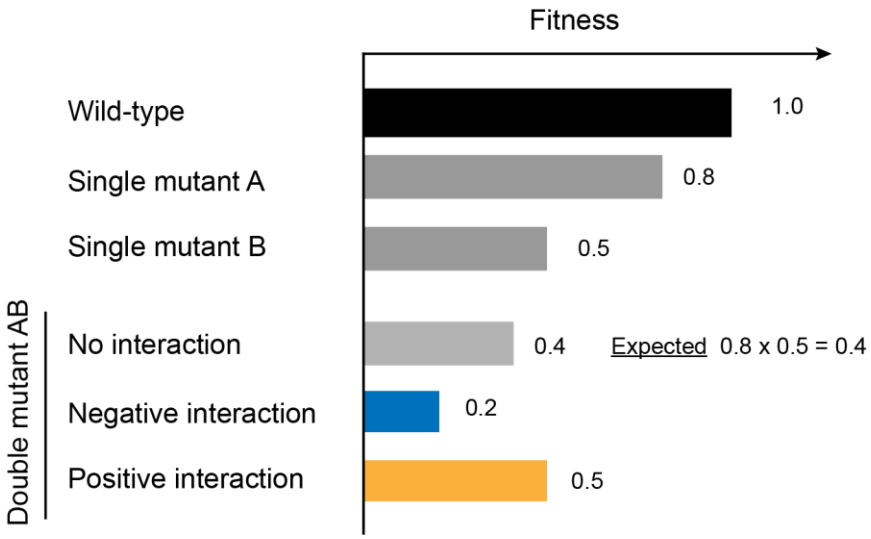


Figure 1.3 Graphical representation of quantitative genetic interactions (GI). Fitness of wild type cells is defined as 1, and single gene mutants exhibit a certain fitness defect. Double mutant fitness is displayed in case of no interaction (according to the multiplicative model), negative, and positive interactions. Image adapted from [82].

Conversely, double mutants for two genes belonging to the same functional complex might display a phenotype less severe than predicted. Analysis of di and tri-genic interactions revealed how genes belonging to the same protein complex or pathway present strong similarities in their GI pattern and, thus, how grouping of genes depending on their interaction profile could be used to predict *de novo* functional modules [86, 88].

With the advances in RNA interference and CRISPR/Cas9 technology, the possibility to experimentally test genetic interactions was extended to mammalian cells. To avoid the practical hurdle of generating double mutant collections in mammalian cells, an indirect method to define "co-essentiality" networks was employed. While in yeast, genetic interactions were assessed in an isogenic background to exclude the confounding effects of natural variants on GI, in mammalian cells the intrinsic differences in gene essentiality across cancer cell lines were exploited to infer the topology of genetic interaction networks [62, 89]. In fact, each cancer cell line is characterised by a unique set of

genomics and transcriptomics imbalances and, as a result of these divergent genetic wirings, per gene fitness score is expected to vary across cell lines. As genes within the same cellular pathway are expected show similar essentiality across all cell lines, two interacting genes will show high correlation in their essentiality pattern within individual cell lines, although their absolute effect across the cell panel will vary. Building on these concepts, an initiative by the Broad and Sanger Institutes performed a series of synthetic lethality screens in cancer cells currently encompassing more than 700 lines [79, 90, 91]. From these data, similarity scores between gene pairs were used to identify functional gene clusters and new protein complex components [92].

In combination with genetic interaction mapping, fitness screens' scope went beyond identifying single gene candidates affecting cellular viability and helped to reconstruct a cellular genetic network map. On the other hand, this approach is only geared towards identifying perturbations affecting cellular fitness and thus cannot be employed for the study of non-lethal, more complex cellular processes.

1.4.2 *High-content genetic screens*

The investigation of cellular phenotypes beyond fitness is made possible by the use of high-content imaging analysis. Advances in automated microscopy allows parallel monitoring of a number of cell phenotypes, ranging from cell shape to quantification of subcellular components through staining with fluorescent dyes [93]. Conversion of visual phenotypes to quantitative data is obtained through standardized image analysis workflows, measuring changes in individual cell states in an objective, reproducible way [94]. High-content screening provided an unparalleled amount of quantitative data on cell phenotypes and were successfully employed to find genetic determinants of complex

morphological processes such as subcellular translocation [95], cell migration [96], and chromosome segmentation in live cells [97]. Acquisition of such detailed information, however, comes at a cost: high-content screens require the mutant pool to be examined in an arrayed format (*e.g.* a multi-well plate), with one mutant per well in a pre-ordered fashion. For larger-scale applications, arrayed screens constitute a more work-intensive and costly option compared to their pooled counterparts as they require 1.) robotic and liquid handler systems to separately prepare and dispense individual reagents, 2.) automated microscopy equipment and 3.) extensive data storage and computing power to collect and analyse the obtained image data [68]. Additionally, while the achievable throughput for pooled screens was significantly increased over the past years with the advances in sequencing technology, the total number of screenable mutants still constitutes a major bottleneck for arrayed screens. This is evident by the fact that only a handful of high-content, genome-wide screens were performed in mammalian cells [95, 96, 98]. Thus, the operational challenges intrinsic to the arrayed screening format favour the use of high-content screens primarily to investigate in detail the phenotype of a subset of gene mutants.

1.4.3 *Enrichment selection screens*

The question of how to screen for non-viability related phenotypes in the more convenient pooled format found an answer in enrichment or marker-based selection screens. A tenet in the genetic screening field is that stringent selection criteria, such as lethality, are required to minimize the risk of passenger mutations or false positives in the selected population [11]. In enrichment selection screens, a cell-autonomous phenotype is translated into a fluorescent signal, easily detectable in high-throughput using Flow

Cytometry (FC). This method, described in detail in **Section 3.1.2**, allows characterisation of cellular properties at single-cell level and can be coupled with sorting of a subpopulation of interest. FC identifies cellular levels of a fluorescent marker by means of a fluorophore-conjugated antibody which recognises a specific surface antigen or, alternatively, by the use a reporter system that encodes an intrinsically fluorescent protein as readout for certain cellular processes. To obtain sufficient separation between the initial and the selected pools, subpopulations displaying the highest (or lowest) fluorescence signal are isolated and returned to culture where they are further expanded. The selection process is repeated two or more times before mutation recovery, mapping and comparing per gene insertions in the selected subpopulation to the initial mutant pool.

This method allowed for the first time the screening for non-viability related phenotypes in a pooled format, requiring only an initial manipulation step for introduction of a reporter system. Enrichment selection screens were used, for example, to identify new component of macroautophagy [99], to discover enhancers of transcription factor POU5F1 in human embryonic stem cells (hESC) [100], and to map WNT signalling in detail [101]. On the other hand, enrichment selection screens are laborious, requiring multiple sequential rounds of fluorescent selection and expansion cycles, and limited to detection of readouts which can be carried out in live cells.

1.4.4 *FACS-based forward genetic screens*

In 2015, Parnas *et al.* published a study in which a CRISPR/Cas9 mutagenized library of primary mouse immune cells was fixed, fluorescently stained for tumour necrosis factor (Tnf) levels and sorted using FACS [102]. It was hypothesized that the sorting bin containing mutants with low fluorescence signal (Tnf^{LOW}) was enriched for sgRNAs

targeting Tnf positive regulators compared to cells in the high fluorescence sorting bin (Tnf^{HIGH}). Conversely, sgRNAs targeting negative regulators were enriched in Tnf^{HIGH} versus Tnf^{LOW} sorted populations [102]. The screen successfully identified multiple components of the Tnf activation cascade although it suffered from a high false positive rate (hit validation rate for positive and negative modulators was 50% and 6%, respectively). This example constitutes a paradigm-shift in the field, allowing for a bi-directional, internally controlled screening approach, here described as FACS-based forward genetic screen. Additionally, by using fixed cells, this screening methodology dramatically broadened the "screenable phenotypic space", for the first time allowing endogenous intracellular markers to be used as readouts in a pooled format.

The same principle was adapted by Brockmann *et al.* to gene-trapped haploid human HAP1 cells (**Figure 1.4**) [103]. Leveraging the significantly higher number of independent mutations per gene obtained through gene-trapping compared to sgRNA integration [76, 77], FACS-based genetic screening in a haploid background allowed for robust statistics and high-confidence identification of genetic modulators. The technology had been successfully used to reconstruct the regulatory network underpinning biological processes such as activation of signalling cascades [103, 104], cholesterol metabolism [105], immune regulation [106, 107, 108] and viral entry [109, 110]. The use of this technology as a discovery tool for mapping intracellular pathways is employed throughout this thesis and its set-up is described in detail in **Chapter 3**.

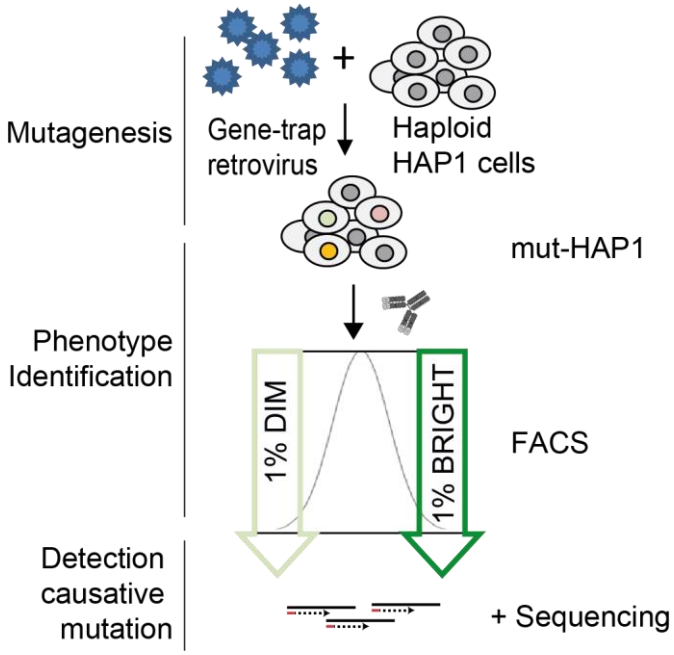


Figure 1.4 Schematic representation of experimental Florescence Activated Cell Sorting (FACS)-based forward genetic screen workflow. HAP1 cells are transduced with gene-trap retrovirus to generate mutagenized HAP1 (mut-HAP1) cells. The knockout pool is expanded and stained for the marker of interest; signal is detected using a fluorescently labelled antibody. Cells in the top and bottom 1% (or 3%) of the fluorescent phenotype are isolated using cell sorting. Regulatory genes are identified by recovering and sequencing genomic DNA from the sorted fractions, followed by mapping of mutations to gene bodies. Per gene significant enrichment of mutations in one sorted bin versus the other identifies disrupted genes as regulators.

1.5 Thesis Aims

In this thesis I employed FACS-based haploid genetic screening to map the regulation of key cellular signalling pathways dysregulated in disease. Specifically, this thesis had four objectives:

- Establish a FACS-based genetic screening workflow according to the protocol from Brockmann *et al.* [103];
- Evaluate the technology for reproducibility and for ability to identify true regulators;
- Employ the technology to identify context-specific pathway regulators through iterative screening in presence of perturbagens;
- Employ the technology to identify novel gene modulators and their interconnectivity for the mTORC1 and the TNFR1/TNFα/NF-κB signalling pathways. Employing the technology in two well studied pathways allowed to validate my findings against pre-existing biological knowledge and, at the same time, unbiasedly identify novel genetic regulators of potential therapeutic interest.

Full list of screens performed in the thesis in **Table 1.2**.

Screen family	Cell background	Treatment	Marker	Comment	Presented in
HIF-1α	Wild type HAP1	-	HIF-1α		**Chapter 3**
HIF-1α	Wild type HAP1	DFOM	HIF-1α		**Chapter 3**
mTORC1	Wild type HAP1	-	p-RPS6	1% gating	**Chapter 4**
mTORC1	Wild type HAP1	-	p-RPS6	3% gating	**Chapter 4**
mTORC1	Wild type HAP1	rapamycin	p-RPS6		**Chapter 4**
mTORC1	ΔLAMTOR4 HAP1	-	p-RPS6		**Chapter 4**
MR1	MR1_HAP1	-	MR1	surface	**Chapter 3**
TNFα-dependent NF-κB activation	Wild type HAP1	+TNFα	IκBα		**Chapter 5**
TNFα-dependent NF-κB activation	ΔQRICH1 HAP1	+TNFα	IκBα		**Chapter 5**
TNFR1	Wild type HAP1	-	TNFR1	surface	**Chapter 5**
TNFR1	ΔQRICH1 HAP1	-	TNFR1	surface	**Chapter 5**

Table 1.2 List of FACS-based forward genetic screens presented in this study. Full hit list for every screen is provided in **Appendices**.

Chapter 2: **Materials and Methods**

2.1 **Antibodies, Plasmids and Reagents**

Target Name	Catalogue Number	Supplier
α-Tubulin	2125	Cell Signaling Technologies
β-Actin	A2066	Sigma Aldrich
FKBP12	2918	Abcam
FLCN	3697	Cell Signaling Technologies
GFP	11814460001	Sigma Aldrich
HIF-1α	610959	BD Biosciences
IκBα	4814	Cell Signaling Technologies
Lamin A/C	2032	Cell Signaling Technologies
LAMTOR4	13140	Cell Signaling Technologies
LAMTOR5	14633	Cell Signaling Technologies
LC3A/B	12741	Cell Signaling Technologies
MEK1/2	9122	Cell Signaling Technologies
MR1	361102	BioLegend
Phospho-RPS6 (Ser235/236)	4858	Cell Signaling Technologies
Phospho-RPS6K1 (Thr389)	9234	Cell Signaling Technologies
QRICH1	HPA037677	Atlas Antibodies
RPS6	2317	Cell Signaling Technologies
RPS6K1	49D7	Cell Signaling Technologies
SEPHS1	HPA037645	Atlas Antibodies

TNFR1	3736	Cell Signaling Technologies
TNFR1/TNFRSF1A	MAB625	R&D Systems
VDAC	4661	Cell Signaling Technologies

Table 2.1 List of primary antibodies used in this study.

Antibody	Catalogue number	Supplier
HRP-conjugated goat-anti-rabbit	1706515	BioRad
HRP-conjugated goat-anti-mouse	1706516	BioRad
Alexa546-conjuagted goat anti-rabbit	A11010	Thermo Fisher Scientific
Alexa488-conjuagted goat-anti-rabbit	A11008	Thermo Fisher Scientific
Alexa488-conjuagted goat-anti-mouse	A11001	Thermo Fisher Scientific
IgG anti-rabbit	12-370	Millipore

Table 2.2 List of secondary antibodies used in this study.

Plasmid	Catalogue Number	Source
pGT-en2-BFP	NA	Gift from T. Brummelkamp
pGag-Pol	NA	Gift from T. Brummelkamp
pAdVantage	NA	Gift from T. Brummelkamp
pVSV.G	14888	Addgene
pCMV-GFP	11153	Addgene
pLentiCRISPR v2	52961	Addgene
FLCN-eGFP	72289	Addgene
pLenti-GFP	17448	Addgene
pLenti-QRICH1	see **Appendix 8.1.2**	GeneScript
pLenti-QRICH1-FLAG	see **Appendix 8.1.2**	GeneScript
pLenti-QRICH1-ΔCARD – FLAG	see **Appendix 8.1.2**	GeneScript
pLenti-QRICH1-ΔNLS – FLAG	see **Appendix 8.1.2**	GeneScript
pMD.G	12259	Gift from M. Gyrd Hansen
psPAX2	12260	Gift from M. Gyrd Hansen

Table 2.3 List of plasmids used in this study. Synthesis of QRICH1 cDNA constructs and cloning in p-LENTI-GFP vector was performed by GeneScript.

Reagent	Catalogue Number	Supplier
Absolute Ethanol (EtOH)	10517694	Thermo Fisher Scientific
Acetyl-6-formylpterin	23303	Cayman Chemicals
Actinomycin D	A1410	Sigma Aldrich
Agarose	1613101	BioRad
Alkaline Phosphatase, Calf Intestinal (CIP)	M0290	New England Biolabs
Ampicillin Sodium Salt	A0839	Applichem
AZD2014 (Vistusertib)	S2783	Selleckchem
Betaine solution	B0300	Sigma Aldrich
Bortezomib	S1013	Selleckchem
Bovine Serum Albumin (BSA)	A3059	Sigma Aldrich
Bromophenol Blue	114391	Sigma Aldrich
BsmBI	R0580S	New England Biolabs
Calcium Chloride ($CaCl_2$)	C/1400/53	Fisher Scientific
Chloroquine	C6628	Selleckchem
Clarity Max Western ECL Substrate	1705062	BioRad
Crystal Violet	32675	Fluka
Cycloheximide	C7698	Sigma Aldrich
4′,6-diamidino-2-phenylindole (DAPI)	62247	Thermo Fisher Scientific
Digitonin	D141	Sigma Aldrich
Distilled Water (H_2O)	15230147	Thermo Fisher Scientific
DL-Dithiothreitol solution	646563	Sigma Aldrich
DMEM, w/o L-Glutamine, w/o amino acids, with 1g/L glucose	C4150	GeneAxxon
DMEM, high glucose, pyruvate	41966029	Thermo Fisher Scientific
DMEM, low glucose, pyruvate	31885023	Thermo Fisher Scientific
dNTP Mix (10 mM)	R0191	Thermo Fisher Scientific
Dynabeads M-270 Streptavidin	65305	Thermo Fisher Scientific
Ethylenediaminetetraacetic acid (EDTA) (0.5 M), pH 8	AM9260G	Thermo Fisher Scientific

EDTA-free Protease Inhibitor Cocktail	11873580001	Roche
Ficoll 400	B22095	Alfa Aesar
Fix Buffer I	557870	BD Bioscience
Foetal Bovine Serum (FCS)	S-001A-BR	Antibody production service
FuGENE HD	E2311	Promega
Gel loading Dye (6X)	B7024S	New England Biolabs
Glycerol	10579570	Thermo Fisher Scientific
HEPES	H3375	Sigma Aldrich
I-Block Protein Based Blocking Reagent	T2015	Applied Biosystems
ICS Fixation Buffer	00-8222-49	eBioscience
IMDM, GlutaMAX Supplement	31980030	Thermo Fisher Scientific
LB Broth	BP1426	Fisher Scientific
Lithium chloride	203637	Sigma Aldrich
Magnesium Chloride ($MgCl_2$)	M8266	Sigma Aldrich
McCoy's 5A Medium	16600082	Thermo Fisher Scientific
MEM Non-Essential Amino Acid Solution (100X)	11140050	Thermo Fisher Scientific
Midori Green	MG 04	Nippon Genetics Europe
MK-2206 2HCl	S1078	Selleckchem
$MnCl_2$	20-309	Merk Millipore
Mowiol	81381	Sigma Aldrich
NEBuffer 3.1	B7203S	New England Biolabs
NuPAGE Sample Reducing Agent	NP0009	Thermo Fisher Scientific
NuPAGE MOPS SDS Running Buffer (20X)	NP0001	Thermo Fisher Scientific
NuPAGE 4-12% Bis-Tris Protein Gels, 1.0 mm, 10/12/15-well	NP0321BOX/ NP0322BOX/ NP0323BOX	Life technologies
OptiMEM	31985062	Thermo Fisher Scientific
PageRuler Plus Prestained Protein Ladder	26619	Thermo Fisher Scientific
Paraformaldehyde solution (PFA) 4% in PBS	sc-281692	Santa Cruz Biotechnology

PBS (1X)	10010023	Thermo Fisher Scientific
Penicillin-Streptomycin-Glutamine (100X)	10378016	Thermo Fisher Scientific
Perm Buffer III	558050	BD Bioscience
Permeabilisation Buffer	00-8333-56	eBioscience
PhosSTOP Phosphatase Inhibitor Cocktail	4906845001	Sigma Aldrich
PMSF Protease Inhibitor	36978	Thermo Fisher Scientific
Poly-L-lysine	P4832	Sigma Aldrich
Polyethylene glycol solution	P1458	Sigma Aldrich
Potassium Chloride (KCl)	P9541	Sigma Aldrich
PowerUp SYBR Green Master Mix	A25741	Thermo Fisher Scientific
Propidium Iodide	P1304MP	Thermo Fisher Scientific
Protamine Sulphate Salt	P4380-25G	MP Biomedicals
Protein A Agarose Beads	16-125	Merk
Puromycin	ant-pr	Invivogen
Quick-Load Purple 1 kb DNA Ladder	N0552	New England Biolabs
Rapamycin (Sirolimus)	S1039	Selleckchem
RIPA Buffer	R0278	Sigma Aldrich
RNase A	A3832	Applichem
RPMI-1640 Medium	11875085	Thermo Fisher Scientific
Sodium Chloride (NaCl)	71382	Sigma Aldrich
Sodium Dodecyl Sulphate solution (10%)	BP2436-1	Thermo Fisher Scientific
Stbl3 Chemically Competent *Escherichia coli*	C737303	Invitrogen
Sucrose	S0389	Sigma Aldrich
T4 DNA Ligase	M0202	New England Biolabs
T4 DNA Ligase Reaction Buffer	B0202	New England Biolabs
T4 Polynucleotide Kinase	M0201	New England Biolabs
TBE Buffer 10X	#1610770	BioRad
Tergitol solution (NP40)	NP405	Sigma Aldrich
TNF (Recombinant human)	300-01A	PeproTech

Trans-Blot Turbo Mini/Midi PVDF Transfer Packs	170-4156/170-4157	BioRad
Triton X-100	X100- 100ML	Sigma Aldrich
Trizma base	T1503	Sigma Aldrich
Trypsin-EDTA	25300096	Thermo Fisher Scientific
TurboFectin 8	TF81001	OriGene
Tween-20	WZ-88248-24	Acros Organics
Western Lightning Plus-ECL	NEL104001EA	Perkin Elmer

Table 2.4 List of reagents used in this study.

Buffer	Composition
1.2% agarose gel	1% w/v agarose powder in 1X TAE Buffer (boiled until dissolved), 0.5% v/v Midori green added
0.05% Triton X-100	0.05% v/v Triton X-100 in 1X PBS
2X binding buffer	6 M LiCl, 10 mM Trizma base (pH adjusted to 7.5), 1 mM EDTA in H2O
2X sample buffer	320 mM Trizma base (pH adjusted to 6.8), 40% glycerol, 16 µg /ml bromophenol blue, 8% SDS
Cytoplasmic extraction buffer (CEB)	10 mM HEPES pH =7.5, 10 mM KCl, 0.1 mM EDTA, 1 mM DTT, 0.5% v/v NP40, 0.5 mM PMSF, 1X PhosSTOP
Digitonin Ficoll extraction buffer (DFEB)	20 mM HEPES pH = 7.5, 6.25% v/v Ficoll 400, 0.27 M Sucrose, 3 mM $CaCl_2$, 2 mM $MgCl_2$, 0.5 mM PMSF, 1X PhosSTOP
Dignam buffer A (modified)	10 mM HEPES (pH adjusted to 8), 1.5 mM $MgCl_2$, 10 mM KCl, 6.25% v/v Ficoll 400, 1X Protease Inhibitor, 1X PhosSTOP
Dignam buffer C	20 mM HEPES (pH adjusted to 8), 25% v/v glycerol, 0.42 M NaCl, 1.5 mM MgCl2, 0.2 mM EDTA, 1X Protease Inhibitor, 1X PhosSTOP
iBlock	0.2% w/v I-Block in 1X PBS (boiled until dissolved), 0.1% v/v Tween-20 added
ILB-E	10 mM Trizma base (pH adjusted to 7.5), 150 mM NaCl, 0.5 mM EDTA 0.5% v/v NP-40
PBS + 0.1% BSA	0.1% w/v BSA in 50 ml PBS
PBS-F	10% Foetal Calf Serum (FCS) in 1X PBS
PBS-T	0.1% v/v Tween-20 in 1X PBS
PEG (Polyethylene glycol) precipitation solution	40% w/w PEG-8000, 3M NaCl

Table 2.5 List of buffers and solutions used in this study.

Kit	Catalogue Number	Supplier
AccuPrime Taq DNA Polymerase High Fidelity (10X Accuprime Buffer II, $MgSO_4$, Accuprime TaqHI)	12346094	Thermo Fisher Scientific
CircLigaseII ssDNA Ligase (CircLigase II, CircLigase II Buffer)	CL9021K	Cambio
DNeasy Blood and Tissue	69506	Qiagen
D1000 ScreenTape Assay	5067-5583	Agilent
GoTaq G2 DNA Polymerase (GoTaq G2 DNA Polymerase, 5X GoTaq Green Reaction Buffer)	M7845	Promega
HiSpeed Plasmid Maxi	12662	Qiagen
MinElute PCR Purification	28004	Qiagen
QIAamp DNA Mini Blood	51104	Qiagen
QIAquick Gel Extraction	28704	Qiagen
QIAquick PCR Purification	28106	Qiagen
QIAprep Spin Miniprep	27104	Qiagen
QuantSeq 3’ mRNA-seq library prep (FWD)	015.96	Lexogen
Qubit dsDNA HS assay	Q32851	Life Technologies
RevertAid RT (5X RT Reaction Buffer, Random Hexamer Primer, dNTP Mix, RiboLock RNase Inhibitor, RevertAid Reverse Transcriptase)	K1691	Thermo Fisher Scientific
RNAeasy Mini	74106	Qiagen
Subcellular Protein Fractionation for Cultured Cells	78840	Thermo Fisher Scientific
TURBO DNA-free (TURBO DNase, 10X TURBO DNase Buffer, DNase Inactivation Reagent)	AM1907	Invitrogen

Table 2.6 List of commercial kits used in this study.

2.2 Cell lines

The haploid human cell line HAP1 was provided by T. Brummelkamp. HAP1 cells were cultured in Iscove's Modified Dulbecco's Medium (IMDM, Thermo Fisher Scientific) supplemented with 10% Foetal Calf Serum (FCS, Antibody Production Service) and 1X Penicillin-Streptomycin-Glutamine (P/S-Glut, Thermo Fisher Scientific). The LAMTOR4 knockout HAP1 clonal cell line, containing a 2 base-pair deletion in exon 2, was obtained from Horizon Genomics (HZGHC000374c009). HEK293T, HeLa, U2OS, HCT116 and ZR-75-1 cells were procured from American Type Culture Collection (ATCC). The TNFR1 knockout HCT116 clonal cell line was a gift from M. Gyrd-Hansen. HEK293T, HeLa and U2OS cells were propagated in Dulbecco's Modified Eagle's Medium (DMEM, Thermo Fisher Scientific) supplemented with 10% FCS and 1X P/S-Glut. HCT116 cells were maintained in McCoy's 5A Modified Medium (Thermo Fisher Scientific) with added 10% FCS and 1X P/S-Glut. ZR-75-1 cells maintained in Roswell Park Memorial Institute's Medium (RPMI-1640, Thermo Fisher Scientific) supplemented with 10% FCS and 1X P/S-Glut. Mycoplasma testing was performed on all cell lines before usage and cells were incubated at 37°C, 5% CO_2 in a humidified incubator.

2.3 Generation of mutagenized HAP1 (mut-HAP1) cells

For gene-trap retroviral production HEK293T cells were grown to approximately 80% confluence in 6 or 12 T175 flasks (Corning). Per each flask, a plasmid mix and a TurboFectin 8 mix are prepared and combined, the resulting solution is incubated at room temperature (RT) for approximately 30 minutes (**Table 2.7**). The mix was added on

HEK293T cells after replacing the standard growth medium with DMEM supplemented with 1X P/S-Glut and 30% FCS.

Plasmid mix	TurboFectin 8 mix
6.02 µg pGag-Pol	200 µl OptiMEM + 45 µl TurboFectin 8
1.4 µg pVSV.G	
0.84 µg pAdVantage	
6.6 µg pGT-en2-BFP	

Table 2.7 Gene-trap retrovirus generation. Mix composition for 1 transfection (1 T175 flask).

Approximately 40 hours after transfection, HEK293T cell supernatant is collected and filtered through mixed cellulose ester 0.45 µm membrane (Merck Millipore). The filtered supernatant is transferred into Ultra-Clear tubes (Beckman Coulter) loaded onto a SW32Ti rotor and spun down at 60.000 rcf for 2 hours at 4°C in an Optima XPN centrifuge. After ultra-centrifugation the clarified supernatant is carefully removed and the viral pellet is resuspended in 200 µl PBS per tube and stored overnight (O/N). Viral supernatant collection is repeated twice daily for the first 3 days, combining the daily harvests.

Concentrated virus is resuspended in IMDM with 1X P/S-Glut + 10% FCS, combined with 8 µg/ml protamine sulphate and added to actively growing HAP1 cells (4 x 10^7 cells per 1 T175 flask, ratio flasks HEK293T: HAP1 cells 3:1). Transduction was performed for three consecutive days after which mut-HAP1 cells were expanded in fresh IMDM + 1X P/S-GLUT + 10% FCS. Transduction efficiency was estimated by comparing gene-trap encoded BFP signal in mut-HAP1 cells to a non-transduced control (wild type HAP1 cells). After trypsinisation, approximately 10^6 wild type and mut-HAP1 cells were washed with 5 ml PBS, spun down at 500 rcf for 5 minutes and resuspend in

200 µl 1:1 Fix Buffer I: PBS solution. Cells were incubated at 37°C for 10 min, spun down at 1.300 rcf for 5 minutes and resuspend in 1 ml PBS-F. Fluorescence was measured on a LSR Fortessa X20 equipped with Violet (405 nm), Blue (488 nm), Yellow-Green (561 nm) and Red (640nm lasers) (BD Biosciences). Mut-HAP1 cells were either aliquoted, frozen, and stored in liquid nitrogen or used directly.

2.4 FACS-based forward genetic screen

Mut-HAP1 cells were expanded to approximately 2 x 10^9 cells and treated according to individual screen protocol. For intracellular reporters, cells were washed once with PBS and detached using Trypsin-EDTA. Cells were resuspended in a solution of PBS-F, spun down at 500 rcf for 10 minutes and pooled together in PBS-F. Mut-HAP1 cell pellet was resuspended in 10 ml 1:1 Fix Buffer I:PBS solution for 10 minutes at 37ºC, washed twice in PBS-F, followed by permeabilisation for 30 minutes at 4ºC in 1:1 Perm Buffer III: PBS. After 2 additional washes in PBS-F with a centrifugation step at 1.300 rcf, mut-HAP1 cells were incubated with a primary antibody dilution in PBS-F for 1 hour. Cell pellet was washed and incubated with 0.8 mg/ml Ribonuclease A (RNase A) for 1.5 hours before 2 additional washing steps and incubation with 10 µg/ml propidium iodide (PI) and Alexa488-conjugated secondary antibody (1:1.000). For surface antigens, cells were detached with PBS supplemented with 1 mM EDTA, pooled in PBS-F before incubation with primary antibody dilution for 1 hour at 4°C. After 2 washes using PBS-F, cells were incubated with Alexa488-conjugated secondary antibody for 45 minutes at 4°C. Cells were then processed in the same way as for intracellular staining undergoing fixation, permeabilisation and RNase A treatment prior to incubation with PI. Notably, in the case of the MR1 screen, mut-HAP1 cells were fixed in ICS Fixation Buffer for 30

minutes at RT, washed once in PBS + 1mM EDTA and once in PBS-F before resuspension and incubation for 10 minutes at RT in 1X Permeabilisation Buffer (diluted in water). According to the manufacturer instruction, the following staining steps (RNase A and PI) were performed in 1X Permeabilisation Buffer. Stained mut-HAP1 cells were finally resuspended in PBS-F + 10 µg/ml PI and stored at 4ºC. Mut-HAP1 cells solution was diluted to a concentration of 20-30 x 10^6 cells/ml and analysed on a LE-SH800 Cell Sorter instrument (Sony) mounted with a 70 nm sorting chip. Both Alexa488 fluorophore and PI can be excited by the 488 nm laser, but they differ in peak emission wavelengths allowing fluorescence to be captured by different detectors (525/50 for Alexa488, 617/30 or 665/30 for PI). After exclusion of doublets [111] and cells with DNA content > 1n, Alexa488 fluorescence was visualized in the selected subpopulation and sorting gates were set to collect approximately 10^7 cells for the lowest (LOW-DIM) and highest (HIGH-BRIGHT) 1-3% of the distribution.

2.5 Insertion sites recovery and mapping

Genomic DNA from the sorted populations was extracted using QIAamp DNA Blood Mini kit. Each genomic pellet was resuspended in 200 µl PBS prior to addition of 20 µl Proteinase K and 200 µl Buffer AL. Samples were pulse vortexed for 15 seconds prior to O/N decrosslinking at 56ºC and 1.100 rpm. After O/N incubation, 200 µl of 100% EtOH were added per sample prior to loading onto a QIAamp spin column. Samples were centrifuged for 1 minute at 8.000 rcf, washed with 500 µl AW1 and then subjected to a second round of centrifugation and washing with 500 µl AW2. Columns were dried by centrifugation for 3 minutes at max speed. Genomic DNA was eluted in a final volume of 100 µl H_2O in 2 sequential steps and quantified using a Nanodrop 8000

Spectrophotometer (Thermo Fisher Scientific). Recovery of gene-trap insertion sites (**Figure 2.1**) was performed as previously reported [103], primers used are listed in **Table 2.8**.

Primer Name	Sequence	Supplier
Dual Biotin Primer	double biotin/GGTCTCCAAATCTCGGTGGAAC	IDT
Phosphorylated ssDNA linker	phospho/ATCGTATGCCGTCTTCTGCTTGACTCAGT AGTTGTGCGATGGATTGATG/dideoxycytidine	IDT
ssDNA pre-adenylated linker	adenyl/ATCGTATGCCGTCTTCTGCTTGACTCAGTA GTTGTGCGATGGATTGATG/dideoxycytidine	IDT
PI LTR primer (P7)	AATGATACGGCGACCACCGAGATCTGATGGTTCT CTAGCTTGCC	Source Bioscience
PII LAM primer (P5)	CAAGCAGAAGACGGCATACGA	Source Bioscience
Custom sequencing primer	CTAGCTTGCCAAACCTACAGGTGGGGTCTTTCA	Source Bioscience

Table 2.8 List of primers used in recovery of gene-trap insertions. All plasmids were diluted in water to 25 µM except dual Biotin primer (0.25 µM) and the custom sequencing primer (100 µM).

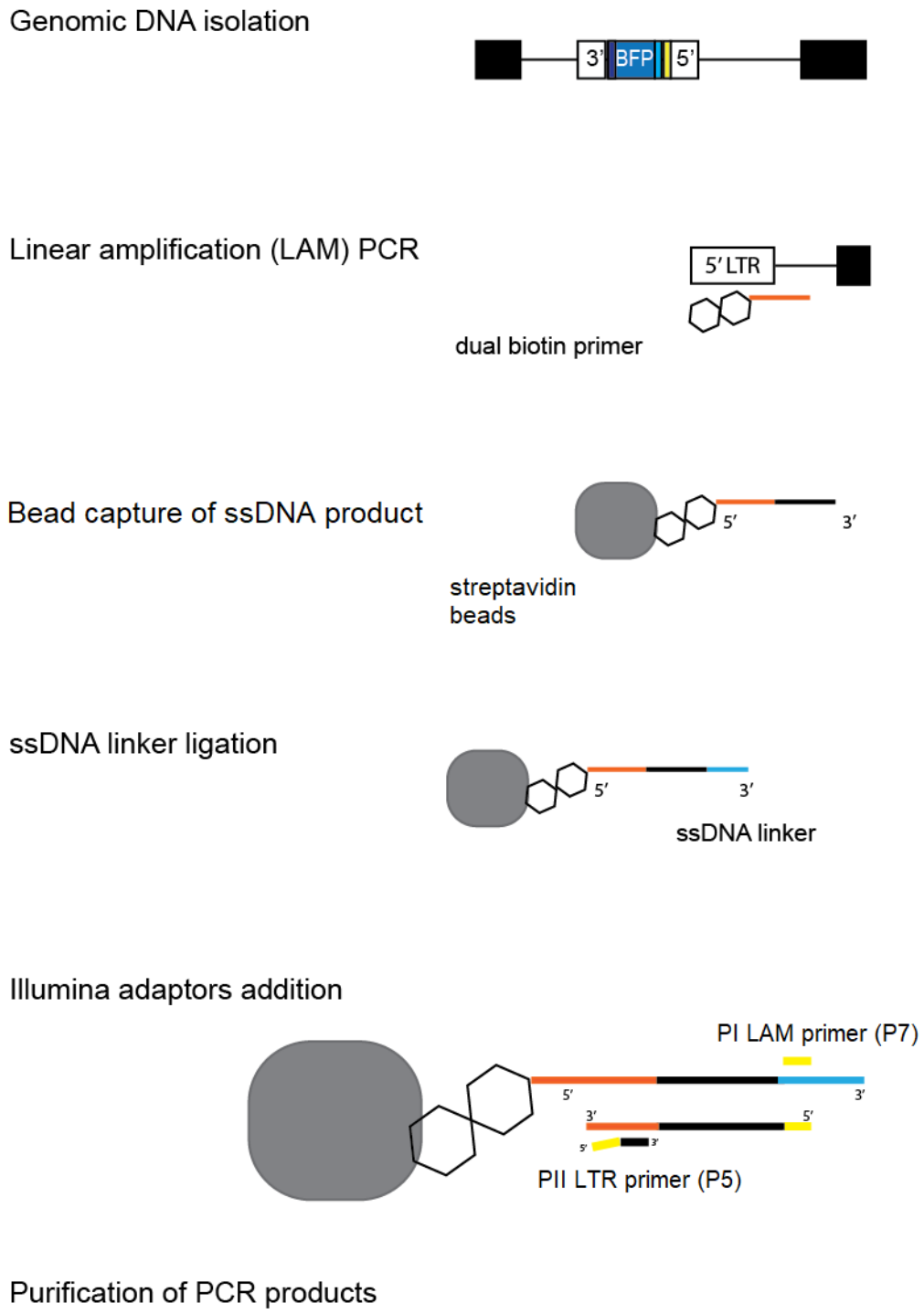


Figure 2.1 Schematic overview of recovery of gene-trap insertion sites workflow. BFP = Blue Fluorescent Protein; LTR = Long Terminal Repeats; ssDNA = single stranded DNA

An initial Linear Amplification (LAM) PCR step was performed: the sample was distributed into N reactions/sample, with N determined to have at least 1 µg genomic DNA/reaction. Reactions were set-up as per **Table 2.9**.

	Amount	Final Concentration
Dual Biotin Primer	3 µl	15 nM
10X AccuPrime Buffer II	5 µl	
$MgSO_4$	1 µl	1 mM
AccuPrime TaqHI	0.4 µl	
Genomic DNA	~ 1 µg	
H_2O	Bring to 50 µl	

Table 2.9 LAM PCR reaction set-up for N = 1.

Samples were amplified for 120 cycles on a Veriti 96-Well Thermal Cycler (Applied Biosciences) according to the following program:

94°C 5 minutes
{94°C 30 seconds
58°C 30 seconds
68°C 1 minutes} x 120
68°C 7 minutes
4°C indefinitely

After the reaction was completed, 2.5 µl of M-270 Streptavidin-coated beads per reaction (N) were washed in 800 µl PBS + 0.1% BSA. Supernatant was removed with the help of a magnetic rack and beads were resuspended in equal volumes of LAM PCR product and 2X binding buffer. In this step, the N LAM PCR reactions pertaining to the same sample (*i.e.* HIGH or LOW) were individually pooled. The mixture was loaded onto a rotating wheel for 2 hours at RT to allow bead capture of ssDNA.

Samples were then washed three times with 0.05% Triton X-100 solution by centrifugation at 8.000 rcf, followed by removal of the unbound fraction with the help of

a magnetic rack. Depending on the number of LAM PCR reactions (N), ligation was set-up in a total volume of 20 µl x (N/2) as shown in **Table 2.10**.

	Amount (µl)	Final Concentration
Betaine	4	1 M
H_2O	11.5	
CircLigase II Buffer	2	
$MnCl_2$	0.5	2.5 mM
Pre-adenylated linker	1	1.25 µM
CircLigase II	1	

Table 2.10 Set-up for 1X 20 µl ssDNA ligation reaction.

After removal of 0.05% Triton X-100 by separating the beads on a magnetic rack, beads were resuspended in DNA ligation mix and incubated at 60°C for 2h. Samples were frequently agitated to avoid beads sedimentation. Reactions were then washed 4 times with 0.05% Triton X-100 as previously described prior to addition of standard Illumina adaptors (PI and PII) via PCR. Depending on the number of LAM PCR reactions (N), ligation was set-up in M=N/2 reactions of 50 µl each (**Table 2.11**).

	Amount (µl)	Final Concentration
H_2O	42.4	
10X Accuprime Buffer II	5	
PI – LTR primer	1	0.5 µM
PII – LAM primer	1	0.5 µM
AccuPrime™ Taq DNA Polymerase	0.6	

Table 2.11 Master mix for 1 standard Illumina adaptors PCR reaction.

The ssDNA fragment bead mixture was resuspended in Illumina adaptors PCR master mix and amplified for 18 cycles on a Veriti 96-Well Thermal Cycler according to the following program:

94°C 2 minutes
{94°C 30 seconds
55°C 30 seconds
68°C 105 seconds} x 18
68°C 7 minutes
4°C indefinitely

The obtained fragment library was purified using QIAquick PCR purification kit according to the manufacturer's specification and eluted in 30 µl H_2O. Overall fragment size of the obtained library was measured on TapeStation 2200 instrument (Agilent) using the Agilent D1000 ScreenTape Assay.

The screen conducted in collaboration with the Brummelkamp lab at the Netherlands Cancer Institute (NKI) was performed using an analogous protocol, as reported in Brockmann *et al.* [103], with two notable differences from what described here. Isolation of the extremes of the fluorescence distribution was performed on a Biorad S3 cell sorter (Biorad). Additionally, ssDNA ligation was performed using the TS2126 thermostable RNA ligase 1 of bacteriophage *Thermus scotoductus* according to the published protocol [103].

2.6 Mutation mapping and analysis

HIGH and LOW libraries were sequenced on HiSeq2500 sequencer (Illumina) using a custom sequencing primer and yielding 50 bp single-end reads. Unique reads were aligned to the human genome (hg19) using Bowtie [112], allowing up to 1 mismatch.

Unambiguously aligned reads were then mapped to a custom reference annotation based on RefSeq coordinates for protein-coding genes. To avoid mapping ambiguity, the custom reference annotation did not consider regions of genetic overlap. Due to the unidirectional design of the gene-trap, only insertions in the same orientation as the gene in which they integrated were extracted after reads mapping: these are further referred to as "sense" insertions. To quantify per gene enrichment for disrupting mutations (INS) in either LOW or HIGH population, a mutational index (MI) was computed. Significance of MI is calculated on a per gene basis using a 2-sided Fisher's exact test. Multiple testing was controlled using False Discovery Rate (FDR) with a threshold of 0.05.

$$MI_{Gene} = \left(\frac{INS_{Gene}}{\sum INS_{AllGenes} - INS_{Gene}} \right)_{HIGH} \Big/ \left(\frac{INS_{Gene}}{\sum INS_{AllGenes} - INS_{Gene}} \right)_{LOW}$$

The p-RPS6 screens obtained using sorting gates of 1 and 3%, were combined by calculating average number of combined per gene insertions. Statistical analysis on the resulting dataset ($p\text{-}RPS6_{combined}$) was performed as mentioned above.

2.7 Delta MI (ΔMI) calculation and insertion location visualisation

To detect significant differences between MIs of the same gene in two screens, it was assumed that the screens were independent and MI was log-transformed; hence, MI differences are expected to be normally distributed. Considering MI as an odds ratio, a standard z-test was applied. Given two screens (1 and 2), for each gene that scored as a significant regulator in at least one of the two screens, the following calculations were performed (SE=standard error, n1-4=contingency table counts, CI=95% confidence interval, p=p value):

$$\Delta MI = \log(MI_{screen1}) - \log(MI_{screen2})$$

$$SE(\Delta) = \sqrt{SE_{screen1}^2 + SE_{screen2}^2}, \quad SE(logMI) = \sqrt{\frac{1}{n1} + \frac{1}{n2} + \frac{1}{n3} + \frac{1}{n4}}$$

$$CI(\Delta) = e^{\Delta \pm z_{\alpha/2} * SE(\Delta)}, \quad p = 2(1 - Z_{table}\frac{\Delta}{SE(\Delta)})$$

Multiple testing correction was applied (FDR < 0.05) to control for false discoveries amongst the rejected hypotheses.

Per gene z-score, representing the deviation of individual gene MIs from the average gene MI in the screen was calculated as follows:

$$z\ score_{Gene} = \frac{log_2(MI_{Gene}) - \mu}{\sigma}$$

with $\mu = \frac{\sum_{i=1}^{N} log_2(MI_i)}{N}$ and $\sigma = \sqrt{\frac{\sum(log_2(MI_{Gene}) - \mu)}{N}}$ with N = total number of genes detected in the screen.

For visualisation of gene-trap locations within the gene body, genomic coordinates of insertions were plotted using the GRCh37 reference genome version. Corresponding protein-coding transcript annotations were obtained from Biomart and labelled according to their Ensembl IDs [113].

2.8 pLentiCRISPR v2- sgRNA cloning strategy

Knockout cell lines were generated using the CRISPR/Cas9 nuclease system employing a single LentiCRISPR v2 plasmid encoding the *S. pyogenes* Cas9 and bearing a gene-specific single guide RNA (sgRNA) sequence. sgRNAs targeting genes of interest were

designed and prioritised using the TKOv3 web tool (TKOv3, www.crispr.ccbr.utoronto.ca/public/library/TKOv3 [114]).

Target gene	# sgRNA	Sequence
LAMTOR4	1	GAGCGAATCCCAGACCAGCT
LAMTOR4	2	GGACCTGGAGAATGATGAGC
LAMTOR5	1	GAAACACGATGGCATCACGG
LAMTOR5	2	TCTGATTCTAGACACACCAC
FKBP1A	1	CACGCAGGTCTGGCCGCGCT
FKBP1A	2	ACCGGTGTAGTGCACCACGC
FLCN	1	CTGGTGGCTGACGTATTTAA
FLCN	2	TCACGCCATTCCTACACCAG
QRICH1	1	GCAGATCCAAATCCAGACCG
QRICH1	2	GCAGACAGCCACCACTACCA
SEPHS1	1	TGTACCTGAAGTCTCCGGGC
SEPHS1	2	GATCGGGTAAATGTAATCTG
ZNF652	1	AAGATGGCACTTGACCACGA
ZNF652	2	GACCTGTGAGAAGTGCCCCA

Table 2.12 List of sgRNAs used in this study.

The cloning strategy for sgRNA insertion into the LentiCRISPR v2 vector was adapted from [60, 115]. First, the sgRNA sequence and its complementary oligonucleotide were synthesized with additional BsmBI-compatible overhangs according to the following design:

Oligo 1: 5'- CACCGNNNNNNNNNNNNNNNNNN – 3'

Oligo 2: 3'- CNNNNNNNNNNNNNNNNNNNCAAA - 5'

Secondly, the LentiCRISPRv2 plasmid backbone was digested and dephosphorylated to prevent re-ligation. To this end, the vector was incubated with restriction enzyme BsmBI

and Alkaline Calf Intestinal Phosphatase (CIP) in NEBuffer 3.1 in presence of 100 µM fresh DL-Dithiothreitol for 2 h at 37˚C. The nicked 11 kb vector backbone was mixed with 6X gel loading dye and separated on a 1.2% agarose gel. Band size was verified using a DNA ladder, visualized using a UV transilluminator (Cleaver Scientific), excised and purified using QIAquick Gel Extraction kit according to the manufacturer's instructions. sgRNAs oligonucleotide pairs (100 µM each) were phosphorylated and annealed through incubation with T4 Polynucleotide Kinase in T4 DNA Ligase Reaction Buffer for 30 minutes at 37˚C, followed by 5 minutes at 95˚C and ramping down to 25˚C at 5 ˚C /minute. A 1:100 dilution of annealed oligonucleotides was incubated with 100 ng digested plasmid with T4 DNA ligase in T4 DNA Ligase Reaction Buffer O/N at 16˚C. The ligation mix was mixed with 25 µl Stbl3 chemically competent *Escherichia coli* for 30 minutes on ice, heat shocked for 45 seconds at 42ºC and then cooled on ice for 2 minutes. Transformed bacteria were spread on ampicillin-LB agar plates. Colonies were picked, grown O/N in LB medium with of 100 µg/ml ampicillin and the plasmid extracted using QIAprep Spin Miniprep kit according to manufacturer's instructions eluting in H_2O. Precise sgRNA integration was confirmed by Sanger sequencing using primer 5'-GACTATCATATGCTTACCGT-3'. Liquid cultures containing the correct LentiCRISPR v2-sgRNAs plasmids were expanded to 200 ml cultures, grown O/N and the plasmid was extracted using HiSpeed Plasmid Maxi kit following manufacturer's specifications.

2.9 Knockout cell generation via transient transfection

HAP1 cells were seeded at a density of 4 x 10^5 cells per well in 6-well plates. The next day, cells were transfected with a mix of 9 µl TurboFectin 8 and 2 µg plasmid of

interest per well. Two separate mixes, TurboFectin 8 mix and plasmid mix, were prepared in 100 and 150 µl OptiMEM respectively, combined and added dropwise to the cells after 30 minutes incubation at RT. Transfected cells were selected with 2 µg/ml puromycin for approximately 36 hours, starting 24 hours after transfection. Approximately 24 hours after the end of selection, 5-10.000 HAP1 cells were seeded in a 10 cm dish for clonal expansion while the pool was used for analysis. This protocol was used in HAP1 cells both for knockout generation using LentiCRISPR v2 constructs (clones and pools) and for reconstitution experiments, all carried out with plasmids bearing puromycin resistance sequences. A single exception was FLCN reconstitution experiment, where transfected cells were not selected but directly expanded for 72 hours before analysis.

HeLa, U2OS and HCT116 cells were plated in 6-well plates at density of 6 x 10^4, 10^5 and 2 x 10^5 cells per well respectively. Transfection was carried out 24 hours later using FuGENE HD at a ratio of 3:1 transfection reagent: DNA. Per well, 3 µg plasmid of interest and 9 µl FuGENE HD were mixed in 155 µl OptiMEM. Following 5 minutes incubation at RT, complexes were added to the cells. Cells were incubated with 2 µg/ml puromycin until death of non-transfected control cells.

2.10 **Knockout cell generation via lentiviral infection**

HEK293T cells were plated at a density of 3.5 x 10^6 in a 10 cm dish in 15 ml DMEM supplemented with 10% FCS, 1X P/S-Glut and non-essential amino acids (NEAA) solution. After 24 hours, cells were transfected with a plasmid mix prepared in 1.5 ml OptiMEM and incubated for 20 minutes at RT before dropwise addition to the cells (**Table 2.13**).

Plasmid mix
6 µg psPAX2
4.5 µg pLentiCRISPR v2 + sgRNA
1.5 µg pMD.G
36 µl FuGENE HD

Table 2.13 Cas9-sgRNA lentivirus generation. Mix composition for 1 transfection (10 cm dish).

After 24 hours, fresh DMEM supplemented with 10% FCS, 1X P/S-Glut and NEAA was added and lentiviral production was sustained for 72 hours. Viral supernatant was filtered using a 0.45 µm cellulose acetate filter unit and precipitated by adding a PEG precipitation solution in a ratio of 1.5:9 to the clarified fraction. After O/N incubation at 4ºC, the virus was precipitated by centrifugation at 3.500 rcf for 15 minutes at 4°C and resuspended in 100 µl PBS. 5 µl of concentrated virus were added to ZR-75-1 cells seeded in 12-well plate at a density of 10^5 per well. Two days after transduction, ZR-75-1 were selected with 1 µg/ml puromycin until death of non-transfected control.

2.11 HAP1 knockout clone generation and characterisation

Approximately one week after end of the puromycin selection, individual colonies derived from single cells were picked under the light microscope, transferred to a 24-well plate, and expanded. Clones were harvested, collected by centrifugation and pellets were either snap-frozen for genomic DNA (gDNA) extraction, fixed in 70% EtOH for ploidy analysis or resuspended in 2X sample buffer for immunoblotting.

Gene	sgRNA	Orientation	Sequence
LAMTOR4	1	forward	GGAAGATCAGTATTGAGGACCATGT
		reverse	GGAAACCAGATAAAAGCCGAGAAAA
LAMTOR4	2	forward	AAGTGTGAGAACCAAGGGGAC
		reverse	AGTCCCAAAGGGAGGAAAGTG
LAMTOR5	1	forward	TTGCAGTGAAGTCCCACTGATTA
		reverse	GACAGGCTGCTGAAGAACAGA
LAMTOR5	2	forward	CAGATGAGCATGCTGGAGTGA
		reverse	CCCCGCCAATTTTACCAGG
FLCN	1	forward	GAAAATGCTCAGCAAGTCCAACAT
		reverse	CCCTGCTTCCCAACTAACAGATTT
FLCN	2	forward	CGGCTAAGGACTGTTCTCCC
		reverse	GCTGGCAGCTTTGGCTTAAA
QRICH1	1	forward	GATTTTCAGTGCTGCCTGGTTC
		reverse	GCGTAGGACACAGTGATGGG
QRICH1	2	forward	AACACTGGTGGTGACTGGAC
		reverse	AGGGTAATTGCTTCTGGGCATT
SEPHS1	2	forward	ACGAGCATGGAACTCGAACA
		reverse	TCCGATACGTCATCTCCCTGA
SEPHS1	3	forward	TGGGGCAGTATAGTCGGGAT
		reverse	CCTGTTCAGAGCACTGGTGA
ZNF652	1	forward	TGGAGATGCGGTTTGCTCAT
		reverse	TTTAAGCCCTGTTTCTTGTGATTT
ZNF652	2	forward	ACCTAAGCGTAAGAAGCGGG
		reverse	TCCCTCTCGGTGATGAAACC

Table 2.14 List of primers for validation of knockout genotype used in this study.

Knockout validation via genotyping was performed by PCR amplification of the genomic region flanking the predicted Cas9 cut site and Sanger sequencing using primers listed in **Table 2.14**. Genomic DNA was isolated using DNeasy Blood and Tissue kit according to the manufacturer's instructions. 100 ng of gDNA was PCR-amplified according to

Table 2.15. PCR products were purified using QIAquick PCR purification kit or MinElute PCR purification kit according to the manufacturer's specifications and analysed via Sanger sequencing using either the forward or reverse PCR primer. Clones bearing frameshift mutations were selected and further expanded.

Reaction set-up		PCR program
GoTaq G2 DNA polymerase	0.25 µl	94ºC 2 minutes {94ºC 30 seconds 55ºC 30 seconds 68ºC 55 seconds} x 35 68ºC 7 minutes 4ºC indefinitely
5X GoTaq Green Reaction Buffer	12.5 µl	
Forward primer (10 µM)	1 µl	
Reverse primer (10 µM)	1 µl	
dNTP Mix	1 µl	
DNA template	100 ng	
H_2O	up to 25 µl	

Table 2.15 Genomic PCR set-up for knockout clones genotyping. Reaction was run on a Veriti 96-Well Thermal Cycler.

Ploidy analysis was performed in EtOH-fixed samples after storage O/N at - 20˚C. Cells were pelleted by centrifugation at 400 rcf for 10 minutes and resuspended in 0.5 mg/ml RNase A in PBS. After 1 hour at RT, samples were stained with 10 µg/ml PI and DNA content was analysed via Flow Cytometry (FC) on a LE-SH800 Cell Sorter instrument.

2.12 Immunoblotting

For immunoblotting sample preparation, cells were collected in RIPA Buffer supplemented with protease and phosphatase inhibitors and lysed for 30 minutes at 4˚C. Samples were spun to separate membrane fraction on a handheld centrifuge for 10 seconds and the supernatant was mixed with 2X sample buffer supplemented with

reducing agent and boiled at 95˚C for 15 minutes. Alternatively, cell pellets were lysed in 2X sample buffer supplemented with reducing agent and denatured as described above. Samples were separated on a Bis-Tris Gradient Gel 4-12% using a prestained protein ladder for size reference. Gel-resolved cell lysates were blotted on a polyvinylidene difluoride (PVDF) membrane using the Trans-Blot Turbo system (Biorad). Membranes were blocked for 1 hour in iBlock to prevent unspecific binding and further incubated O/N at 4ºC with primary antibodies. Membranes were washed three times in PBS-T before incubation with species-specific horseradish peroxidase (HRP)-conjugated antibodies for 1 hour at RT under agitation. After washing with PBS-T, signal was detected using enhanced chemiluminescence reagents on a Universal Hood III machine (Bio-Rad). Images were processed and quantified using ImageJ software. All immunoblots presented in this thesis are representative of n = 3 independent experiments unless stated otherwise.

2.13 **Flow Cytometry**

Approximately 3 x 10^6 HAP1 cells per sample were harvested after dissociation with either 0.05% Trypsin-EDTA or PBS + 1mM EDTA. After resuspension in a constant volume of complete IMDM (IMDM + 10% FCS + 1X P/S-Glut), cells were counted using a TC20 automated cell counter (Bio-Rad) and cell number were normalised by volume adjustment. Staining was performed as described in **Section 2.4**. For each staining, a "secondary only" control was included to determine baseline fluorescence. Cells were analysed on a LE-SH800 Cell Sorter (Sony) fitted with Blue laser (488nm) or on LSR Fortessa X-20 (BD Biosciences) equipped with Violet (405 nm), Blue (488 nm), Yellow-

Green (561 nm) and Red (640nm) lasers. 15-30.000 events were recorded per sample. Data were analysed using FlowJo software v8.

2.14 RNA isolation and quantitative Real Time PCR (qRT-PCR)

HAP1 cells were seeded at a density of 2.5 x 10^5 cells per well in a 12-well plate and expanded O/N. The following day cells were rinsed twice with ice cold PBS and the plates snap frozen and stored at -80ºC for at least 24 hours. Total RNA was isolated using RNeasy Mini kit according to manufacturer's instructions eluting in 30 µl of H_2O. DNA contamination was removed via incubation at 37ºC for 30 minutes with 3 µl TURBO DNase Buffer 10X and 0.7 µl TURBO DNase. After addition of DNase Inactivation Reagent, samples were centrifuged at 1.500 rcf for 90 seconds and the RNA-containing supernatant was collected on ice and quantified using a Nanodrop 8000 spectrophotometer.

cDNA synthesis was performed with 500 ng of RNA using RevertAid RT kit. First, the RNA was incubated with 2.5 µl Random Hexamer Primer in a total volume of 10 µl. The annealing step was performed at 65ºC for 5 minutes. cDNA synthesis was performed by adding the RT master mix to each RNA sample as described in **Table 2.16**.

RT master mix		PCR program
5X RT Reaction Buffer	4 µl	25ºC 10 minutes 42ºC 60 minutes 70ºC 10 minutes 4ºC indefinitely
dNTP Mix	2 µl	
RiboLock RNase Inhibitor	1 µl	
RevertAid Reverse Transcriptase	1 µl	
H_2O	9.5 µl	

Table 2.16 cDNA synthesis reaction set-up. Reaction was run on a Veriti 96-Well Thermal Cycler.

The resulting cDNA was used to perform quantitative Real Time PCR (qRT-PCR). Reactions were assembled in a MicroAmp Optical 96-Well plate (Applied Biosystems) to a final volume of 10 µl and run according to **Table 2.17**.

Reaction set-up		**qRT-PCR program**
SYBR Green Master Mix 2X	5 µl	Amplification: 95ºC 3 minutes {95ºC 3 seconds 60ºC 30 seconds} x 35/40 Melting curve: 95ºC 1 minute 55ºC 30 sec Ramp up to 95ºC (0.1ºC/second)
Forward primer (10 µM)	0.2 µl	
Reverse primer (10 µM)	0.2 µl	
cDNA	1 µl	
H_2O	3.6 µl	

Table 2.17 qRT PCR set-up. Reaction was run on a StepOnePlus Real-Time PCR System (Applied Biosciences).

qRT-PCR primers used in this thesis were designed using the PrimerBank web tool (PrimerBank, www.pga.mgh.harvard.edu/primerbank [116]) and are listed in **Table 2.18**. For each qRT-PCR run, a melting curve was determined after signal amplification to assess the specificity of primers. From the resulting cycle threshold value (Ct), relative gene expression values were calculated for each gene via normalisation to GAPDH as internal control (ΔCt). Fold change across conditions was determined by comparing ΔCt values (ΔΔCt). Data were plotted as fold change difference from control (set to 1) and statistical analysis was performed using GraphPad Prism v8.

Gene	Orientation	Sequence
FLCN	Forward	TCTTCAGCATTGTCCGCCAG
	Reverse	AGTTGATGAGGTAGATCCGGTC
TNFR1	Forward	TCACCGCTTCAGAAAACCACC
	Reverse	GGTCCACTGTGCAGAAGAGA
RELB	Forward	CCATTGAGCGGAAGATTCAACT
	Reverse	CTGCTGGTCCCGATATGAGG
GAPDH	Forward	CGAGCCACATCGCTCAGACA
	Reverse	GGCGCCCAATACGACCAAAT

Table 2.18 List of qRT PCR primers used in this study.

2.15 RNA sequencing and analysis

Total RNA was isolated from wild type and knockout HAP1 cells using RNeasy Mini kit according to manufacturer's instructions eluting in 30 µl H_2O. 500 ng of total RNA were used for preparation of Illumina-compatible library from polyadenylated RNA using QuantSeq 3' mRNA-seq library kit. Barcoded libraries were generated from up to 96 samples according to the manufacturer's specifications with the exclusion of the library amplification and barcode introduction PCR step, which was modified to 14 cycles. Resulting barcoded cDNA samples were quantified using a Qubit High Sensitivity dsDNA quantification assay on a Qubit fluorimeter (Thermo Fisher Scientific) and equal amounts from all samples were pooled. The overall fragment sizes of the obtained library were measured on TapeStation 2200 instrument (Agilent) using Agilent D1000 ScreenTape Assay. Sequencing was conducted on a single HiSeq 3000 or 4000 lane using standard Illumina sequencing primer and 50 bp single ends reads were generated and subsequently demultiplexed.

Data processing, alignment and scoring was performed as described in Gapp *et al.* [117] using an automated analysis pipeline built by T. Konopka. A per gene differential expression (DE) score was obtained by weighing effect sizes (fold change in sample versus wild type control) and uncertainty level (z-score).

2.16 Immunofluorescence microscopy

Micro-coverslips were coated with 0.1% poly-L-lysine by incubation in the solution for 10 minutes. Coated coverslips were transferred to a 24 well plate and HAP1 cells were seeded on top at a density of 1.5 x 10^5 cells per well. After 24 hours, cells were rinsed with PBS and fixed in 4% PFA for 10 minutes. Prior to antibody staining, cells were washed twice with PBS and permeabilized with 0.05% Triton X-100 for 5 minutes. Cells were incubated for 1 hour at RT in primary antibody diluted in PBS-T followed by three washes using PBS-T 45 minutes incubation in the dark in with species-specific secondary antibody and DNA intercalating dye DAPI. Unbound antibody was removed by 3 washes in PBS-T, coverslips were rinsed with H_2O and mounted on glass microscope slides (VWR) using Mowiol. Confocal images were acquired using a Zeiss LSM710 microscope and analysed using Zen software.

2.17 Cell Fractionation

Approximately 10^7 HAP1 cells per condition were rinsed twice with ice-cold PBS and resuspended in 0.6 ml of ice-cold cytoplasmic extraction buffer (CEB) or Digitonin Ficoll extraction buffer (DFEB). The lysate was incubated on ice for 15 minutes with frequent rotation before centrifugation at 13.000 rcf for 5 minutes to sediment the insoluble fraction. The supernatant containing the soluble fraction was collected and the

pellet was washed four times with CEB/DFEB. After the last wash, the pellet was resuspended in 2x sample buffer and processed for immunoblotting as described above. Alternatively, the cell lysate was centrifuged at 1.000 rcf for 5 minutes to exclusively sediment the nuclear fraction, while the supernatant was further centrifuged at 13.000 rcf to separate the insoluble fraction. Cellular fractionation was also performed with Subcellular Protein Fractionation kit for Cultured Cells according to the manufacturer's protocol.

2.18 **Immunoprecipitation**

8 x 10^6 HAP1 cells per condition were rinsed twice with ice-cold PBS and lysed at 4°C either in ILB-E for 5 minutes or in DFEB following the protocol used for cell fractionation. For ILB-E-sample, the pellet was removed by centrifugation at 13.000 rcf for 5 minutes and a 10% of the supernatant was collected as input. For DFEB-sample, the pellet was thoroughly resuspended in 300 µl of modified Dignam buffer C and spun at 13.000 rcf for 5 minutes [118]. The supernatant was diluted in 600 µl of modified Dignam buffer A and a 10% fraction was set aside as input control sample. Soluble fractions obtained with either cell permeabilisation method were incubated with anti-QRICH1, -SEPHS1 or -IgG antibodies at a final concentration of 1 µg/ml for 1 hour on ice with intermittent mixing. Afterwards, lysates were incubated with 15 µl Protein A agarose beads that had already been prewashed in ILB-E or in Buffer C/A (1:2 mix), for up to 3 hours on a rotating wheel at 4˚C. Beads were pelleted by centrifugation at 2.500 rcf for 2 minutes and washed with ILB-E or Buffer C/A for a total of 4 washes. Beads were resuspended in 2X sample buffer and fractions were boiled at 95˚C for 5 minutes for immunoblotting.

2.19 Amino acid starvation

HAP1 cells were seeded at 7 x 10^5 cells per well in a 6-well plate 24 hours before the start of the experiment. Cells were rinsed once with PBS and medium was replaced with DMEM without L-Glutamine, without amino acids (AAs) and with 1g/L glucose for 2 hours. Effect of AA reconstitution was assessed by replacing the medium with DMEM with L-Glutamine, with AA, with 1g/L glucose for 1 hour before harvest. Samples were collected for immunoblotting as previously described.

2.20 Colony formation assay

2.5 x 10^5 HAP1 cells per well were seeded in a 6-well plate. 24 hours after seeding, cells were either treated with rapamycin or with DMSO and allowed to proliferate for 96 hours. Cells were washed in PBS and fixed by addition of 4% PFA solution for 10 minutes. Colonies were visualized by staining with a solution of 1% crystal violet in 10% EtOH for 1 hour. Excess staining solution was washed away in H_2O and plates were imaged using a Universal Hood III instrument (Bio-Rad). Images were processed using ImageJ software.

2.21 Protein stability and half-life measurement

One day after seeding at a density of 7 x 10^5 cells per well in a 6-well plate, HAP1 cells were treated with either 100 μM bortezomib (Selleck Chemicals) for up to 6 hours to block proteasomal degradation or 250 μM chloroquine (Sigma Aldrich) for 16 hours to block lysosomal degradation. The half-life of protein of interest was investigated by treating HAP1 cells with 100 μM cycloheximide (Sigma Aldrich) for up to 8 hours.

Lysates were immunoblotted for the protein of interest and quantified using Image Lab software after normalisation to protein levels in wild type cells.

2.22 mRNA stability measurement

HAP1 cells were seeded at a density of 3 x 10^5 cells per well in a 12-well plate and treated with 3 μg/ml Actinomycin D for up to 6 hours. Longer treatment affected cell viability. Total RNA was extracted and mRNA levels for gene of interest were measured by qRT-PCR as described. Levels of gene of interest mRNA were normalised to GAPDH as internal control and ΔΔCt values were plotted against treatment time using GraphPad Prism 8.

2.23 TIDE analysis

Cell pellet was isolated from wild type and ΔFLCN HAP1 cell pools transfected with pLentiCRISPR v2 either carrying a scrambled sgRNA sequence (empty) or LAMTOR4 sgRNA 1 were collected. Genomic DNA (gDNA) extraction was performed using DNeasy Blood and Tissue kit at multiple time points and the region containing the predicted cut site was PCR amplified using genomic LAMTOR4 primers as described in **Section 2.11**. Sanger Sequencing traces were uploaded to the Tracking of Indels Decomposition (TIDE) web tool (TIDE, www.tide.deskgen.com [119]) and decomposed. For each sample, the frequency of unedited and in-frame insertion-deletions (indels) was expressed as a percentage of the total measured indels within the sample. Only indels with a p value < 0.001 were considered for analysis.

2.24 Data plotting

Regulator maps and volcano plots were generated in RStudio 1.2.5033 using the ggplot2 package. Forest plots and insertion location images were created using the Rbase package.

2.25 Statistical Analysis

Data were represented as Mean ± SEM (Standard Error of the Mean) of multiple biological replicates. Statistical significance was assessed using ANOVA (Analysis of Variance) followed by Dunnett's post hoc test for multiple comparisons. Either one-way or two-way ANOVA was used depending on whether the difference in measured parameter was assessed between two groups differing for one (knockout backgrounds) or more (treatment on knockout backgrounds) variable.

Chapter 3: **FACS-based forward genetic screening technology**

3.1 **Introduction**

Forward genetic screening constitutes a systematic and comprehensive approach to map the multiple genetic components involved in a phenotype of interest in an unbiased manner [11]. In general, the screening workflow is comprised of three key aspects, namely: 1.) efficient generation of mutants, 2.) robust identification of the phenotype of interest and 3.) sensitive detection of causative mutation(s) [120].

In this Chapter I detail a forward genetic screening approach that that I transferred from the Netherlands Cancer Institute (NKI) and successfully established in Oxford, which employs near-random insertional mutagenesis on haploid human cells [103]. In this approach, Fluorescence Activated Cell Sorting (FACS) is used to measures protein abundance (or level of post-translational modifications thereof) in individual cells, which serves as a proxy to describe a variety of cellular phenotypes of interest. After describing the set-up, I present two experiments detailing the robustness and reproducibility of the FACS-based forward genetic screening approach and I employ the technology to generate comprehensive regulatory maps of two example readouts.

3.1.1 *Mutagenesis: gene-trapping on haploid cell line*

As described in **Chapter 1**, a number of available manipulation strategies can be employed to block gene function, including insertion of a gene-trap cassette. Gene-trapping is a genome-wide mutagenesis technique based on near-random insertion of an engineered DNA sequence in order to disrupt endogenous coding sequences [13]. As protein-coding exons represent only a small portion of the total human genome (approximately 1.1%), inactivating insertions within gene bodies are more likely to land within intronic regions, which span approximately 24% of the mammalian genome [7]. In order to render the mutagenesis more efficient, gene-trap vectors therefore typically contain one or more strong splice acceptor sites and a polyadenylation (PolyA) tail, ensuring that genomic integrations will result in premature mRNA termination also when the cassette inserts in intronic regions [13, 121]. The cassette can be inserted in two orientations with equal probabilities: either matching the direction of transcription of the gene it inserts into (sense) or opposite to it (antisense), with effective gene-trapping limited to sense insertions [13]. Of the different strategies that can be employed to introduce gene-trap cassettes in eukaryotic cells, retroviral infection is usually preferred over direct electroporation of gene-trap plasmid as integration in the genome is 1.) facilitated by retroviral integrase [122] and 2.) occurs preferentially at the 5' end of a gene, overlapping with regions of open chromatin, thereby increasing the chances of functional gene disruption [123, 124].

In practice, the efficiency of gene-trap mutagenesis is hindered by somatic cells carrying two copies of each chromosome. While the presence of two alleles buffers the effect of potential deleterious mutation and promotes fitness under physiological conditions, a diploid background is less suitable for genetic manipulation experiments [80].

This limitation was overcome following the discovery of naturally occurring sub-diploid genomes in some human tumours [125-127] and the subsequent isolation of a near-haploid cell line, KBM7, from a chronic myeloid leukaemia patient [128]. The KBM7 karyotype revealed a disomy restricted to chromosome 8 and a part of chromosome 15, in addition to harbouring the reciprocal translocation involving chromosome 9 and 22 giving rise to the BCR-ABL fusion protein [129]. A re-programming effort on KBM7 cells produced a fibroblast-like cell line named HAP1 [130]. Compared to the parental line, HAP1 cells were haploid for chromosome 8 and lost their hematopoietic features together with the dependency on BCR-ABL oncogenic signalling. A fully haploid HAP1 cell line was later obtained by CRISPR/Cas9-mediated deletion of the extra chromosome 15 fragment [131]. In the last 10 years, gene-trapped KBM7 and HAP1 cells collections were extensively used for functional gene annotation [69, 101, 132-136]. The gene-trap constructs used in these studies were derived from Murine Leukaemia Virus (MLV) as MLV and other γ-retroviruses tend to integrate in regions of open chromatin (*e.g.* around the transcriptional start site (TSS) and in regions rich in CpG dinucleotide repeats), providing a useful tool for genome-wide mutagenesis applications [137]. In fact, previous reports studying the insertion pattern of MLV-derived gene-trap cassette in KBM7 and HAP1 cells indicated a bias towards RefSeq annotated genes and long intergenic non-coding RNAs (lincRNAs) with a preference towards highly-expressed gene products [132, 138, 139]. In this thesis, HAP1 cells, mutagenized using an MLV-derived gene-trap cassette, were used as a cell model for genome-wide screening.

3.1.2 *Identification of phenotype of interest: Fluorescence Activated Cell Sorting (FACS)*

In a pooled screen setting, non-lethal phenotypes are usually identified through Flow Cytometry (FC), where cell-autonomous traits are measured using fluorescence, either derived from labelling an endogenous antigen or from a reporter system. FC is an established technology used to detect intrinsic cellular properties, such as size and granularity, together with extrinsic subcellular characteristics through use of fluorescent biochemical labels [140].

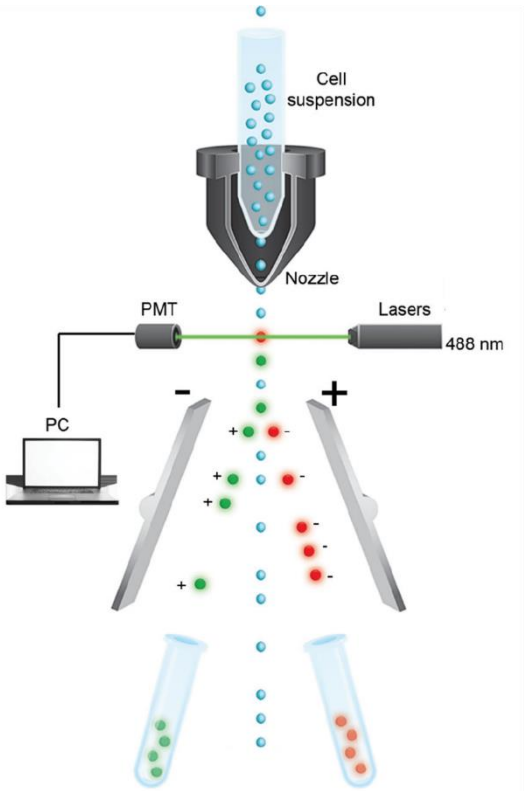


Figure 3.1 Fluorescence Activated Cell Sorting principle. A fluorescent cell suspension flows through a nozzle vibrating at high frequency, breaking the fluid stream into droplets typically containing up to one cell. Droplets travel through a laser beam, where cells scatter the light depending to their intrinsic characteristics (*i.e.* size and granularity) and where, if present, a fluorescent marker is excited and emits light at a known wavelength. Output signals are detected using photomultipliers (PMTs) and processed by a computer. For sorting, droplets with the required characteristics are electrically charged and, by passing through an electric field, are deflected into up to two outlets depending on their charge. Image adapted from [141].

FC allows accurate per-cell measurements in a high-throughput format (simultaneous fluorescence measurements can be performed for each cell at a speed of up to 10.000 events per second [140]) and is, as such, particularly suitable for pooled genetic screens, where mutant libraries of up to billions of cells are investigated.

The combination of FC analysis with the ability to isolate selected subpopulations give raise to Fluorescence Activated Cell Sorting (FACS) [142]. In this application, a fluorescently labelled cell suspension is parcelled out, the resulting droplets are excited at the appropriate wavelength and, depending on whether they contain a cell within the desired fluorescence range, electrically charged (**Figure 3.1**) [143]. Two high voltage deflection plates attract or repel droplets based on their charge, allowing collection into up to two separate tubes. In FACS-based forward genetic screens, the sorting step is performed with fixed, permeabilized and RNase-treated cells, thus permitting straightforward downstream processing.

3.1.3 *Detection of causative mutation: sequencing and mapping*

While multiple options are available when it comes to the choice of a mutagenesis protocol, analysis of causative mutations in forward genetic screens is consistently conducted via next-generation sequencing, which allows parallel mapping of millions of mutations [120]. With the exclusion of radiation and chemical mutagenesis methods, all other untargeted mutagenesis approaches are engineered to contain a set of molecular markers within the inserted cassette. Thus, the genomic location flanking the gene-trap sequence can be detected either by using enzymatic restriction/ligation methods (*e.g.* Splinkerette PCR [144] and inverse PCR [145]) or by amplifying the flanking genomic region

using a cassette-specific primer (Linear Amplification (LAM) PCR [146]). Among the different methods for library preparations from purified DNA of isolated cells, LAM-PCR has the ability of characterising unknown flanking DNA regions in complex samples with multiple insertion sequences and was thus employed in this thesis.

While a detailed description of the experimental details of the FACS-based genetic screening methodology is provided in **Chapter 2**, this Chapter critically discusses requirements for each stage, presents optimisation experiments and highlights quality control steps. Additionally, the robustness of the screening methodology is critically assessed both by fine-tuning internal screen parameters and by comparing screen replicates across two different laboratories: S. Nijman lab (Oxford University, OX) and T. Brummelkamp lab (Netherlands Cancer Institute, NKI), where the technology was developed [103]. Finally, this Chapter explores application of this technology to unveil the regulatory network underlying two biological processes: 1.) the regulation of hypoxia-inducible factor 1α (HIF-1α) and 2.) the surface presentation of major histocompatibility complex, class I-related protein (MR1), performed in collaboration with V. Cerundolo (Weatherall Institute of Molecular Medicine (WIMM), Oxford).

3.2 **Results**

3.2.1 *Selection and validation of a reporter system*

The first step in the set-up of any genetic screen is identifying an actionable cellular readout that recapitulates the phenotype of interest. For FACS-based screens such readout needs to be converted into a fluorescent signal either by introduction of a fluorescent reporter gene system, expression of a tagged protein, or by recognition using a fluorophore-conjugated antibody [135, 147]. While arguably a cell-intrinsic readout best describes the regulatory networks in physiological conditions and constitutes a preferred choice, it also imposes some limitations. Specifically, an endogenous marker needs to 1.) be expressed at detectable level and be active in the cell model system and 2.) be recognised by a FC-compatible antibody.

Assessing the endogenous level of the chosen readout and the readout's functionality in the cell model of choice is thus crucial and is usually performed in two steps. An initial indication can be obtained through available cell line data (*e.g.* proteomic or transcriptomic profile or literature) followed by an experimental validation step. In the case of well-characterised HAP1 cells, the expression levels of endogenous readouts can be predicted from multiple available datasets exploring cells' transcriptomic [148, 149], mutational [148, 150] and proteomic [151] profile. With the exception of the MR1 screen (see **Section 3.2.10**) all screens presented in this thesis were performed using endogenous marker, detected through staining with fluorophore-conjugated antibodies.

Experimental confirmation of readout levels in a selected cell line necessarily includes testing of whether the signal can be confidently measured by FC using a fluorescently labelled antibody. While the extensive use of FACS for phenotyping of

immune cells resulted in a plethora of FC-optimized antibodies targeting immunological markers, antibodies raised against intracellular proteins are often validated only for immunoblotting applications [152].

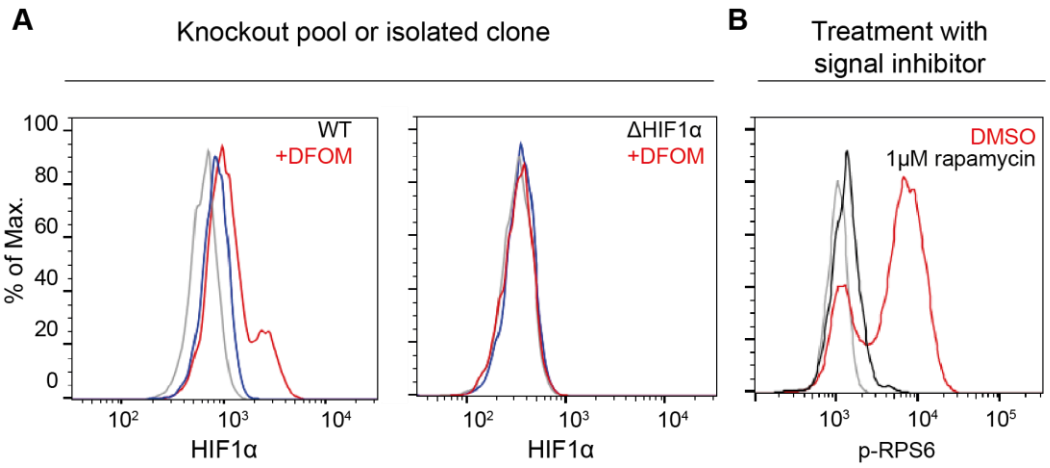


Figure 3.2 Antibody testing for FC. Antibodies for selected proteins were tested by FC using either knockout cells or well-described inhibitors as negative controls. **A.** Hypoxia-inducible factor 1-alpha (HIF-1α) levels in wild type versus ΔHIF1A HAP1 cells and after stimulation with 50 μM deferoxamine (DFOM) for 6 hours. **B.** Phosphorylation levels of ribosomal protein S6 (p-RPS6) at Ser235/236 after treatment with 1μM rapamycin for 6 hours compared to DMSO-treated control. Secondary antibody background is depicted in grey. WT = wild type.

As antibodies obtained for one application are not guaranteed to work in a different one, preventive testing is required [153]. For each target, candidate antibodies inducing a measurable shift in fluorescence signal were tested for specificity. This was achieved by confirming a decrease in the fluorescent signal either in a knockout background for the tested cell marker or following its pharmacological inhibition compared to control cells (**Figure 3.2**). This validation process, performed for every endogenous reporter presented in this thesis, ensured the accuracy of the resulting regulatory maps.

3.2.2 *Generation of mutagenized HAP1 (mut-HAP1) cells*

In order to generate a genome-wide mutagenized pool, insertional mutagenesis was performed on a population of haploid HAP1 cells utilizing a gene-trapping cassette featuring a promoterless Blue Fluorescent Protein (BFP) gene, a PolyA tail for transcription termination and two splice acceptors that ensured gene disruption when the cassette was inserted in sense orientation (**Figure 3.3A**).

In the past, gene-trap mutagenesis included a selection step whereby cells that failed to display activation of the reporter gene embedded in the gene-trap cassette were excluded from downstream applications [13]. While on the one hand this step removed untransduced cells, which would display a wild type phenotype, on the other hand it depleted the mutagenized pool of mutants where the gene-trap cassette had integrated into silent or poorly expressed genes [154]. To maintain a genome-wide overview of the genes implicated in the phenotype, the selection step was therefore omitted and an estimation of transduction efficiency in mut-HAP1 cells was obtained by measuring gene-trap-encoded BFP signal compared to wild type HAP1 cells.

Notably, the expression levels of gene-trap-encoded BFP are not driven by a promoter embedded in the cassette but are dictated by endogenous gene expression at the site of insertion. In addition, the low intrinsic brightness of BFP can lead to an underestimation of the fraction of transduced cells [155]. Thus, I hypothesized that the detected percentage of BFP^+ mut-HAP1 cells, ranging between 30 and 65% for different mutagenesis experiments, was underestimating the true library complexity (**Table 3.1**). To test this, the fraction of BFP^+ cells was additionally assessed in a mut-HAP1 cell pool after staining with anti-GFP antibody to amplify the signal. Structurally, BFP and GFP proteins only differ by the residues in the catalytic site while the β-barrel structure around

the fluorescent core is unchanged [156]. Hence, the anti-GFP antibody can equally well recognise the two fluorescent proteins, as it is directed towards the conserved, exposed protein structure.

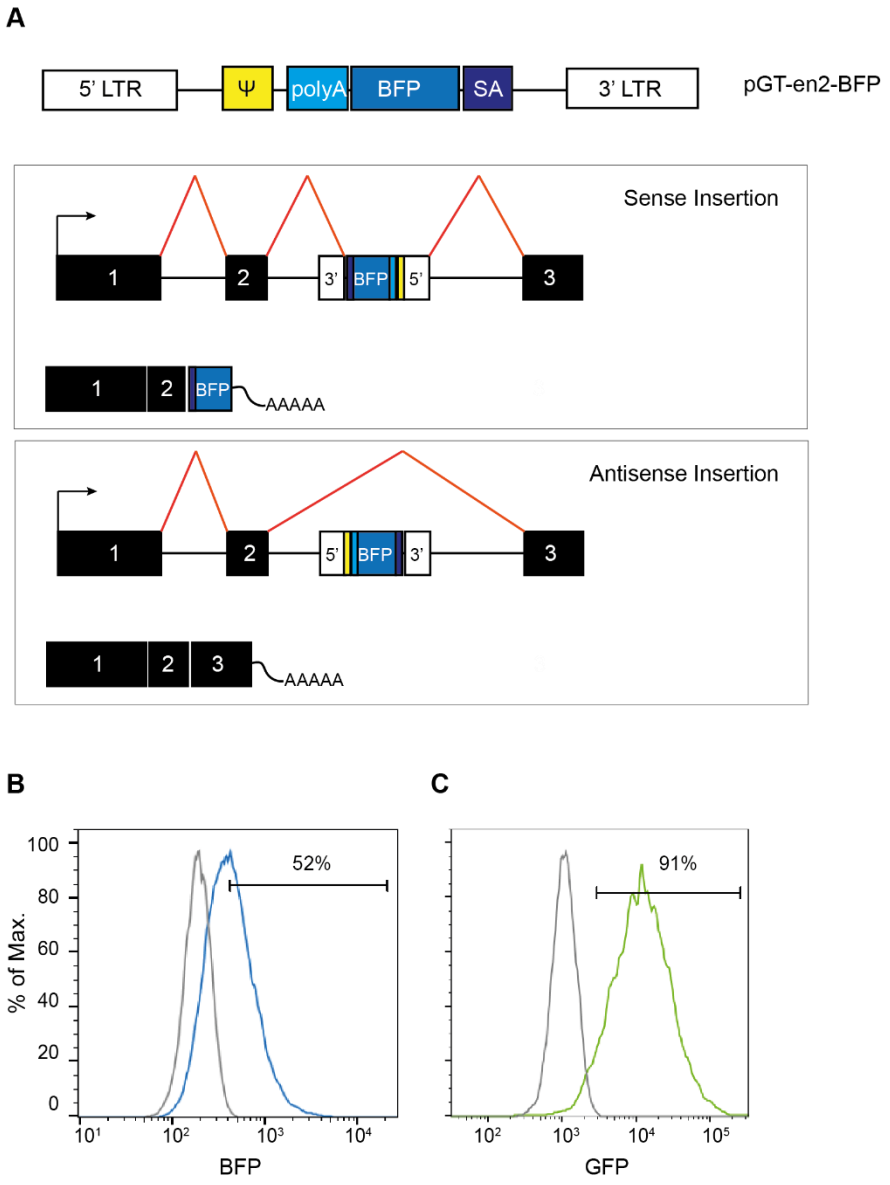


Figure 3.3 Gene-trap mutagenesis on HAP1 cells. A. Schematic visualisation of gene-trap cassette in pGT-en2-BFP and predicted transcriptional products. LTR = Long Terminal Repeats; Ψ = packaging signal; SA = Adenovirus 40 (Ad-40) and engrailed-2 splice acceptors. mRNA splicing sites are indicated in red. **B.** HAP1 cells were transduced with gene-trap containing retrovirus for 3 days. Percentage of BFP positive cells was detected via FC either via BFP fluorescence (LSR Fortessa X20, excitation 406 nm) or **C.** after signal amplification using anti-

GFP antibody and detection via Alexa488-conjugated secondary antibody (LE-SH800, excitation 488 nm).

The analysis revealed that in the same mut-HAP1 cell pool, transduction efficiency was 52% when BFP-positivity was assessed while the percentage reached 90%, when the signal was detected and amplified using the anti-GFP antibody (**Figure 3.3B**). With an extrapolated GFP/BFP ratio of approximately 1.7, these data indicated that, to reach an arbitrary minimum threshold of 80% truly mutagenized cells, a minimum of 45% BFP^+ mut-HAP1 cells were required. Accordingly, only mutagenesis rounds yielding above 50% of BFP^+ cells were further used for screening.

Mutagenesis date	BFP^+ mut-HAP1 cells	"Quality control" result
October 2016	68%	PASS
February 2017	52%	PASS
August 2017	54%	PASS
May 2018	30%	FAIL
March 2019	63%	PASS

Table 3.1 Summary table of mutagenesis experiments. Percentage of BFP positive cells was calculated using untransduced HAP1 cells as a control. FC analysis was performed on LSR Fortessa X20 instrument. At least 30.000 events were collected per experiment.

3.2.3 *mut-HAP1 cells expansion*

Published screens using insertional mutagenesis on HAP1 cells showed near-saturating mutational genome coverage from a mutant library of 10^8 cells, with a number of independent lesions per gene ranging from less than ten up to thousands [77]. The variability in the number of insertions per gene depends mainly on two factors: gene length and its expression levels. As reported by Yu *et al.* [139], longer genes have more chances to be targeted by the gene-trap cassette, which, additionally tends to integrate in regions of open chromatin often corresponding with (or being near to) the TSS of highly

expressed genes. This latter feature is particularly useful as gene expression was found to be a requirement for phenotypic contribution: in fact, insertions tend to be naturally biased towards genes modulating biological processes [103].

Following the protocol used in Brockmann *et al.* [103], where between 0.8 and 2 x 10^7 cells were isolated for each end of the fluorescence distribution for a given marker, I aimed to sort 10^7 cells for each channel, corresponding to the extreme 1% of mut-HAP1 cells distribution. This in turn required an initial mut-HAP1 cell pool of no less than 10^9 cells. To conservatively account for cell loss during collection, staining and sorting steps, mut-HAP1 cell libraries were expanded to 2-3 x 10^9 cells prior to harvest and staining. Notably, mut-HAP1 cells expansion was kept to a minimum as, over time, mutants bearing disrupting insertions in an essential genes are depleted from the pool, thus hampering the classification of essential genes as modulators of the phenotype of interest [76, 77].

3.2.4 *mut-HAP1 cells screen harvest and staining*

As described in the following Chapters, FACS-based forward genetic screening can be used to identify genetic modulators of total protein abundance for an intracellular marker (HIF-1α, IκBα) and for a cell surface receptor (MR1, TNFR1). Of note, distinct harvest and staining protocols were applied depending on whether the readout was localised intracellularly or on the cell surface (**Table 3.2**). In fact, due to their localisation, surface proteins are more sensitive to common cell harvesting protocols that are based on proteolytic cleavage of cell focal adhesions. In this case, a solution of PBS supplemented with chelating agent EDTA was preferred to preserve integrity of surface antigens. Additionally, antibodies recognising cell membrane antigen generally recognise the folded, naturally-occurring protein conformation and, as such, usually lack the ability to

bind to their cognate epitope after fixation [157]. Thus, membrane antigen staining required incubation of the targeting antibody with live cells, a step performed at 4ºC to inhibit dynamic receptor recycling [158].

Screen marker localisation	Intracellular	Cell Surface
Harvest	Trypsin-EDTA	PBS + 1 mM EDTA
Staining	- Fixation - Permeabilisation - Primary antibody staining - RNase A treatment - Secondary antibody + PI staining	- Primary antibody staining - Secondary antibody staining - Fixation - Permeabilisation - RNase A treatment - PI staining

Table 3.2 Harvesting and staining workflow for intracellular and surface markers.

Mut-HAP1 cells staining was consistently performed using a two-step process, in which an unconjugated primary antibody, whose concentration was experimentally optimized to obtain the best balance between signal to background ratio and cost (**Figure 3.4**), was recognised by a species-specific Alexa488-conjugated secondary antibody. The fluorophore was chosen for its brightness, photostability, and excitation wavelength compatible with blue laser excitation (488 nm) [159]. Furthermore, mut-HAP1 cells were stained using the DNA-intercalating dye propidium iodide (PI). Published observations highlighted how rare diploidisation events in HAP1 cells can give raise to faster growing diploid clones which, over time, supplant their haploid counterparts [160]. If occurring prior to mutagenesis, diploidisation might lead to a sub-population of cells heterozygous for gene-trapped alleles, where loss-of-function cannot be confidently established. To minimize such confounding effects, DNA content in mut-HAP1 cells was visualized using PI and only cells corresponding to 1n DNA content peak were further investigated for expression of the marker of interest. As PI intercalates indiscriminately into DNA and

RNA, to correctly identify cell DNA content, mut-HAP1 cells were pre-treated with RNase A [161].

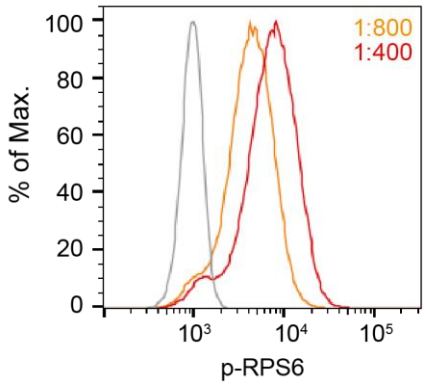


Figure 3.4 Primary antibody titration. Optimal primary antibody dilution was experimentally determined for each screen. Titration for anti-p-RPS6 antibody is used as example. Secondary antibody background is represented in grey.

3.2.5 *mut-HAP1 cells sorting*

After staining, mut-HAP1 cells were sequentially gated to exclude cell aggregates (retaining so-called "singlets") and cells with DNA content > 1n (**Figure 3.5**). From the resulting subpopulation, mutants at the brighter (HIGH) and dimmer (LOW) end of the Alexa488 distribution were selected and sorted out.

Due to the comparative nature of the two-tailed sorting approach described here, the quality of screening data depended largely on the accurate separation of sorted cell populations, or, in other words, on the error rate tolerated during the sorting. At any given time, the two collection tubes for the sorted populations contain true positives (cells inside the selected sorting gates) and false positives (cells erroneously isolated by the sorter).

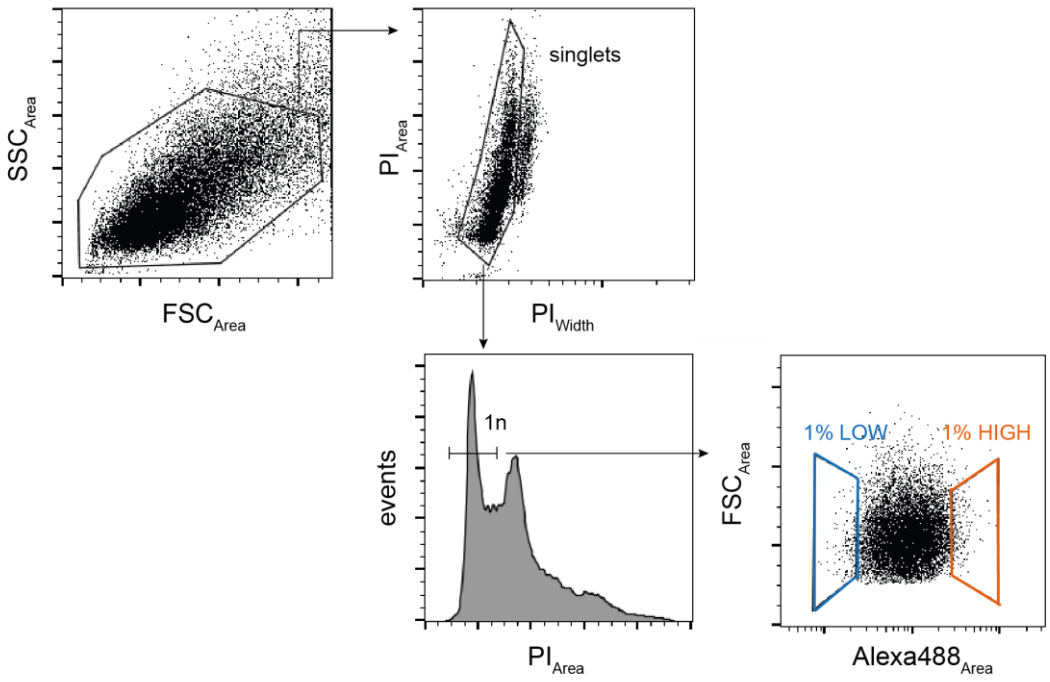


Figure 3.5 FACS sorting workflow. Example representation of sequential gating on mut-HAP1 cells to specifically select single cell (singlets) with 1n DNA content. The resulting population is gated for cells displaying lower and higher intensity fluorescence signal. At each end of the distribution, 1% of total mutant population was sorted. FSC = forward scatter, SSC = side scatter, PI = propidium iodide.

The LE-SH800 sorter designates this ratio as "purity", a parameter which can be interpreted as a user-defined level of tolerance for false positives. In fact, when the sorter is faced with a "conflicting event" (*i.e.* it is uncertain whether to treat it as positive or negative event), it can either sort the containing droplet (favouring yield) or discard it (favouring purity). During sorting, depending on factors such as nozzle size, flow rate, and sample concentration, one or more cells can be incorporated in the same droplet creating such conflicting events [162]. Thus, sorting purity is closely related to other two parameters: efficiency and speed (**Figure 3.6A**). Efficiency is defined by the ratio of true events sorted compared to true events detected and speed refers to the number of events

per seconds (eps) processed by the sorter. Processing a large number of events with high purity setting translates into exclusion of a consistent number of positive events – thus lowering the sort efficiency. In turn, a sort requiring high purity and high efficiency can only be performed at low speed, affecting the experiment length [163].

I set out to systematically alter purity and speed parameters of the sort to find the optimal setting to perform the screen sorting step. To this end, a population of fixed and permeabilized wild type HAP1 cells was immunostained using an antibody against the phosphorylated form of RPS6 (p-RPS6). HIGH and LOW fractions were collected for a number of combinations of speed and purity settings. Post-sort analysis was performed by re-analysing isolated cell populations to calculate the percentage of spillover, defined as the percentage of cells that, at re-run, was classified as belonging to the opposite gate.

Initial sorting conditions at "normal" purity level and 9.000 eps resulted in a maximum spillover of around 2%. The level of technical contamination affected the sensitivity window for detecting enrichment: in this case, for every 49 events sorted correctly, one was mistakenly collected in the opposite tube. It follows logically that the maximum detectable enrichment in disrupting insertions per every individual gene was 50 folds. Thus, minimizing the sorting error would increase the accurateness of the resulting regulatory map. As shown in **Figure 3.6B**, decreasing the sorting speed from 9.000 eps to 5.000 eps lowered the spillover to less than 1% in each gate, and a higher purity setting ("semi-purity", "purity") also led to an overall lower spillover, albeit at the cost of efficiency. Further tweaking of purity stringency ("ultra-purity") and speed (to 3.000 eps) did not further affect spillover, possibly indicating hardware limitations. Overall, sorting at 5.000 eps using a semi-purity setting led to an acceptable efficiency

(approximately 70%), a spillover of less than 1%, and tolerable reduction in sorting speed.

These parameters were used for the sorting of screens presented in this thesis

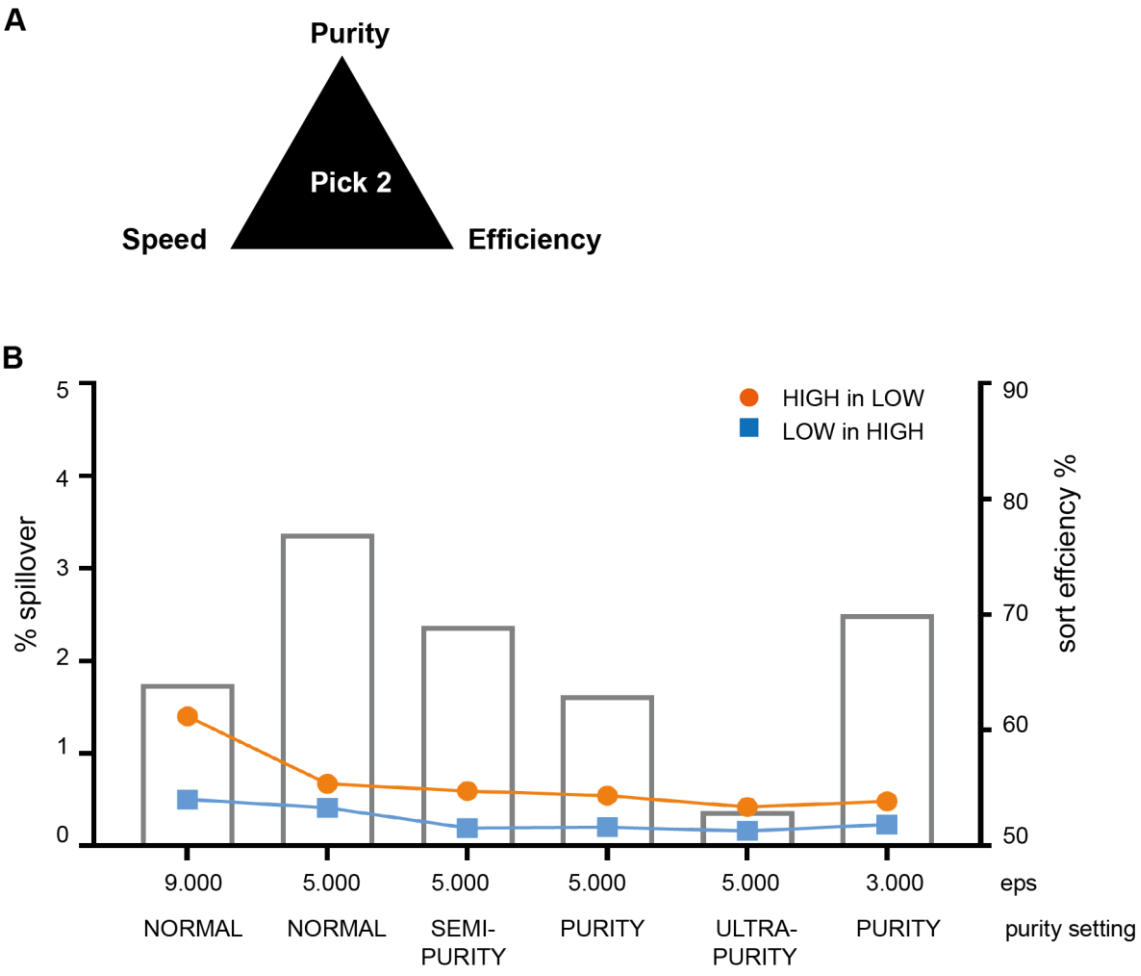


Figure 3.6 Sorting parameters optimisation. A. Graphical representation of the interconnectedness of sorting purity, speed, and efficiency parameters. **B.** Post-sort analysis of isolated cell populations corresponding to the brightest and dimmest 3% of p-RPS6 fluorescence distribution. Sort efficiency (right axis, indicated by grey bars) and spillover among sorted fractions (left axis, indicated by symbols) were examined for a series of speed (eps) and sorting stringency (purity settings) conditions. In orange, percentage of sorted cells in HIGH population found in the lowest 3% gate after post-sort analysis. In blue, cells sorted in LOW population found in the highest 3% in post-sort run. Purity parameters as defined in LE-SH800 sorter in ascending order of "stringency": "normal" < "semi-purity" < "purity" < "ultra-purity".

3.2.6 *Recovery of insertion sites and bioinformatic analysis*

Stable integration of the retroviral gene-trap cassette in mut-HAP1 cell pool allows mutation mapping via recovery, sequencing, and genome mapping of the DNA region immediately next to the integration site. The first step to identify disrupted genes was the isolation of genomic DNA from HIGH and LOW mut-HAP1 sorted cell fractions. Across a number of screens, around 7-12 µg genomic DNA was isolated from 10^7 sorted cells (**Figure 3.7A**). Assuming DNA mass for haploid cell being half of the accepted value of 6 x 10^{-12} g for a diploid cell [164], theoretical DNA yield from 10^7 haploid cells should be around 30 µg. The DNA loss could likely be attributed to the mechanical disruption of the permeabilized cell membrane during sorting and pooling of different fractions. In fact, the use of harsher fixation and permeabilization reagents in the MR1 screen while maintaining all other parameters unchanged, led to a 50% decrease in recovered DNA (see **Section 2.4**).

Genomic locations flanking the gene-trap cassette were recovered using LAM PCR. By using a primer specific for the inserted 5' LTR and a high-fidelity polymerase, the DNA neighbouring the gene-trap cassette was amplified [165]. By accounting for the enzyme processivity (1 kb/minute) and the duration of the PCR elongation step (1 minute), the expected LAM result was a fragment library of a continuous size distribution up to approximately 1 kb. This feature was used at the end of the recovery procedure to assess the quality of the prepared library prior to sequencing. Inefficient genomic library amplification or contamination with an exogenous 5' LTR-containing sequence were expected to significantly alter the fragment distribution and affect sequencing quality.

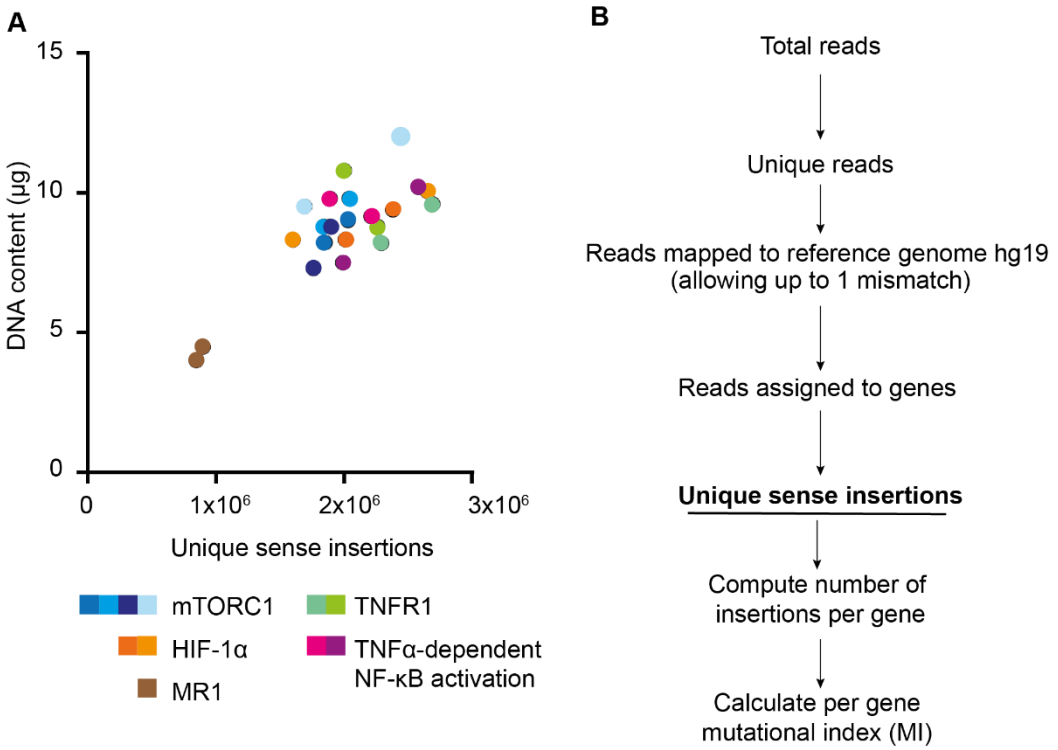


Figure 3.7 Recovery of insertion sites and bioinformatic analysis workflow. A. DNA content (in µg) extracted from HIGH and LOW sorted mut-HAP1 cell populations is plotted against the obtained unique sense integration in the same fraction. Results are reported per each screen for HIGH and LOW populations (*i.e.* 2 values/screen). Dots are coloured according to the legend. For full list of screens, refer to **Table 1.2**. **B.** Workflow containing bioinformatics analysis steps performed for each screen. Detailed description in **Section 2.6**.

For each fragment library (deriving from HIGH and LOW populations), between 2.1 and 2.7 x 10^8 50 bp single end reads were generated (**Figure 3.7B**). Sequencing was performed using a custom primer that annealed to the 5' end of the gene-trap 5' LTR, thus ensuring the reads only spanned the DNA sequence flanking the inserted cassette. Around 25% of the total reads was uniquely represented in the sample (unique reads). After mapping to the genome, only reads that aligned with 0 and 1 mismatch were considered and duplicates removed. Removal of duplicates was required as reads that align uniquely to a genomic region without mismatches might map to two different regions when allowing for 1 mismatch. From an initial sorted population of 10^7 mut-

HAP1 cells, the expected number of unique reads was around 10^7, while a higher number would suggest that some cells contained more than one gene-trap cassette.

Unambiguously aligned reads were mapped to a custom reference annotation based on RefSeq coordinates for protein-coding genes. Overall, only about 45% of uniquely aligned reads mapped to protein-coding genes. Finally, only insertions whose directionality matches the gene they were inserted in were considered (*i.e.* sense), as they were the ones most likely to disrupt the open reading frame. On average, only 1 out of 5 uniquely aligned sequences were considered disruptive, leading to a median of approximately 2 x 10^6 inactivating insertions per sorted population (*i.e.* HIGH or LOW) across screens (**Figure 3.7A**). Each screen thus retrieved a median of 4 x 10^6 unique sense insertions (HIGH + LOW) which mapped to approximately 17.400 genes, in line with what was reported by Brockmann *et al.* [103]. Of note, isolated DNA content is correlated to the number of inactivating insertions as shown by a lower number of unique, sense reads in MR1 screen (**Figure 3.7A**, see **Section 3.2.10**). After computing the total number of insertions per gene, positive and negative regulators for the phenotype of interest were identified by calculating the enrichment of disrupting insertions in HIGH and LOW channel. As in the same screen the total number of unique aligned sense reads in HIGH and LOW populations might differ, insertions were first "normalised" within each sorted population. Per gene mutational index (MI) was then calculated as the ratio of the resulting normalised insertions in HIGH versus LOW sorted population (see **Section 2.6**).

3.2.7 *Screen reproducibility*

To be able to understand how signalling networks get re-wired in response to genetic and chemical perturbations, a screen for a relevant marker can be iteratively repeated in presence of distinct perturbagens. This step is then followed by comparison among the resulting screens to highlight similarities and differences (see **Chapter 4**). In order to allow direct comparison between two screens, the robustness and quantitative nature of the screening technology is critical.

To this end, I assessed the performance of completely independent biological replicate FACS-based forward genetic screens by conducting the same experiment in two different laboratories (S. Nijman's (Oxford University, OX) and T. Brummelkamp's (Netherlands Cancer Institute, NKI)) without explicit standardisation of mutagenesis, culture conditions, FACS settings or library preparation. The two screens used phosphorylation of ribosomal protein S6 (p-RPS6) as a marker (p-RPS6 NKI and p-RPS6 OX, see **Appendices 8.2.1** and **8.2.2**). First, I assessed the reproducibility of the mutagenesis as mut-HAP1 cells employed in the two screens originated from two independent batches of mut-HAP1 cells. Across the genome, the number of per gene insertions was highly consistent between laboratories (Spearman Rho = 0.98), indicating the mutagenesis process was highly consistent (**Figure 3.8A**). To assess the reproducibility in identifying significant regulators, MI z-scores were calculated for gene hits in each screen and compared for the union of the two screens' hits. I reasoned that although the absolute value of per gene MI might be influenced by screen intrinsic biological variability and technical aspects, the relative magnitude and directionality of gene regulatory effects would be retained. The comparison showed a high agreement in

MI z-scores across laboratories (Spearman Rho = 0.92) supporting the feasibility of direct comparison across screens (**Figure 3.8B**).

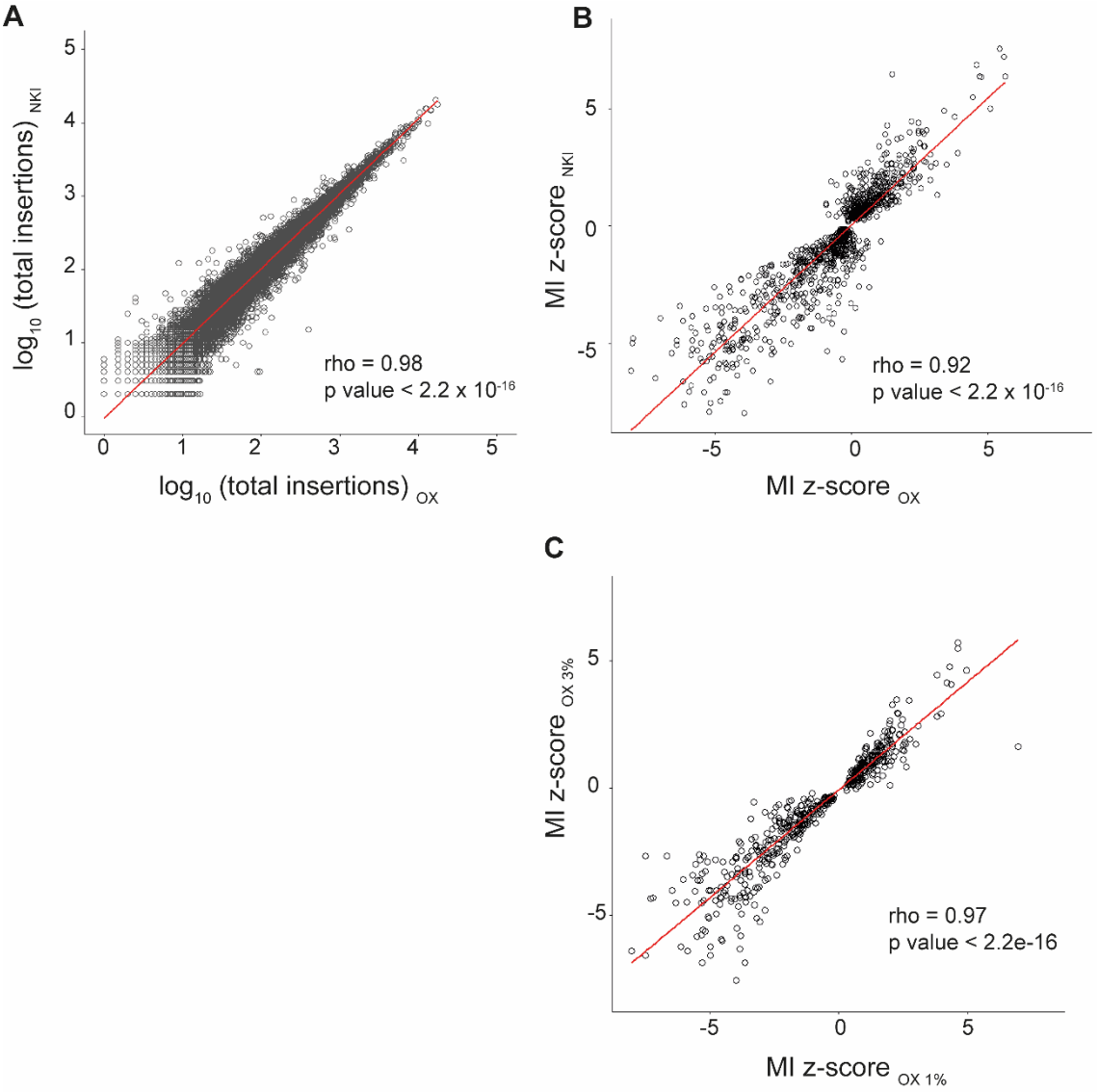


Figure 3.8 Screen reproducibility. A. Comparison between number of trapping insertions mapped per gene in two screens performed without explicit standardisation in two separate laboratories from independently mutagenized mut-HAP1 cells batches. Screens used phosphorylation of RPS6 as a readout. Screens were conducted in S. Nijman's (Oxford University, p-RPS6 OX) and in T. Brummelkamp's (Netherlands Cancer Institute, p-RPS6 NKI) laboratories. **B.** Correlation of MI z-scores for each gene that scored as a significant regulator in at least one of the two screens. **C.** Correlation of MI z-scores for genes scoring as hits in at least

one of the two screens (p-RPS6 1% and p-RPS6 3%) obtained by varying the sorting gates. Spearman Rho is calculated for each comparison.

I then investigated whether the major bottleneck in FACS-based genetic screens, the sorting step, could be improved. At an event rate of 5.000 eps and a sorting efficiency of approximately 70%, isolation of 1% of the population translated to isolation of 35 events per second (see **Section 3.2.5**). This implies that the total sorting time to collect 10^7 cells would exceed 70 hours. To test whether the sorting duration could be reduced without affecting the identification of pathway regulators, I determined the effects of increasing the sorting gates from 1 to 3%, whilst keeping all other variables identical. From an initial batch of mut-HAP1 cells stained for p-RPS6 levels, I sequentially isolated fractions of 10^7 cells corresponding to the extreme 1% and 3% of the distribution (p-RPS6 1% and p-RPS6 3%, see **Appendices 8.2.2** and **8.2.3**). Comparison of MI z-score for gene hits in the two screens showed a high correlation (Spearman Rho = 0.97), indicating that the variability in the size of the sorting gate has a minimal impact on the outcome of the screen (**Figure 3.8C**). Additionally, as the use of 3% sorting gate alleviated the sorting duration bottleneck (24 hours versus 70 hours), therefore following screens were performed with sorting parameters between 1.5% and 3%. These results highlighted the reproducibility of the technology both inter- and intra-laboratories, even after modification of the sorting parameters.

3.2.8 *Screen hits prioritisation*

A crucial step in the analysis of any high-dimensional dataset is the assessment of the experiment performance by comparing the results against a control dataset. In the case of FACS-based genetic screens, this step verified 1.) that the gene encoding the marker itself scored as a positive regulator and 2.) that genes known to interact and associate with the marker of interest were also found among the hits. This step, referred to as "benchmarking", established whether the screen was able to identify true regulators.

This first, qualitative assessment was followed by an extensive hit prioritization step aimed at maximising the success of downstream experimental validation. The challenge of effective gene prioritisation is pervasive in the interpretation of high-dimensional genomic datasets and, depending on the specific experimental context, different gene prioritization principles can be employed [166]. In this section I discuss a number of criteria I considered to prioritize hits of FACS-based genetic screens for downstream validation.

3.2.8.1 Degree of connection with the phenotype ("guilt by association")

Often, gene prioritisation is based on the "guilt by association" assumption according to which hits linked to genes previously connected with the phenotype are more likely to be true positives [167]. In this approach screen data were evaluated according to available knowledge about both the individual gene hit and the phenotype investigated in the screen, combining evidences from gene sequence (UniProt, www.uniprot.org [168]), functional annotation (Gene Ontology, www.geneontology.org [169]; Reactome, www.reactome.org [170]) genetic association (DepMap, www.depmap.org [90]), differential expression (Gene Expression Omnibus, www.ncbi.nlm.nih.gov/geo [171]; Human Protein Atlas, www.proteinatlas.org [172]), co-expression (COXPRESdb, www.coxpresdb.jp [173])

and physical protein-protein interaction datasets (Bioplex 2.0, www.bioplex.hms.harvard.edu [174]; IntAct, www.ebi.ac.uk/intact [175]; BioGrid, www.thebiogrid.org [176]). As no individual data type could be expected to be exhaustive, all the above-mentioned resources had to be considered alongside information extracted directly from literature.

3.2.8.2 Effect size

Generally, the effect size in the screen correlates with the strength of the phenotype upon validation. Thus, genes displaying a higher absolute log_2MI values ($|log_2MI|$) were usually prioritised over genes with a lower $|log_2MI|$. The $|log_2MI|$ can be visualized as the magnitude of the deviation of the distribution for a specific gene knockout/down mutant from the general mutagenized pool distribution. Thus, it is logical to assume that, on average, the extent of such deviation is greater for mutants eliciting a strong effect on the measured phenotype.

3.2.8.3 Pattern of insertions within the gene body

The MI parameter does not take into account technical biases such as inefficient mutagenesis, for instance due to large introns or alternative splicing, which can result in underestimating the effect size [177]. To increase the confidence that a putative genetic regulator is a true hit, the gene-trap integration sites across the gene body were analysed to assess whether the pattern was compatible with loss-of-function mutations (*e.g.* insertions concentrated around the TSS of the gene).

3.2.8.4 Promiscuity across multiple screens

Another aspect that requires consideration is the specificity for a certain cellular phenotype. Knockout of genes involved in central processes aimed at maintaining protein

homeostasis, such as chromatin remodelling, cell growth and proteasomal degradation, are expected to be "promiscuous", *i.e.* score as regulators in multiple screens, independent of the protein phenotype being investigated. These genes, although being true positives, might impede the identification of context-specific hits. A powerful method to recognise these "frequent hitters" is to perform comparisons of hits across a combined set of > 20 FACS-based genetic screens that were performed with different reporters (Phenosaurus, www.phenosaurus.nki.nl [103]). Analysis of per gene pattern (*i.e.* scoring as a positive, negative, or non-significant regulator across multiple independent screens) indicated mutants consistently affecting disparate and independent phenotypes and allowed to make an informed choice whether to include them in the validation step. Importantly, this filtering step would become more powerful with increasing numbers of screens across a diverse set of phenotypes.

Collectively, these four criteria, together with practical considerations in terms of novelty and biological significance of the finding, were used to identify the most promising hits for downstream validation.

3.2.9 *Screen example #1: HIF-1α regulation*

HIF-1α is the hypoxia-inducible α subunit of transcription factor complex HIF-1 and plays a major role at cellular and systemic level in response to low oxygen conditions [178]. Under normoxic conditions, cells constantly synthesize and degrade HIF-1α through a post-translational mechanism (**Figure 3.9**) [179]. In presence of molecular oxygen, two HIF-1α prolyl residues are hydroxylated by the HIF-modifying enzymes prolyl hydroxylase domain 1-3 (PHD1–PHD3) (reviewed in [180]). The hydroxylated form of HIF-1α is recognised by the von Hippel–Lindau tumour suppressor (VHL) protein, an E3 ubiquitin ligase complex subunit that tags HIF-1α for proteolysis. A number of studies showed HIFα involvement in various pathogenic conditions such as kidney cancer, pulmonary hypertension, and ischemic cardiovascular disorders (reviewed in [181]). Therefore, using haploid genetic screening to gain a better understanding of its upstream regulatory signalling could have therapeutic implications.

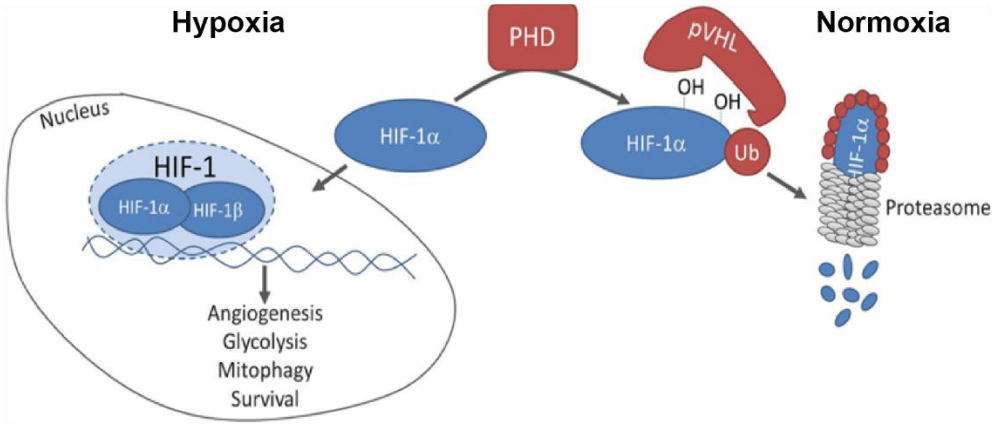


Figure 3.9 Regulation of HIF-1α stability in normoxia and hypoxia. HIF-1β = transcription factor complex HIF-1, subunit β; Ub = ubiquitin. Image adapted from [182].

As HIF-1α was degraded under normoxic conditions, a genetic screen performed at 21% oxygen was expected to only highlight negative regulators stabilizing the HIF-1α

protein (see **Appendix 8.2.4**). To improve the sensitivity towards proteins promoting HIF-1α downregulation, a second screen was performed in presence of a hypoxia mimetic compound, the iron chelator deferoxamine (DFOM) (see **Appendix 8.2.5**) [183].

By sequestering the PHD co-factor, Fe^{2+}, treatment with 50 μM DFOM for 6 hours led to an increase in HIF-1α levels (**Figure 3.2A**). For each screen, per gene relative enrichment of trapping sense insertion in the HIF-$1\alpha^{HIGH}$ versus HIF-$1\alpha^{LOW}$ sorted cells (MI) was plotted against the number of unique sense insertion recovered collectively in both channels. Genes displaying a significant enrichment (FDR < 0.05) in either channel were displayed in orange (negative regulators) or light blue (positive regulators).

As expected, in the untreated HIF-1α screen, HIF1A gene did not score as a hit, confirming the challenge to identify true positive regulators in this specific set-up (**Figure 3.10A**). Among known HIF-1α negative regulators, the E3 ubiquitin ligase gene VHL was identified as the strongest hit ranked by MI (MI = 16.5). On the other hand, the prolyl hydroxylases did not score as significant negative regulators. While PHD1 (EGLN2) was not detected at protein level in HAP1 cells [151], EGLN1 and EGLN3 (coding, respectively for PHD2 and PHD3) were not identified as hits, possibly due to partial functional redundancy [184].

In the DFOM-treated screen, HIF1A gene scored as positive regulator, reflecting, as expected, that cells containing inactivating insertions in HIF1A are enriched in HIF-$1\alpha^{LOW}$ (dimmest 1%) versus HIF-$1\alpha^{HIGH}$ (brightest 1%) sorted cells (**Figure 3.10B**). Visualisation of disrupting insertions in HIF1A gene revealed that most gene-traps inserted close to the 5' end of the gene, where they were most likely to give rise to inactive mutants (**Figure 3.10C**). By blocking PHD activity using DFOM, VHL, whose effect on

HIF-1α stabilisation depended on prolyl hydroxylation, was not expected among negative regulators.

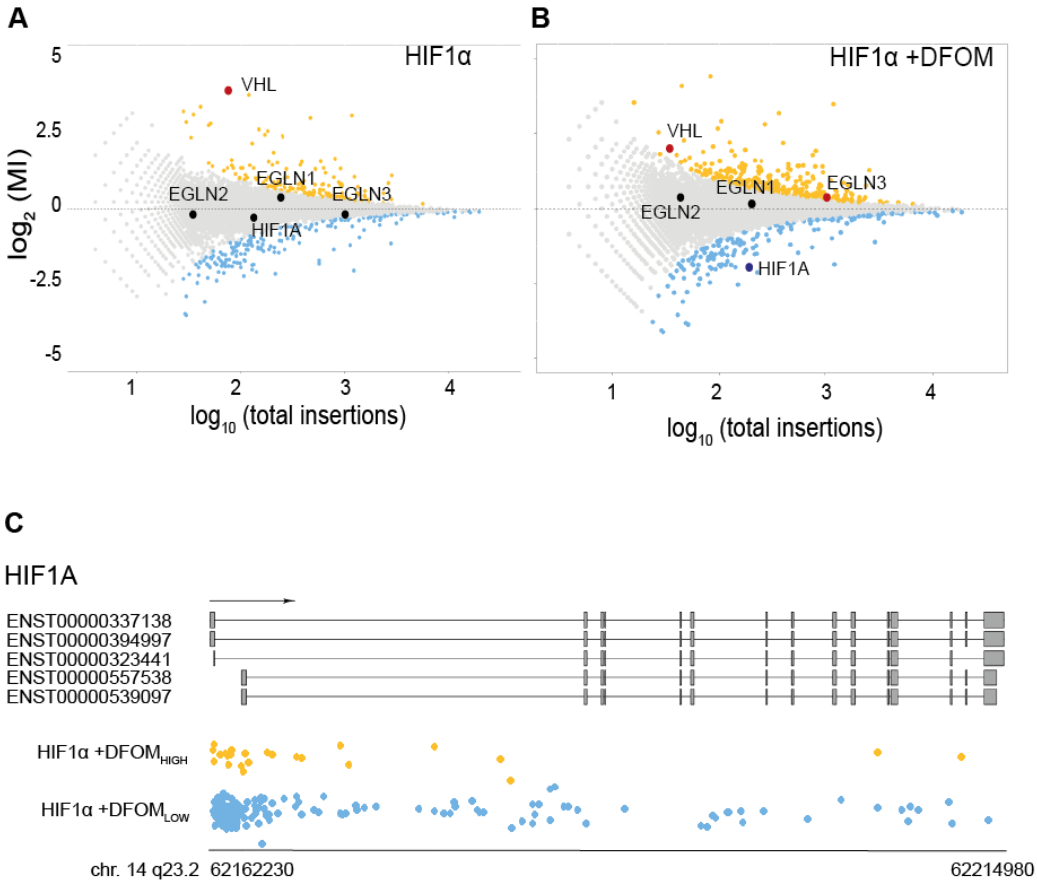


Figure 3.10 Regulator maps for total levels of HIF-1α. A. Regulatory maps for HIF-1α protein level under steady-state conditions and **B.** after 6 hours treatment with 50 μM DFOM. Shown is per gene $\log_2$(MI) (y-axis) as a function of number of independent per gene insertions (x-axis). Significant regulators (FDR < 0.05) are highlighted in orange (or red, negative) and light blue (or blue, positive). Selected genes are labelled. **C.** Location of unique gene-trap insertions in HIF1A gene in HIGH and LOW sorted populations in the HIF-1α+DFOM screen. Colour coding as in **A.** Ensembl IDs for HIF1A protein-coding transcripts are reported. Grey boxes represent exons and arrow indicating transcription direction.

Possibly as result of incomplete blockade of the pathway by DFOM (**Figure 3.2**), both VHL and PHD3 scored weakly as hits. PHD3 differs from its paralogue PHD2 in being strongly induced even after short exposure to hypoxia [185]. It is likely that, due to

incomplete DFOM-mediated HIF-1α stabilisation, this negative feedback loop was absent in PHD3-null cells and led to a modest increase in HIF-1α levels.

Collectively, these data indicated that FACS-based genetic screening could unbiasedly detect known regulators of HIF-1α signalling pathway both under steady-state and after chemical treatment. However, in this specific case, analysis of other screen hits did not highlight novel, high confidence candidates for further biological investigation.

3.2.10 *Screen example #2: MR1 surface presentation*

MR1 is a MHC class I molecule that presents microbial-generated neoantigens to unconventional T cells called "mucosal-associated invariant T" (MAIT) cells inducing their activation [186]. Under steady-state conditions, MR1 resides in the endoplasmic reticulum (ER) and is trafficked to the cell surface upon binding with riboflavin-derived metabolites [187]. Despite being described for the first time in 1995 [188], very little is known about the mechanism underlying MR1 surface presentation. A recent report identified MR1 as a tumour-associated antigen (TAA) presenting molecule restricted to cancer cells. MR1-TAA complex presentation in turn led to recognition and killing by clonally expanded T cells [189]. Thus, dissecting the mechanism regulating MR1 surface presentation can lead to the identification of new immunoncology targets. This screen was conducted in collaboration with the lab of professor V. Cerundolo (WIMM, Oxford), where selected hits are being followed up functionally.

Although MR1 was reported to be expressed at low level in a variety of cell lines [190], it is not detected in wild type HAP1 cells [151]. Thus, a cassette bearing MR1 cDNA under the control of a strong silencing-prone spleen focus forming virus (SFFV) promoter was stably inserted in HAP1 cells using a lentiviral vector, generating an engineered

isogenic haploid cell line named MR1_HAP1. This step was performed by C. Kulicke (WIMM, Oxford) [191]. Mutagenesis was performed on an isolated MR1_HAP1 clone and a genetic screen for MR1 surface levels was conducted in presence of acetyl-6-formylpterin (Ac-6-FP) [192], a known MR1 ligand promoting receptor stabilisation and surface presentation (**Figure 3.11**) (see **Appendix 8.2.6**).

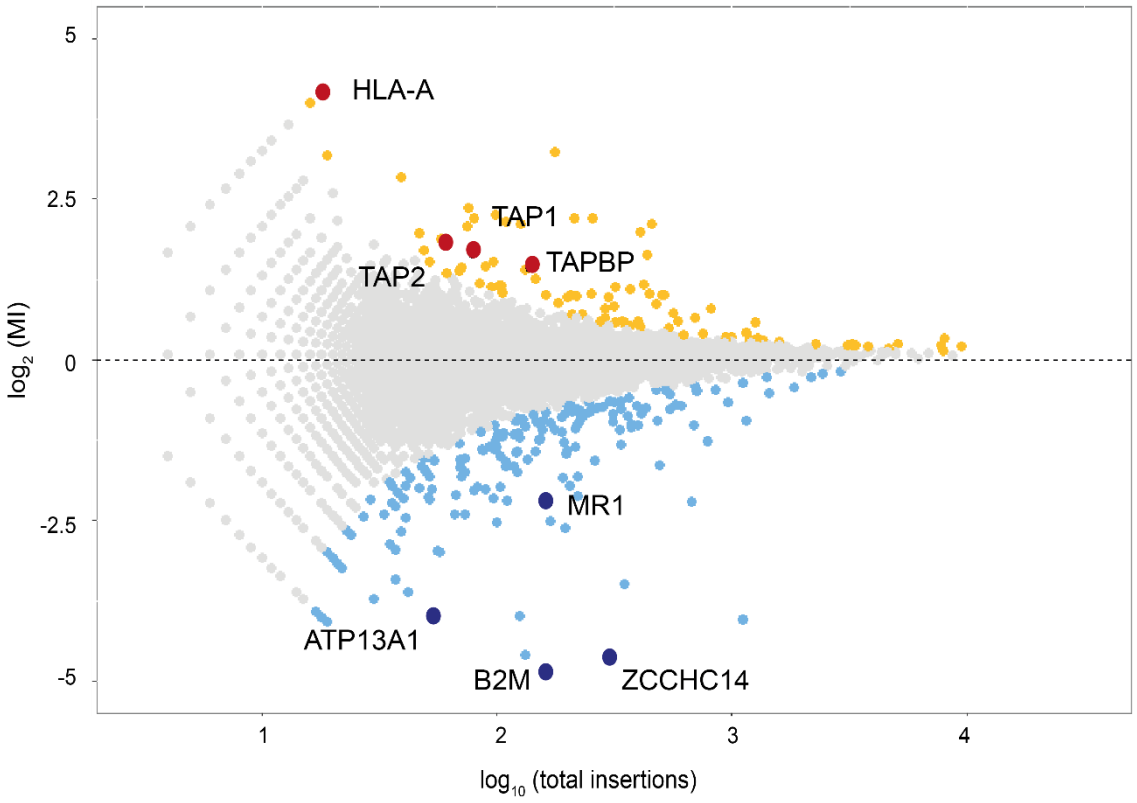


Figure 3.11 Regulatory map for MR1 surface levels. Regulatory map of MR1 surface level after 5 hours treatment with 5 µg/ml acetyl-6-formylpterin. Significant regulators ($p < 0.05$) are highlighted in orange (or red, negative) and light blue (or blue, positive). Selected genes are labelled. MR1_HAP1 cells were generated by C. Kulicke.

As shown previously, the number of mapped insertions in this screen was below average (**Figure 3.7A**). To examine whether this significantly affected the ability to identify genetic regulators, I compared the number of mutagenized genes in the MR1 experiment to the screen average. Reassuringly, a total of 16.900 genes were trapped with

at least 1 insertion (compared to a screen average of 17.400) indicating that the lower number of total insertions only marginally affected the screen ability to identify genome-wide MR1 regulators.

Overall, the screen identified a total of 273 significant regulators (FDR < 0.05) among which the known regulator β-2-microglobulin (B2M) and MR1 itself were found. β-2-microglobulin, a component of MHC class I complex that was shown to heterodimerize with MR1 to form an antigen presenting molecule [193] was detected as the strongest positive regulator (MI = 0.03). Interestingly, one of the classical MHC class I genes, the human leukocyte antigen A (HLA-A) scored as a negative regulator together with transporter associated with antigen processing 1 and 2 (TAP1, TAP2) and TAP binding protein (TAPBP). Contrary to other MHC class I molecules, MR1 antigen processing was demonstrated to be TAP-independent (*i.e.* not requiring TAP proteins for antigen loading) [190]. Thus, increased MR1 surface presentation following inactivation of HLA-A and TAP suggested that MR1 molecules likely competed with HLA-A for β-2-microglobulin binding.

It is worth noticing that MR1_HAP1 cells contained two versions of the MR1 gene: the non-expressed endogenous one and the integrated cDNA which only contains exons. As only the exogenous construct expressed MR1 in edited cells, the MI, calculated using sense insertions number across the whole gene body, underestimated the true gene enrichment in the $MR1^{LOW}$ fraction (MI = 0.44, FDR = 7.27×10^{-8}). Thus, MR1 MI was re-calculated by considering only insertions in exons (MI = 0.21, FDR = 2.9×10^{-14}). In addition, the screen identified a number of novel, little studied genetic regulators such as manganese-transporting ATPase 13A1 (ATP13A1), whose role as regulator was validated in both HAP1 and THP1 cells in V. Cerundolo's laboratory and is being further

characterised at functional level [191]. Of note, the screen also identified genes coding for DNA-binding molecules, such as zinc finger CCHC-type containing 14 (ZCCHC14). However, these hits would require more careful validation in a different MR1_HAP1 clone to ascertain that the effect was not limited to regulation of the transgenic MR1 cDNA.

Overall, this screen retraced and significantly expanded the current knowledge of MR1 surface presentation, suggesting the involvement of a number of novel regulators.

3.3 Discussion

First described 5 years ago, genetic screens using Fluorescence Activated Cell Sorting played a key role in furthering the understanding of basic biology [104, 194] and therapeutic target discovery [106, 108], allowing the investigation of cellular phenotypes beyond viability. In particular, analysis of "protein state", an umbrella term encompassing protein abundance, splicing and post-translational modification, proved to be an effective proxy to describe a number of cellular phenotypes [103]. While such a continuous readout confers a clear advantage in terms of the breadth of biological questions that can be addressed, it also brings along some technical challenges. Fitness screens rely on strong selective pressure to unambiguously separate mutants with phenotypic advantage from the initial pool. On the other hand, FACS-based genetic screens can isolate cells in arbitrarily selected gates, for instance at the extremes of a continuous phenotypic distribution. In positive selection fitness screens, disrupted genes causing the investigated phenotype are identified by comparison of inactivating mutations in two populations separated by multiple days or weeks of selection. In contrast in FACS-based screens mutant cell pools undergoing comparison are separated by few-fold median fluorescence intensity (MFI). It follows that sensitivity and robustness of FACS-based genetic screens strongly depend on 1.) the signal to background ratio for the fluorescent screen reporter and 2.) the confidence that can be attached to the comparison. As highlighted in the following sections, the first parameter is intrinsic to the readout signal, the second one is affected by technical parameters such as the reliability of the sorting method, the knockout efficiency in the mutant pool and the number of recorded events.

3.3.1 *Choice of screen reporter system*

By using known pathway regulators as benchmark, I demonstrated the performance of the FACS-based approach in two example screens using either an antibody recognising an internal marker (HIF-1α) or an exogenous reporter system (MR1). While the choice of endogenous versus exogenous reporter needs to be made for each individual screen, some considerations can be put forward to drive the decision. On the one hand, phenotype detection using an endogenous marker better reflects cell-intrinsic phenotypes, ensures the intactness of cognate regulatory signalling, and requires minimum protocol optimisation. On the other hand low intrinsic expression levels of the marker of interest may affect screen sensitivity. For instance, the screen for HIF-1α regulation performed in normoxia lacked the sensitivity to identify HIF-1α positive regulators due to degradation of the target marker. This limitation can, in some cases, be addressed by treating HAP1 cells with chemical (DFOM) or biological stimuli increasing the level of endogenous marker. For instance, interferon γ (IFN-γ) treatment was used to stimulate CD274 expression in mut-HAP1 cells prior to performing a forward genetic screen [106]. This approach, while expanding the repertoire of interrogable phenotypes, also introduces another layer of complexity by returning treatment-specific modifiers in addition to target-specific regulators, creating an opportunity to identify modulators of drug response, further discussed in **Chapter 4:**.

Alternatively, cell-extrinsic phenotypes can be successfully studied by introduction of a fluorescent reporter system as exemplified by the MR1 screen. This approach is more laborious, requiring cloning and transduction of cDNA of interest and selection of transduced clones for concomitant reporter expression and 1n DNA content. Additionally, a screen performed in an engineered background (*i.e.* in HAP1 cells carrying a reporter

system under the control of an exogenous promoter) is able to confidently identify only genetic elements involved in post-transcriptional regulatory processes, as transgene expression is likely regulated differently than the endogenous gene.

3.3.2 *Choice of cell system and mutagenesis approach*

Crucially, mapping of regulators of the phenotype of interest is only feasible when the interrogated pathway is intact and functional in the cell model employed. As a result, screenable space is limited to biological processes active in the cell line of choice. This was long considered the main drawback of haploid genetics, as highly specialized pathways cannot be studied using KBM7 cells and their derivative, the HAP1 cell line [80]. An extensive analysis of KBM7 cells revealed that for approximately 75% of Kyoto Encyclopaedia of Genes and Genomes (KEGG) pathways, about half of the annotated signalling components are expressed, a percentage matched by other frequently used cell lines [148]. The constraint on cell type was partially overcome by the isolation of human haploid embryonic stem cells (haESC) and their successful somatic differentiation into neuronal, cardiomyocyte, endodermal and pancreatic lineages [195]. While this approach poses substantial limitations for the achievable scale of the screenable mutant pool, mammalian haESCs were successfully employed to investigate cell differentiation process [196, 197], chromosome X inactivation [198] and to identify drug targets [199, 200].

Alternative mutagenesis methods such as RNA interference and CRISPR/Cas9 allow genome-wide editing in a variety of somatic cell lines. These approaches, while paving the way to functional genomic interrogation in highly specialized cells and in primary cultures [201-203], nonetheless carry their own set of limitations. In general, knockout efficiency and off-target effects constitute a major challenge for RNAi screens

[52]. To some extent, the problem is shared by CRISPR/Cas9 screens, where recovery of sgRNAs through sequencing is taken as indication of targeted gene knockout. While the problem is now being addressed by the development of highly optimized sgRNA libraries [114, 204], in the past variable editing efficiency of individual sgRNAs constituted a significant technical limitation of CRISPR/Cas9 screens [68]. On the other hand, haploid genetics is much less sensitive to incomplete gene loss-of-function than CRISPR/Cas9 system. Whereas the genomic lesions induced by an individual sgRNA can differ among transfected cells, with the same guide also potentially generating neutral in-frame insertion or deletion (indels) on one or both alleles [80], gene-trap sense integrations in a particular location lead to equal and reproducible perturbations. As independent integrations are considered separately, hypomorphic alleles and incomplete loss-of-function gene products only partially affect the counting of true knockout events [80]. An elegant study performed in KBM7 cells directly compared gene-trapping and CRISPR/Cas9 mutagenesis protocols in a sequential FACS-enrichment screen for components of the endoplasmic-reticulum-associated protein degradation (ERAD) pathway and showed vast overlap (70%) in the identified hits [205]. Further analysis of non-shared hits indicated that each methodology fell short in identifying true hits due to either poorly effective sgRNAs (in the CRISPR/Cas9 iteration) or insertion bias (in haploid genetics).

3.3.3 *Gene-trapping versus CRISPR/Cas9 mutagenesis for FACS-based forward genetic screening*

Both CRISPR/Cas9 technology and haploid genetics are used to generate mutagenized pools for FACS-based forward genetic screens [102-108, 194, 206-209]. In general, analysis of CRISPR/Cas9 screens relies on counting sgRNA enrichment in a selected population versus a control sample. A score is then obtained by averaging the effects of multiple sgRNAs (usually between 4 and 10) targeting one gene, with varying corrections depending on the statistical analysis employed [210]. In an early example of FACS-based genetic screen using a CRISPR/Cas9 mutagenized library, the quality of the results was strongly affected by the variability in individual sgRNA performance [102]. Since then, CRISPR/Cas9 screens performance and reproducibility improved. For instance, replicate CRISPR/Cas9 fitness screens performed in the same laboratory [211] and even in two separate locations [91] displayed high concordance in gene mean scores. However, correlation between replicates was less striking in examples of CRISPR/Cas9 mutagenized pools used for FACS-based screening, presumably as fluorescence levels readouts are more prone to technical variability compared to cellular fitness [207, 209].

On the other hand, in this Chapter I presented how comparison of FACS-based haploid screens (which used level of phosphorylation of RPS6 protein as a readout) showed a high degree of concordance even when conducted without explicit standardisation across laboratories (**Figure 3.8B**). This robust performance is likely due to two reasons. First, although the gene-trap cassette has intrinsic integration biases, its insertion pattern is highly consistent across different mutagenesis rounds, generating remarkably similar mut-HAP1 cells populations. Secondly, haploid screening relies on

dozens, and in some cases, thousands independent insertions per gene which allows robust and straightforward hits calling [103].

Thus, while both mutagenesis approaches (haploid genetics and CRISPR/Cas9) remain valid and effective, my data indicate that the robustness and consistency of haploid genetics render them especially suited for screening of continuous phenotypes not driven by a strong selective pressure.

3.3.4 *Hit prioritisation for validation*

Genetic screens usually return between tens and hundreds of hits which pass the significance cut-off and are predicted to affect, to a varying degree, the phenotype studied. As generation and testing of a large number of knockouts for single-well validation experiments is laborious, the hit validation step is preceded by compiling a ranking of gene candidates according to 1.) their likelihood to be specifically associated with the phenotype and 2.) their novelty and/or the ability to formulate hypotheses around their link to the phenotype. Thus, although every hit is carefully evaluated both on its own merit and in connection with the screen reporter, studies starting with genetic screens ultimately focus on a small number of regulators, investigating them in depth. Similarly, for the screens presented in this thesis, when confronted with a number of possible research paths, I followed up on a subset of hits which, according to aggregated data from a number of different sources, were identified as most promising (see **Section 3.2.8**).

Despite the availability of a number of gene prioritisation tools designed to combine knowledge sources and offer standardized scoring systems [212], this step still requires extensive manual curation. While machines are faster and more efficient than humans in finding and incorporating information from a number of databases, algorithms built

around knowledge bases are of limited use in the discovery of new biology. In fact, genetic screens often identify novel, poorly characterised genes as hits and researchers are faced with the task of "deorphanizing" them. Due to the genetic "information asymmetry" (according to which 75% of research focuses on 10% of the genes [213]), genes that were historically extensively investigated are very likely to outrank poorly-studied genes in hits lists that are fed to a prioritisation tool.

Collection and ranking of gene-specific information thus follows a non-standardized, flexible procedure at least as much centred on the hit gene itself as on the phenotype. In this context, analysis of on-line repositories of raw data such as protein-protein interactions, expression data and genetic screen hit lists is of greater importance to form novel predictions without *a priori* knowledge. In particular, the structure of protein or gene interaction networks can help gene prioritisation by revealing interactions among gene hits [214]. In fact, the probability of two or more related genes scoring as hits by chance is much lower than for an individual gene, revealing a probable link between a protein complex and the tested phenotype.

3.3.5 *Future perspectives*

3.3.5.1 Technology advances

Fluorescence Activated Cell Sorting constitutes the gold standard for phenotypic pooled screening applications, offering unparalleled flexibility and the option to fine-tune sorting parameters in real time. However, it is undisputable that sorting constitutes the main bottleneck in genetic screens workflow, requiring the analysis of hundreds of millions of cells. This drawback can be overcome in various ways. As demonstrated in **Section 3.2.7**, the quality of the regulatory map is not affected by increasing sorting gates

3-fold to 3%, in line with previous reports where successful identification of genetic regulators was performed by isolation and comparison of the top and bottom 10-25% of the fluorescent distribution [207, 208]. Besides setting more permissive sorting gates, sorting time can be reduced by employing a more precise and powerful sorter, or substituting FACS with a faster high-throughput screening methodology. Recently, magnetic cell labelling using antibody conjugated beads was optimized for genetic screening applications [215]. This technique, called microfluidic immunomagnetic cell sorting (MICS) allowed sorting of up to 10^8 live cells in 1 hour, constituting approximately a 5-fold improvement over the 1.8 x 10^7 reported here. However, the speed and affordability of the application came at the cost of flexibility in sort settings and the need of a more extensive set-up optimisation per each screen [216]. Currently, no other technology allows cellular phenotype analysis to a comparable throughput in a format compatible with pooled screens. This notion suggests that fluorescence (or magnetic)-based cell sorting will continue to play a prominent role in the functional genomics toolbox.

Furthermore, adaptation of FACS-based forward genetic screening set-up to 1.) exploit the simultaneous detection of multiple fluorescent parameters and 2.) expand the screen-able space, can be envisioned. Multi-colour FACS was already described to investigate genetic factors concomitantly affecting NF-κB and MHC class I expression in neuroblastoma [107]. This application could further prove useful in detecting regulation of known feedback loops where expression of one marker is increased in response to downregulation of a second one. Additionally, application of already existing protocols coupling FACS with RNA-detection methods (Flow-FISH) [217] could yield an unprecedented insight in the regulation of RNA-dependent cellular phenotypes such as aberrant RNA splicing and lncRNA transcription.

3.3.5.2 Building a genetic interaction map from FACS-based genetic screens

Following the example set by collections of fitness screens in yeast [86, 87] and mammalian cells [90], comparison of a number of FACS-based screens could be instrumental in the inference of novel protein networks. As discussed in **Chapter 1**, genetic interaction approaches in mammalian cells exploited the correlation among gene essentiality scores of elements belonging to a functional module across different backgrounds [62]. In other words, a number of different cellular backgrounds was investigated for a single phenotype (*i.e.* lethality). The approach could be reversed in haploid FACS-based genetic screens with the same genetic background (HAP1 cells) being investigated for multiple phenotypes to reconstruct genetic interactions.

The feasibility of such approach is supported by data published by Brockmann *et al.*: when regulatory patterns of genes known to belong to the same functional unit were compared across ten independent FACS-based genetic screens, subunits of known complexes displayed consistent behaviour [103]. This result suggested how haploid genetic screens not only constitute a rich resource of regulators for the phenotype of interest but, when integrated, they might help refine the mammalian genetic interaction map, by validating and expanding on known cell circuitry revealed by other biochemical and genetic interaction approaches.

Collectively, in this Chapter I described a robust and flexible genome-scale phenotypic screening approach. For a defined continuous phenotype of interest such as protein state or activation of a reporter system (HIF-1α, MR1), this technology accurately reconstructed the underlying regulatory network of cells presenting an altered phenotype. When coupled to haploid genetics, FACS-based forward genetic screening displayed high

reproducibility even across replicates performed in different laboratories, marking it as a powerful tool to iteratively study a phenotype of interest in basal and perturbed states.

Chapter 4: A Ragulator-FLCN compensatory mechanism regulates mTORC1 activation

4.1 Introduction

The mammalian target of rapamycin complex 1 (mTORC1) acts as the cell's gatekeeper, activating either growth or autophagy programs in response to external cues. While there is a good understanding around core mTORC1 pathway components, less is known about how the different regulatory layers are interconnected and how they get rewired under stress conditions or in a mutated genetic background. In the past, genetic screens aiming to identify novel components of mTORC1 pathway were often biased because they only targeted a small number of pre-selected genes or were performed in highly specialized cellular systems, failing to take the full complexity of the pathway into account [218-221]. In this Chapter I employ FACS-based haploid genetic screening to iteratively interrogate mTORC1 activation in basal condition and in presence of relevant pharmacological and genetic alterations. This approach highlights a differential requirement for the Ragulator subunits LAMTOR4 and LAMTOR5 in maintaining mTORC1 activation. Additionally, LAMTOR4 and the tumour suppressor FLCN are found to be involved in a "synthetic sick" interaction, with possible translational applications. Together, this Chapter describes how iterative screening allows for dissection of the mTORC1 signalling pathway, uncovering regulatory mechanisms and their interconnectivity that are usually overshadowed by the core regulatory module.

4.1.1 *Mammalian target of rapamycin complex 1 (mTORC1)*

The mammalian target of rapamycin complex 1 (mTORC1) is a multiprotein complex playing a key role in directing cell fate towards growth or autophagy in response to a number of external cues such as growth factors, AA, oxygen, and other nutrients [222]. External signals converge on mTORC1 which directs cell fate by activating anabolic or catabolic pathways through the phosphorylation of multiple downstream effectors. The kinase activity of the mTORC1 complex is mediated by a conserved serine/threonine protein kinase, mTOR, after which the complex is named. The kinase owes its name to rapamycin, a naturally-occurring compound first isolated on the Rapa Nui island from *Streptomyces hygroscopius* [223]. Rapamycin (sirolimus) was later shown to physically bind to and inhibit mTOR activity [224-226]. mTOR is part of two distinctive, yet functionally interconnected complexes, namely mTORC1, which will be the focus of this Chapter, and mTORC2. Both complexes play a role in regulating cell survival, but mTORC1 specifically orchestrates cell growth and metabolism, and mTORC2 coordinates the cellular response to a set of growth factors, such as insulin, primarily through activation serine/threonine-specific protein kinase AKT [227]. In the mTORC1 complex, mTOR associates with four other proteins: proline-rich AKT substrate 40 kDa (PRAS40, also known as AKT1S1), DEP domain-containing mTOR-interacting protein (DEPTOR), regulatory-associated protein of mTOR (RAPTOR) and mammalian lethal with Sec13 protein 8 (mLST8) [228, 229] all of which play a role in modulating downstream signalling.

4.1.2 *mTORC1 regulation*

Since its discovery more than 25 years ago, a wealth of studies focused on understanding the intricate regulation of mTORC1 complex (reviewed in [89]). Activation of mTORC1 requires the convergence of two types of pro-growth inputs: nutrients, such as growth factors, and essential AAs. The two arms converge on the lysosomal membrane, where mTORC1 activation takes place (

Figure 4.1 and **Figure 4.2C**).

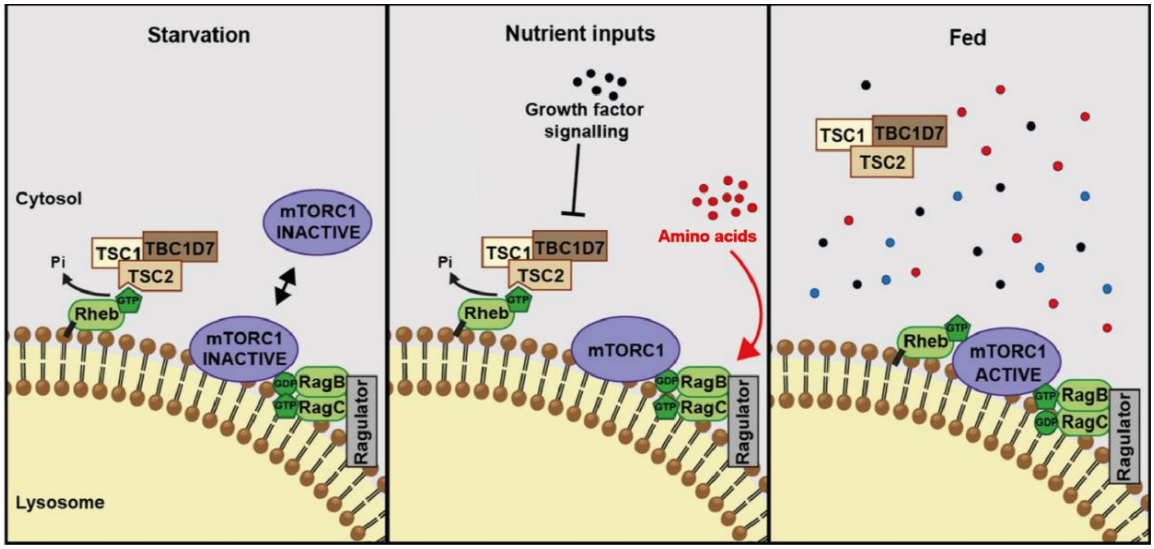


Figure 4.1 mTORC1 activation requires both nutrient and AA sufficiency cues. Image adapted from [230].

4.1.2.1 The nutrient-sensing arm

mTORC1 activation is regulated by a series of small GTPases acting as molecular switches depending on their guanosine diphosphate/triphosphate (GDP/GTP) loading status. In particular, when mTORC1 comes into contact with the lipid-anchored GTP-binding protein RHEB (Ras homologue enriched in brain) on the lysosome, RHEB promotes mTOR auto-phosphorylation and subsequent activation, although the exact

mechanism remains unknown [231, 232]. Studies in *Drosophila melanogaster* showed that overexpression of dRheb led to increased cell size in both in cultured cells and *in vivo*, a phenotype that could be reversed *in vitro* by treatment with rapamycin [233]. Buerger *et al.* showed that Rheb localisation on the lysosomal surface was critical for mTORC1 activation and depended on its post-translational modification; in fact, disruption of Rheb's C-terminal CAAX farnesylation motif severely reduced mTORC1 activation in HEK293 cells [234]. Rheb's GDP/GTP loading status is regulated by the tuberous sclerosis complex (TSC) which promotes the hydrolysis of GTP to GDP [235], [236, 237]. Growth factor signalling and environmental stresses, such as low energy and hypoxia, converge on the TSC, which is composed of the scaffolding protein TSC1, the catalytic subunit TSC2 and the Tre2-Bub2-Cdc16-1 domain family member 7 (TBC1D7) [238]. The above-mentioned pro-growth signals are usually transmitted to the TSC through various intracellular phosphorylation cascades such as the serine/threonine kinases PI3K and AKT in response to insulin [239] and the 5' AMP-activated protein kinase (AMPK) in response to stimulation of WNT (wingless and int-1) signalling [240].

4.1.2.2 The amino acid (AA) sensing arm

mTORC1 can be activated in response to intracellular AA levels, which promote complex localisation to the lysosome by the action of a family of four Ras related GTP binding proteins (the "Rags") [241]. Rag GTPases exist in two possible heterodimeric forms, with Rag A or Rag B interacting with either Rag C or Rag D [242]. In the active state, the two subunits are loaded with the phosphorylated forms of guanosine nucleotide: Rag A/B is GTP loaded while Rag C/D is GDP loaded. mTORC1 is recruited to the lysosomal surface by the active conformation of Rag GTPases where it can be activated by GTP-

loaded Rheb, indicating a logical "AND-gate" type of regulation, *i.e.* both activation signals are required.

Rag heterodimers are tethered to the lysosomal surface by the pentameric Ragulator complex, composed of five subunits named late endosomal/lysosomal adaptor, MAPK and MTOR activator proteins (LAMTORs): p18/LAMTOR1, p14/LAMTOR2, MP1/LAMTOR3, C7orf59/LAMTOR4 and HBXIP/LAMTOR5 [243, 244]. Recently, the basic structure of the Ragulator complex was solved: the lysosome-bound subunit p18/LAMTOR1, wraps around obligate heterodimers p14/MP1 (LAMTOR2/3) and C7orf59/HBXIP (LAMTOR4/5), while its N-terminal region, together with two helices of p14/MP1 (LAMTOR2/3), is involved in recruitment of Rag GTPases [245-247]. Besides its structural role, the Ragulator complex and its subunits are linked to a series of cellular phenotypes both related and unrelated to mTORC1 signalling (**Table 4.1**).

Gene	Molecular phenotypes	Mouse phenotypes	Human disease phenotypes
LAMTOR1 (p18)	Activation of RhoA and regulation of actin cytoskeleton [248]	Embryonic lethal (IMPC, [249])	NA
	Regulation of lysosomal catabolism and positioning [250]	Impairment of M2 polarisation in macrophages-specific knockout [251],	
		Reduction in proliferation and suppressive T cell function in CD4-specific knockout [252]	
LAMTOR2 (P14)	Regulation of endosomal trafficking and cell proliferation [253]	Embryonic lethal (IMPC, [249])	Mutations cause primary immunodeficiency syndrome. Perturbed distribution of late endosomes [254]
		Impaired defence against Salmonella in macrophage-specific knockout mice [255]	Polymorphisms do not play a role in breast cancer [256]
LAMTOR3 (MP1)	MEK binding partner and regulation of MEK/ERK activation cascade [257]	NA	Polymorphisms do not play a role in breast cancer [256],
LAMTOR4 (C7orf59)	Regulation of microglia development [258]	NA	NA
LAMTOR5 (HBXIP)	Hepatitis B virus binding and replication inhibition [259]	Embryonic lethal (IMPC, [249])	NA
	Regulation centrosome dynamics and spindle assembly [260]	Higher fasting glucose levels and lower glucose tolerance in pancreatic β-cell-specific knockout mice [221]	
	Cofactor in apoptosis suppression [261]		

Table 4.1 List of molecular and phenotypic characteristics related to Ragulator components. IMPC = International Mouse Phenotypic Consortium.

Over the years, biochemical studies uncovered multiple proteins acting as GDP/GTP exchange factors for the Rags. While contrasting reports exist on the role of Ragulator as Guanosine Exchange Factor (GEF) towards Rag A/B, supposedly promoting its GTP-loading [243, 247], multiple studies describe how Rag A/B cycles to its GDP-bound inactive form by action of the trimeric complex GATOR1 (GAP activity toward the Rag GTPases 1) [262]. Loss of any of the three GATOR1 components, DEP domain containing 5 (DEPDC5), NPR2- and NPR3-like proteins (NPRL2 and NPRL3), prevents mTORC1 inactivation in the absence of AAs [262]. Recently, a complex composed of KPTN, ITFG2, C12orf66 and SZT2, named KICSTOR, was identified acting as a scaffold for GATOR1 on the lysosome [263, 264]. KICSTOR localises on the lysosomes in an AA-independent manner and, similar to GATOR1, its loss is sufficient to cause mTORC1 lysosomal localisation in AA starved conditions [263]. GATOR1 activity is additionally antagonized by a pentameric complex named GATOR2 (composed of MIOS, SEH1L, WDR59, SEC13 and WDR24 proteins). GATOR2 acts upstream of GATOR1, and in line with its role of activator of the pathway, depletion of four out of five of its components blunted AA-mediated mTORC1 activation [262].

Rag C/D nucleotide loading status is regulated by a protein called folliculin (FLCN) together with its partner Folliculin Interacting Protein 2 (FNIP2), which was demonstrated to interact with the γ-1 subunit of AMPK [265-267]. Co-immunoprecipitation experiments in HEK293T cells showed AA-sensitive interactions of FLCN-FNIP2 complex with the Rags, with a preference for GTP-loaded Rag C, suggesting a GTPase role for FLCN. Biochemical studies thus support a role of FLCN as a positive regulator of mTORC1, in line with genetic experiments performed in fission yeast highlighting the opposing roles of FLCN and TSC1/2 orthologues on expression levels of genes involved

in AA homeostasis [268]. Under fully fed conditions, FLCN is diffused throughout the cytoplasm and only localises on the lysosome upon AA starvation, possibly facilitating re-activation of mTORC1 [265]. Interestingly, germline mutations in FLCN gene cause Birt-Hogg-Dubé (BHD) syndrome, an autosomal dominant condition characterised by benign tumours of the hair follicle, lung cysts, spontaneous pneumothorax, and predisposition for kidney tumours (reviewed in [266]). In order to study FLCN function, deletion experiments were conducted both *in vitro* and *in vivo* with the generation of FLCN knockout mice. In these studies, conflicting results for activation of the mTORC1 pathway in tumours were reported, highlighting the complexity of FLCN- mTORC1 axis [269, 270].

Although mTORC1 recruitment to the lysosome and its activation in AA sufficiency is well characterised, the exact mechanism of AA sensing remained, until recently, uncharacterized. Recent studies pointed to an important role of the vacuolar-type H^+-ATPase (v-ATPase) complex [220] and solute carrier family 38 member 9 (SLC38A9) in detecting AA accumulation in the lysosomal lumen [271-273]. Additionally, co-immunoprecipitation experiments further underlined the pathway's interconnectivity, suggesting an interaction between members of the Ragulator complex, v-ATPase subunits in the membrane spanning region and AA transporter SLC38A9 [220, 271].

4.1.3 *mTORC1 effectors*

The molecular architecture underlying mTORC1-dependent regulation of anabolic and catabolic cellular processes including protein synthesis and turnover was extensively studied and depends on mTORC1-mediated phosphorylation of a number of downstream effectors [274]. Protein translation in mammalian cells is a highly regulated process that

includes several control checkpoints to avoid aberrant activation. Translation is initiated by the recruitment of the small ribosome subunit together with the eukaryotic initiation factor 4F (eIF4F) complex to the 5' end of an mRNA molecule. By modulating the assembly of the eIF4F complex, composed of the three initiation factors eIF4E, eIF4G and eIF4A, cells exert a tight control over protein synthesis. mTORC1 acts through phosphorylation of eIF4E-binding protein 1 (4E-BP1), which in turn releases eIF4E, thereby promoting eIF4F complex formation and activating translation [274]. While eIF4F is required for mRNA translation in general, it was shown to be particularly important for mRNAs containing a 5' terminal oligopyrimidine (TOP) tract [275, 276]. In agreement with these findings, two independent groups reported translation of 5' TOP mRNAs to be highly sensitive to competitive mTORC1 inhibition through a mechanism partly relying on regulation of eIF4E by 4E-BP1 [277, 278]. As the TOP tract is a feature characteristic of mRNAs encoding ribosomal proteins and components of the translational machinery, this highlights mTORC1's control of protein synthesis.

Another downstream effector through which mTORC1 modulates protein synthesis is p70S6 kinase 1 (RPS6K1). Phosphorylation of RPS6K1 at Thr389 activates its kinase activity towards a number of substrates promoting mRNA translation initiation. In particular, phosphorylation of ribosomal protein S6 (RPS6), a component of the 40S subunit of the ribosome, at Ser235/236 is indicative of increased protein synthesis [279]. A growing body of evidence points towards additional mechanisms by which RPS6K1 can regulate translation such as RPS6K1 promoting eIF4A helicase activity against structured 5'UTR regions of mRNAs [274].

Translation is differentially regulated by treatment with allosteric and ATP-competitive mTORC1 inhibitors. In fact, short term treatment (< 6 hours) with allosteric

inhibitor rapamycin does not affect 4E-BP1 phosphorylation, while treatment using competitive inhibitor Torin-1 induce changes in protein synthesis already after 2 hours [278]. Rapamycin, acting in complex with the FK506-binding protein 12 (FKBP12) [280], was shown to perform its mTORC1 inhibitory activity by sterically hindering substrate recruitment and preventing contact with the kinase active site, selectively restricting RPS6K1 phosphorylation while failing to affect 4E-BP1 [281].

4.1.4 *mTORC1 in cancer*

As a result of the central role of mTOR in the cell, genetic alterations causing aberrant mTORC1 signalling were linked to a number of pathological conditions ranging from neurological disorders to impaired glucose homeostasis and cancer [222]. In particular, mutations in upstream regulators of mTORC1 pathway, such as within TSC1, TSC2 and FLCN genes, were linked to a variety of familial cancers (reviewed in [282]). These data, together with low frequency mutations in GATOR1 components in glioblastoma [262], alterations in RRAGC in follicular lymphoma [283] and activating mutations in MTOR itself [284] strongly support a role for mTORC1 in tumorigenesis.

Chronic use of mTOR pharmacological inhibitors in both animal models and in clinical setting is fraught with limitations due to multiple, still poorly understood feedback loops and crosstalk between signalling arms within the mTORC1 pathway [285]. In short-term *in vitro* experiments rapamycin and its closely related analogues (rapalogues) were shown to block cell growth in various cancer cell lines, including acute lymphoblastic leukaemia, prostate, breast and small cell lung cancer [286]. However, when the findings were translated into clinical settings, patients treated with rapalogues reported only limited therapeutic benefits [287, 288]. Subsequent molecular studies showed

how sustained mTORC1 blockade triggered a feedback loop activating pro-growth insulin receptor substrate 1 (IRS1)/PI3K/AKT signalling [289]. Moreover, a collection of *in vitro* and *in vivo* data demonstrated how hyperactivation of the rapamycin-insensitive eIF4E/4-EBP1 axis drives cell proliferation in ERK- and AKT-dependent cancers [277, 290, 291].

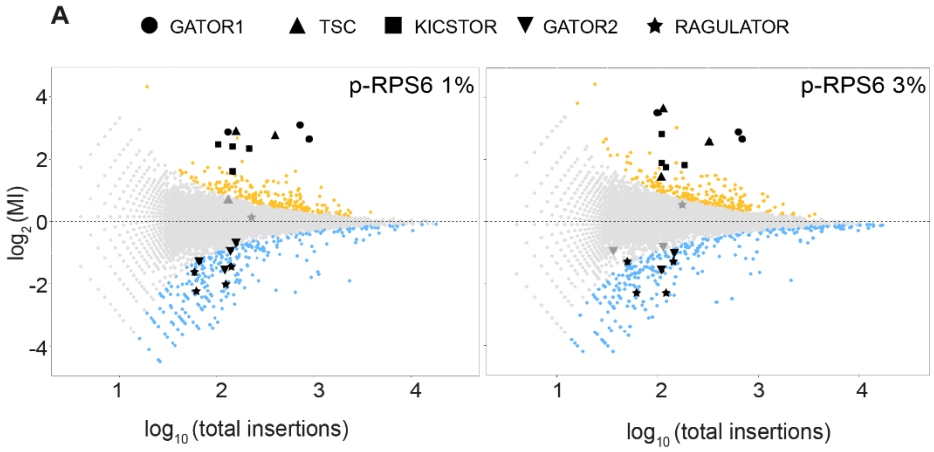
Underwhelming results of anti-cancer clinical trials using rapalogues highlighted the need for a molecular, in-depth understanding of how different inputs collectively regulate mTORC1. By using a set of robust, quantitative forward genetic screens the work presented in this Chapter uncovers a fine-tuned regulation of the mTORC1 pathway through a feedback loop between the Ragulator subunit LAMTOR4 and the tumour suppressor FLCN.

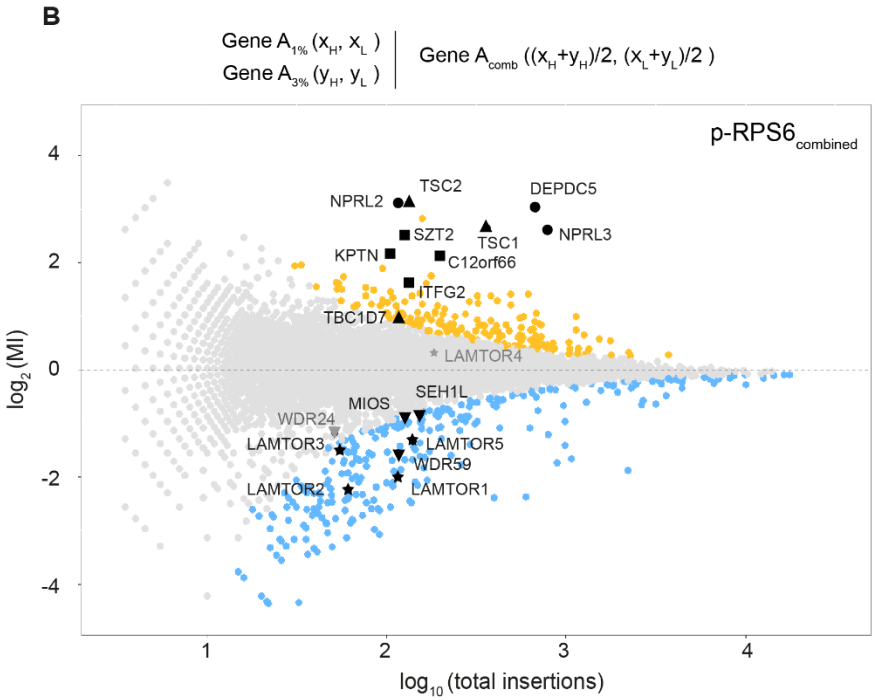
4.3 **Results**

4.3.1 *Haploid genetic screen for mTORC1 activation*

Under steady-state culturing conditions (*i.e.* in medium supplemented with nutrients and AAs), mTORC1 activates cellular anabolic signalling through phosphorylation of a number of effectors. As previously shown by others, the phosphorylation of mTORC1's immediate downstream proteins constitutes a sensitive and dynamic readout for pathway activation [292]. Hence, I utilized the phosphorylation of ribosomal protein S6 (p-RPS6) at Ser235/236, a key effector of mTORC1 closely implicated in protein translation, as readout for FACS-based genetic screen [279].

I conducted two screens to identify regulators of p-RPS6 (and thus mTORC1), isolating mut-HAP1 cells in the extreme 1 and 3% of the fluorescence distribution to determine the effect of varying the sorting gate (**Figure 3.8C**, see **Appendices 8.2.2** and **8.2.3**). The retrieved inactivating insertions mapped, in both instances, to approximately 16.000 genes, which cover a significant portion (approximately 95%) of the expressed HAP1 cell transcriptome [103]. As shown in **Figure 3.8C**, MI z-scores of hits were highly concordant between the 1% and 3%-gated screens (Spearman Rho =0.98). I reasoned that these screens could hence be treated as quasi-replicates, effectively representing sorting of 2 x 10^7 cells for each end of the p-RPS6 distribution (obtained through a variable gating). Thus, I combined the two datasets, calculating average number of combined per gene insertions and performing a new statistical analysis on the combined dataset (**Figure 4.2A-C**, see **Appendix 8.2.7**).


A
GATOR1
TSC
KICSTOR
GATOR2
RAGULATOR
p-RPS6 1%
p-RPS6 3%
log2 (MI)
log10 (total insertions)
log10 (total insertions)


B
Gene A1% (xH, xL)
Gene A3% (yH, yL)
Gene Acomb ((xH+yH)/2, (xL+yL)/2)
p-RPS6combined
NPRL2
TSC2
DEPDC5
SZT2
TSC1
NPRL3
KPTN
C12orf66
ITFG2
TBC1D7
LAMTOR4
SEH1L
MIOS
WDR24
LAMTOR3
LAMTOR5
WDR59
LAMTOR2
LAMTOR1
log2 (MI)
log10 (total insertions)

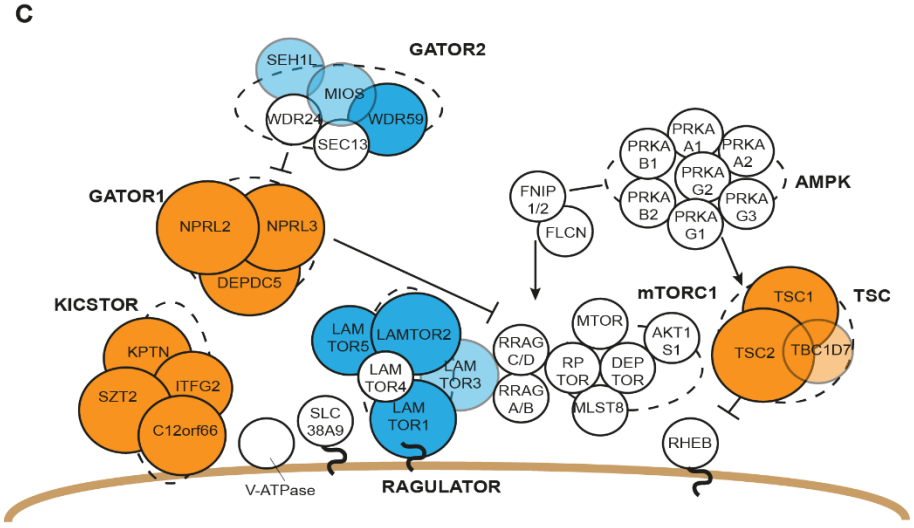

C
GATOR2
SEH1L
MIOS
WDR24
WDR59
SEC13
GATOR1
NPRL2
NPRL3
DEPDC5
KICSTOR
KPTN
SZT2
ITFG2
C12orf66
LAM TOR5
LAMTOR2
LAM TOR4
LAM TOR3
LAM TOR1
SLC 38A9
V-ATPase
RAGULATOR
FNIP 1/2
FLCN
PRKA B1
PRKA A1
PRKA A2
PRKA G2
PRKA B2
PRKA G3
PRKA G1
AMPK
mTORC1
MTOR
AKT1 S1
RRAG C/D
RP TOR
DEP TOR
RRAG A/B
MLST8
TSC
TSC1
TSC2
TBC1D7
RHEB

Figure 4.2 FACS-based forward genetic screens on mTORC1 activation. A. Regulatory maps for mTORC1 activation obtained through FACS separation and analysis of the extreme 1% (left panel) and 3% (right panel) of the p-RPS6 distribution in a mut-HAP1 cell pool. Only significant regulators are coloured (orange and light blue for negative and positive regulators respectively), non-significant genes are represented in grey. Symbols are used to highlight genes belonging to selected pathways. **B.** p-RPS6$_{combined}$ map obtained by calculating per-channel, gene average insertions across 1% and 3% screens. Colouring and symbols as in **A.**, names for selected genes are displayed. Of note, SEC13 is not represented as insertion numbers are below graph limit ($n < 5$). **C.** Schematic representation of major known mTORC1 regulators (image adapted from [293]). Gene products are represented as circles; genes scoring as regulators are coloured (darker shade for FDR < 0.001, lighter colouring for FDR < 0.05) orange and light blue are used for negative and positive regulators respectively. Circle diameter reflects absolute log_2MI value.

The resulting regulatory map for p-RPS6$_{combined}$ contained hundreds of genes whose inactivation affected p-RPS6 levels in HAP1 cells to a varying degree, as expected for a central cellular signalling hub. In particular, the screen identified a number of well-characterised mTORC1 regulators from both the nutrient- and AA-sensing arms, benchmarking the screen results (**Figure 4.2B**, **C**). In particular, all genes known to belong to the mTORC1 upstream negative regulatory complexes GATOR1, KICSTOR and TSC were identified as highly significant.

Among positive regulators, the majority of genes (154 out of 277, 55%) were annotated to mitochondrial processes (**Figure 4.3A**). Accordingly, pathways related to mitochondrial function, and in particular to mitochondrial translation, were strongly represented among the top Reactome terms enriched in the positive regulators list (**Figure 4.3B**). Impairment in mitochondrial homeostasis can lead to a drop in membrane potential which in turns affects cell growth and, ultimately, viability [294]. As mTORC1 senses the cell's energy state, it was not surprising to find that loss of mitochondrial proteins lowered mTORC1 activation.

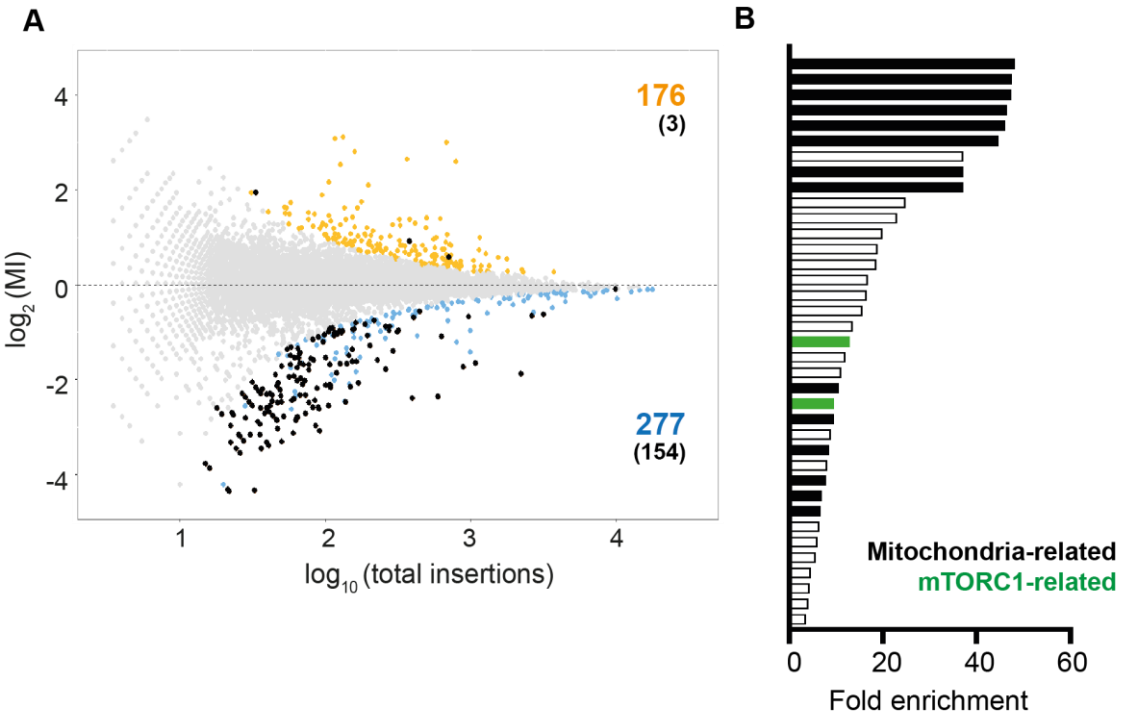


Figure 4.3 Mitochondrial gene enrichment among mTORC1 positive regulators. A. Map of p-RPS6$_{combined}$ regulators with mitochondrial hits (Human MitoCarta 2.0, [295]) highlighted in black. Negative regulators are highlighted in orange (n = 176) and positive regulators in light blue (n = 277): for each channel, the number of mitochondrial hits is displayed in brackets. **B.** Reactome pathways enriched among positive regulators of p-RPS6$_{combined}$, ordered by fold enrichment (FDR < 0.05 and fold enrichment > 1). Pathways related to mitochondrial processes are displayed in black, mTORC1-related pathways are displayed in green.

Additionally, insertions in four of the five genes coding for components of the Ragulator complex (LAMTOR1-3, LAMTOR5) were statistically enriched in cells displaying lower p-RPS6 fluorescence. The screen additionally identified MIOS, SEH1L and WDR59 genes, coding for well-described subunits of GATOR2, as positively regulating mTORC1 activation when disrupted. The other two GATOR2 complex components, SEC13 and WDR24, were previously reported to have complex-independent functions and were thus less likely to score as positive regulators (SEC13 was additionally poorly hit by gene-trap insertions, n < 5) [262, 296].

Of note, as displayed in **Figure 4.2C**, not all pathway components described in the literature scored as hits. This observation reflected a limitation intrinsic of all genetic screens according to which genes strictly required for viability, those with redundant functions or paralogues cannot be detected. Additionally, haploid genetic applications also miss genes constituting "cold spots" for gene-trap integration. Thus, genes encoding other positive modulators, such as the Rags proteins and the subunits of the v-ATPase complex, presumably failed to score due to their functional redundancy while for essential genes, such as MTOR itself, the number of insertions was too low to obtain meaningful statistics [77]. Overall, by using p-RPS6 as a readout, the FACS-based screening approach presented here successfully mapped the regulatory network modulating mTORC1 activation. While functional investigation of mTORC1 upstream modulators is usually performed under stress conditions, such as AA withdrawal or other types of starvation in order to increase observable differences [262], the obtained regulatory map was generated in complete medium, demonstrating the sensitivity of the approach.

4.3.2 *Pharmacological modifier screen: mTORC1 activation in presence of rapamycin*

Cellular systems, especially in higher eukaryotes, tend to be highly adaptable, maintaining homeostasis through functional redundancy and feedback loops. Perturbations, whether pharmacological or genetic, modify the system's steady-state and can induce extensive molecular rewiring to reach a new equilibrium. Genetic screening can be used to dissect these additional regulatory layers as shown by extensive work on synthetic lethal interactions (reviewed in [297]). Here, I applied this concept to the mTORC1

pathway, investigating how treatment with a perturbagen affects upstream signalling architecture.

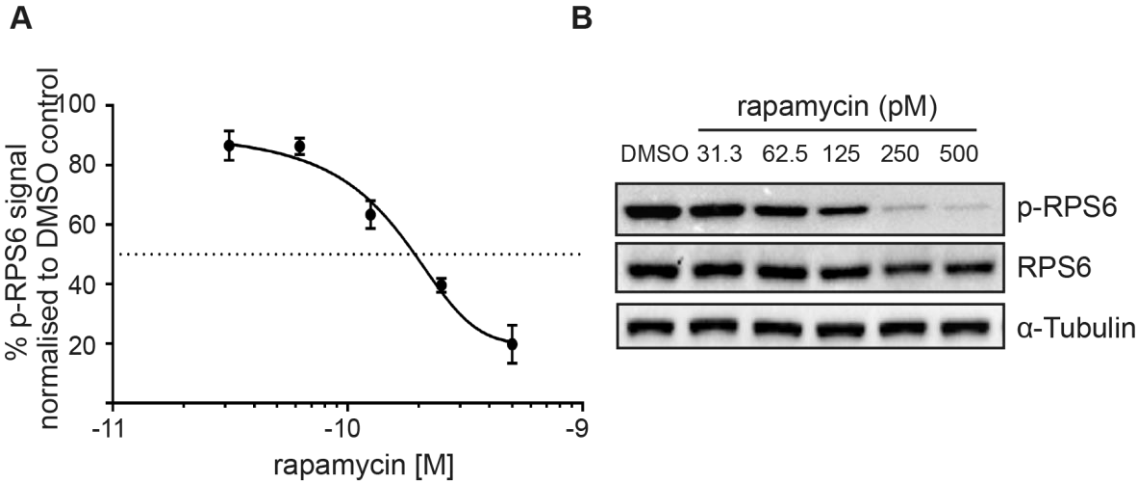


Figure 4.4 Rapamycin dose finding. A. HAP1 cells were treated with rapamycin for 6 hours at the indicated concentrations. Phosphorylation of RPS6 was measured by FC and **B.** immunoblotting using the indicated antibodies.

The screen was thus repeated in presence of the well-studied allosteric mTORC1 inhibitor rapamycin, maintaining p-RPS6 levels as readout ($p\text{-}RPS6_{rapamycin}$, see **Appendix 8.2.8**). To capture alterations of both positive and negative regulators, mut-HAP1 cell pool was treated with 125 pM rapamycin for 6 hours, a dose resulting in approximately 50% inhibition in p-RPS6 signal (**Figure 4.4A**, **B**). Such reduction was shown to provide a "sensitivity window" to detect functionally distinct classes of drug-dependent regulators, both inducing and suppressing drug action [298]. In order to compare whether the role of every individual gene in mTORC1 activation was altered upon rapamycin treatment, I employed a statistical metric, defined as "Delta MI" (ΔMI) assessing significant differences in gene MIs across screens (see **Section 2.7**).

Direct comparison of $p\text{-}RPS6_{combined}$ and $p\text{-}RPS6_{rapamycin}$ (**Figure 4.5A**, **B**) identified four genes with significantly different MI values ($\Delta MI > |1.5|$, FDR < 0.05) (**Figure 4.5C**,

D, see **Appendix 8.2.9**). In particular, FKBP1A, which encodes the well-known rapamycin-binding protein FKBP12 [299], scored as the strongest differential hit which suppressed rapamycin activity. While FKBP1A inactivation did not affect mTORC1 signalling under steady-state conditions (MI = 1.4; FDR = 0.56), gene knockout in p-$RPS6_{rapamycin}$ led to a blockade of the drug's effect on mTORC1 (MI = 3.83, FDR = 2.44 x 10^{-13}). Unbiased identification of FKBP1A benchmarked the ΔMI metric and supported the ability of this measure to identify true differential mTORC1 regulators.

The other three genes identified through ΔMI calculation as potentiating the effect of rapamycin were LAMTOR4, KIAA1033 and SPTLC1 (**Figure 4.5C**, **D**). LAMTOR4 was particularly interesting, as it was the only Ragulator subunit scoring significantly solely in presence of rapamycin, while inactivation of the other four complex components inhibited mTORC1 activation both in presence and in absence of the drug. Analysis of the gene-trap insertion profile for LAMTOR4 in both screens showed a comparable pattern, with mutations accumulating towards the TSS, ruling out that the result was due to a difference in mutagenesis efficiency, as the two screens were performed using two different batches of mut-HAP1 cells (**Figure 4.5E**). These result suggested that LAMTOR4 only affected mTORC1 activation in presence of rapamycin in contrast to a previous report describing all Ragulator subunits to be required for AA-dependent mTORC1 activation [244].

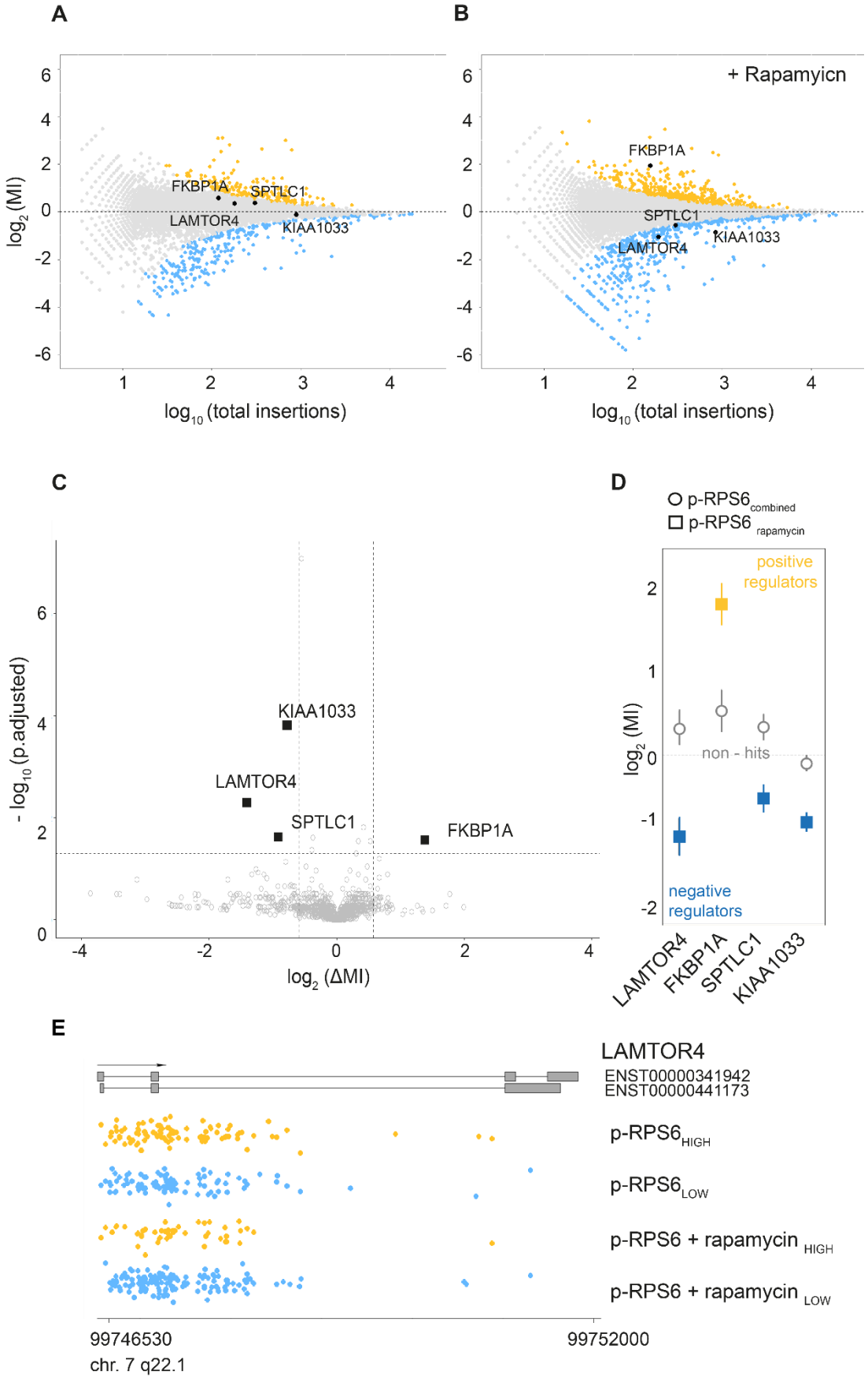

A
B
+ Rapamyicn
FKBP1A
SPTLC1
LAMTOR4
KIAA1033
log2 (MI)
log10 (total insertions)
C
D
- log10 (p.adjusted)
log2 (ΔMI)
p-RPS6combined
p-RPS6rapamycin
positive regulators
non - hits
negative regulators
E
LAMTOR4
ENST00000341942
ENST00000441173
p-RPS6HIGH
p-RPS6LOW
p-RPS6 + rapamycin HIGH
p-RPS6 + rapamycin LOW
99746530
99752000
chr. 7 q22.1

Figure 4.5 Pharmacological modifier screen identifies rapamycin-dependent effects involving FKBP1A and LAMTOR4. A. Regulatory maps for phosphorylation of RPS6 under steady-state conditions and **B.** after 6 hours treatment with 125 pM rapamycin. Colouring as in **Figure 4.2**, selected regulators are highlighted. **C.** Per gene ΔMI and relative significance between p-RPS6$_{combined}$ and p-RPS6$_{rapamycin}$ are plotted. Genes with significantly divergent MI values (ΔMI > |1.5|, FDR < 0.05) are labelled. **D.** Representation of MI values with standard errors (SE, see **Section 2.7**) in p-RPS6$_{combined}$ and p-RPS6$_{rapamycin}$ screens for genes highlighted in panel **C.** Colouring as per above. **E.** Location of gene-trap insertions in the LAMTOR4 gene for p-RPS6$_{combined}$ and p-RPS6$_{rapamycin}$ screens. Colouring and details as in **Figure 3.10**.

4.3.3 *LAMTOR4 hit validation*

To validate LAMTOR4's distinct role in mTORC1 signalling under pharmacological perturbation, I used the CRISPR/Cas9 genome editing system to generate polyclonal LAMTOR4 knockout (KO) pools in HAP1 cells. To verify the unique behaviour of LAMTOR4 in the Ragulator complex, LAMTOR5 knockout pools were generated as controls. LAMTOR5 was described as LAMTOR4's obligate heterodimeric partner and *in vitro* binding studies had shown that the two proteins form a complex [244]. After confirming a high knockout efficiency for both genes (**Figure 4.6A**), knockout pools were tested for p-RPS6 levels using FC. As expected, under steady-state conditions, only LAMTOR5 knockout resulted in a statistically significant reduction in mTORC1 activation while, in line with the screen results, p-RPS6 levels in the LAMTOR4-null background were comparable to wild type control (**Figure 4.6B**, **C**). Conversely, inactivation of both genes enhanced rapamycin-inhibitory effect.

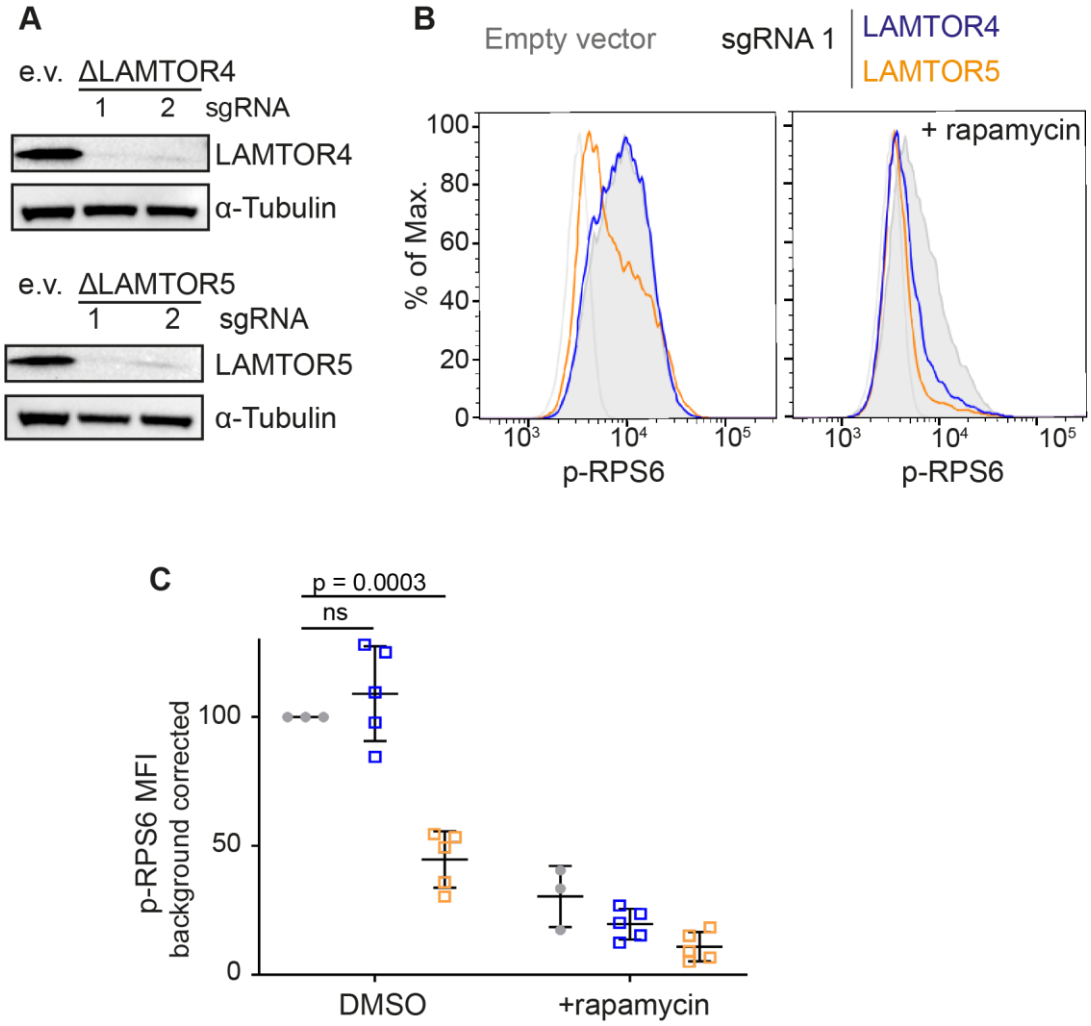


Figure 4.6 LAMTOR4 regulates mTORC1 activation only in presence of rapamycin. **A.** Efficiency of LAMTOR4 and LAMTOR5 knockout in a polyclonal HAP1 cell pool was tested via immunoblotting with the respective antibodies. CRISPR/Cas9 genome editing was performed with two sgRNAs per gene. Empty pLentiCRISPR-v2 was used as control (e.v.). **B.** Phosphorylation of RPS6 in LAMTOR4 and LAMTOR5 polyclonal pools was compared with empty pLentiCRISPR-v2 (e.v.) - transfected HAP1 cells under steady-state conditions and after 6 hours of treatment with 125 pM rapamycin. Representative FC data obtained with two sgRNA each for LAMTOR4 and LAMTOR5 are shown. **C.** Quantification of p-RPS6 median fluorescence intensity (MFI) from data in **B**. Statistical analysis was performed using 2-way ANOVA followed by Dunnett's post hoc test. Data for n = 3 independent experiments are shown, one replicate was performed with only sgRNA1 for both genes.

To further investigate the divergent roles of these two genes, independent HAP1 knockout clones for LAMTOR4 and LAMTOR5 were isolated (**Table 4.2**).

Immunoblotting confirmed the lower levels of p-RPS6 phosphorylation in ΔLAMTOR5 clones, while total RPS6 protein levels were unchanged (**Figure 4.7A**).

Gene	sgRNA	Clone #	Genotype	Validated via immunoblotting?
LAMTOR4	1	1	2 bp deletion*	YES
	1	2	25 bp deletion	YES
	1	3	1 bp insertion	YES
LAMTOR5	2	1	5 bp deletion	YES
	2	2	1 bp deletion	YES
	1	3	13 bp deletion	YES

Table 4.2 Genotype information for LAMTOR4 and LAMTOR5 knockout clones employed in the study. * clone was obtained from Horizon Genomics.

As expected, p-RPS6 reduction was not observed in ΔLAMTOR4. Moreover, inactivation of either Ragulator subunit led to decreased expression of the other, the effect being more pronounced in LAMTOR5 knockouts. The two proteins thus behave as expected for obligate heterodimers, likely affecting each other's stability [244].

To confirm that the LAMTOR4 response to rapamycin was due to an FKBP12-dependent mechanism I generated knockout pools for FKBP12 coding gene FKBP1A in wild type and LAMTOR4-null background (**Figure 4.7B**). In both cases, the deletion of FKBP1A gene abolished rapamycin sensitivity, measured as p-RPS6 levels, indicating that the heightened rapamycin effect in LAMTOR4 knockout is downstream of FKBP12 (**Figure 4.7C**). Furthermore, I asked whether ΔLAMTOR4 cells "hypersensitivity" was limited to the allosteric inhibitor rapamycin or could be recapitulated using other well-known mTORC1 inhibitors. To this end, I treated wild type and ΔLAMTOR4 cells with the mTORC1 competitive inhibitor AZD2014, the AKT-inhibitor MK2206 and rapamycin at concentrations causing approximately 50% reduction in p-RPS6 signal in wild type HAP1 cells.

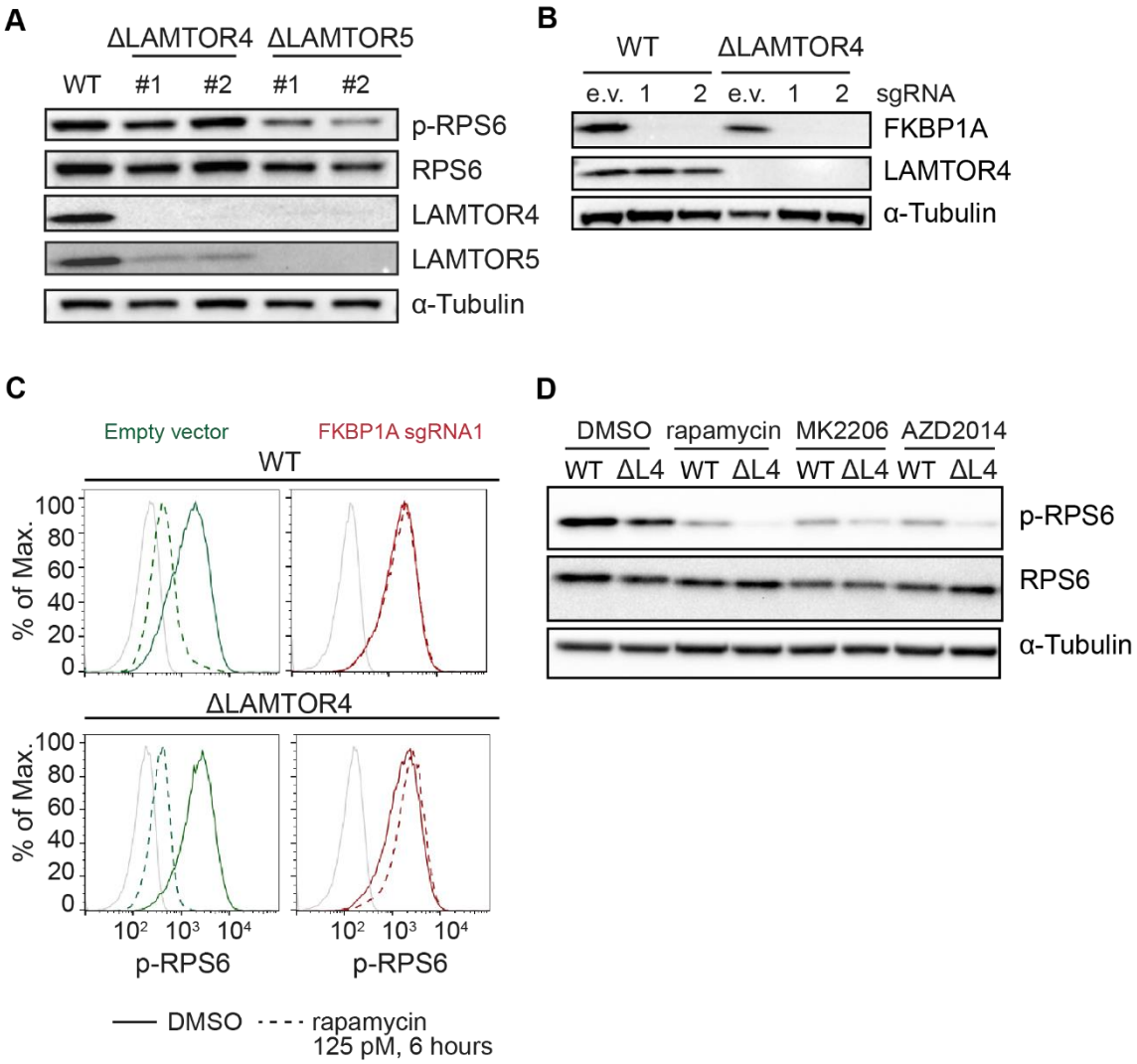


Figure 4.7 Functional effect of LAMTOR4 inactivation. A. Cell lysates from ΔLAMTOR4 and ΔLAMTOR5 HAP1 clones were immunoblotted alongside wild type cells using the indicated antibodies. **B.** Polyclonal HAP1 cell pools resulting from inactivation of FKBP1A with two independent sgRNAs in wild type and LAMTOR4-null background were tested via immunoblotting to determine knockout efficiency. Cells transfected with empty pLentiCRISPR-v2 were used as controls (e.v.). **C.** Phosphorylation of RPS6 was analysed using FC in FKBP1A knockout pools generated in wild type and ΔLAMTOR4 backgrounds, in presence of DMSO or rapamycin treatment (6 hours, 125 pM). **D.** Wild type and ΔLAMTOR4 cells were treated for 6 hours with DMSO, rapamycin (125 pM), MK2206 (750 nM) or AZD2014 (100 nM). Cell lysates were collected and immunoblotted using the indicated antibodies. Experiment conducted with the support of S. Militi. WT = wild type; ΔL4 = ΔLAMTOR4.

All treatments caused a more pronounced inhibition in the ΔLAMTOR4 cells, indicating that the effect is not rapamycin-specific but underlies a more general sensitivity of knockout cells to pharmacological treatment (**Figure 4.7D**).

As phosphorylation of the RPS6K1/RPS6 axis by mTOR regulates pro-growth signals, I functionally characterised ΔLAMTOR4 and ΔLAMTOR5 clones for their colony-forming ability. As expected, in the DMSO-treated control, LAMTOR4 knockout grew comparably to the wild type control and marginally faster than LAMTOR5 knockout cells (**Figure 4.8A**). However, when a low dose of rapamycin (100 pM) was added to the culture medium, as expected, the growth of both knockouts was impaired compared to wild type cells, with ΔLAMTOR5 cells displaying a more pronounced effect.

Next, I tested whether the ΔLAMTOR4 cells "hypersensitivity" was also observed under stress conditions other than treatment with a pharmacological inhibitor. As ablation of the Ragulator complex was shown to affect cell's ability to recover after AA starvation [243], I tested the ability of ΔLAMTOR4 and ΔLAMTOR5 cells to reactivate mTORC1 signalling after incubation in AA-depleted medium. As expected, ΔLAMTOR5 clones failed to efficiently phosphorylate RPS6K1 upon re-feeding (**Figure 4.8B**). Conversely, p-RPS6 levels in ΔLAMTOR4 clones after incubation in full medium were similar wild type control, indicating full recovery.

Taken together, these results indicated that LAMTOR4, distinctively from its heterodimeric partner LAMTOR5, was dispensable for mTORC1 activation under steady-state conditions in HAP1 cells with no appreciable effects on RPS6 phosphorylation, cell proliferation and ability to recover from AA starvation. However, LAMTOR4 was required in presence of a pharmacological stressor.

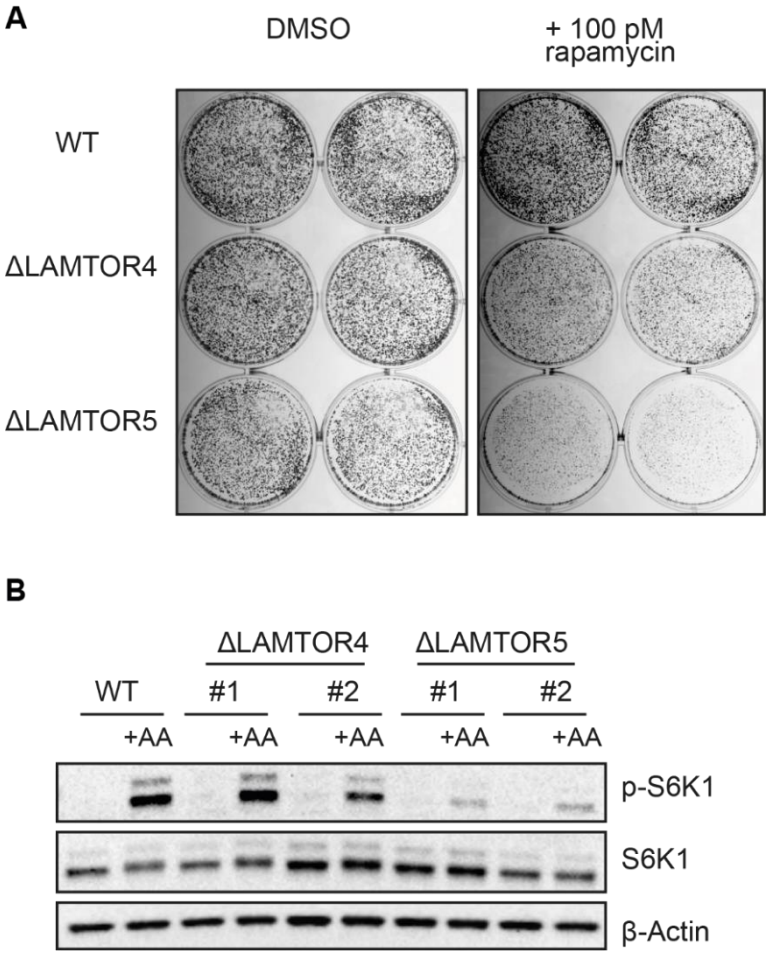


Figure 4.8 Functional consequences of LAMTOR4 loss. A. ΔLAMTOR4, ΔLAMTOR5 and wild type cells were cultured for 96 hours either in presence of DMSO or rapamycin. Colonies were visualized using crystal violet. Images are representative of 3 independent replicates. **B.** ΔLAMTOR4, ΔLAMTOR5 and wild type (WT) cells were grown absence of AA for 120 minutes before recovery in full medium for 60 minutes (indicated as "+AA"). Cell lysates were immunoblotted with the indicated antibodies.

4.3.4 *Genetic modifier screen: mTORC1 activation in ΔLAMTOR4 background*

Data generated so far indicated that HAP1 cells mutant for LAMTOR4 maintain a level of mTORC1 activation comparable to wild type control. This result suggests that compensatory mechanisms are activated in LAMTOR4 knockout cells to promote mTORC1 signalling. To test this hypothesis and investigate the molecular basis of the

persistence of RPS6 phosphorylation, the screen was repeated in ΔLAMTOR4 mut-HAP1 cells (p-RPS6$_{\Delta LAMTOR4}$, see **Appendix 8.2.10**). Interestingly, the per gene effects for components of the GATOR 1 and 2 and KICSTOR complexes were markedly reduced in p-RPS6$_{\Delta LAMTOR4}$ compared to p-RPS6$_{combined}$ screen (**Figure 4.9A**). This result indicated that further inactivation of the AA sensing arm feeding into mTORC1 pathway only minimally affected RPS6 phosphorylation in a LAMTOR4-null background. On the other hand, components of the tuberous sclerosis complex (*i.e.* TSC1, TSC2 and TBC1D7) scored as strong negative regulators in line with the results obtained in a wild type background. These data are in agreement with the accepted two-branched structure of mTORC1 upstream regulation, where KICSTOR/GATOR/Ragulator on one side, and TSC on the other, convey largely independent signals [300]. Thus, the ability to detail general features of the mTORC1 signalling network architecture in an unbiased manner highlighted how iterative genetic screening could be employed to dissect complex signalling pathways.

To identify genetic components that maintain mTORC1 signalling in absence of LAMTOR4, I identified genes whose inactivation lowered p-RPS6 level only in LAMTOR4-null background. Gene Ontology analysis for pathway components run on positive regulators specific for p-RPS6$_{\Delta LAMTOR4}$ showed strong enrichment for gene encoding subunits of AP-3 (AP3B1 and AP3D1), HOPS (VPS16, VPS18, VSP33A and VPS41) and BLOC-1 (BLOC1S1 and BLOC1S2) complexes (**Figure 4.9B, C**). Collectively, these genes were reported to regulate lysosome-related processes, such as biogenesis and vesicular trafficking [301-303].

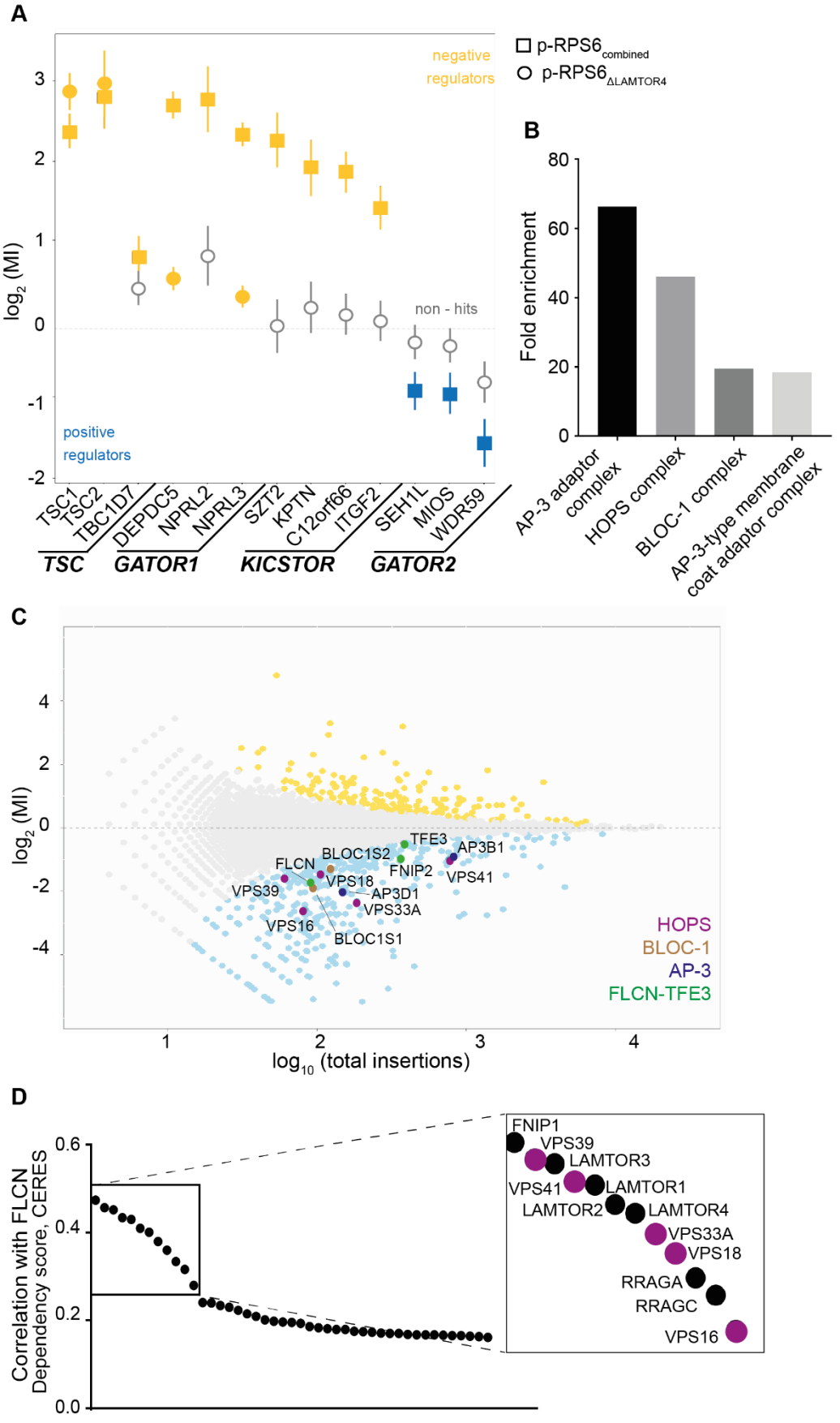

A
p-RPS6combined
p-RPS6ΔLAMTOR4
negative regulators
non - hits
positive regulators
log2 (MI)
TSC1
TSC2
TBC1D7
DEPDC5
NPRL2
NPRL3
SZT2
KPTN
C12orf66
ITGF2
SEH1L
MIOS
WDR59
TSC
GATOR1
KICSTOR
GATOR2
B
Fold enrichment
AP-3 adaptor complex
HOPS complex
BLOC-1 complex
AP-3-type membrane coat adaptor complex
C
log2 (MI)
log10 (total insertions)
TFE3
AP3B1
BLOC1S2
FLCN
FNIP2
VPS41
VPS18
VPS39
AP3D1
VPS33A
VPS16
BLOC1S1
HOPS
BLOC-1
AP-3
FLCN-TFE3
D
Correlation with FLCN Dependency score, CERES
FNIP1
VPS39
LAMTOR3
VPS41
LAMTOR1
LAMTOR2
LAMTOR4
VPS33A
VPS18
RRAGA
RRAGC
VPS16

Figure 4.9 FACS-based genetic screen in LAMTOR4-null background identifies additional layers of mTORC1 regulation. A. MI values for components of TSC, GATOR1 and 2 and KICSTOR complexes in p-RPS6 (squares) and p-RPS6$_{\Delta LAMTOR4}$ screens (circles). Genes scoring as positive regulators are represented in orange, negative regulators in light blue, empty symbols in grey indicate non-hits. Standard error for $\log_2$(MI) was estimated as described in **Section 2.7**. **B.** Gene Ontology (GO) analysis was performed on positive regulators specific for p-RPS6$_{\Delta LAMTOR4}$ using GO web tool (www.geneontology.org [169]). Top cellular components by fold enrichment are displayed. **C.** Regulatory map for p-RPS6$_{\Delta LAMTOR4}$; significant (FDR < 0.05) positive (light blue) and negative regulators (light orange) are indicted. Paler shades were used for readability. Positive regulators belonging to indicated complexes (HOPS, BLOC-1, AP-3 and FLCN-TFE3) are highlighted. Colour scheme matches complex name labels. **D.** Top 45 genes ordered by decreasing correlation in dependency score with FLCN are represented. In insert, top twelve genes are shown and genes belonging to the HOPS complex are coloured in purple. Data extracted from DepMap web tool (www.depmap.org [90]).

Lysosomes play an important role in mTORC1 regulation, not only by serving as anchorage but also by providing information about nutrient status [304]. Thus, it is logical to infer that in response to perturbation of Ragulator function (*i.e.* LAMTOR4 knockout), cells increasingly rely on lysosomal-related processes to maintain mTORC1 activation.

Interestingly, a functional module comprised of folliculin (FLCN), its binding partner folliculin interacting protein 2 (FNIP2) and transcription factor binding to IGHM enhancer 3 (TFE3) appeared among positive regulators specifically enriched in the LAMTOR4-null background (**Figure 4.9C**). In addition to its GTPase function [265, 305], FLCN is associated with lysosomal biology and endosomal trafficking through its connection with the lysosomal- and mitochondrial- biogenesis activating transcription factor TFE3 [306]. Additionally, an independent analysis of FLCN co-dependency patterns in the DepMap data showed a high concordance with HOPS complex subunits scoring as specific hits in p-RPS6$_{\Delta LAMTOR4}$ (**Figure 4.9D**). Overall, these observations suggested that existence of a FLCN/lysosomal axis could compensate for mTORC1 activation upon partial Ragulator perturbation.

4.3.5 *ΔLAMTOR4 cells require FLCN to maintain mTORC1 activation*

To better understand the link between FLCN and LAMTOR4, I generated HAP1 knockout clones for FLCN both in wild type and ΔLAMTOR4 background (**Table 4.3**).

Gene	sgRNA	Clone #	Genotype	Validated via immunoblotting?
FLCN	1	1	1 bp deletion	YES
	2	2	Failed to align	YES
FLCN in ΔLAMTOR4	2	1	11 bp deletion	YES
	2	2	35 bp deletion	YES

Table 4.3 Genotype information for FLCN and LAMTOR4-FLCN knockout clones generated in the study.

In line with the screen results, inactivation of FLCN alone did not affect p-RPS6 levels, while a strong reduction was observed in double knockout (dKO) clones (ΔLAMTOR4ΔFLCN) (**Figure 4.10A**). To investigate the functional consequences of FLCN inactivation in a LAMTOR4-null background, I tested the dKO's ability to recover RPS6K1 phosphorylation after AA starvation. While single knockout cells for either FLCN or LAMTOR4 were able to reactivate mTORC1 signalling after transient AA withdrawal to a degree similar to wild type, RPS6K1 was not re-phosphorylated in dKO cells (**Figure 4.10B**). To further investigate whether FLCN was specifically required to maintain mTORC1 activation in a ΔLAMTOR4 background, a GFP-tagged form of FLCN (FLCN-eGFP) was expressed in wild type, ΔFLCN and dKO HAP1 cells.

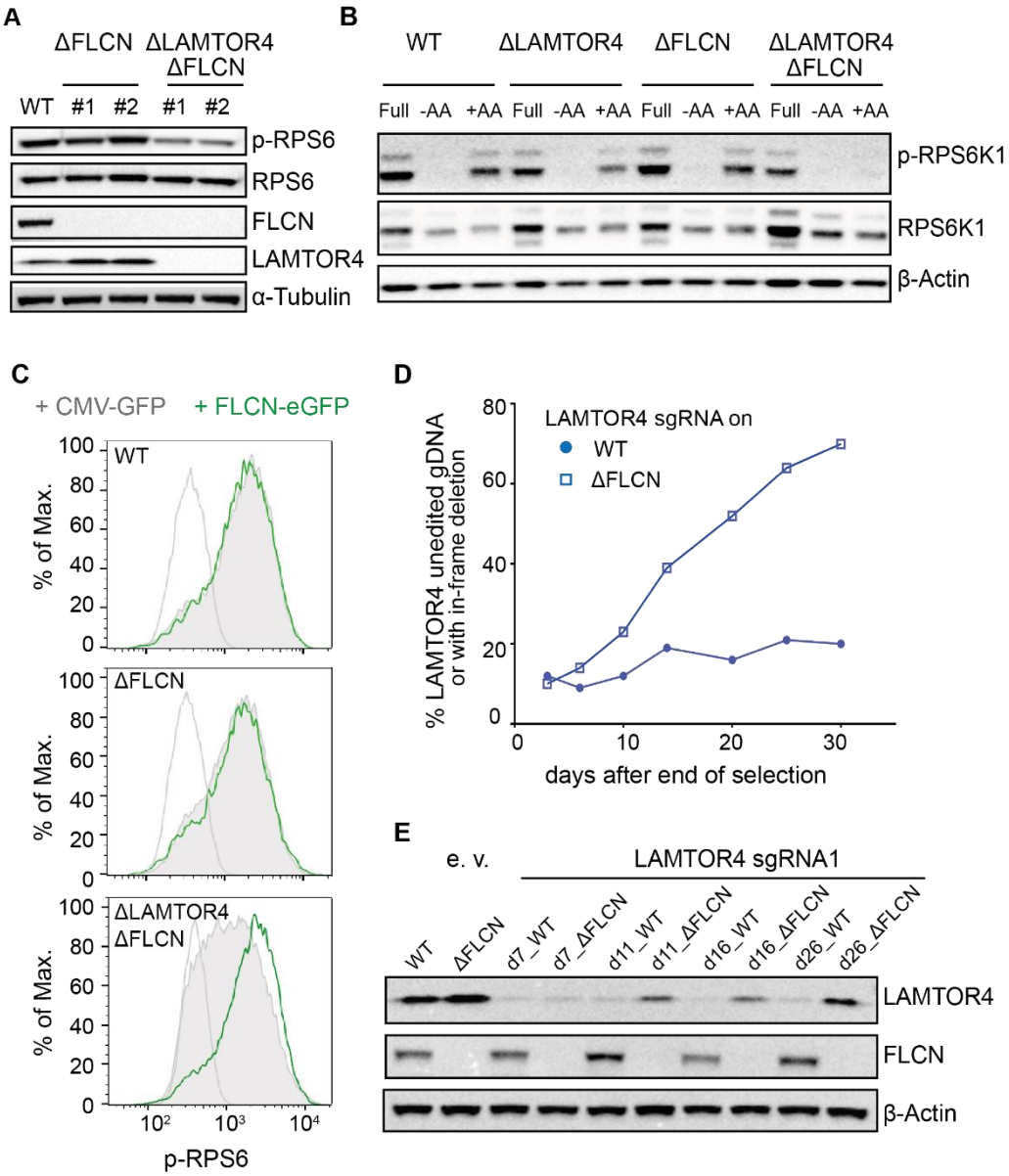


Figure 4.10 ΔLAMTOR4 HAP1 cells depend on FLCN to maintain mTORC1 signalling. A. Cell lysates for wild type, ΔLAMTOR4 and ΔLAMTOR4ΔFLCN clones were immunoblotted using the indicated antibodies. **B.** Single and double knockouts for LAMTOR4 and FLCN were starved for AAs alongside wild type HAP1 cells for 120 minutes. After 60 minutes re-feeding, cell lysates were collected and immunoblotted for p-RPS6K1, RPS6K1 and β-Actin as loading control. **C.** Plasmid expressing FLCN-eGFP was transfected into wild type, ΔFLCN and ΔLAMTOR4ΔFLCN cells. A CMV-GFP vector was used as control. After 3 days, cells were collected and levels of p-RPS6 were analysed by FC in the GFP^+ population (15.000 events were recorded for GFP^+ cells). Secondary antibody only staining is used as background (grey traces). **D.** LAMTOR4 gene editing in wild type and ΔFLCN was evaluated over 30 days. After transfection with LAMTOR4 sgRNA, pools were selected for 36 hours with puromycin, followed by expansion in full medium. Aliquots of the population were taken at the indicated time points, the sgRNA target locus in LAMTOR4 gene was PCR amplified from genomic DNA

(gDNA). Editing was measured by Sanger sequencing and traces were analysed using the TIDE web tool (www.tide.deskgen.com [119]). Percentage of cells containing unedited or in-frame mutants of LAMTOR4 are reported as function of time in each background. **E.** Pools transfected with LAMTOR4 sgRNA were collected at 7, 11, 16 and 26 days after the end of selection and were examined for LAMTOR4 protein levels in both wild type and FLCN backgrounds by immunoblotting. Empty pLentiCRISPR-v2 vector transfected counterparts were used as control (e.v.). Experiment representative of n = 3 independent biological replicates, samples were collected for immunoblotting in 2 out of 3 biological replicates. WT = wild type.

4.3.6 *LAMTOR4/FLCN synthetic sick interaction*

The reliance of LAMTOR4-perturbed cells on FLCN for RPS6 phosphorylation confirmed a bona fide genetic interaction (*i.e.* no effect in the individual single mutants) between these two genes. The epistatic link between LAMTOR4 and FLCN is compelling, as spontaneous inactivation of FLCN in familial Birt-Hogg-Dubé (BHD) syndrome was shown to significantly increase the risk of developing kidney tumours [266] and concomitant LAMTOR4 inactivation could therefore have therapeutic implications.

Thus, I investigated whether simultaneous inactivation of FLCN and LAMTOR4 in HAP1 cells resulted in decreased viability. Using CRISPR/Cas9 genome editing, LAMTOR4 was inactivated in a wild type or ΔFLCN background. Percentage of LAMTOR4 knockout cells in polyclonal pools was followed over 30 days by Sanger sequencing and deconvolution of LAMTOR4 genomic traces using the Tracking of Indels Decomposition software (TIDE, www.tide.deskgen.com [119]). In wild type background, the fraction of cells carrying LAMTOR4 inactivating mutations did not show a defect in proliferation was approximately stable for four weeks, as LAMTOR4 null cells do not show a growth defect under steady-state conditions. On the other hand, cells with LAMTOR4 perturbations in a FLCN-null background were depleted over time indicating a proliferation defect of dKO cells (reduction from 90% to less than 30%, **Figure 4.10D**,

E). Of note, this negative selective pressure on dKO cells did not affect detection of FLCN inactivation in p-RPS6$_{\Delta LAMTOR4}$ screen as ΔLAMTOR4 mut-HAP1 cell pool had only been expanded for 12 days after mutagenesis. Together, these results confirmed a synthetic sick interaction between FLCN and LAMTOR4.

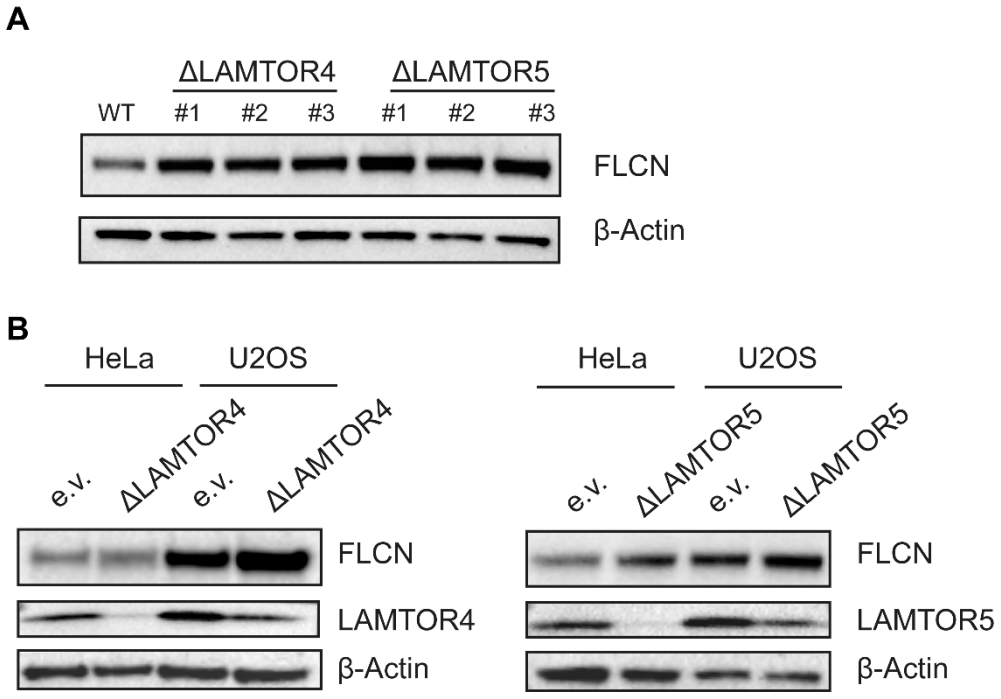


Figure 4.11 FLCN upregulation in Ragulator-null background. A. Cell lysates for wild type (WT) HAP1 cells, and multiple ΔLAMTOR4 and ΔLAMTOR5 clones were immunoblotted for FLCN levels alongside loading control. **B.** Knockout pools in HeLa and U2OS cells were generated by transfection of empty pLentiCRISPR-v2 (e.v.) or bearing LAMTOR4/LAMTOR5 sgRNAs. Cell lysates were immunoblotted with indicated antibodies.

4.3.7 *LAMTOR4/FLCN compensatory mechanism*

Next, I set out to investigate the mechanism by which FLCN promotes phosphorylation of RPS6 upon LAMTOR4 loss. Surprisingly, the ablation of Ragulator components LAMTOR4 and LAMTOR5 induced a notable increase in FLCN level in HAP1 cells (**Figure 4.11A**).The effect was recapitulated in other cell lines such as HeLa

and U2OS, indicating that FLCN upregulation is a general response mechanism to Ragulator perturbation (**Figure 4.11B**). To further investigate whether the effect was due to FLCN protein stabilisation, I treated ΔLAMTOR4 and ΔLAMTOR5 cells with the proteasome inhibitor bortezomib. In fact, a previous study showed that FLCN protein degradation could be halted by proteasome blockade [307]. FLCN levels were not significantly altered in both knockout and wild type background after 5 hours indicating that the change in total protein levels was not due to dysregulated protein degradation (**Figure 4.12A**). Moreover, the stability of FLCN was tested by treating ΔLAMTOR4 and ΔLAMTOR5 cells and wild type HAP1 cells with the translation inhibitor cycloheximide. Protein half-life was comparable between HAP1 wild type cells and LAMTOR4 or LAMTOR5-null cells, thus excluding altered stability as a reason for the observed increase (**Figure 4.12B**, **C**). Interestingly, FLCN transcript levels were increased in LAMTOR4 and LAMTOR5 knockout cells, correlating with FLCN protein abundance (**Figure 4.12D**).

Overall, these results suggested that an increase in FLCN transcription is part of a compensatory mechanism in response to Ragulator perturbation.

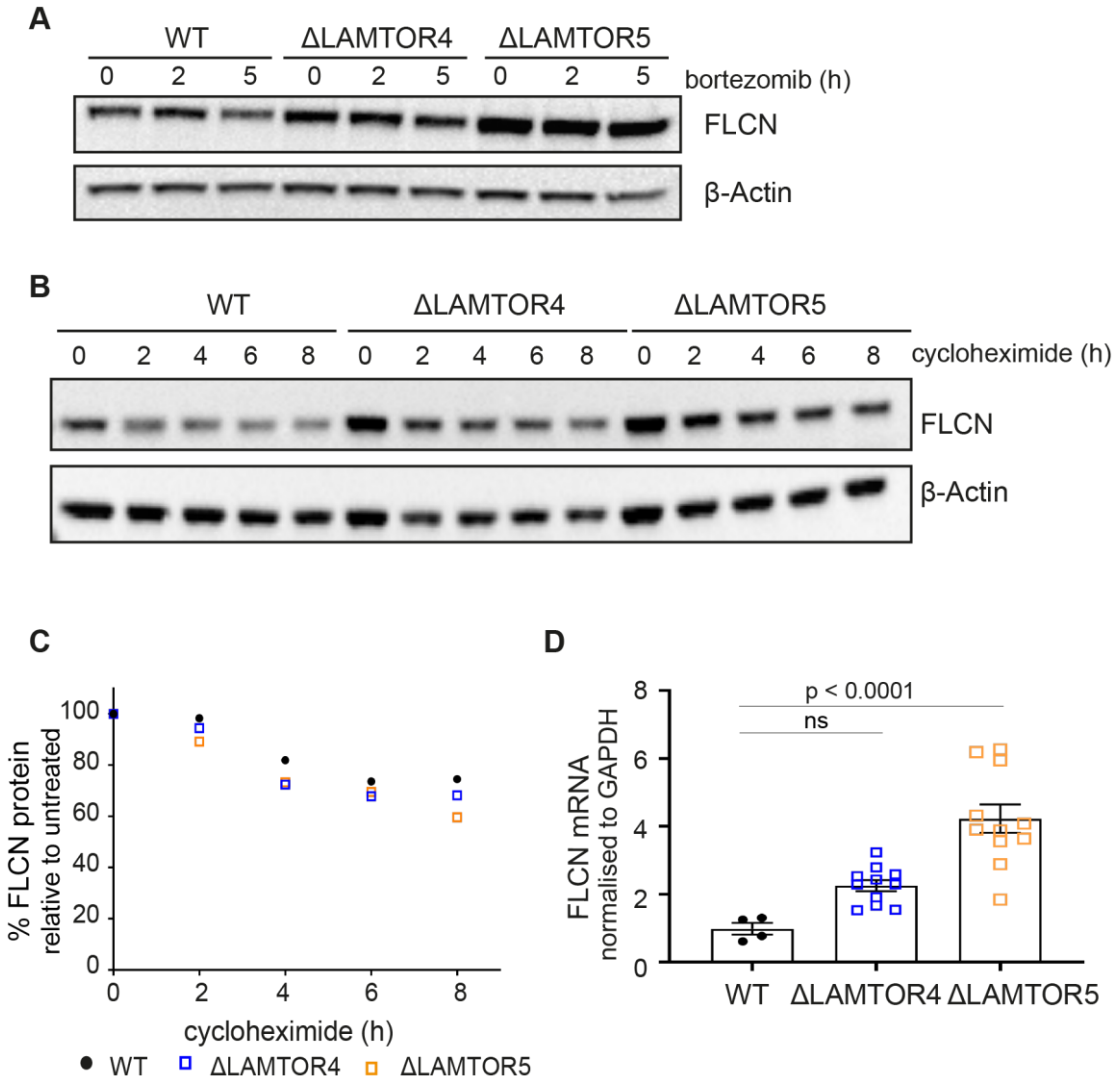


Figure 4.12 Transcriptional upregulation of FLCN in Ragulator-null cells. A. HAP1 wild type (WT), ΔLAMTOR4 and ΔLAMTOR5 clones were treated with 100 μM proteasome inhibitor bortezomib or **B.** 100 μM translation inhibitor cycloheximide for the indicated time. Cell lysates were immunoblotted for FLCN and β-actin as loading control. **C.** Quantification of bands for FLCN protein levels after cycloheximide treatment was plotted relative to wild type untreated levels at t=0. **D.** FLCN mRNA levels were measured in wild type HAP1 cells and in independent knockout clones for LAMTOR4 and LAMTOR5. Statistical analysis was performed using 1-way ANOVA followed by Dunnett's post hoc test. Data obtained from a minimum two independent clones per gene were pooled. Experiment was performed n = 2.

4.4 Discussion

In this Chapter I described how an iterative genetic screening approach in presence of pharmacological and genetic inhibition could be used to tease apart the multi-layered signalling upstream of mTORC1. An analysis of context-specific regulators revealed a novel, distinct role of the Ragulator component LAMTOR4 and the existence of a regulatory feedback loop between Ragulator and FLCN.

4.4.1 *Comparative genetic screening*

In **Section 3.2.8** I discussed the challenge of prioritising screen hits for downstream validation. This step is particularly arduous for screens returning many hits, as this complicates the mechanistic interpretation of the results. A single stand-alone screen, in fact, can neither address whether an individual hit is context-specific or commonly involved in signalling, nor can it assign hits to specific pathway branches without recurring to additional validation experiments. Such questions, growing in complexity from "What genes affect the cellular phenotype?" to "How are these genes interconnected?", can however be addressed in comparative terms, identifying specific signalling modules that vary across multiple screen iterations.

The concept of iterative genetic screening is not new, although to my knowledge, there are only a handful of examples where this was applied to genetic screens using a continuous readout. To dissect the regulation of biogenesis and trafficking of glycophosphatidylinositol (GPI)-anchored proteins, Davis *et al.* performed two haploid enrichment-based genetic screens for two functionally unrelated GPI-anchored proteins: prion protein (PrP) and the immune molecule CD59 [308]. After normalisation of per gene

insertions within screens, hits were intersected and differential requirements for several components of the GPI synthesis machinery were highlighted. By using this comparative screening approach, the study revealed the existence of divergent branches within the GPI-dependent processing pathway.

A more exhaustive approach was taken in Lebensohn *et al.*, where a series of genetic screens were performed in HAP1 cells to dissect WNT signalling [101]. There, a fluorescent protein under control of a WNT-responsive element was used as a reporter for pathway activation in presence of the cognate signalling molecule WNT3A. "Perturbed" screens were performed in two mutant backgrounds leading to constitutive activation of WNT signalling and in presence of a WNT pathway potentiator. The baseline WNT3A-stimulated screen was compared to its perturbed iterations using a metric based on the sense/antisense ratio of trapping cassettes in gene introns thus highlighting treatment-specific and genotype-specific rewiring.

In a similar way, in this Chapter I applied a robust comparative approach to study mTORC1 pathway rewiring after genetic- and drug-induced perturbations. However, in contrast to previous examples, where per sense/antisense ratio gene scores were qualitatively compared, the reproducibility of FACS-based genetic screening allowed to quantitatively measure inter-screen differences using the ΔMI metric.

4.4.2 *Pharmacologically perturbed p-RPS6 screen*

In general, genetic screens conducted in presence of a certain stimulus reveal both context-specific responses to the stimulus and requirements of the system itself. Thus, the comparison of the p-RPS6$_{combined}$ and p-RPS6$_{rapamycin}$ screens unbiasedly identified FKBP1A, a stimulus-specific regulator, and LAMTOR4, a pathway-specific modulator.

This modulation is not rapamycin-specific but can be recapitulated by other pharmacological inhibitors such as MK2206 and AZD2014.

In this study I focused on LAMTOR4, for which I demonstrated a novel, divergent role compared to the other closely-related Ragulator subunit LAMTOR5. These results were unexpected as in another cell model all members of Ragulator were shown to be required for an efficient tethering of Rag proteins to the lysosome [244]. It had been previously shown that mTORC1 pathway wiring differs slightly among different cell lines [230, 309]. As such, the mTORC1 map described here does not constitute a definitive version but one of the naturally occurring alternatives, and testing and validation in different cell models is required.

In addition to LAMTOR4, loss of two other genes was predicted to enhance the rapamycin effect on p-RPS6 albeit to a smaller degree: KIAA1033 and serine palmitoyltransferase long chain base subunit 1 (SPTLC1). KIAA1033 is a subunit of the WASH complex that regulates endosomal transport [310]. While no direct connection between KIAA1033 and the mTORC1 complex was reported, the crosstalk between mTORC1 and the endosomal compartment is well documented [311]. On the other hand, hematopoietic mouse stem cells lacking sptlc1 gene were reported to have dysregulated mTORC1 and proto-oncogene MYC signalling [312]. While these initial observations are promising, further research is needed to validate and understand the physiological implications of rapamycin-sensitising effects on mTORC1 activation in KIAA1033 and SPTLC1-null backgrounds.

4.4.3 *Genetically perturbed p-RPS6 screen*

Genetic screens performed in a null background, called "suppressor screens", are generally employed to investigate cellular rewiring in response to a pathological mutation. However, in this case, genetic screening in the LAMTOR4-null background was motivated by its divergent behaviour from other Ragulator components. While a variable level of network rewiring takes place upon mutation of any mTORC1 modulator, in the case of ΔLAMTOR4, such alterations maintain high level of pathway activation. Hence, a suppressor screen performed in a LAMTOR4-null background constituted a good entry point to study additional layers of pathway regulation, providing sufficient sensitivity to detect both positive and negative modulators.

Among positive regulators in the LAMTOR4-null background I found a number of proteins belonging to the vesicular transport pathway. This is not surprising, as the late endosome and lysosome are crucial for mTORC1 positioning and signalling [220, 311]. A small body of evidence suggested that this effect could be, at least partially, mediated through Ragulator. In fact, a number of molecular phenotypes not directly linked to mTORC1 signalling were ascribed to Ragulator components and, interestingly, many of them were linked to lysosomal/endosomal regulation (**Table 4.1**). *In vitro* experiments suggested the existence of two distinct pools of Ragulator, of which one constitutes a docking platform for the Rags while the other interacts with the BLOC-1 complex and determines lysosomal positioning within the cell [313]. Additionally, a recent report showed the yeast equivalent of the AP-3 adaptor complex was required to deliver the Ragulator complex orthologue from the trans-Golgi network to the vacuole, where the HOPS complex mediates the homotypic fusion process [314]. These data are in line with a mechanistic model where a LAMTOR4-null Ragulator complex is still partially active,

and the lysosomal trafficking and biogenesis pathways promote its shuttling and localisation to activate mTORC1. In a cell-free experiment, a "minimal Ragulator" complex, only composed of LAMTOR1-3, interacted weakly with the Rags [243].

Together with vesicular transport genes, lysosomal- and mitochondrial- biogenesis activating transcription factor TFE3 and tumour suppressor FLCN also scored as positive regulators in the LAMTOR4-null background [315]. Although the canonical FLCN function is still being investigated, its involvement in a number of pathways related to energy sensing, metabolism and autophagy was shown (reviewed in [266]). Analysis of genetic dependencies profiles suggested that FLCN likely interact with the Ragulator complex, the Rags and the HOPS complex, which mediates autophagosome-lysosome fusion (**Figure 4.9D**). This hypothesis is supported by biochemical experiments indicating that, in nutrient-depleted conditions, FLCN is recruited to the lysosomal membrane where Ragulator and Rags proteins reside, and acts as a GTPase, ultimately promoting mTORC1 activation [265]. However, the signalling cues driving FLCN lysosomal recruitment are still unclear, even though a potential mechanism involving the degradation of FLCN-binding protein FNIP2 was recently proposed [316].

4.4.4 *Future perspectives*

Recently, a mTORC1 activation feedback loop involving the yeast orthologues for FLCN and FNIP (Lst7 and Lst4) was reported [317]. In fully-fed conditions, mTOR phosphorylates the Lst7/4 complex to displace it from its vacuolar localisation, which is likely to block pathway hyper-activation. Analysis of Ragulator-null clones described in this Chapter revealed an additional feedback loop involving FLCN, in the form of a synthetic sick relationship with LAMTOR4. Although no LAMTOR4/Ragulator inhibitor

exists today, critical reliance on Ragulator in cancer cells lacking FLCN could provide an actionable therapeutic strategy.

It is tempting to speculate that FLCN transcriptional increase has a functional role in maintaining mTORC1 signalling. To this end, the use of RNA interference or CRISPRi to achieve precise reduction of FLCN transcript levels in ΔLAMTOR4 cells to wild type levels could provide valuable insights. In this context, further exploration of the mechanism underlying FLCN transcription in absence of Ragulator would be of interest. Previous reports showed that TFE3, which scores in p-RPS6$_{\Delta LAMTOR4}$ as positive regulator, is required for a starvation-induced increase in FLCN levels, although not through direct control of transcription [306, 318]. Thus further studies might generate ΔLAMTOR4ΔTFE3 HAP1 cells and investigate their FLCN levels.

Additionally, the iterative screening paradigm described in this Chapter lends itself to define context-specific regulators of other mTORC1 perturbations. For instance, iteration of the current screen in loss-of-function cells for pathway components mutated in human disease (*e.g.* FLCN, TSC and KICSTOR components) could reveal context-specific regulators that are therapeutically actionable. Additionally, this approach could be used to further study mTORC1 AA sensing. Recent biochemical studies, aided by proteomics screens, uncovered AA sensor mechanisms upstream of the GATOR1/GATOR2 complexes [319-321]. By comparing modulators of pathway activation under starvation and following single AA reconstitution, iterative FACS-based forward genetic screens could constitute a systematic approach to uncover yet uncharacterised AA sensing mechanisms.

Overall, the data presented in this Chapter shed light on the composition of the multi-layered regulatory network upstream of mTORC1. Crucially, the quantitative, comparative methodology described here could be readily applied to dissect other complex intracellular pathways. The study uncovered a unique, dispensable function for the Ragulator subunit LAMTOR4 under steady-state conditions and further revealed how proliferation of LAMTOR4 mutants relied on compensatory induction of FLCN and, possibly, on lysosomal biogenesis. The regulatory maps presented here described the most comprehensive set of genome-wide screens conducted on mTORC1 to date and constituted a valuable resource for future investigation.

Chapter 5: QRICH1 and SEPHS1 work together to regulate TNFR1 level in HAP1 cells

5.1 Introduction

Tumour Necrosis Factor α (TNFα) is a potent mediator of inflammation and anti-microbial immunity that also plays an important role in driving physiological functions [322]. TNFα acts principally through binding TNF receptor 1 (TNFR1) on the cell surface to activate pro-inflammatory NF-κB signalling. While blockade of the TNFα/TNFR1/NF-κB axis using anti-TNFα biologics was proven effective as a therapy for autoimmune pathologies, at the same time, it could lead to paradoxical increased inflammation and long-term intolerance [323]. In this context, a complementary/alternative treatment paradigm based on the reduction of cell surface levels of TNFR1 was suggested. However, despite its centrality in orchestrating the TNFα cellular response, very little is known about the regulatory mechanisms of TNF receptor 1 itself.

In this Chapter I describe the identification of regulators of the TNFα/TNFR1/NF-κB cascade and surface levels of TNFR1 in HAP1 cells using a series of FACS-based forward genetic screens. Overall, the screens identify three poorly-studied genes, glutamine rich protein 1 (QRICH1), selenophosphate synthetase 1 (SEPHS1) and zinc finger protein 652 (ZNF652), whose disruption severely curtails TNFR1 at transcriptional level both in presence and in absence of TNFα stimulation. In addition, ablation of QRICH1 and SEPHS1 lead to similar transcriptional responses, indicating that the two genes belong to the same functional module. Furthermore, initial observations suggest a

physical interaction between QRICH1 and SEPHS1. This additional understanding of the TNFR1 regulatory network could be used to devise new therapeutic strategies.

5.1.1 *Tumour Necrosis Factor α (TNFα)*

Initially identified as a circulating factor capable of inducing tumour necrosis [324], TNFα was since implicated in a plethora of physiological and pathological processes ranging from formation of lymph nodes and neurite outgrowth on one side [322, 325] to inflammation and cell death on the other [322, 326, 327]. In particular, the critical role of TNFα in inflammation is underscored by the success of anti-TNFα biologics (antibodies or soluble TNF receptors) in the treatment of autoimmune pathologies such as rheumatoid arthritis [323].

From its immature transmembrane form, the pro-TNFα protein is cleaved by the ADAM metallopeptidase domain 17 (ADAM17) to generate a 17 kDa soluble active molecule [328]. Synthesized mainly by cells of the monocytic lineage, soluble TNFα assembles as a homotrimer into its active form [329]. TNFα binds to two distinct transmembrane receptors, namely TNFR1, a pleiotropic death-domain-containing protein which mediates most of the biological TNFα responses [329, 330], and TNFR2, whose expression is restricted to specific immune cell lineages [331]. While TNFR1 can be activated by both soluble and membrane-bound TNFα, TNFR2 can only be activated in an autocrine fashion, by binding of pro-TNFα [332].

5.1.2 *TNFα-dependent NF-κB pro-inflammatory signalling*

Binding of TNFα to TNFR1 regulates two divergent signalling pathways, triggering either cell death or an inflammatory response. The balance between these two fates is

determined, among others factors by cell-type and activation status and levels of intracellular downstream signalling proteins [331, 333]. In this Chapter, I focus on the pro-inflammatory TNFα/TNFR1 arm, where binding of TNFα to TNFR1 ultimately leads to the transcription of a number of inflammatory genes by activating the nuclear factor kappa-light-chain-enhancer of activated B cells (NF-κB)/REL family of dimeric transcription factors.

In unstimulated conditions, NF-κB/REL proteins are bound and inhibited by NF-κB inhibitor alpha (IκBα). When TNFα binds to TNFR1 it induces receptor homotrimerisation; the resulting conformational change in the receptor intracellular domain then recruits the adapter molecule TNFRSF1A-associated via death domain (TRADD) through homotypic interaction between the proteins' death domains (DD) (**Figure 5.1**) [334]. TRADD recruits TNFR associated factor 2 or 5 (TRAF2/5), cellular inhibitor of apoptosis 1/2 (cIAP1/2, BIRC2/3) and receptor interacting protein kinase 1 (RIPK1) to form the signal complex I [335]. This event is followed by extensive ubiquitination of TNFR1 complex components resulting in the recruitment of three additional multi-protein complexes: 1.) TGF activated kinase 1 (TAK1/MAP3K7) with TAK1 binding protein 1-3 (TAB1-3); 2.) the linear ubiquitin chain assembly complex (LUBAC), comprised of heme-oxidised IRP2 Ub ligase 1 (HOIL-1/RBCK1), SHANK-associated RH domain interactor (SHARPIN), and HOIL-1 interacting protein (HOIP/RNF31) and 3.) the inhibitor of κB Kinase (IKK) complex, composed of IKKα/CHUK, IKKβ/IKBKB, and NF-κB essential modulator NEMO/IKBKG [336]. Both LUBAC and MAP3K7 activity are required for productive pro-inflammatory signalling, acting through NEMO to ultimately activate the IKK complex. Upon IKK activation, IκB

kinases phosphorylate IκBα, targeting it for degradation. The now released NF-κB/REL dimers can translocate into the nucleus and induce transcription of target genes.

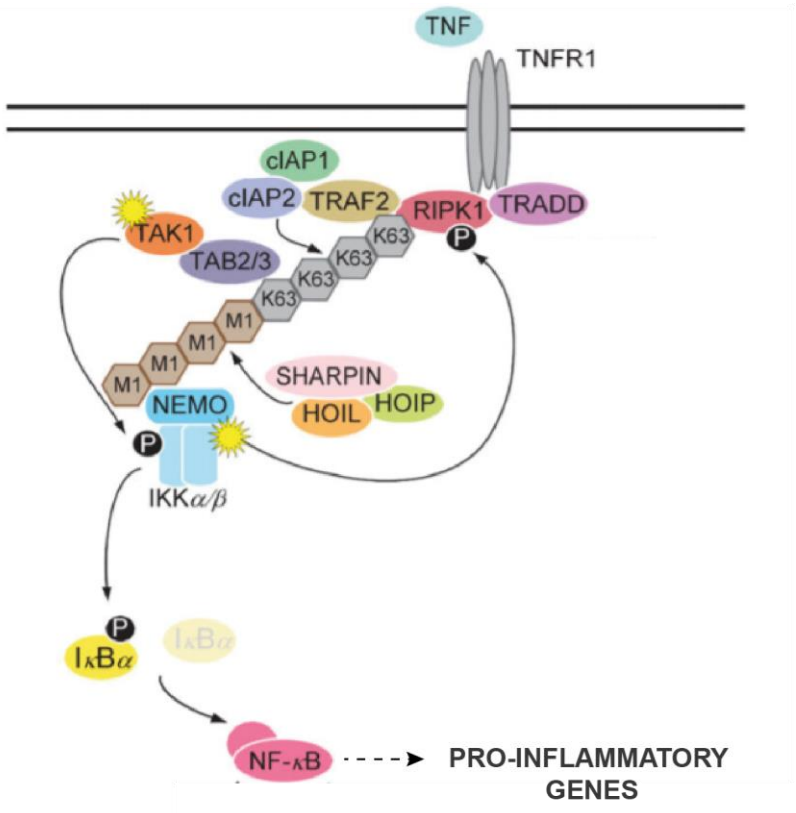


Figure 5.1 Schematic representation of the TNFα/TNFR1/NF-κB signalling axis. After TNFR1 receptor homotrimerisation, the adaptors TRADD, RIPK1 and TRAF2 are recruited and the complex is ubiquitinated by cIAP1/2 generating Lys-63 linked ubiquitin chains, K63. Further recruitment of TAK1, the SHARPIN/HOIP/HOIL complex (generating Met-1 linked ubiquitin chains, M1) and the IKK complex promotes IκBα phosphorylation and degradation, releasing NF-κB dimers into the nucleus. Image adapted from [337].

5.1.3 *TNFR1 regulation*

TNFR1 is absolutely required to mediate TNFα pleiotropic signalling as highlighted by a number of *in vivo* studies. Mice engineered to display higher cell surface levels of TNFR1 fared better in pathogen clearance than mice with wild type TNFR1 levels, albeit at the cost of developing spontaneous inflammatory conditions [338]. On the other hand, mice expressing 50% lower TNFR1 levels were protected against TNFα-induced lethal inflammation [339]. In humans, more than 100 mutations affecting the TNFR1 extracellular domain were linked to the TNFR-associated periodic syndrome (TRAPS), a condition characterised by periodic high fever attacks and localised inflammation [340] [341]. Additionally, dysregulated TNF receptor 1 levels were detected in patients suffering from a range of autoimmune and inflammatory diseases [342].

Membrane display of TNFR1 is post-translationally regulated through receptor shedding and receptor recycling mechanisms. TNFR1 is cleaved by the endoplasmic reticulum aminopeptidase (ERAP1) [343] and the ADAM17 [344], a process enhanced by a series of pro-inflammatory mediators (TNFα, IFN-γ), G protein-coupled receptor's ligands (such as thrombin) and oxidative stress [345]. TNFα stimulation also induces reduction of surface TNFR1 by promoting receptor internalisation and degradation through the endo-lysosomal pathway as part of a negative feedback loop [346, 347].

On the other hand, little is known about transcriptional regulation of TNFR1 coding gene TNFRSF1A, which was initially considered to be a housekeeping gene as its promoter drives transcription from multiple start points and lacks a canonical TATA box motif [348]. However, over the years, a handful of studies reported control of TNFR1 expression by the transcription factors CCAAT-enhancer-binding proteins (C/EBP) [349], NF-κB [350], signal transducer and activator of transcription 3 (STAT3) which binds in

intron 1 [351] and histone deacetylase 5 (HDAC5) [352] (**Figure 5.2**). Additionally, the TNFRSF1A gene contains nucleotide sequences deputed to RNA-protein complex formation and stimulation with phorbol esters was shown to ablate surface localisation of the receptor by destabilizing mRNA binding to uncharacterised RNA-interacting proteins [353].

CTTTTCACTGCTGTGATCCATCTGGGAAAGGCTAGTGATGTGGGCAAGGGGCTTATTGCCCCTT
GGTGTTTGGTTGGGAGTGGTCGGATTGGTGGGTTGGGGGCACAAGGCAGCCAGATCTGGGACTC
CTGTGCTTGTGACTGGACTACAAAGAGTTAAAGAACGTTGGGCCTCCTCCTCCCGCCTCCTGTG
GCCTCCTCCTCCAGCTCTTCCTGTCCCGCTGTTGCAACACTGCCTCACTCTTCCCCTCCCACCT
TCTCTCCCCTCCTCTCTGCTTTAATTTTCTCAGAATTCTCTGGACTGAGGCTCCAGTTCTGGCC
TTTGGGGTTCAAGATCACTGGGACCAGGCCGTGATCTCTATGCCCGAGTCTCAACCCTCAACTG
TCACCCCAAGGCACTTGGGACGTCCTGGACAGACCGAGTCCCGGGAAGCCCCAGCACTGCCGCT
GCCACACTGCCCTGAGCCCAAATGGGGGAGTGAGAGGCCATAGCTGTCTGGCATG

Figure 5.2 DNA sequence 500 bp upstream of the TNFRSF1A start codon. The ZNF652 putative binding motif is highlighted in orange (see **Section 5.1.7**), the C/EBP binding site [349] in blue, the putative 5' UTR start in magenta and the ATG start codon in green. Assembly GRCh38.p13, sequence extracted from National Center for Biotechnology Information (NCBI) website (www.ncbi.nlm.nih.gov/nuccore [354]).

5.1.4 *Anti-TNFR1 therapy*

The advent of anti-TNFα therapies led to a major quality of life improvement in patients suffering from conditions such as rheumatoid arthritis, inflammatory bowel disease and psoriasis [323]. However, meta-analysis and retrospective studies highlighted some drawbacks arising from continuous TNFα blockade such as enhanced risk of infections [355], development of paradoxical inflammation [356], and moderately increased incidence of haematological malignancies [357] and neuropathies [358]. A body of evidence collected in recent years shed light on both the intricacy of TNFα-dependent effects in physiological and pathological settings, and the protective role of TNFR2 against autoimmune diseases (reviewed in [359]). Thus, to circumvent adverse effects of anti-TNFα therapy, new strategies were suggested, aiming at specific blockade of pro-inflammatory

TNFR1 signalling, while leaving "beneficial" TNFR2 untouched [339, 360, 361]. In this context, the efficacy and safety of TNFR1-selective antagonistic antibodies and antisense oligonucleotides were described [339, 362]. Nonetheless, a better understanding of endogenous mechanisms of TNFR1 regulation could identify additional actionable therapeutic targets.

5.1.5 *Glutamine rich protein 1 (QRICH1)*

Glutamine rich protein 1 (QRICH1) is a poorly characterised protein ubiquitously expressed in human tissues (Human Protein Atlas, www.proteinatlas.org [172, 363]). Initially identified in a yeast two-hybrid screen for binding amyloid β peptide (Aβ1-42) and thus originally named Aβ-related death inducing protein (AB-DIP), QRICH1 caused cell death when overexpressed in the human neuroblastoma SH-SY5Y cell line [364]. The initial characterisation effort described a 97 kDa protein containing a N-terminal caspase recruitment domain (CARD), a nuclear targeting sequence and a conserved domain of unknown function 3504 (DUF3504) at the C-terminus. QRICH1 is one of 33 CARD-containing proteins in humans. Its CARD is classified as a "longhair CARD" as the domain is followed by a long sequence of unknown function [365] (**Table 5.1**). CARD domains are one of the four domain types that are part the death-fold superfamily, a group of structurally homologous motifs engaging in homotypic interactions [366]. Together with the DDs, the Death Effector Domains (DEDs) and the PYrin Domains (PYDs), proteins containing CARD domains play a role in the assembly of complexes involved in apoptosis and inflammation [367].

Protein	Function	Signalling complex
APAF1	Caspase-9 activation	Apoptosome
NLRC4/IPAF/CARD12	Caspase-1 activation	Inflammasome
NLRP1/NALP1/CARD7	Caspase-1 activation	Inflammasome
NOD1/CARD4	NF-κB activation	Nodosome
NOD2/CARD15	NF-κB activation	Nodosome
CARD9	NF-κB activation	CBM complex
CARD11/CARMA1	NF-κB activation	CBM complex
CARD14/CARMA2	NF-κB activation	CBM complex
CARD10/CARMA3	NF-κB activation	CBM complex
DLG5	Unknown	Unknown
cIAP1/BIRC2	NF-κB activation, Caspase inhibition	TRAF2 complex
cIAP2/BIRC3	NF-κB activation, Caspase inhibition	TRAF2 complex
IFIH1/MDA5	NF-κB activation	MAVS signalosome
DDX58/RIG-I	NF-κB activation	MAVS signalosome
PYCARD/ASC	Caspase-1 activation	Inflammasome
CARD8/CARDINAL	Inhibition of NF-κB activation, Inhibition of Caspase-9 activation	Inflammasome
CASP1	Inflammation	Inflammasome
CASP4	Inflammation	Inflammasome
CASP5	Inflammation	Inflammasome
CASP12	Inflammation	Inflammasome
CASP2	Apoptosis	PIDDosome
CASP9	Caspase activation	Apoptosome
RAIDD/CRADD	Caspase-2 activation	PIDDosome
RIPK2/RICK/RIP2	NF-κB activation	Nodosome
BCL10	NF-κB activation	CBM complex
C9orf89/CARD19/binCARD	Inhibition of NF-κB activation	CBM complex
CARD16/COP	Inhibition of Caspase-1 activation	Inflammasome
CARD17/INCA	Inhibition of Caspase-1 activation	Inflammasome
CARD18/ICEBERG	Inhibition of Caspase-1 activation	Inflammasome
NOL3/ARC	Inhibition of Caspase-2, -8 activation	Unknown
CARD6	NF-κB activation	Unknown
MAVS	NF-κB activation	MAVS signalosome
QRICH1	Unknown	Unknown

Table 5.1 Classification of human CARD-containing proteins by function and signalling complex. Proteins expressed under steady-state conditions in HAP1 cells are shown in bold, data obtained from [148]. CBM = CARD11-BCL10-MALT1 complex. MAVS = mitochondrial antiviral signalling protein. Table adapted from [365].

Recently, two research groups linked mutations in the QRICH1 gene with a clinical phenotype characterized by mild developmental delay, impaired intellectual development and chondrodysplasia (**Table 5.2**) [368, 369]. Point mutations are enriched in the proximity of the C-terminal DUF3504 domain and lead to QRICH1 loss-of-function either by nonsense-mediated decay (NMD) or protein truncation [368]. To validate the role of QRICH1 in skeletal development, Lui *et. al* knocked down QRICH1 in mouse epiphyseal chondrocytes. The experiment returned a number of downregulated genes linked to chondrocyte hypertrophic differentiation, including Collagen type X alpha 1 chain (Col10a1), nonetheless failing to elucidate the mechanistic basis of the phenotype [369].

Mutation	Comments	Mutant length (AA)	Reference
1954C > T: p. Arg652X	Nonsense substitution	652	[368]
1953dup: p. Arg652Alafs	Frameshift (fs) leading to STOP codon 8 residues downstream	652	[368]
138_139delinsTT: p. Gln46_Gln47delinsHisX	Nonsense substitution	47	[368]
1606C > T: p. Arg536X	Nonsense substitution	536	[369]
1531C > T: p. Arg511X	Nonsense substitution	511	[369]

Table 5.2 Summary of reported QRICH1 pathogenic mutations in humans. X = termination

5.1.6 *Selenophosphate synthetase 1 (SEPHS1)*

Selenium is an essential trace element, required in the human diet. In fact, selenium, in the form of the rare AA selenocysteine (Sec), is incorporated at the active site of a group of proteins aptly named selenoproteins [370]. Cells contain a specialized translation machinery for the synthesis of selenocysteyl-tRNA $^{[Ser]Sec}$ in which selenium, in the form of selenophosphate, is loaded onto an intermediate form of serine-tRNA [371]. The enzyme required for the synthesis of selenophosphate from the selenium anion selenide (Se^{2-}) was

initially identified in prokaryotes as selenophosphate synthetase (SelD) which carries out the two-step reaction:

$SelD + ATP \rightarrow SelD:PO_4 + ADP$

$SelD:PO_4 + Selenide \rightarrow SelD + Selenophosphate$

SelD has two highly conserved orthologues in eukaryotes, namely SEPHS1 and SEPHS2. The two enzymes contain a conserved domain of unknown function in addition to an ATP- and a Mg^{2+} -binding sites, but only SEPHS2 has either a cysteine (Cys) or a Sec residue in its catalytic site [372]. A body of evidence, generated both *in vitro* and *in vivo* using fruit fly and mouse orthologues, indicates that only SEPHS2 is crucial for selenophosphate synthesis [373, 374]. Although some evidence points to a role in selenocysteine recycling and partial SEPHS2 complementation, the primary function of SEPHS1 remains unclear [371]. SEPHS1 is ubiquitously expressed in human tissue and its main isoform is found both in the nucleus and the cytoplasm [371]. Systemic removal of SEPHS1 is embryonic lethal both in fruit fly and mouse, while liver-specific knockout leads to viable offspring [375]. Analysis of primary mouse hepatocytes knockout for Sephs1 indicates accumulation of reactive oxygen species and downregulation of a number of redox-related enzymes, a phenotype partly recapitulated in the F9 mouse cancer cell line knockdown for Sephs1 [375].

5.1.7 *Zinc Finger Protein 652 (ZNF652)*

ZNF652 was initially identified in a yeast two-hybrid screen for binding to CBFA2 partner transcriptional co-repressor 3 (CBFA2T3) [376]. Co-immunoprecipitation analysis identified the ZNF652 C-terminus as required for CBFA2T3 binding while its multiple

zinc- finger domains located between residues 245 and 492 mediate DNA binding [377]. It was suggested that ZNF652 acts together with CBFA2T3 as a transcriptional corepressor, downregulating the expression of the endogenous helix-loop-helix transcription factor 4 (HEB4) [377]. Interestingly, a genome-wide chromatin immunoprecipitation (ChIP) study mapping genome-wide ZNF652-binding sites and found a peak indicating binding upstream of the TNFR1 promoter [378]. Its target sequence (AAAGAGTTAA) was positioned 10 nucleotides upstream the putative 5' UTR and had high homology (approximately 80%) with the ZNF652 *in-silico* predicted binding site, suggesting that the zinc finger could be involved in transcriptional regulation of TNFR1 (**Figure 5.2**).

In this Chapter I employ FACS-based genetic screening technology to identify genes modulating both TNFR1 surface levels and its ability to mediate TNFα-induced pro-inflammatory responses (TNFα/TNFR1/NF-κB signalling axis). The overlap between the two screens reveals a novel role for three poorly-characterised genes, QRICH1, SEPHS1 and ZNF652, as positive modulators of TNFR1 expression.

5.2 Results

5.2.1 *HAP1 cells as a model for TNFR1 surface level and TNFα-dependent NF-κB activation*

While a number of genetic screens was performed to study TNFα-stimulated NF-κB activation [379-382], relatively little is known about regulation of TNFR1 itself. As TNFα binding to the extracellular domain of TNF receptor 1 activates a downstream pro-inflammatory response, it derives logically that the level of TNFR1 receptor on the cell surface affects, to some degree, the cellular response to TNFα. Hence, the cellular network impinging on TNFR1 membrane presentation can also modulate the activation of TNFα-mediated NF-κB signalling.

To selectively map genetic modulators that affect TNFR1 localisation on the cell surface **and** activation of the TNFα/ NF-κB axis, I set out to perform two screens: one for TNFR1 surface levels and one for TNFα-dependent NF-κB activation, focussing on the overlapping hits. First, I validated HAP1 cells as a suitable model for TNFR1 screens by examining the expression levels of TNFα-related genes. Publicly available data indicated that TNFRSF1A expression can be detected in HAP1 cells both at mRNA and protein level (**Table 5.3**) [148, 151]. Of note, HAP1 cells displayed no detectable expression of TNF and TNFRSF1B (which codes for TNFR2), eliminating possible confounding effects of TNFα autocrine signalling and TNFR2 activation.

Gene	mRNA (FPKM)	Found in proteome
TNF (TNFα)	0.01 ± 0.01	No
TNFRSF1A (TNFR1)	13.97 ± 0.06	Yes
TNFRSF1B (TNFR2)	1.08 ± 0.17	No

Table 5.3 TNFα/TNFR expression and protein level in HAP1 cells. Data obtained from [148, 151]. FPKM values are represented as Mean ± standard deviation from two independent replicates.

Immunoblotting of cellular lysates with anti-TNFR1 antibody returned a band at the expected molecular weight of approximately 55 kDa (**Figure 5.3A**). Next, I investigated whether TNFR1 was expressed on the cell surface and whether its levels could be detected by FC in HAP1 cells. The specificity of commercial anti-TNFR1 antibody was tested by staining HCT116 wild type and ΔTNFR1 cells for FC. As expected, fluorescent surface signal was lost in a TNFR1 knockout clone as compared with wild type cells, thus validating the antibody for FACS-based application (**Figure 5.3B**). When the staining was performed in HAP1 cells, the signal for surface TNFR1 was low but consistent among multiple experiments (n = 4, **Figure 5.3C**).

I then tested whether TNFR1 was functionally active by mapping the cellular response to TNFα stimulation in HAP1 cells. According to previous reports, stimulation of HAP1 cells with lymphotoxin α (a well-described TNF receptor ligand) induced activation of the NF-κB pathway [383] and, additionally, KBM-7 cells, the HAP1 parental cell line, were shown to be sensitive to TNFα [148, 384]. It is well documented that degradation of the cytoplasmic protein IκBα, which normally prevents NF-κB migration into the nucleus, is a quantitative and dynamic marker of TNFα signalling activation [385]. Hence, TNFα-dependent NF-κB activation in HAP1 cells was tested via a time course experiment quantifying reduction of IκBα after addition of 10 ng/ml TNFα. The IκBα signal was decreased up to approximately 50%, peaking 30 minutes after treatment as

shown by immunoblotting and FC, confirming that HAP1 cells harbour a functionally active TNFα/TNFR1/NF-κB signalling axis (**Figure 5.3D**, **E**).

Collectively these results established HAP1 cells as a suitable model for the investigation of TNFR1 expression and TNFα-mediated NF-κB activation through FACS-based forward genetic screens.

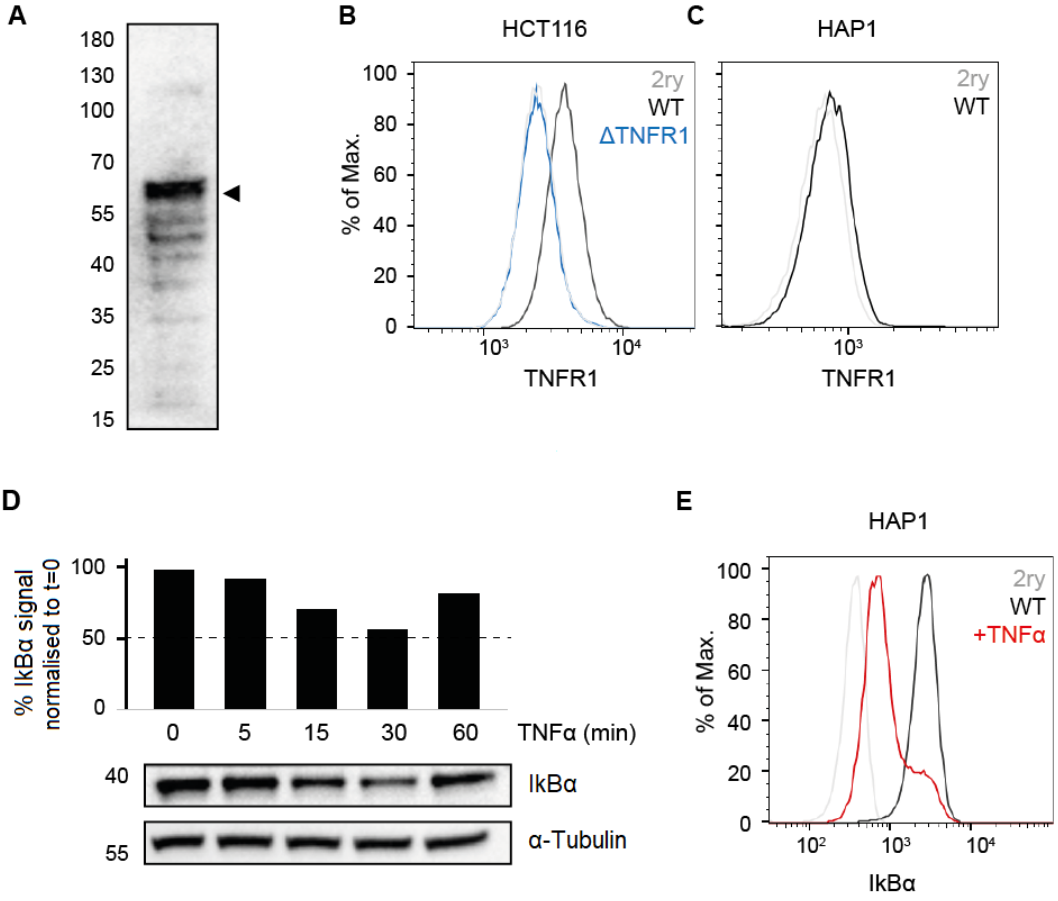


Figure 5.3 Validation of HAP1 cells as a model for investigating TNFR1 expression and TNFα-mediated NF-κB activation. A. Immunoblotting of HAP1 cell lysate with anti-TNFR1 antibody, expected band at approximately 55 kDa is indicated with an arrow. **B.** Wild type and ΔTNFR1 HCT116 cells were stained alongside HAP1 cells (**C.**) for surface expression of TNFR1 and analysed by FC. Staining with Alexa488-conjugated secondary antibody is used as control ("2ry"). **D.** HAP1 cells were treated with 10 ng/ml TNFα for the indicated time. Lysates were collected and immunoblotted for IκBα; α-Tubulin was used as loading control. IκBα signal was quantified after normalisation to protein levels before treatment (t=0). Experiment was performed in n = 2 independent biological replicates. **E.** HAP1 cells ± 10 ng/ml TNFα were stained for IκBα and analysed by FC. WT = wild type.

5.2.2 *Haploid genetic screen for TNFR1 surface levels*

To map regulators affecting TNFR1 surface presentation, I performed a FACS-based forward genetic screen by staining live mut-HAP1 cells for TNFR1 and isolating cells at the extremes of the fluorescence distribution (**Figure 5.4A**). The gene encoding for the screen marker itself (TNFRSF1A) served as internal screen quality control, expected to score as positive signal modulator. Overall, positive regulators displayed modest MIs, likely due to the limited shift in median fluorescence intensity of the TNFR1 signal compared to background (**Figure 5.3C**). Notwithstanding, TNFRSF1A knockout cells were enriched in the lower end of the distribution (MI = 0.41), confirming the exquisite sensitivity of the screening approach.

Among the 512 hits, proteins involved in TNFR1 post-translational regulation such as charged multivesicular body protein 3 and 5 (CHMP3/5), two core components of classic receptor-mediated internalisation pathway previously linked to TNFR1 internalisation were found [347]. Of note, ADAM17 and ERAP1, two proteins known to control surface TNFR1 levels through ectodomain shedding, did not score as modulators in the screen. While it is well known that proteolytic cleavage of cell surface TNFR1 plays an important role in response to pro-inflammatory stimuli [342], the screen confirmed that it does not contribute to surface receptor level in basal conditions in HAP1 cells.

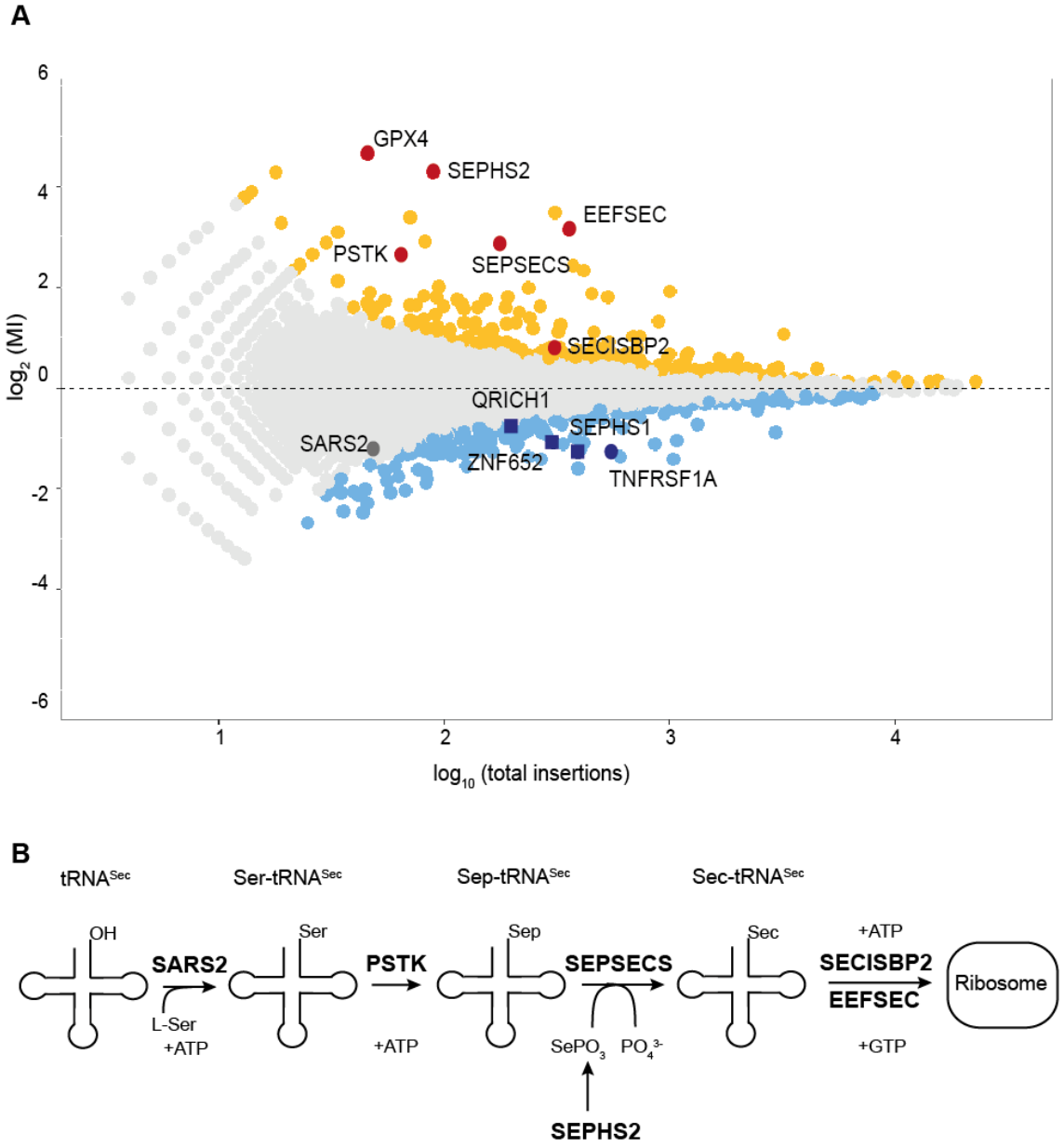


Figure 5.4 Forward genetic screen for TNFR1 surface level. A. Regulatory map of TNFR1 surface expression. Genetic regulators (FDR < 0.05) are represented in orange (negative regulators) and light blue (positive regulators). Highlighted are TNFRSF1A (blue circle), QRICH1, SEPHS1, ZNF652 (blue squares) and selenium biosynthesis genes (red squares). **B.** Schematic representation of synthesis and incorporation of selenocysteine. Image adapted from [386].

Interestingly, selenium biosynthesis genes SEPHS2, phosphoseryl-tRNA kinase (PSTK), o-Phosphoseryl-tRNA^{Sec} selenium transferase (SEPSECS), Sec insertion sequence-binding protein 2 (SECISBP2) and Sec-specific elongation factor (EEFSEC)

featured prominently among TNFR1 negative modulators together with selenocysteine-containing glutathione peroxidase 4 (GPX4) (**Figure 5.4B**) [386]. This result was intriguing, as the selenocysteine pathway had not been previously linked to TNFR1 regulation.

In addition to the above-mentioned notable hits, the screen revealed a number of novel putative regulators (see **Appendix 8.2.11**) of TNFR1 surface level in HAP1 cells. Crucially, screening results did not discriminate mutants which affected receptor conformation and antibody binding, but left the actual level of TNFR1 unchanged. Thus, to identify genes whose regulation of TNFR1 surface levels led to functional consequences on TNFα-mediated downstream NF-κB activation, I performed a companion screen, where mutant pools were tested for activation of TNFα signalling and mapped the hits overlap.

5.2.3 *Haploid genetic screen for TNFα-dependent NF-κB activation*

I set out to identify modulators of TNFR1-dependent NF-κB activation by quantitative haploid genetic screening using IκBα as a readout (see **Section 5.2.1**). As prerequisite for mapping TNFR1 downstream pathway activation, mut-HAP1 cells required stimulation with TNFα. To maximise the sensitivity towards both positive and negative regulators of TNFα-dependent NF-κB activation, the screen was stimulated with TNFα for 15 minutes before cell harvesting and downstream processing (**Figure 5.3E**). For interpreting the resulting regulatory map (**Figure 5.5A,** see **Appendix 8.2.12**), it is worth pointing out that IκBα levels are inversely correlated with NF-κB activation and, as such, negative regulators for TNFα/TNFR1/NF-κB signalling axis appear in the lower half of the regulatory map and positive regulators in the top half.

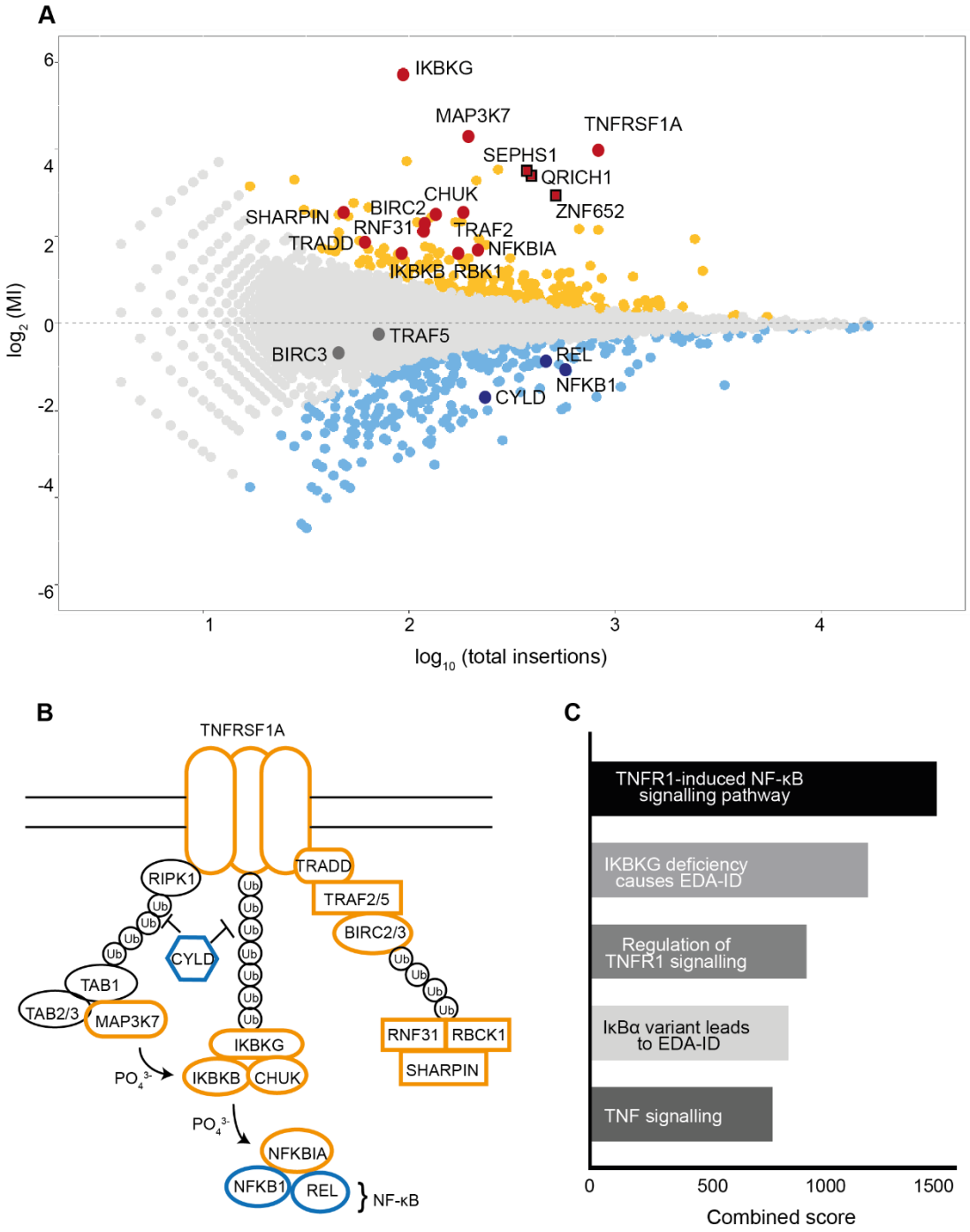


Figure 5.5 Forward genetic screen for TNFα-dependent NF-κB activation. A. Regulatory map of TNFα-dependent NF-κB activation. Mut-HAP1 cells were treated for 15 minutes with 10 ng/ml TNFα prior to harvest, permeabilisation and staining with anti-IκBα antibody. Genes scoring as significant regulators for IκBα levels (FDR < 0.05) are represented in orange (negative regulators) and light blue (positive regulators). Red, blue, and dark grey circles highlight components of TNFα activation pathway highlighted in (**B.**). Red squares represent QRICH1, SEPHS1 and ZNF652. **B.** Schematic representation of the TNFα-dependent NF-κB

activation pathway. Highlighted are genes scoring as hits in the IκBα screen, colour indicates positive (light blue) and negative (orange) regulators. Image adapted from [387]. **C.** Top five Reactome pathways enriched among negative regulators for TNFα-dependent NF-κB activation screen (207 genes) ordered by decreasing "combined score", calculated as ln (p) * z, with p = p value from Fisher exact test and z = z-score of the deviation from the expected rank. EDA-ID = anhidrotic ectodermal dysplasia with immunodeficiency. Analysis was conducted using Enrichr web tool (www.amp.pharm.mssm.edu/Enrichr [388]).

Hits recovered from the screen were enriched for known components of the TNFR1/NF-κB signalling cascade (**Figure 5.5B**) as highlighted by the top Reactome pathways overrepresented within the screen's negative regulators (**Figure 5.5C**). Hits included genes encoding all three subunits of the IKK complex (IKBKG, CHUK, IKBKB) [389], MAP3K7, and the gene coding for the receptor itself. As expected, TNFRSF1A was found among IκBα negative regulators, as cells mutant for TNFR1 would be refractory to TNFα activation. Notably, the screen also identified NFKBIA, the gene coding for IκBα, as a negative regulator. This result, shared with another NF-κB genetic screen [382], could be explained by an incomplete NFKBIA gene knockout. IκBα loss, in fact, results in continuous NF-κB activation and triggers a negative feedback loop thus possibly increasing hypomorphic IκBα levels [390].

Of note, not all genes annotated in TNFR1-induced NF-κB pathway appeared in the hit list (**Figure 5.6A**). Of these, some are partially redundant paralogues of screen hits (BIRC2/3 [391] and TRAF2/5 [392]), some are involved in post-translational regulation of the NF-κB complex itself (ubiquitin A52, B and C (UBA52, UBB, UBC) and ribosomal protein 27A (RPS27A)[393]) and as such are unlikely to score in a screen that uses IκBα as a readout, and others' involvement in the pathway is controversial (TAB1/2 [394]). Overall, the FACS-based screening approach was able to unbiasedly highlight numerous known

components of the TNFR1-induced NF-κB pathway, by mapping modulators of IκBα degradation after TNFα stimulation,

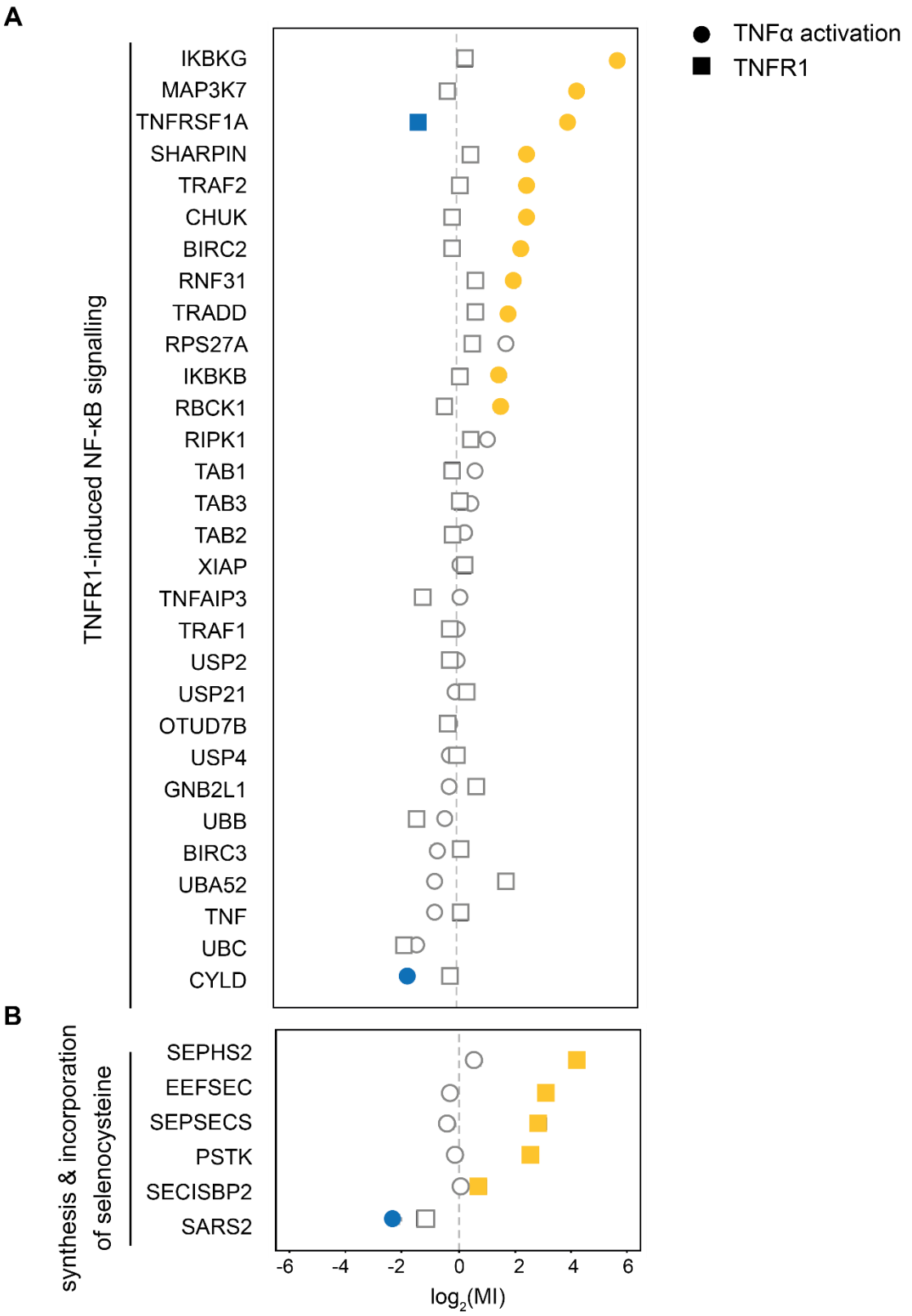


Figure 5.6 MI comparison for selected gene in TNFR1 and TNFα-dependent NF-κB pathway activation. A. MI of genes belonging to the "TNFR1-induced NF-κB signalling

pathway" (Reactome pathway R-HSA-5357956) and **B.** genes involved in the selenium biosynthesis and incorporation in both TNFR1 and TNFα-dependent NF-κB activation screens.

5.2.4 *Identification of hits' overlap between TNFR1 surface level and TNFα-dependent NF-κB activation screens*

Next, I investigated the hits' overlap between the two screens. With the exception of TNFRSF1A, genes belonging to the TNFR1-induced NF-κB signalling pathway were unique to the TNFα-dependent NF-κB activation screen (**Figure 5.6**). Similarly, selenium biosynthesis genes which scored as TNFR1 negative regulators failed to affect IκBα levels in the TNFα-dependent NF-κB activation screen (with the exception of seryl-tRNA synthetase 2, SARS2).

Collectively these results indicated that: 1.) basal TNF receptor 1 regulation was largely independent from its signalling activity and 2.) upregulation of surface TNFR1 through blockade of selenium biosynthesis did not have functional consequences on TNFα signalling in the current set-up.

Genes whose effect on TNF receptor 1 reverberates on NF-κB activation would score as hits in both screens, albeit with opposite MI values. To unbiasedly detect such genes, I overlapped the hit list from the two screens and selected genes whose knockout elicited a minimum 2-fold change over baseline level in either of the phenotypes tested (MI > 2 or < 0.5 in either screen). The resulting list comprised 10 genes: among them appeared TNFRSF1A, underscoring the validity of the analysis (**Table 5.4**). Intriguingly the same pattern was shared by four poorly characterised genes: QRICH1, SEPHS1, ZNF652 and carnosine methyltransferase (CARNMT1). I decided to focus on the first three as they all scored as very strong regulators in the TNFα-dependent NF-κB activation screen (**Figure 5.5A**).

	TNFα-mediated NF-κB activation		TNFR1	
Gene	**FDR**	**MI**	**FDR**	**MI**
TNFRSF1A	2.58×10^{-183}	15.89	9.15×10^{-20}	0.41
QRICH1	2.44×10^{-71}	10.67	1.73×10^{-2}	0.59
SEPHS1	3.51×10^{-72}	10.58	1.56×10^{-13}	0.41
ZNF652	4.60×10^{-79}	7.57	6.58×10^{-8}	0.47
CARNMT1	2.19×10^{-3}	2.34	4.85×10^{-2}	0.57
EIF4E2	3.37×10^{-3}	0.42	4.50×10^{-3}	2.23
VPS45	9.92×10^{-7}	0.39	7.38×10^{-15}	3.03
RANBP3	1.04×10^{-17}	0.33	2.22×10^{-4}	1.72
GIGYF2	2.85×10^{-41}	0.26	1.42×10^{-79}	3.74
CHMP5	2.05×10^{-6}	0.11	9.54×10^{-12}	10.33

Table 5.4 List of genes concomitantly affecting TNF receptor 1 surface levels and TNFα-dependent NF-κB activation. Overlap of gene hits in TNFR1 and TNFα-mediated NF-κB activation screens. Only hits with FDR < 0.05 in both screens and MI > 2 or < 0.5 in either screen were considered. MI values colour identifies positive (light blue) and negative (orange) regulators.

To exclude that the result was due to a technical artefact, I inspected gene the trap cassette insertion profiles in QRICH1, SEPHS1 and ZNF652 in addition to TNFRSF1A. As shown in **Figure 5.7**, independent insertions in sense orientation were preferentially located at the gene start or within the first intron, most likely resulting in a complete loss-of-function. These data indicated that QRICH1, SEPHS1 and ZNF652 are likely positive regulators of TNFR1 surface level and activation.

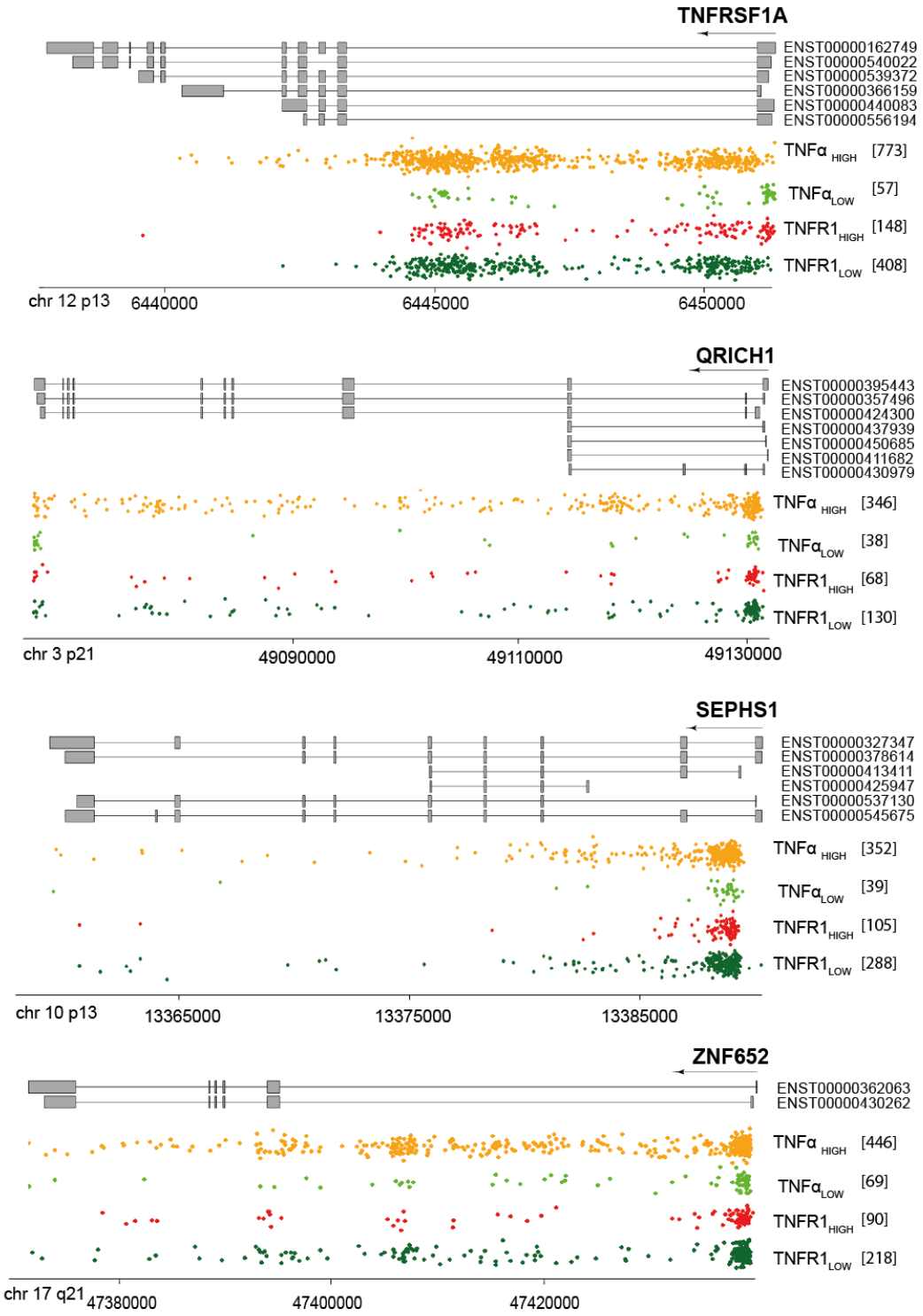


Figure 5.7 Location of independent sense gene-trap insertions in TNFRSF1A, QRICH1, SEPHS1 and ZNF652. Gene-trap insertions for the indicated genes are shown for the HIGH and LOW sorted cell populations. Insertions in TNFα-dependent NF-κB activation (TNFα, orange and light green) and surface TNFR1 expression (red and dark green) screens are shown. Figure details as in **Figure 3.10**

5.2.5 *QRICH1, SEPHS1 and ZNF652 hit validation*

To validate the phenotype associated with QRICH1, SEPHS1 and ZNF652 loss, I generated knockout clones in HAP1 cells using the CRISPR/Cas9 system with two validated, independent sgRNAs per gene. Gene editing was confirmed by genotyping and, when possible, immuno-blotting for lack of the disrupted protein. Knockout clones used in the study are listed in **Table 5.5**.

Gene	sgRNA	Clone #	Genotype	Validated via immunoblotting?
QRICH1	1	1	Sequence failed to align	YES
	2	2	10 bp deletion	YES
	1	3	2 bp insertion	YES
	1	4	4 bp deletion	YES
SEPHS1	1	1	11 bp deletion	YES
	2	2	1 bp insertion	YES
	1	3	Sequence failed to align	YES
ZNF652	1	1	87 bp insertion	NA
	2	2	8 bp deletion	NA
	2	3	1 bp deletion	NA

Table 5.5 Genotype information for QRICH1, SEPHS1 and ZNF652 knockout clones used in the study.

First, I stained QRICH1, SEPHS1 and ZNF652 knockout clones for surface expression of TNFR1 using the same protocol employed in the screen. In all tested clones, TNFR1 signal consistently dropped close to background level (**Figure 5.8A**). A logical consequence of low surface levels of TNFR1 in ΔQRICH1, ΔSEPHS1 and ΔZNF652 cells was defective TNFα signalling, as highlighted by the TNFα-dependent NF-κB activation screen (**Figure 5.5A**). I validated these observations by treating the knockout clones with 10 ng/ml TNFα for 15 minutes and immunoblotting lysates for IκBα (**Figure 5.8B**). As expected, IκBα levels did not significantly change after stimulation in knockout

cells. Collectively these data indicated that ablation of QRICH1, SEPHS1 and ZNF652 resulted in reduction of surface TNFR1 levels below the activation threshold for the TNFα/TNFR1/NF-κB axis.

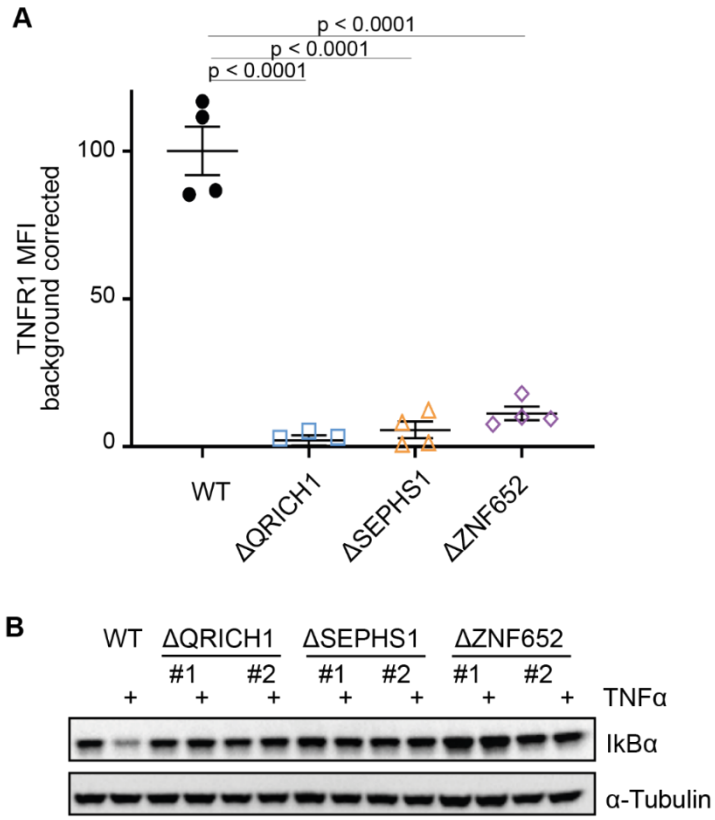


Figure 5.8 QRICH1, SEPHS1 and ZNF652 hit validation. A. QRICH1, SEPHS1 and ZNF652 HAP1 knockout clones were stained for surface expression of TNFR1 alongside wild type cells. Analysis was performed by FC. Displayed is in the quantification of TNFR1 signal (MFI, normalised to wild type control and corrected for secondary antibody). Two clones per gene were tested, experiment was performed in n =2 biological replicates. Statistical analysis was performed using 1-way ANOVA followed by Dunnett's post hoc test. **B.** ΔQRICH1, ΔZNF652, ΔSEPHS1 and wild type HAP1 cells were stimulated with 10 ng/ml TNFα for 15 minutes. Lysates of unstimulated and stimulated cells were probed for IκBα level. α-Tubulin was used as loading control. WT = wild type.

5.2.6 *QRICH1, SEPHS1 and ZNF652 regulation of TNFR1*

To further investigate whether ablation of QRICH1, SEPHS1 and ZNF652 induced changes in total TNFR1 levels or only in its surface expression, I subjected knockout lysates to immunoblotting for TNF receptor 1. All knockout clones presented a drastically decreased level of TNFR1, indicating that the defect was not restricted to surface presentation (**Figure 5.9A**). I then asked whether the effect was due to destabilisation of the receptor and a shorter half-life. Since TNFR1 is principally degraded through the endo/lysosomal pathway [346], I treated the cells for 16 hours with chloroquine, a chemical that blocks endosomal acidification, using cleavage of Light Chain 3 A/B (LC3A/B) as a positive control. TNFR1 protein accumulation after chloroquine treatment was observed in wild type HAP1 cells and, to a much lower degree, in a ΔZNF652 clone but still undetectable in ΔQRICH1 and ΔSEPHS1 clones (**Figure 5.9B**). These results suggested that decreased TNF receptor level in the knockout clones was not due to receptor degradation.

I then examined whether knockout of QRICH1, SEPHS1 and ZNF652 affected TNFR1 at transcriptional level. To this end, isolated total RNA from three independent clones for each gene was assayed for TNFR1 mRNA levels using qRT-PCR. The results showed a significant reduction (> 10 fold) in TNFR1 mRNA across all clones, with a weaker effect in ΔZNF652 clones (**Figure 5.9C**).

To test whether such an effect was caused by impairment of mRNA stability, *de novo* mRNA synthesis was blocked with transcription inhibitor Actinomycin D and TNFR1 mRNA levels were followed for 6 hours (**Figure 5.9D**). Relative mRNA levels were highly comparable between wild type and knockout samples, suggesting QRICH1, SEPHS1 and ZNF652 did not play a role in transcript stability. These data indicated that

QRICH1, SEPHS1 and possibly ZNF652 presence was required for baseline TNFR1 transcription in HAP1 cells.

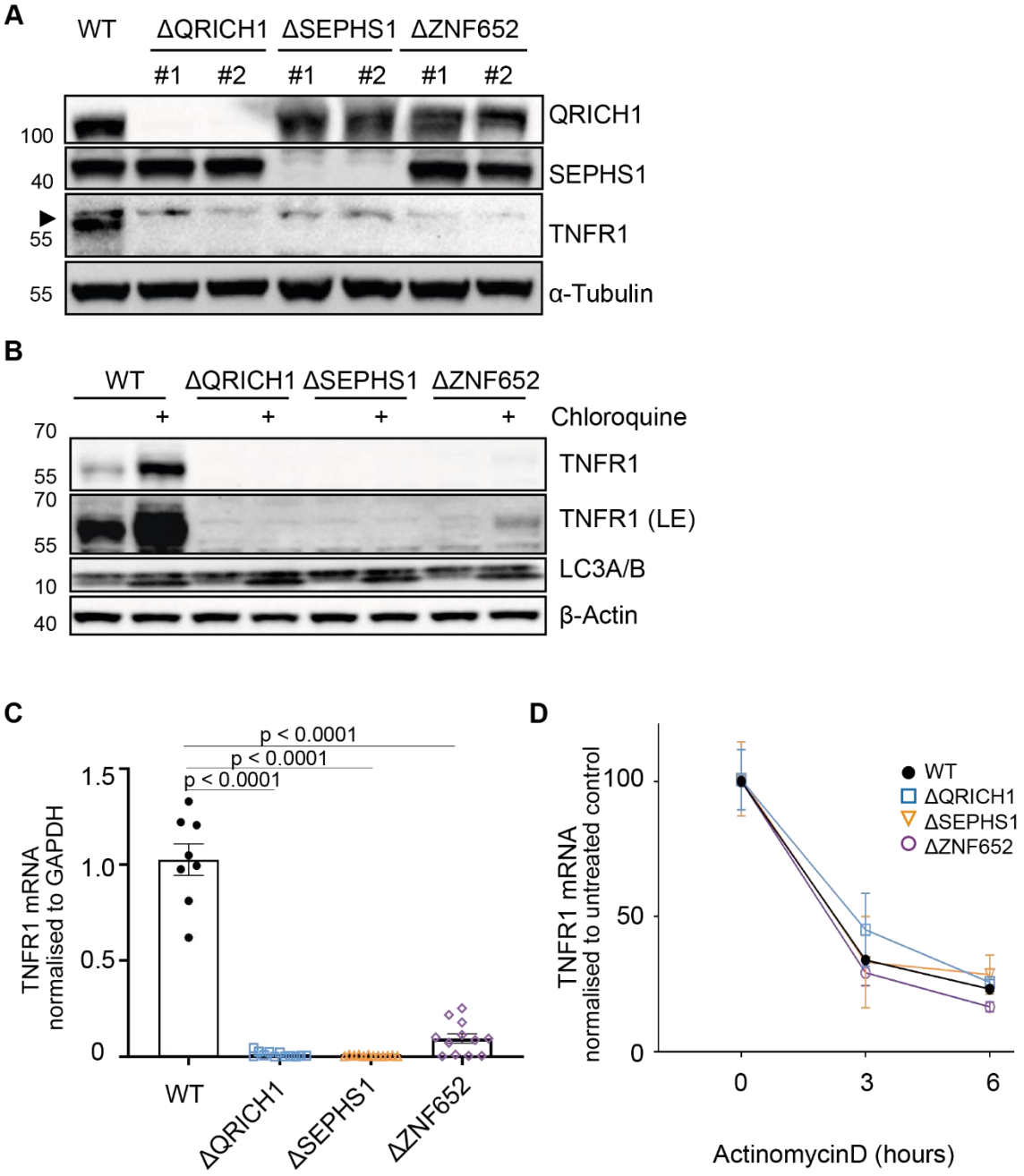


Figure 5.9 QRICH1, SEPHS1 and ZNF652 regulate TNFR1 at transcriptional level. **A.** Lysates from ΔQRICH1, ΔSEPHS1, ΔZNF652 clones and wild type HAP1 cells were collected. TNFR1 total protein was detected by immunoblotting, α-Tubulin was used as loading control. WT = wild type. **B.** HAP1 wild type and knockout clones for QRICH1, SEPHS1 and ZNF652 were treated with chloroquine for 16 hours. Lysates were immunoblotted using the

indicated antibodies. LE = long exposure. Immunoblot representative of n = 2 independent biological replicates. **C.** TNFR1 mRNA levels were measured by qRT PCR. Data obtained from three independent clones per gene were pooled. Experiment was performed in n≥3 biological replicates. Statistical analysis was performed using 1-way ANOVA followed by Dunnett's post hoc test**. D.** Wild type, ΔQRICH1, ΔSEPHS1 and ΔZNF652 cells were treated with 3 µg/ml transcription inhibitor actinomycin D for the indicated time-points. TNFRSF1A mRNA levels were quantified using qRT-PCR. For each clone, mRNA level was normalised to t=0 level.

5.2.7 *Haploid genetic screens for TNFα-dependent NF-κB activation and TNFR1 surface level in ΔQRICH1 background*

Next, I wondered whether the three genes might work together to downregulate TNFR1. An elegant and unbiased method to gather information on gene co-dependencies is a suppressor screen, where a forward genetic screen is repeated in a knockout background of interest and results are compared with the original wild type screen. While inactivation of a gene of interest (in this case QRICH1) in wild type cells affects the TNFR1 phenotype, in a ΔQRICH1 background further trapping of QRICH1 has no effect on TNFR1 levels. In this scenario, genes that associated with, depended on, or working in coordination with the background-inactivated gene are also expected to lose their role as regulators in the suppressor screen. Thus, I repeated both the TNFR1 screen and the TNFα-dependent NF-κB activation screens in ΔQRICH1 cells and unbiasedly identified genes displaying QRICH1-analogous pattern compared to wild type screens (

Figure 5.10, see **Appendices 8.2.13** and **8.2.14**). To this end, I used ΔMI, a statistical metric to calculate significant shifts in MI on a per gene basis (see **Section 2.7**).

In total, 291 genes displayed significant ΔMI in both screen pairs: TNFα-dependent NF-κB activation in wild type versus ΔQRICH1 ($\Delta MI_{TNF\alpha}$) and TNFR1 surface level in wild type versus ΔQRICH1 background (ΔMI_{TNFR1}) (see **Appendices 8.2.15** and **8.2.16**).

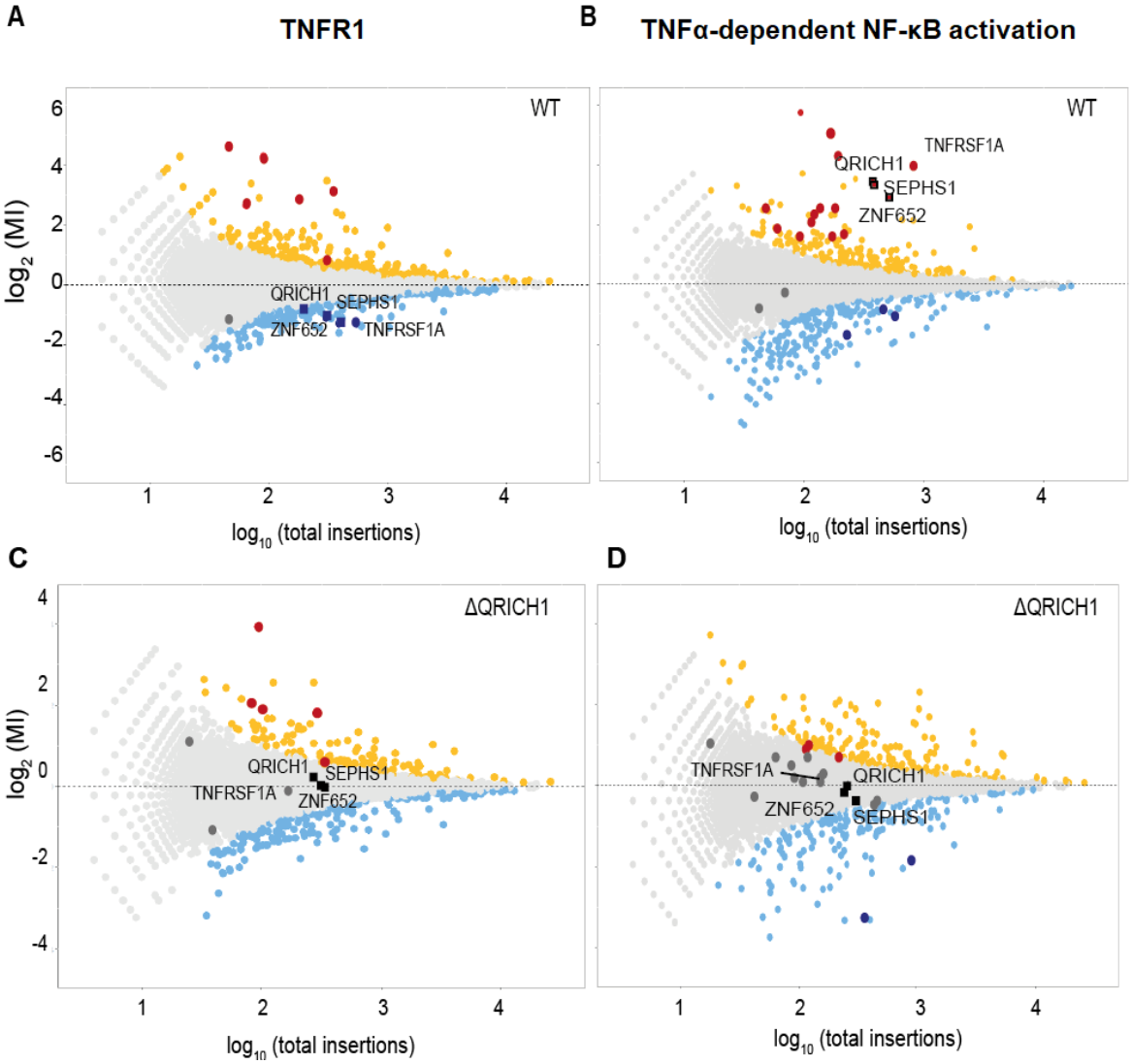


Figure 5.10 Haploid genetic screens for TNFα-dependent NF-κB activation and TNFR1 surface level in wild type and ΔQRICH1 cells. A. Regulatory maps of TNFR1 surface expression in wild type and **C.** ΔQRICH1 cells. Genes scoring as significant regulators (FDR < 0.05) are represented in orange (negative regulators) and light blue (positive regulators). Red and dark grey circles represent components of selenocysteine synthesis and incorporation pathway as described in **Figure 5.4**. **B.** Regulatory maps of TNFα-dependent NF-κB activation in wild type and **D.** ΔQRICH1. Genes scoring as significant regulators (FDR < 0.05) are represented in orange (negative regulators) and light blue (positive regulators). Red, dark grey and blue circles indicate components of TNFR1-mediated NF-κB signalling pathway as detailed in **Figure 5.5**. Colouring indicates role as negative, positive, and non-significant regulator, respectively. In all maps, QRICH1, SEPHS1 and ZNF652 are represented using square symbols.

Notably, only 8 genes exhibited a pattern comparable to QRICH1 ($\Delta MI_{TNF\alpha} < 1$ & $\Delta MI_{TNFR1} > 1$): among those, ZNF652, SEPHS1 and TNFRSF1A display the highest

|ΔMI| (**Figure 5.11**). Overall, this analysis supported the existence of a functional link between QRICH1, ZNF652 and SEPHS1 in HAP1 cells, all behaving as positive regulators of TNFR1 surface expression and activation.

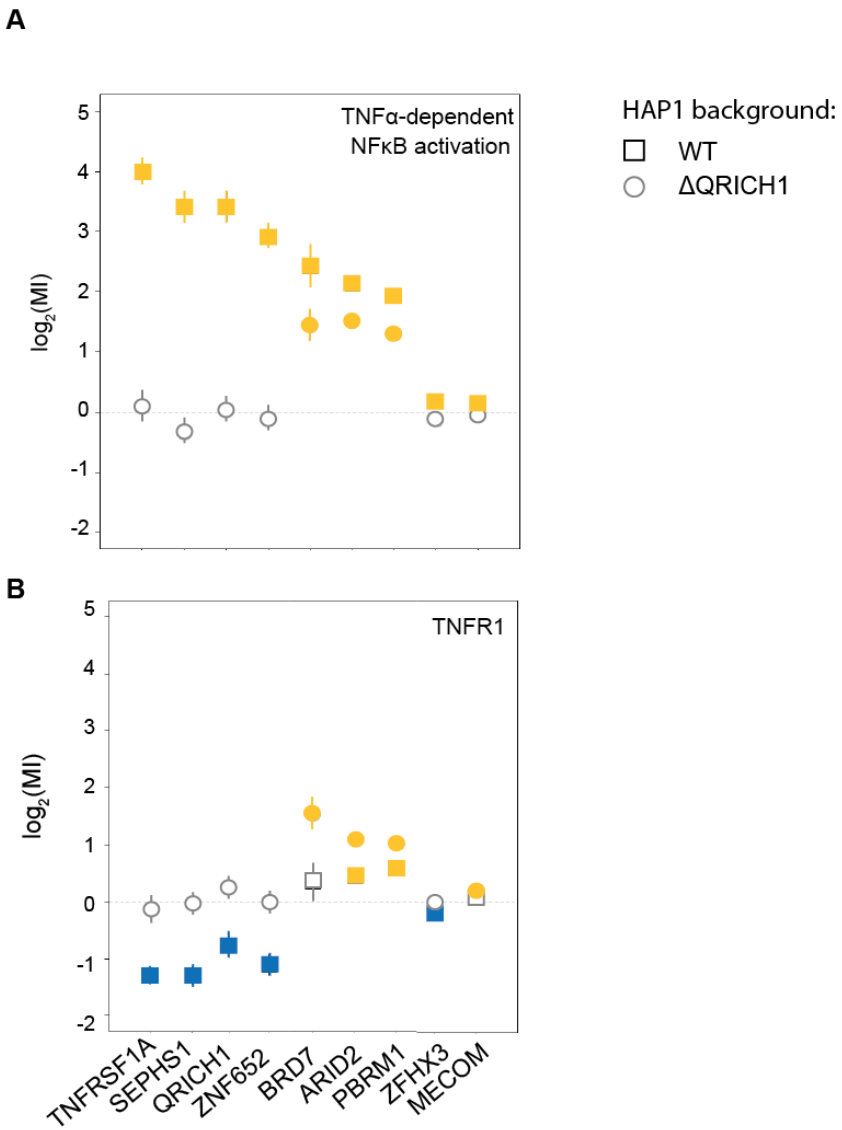


Figure 5.11 Unbiased genome-wide analysis of ΔMI in TNFα-dependent NF-κB activation and TNFR1 screen pairs. A. Per gene ΔMI was calculated for each screen pair (wild type versus ΔQRICH1). Among genes with a significant ΔMI (FDR < 0.05), the ones showing similarities with the QRICH1 ΔMI pattern ($\Delta MI_{TNF\alpha} < 1$ and $\Delta MI_{TNF\alpha} > 1$) are shown. Per gene $\log_2$(MI) in wild type (circles) and ΔQRICH1 background (squares) is displayed for TNFα-dependent NF-κB activation screen and **B.** TNFR1 screen. Standard error for $\log_2$(MI) was estimated as described in **Section 2.7**. Positive regulators are represented in blue, negative

regulators in orange. Filled symbols indicate that the gene is a significant regulator in the screen (FDR < 0.05).

5.2.8 *Data mining for QRICH1, SEPHS1 and ZNF652 interactions*

To corroborate these findings, I investigated whether interactions among QRICH1, SEPHS1 and ZNF652 had been previously described. Intriguingly, SEPHS1 and QRICH1 were reported to physically interact (IntAct, www.ebi.ac.uk/intact [175]). The interaction was observed in a systematic screen of the human interactome using a yeast two-hybrid screen on a full-length cDNA library [395]. Furthermore, DepMap dependency scores (copy-number weighted gene-essentiality) for QRICH1 and SEPHS1 were highly correlated (Pearson Rho = 0.58), a feature characteristic of functionally related genes, while correlation of either of them with ZNF652 was less striking (**Figure 5.12**).

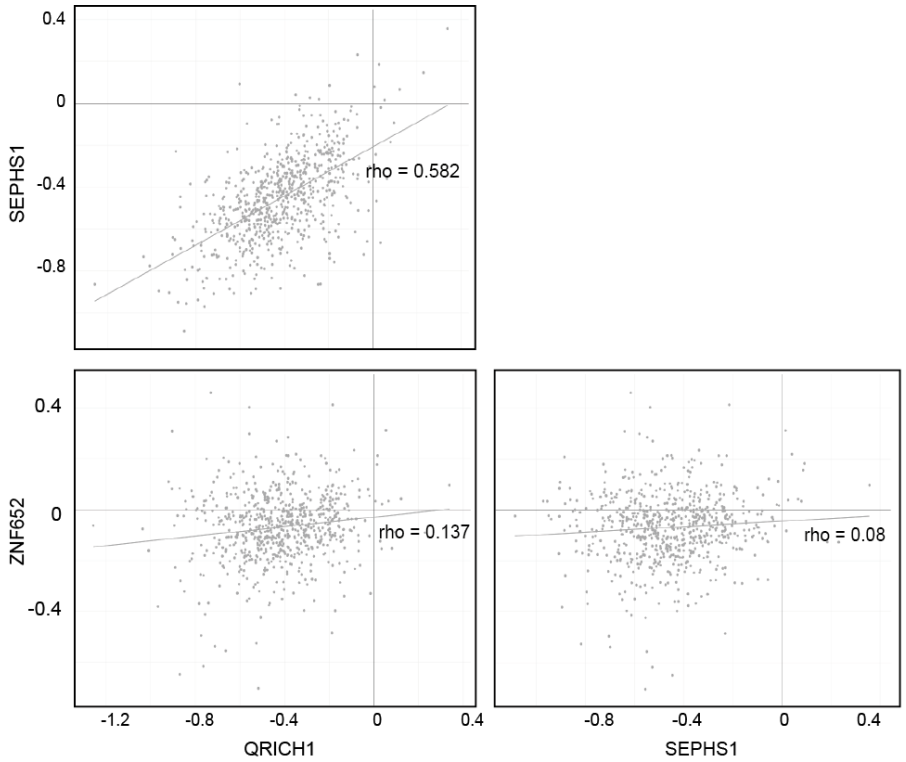


Figure 5.12 Correlation of dependency scores for QRICH1, SEPHS1 and ZNF652 (DepMap). Cell-line specific, per gene dependency scores for QRICH1, SEPHS1 and ZNF652 were obtained from DepMap (www.depmap.org/portal/depmap [90]). Correlation of dependency

scores among each gene pair is plotted. Trend line and Pearson correlation coefficient are indicated. Images adapted from the DepMap online visualisation tool.

Taken together, these data suggested a probable functional and biochemical interaction between QRICH1 and SEPHS1. On the other hand, the lack of evidence linking ZNF652 to either of the other two proteins in publicly available databases, in addition to the lack of reliable commercial antibodies, led me to focus only on QRICH1 and SEPHS1 for the remainder of the study.

5.2.9 *Subcellular localisation of QRICH1*

One of the sources of false positives in yeast two-hybrid screen system is the forced localisation of bait and/or prey in a compartment different from their natural subcellular localisation [396]. Thus, the first step to validate an endogenous QRICH1 and SEPHS1 interaction was to examine whether the two proteins co-localise. While SEPHS1's multiple isoforms are found both in the nucleoplasm and the cytosol [371], QRICH1 is expected to localise in the nucleoplasm due to a putative nuclear localisation sequence (NLS) at residues 234-250 [364, 397]. However, cellular fractionation data in HEK293 cells reported QRICH1 in cytoplasmic, membrane and nuclear soluble fraction [369].

First, I stained wild type and ΔQRICH1 HAP1 cells to verify anti-QRICH1 antibody specificity (**Figure 5.13A**). Immunofluorescence analysis revealed a highly specific QRICH1 signal co-localised with DAPI in the nucleus. Next, I performed a cell fractionation experiment on HAP1 cells, separating the cytoplasmic from the insoluble fraction, containing membrane and mitochondria, and investigating QRICH1 localisation. Unexpectedly, QRICH1 was mainly found in the cytoplasm (**Figure 5.13B**). The same result was obtained with a commercial cell fractionation kit (results not shown). Isolated

studies reported protein leakage from the nucleus during cell fractionation [398, 399]; in such cases, detection of the true localisation was restored by modifying the cell fractionation buffers, for instance by supplementing the lysis buffer with high concentrations of inert polymers and/or using a detergent specific for the plasma membrane. To investigate whether the concentration of macromolecules in solution (also defined as "macromolecular crowding") affected QRICH1 localisation, I repeated the fractionation in presence of 6.25% of highly branched polymer Ficoll 400. In addition, I substituted the detergent NP-40 with the steroid glycoside digitonin which creates pores in the cholesterol-rich cell membrane while leaving the nuclear membrane intact [400]. As shown in **Figure 5.13C,** cellular fractionation in Digitonin-Ficoll extraction buffer (DFEB) clearly showed QRICH1 primarily localised in the insoluble fraction. Furthermore, SEPHS1 shows the same trend.

Next, I asked whether either Ficoll 400 or digitonin alone or a combination of both reagents was instrumental in preventing QRICH1 and SEPHS1 leakage in the cytoplasm. I designed an experiment where HAP1 cells were lysed with either the "full" DFEB or in absence of either Ficoll 400, sucrose or digitonin. In the lysis buffer without digitonin, detergent NP-40 was used to ensure membrane lysis. Additionally, the fractionation protocol was slightly altered to further separate nuclear and insoluble fraction. Notably, Ficoll 400 was the crucial component for QRICH1 retention in the nuclear fraction, while absence of sucrose or digitonin did not affect subcellular protein localisation (**Figure 5.13D**).

Together, these data offered a solution for the published discrepancy in QRICH1 protein localisation between immunofluorescence and cell fractionation, suggesting that macromolecular crowding played a pivotal role in the process.

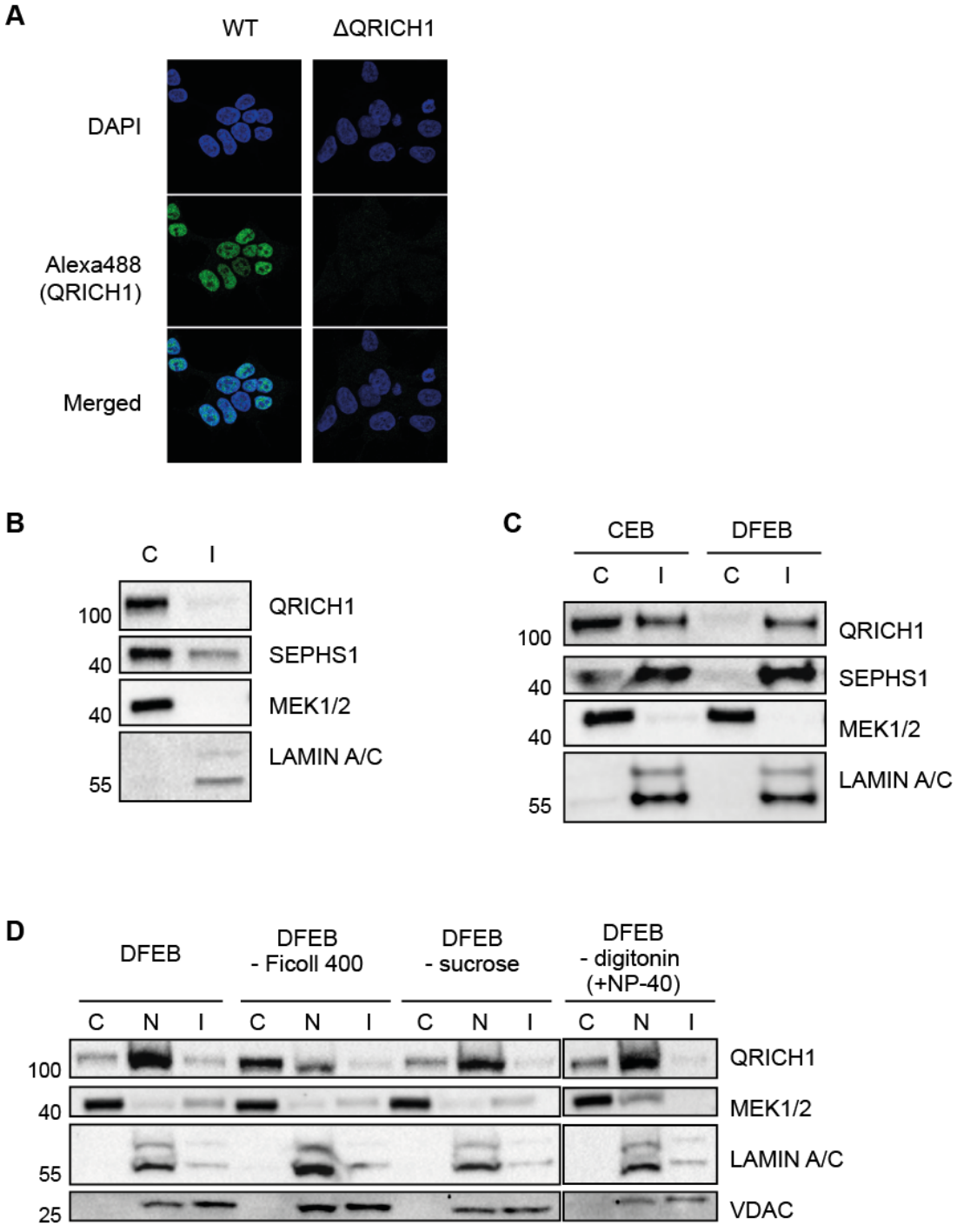


Figure 5.13 QRICH1 localises in the nucleoplasm. A. After fixation, wild type and ΔQRICH1 HAP1 cells were stained with anti-QRICH1 antibody (Alexa 488) and DAPI. WT = wild type. **B.** Wild type HAP1 cells were fractionated using cytoplasmic extraction buffer (CEB) and separated into cytosolic lysate (C) and insoluble fraction (I). Fractions were loaded on a gel and immunoblotted using the indicated antibodies. MEK1/2 and Lamin A/C are used, respectively, as cytoplasmic and nuclear markers. **C.** Wild type HAP1 cells were fractionated using either CEB of DFEB. Proteins of interest were detected by immunoblotting with the

appropriate antibodies. **D.** "Full" DFEB or DFEB lacking either sucrose, Ficoll 400 or digitonin was used to fractionate HAP1 wild type cells in cytoplasmic (C), nuclear (N) and insoluble fractions (I). Voltage-dependent anion channel (VDAC) was used as marker for the insoluble fraction. Fractions were immunoblotted for proteins of interest. Immunoblot representative of n = 2 independent biological replicates.

5.2.10 *Co-immunoprecipitation of QRICH1 and SEPHS1*

Having established that QRICH1 and SEPHS1 reside in the same subcellular compartment, the next step was to investigate whether they physically interacted in physiological conditions. I started by testing whether anti-QRICH1 and anti-SEPHS1 antibodies could be used to efficiently precipitate the respective endogenous protein. As shown in **Figure 5.14A**, both proteins were efficiently enriched using 1 μg/ml of the cognate antibody but no co-immunoprecipitation was detected. Notably, when comparing protein ratios of the immunoprecipitated fraction versus the initial lysate, immunoprecipitation of QRICH1 led to a more significant enrichment, prompting me to choose a QRICH1 pulldown – SEPHS1 detection strategy.

I showed earlier that standard cell fractionation methods led to QRICH1 protein mislocalisation. It is reasonable to assume that, under such non physiological conditions, endogenous protein associations can be affected alongside subcellular localisation. Thus, I re-designed the standard immunoprecipitation protocol to consist of two steps, namely nuclear isolation with DFEB and nuclear extraction using modified Dignam buffer. Notably, both steps were carried out in presence of Ficoll 400. Under these conditions, I was able to detect an enrichment in SEPHS1 signal in the QRICH1-immunoprecipitated fraction compared to the IgG control (**Figure 5.14B**). These results supported publicly available data on QRICH1-SEPHS1 interaction and suggested that a physical interaction

between the two endogenous proteins could be detected as long as the system was kept in near-physiological conditions.

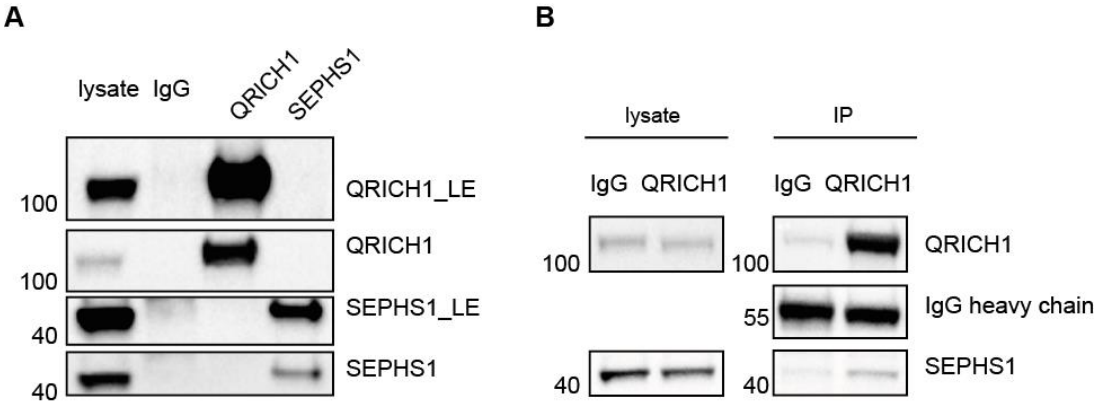


Figure 5.14 QRICH1- SEPHS1 co-immunoprecipitation. **A.** HAP1 cells were lysed using ILB-E. Supernatant was incubated with anti-QRICH1, -SEPHS1 or -IgG antibodies followed by pull-down with Protein A agarose beads. Samples were boiled and supernatants were immunoblotted for proteins of interest. LE = long exposure. Immunoblot representative of n = 2 independent biological replicates **B.** HAP1 cells were lysed using DFEB and modified Dignam nuclear extraction Buffer in presence of Ficoll 400. Extracts were incubated with anti-QRICH1 or -IgG antibodies and precipitated using Protein A beads. After boiling, samples were immunoblotted using the indicated antibodies.

5.2.11 *Transcriptional signature in ΔQRICH1 and ΔSEPHS1 background*

It is well accepted that perturbations, either pharmacological or genetic, can induce specific changes in cellular transcriptional profile. These transcriptional changes, collectively named "signatures", are collected in publicly available databases such as the Connectivity Map (www.clue.io [401]). Analysis of these compendia revealed that treatment with related perturbagens (*e.g.* functionally related genes or drugs targeting the same pathway) induced similar transcriptional signatures [402, 403]. Thus, comparison of the specific transcriptional changes induced by inactivation of a gene of interest with a compendium of perturbational signatures could be used to link the gene to a physiological process, disease, or drug by "guilt-by-association".

As shown previously, both QRICH1 and SEPHS1 affect TNFR1 transcription either directly or indirectly in HAP1 cells (see **Section 5.2.6**). It is reasonable to assume that knockout clones for these two genes present other transcriptional changes in addition to TNFRSF1A downregulation, and analysis of these perturbational signatures could help reconstruct the QRICH1- SEPHS1 pathway. As it could not be excluded that the two proteins played additional independent physiological roles, identifying common differentially regulated genes, would likely give an indication of processes affected by both QRICH1 and SEPHS1.

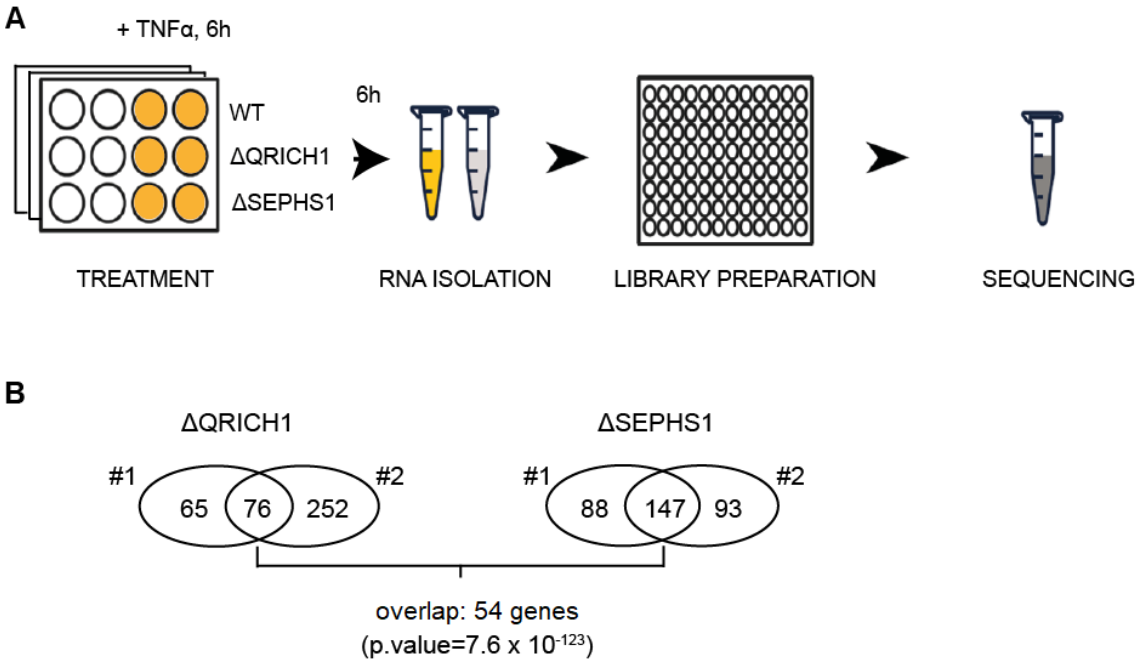


Figure 5.15 RNA sequencing workflow for ΔQRICH1 and ΔSEPHS1 clones. A. Schematic representation of RNA-seq experiment set-up. For each gene, two independent clones were used. RNA from TNFα-treated and untreated samples was isolated and quantified. Multiplexed library was prepared using the Lexogen 3' QuantSeq kit and resulting libraries were sequenced. Image adapted from www.lexogen.com. WT = wild type. **B.** Venn diagram representing size and overlap of gene signatures among independent ΔQRICH1 and ΔSEPHS1 clone pairs. Likelihood that observed overlap was due to chance was calculated with hypergeometric test starting form a theoretical maximum of 42.784 detected transcripts; p value shown. The hypergeometric test was performed with the help of R. Li.

Thus, I performed a global transcriptome analysis by RNA sequencing (RNA-seq), comparing gene expression profiles of two independent knockout clones (*i.e.* obtained with different sgRNAs) for each QRICH1 and SEPHS1 genes using wild type HAP1 cells as controls (**Figure 5.15A**).Independent knockout clones for the same gene displayed a considerable overlap of differentially expressed genes (DEGs) compared to wild type in unstimulated samples (23-62%) (**Figure 5.15B**). I then investigated whether any DEG were shared between QRICH1 and SEPHS1 common genes (76 and 147 genes, respectively) and found 54 concordant genes shared among all four clones (**Table 5.6**, **Figure 5.16A**). As the probability of such overlap occurring by chance is minimal (p value = 7.6×10^{-123}), these data supported once again the notion of a functional relationship among QRICH1 and SEPHS1 (**Figure 5.15B**).

Gene	DE score ΔQRICH1	DE score ΔSEPHS1	Description
COL11A1	-4.2	-3.1	Collagen type XI alpha 1 chain
HAPLN3	-3.2	-3.9	Hyaluronan and proteoglycan link protein 3
TESC	-3	-3.7	Tescalcin
TNFRSF1A	-2.8	-3	TNF receptor superfamily member 1A
FAM127B	-2.8	-2	NA
GALNT5	-2.5	-1.8	Polypeptide N-acetylgalactosaminyltransferase 5
TAL1	-2.3	-2	TAL bHLH transcription factor 1, erythroid differentiation factor
SERPINF1	-2.2	-2.3	Serpin family F member 1
MAP1A	-2.1	-1.8	Microtubule associated protein 1A
PDE4A	-2	-2.3	Phosphodiesterase 4A
CITED1	-2	-2.6	Cbp/p300 interacting transactivator with Glu/Asp rich carboxy-terminal domain 1
SUSD5	-1.9	-3	Sushi domain containing 5
RASL10B	-1.9	-3.6	RAS like family 10 member B

MB21D1	-1.8	-1.4	Mab-21 domain containing 1
PSTPIP2	-1.8	-3.4	Proline-serine-threonine phosphatase interacting protein 2
CYP26B1	-1.7	-1.9	Cytochrome P450 family 26 subfamily B member 1
SLC4A11	-1.7	-2	Solute carrier family 4, member 11
AC091493.2	-1.5	-1.3	NA
SIDT2	-1.4	-1.6	SID1 transmembrane family member 2
CXXC5	-1.4	-1.3	CXXC finger protein 5
SLC2A3	-1.4	-1.4	Solute carrier family 2, member 3
KCNC1	-1.4	-1.6	Potassium voltage-gated channel subfamily C member 1
PPP1R1A	-1.4	-1.2	Protein phosphatase 1 regulatory inhibitor subunit 1A
GPR124	-1.3	-1.9	NA
ABL1	-1.3	-1.7	ABL proto-oncogene 1, non-receptor tyrosine kinase
JAKMIP2	-1.3	-1.3	Janus kinase and microtubule interacting protein 2
SYTL4	-1.3	-2.5	Synaptotagmin like 4
NEIL1	-1.3	-1.1	Nei like DNA glycosylase 1
FBXL7	-1.2	-1.9	F-box and leucine rich repeat protein 7
GNAL	-1.2	-1.9	G protein subunit alpha L
KCNMB2	-1.2	-1.2	Potassium calcium-activated channel subfamily M regulatory beta subunit 2
COL26A1	-1.2	-1.1	Collagen type XXVI alpha 1 chain
MYO5C	-1.2	-1.1	Myosin VC
CENPM	-1.2	-1.1	Centromere protein M
SLC16A3	-1.2	-1.2	Solute carrier family 16, member 3
CCDC106	-1.2	-1.3	Coiled-coil domain containing 106
CACNG7	-1.1	-1.9	Calcium voltage-gated channel auxiliary subunit gamma 7
PCSK5	-1.1	-1	Proprotein convertase subtilisin/kexin type 5
GLRX	-1.1	-1.2	Glutaredoxin

NPTXR	-1.1	-1.1	Neuronal pentraxin receptor
CCDC69	-1.1	-1.4	Coiled-coil domain containing 69
MMP15	-1.1	-1.3	Matrix metallopeptidase 15
MAGI1	-1.1	-0.8	Membrane associated guanylate kinase, WW and PDZ domain containing 1
WSCD1	-1.1	-2.2	WSC domain containing 1
FAN1	-1.1	-1.2	FANCD2 and FANCI associated nuclease 1
NES	-1.1	-0.8	Nestin
GATSL3	-1	-1.1	NA
ITPRIP	-0.9	-0.9	Inositol 1,4,5-trisphosphate receptor interacting protein
PXMP2	-0.9	-2.9	Peroxisomal membrane protein 2
CSRP2BP	-0.9	-1.4	NA
TRIM44	-0.8	-1.3	Tripartite motif containing 44
SYPL2	-0.8	-1	Synaptophysin like 2
MGAT4B	-0.8	-1.2	Mannosyl (alpha-1,3-)-glycoprotein beta-1,4-N-acetylglucosaminyltransferase, isozyme B
CCKBR	0.9	1.1	Cholecystokinin B receptor

Table 5.6 List of 54 differentially expressed genes shared in the four independent ΔQRICH1 and ΔSEPHS1 clones. Differential expression (DE) score is obtained as average of DE scores for two independent ΔQRICH1 and two independent ΔSEPHS1 clones. Gene description was obtained from Biomart.

As expected, TNFRSF1A scored as one of the strongest downregulated genes in QRICH1 and SEPHS1 knockout clones, confirming the previously obtained qRT-PCR data (**Figure 5.16B**). Intriguingly, TNFRSF1A was not the only immune gene present in the dataset. MB21D1, coding for the cytosolic sensor and immune activator cyclic GMP-AMP synthase (CGAS), was also strongly downregulated, suggesting that loss of QRICH1 or SEPHS1 might induce an "immune-dampened" cellular phenotype (**Figure 5.16B**).

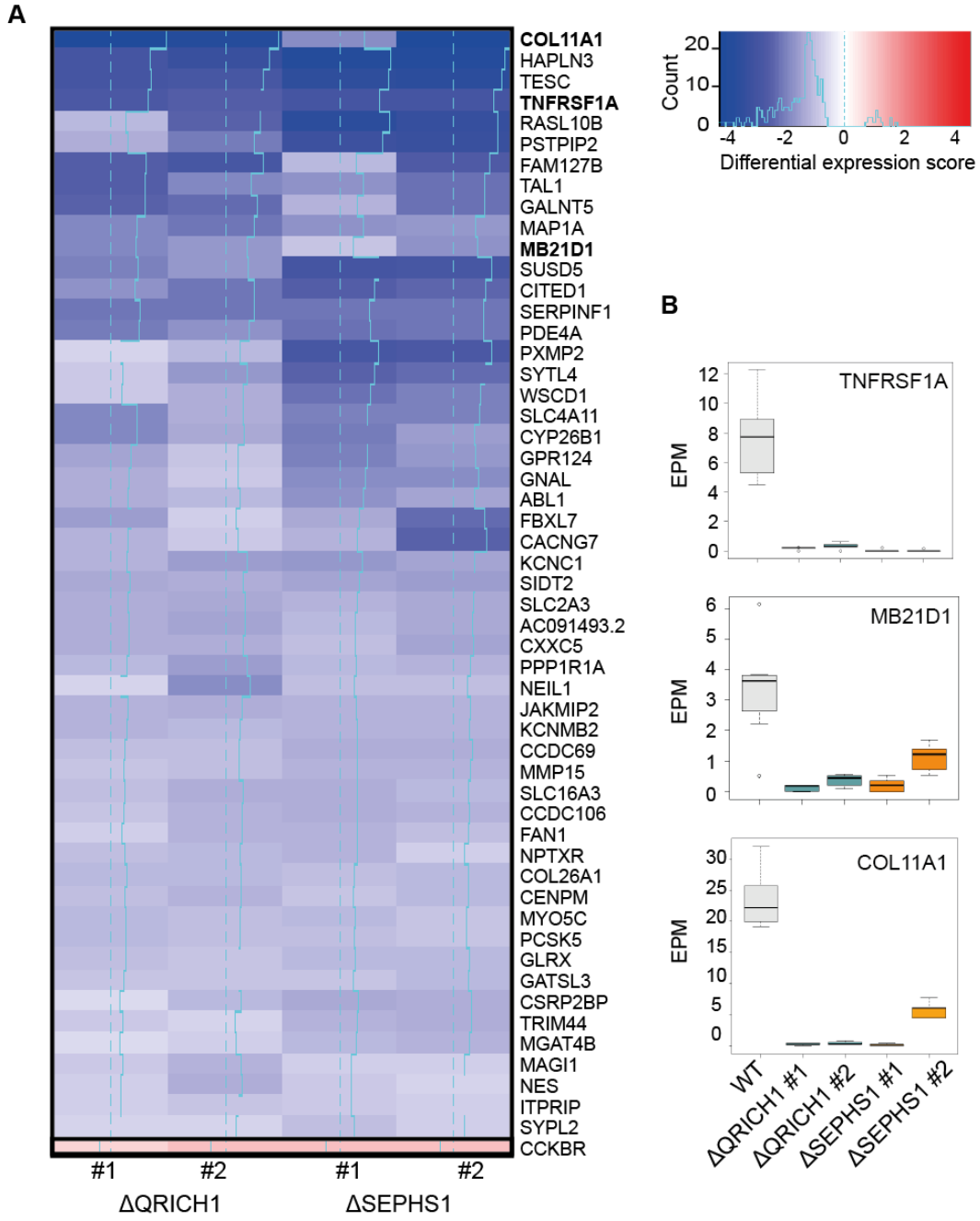


Figure 5.16 Differentially regulated genes in unstimulated ΔQRICH1 and ΔSEPHS1 background. A. Heatmap showing differential expression (DE) score of the 54 common genes in ΔQRICH1 and ΔSEPHS1 clones. Negative differential expression score indicates gene downregulation compared to wild type (WT) control. Rows were re-ordered by average gene DE score; cerulean trace line represents DE score rank within each knockout clone. **B.** Expression levels of TNFRSF1A, MB21D1 and COL11A1 in unstimulated wild type, ΔQRICH1 (blue) and ΔSEPHS1 (orange) clones. Boxes represent the 25th and 75th percentile. Whiskers extend to 1.5 x the interquartile range (IQR).

Of note, the collagen type XI alpha 1 chain (COL11A1) was strongly repressed in all knockout clones (**Figure 5.16B**). This result was in line with QRICH1 knockdown experiment conducted in mouse epiphyseal chondrocytes resulting in downregulation of Col10a1 [369]. Of note Col110a1 orthologue was not expressed at detectable levels in HAP1 cells [148]. Comparison of the common DEGs to published perturbational signatures in Connectivity Map (www.clue.io [401]) and Gene Set Enrichment Analysis tool (GSEA, www.gsea-msigdb.org [404, 405]) failed to identify similar phenotypes (not shown). Overall, the analysis of transcriptional signatures in null-backgrounds indicated a strong functional link between ΔQRICH1 and ΔSEPHS1 clones and validated my previous findings. Additionally, as the great majority of genes shared among independent clones was downregulated (53/54), these results suggested that QRICH1 and SEPHS1 may act as transcriptional activators.

5.2.12 *TNFα-dependent transcriptional response in ΔQRICH1 and ΔSEPHS1 background*

So far, I used IκBα degradation as the only proxy for TNFα-dependent NF-κB activation. To further validate the effect of QRICH1 and SEPHS1 ablation on the NF-κB-mediated pro-inflammatory response, the transcriptional profiles of TNFα-stimulated clones were compared to wild type cells. In a pilot experiment, the dose and length of TNFα treatment were optimized to detect the upregulation of the NF-κB early response NF-κB subunit RELB gene (**Figure 5.17A**). Cells were then stimulated with 25 ng/ml TNFα for 6 hours, prior to RNA isolation and sequencing as described above. As expected, classical TNFα response genes (RELB, TNFα induced protein 3 (TNFAIP3), NF-κB subunit 1 (NFKB1)) failed to be upregulated in ΔQRICH1 and ΔSEPHS1 clones

after TNFα stimulation (**Figure 5.17B**, **C**), indicating that downregulation of TNFR1 completely inhibited the pro-inflammatory response.

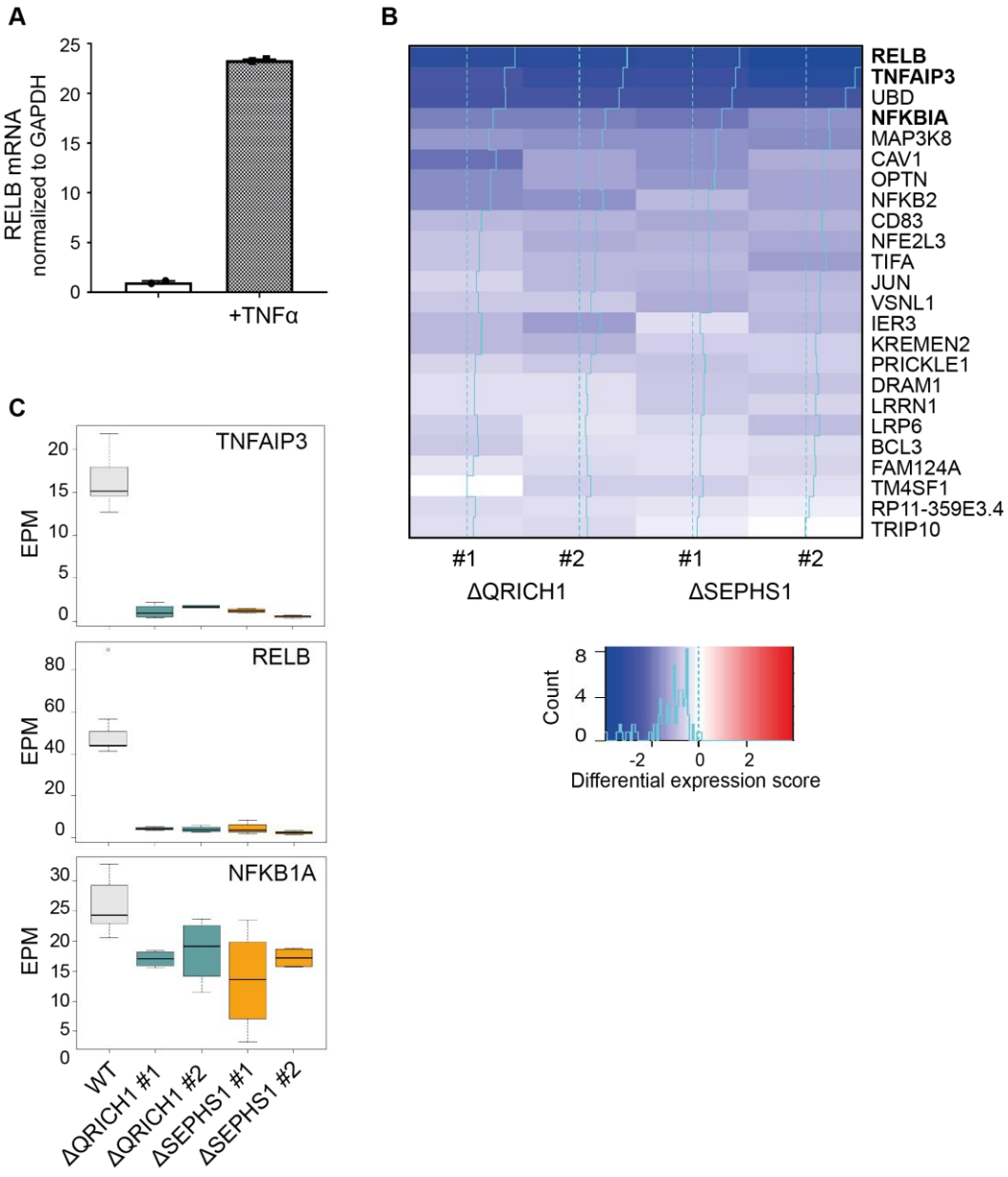


Figure 5.17 Differentially Regulated Genes in TNFα-stimulated ΔQRICH1 and ΔSEPHS1 background. A. Fold increase in expression of the TNFα-response gene RELB after 6 hours treatment with 25 ng/ml TNFα. The same TNFα concentration was used for RNA-seq experiment. **B.** Heatmap showing differential expression scores for 24 genes exclusively scoring as DEGs in stimulated ΔQRICH1 and ΔSEPHS1 clones. Negative differential expression score (DE) indicates gene downregulation compared to TNFα-stimulated wild type (WT) control. Rows were re-ordered by average gene DE score; cerulean trace line represents DE score rank within

each knockout. **C.** mRNA levels for the TNFα-response genes TNFAIP3, RELB and NFKB1 in stimulated wild type, QRICH1 (blue) and SEPHS1 (orange) knockout clones. Boxes represent the 25th and 75th percentile. Whiskers extend to 1.5 x the interquartile range (IQR).

5.2.13 *Validation of ΔQRICH1 phenotype in other human cell lines*

It is well known that intrinsic variability among cell lines often results in differences in regulatory maps for a shared pathway, including the in case of NF-κB [382]. It is reasonable to speculate that such limitations had prevented the characterisation of the phenotype associated with QRICH1/SEPHS1 loss, as only a limited number of cell lines might recapitulate the findings described in this Chapter. To test the generalisability of my findings, QRICH1 knockout pools were generated for several cell lines using CRISPR-Cas9 as described for HAP1 cells and TNFR1 levels measured (**Figure 5.18A**). Preliminary data indicated that the phenotype was recapitulated in breast cancer cell line ZR-75-1, where total TNFR1 protein level decreased, while QRICH1 loss in HCT116 and HeLa cell lines did not induce any significant reduction (**Figure 5.18B**). Quantification of TNFR1 mRNA levels in ZR-75-1 QRICH1 knockout pools showed a decrease compared to wild type cells (**Figure 5.18C**). Of note, all three tested cell lines are at least diploid for TNFRSF1A and thus knockout efficiency is expected to be lower compared to haploid HAP1 cells. I reasoned that an analysis of the transcriptional signature derived from a confirmed QRICH1 knockout clone in ZR-75-1 cells would confirm this initial observation and help refine the 54-gene QRICH1-SEPHS1 transcriptional signature by excluding HAP1 cells-specific effects. However, despite my efforts, it was not possible to generate single clones from slow growing ZR-75-1 cells (doubling time 80 hours). Overall, these preliminary observations indicated that the QRICH1 and SEPHS1 TNFR1-related phenotype was restricted to specific cell models.

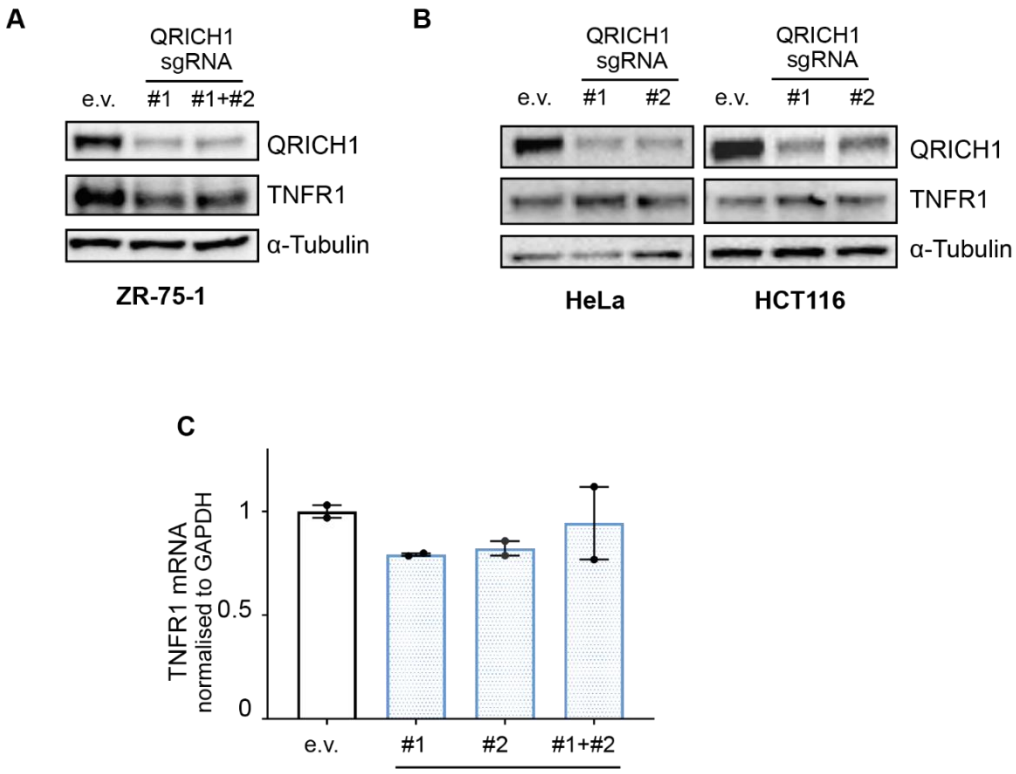


Figure 5.18 QRICH1-dependent TNFR1 downregulation in other cell lines. A. ZR-75-1, **B.** HeLa and HCT116 cell lines were transfected either with empty pLentiCRISPR-v2 vector (e.v.) or a vector bearing an sgRNA targeting QRICH1. Obtained cell pools were lysed and immunoblotted using the indicated antibodies. Immunoblots for HeLa and HCT116 representative of n = 2 independent biological replicates**. C.** Total RNA was isolated from ZR-75-1 QRICH1 knockout pools. TNFR1 mRNA was quantified via qRT-PCR.

5.2.14 *QRICH1 reconstitution*

Finally, I investigated whether TNFR1 expression and functionality could be rescued by QRICH1 (Q and Q_{FLAG}) reconstitution in ΔQRICH1 knockout cells. In addition, I tested QRICH1 mutants lacking the N-terminal CARD domain (Q_{CARD}) or NLS sequence (Q_{NLS}) to investigate whether presence of the CARD domain or nuclear localisation were required for signal reconstitution (see **Appendix 8.1.2**).

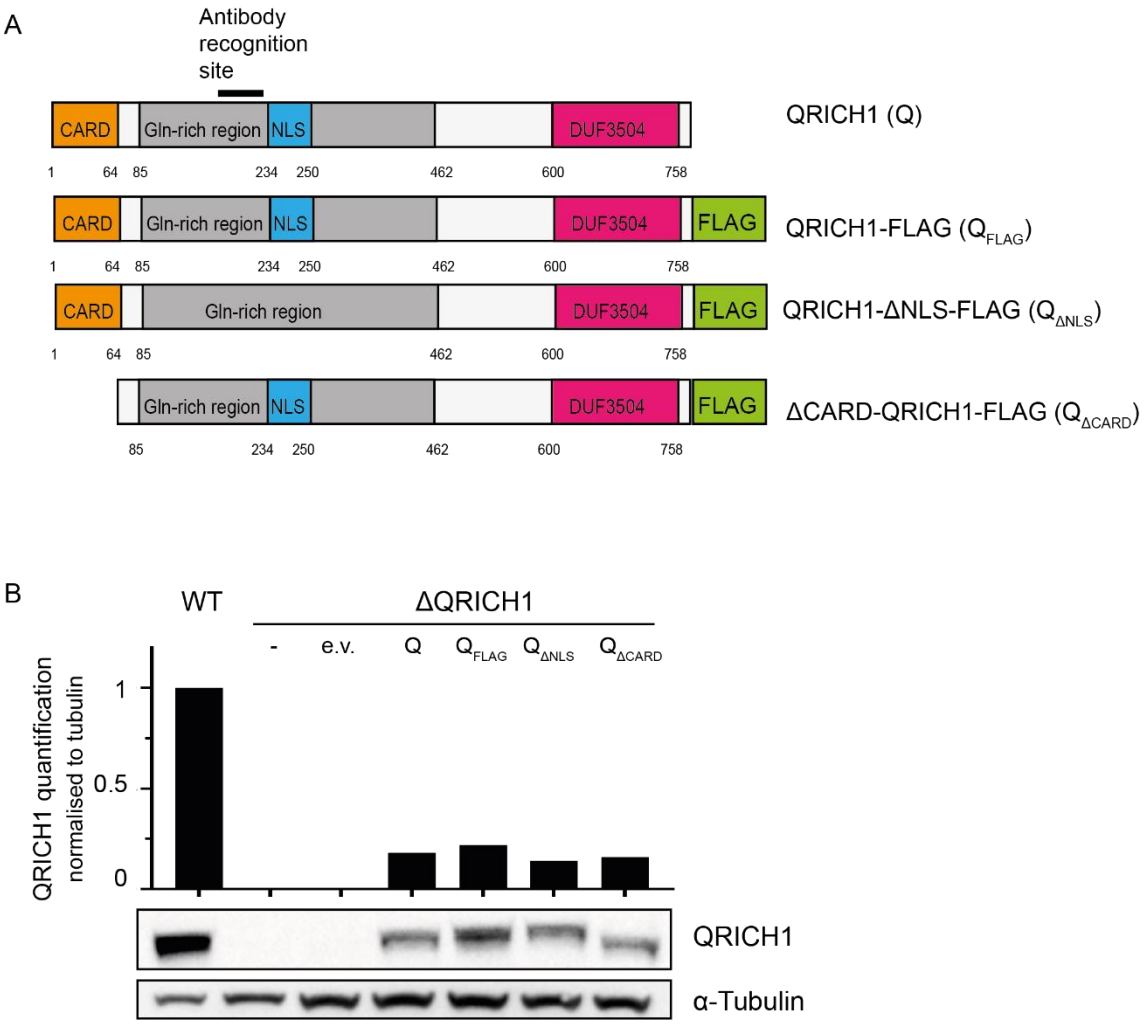


Figure 5.19 QRICH1 full length and mutant reconstitution in ΔQRICH1 HAP1 cells. **A.** Schematic representation of engineered cDNA constructs of the QRICH1 gene. NLS, nuclear localisation sequence. **B.** ΔQRICH1 HAP1 cells were transiently transfected with pLenti vectors containing QRICH1 cDNA constructs described in (**A.**) or an empty pLentiCRISPR-v2 (e.v.) control. After puromycin selection, lysates were collected and immunoblotted for QRICH1 expression. QRICH1 levels are normalised to α-Tubulin loading control and displayed relative to wild type (WT) HAP1 cells. Quantification of band intensity was performed using Image J. Immunoblot representative of n = 2 independent biological replicates.

Q_{CARD} was obtained by deleting the 64 N-terminal AA corresponding to the CARD domain (InterPro, www.ebi.ac.uk/interpro [406]), while Q_{NLS} was generated by deleting the first basic AA patch (2 Arg residues) of the bipartite nuclear localisation sequence [407]. ΔQRICH1 cells were transiently transfected with the constructs in **Figure 5.19A** and

underwent antibiotic selection. A low, but consistent level of reconstitution (14-22%) was detected for all QRICH1 constructs, allowing a direct comparison of functional effects (**Figure 5.19B**). As expected, bands relative to FLAG-tagged constructs migrated at a slightly higher molecular weight than untagged QRICH1 protein while the Q_{CARD} construct, with a 64 AA deletion, ran lower than the other (near-) full-length protein versions.

The subcellular localisation of exogenous QRICH1 protein was tested in reconstituted cells. Surprisingly, immunofluorescence results indicated sub-optimal transfection efficiency even after antibiotic selection, with only a fraction of HAP1 cells displaying expression of QRICH1 (**Figure 5.20A**). Disappointingly, the Q_{NLS} construct retained its nuclear localisation, suggesting that the nuclear localisation sequence was still functional or that other non-annotated NLS(s) existed in the protein, and was excluded from the following experiments. mRNA from QRICH1-reconstituted cells in basal conditions and in presence of TNFα stimulation was isolated and quantified for TNFR1 and TNFα-response gene RELB. Preliminary data indicated that full length QRICH1 reconstitution led to partial recovery of TNFR1 expression (**Figure 5.20B**). In contrast, no increase in TNFR1 mRNA was detected for the CARD-deleted QRICH1 variant.

In agreement with these results, TNFα addition to QRICH1-reconstituted cells resulted in an increase in RELB transcripts, while this increase was lost in Q_{CARD} expressing cells (**Figure 5.20C**). Collectively, these results further reiterated the essential role of QRICH1 in transcriptional regulation of TNFR1 and further suggest that the QRICH1 CARD domain might be required.

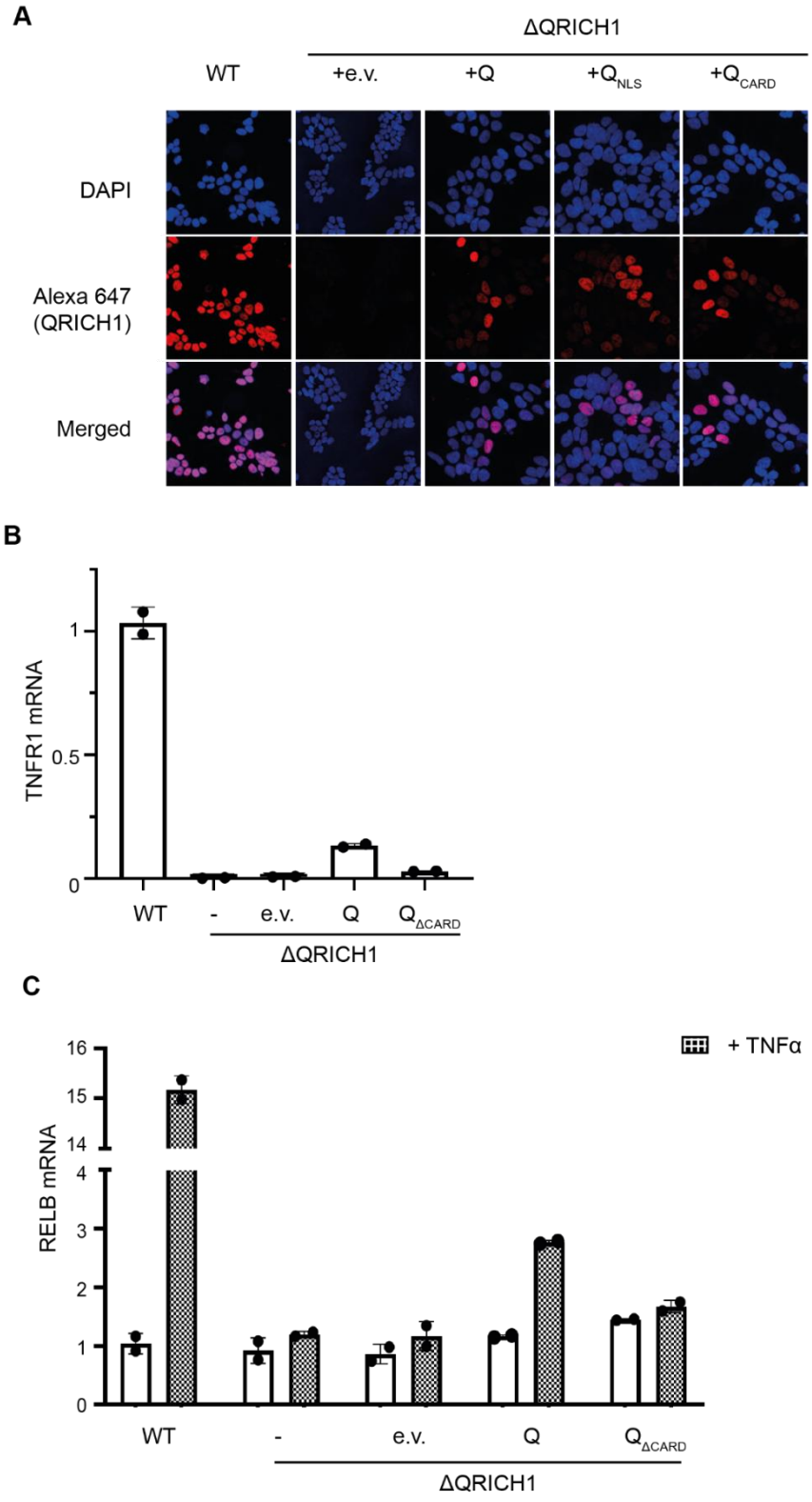


Figure 5.20 Analysis of TNFR1 expression and NF-κB activation in reconstituted ΔQRICH1 cells. A. Reconstituted cells were analysed by immunofluorescence for QRICH1 expression and localisation. Anti-QRICH1 antibody was detected with Alexa647, DAPI was used

to stain nuclei. **B.** Total RNA was isolated from wild type, ΔQRICH1 and reconstituted ΔQRICH1 cells either in basal conditions or after 6 hours treatment with 10 ng/ml TNFα. mRNA levels for TNFR1 in unstimulated samples and **C.** RELB upregulation after TNFα treatment were quantified. TNFR1 mRNA in reconstituted cells was measured in two independent biological replicates. Stimulation on reconstituted ΔQRICH1 was performed only once and is thus not fully conclusive. WT = wild type. Immunofluorescence and qRT -PCR data for QRICH1-FLAG were in line with QRICH1 (Q_{FLAG} not shown).

5.3 Discussion

By employing a dual forward genetic screening approach in HAP1 cells, this study uncovered novel genetic regulators that act at transcriptional level to govern TNF receptor 1 expression. Ablation of QRICH1, SEPHS1 and ZNF652 resulted in strong TNFR1 transcriptional repression and initial observations indicate that the QRICH1 CARD domain might be required for this process. Furthermore, biochemical data point to a functional interaction among QRICH1 and SEPHS1 driving physiological effects beside TNFR1 regulation and suggest the two proteins might act together in a complex. Following my observations, two alternative models can be suggested: the three proteins could act directly as transcriptional activators of TNFRSF1A (**Figure 5.21A**) or they could block/sequester an intrinsic transcriptional repressor complex (**Figure 5.21B**).

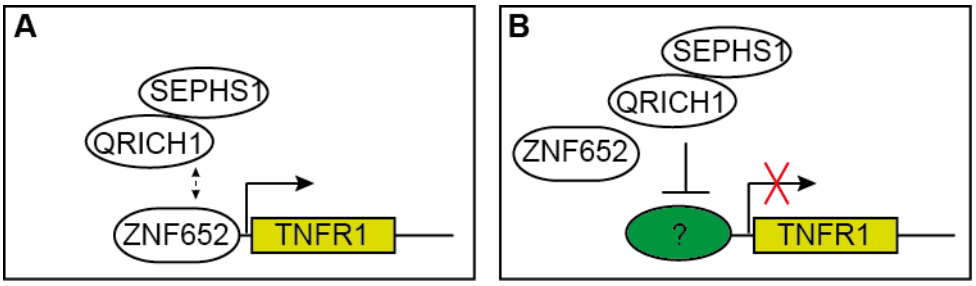


Figure 5.21 Schematic representation of two possible mechanisms of QRICH1-SEPHS1- and ZNF652-dependent TNFRSF1A transcriptional control.

5.3.1 *QRICH1, SEPHS1 and ZNF652*

QRICH1 is a largely uncharacterized member of the CARD-containing protein family, whose components are known to be involved in inflammatory phenotypes and innate immune response. One report identified QRICH1 as co-immunoprecipitating with membrane TNFR1 in absence of TNFα stimulation [408]. This result was in contrast with

both *in silico* predictions and immunofluorescence data showing nuclear localisation of QRICH1 in multiple cell lines (Human Protein Atlas, www.proteinatlas.org [172,364]). In this Chapter, I demonstrated how physiological QRICH1 localisation was lost by conventional subcellular fractionation protocols, which caused protein leakage into the cytoplasm (**Figure 5.13C**). It is unknown whether this might be part of a physiological translocation in response to hypotonic stress or an artefact caused by the loss of subcellular compartmentalisation [398, 409]. It is tempting to speculate that QRICH1 mislocalisation caused spurious CARD domain-mediated binding to other death-domains-containing proteins naturally located in the cytoplasm. Disappointingly, the reconstitution experiment set-up to test the requirement for QRICH1 nuclear localisation failed as the NLS mutant protein was retained in the nucleus.

Despite Gene Ontology annotation of QRICH1 as DNA-binding protein with transcriptional activity, it is unlikely that TNFR1 regulation is achieved through QRICH1 directly binding DNA. In fact, QRICH1's DNA binding molecular function was inferred phylogenetically from the *Drosophila melanogaster* ancestor gene "without children" (woc) (FlyBase, www.flybase.org [410]) which contains both an MYM-type zinc finger DNA binding domain and the uncharacterised DUF3504 domain, only the latter of which was inherited by QRICH1 [411]. However, multiple proteins belonging to the DD-fold superfamily were found to be involved in the transcriptional regulation of immune-related genes [412]. Although the role of DD-fold in mediating transcription is not clear, functional studies performed with mutant NLR Family CARD domain containing 5 (NLRC5) protein indicated that the putative CARD domain was required for both nuclear localisation and transcriptional activation [413]. In line with this finding, preliminary data

presented in this Chapter suggested that CARD domain is required for QRICH1-mediated transcriptional activation of TNFR1.

While SEPHS1 is thought to belong to a family of selenium biosynthesis genes, screen results for genetic regulators of TNFR1 surface expression indicated that SEPHS1 and SEPHS2 had divergent functions, with only the latter scoring together with genes of the selenium biosynthesis pathway (**Figure 5.3**). This is in agreement with reports of SEPHS1 lacking selenophosphate synthetase activity [373, 374] and my own data showing that loss of QRICH1- (and possibly SEPHS1-) dependent regulation of TNFR1 did not affect the influence of selenium biosynthesis genes on receptor surface presentation (

Figure 5.10).

Two previous screens investigating innate immune regulation reported a role for SEPHS1. An RNAi screen for NOD2/NF-κB-dependent production of interleukin 8 (IL-8) in human cells identified SEPHS1 as a negative signal regulator, although the data were confounded by increased cell proliferation of SEPHS1 knockout cells [414]. In a series of *in vivo* CRISPR-Cas9 screens, tumour immune evasion was shown to be augmented by the loss of the TNFR1 signalling pathway [415]. Interestingly, in two out of three animals tested, analysis of knockout tumour cells escaping $CD8^+$ T-cell-mediated killing activity found Sephs1 among the top four enriched sgRNAs. This result was in line with findings presented here (*i.e.* SEPHS1 loss decreasing TNFR1 signalling), although the published study did not clarify whether a proliferation control was used. While I did not specifically test cell proliferation rates upon SEPHS1 loss, the forward genetic screening approach described here measured relative enrichment of independent insertions between two populations in the same screen (MI) and thus was internally controlled for proliferation bias.

Alone of the three novel TNFR1 regulator identified in this study, SEPHS1 contains a druggable pocket which could be targeted by a small molecule inhibitor [416]. This could be of potential interest in the future for therapeutic modulation of QRICH1-SEPHS1/TNFR1 axis. However, as no clear enzymatic activity was described for SEPHS1, "lead discovery" efforts would first need to investigate whether targeting the protein druggable pocket would phenocopy SEPHS1 loss-of-function.

Two independent ChIP-Seq studies reported ZNF652 binding to the TNFRSF1A promoter (ENCODE, www.encodeproject.org [417,378]) suggesting a model in which the zinc-finger protein would bind to the TNFRSF1A promoter sequence and mediate transcriptional activation in presence of QRICH1 and SEPHS1. In agreement with this, I identified QRICH1-dependent reduction of TNFR1 in the ZR-75-1 breast cancer cell line where ZNF652 binding to TNFRSF1A promoter was first reported [378]. However, genotype-validated ΔZNF652 HAP1 clones displayed a weaker transcriptional effect, compared to QRICH1 and SEPHS1 (**Figure 5.8** and **Figure 5.9**) which is in contrast with the hypothesis of ZNF652 functioning as "gatekeeper" for QRICH1/SEPHS1-mediated TNFR1 regulation (**Figure 5.21**). If the model is indeed correct, there are two possible explanations for such discrepancies. First, due to the unavailability of a reliable commercial antibody, it was not possible to validate ΔZNF652 clones at protein level and thus, the generation of mutant, shorter isoforms retaining DNA binding activity cannot be excluded. In fact, generation of partial loss-of-function isoforms using CRISPR/Cas9 was recently reported [418, 419]. Secondly, a ZNF652 paralogue (ZNF651/ZBTB47) which shares the same target DNA binding site, had been described [420]. It is possible to hypothesize that ΔZNF652 clonal expansion selected for concomitant high expression of its paralogue, resulting in a weaker TNFR1 suppression phenotype. Further studies will

require a more extensive validation of ZNF652 knockout cells by obtaining non-commercially available antibodies from the academic lab where the protein was first characterised and by testing the expression levels of genes possibly complementing ZNF652 loss.

5.3.2 *Other regulatory mechanisms*

In addition to identifying QRICH1, SEPHS1 and ZNF652, the screening approach uncovered other putative TNFR1 regulatory mechanisms. For example, a role in general translational repression had been previously described for the 4EHP-GIGYF2 complex, composed of eukaryotic translation initiation factor EIF4E2 (EIF4E2), GRB10-interacting GYF protein 2 (GIGYF2) and zinc-finger protein 598 (ZNF598) [421]. Interestingly, EIF4E2 and GIGYF2 belonged to the list of genes affecting both TNFR1 level and downstream NF-κB activation (**Table 5.4**). Loss of either gene in the complex resulted in upregulation of TNFR1 indicating that the complex might play a role in the translational initiation of either the receptor itself or one of its positive regulators. Knockout studies using ribosome profiling techniques could identify the protein responsible for the 4EHP-GIGYF2 complex effect on TNFR1.

Less clear is the role CARNMT1 in TNFR1 regulation. Similar to QRICH1, SEPHS1 and ZNF652, ablation of CARNMT1 caused a decrease in TNFR1 levels. CARNMT1 converts carnosine to anserine, a dipeptide abundant in brain and skeletal muscle [422]. L-carnosine was reported to have anti-oxidative and anti-inflammatory properties through suppression of NF-κB both *in vitro* and in clinical settings [423, 424]. It is tempting to speculate that disrupting the cellular carnosine/anserine balance affects pro-

inflammatory signalling, however additional studies are needed to clarify the connection with TNFR1.

Additionally, haploid genetic screen for TNFR1 surface presentation uncovered a role for the selenium biosynthetic pathway (**Figure 5.4**). Selenium-containing proteins are broadly classified as anti-oxidants and include, among others, glutathione peroxidases and thioredoxin reductases [425]. Through the action of selenium-containing proteins, selenium levels can affect activation, differentiation, and proliferation of immune cells (reviewed in [426]). Alteration of the reducing cellular environment was already linked to the NF-κB pathway via modification of the disulphide bond equilibrium in the transcription factor p50 subunit [427]. More recently, defective disulphide-mediated oligomerisation within TNFR1 cysteine-rich domain was shown to alter ER retention and signalling of the receptor [428]. It is possible that the negative regulatory role of selenium biosynthetic pathway on TNFR1 is linked to altered anti-oxidant levels in the cell, affecting receptor folding and oligomerisation. Along these lines, a study in oesophageal carcinoma showed that knockout of glutathione peroxidase 7 (GPX7) promoted TNFR1 protein degradation (GPX7 does not contain glutathione-binding selenocysteine) [429].

As increase of TNFR1 levels at the cell membrane in mutants for selenoprotein biosynthesis pathway was not translated into increased pathway activation, it is possible to speculate that additional surface receptor does not augment NF-κB response (*i.e.* TNFR1 is not the limiting factor for the driving downstream pro-inflammatory response) or, alternatively, that the surplus of TNFR1 on the surface is not functional (*e.g.* incorrectly folded or not matured by proteolytic cleavage), but still recognised by the cognate antibody. As selenoprotein expression is generally regulated by selenium

bioavailability in the body or in the culture medium [430], it would be interesting to test: 1.) whether manipulation of selenium levels could affect TNFR1 expression, 2.) which cell types would display this type of response and 3.) whether selenium sensitivity is accompanied by alteration in reactive oxygen species levels. However, HAP1 cells are not a suitable model for such experiments, as selenium, in the form of sodium selenite, is included in the formulation of HAP1 cells optimal growth medium IMDM.

5.3.3 *Future perspectives*

In order to fully understand the regulatory relationship between TNFR1 signalling and QRICH1, SEPHS1 and ZNF652, a number of questions remain to be addressed. First, do QRICH1, SEPHS1 and ZNF652 block transcription by interacting directly with the DNA (alone or with other co-factors) or as part of a signalling cascade? To this end, mass spectrometry analysis of QRICH1 immunoprecipitates could validate the interaction with SEPHS1 (**Figure 5.14**) and identify additional co-factors. Furthermore, a targeted ChIP experiment on the TNFR1 promoter could reveal unequivocally whether QRICH1, SEPHS1 and ZNF652 indeed form a complex that directly regulates transcription and if so, identify the binding sequence.

Secondly, what are the physiological implications of this transcriptional repression mechanism of TNF receptor 1 and how does the regulatory circuitry upstream of QRICH1 and SEPHS1 transmit the relevant environmental cues? Unfortunately, comparison of transcriptional signatures associated with the ablation of either gene with public datasets failed to provide any indication on related cellular phenotypes and upstream regulatory signalling. Further investigation in this direction could analyse the full list of genes concomitantly regulated by both QRICH1 and SEPHS1 one-by-one to identify a gene

candidate that could be used as a readout in further genetic screening. By performing two companion screens for the selected gene candidate in wild type and ΔQRICH1 cells, additional components of the QRICH1 functional module could be uncovered.

Finally, what is the molecular basis for the restriction of QRICH1, SEPHS1 and ZNF652 regulation of TNFR1 to a subset of cell lines? It is possible that the variable response across cell lines is the result of intrinsic differences at proteomic and transcriptomic level. Compared to other breast cancer cell lines, ZR-75-1 cells contain six copies of TNFRSF1A and express high levels of TNF receptor 1 protein [431]. Additionally, DepMap data indicate that ZR-75-1 cells viability is strongly affected by QRICH1 and SEPHS1 knockout (www.depmap.org [90]). Thus, is tempting to speculate that the ZR-75-1 response is linked to addiction to TNFR1 and cell lines with similar profiles (*i.e.* sensitivity to loss of QRICH1 and SEPHS1 and high TNFR1 levels) could be prioritised in future testing. Alternatively, to identify cell-type specific vulnerabilities to QRICH1-dependent TNFR1 regulation, CRISPR/Cas9 screens could be performed in non-responsive cells (*e.g.* HCT116 or HeLa, **Figure 5.18**). In this context, it would be possible to identify genes that buffer the effect of QRICH1 loss on TNFR1 levels.

Of the novel TNFR1 regulators, only QRICH1 was found to be mutated in humans. The resulting phenotype was linked with developmental delay and cognitive impairment in a syndrome named Ververi-Brady [368]. While a number of downregulated genes in ΔQRICH1 cells were possibly in agreement with the human phenotype (*e.g.* coding for the extracellular structural proteins COL11A1 and HAPLN3 or brain-enriched genes like MAP1A and KCNC1), no immune phenotype was described for the five human patients [368, 369].

Overall, this Chapter described a novel mechanism regulating TNFR1 transcription in HAP1 cells by the action of three poorly described proteins, CARD-containing QRICH1, the selenophosphate synthetase SEPHS1 and the zinc-finger protein ZNF652. Biochemical and genomics data indicated that QRICH1 and SEPHS1 constitute a functional module and are likely to interact. These findings are extremely relevant, possibly indicating a novel therapeutic avenue to treat auto-immune pathologies characterised by elevated TNFα levels, possibly through the blockade of SEPHS1 druggable pocket. However, further studies are required to elucidate the mechanism of action of the QRICH1-SEPHS1-ZNF652 axis and its significance for TNFR1 modulation and beyond.

Chapter 6: **Final discussion: the future of genetic screening technologies**

Since their inception in the 1930s, genetic screening technologies have benefitted from massive advances in the precision and throughput of molecular manipulation tools. From investigation of genetic determinants of phenotypes at whole organism level, the field moved to interrogate flexible *in vitro* models such as *Saccharomyces cerevisiae* and, finally, mammalian cell cultures. The reduction in the complexity of model systems was compensated by the ability to finely control and manipulate the host, and the field was rewarded by detailed understanding of a variety of subcellular phenotypes.

The trade-off between feasibility of genetic manipulation and interrogable phenotypic complexity is at the core of functional genomics and its reconciliation will constitute the field's main challenge in the next years. Following new and sensitive approaches to identify functionally relevant phenotypes, as described in this thesis, I foresee further technical advances in the ability to define and interrogate complex cell states. In particular, I expect two driving forces to play a major role in the field's evolution in coming years:

- Definition of biologically relevant, granular phenotypes and
- Capability to test multimodal cell states in high-throughput.

6.1 **Towards complex phenotypes**

Until recently, the pooled screening format was limited to positive and negative selection. In 2015, screening readouts based on the relative level of a fluorescent selection

marker within a mutant population were first introduced and constitute the major focus of this thesis. The screenable space significantly expanded, allowing sensitive and specific interrogation of a number of signalling pathways through measurement of a marker protein abundance and/or the levels of its post-translational modifications.

This approach can offer valuable translational insight when applied to a molecular feature known to be driving a cellular phenotype (*e.g.* cancer driver mutations or monogenic diseases). Nevertheless, these examples constitute exceptions in biology, as characteristics defining a cell state in disease and development can rarely be reduced to the influence of a single genetic component. In this sense, genetic screens tracking a single parameter can be grouped together with cell fitness as employing "low-complexity" readouts [382].

To truly realise the ambition to link phenotype-to-genotype, complex phenotypes first need to be deconvoluted in sets of manageable and measurable features. Thanks to many decades of technical advances, today's molecular toolbox encompasses a number of experimental and computational methods to generate global profiles of cell states [75, 432]. In particular, the advances in single cell transcriptomics, epigenomics, and imaging generated a wealth of complex and granular information [433-435]. The challenge now resides in "sifting" through the data and combining multimodal measurements at single cell level to identify minimal marker combinations that recapitulate a given phenotype.

While this constitutes a daunting task for a human operator, the use of newly developed data-analysis techniques to find patterns in complex data renders the challenge approachable [436]. The branch of computer science that analyses association among features in a dataset to build predictive outcome models is known as Machine Learning (ML). ML's inherent ability to catalogue and integrate complex molecular data to define

new phenotypes is proving disruptive in the biomedical field when applied to problems such as characterisation of transcriptional networks [437], metabolic profiling of bacterial communities [438] or protein binding site prediction [439]. In general, ML workflows re comprised of four phases: processing an input dataset, extracting features, training a statistical model on such features, and finally using the model to make a prediction on new data. The successful interplay between ML and biology was fostered by the availability of large, high quality "-omics" datasets [436]. With increasing frequency, the data are generated by dedicated consortia that also develop standardisation methods and share their raw measurements with the wider scientific community for re-analysis (reviewed in [440]). As ML algorithms are trained on a set of experimental results, the quality, annotation, and reproducibility of input data are of pivotal importance (synthesised in the famous "garbage-in, garbage out" concept) [436].

When applied to the challenge at hand, ML algorithms could play a crucial role in two ways. First by identification of a number of subcellular markers that set apart healthy and diseased tissue and/or cells without any *a priori* knowledge. Secondly, using the identified subcellular markers to reconstruct a "minimal signature" that would recapitulate the variability of a complex phenotype using a small set of traits. Early examples of ML applied to biological network organisation successfully recognised a subgroup of features whose level of connectivity set apart healthy and disease cell states and identified tissue-specific differences in genetic network interactions [441, 442].

The process of combining different types of subcellular features might offer a new concept of "phenotype", likely requiring simultaneous screening for different types of phenotypic traits (*e.g.* morphological, transcriptional, and proteomic characteristics). In

this scenario, screening techniques capable of handling multi-parametric phenotypes are required. Advances in this field are discussed the next section.

6.2 High-throughput genetic screening for multi-modal phenotypes

Recent proof-of-concept studies reported the coupling of pooled genetic screens with detection of highly complex phenotypes such as transcriptomics and high-content imaging. Despite the sub-genome complexity of the analysed mutagenized pools, these new approaches provide a framework for the development of high-throughput multi-modal phenotypic screens.

6.2.1 *Single cell transcriptomics*

In 2016, four groups independently developed methodologies to couple transcriptome analysis of single cell RNA sequencing (scRNA-seq) to CRISPR/Cas9 screens [443-446]. In these approaches, gene inactivation is linked with an "high-dimensional" phenotype, *i.e.* global transcriptome changes. The common underlying technical innovation was the detection of sgRNAs by deep sequencing in parallel with the transcriptome. This was achieved, for instance, by concomitant expression of a polyA-mRNA barcode for each sgRNA [443]. Besides the obvious increase in the number of readouts, this application offers the additional advantage of tracking cell-to-cell differences in a knockout subpopulation, thus revealing interactions likely hidden at population level [65, 447]. In a study by Adamson *et al.*, 80 genes involved in the unfolded protein response (UPR) were identified in an initial CRISPR/Cas9 screen and interrogated using scRNA-seq screening. The analysis of the transcriptomes of approximately 65.000

single cells successfully assigned each of the 80 query genes to one or more of the three UPR pathway branches [443].

In another recent report, the detection of CRISPR-mediated perturbations was coupled to the measurement of single cell transcriptomes and with spatial information to study the acquisition of invasive properties by epithelial cells [448]. In particular, the researchers employed a scRNA-seq CRISPR/Cas9 screen to study the effect of mutations on a cell's invasiveness in an *in vitro* epithelial-to-mesenchymal transition (EMT) assay. Single cell transcriptome data were gathered for individual mutants at different radii from the centre, representing different stages of invasiveness in the EMT continuum. The results showed that knockout cells for certain receptors and transcription factors accumulated at different stages in the EMT program, suggesting the existence of "checkpoints" driving the transcriptional continuum. This study suggested a new way to interpret cellular heterogeneity where effects of genetic perturbations could be simultaneously studied across cell sub-populations.

In the most advanced attempt to date, Mimitou *et al.* described the concurrent quantification of proteins and transcripts in a CRISPR-perturbed pool [449]. First reported in 2017, Cellular Indexing of Transcriptomes and Epitopes by sequencing (CITE-Seq) couples antigen detection using DNA-barcoded antibodies with single cell transcriptome analysis, whereby antibody binding can also be read out by sequencing [450, 451]. The expanded CRISPR-compatible CITE-Seq (ECCITE-Seq) method allowed the simultaneous analysis of CRISPR-induced perturbations of 13 genes and linked the loss-of-function genotype with proteomic and transcriptomic single cells characterisation [449].

Although yielding encouraging results, analysis of multi-modal phenotypes at single cell level in perturbed cell pools presents consistent challenges. scRNA-seq data is

inherently noisy (not every transcript will be captured in every cell), and only approximately 80% of cells containing an sgRNA also carry the corresponding gene inactivation [447]. Analysis of scRNA-seq data thus requires a laboratory to have the computational expertise to develop custom analytical methods and robustly process the data. Additionally, all the described methods coupling sequencing readouts with genetic perturbations require analysis of the whole mutant pool. Phenotypes of interest can thus only be reconstructed though a downstream computational analysis, instead of being robustly selected for *a priori* as it happens in fitness and FACS-based screens. This translates into the need to screen a high number of mutant cells, rendering multi-modal approaches costly and, so far, limiting the number of genes that can be studied.

6.2.2 *High-content imaging in pooled screening format*

In 2017 two proof-of-concept studies demonstrated the feasibility of high-throughput screening with pooled genetic libraries and image-based phenotypic characterisation [452, 453]. Both approaches transfected libraries of barcoded genetic variants into *Escherichia coli* and interrogated the system for genetic determinants of growth [453] or brightness and photostability of a fluorescent protein [452]. Genotype –phenotype links were analysed *in situ* through identification of the barcode sequence using sequential rounds of multiplexed fluorescence in situ hybridisation (FISH). This solution first bridged the gap between the scalability of pooled screening and phenotypic complexity captured by an image-based approach, allowing the identification of the precise perturbation of individual cells in a given image. Moreover, loading of pooled *Escherichia coli* libraries onto a microfluidic device such that each strain occupies a spatially separate “trap”, allowed researchers to follow the phenotype of interest over time

[454]. However, these hybridisation-based detection methods showed limitations in terms of throughput, requiring high-magnification imaging (60X) which renders them unsuitable for mammalian cell screening applications.

In a recent report describing the first example of high-content imaging applied to pooled screens in mammalian cells, the throughput bottleneck was circumvented by determining sgRNA-coupled barcodes using *in situ* sequencing [382]. The protocol for *in situ* sequencing allows for sequencing of RNA in morphologically intact fixed cells using of an epifluorescence microscope and is, as such, compatible with high-content microscopy analysis [455]. Compared to the previously adopted FISH protocol to detect individual cell barcodes, *in situ* sequencing offered improvements in terms of synthesis cost of annealed barcodes and the magnification required to detect fluorescence signal. The ability to couple dynamic, spatially-resolved information to a genetic perturbation was used to detect modifiers of p65 nuclear translocation in a pool of 3.063 sgRNAs targeting approximately 1.000 genes [382]. Despite the importance of the study, this advance in phenotype granularity is still far from a genome-wide scale, confirming that optical pooled screens are currently more suitable as secondary screening tool. This approach is however extremely promising for integrating morphological information with other -omics readouts and phenotypes.

Collectively, the approaches developed in the last five years paved the way to the simultaneous investigation of different types of readouts at single cell level (e.g. transcriptomics together with a protein marker) and moved beyond the typical arrayed format for high-content screening applications. In the coming years, I expect further advancements in the throughput of these technologies and a general drop in costs, driven by single cell sequencing becoming more affordable. However, the success of these

applications in unveiling new biology will be inextricably linked with the definition of biologically relevant, granular phenotypes that cannot be investigated with cheaper, simpler approaches.

Chapter 7: **Bibliography**

1. Schwartz, S. The Differential Concept of the Gene: Past and Present, in *The Concept of the Gene in Development and Evolution: Historical and Epistemological Perspectives* (Cambridge University Press, Cambridge; 2000).
2. Ewing, B. & Green, P. Analysis of expressed sequence tags indicates 35,000 human genes. *Nat Genet* **25**, 232-234 (2000).
3. Goffeau, A. *et al.* Life with 6000 genes. *Science* **274**, 546, 563-547 (1996).
4. Adams, M.D. *et al.* The genome sequence of Drosophila melanogaster. *Science* **287**, 2185-2195 (2000).
5. Consortium, C.e.S. Genome sequence of the nematode C. elegans: a platform for investigating biology. *Science* **282**, 2012-2018 (1998).
6. Salzberg, S.L. Open questions: How many genes do we have? *BMC Biol* **16**, 94 (2018).
7. Venter, J.C. *et al.* The sequence of the human genome. *Science* **291**, 1304-1351 (2001).
8. Lander, E.S. *et al.* Initial sequencing and analysis of the human genome. *Nature* **409**, 860-921 (2001).
9. International Human Genome Sequencing, C. Finishing the euchromatic sequence of the human genome. *Nature* **431**, 931-945 (2004).
10. Ochsner, S.A. *et al.* The Signaling Pathways Project, an integrated 'omics knowledgebase for mammalian cellular signaling pathways. *Sci Data* **6**, 252 (2019).
11. Nurse, P. & Hayles, J. Using genetics to understand biology. *Heredity (Edinb)* **123**, 4-13 (2019).
12. Martin, A. & Orgogozo, V. The Loci of repeated evolution: a catalog of genetic hotspots of phenotypic variation. *Evolution* **67**, 1235-1250 (2013).
13. Stanford, W.L., Cohn, J.B. & Cordes, S.P. Gene-trap mutagenesis: past, present and beyond. *Nat Rev Genet* **2**, 756-768 (2001).
14. Muller, H.J. Artificial Transmutation of the Gene. *Science* **66**, 84-87 (1927).
15. You, Y. *et al.* Chromosomal deletion complexes in mice by radiation of embryonic stem cells. *Nat Genet* **15**, 285-288 (1997).
16. Kutscher, L.M. & Shaham, S. Forward and reverse mutagenesis in C. elegans. *WormBook*, 1-26 (2014).
17. Lewis, E.B. A gene complex controlling segmentation in Drosophila. *Nature* **276**, 565-570 (1978).

18. Lewis, E.B. & Bacher, F. Methods of feeding ethyl methane sulphonate (EMS) to Drosophila males. *Drosophila Information Service* **43**, 193 (1968).

19. Russell, L.B. *et al.* Chlorambucil effectively induces deletion mutations in mouse germ cells. *Proc Natl Acad Sci U S A* **86**, 3704-3708 (1989).

20. St Johnston, D. The art and design of genetic screens: Drosophila melanogaster. *Nat Rev Genet* **3**, 176-188 (2002).

21. Nusslein-Volhard, C. & Wieschaus, E. Mutations affecting segment number and polarity in Drosophila. *Nature* **287**, 795-801 (1980).

22. Brenner, S. The genetics of Caenorhabditis elegans. *Genetics* **77**, 71-94 (1974).

23. Nolan, P.M. *et al.* A systematic, genome-wide, phenotype-driven mutagenesis programme for gene function studies in the mouse. *Nat Genet* **25**, 440-443 (2000).

24. Jaenisch, R. Germ line integration and Mendelian transmission of the exogenous Moloney leukemia virus. *Proc Natl Acad Sci U S A* **73**, 1260-1264 (1976).

25. Spradling, A.C. *et al.* The Berkeley Drosophila Genome Project gene disruption project: Single P-element insertions mutating 25% of vital Drosophila genes. *Genetics* **153**, 135-177 (1999).

26. Bessereau, J.L. Insertional mutagenesis in C. elegans using the Drosophila transposon Mos1: a method for the rapid identification of mutated genes. *Methods Mol Biol* **351**, 59-73 (2006).

27. Spradling, A.C. & Rubin, G.M. Transposition of cloned P elements into Drosophila germ line chromosomes. *Science* **218**, 341-347 (1982).

28. Hacker, U., Nystedt, S., Barmchi, M.P., Horn, C. & Wimmer, E.A. piggyBac-based insertional mutagenesis in the presence of stably integrated P elements in Drosophila. *Proc Natl Acad Sci U S A* **100**, 7720-7725 (2003).

29. Vallin, E. *et al.* A genome-wide collection of Mos1 transposon insertion mutants for the C. elegans research community. *PLoS One* **7**, e30482 (2012).

30. O'Kane, C.J. & Gehring, W.J. Detection in situ of genomic regulatory elements in Drosophila. *Proc Natl Acad Sci U S A* **84**, 9123-9127 (1987).

31. Allen, N.D. *et al.* Transgenes as probes for active chromosomal domains in mouse development. *Nature* **333**, 852-855 (1988).

32. Zambrowicz, B.P. *et al.* Disruption and sequence identification of 2,000 genes in mouse embryonic stem cells. *Nature* **392**, 608-611 (1998).

33. Amsterdam, A. *et al.* A large-scale insertional mutagenesis screen in zebrafish. *Genes Dev* **13**, 2713-2724 (1999).

34. Skarnes, W.C. *et al.* A public gene trap resource for mouse functional genomics. *Nat Genet* **36**, 543-544 (2004).

35. Housden, B.E. *et al.* Loss-of-function genetic tools for animal models: cross-species and cross-platform differences. *Nat Rev Genet* **18**, 24-40 (2017).

36. Kumar, A. & Snyder, M. Emerging technologies in yeast genomics. *Nat Rev Genet* **2**, 302-312 (2001).

37. Winzeler, E.A. *et al.* Functional characterization of the S. cerevisiae genome by gene deletion and parallel analysis. *Science* **285**, 901-906 (1999).

38. Golic, K.G. & Lindquist, S. The FLP recombinase of yeast catalyzes site-specific recombination in the Drosophila genome. *Cell* **59**, 499-509 (1989).

39. Lewandoski, M. Conditional control of gene expression in the mouse. *Nat Rev Genet* **2**, 743-755 (2001).

40. Bouabe, H. & Okkenhaug, K. Gene targeting in mice: a review. *Methods Mol Biol* **1064**, 315-336 (2013).

41. International Mouse Knockout, C., Collins, F.S., Rossant, J. & Wurst, W. A mouse for all reasons. *Cell* **128**, 9-13 (2007).

42. Xu, T., Wang, W., Zhang, S., Stewart, R.A. & Yu, W. Identifying tumor suppressors in genetic mosaics: the Drosophila lats gene encodes a putative protein kinase. *Development* **121**, 1053-1063 (1995).

43. Porteus, M. Using homologous recombination to manipulate the genome of human somatic cells. *Biotechnol Genet Eng Rev* **24**, 195-212 (2007).

44. Fire, A. *et al.* Potent and specific genetic interference by double-stranded RNA in Caenorhabditis elegans. *Nature* **391**, 806-811 (1998).

45. Ketting, R.F. The many faces of RNAi. *Dev Cell* **20**, 148-161 (2011).

46. Bobbin, M.L. & Rossi, J.J. RNA Interference (RNAi)-Based Therapeutics: Delivering on the Promise? *Annu Rev Pharmacol Toxicol* **56**, 103-122 (2016).

47. Boutros, M. & Ahringer, J. The art and design of genetic screens: RNA interference. *Nat Rev Genet* **9**, 554-566 (2008).

48. Mohr, S., Bakal, C. & Perrimon, N. Genomic screening with RNAi: results and challenges. *Annu Rev Biochem* **79**, 37-64 (2010).

49. Agaisse, H. *et al.* Genome-wide RNAi screen for host factors required for intracellular bacterial infection. *Science* **309**, 1248-1251 (2005).

50. Li, T. *et al.* Identification of the gene for vitamin K epoxide reductase. *Nature* **427**, 541-544 (2004).

51. Brummelkamp, T.R., Nijman, S.M., Dirac, A.M. & Bernards, R. Loss of the cylindromatosis tumour suppressor inhibits apoptosis by activating NF-kappaB. *Nature* **424**, 797-801 (2003).

52. Kaelin, W.G., Jr. Molecular biology. Use and abuse of RNAi to study mammalian gene function. *Science* **337**, 421-422 (2012).

53. Carroll, D. Genome engineering with zinc-finger nucleases. *Genetics* **188**, 773-782 (2011).

54. Joung, J.K. & Sander, J.D. TALENs: a widely applicable technology for targeted genome editing. *Nat Rev Mol Cell Biol* **14**, 49-55 (2013).

55. Kim, Y. *et al.* A library of TAL effector nucleases spanning the human genome. *Nat Biotechnol* **31**, 251-258 (2013).

56. Barrangou, R. *et al.* CRISPR provides acquired resistance against viruses in prokaryotes. *Science* **315**, 1709-1712 (2007).

57. Jinek, M. *et al.* A programmable dual-RNA-guided DNA endonuclease in adaptive bacterial immunity. *Science* **337**, 816-821 (2012).

58. Cong, L. *et al.* Multiplex genome engineering using CRISPR/Cas systems. *Science* **339**, 819-823 (2013).

59. Wang, T., Wei, J.J., Sabatini, D.M. & Lander, E.S. Genetic screens in human cells using the CRISPR-Cas9 system. *Science* **343**, 80-84 (2014).

60. Shalem, O. *et al.* Genome-scale CRISPR-Cas9 knockout screening in human cells. *Science* **343**, 84-87 (2014).

61. Tzelepis, K. *et al.* A CRISPR Dropout Screen Identifies Genetic Vulnerabilities and Therapeutic Targets in Acute Myeloid Leukemia. *Cell Rep* **17**, 1193-1205 (2016).

62. Wang, T. *et al.* Gene Essentiality Profiling Reveals Gene Networks and Synthetic Lethal Interactions with Oncogenic Ras. *Cell* **168**, 890-903 e815 (2017).

63. Jain, I.H. *et al.* Hypoxia as a therapy for mitochondrial disease. *Science* **352**, 54-61 (2016).

64. Park, R.J. *et al.* A genome-wide CRISPR screen identifies a restricted set of HIV host dependency factors. *Nat Genet* **49**, 193-203 (2017).

65. Kampmann, M. CRISPRi and CRISPRa Screens in Mammalian Cells for Precision Biology and Medicine. *ACS Chem Biol* **13**, 406-416 (2018).

66. Gilbert, L.A. *et al.* Genome-Scale CRISPR-Mediated Control of Gene Repression and Activation. *Cell* **159**, 647-661 (2014).

67. Hunter, P. The paradox of model organisms. The use of model organisms in research will continue despite their shortcomings. *EMBO Rep* **9**, 717-720 (2008).

68. Shalem, O., Sanjana, N.E. & Zhang, F. High-throughput functional genomics using CRISPR-Cas9. *Nat Rev Genet* **16**, 299-311 (2015).

69. Carette, J.E. *et al.* Haploid genetic screens in human cells identify host factors used by pathogens. *Science* **326**, 1231-1235 (2009).

70. Rosmarin, D.M. *et al.* Attachment of Chlamydia trachomatis L2 to host cells requires sulfation. *Proc Natl Acad Sci U S A* **109**, 10059-10064 (2012).

71. Marceau, C.D. *et al.* Genetic dissection of Flaviviridae host factors through genome-scale CRISPR screens. *Nature* **535**, 159-163 (2016).

72. Birsoy, K. *et al.* MCT1-mediated transport of a toxic molecule is an effective strategy for targeting glycolytic tumors. *Nat Genet* **45**, 104-108 (2013).

73. Hou, P. *et al.* A Genome-Wide CRISPR Screen Identifies Genes Critical for Resistance to FLT3 Inhibitor AC220. *Cancer Res* **77**, 4402-4413 (2017).

74. Krall, E.B. *et al.* KEAP1 loss modulates sensitivity to kinase targeted therapy in lung cancer. *Elife* **6** (2017).

75. Sharma, S. & Petsalaki, E. Application of CRISPR-Cas9 Based Genome-Wide Screening Approaches to Study Cellular Signalling Mechanisms. *Int J Mol Sci* **19** (2018).

76. Wang, T. *et al.* Identification and characterization of essential genes in the human genome. *Science* **350**, 1096-1101 (2015).

77. Blomen, V.A. *et al.* Gene essentiality and synthetic lethality in haploid human cells. *Science* **350**, 1092-1096 (2015).

78. Hart, T. *et al.* High-Resolution CRISPR Screens Reveal Fitness Genes and Genotype-Specific Cancer Liabilities. *Cell* **163**, 1515-1526 (2015).

79. Meyers, R.M. *et al.* Computational correction of copy number effect improves specificity of CRISPR-Cas9 essentiality screens in cancer cells. *Nat Genet* **49**, 1779-1784 (2017).

80. Elling, U. & Penninger, J.M. Genome wide functional genetics in haploid cells. *FEBS Lett* **588**, 2415-2421 (2014).

81. Evers, C.H., Luiken, J.A., Bolhuis, P.G. & Kegel, W.K. Self-assembly of microcapsules via colloidal bond hybridization and anisotropy. *Nature* **534**, 364-368 (2016).

82. Costanzo, M. *et al.* Global Genetic Networks and the Genotype-to-Phenotype Relationship. *Cell* **177**, 85-100 (2019).

83. Phillips, P.C. Epistasis--the essential role of gene interactions in the structure and evolution of genetic systems. *Nat Rev Genet* **9**, 855-867 (2008).

84. Bateson, M.A., Saunders, E.R. & Punnett, M.A. in Reports to the Evolution Committee of the Royal Society (1905).

85. Tong, A.H. *et al.* Global mapping of the yeast genetic interaction network. *Science* **303**, 808-813 (2004).

86. Costanzo, M. *et al.* A global genetic interaction network maps a wiring diagram of cellular function. *Science* **353** (2016).

87. Kuzmin, E. *et al.* Systematic analysis of complex genetic interactions. *Science* **360** (2018).

88. Usaj, M. *et al.* TheCellMap.org: A Web-Accessible Database for Visualizing and Mining the Global Yeast Genetic Interaction Network. *G3 (Bethesda)* **7**, 1539-1549 (2017).

89. Kim, E. *et al.* A network of human functional gene interactions from knockout fitness screens in cancer cells. *Life Sci Alliance* **2** (2019).

90. Tsherniak, A. *et al.* Defining a Cancer Dependency Map. *Cell* **170**, 564-576 e516 (2017).

91. Dempster, J.M. *et al.* Agreement between two large pan-cancer CRISPR-Cas9 gene dependency data sets. *Nat Commun* **10**, 5817 (2019).

92. Pan, J. *et al.* Interrogation of Mammalian Protein Complex Structure, Function, and Membership Using Genome-Scale Fitness Screens. *Cell Syst* **6**, 555-568 e557 (2018).

93. Boutros, M., Heigwer, F. & Laufer, C. Microscopy-Based High-Content Screening. *Cell* **163**, 1314-1325 (2015).

94. Eliceiri, K.W. *et al.* Biological imaging software tools. *Nat Methods* **9**, 697-710 (2012).

95. Hasson, S.A. *et al.* High-content genome-wide RNAi screens identify regulators of parkin upstream of mitophagy. *Nature* **504**, 291-295 (2013).

96. Williams, S.P. *et al.* Systematic high-content genome-wide RNAi screens of endothelial cell migration and morphology. *Sci Data* **4**, 170009 (2017).

97. Neumann, B. *et al.* High-throughput RNAi screening by time-lapse imaging of live human cells. *Nat Methods* **3**, 385-390 (2006).

98. Chia, N.Y. *et al.* A genome-wide RNAi screen reveals determinants of human embryonic stem cell identity. *Nature* **468**, 316-320 (2010).

99. Morita, K. *et al.* Genome-wide CRISPR screen identifies TMEM41B as a gene required for autophagosome formation. *J Cell Biol* **217**, 3817-3828 (2018).

100. Diao, Y. *et al.* A new class of temporarily phenotypic enhancers identified by CRISPR/Cas9-mediated genetic screening. *Genome Res* **26**, 397-405 (2016).

101. Lebensohn, A.M. *et al.* Comparative genetic screens in human cells reveal new regulatory mechanisms in WNT signaling. *Elife* **5** (2016).

102. Parnas, O. *et al.* A Genome-wide CRISPR Screen in Primary Immune Cells to Dissect Regulatory Networks. *Cell* **162**, 675-686 (2015).

103. Brockmann, M. *et al.* Genetic wiring maps of single-cell protein states reveal an off-switch for GPCR signalling. *Nature* **546**, 307-311 (2017).

104. Nieuwenhuis, J. *et al.* Vasohibins encode tubulin detyrosinating activity. *Science* **358**, 1453-1456 (2017).

105. Loregger, A. *et al.* Haploid Mammalian Genetic Screen Identifies UBXD8 as a Key Determinant of HMGCR Degradation and Cholesterol Biosynthesis. *Arterioscler Thromb Vasc Biol* **37**, 2064-2074 (2017).

106. Mezzadra, R. *et al.* Identification of CMTM6 and CMTM4 as PD-L1 protein regulators. *Nature* **549**, 106-110 (2017).

107. Spel, L. *et al.* Nedd4-Binding Protein 1 and TNFAIP3-Interacting Protein 1 Control MHC-1 Display in Neuroblastoma. *Cancer Res* **78**, 6621-6631 (2018).

108. Logtenberg, M.E.W. *et al.* Glutaminyl cyclase is an enzymatic modifier of the CD47- SIRPalpha axis and a target for cancer immunotherapy. *Nat Med* **25**, 612-619 (2019).

109. Staring, J. *et al.* PLA2G16 represents a switch between entry and clearance of Picornaviridae. *Nature* **541**, 412-416 (2017).

110. Hoffmann, H.H. *et al.* Diverse Viruses Require the Calcium Transporter SPCA1 for Maturation and Spread. *Cell Host Microbe* **22**, 460-470 e465 (2017).

111. Wersto, R.P. *et al.* Doublet discrimination in DNA cell-cycle analysis. *Cytometry* **46**, 296-306 (2001).

112. Langmead, B., Trapnell, C., Pop, M. & Salzberg, S.L. Ultrafast and memory-efficient alignment of short DNA sequences to the human genome. *Genome Biol* **10**, R25 (2009).

113. Smedley, D. *et al.* The BioMart community portal: an innovative alternative to large, centralized data repositories. *Nucleic Acids Res* **43**, W589-598 (2015).

114. Hart, T. *et al.* Evaluation and Design of Genome-Wide CRISPR/SpCas9 Knockout Screens. *G3 (Bethesda)* **7**, 2719-2727 (2017).

115. Sanjana, N.E., Shalem, O. & Zhang, F. Improved vectors and genome-wide libraries for CRISPR screening. *Nat Methods* **11**, 783-784 (2014).

116. Spandidos, A., Wang, X., Wang, H. & Seed, B. PrimerBank: a resource of human and mouse PCR primer pairs for gene expression detection and quantification. *Nucleic Acids Res* **38**, D792-799 (2010).

117. Gapp, B.V. *et al.* Parallel reverse genetic screening in mutant human cells using transcriptomics. *Mol Syst Biol* **12**, 879 (2016).

118. Dignam, J.D., Lebovitz, R.M. & Roeder, R.G. Accurate transcription initiation by RNA polymerase II in a soluble extract from isolated mammalian nuclei. *Nucleic Acids Res* **11**, 1475-1489 (1983).

119. Brinkman, E.K., Chen, T., Amendola, M. & van Steensel, B. Easy quantitative assessment of genome editing by sequence trace decomposition. *Nucleic Acids Res* **42**, e168 (2014).

120. Grimm, S. The art and design of genetic screens: mammalian culture cells. *Nat Rev Genet* **5**, 179-189 (2004).

121. Ishida, Y. & Leder, P. RET: a poly A-trap retrovirus vector for reversible disruption and expression monitoring of genes in living cells. *Nucleic Acids Res* **27**, e35 (1999).

122. Craigie, R., Fujiwara, T. & Bushman, F. The IN protein of Moloney murine leukemia virus processes the viral DNA ends and accomplishes their integration in vitro. *Cell* **62**, 829-837 (1990).

123. Vijaya, S., Steffen, D.L. & Robinson, H.L. Acceptor sites for retroviral integrations map near DNase I-hypersensitive sites in chromatin. *J Virol* **60**, 683-692 (1986).

124. Bushman, F. *et al.* Genome-wide analysis of retroviral DNA integration. *Nat Rev Microbiol* **3**, 848-858 (2005).

125. Kessous, A., Colombies, P., Pris, J. & Clement, D. Near haploid cell line in lymphoid blast crisis of Ph1-positive chronic myeloid leukemia. *Cancer Res* **40**, 1354-1359 (1980).

126. Najafzadeh, T.M., Dumars, G.E., Dumars, K.W., Simpkins, H. & Katz, J. Near-haploid cell line in the blastic crisis of chronic myelogenous leukemia: a possible marker for lymphoid malignancy. *Cancer Genet Cytogenet* **9**, 333-339 (1983).

127. Drouin, V., Viguie, F. & Debesse, B. Near-haploid karyotype in a squamous cell lung carcinoma. *Genes Chromosomes Cancer* **7**, 209-212 (1993).

128. Andersson, B.S. *et al.* KBM-7, a human myeloid leukemia cell line with double Philadelphia chromosomes lacking normal c-ABL and BCR transcripts. *Leukemia* **9**, 2100-2108 (1995).

129. Kotecki, M., Reddy, P.S. & Cochran, B.H. Isolation and characterization of a near-haploid human cell line. *Exp Cell Res* **252**, 273-280 (1999).

130. Carette, J.E. *et al.* Generation of iPSCs from cultured human malignant cells. *Blood* **115**, 4039-4042 (2010).

131. Essletzbichler, P. *et al.* Megabase-scale deletion using CRISPR/Cas9 to generate a fully haploid human cell line. *Genome Res* **24**, 2059-2065 (2014).

132. Carette, J.E. *et al.* Ebola virus entry requires the cholesterol transporter Niemann-Pick C1. *Nature* **477**, 340-343 (2011).

133. Lee, C.C., Carette, J.E., Brummelkamp, T.R. & Ploegh, H.L. A reporter screen in a human haploid cell line identifies CYLD as a constitutive inhibitor of NF-kappaB. *PLoS One* **8**, e70339 (2013).

134. Jae, L.T. *et al.* Virus entry. Lassa virus entry requires a trigger-induced receptor switch. *Science* **344**, 1506-1510 (2014).

135. Tchasovnikarova, I.A. *et al.* GENE SILENCING. Epigenetic silencing by the HUSH complex mediates position-effect variegation in human cells. *Science* **348**, 1481-1485 (2015).

136. Burr, S.P. *et al.* Mitochondrial Protein Lipoylation and the 2-Oxoglutarate Dehydrogenase Complex Controls HIF1alpha Stability in Aerobic Conditions. *Cell Metab* **24**, 740-752 (2016).

137. Wu, X., Li, Y., Crise, B. & Burgess, S.M. Transcription start regions in the human genome are favored targets for MLV integration. *Science* **300**, 1749-1751 (2003).

138. Lewinski, M.K. *et al.* Retroviral DNA integration: viral and cellular determinants of target-site selection. *PLoS Pathog* **2**, e60 (2006).

139. Yu, J. & Ciaudo, C. Vector Integration Sites Identification for Gene-Trap Screening in Mammalian Haploid Cells. *Sci Rep* **7**, 44736 (2017).

140. Black, C.B., Duensing, T.D., Trinkle, L.S. & Dunlay, R.T. Cell-based screening using high-throughput flow cytometry. *Assay Drug Dev Technol* **9**, 13-20 (2011).

141. Hodne, K. & Weltzien, F.A. Single-Cell Isolation and Gene Analysis: Pitfalls and Possibilities. *Int J Mol Sci* **16**, 26832-26849 (2015).

142. Bonner, W.A., Hulett, H.R., Sweet, R.G. & Herzenberg, L.A. Fluorescence activated cell sorting. *Rev Sci Instrum* **43**, 404-409 (1972).

143. Herzenberg, L.A., Sweet, R.G. & Herzenberg, L.A. Fluorescence-activated cell sorting. *Sci Am* **234**, 108-117 (1976).

144. Uren, A.G. *et al.* A high-throughput splinkerette-PCR method for the isolation and sequencing of retroviral insertion sites. *Nat Protoc* **4**, 789-798 (2009).

145. Ochman, H., Gerber, A.S. & Hartl, D.L. Genetic applications of an inverse polymerase chain reaction. *Genetics* **120**, 621-623 (1988).

146. Schmidt, M. *et al.* High-resolution insertion-site analysis by linear amplification-mediated PCR (LAM-PCR). *Nat Methods* **4**, 1051-1057 (2007).

147. Duncan, L.M. *et al.* Fluorescence-based phenotypic selection allows forward genetic screens in haploid human cells. *PLoS One* **7**, e39651 (2012).

148. Burckstummer, T. *et al.* A reversible gene trap collection empowers haploid genetics in human cells. *Nat Methods* **10**, 965-971 (2013).

149. Gapp, B.V. *et al.* Parallel reverse genetic screening in mutant human cells using transcriptomics. *Mol Syst Biol* **12**, 879 (2016).

150. Moder, M. *et al.* Parallel genome-wide screens identify synthetic viable interactions between the BLM helicase complex and Fanconi anemia. *Nat Commun* **8**, 1238 (2017).

151. Lee, S.E. *et al.* Proteogenomic Analysis to Identify Missing Proteins from Haploid Cell Lines. *Proteomics* **18**, e1700386 (2018).

152. BCSH, G.H.T.F.o. Immunophenotyping in the diagnosis of chronic lymphoproliferative disorders. *J Clin Pathol* **47**, 871-875 (1994).

153. Acharya, P., Quinlan, A. & Neumeister, V. The ABCs of finding a good antibody: How to find a good antibody, validate it, and publish meaningful data. *F1000Res* **6**, 851 (2017).

154. Carette, J.E. *et al.* Global gene disruption in human cells to assign genes to phenotypes by deep sequencing. *Nat Biotechnol* **29**, 542-546 (2011).

155. Lee, S., Lim, W.A. & Thorn, K.S. Improved blue, green, and red fluorescent protein tagging vectors for S. cerevisiae. *PLoS One* **8**, e67902 (2013).

156. Subach, O.M. *et al.* Conversion of red fluorescent protein into a bright blue probe. *Chem Biol* **15**, 1116-1124 (2008).

157. Menon, V., Thomas, R., Ghale, A.R., Reinhard, C. & Pruszak, J. Flow cytometry protocols for surface and intracellular antigen analyses of neural cell types. *J Vis Exp* (2014).

158. Hoxie, J.A. *et al.* Internalization and recycling of activated thrombin receptors. *J Biol Chem* **268**, 13756-13763 (1993).

159. Panchuk-Voloshina, N. *et al.* Alexa dyes, a series of new fluorescent dyes that yield exceptionally bright, photostable conjugates. *J Histochem Cytochem* **47**, 1179-1188 (1999).

160. Olbrich, T. *et al.* A p53-dependent response limits the viability of mammalian haploid cells. *Proc Natl Acad Sci U S A* **114**, 9367-9372 (2017).

161. Cui, H.H., Valdez, J.G., Steinkamp, J.A. & Crissman, H.A. Fluorescence lifetime-based discrimination and quantification of cellular DNA and RNA with phase-sensitive flow cytometry. *Cytometry A* **52**, 46-55 (2003).

162. Ormerod, M.G. *Flow cytometry: a practical approach*. (OUP, Oxford; 1994).

163. Eich, M. (The Heidelberg Flow Cytometry Workshop, https://flowcytometry-embl.de/; 2016).

164. Russo, J. & Russo, I. Methodology for Studying the Compartments of the Human Breast, in *Techniques and Methodological Approaches in Breast Cancer Research* (Springer, New York; 2014).

165. McInerney, P., Adams, P. & Hadi, M.Z. Error Rate Comparison during Polymerase Chain Reaction by DNA Polymerase. *Mol Biol Int* **2014**, 287430 (2014).

166. Moreau, Y. & Tranchevent, L.C. Computational tools for prioritizing candidate genes: boosting disease gene discovery. *Nat Rev Genet* **13**, 523-536 (2012).

167. Oti, M. & Brunner, H.G. The modular nature of genetic diseases. *Clin Genet* **71**, 1-11 (2007).

168. UniProt, C. UniProt: a worldwide hub of protein knowledge. *Nucleic Acids Res* **47**, D506-D515 (2019).

169. Ashburner, M. *et al.* Gene ontology: tool for the unification of biology. The Gene Ontology Consortium. *Nat Genet* **25**, 25-29 (2000).

170. Fabregat, A. *et al.* The Reactome pathway Knowledgebase. *Nucleic Acids Res* **44**, D481-487 (2016).

171. Edgar, R., Domrachev, M. & Lash, A.E. Gene Expression Omnibus: NCBI gene expression and hybridization array data repository. *Nucleic Acids Res* **30**, 207-210 (2002).

172. Thul, P.J. *et al.* A subcellular map of the human proteome. *Science* **356** (2017).

173. Obayashi, T., Kagaya, Y., Aoki, Y., Tadaka, S. & Kinoshita, K. COXPRESdb v7: a gene coexpression database for 11 animal species supported by 23 coexpression platforms for technical evaluation and evolutionary inference. *Nucleic Acids Res* **47**, D55-D62 (2019).

174. Huttlin, E.L. *et al.* Architecture of the human interactome defines protein communities and disease networks. *Nature* **545**, 505-509 (2017).

175. Orchard, S. *et al.* The MIntAct project--IntAct as a common curation platform for 11 molecular interaction databases. *Nucleic Acids Res* **42**, D358-363 (2014).

176. Stark, C. *et al.* BioGRID: a general repository for interaction datasets. *Nucleic Acids Res* **34**, D535-539 (2006).

177. McClive, P. *et al.* Gene trap integrations expressed in the developing heart: insertion site affects splicing of the PT1-ATG vector. *Dev Dyn* **212**, 267-276 (1998).

178. Ratcliffe, P.J., O'Rourke, J.F., Maxwell, P.H. & Pugh, C.W. Oxygen sensing, hypoxia-inducible factor-1 and the regulation of mammalian gene expression. *J Exp Biol* **201**, 1153-1162 (1998).

179. Jewell, U.R. *et al.* Induction of HIF-1alpha in response to hypoxia is instantaneous. *FASEB J* **15**, 1312-1314 (2001).

180. Weidemann, A. & Johnson, R.S. Biology of HIF-1alpha. *Cell Death Differ* **15**, 621-627 (2008).

181. Semenza, G.L. HIF-1 and human disease: one highly involved factor. *Genes Dev* **14**, 1983-1991 (2000).

182. Iommarini, L., Porcelli, A.M., Gasparre, G. & Kurelac, I. Non-Canonical Mechanisms Regulating Hypoxia-Inducible Factor 1 Alpha in Cancer. *Front Oncol* **7**, 286 (2017).

183. An, W.G. *et al.* Stabilization of wild-type p53 by hypoxia-inducible factor 1alpha. *Nature* **392**, 405-408 (1998).

184. Berra, E. *et al.* HIF prolyl-hydroxylase 2 is the key oxygen sensor setting low steady-state levels of HIF-1alpha in normoxia. *EMBO J* **22**, 4082-4090 (2003).

185. Walmsley, S.R. *et al.* Prolyl hydroxylase 3 (PHD3) is essential for hypoxic regulation of neutrophilic inflammation in humans and mice. *J Clin Invest* **121**, 1053-1063 (2011).

186. Corbett, A.J. *et al.* T-cell activation by transitory neo-antigens derived from distinct microbial pathways. *Nature* **509**, 361-365 (2014).

187. McWilliam, H.E. *et al.* The intracellular pathway for the presentation of vitamin B-related antigens by the antigen-presenting molecule MR1. *Nat Immunol* **17**, 531-537 (2016).

188. Hashimoto, K., Hirai, M. & Kurosawa, Y. A gene outside the human MHC related to classical HLA class I genes. *Science* **269**, 693-695 (1995).

189. Crowther, M.D. *et al.* Genome-wide CRISPR-Cas9 screening reveals ubiquitous T cell cancer targeting via the monomorphic MHC class I-related protein MR1. *Nat Immunol* **21**, 178-185 (2020).

190. Huang, S. *et al.* MR1 uses an endocytic pathway to activate mucosal-associated invariant T cells. *J Exp Med* **205**, 1201-1211 (2008).

191. Kulicke, C. (Oxford University, DPhil thesis; 2019).

192. Patel, O. *et al.* Recognition of vitamin B metabolites by mucosal-associated invariant T cells. *Nat Commun* **4**, 2142 (2013).

193. Miley, M.J. *et al.* Biochemical features of the MHC-related protein 1 consistent with an immunological function. *J Immunol* **170**, 6090-6098 (2003).

194. Bailis, W. *et al.* Distinct modes of mitochondrial metabolism uncouple T cell differentiation and function. *Nature* **571**, 403-407 (2019).

195. Sagi, I. *et al.* Derivation and differentiation of haploid human embryonic stem cells. *Nature* **532**, 107-111 (2016).

196. Leeb, M., Dietmann, S., Paramor, M., Niwa, H. & Smith, A. Genetic exploration of the exit from self-renewal using haploid embryonic stem cells. *Cell Stem Cell* **14**, 385-393 (2014).

197. Liu, G. *et al.* Arrayed mutant haploid embryonic stem cell libraries facilitate phenotype-driven genetic screens. *Nucleic Acids Res* **45**, e180 (2017).

198. Monfort, A. *et al.* Identification of Spen as a Crucial Factor for Xist Function through Forward Genetic Screening in Haploid Embryonic Stem Cells. *Cell Rep* **12**, 554-561 (2015).

199. Forment, J.V. *et al.* Genome-wide genetic screening with chemically mutagenized haploid embryonic stem cells. *Nat Chem Biol* **13**, 12-14 (2017).

200. Horn, M. *et al.* Unbiased compound-protein interface mapping and prediction of chemoresistance loci through forward genetics in haploid stem cells. *Oncotarget* **9**, 9838-9851 (2018).

201. Chen, L. *et al.* CRISPR-Cas9 screen reveals a MYCN-amplified neuroblastoma dependency on EZH2. *J Clin Invest* **128**, 446-462 (2018).

202. Kramer, N.J. *et al.* CRISPR-Cas9 screens in human cells and primary neurons identify modifiers of C9ORF72 dipeptide-repeat-protein toxicity. *Nat Genet* **50**, 603-612 (2018).

203. Shifrut, E. *et al.* Genome-wide CRISPR Screens in Primary Human T Cells Reveal Key Regulators of Immune Function. *Cell* **175**, 1958-1971 e1915 (2018).

204. Sanson, K.R. *et al.* Optimized libraries for CRISPR-Cas9 genetic screens with multiple modalities. *Nat Commun* **9**, 5416 (2018).

205. Timms, R.T. *et al.* Genetic dissection of mammalian ERAD through comparative haploid and CRISPR forward genetic screens. *Nat Commun* **7**, 11786 (2016).

206. Pusapati, G.V. *et al.* CRISPR Screens Uncover Genes that Regulate Target Cell Sensitivity to the Morphogen Sonic Hedgehog. *Dev Cell* **44**, 113-129 e118 (2018).

207. Fang, Z. *et al.* Single-Cell Heterogeneity Analysis and CRISPR Screen Identify Key beta-Cell-Specific Disease Genes. *Cell Rep* **26**, 3132-3144 e3137 (2019).

208. Bassaganyas, L. *et al.* New factors for protein transport identified by a genome-wide CRISPRi screen in mammalian cells. *J Cell Biol* **218**, 3861-3879 (2019).

209. Leto, D.E. *et al.* Genome-wide CRISPR Analysis Identifies Substrate-Specific Conjugation Modules in ER-Associated Degradation. *Mol Cell* **73**, 377-389 e311 (2019).

210. Miles, L.A., Garippa, R.J. & Poirier, J.T. Design, execution, and analysis of pooled in vitro CRISPR/Cas9 screens. *FEBS J* **283**, 3170-3180 (2016).

211. Horlbeck, M.A. *et al.* Mapping the Genetic Landscape of Human Cells. *Cell* **174**, 953-967 e922 (2018).

212. Zolotareva, O. & Kleine, M. A Survey of Gene Prioritization Tools for Mendelian and Complex Human Diseases. *J Integr Bioinform* **16** (2019).

213. Edwards, A.M. *et al.* Too many roads not taken. *Nature* **470**, 163-165 (2011).

214. Lage, K. Protein-protein interactions and genetic diseases: The interactome. *Biochim Biophys Acta* **1842**, 1971-1980 (2014).

215. Mair, B. *et al.* High-throughput genome-wide phenotypic screening via immunomagnetic cell sorting. *Nat Biomed Eng* **3**, 796-805 (2019).

216. Legut, M. & Sanjana, N.E. Immunomagnetic cell sorting. *Nat Biomed Eng* **3**, 759-760 (2019).

217. Arrigucci, R. *et al.* FISH-Flow, a protocol for the concurrent detection of mRNA and protein in single cells using fluorescence in situ hybridization and flow cytometry. *Nat Protoc* **12**, 1245-1260 (2017).

218. Stocker, H. *et al.* Rheb is an essential regulator of S6K in controlling cell growth in Drosophila. *Nat Cell Biol* **5**, 559-565 (2003).

219. Kim, E., Goraksha-Hicks, P., Li, L., Neufeld, T.P. & Guan, K.L. Regulation of TORC1 by Rag GTPases in nutrient response. *Nat Cell Biol* **10**, 935-945 (2008).

220. Zoncu, R. *et al.* mTORC1 senses lysosomal amino acids through an inside-out mechanism that requires the vacuolar H(+)-ATPase. *Science* **334**, 678-683 (2011).

221. Li, M. *et al.* Genome-wide CRISPR-KO Screen Uncovers mTORC1-Mediated Gsk3 Regulation in Naive Pluripotency Maintenance and Dissolution. *Cell Rep* **24**, 489-502 (2018).

222. Saxton, R.A. & Sabatini, D.M. mTOR Signaling in Growth, Metabolism, and Disease. *Cell* **168**, 960-976 (2017).

223. Baker, H., Sidorowicz, A., Sehgal, S.N. & Vezina, C. Rapamycin (AY-22,989), a new antifungal antibiotic. III. In vitro and in vivo evaluation. *J Antibiot (Tokyo)* **31**, 539-545 (1978).

224. Heitman, J., Movva, N.R. & Hall, M.N. Targets for cell cycle arrest by the immunosuppressant rapamycin in yeast. *Science* **253**, 905-909 (1991).

225. Brown, E.J. *et al.* A mammalian protein targeted by G1-arresting rapamycin-receptor complex. *Nature* **369**, 756-758 (1994).

226. Sabatini, D.M., Erdjument-Bromage, H., Lui, M., Tempst, P. & Snyder, S.H. RAFT1: a mammalian protein that binds to FKBP12 in a rapamycin-dependent fashion and is homologous to yeast TORs. *Cell* **78**, 35-43 (1994).

227. Sarbassov, D.D., Guertin, D.A., Ali, S.M. & Sabatini, D.M. Phosphorylation and regulation of Akt/PKB by the rictor-mTOR complex. *Science* **307**, 1098-1101 (2005).

228. Wang, L., Harris, T.E., Roth, R.A. & Lawrence, J.C., Jr. PRAS40 regulates mTORC1 kinase activity by functioning as a direct inhibitor of substrate binding. *J Biol Chem* **282**, 20036-20044 (2007).

229. Sengupta, S., Peterson, T.R. & Sabatini, D.M. Regulation of the mTOR complex 1 pathway by nutrients, growth factors, and stress. *Mol Cell* **40**, 310-322 (2010).

230. Carroll, B. *et al.* Control of TSC2-Rheb signaling axis by arginine regulates mTORC1 activity. *Elife* **5** (2016).

231. Saucedo, L.J. *et al.* Rheb promotes cell growth as a component of the insulin/TOR signalling network. *Nat Cell Biol* **5**, 566-571 (2003).

232. Long, X., Lin, Y., Ortiz-Vega, S., Yonezawa, K. & Avruch, J. Rheb binds and regulates the mTOR kinase. *Curr Biol* **15**, 702-713 (2005).

233. Patel, P.H. *et al.* Drosophila Rheb GTPase is required for cell cycle progression and cell growth. *J Cell Sci* **116**, 3601-3610 (2003).

234. Buerger, C., DeVries, B. & Stambolic, V. Localization of Rheb to the endomembrane is critical for its signaling function. *Biochem Biophys Res Commun* **344**, 869-880 (2006).

235. Garami, A. *et al.* Insulin activation of Rheb, a mediator of mTOR/S6K/4E-BP signaling, is inhibited by TSC1 and 2. *Mol Cell* **11**, 1457-1466 (2003).

236. Inoki, K., Li, Y., Xu, T. & Guan, K.L. Rheb GTPase is a direct target of TSC2 GAP activity and regulates mTOR signaling. *Genes Dev* **17**, 1829-1834 (2003).

237. Zhang, Y. *et al.* Rheb is a direct target of the tuberous sclerosis tumour suppressor proteins. *Nat Cell Biol* **5**, 578-581 (2003).

238. Inoki, K., Li, Y., Zhu, T., Wu, J. & Guan, K.L. TSC2 is phosphorylated and inhibited by Akt and suppresses mTOR signalling. *Nat Cell Biol* **4**, 648-657 (2002).

239. Menon, S. *et al.* Spatial control of the TSC complex integrates insulin and nutrient regulation of mTORC1 at the lysosome. *Cell* **156**, 771-785 (2014).

240. Inoki, K. *et al.* TSC2 integrates Wnt and energy signals via a coordinated phosphorylation by AMPK and GSK3 to regulate cell growth. *Cell* **126**, 955-968 (2006).

241. Sancak, Y. *et al.* The Rag GTPases bind raptor and mediate amino acid signaling to mTORC1. *Science* **320**, 1496-1501 (2008).

242. Sekiguchi, T., Hirose, E., Nakashima, N., Ii, M. & Nishimoto, T. Novel G proteins, Rag C and Rag D, interact with GTP-binding proteins, Rag A and Rag B. *J Biol Chem* **276**, 7246-7257 (2001).

243. Sancak, Y. *et al.* Ragulator-Rag complex targets mTORC1 to the lysosomal surface and is necessary for its activation by amino acids. *Cell* **141**, 290-303 (2010).

244. Bar-Peled, L., Schweitzer, L.D., Zoncu, R. & Sabatini, D.M. Ragulator is a GEF for the rag GTPases that signal amino acid levels to mTORC1. *Cell* **150**, 1196-1208 (2012).

245. Su, M.Y. *et al.* Hybrid Structure of the RagA/C-Ragulator mTORC1 Activation Complex. *Mol Cell* **68**, 835-846 e833 (2017).

246. Yonehara, R. *et al.* Structural basis for the assembly of the Ragulator-Rag GTPase complex. *Nat Commun* **8**, 1625 (2017).

247. Zhang, T. *et al.* Structural basis for Ragulator functioning as a scaffold in membrane-anchoring of Rag GTPases and mTORC1. *Nat Commun* **8**, 1394 (2017).

248. Hoshino, D., Tomari, T., Nagano, M., Koshikawa, N. & Seiki, M. A novel protein associated with membrane-type 1 matrix metalloproteinase binds p27(kip1) and regulates RhoA activation, actin remodeling, and matrigel invasion. *J Biol Chem* **284**, 27315-27326 (2009).

249. Meehan, T.F. *et al.* Disease model discovery from 3,328 gene knockouts by The International Mouse Phenotyping Consortium. *Nat Genet* **49**, 1231-1238 (2017).

250. Malek, M. *et al.* LAMTOR1 depletion induces p53-dependent apoptosis via aberrant lysosomal activation. *Cell Death Dis* **3**, e300 (2012).

251. Kimura, T. *et al.* Polarization of M2 macrophages requires Lamtor1 that integrates cytokine and amino-acid signals. *Nat Commun* **7**, 13130 (2016).

252. Hosokawa, T. *et al.* Lamtor1 Is Critically Required for CD4(+) T Cell Proliferation and Regulatory T Cell Suppressive Function. *J Immunol* **199**, 2008-2019 (2017).

253. Teis, D. *et al.* p14-MP1-MEK1 signaling regulates endosomal traffic and cellular proliferation during tissue homeostasis. *J Cell Biol* **175**, 861-868 (2006).

254. Bohn, G. *et al.* A novel human primary immunodeficiency syndrome caused by deficiency of the endosomal adaptor protein p14. *Nat Med* **13**, 38-45 (2007).

255. Taub, N. *et al.* The late endosomal adaptor p14 is a macrophage host-defense factor against Salmonella infection. *J Cell Sci* **125**, 2698-2708 (2012).

256. De Araujo, M.E. *et al.* Polymorphisms in the gene regions of the adaptor complex LAMTOR2/LAMTOR3 and their association with breast cancer risk. *PLoS One* **8**, e53768 (2013).

257. Schaeffer, H.J. *et al.* MP1: a MEK binding partner that enhances enzymatic activation of the MAP kinase cascade. *Science* **281**, 1668-1671 (1998).

258. Shen, K., Sidik, H. & Talbot, W.S. The Rag-Ragulator Complex Regulates Lysosome Function and Phagocytic Flux in Microglia. *Cell Rep* **14**, 547-559 (2016).

259. Melegari, M., Scaglioni, P.P. & Wands, J.R. Cloning and characterization of a novel hepatitis B virus x binding protein that inhibits viral replication. *J Virol* **72**, 1737-1743 (1998).

260. Fujii, R. *et al.* HBXIP, cellular target of hepatitis B virus oncoprotein, is a regulator of centrosome dynamics and cytokinesis. *Cancer Res* **66**, 9099-9107 (2006).

261. Marusawa, H. *et al.* HBXIP functions as a cofactor of survivin in apoptosis suppression. *EMBO J* **22**, 2729-2740 (2003).

262. Bar-Peled, L. *et al.* A Tumor suppressor complex with GAP activity for the Rag GTPases that signal amino acid sufficiency to mTORC1. *Science* **340**, 1100-1106 (2013).

263. Wolfson, R.L. *et al.* KICSTOR recruits GATOR1 to the lysosome and is necessary for nutrients to regulate mTORC1. *Nature* **543**, 438-442 (2017).

264. Peng, M., Yin, N. & Li, M.O. SZT2 dictates GATOR control of mTORC1 signalling. *Nature* **543**, 433-437 (2017).

265. Tsun, Z.Y. *et al.* The folliculin tumor suppressor is a GAP for the RagC/D GTPases that signal amino acid levels to mTORC1. *Mol Cell* **52**, 495-505 (2013).

266. Schmidt, L.S. & Linehan, W.M. FLCN: The causative gene for Birt-Hogg-Dube syndrome. *Gene* **640**, 28-42 (2018).

267. Baba, M. *et al.* Folliculin encoded by the BHD gene interacts with a binding protein, FNIP1, and AMPK, and is involved in AMPK and mTOR signaling. *Proc Natl Acad Sci U S A* **103**, 15552-15557 (2006).

268. van Slegtenhorst, M. *et al.* The Birt-Hogg-Dube and tuberous sclerosis complex homologs have opposing roles in amino acid homeostasis in Schizosaccharomyces pombe. *J Biol Chem* **282**, 24583-24590 (2007).

269. Hasumi, Y. *et al.* Homozygous loss of BHD causes early embryonic lethality and kidney tumor development with activation of mTORC1 and mTORC2. *Proc Natl Acad Sci U S A* **106**, 18722-18727 (2009).

270. Hartman, T.R. *et al.* The role of the Birt-Hogg-Dube protein in mTOR activation and renal tumorigenesis. *Oncogene* **28**, 1594-1604 (2009).

271. Jung, J., Genau, H.M. & Behrends, C. Amino Acid-Dependent mTORC1 Regulation by the Lysosomal Membrane Protein SLC38A9. *Mol Cell Biol* **35**, 2479-2494 (2015).

272. Rebsamen, M. *et al.* SLC38A9 is a component of the lysosomal amino acid sensing machinery that controls mTORC1. *Nature* **519**, 477-481 (2015).

273. Wang, S. *et al.* Metabolism. Lysosomal amino acid transporter SLC38A9 signals arginine sufficiency to mTORC1. *Science* **347**, 188-194 (2015).

274. Ma, X.M. & Blenis, J. Molecular mechanisms of mTOR-mediated translational control. *Nat Rev Mol Cell Biol* **10**, 307-318 (2009).

275. Avni, D., Biberman, Y. & Meyuhas, O. The 5' terminal oligopyrimidine tract confers translational control on TOP mRNAs in a cell type- and sequence context-dependent manner. *Nucleic Acids Res* **25**, 995-1001 (1997).

276. Meyuhas, O. Synthesis of the translational apparatus is regulated at the translational level. *Eur J Biochem* **267**, 6321-6330 (2000).

277. Hsieh, A.C. *et al.* The translational landscape of mTOR signalling steers cancer initiation and metastasis. *Nature* **485**, 55-61 (2012).

278. Thoreen, C.C. *et al.* A unifying model for mTORC1-mediated regulation of mRNA translation. *Nature* **485**, 109-113 (2012).

279. Gressner, A.M. & Wool, I.G. The phosphorylation of liver ribosomal proteins in vivo. Evidence that only a single small subunit protein (S6) is phosphorylated. *J Biol Chem* **249**, 6917-6925 (1974).

280. Choi, J., Chen, J., Schreiber, S.L. & Clardy, J. Structure of the FKBP12-rapamycin complex interacting with the binding domain of human FRAP. *Science* **273**, 239-242 (1996).

281. Aylett, C.H. *et al.* Architecture of human mTOR complex 1. *Science* **351**, 48-52 (2016).

282. Laplante, M. & Sabatini, D.M. mTOR signaling in growth control and disease. *Cell* **149**, 274-293 (2012).

283. Okosun, J. *et al.* Recurrent mTORC1-activating RRAGC mutations in follicular lymphoma. *Nat Genet* **48**, 183-188 (2016).

284. Sato, T., Nakashima, A., Guo, L., Coffman, K. & Tamanoi, F. Single amino-acid changes that confer constitutive activation of mTOR are discovered in human cancer. *Oncogene* **29**, 2746-2752 (2010).

285. Dancey, J. mTOR signaling and drug development in cancer. *Nat Rev Clin Oncol* **7**, 209-219 (2010).

286. Hare, S.H. & Harvey, A.J. mTOR function and therapeutic targeting in breast cancer. *Am J Cancer Res* **7**, 383-404 (2017).

287. Cloughesy, T.F. *et al.* Antitumor activity of rapamycin in a Phase I trial for patients with recurrent PTEN-deficient glioblastoma. *PLoS Med* **5**, e8 (2008).

288. O'Reilly, K.E. *et al.* mTOR inhibition induces upstream receptor tyrosine kinase signaling and activates Akt. *Cancer Res* **66**, 1500-1508 (2006).

289. Sun, S.Y. *et al.* Activation of Akt and eIF4E survival pathways by rapamycin-mediated mammalian target of rapamycin inhibition. *Cancer Res* **65**, 7052-7058 (2005).

290. Choo, A.Y., Yoon, S.O., Kim, S.G., Roux, P.P. & Blenis, J. Rapamycin differentially inhibits S6Ks and 4E-BP1 to mediate cell-type-specific repression of mRNA translation. *Proc Natl Acad Sci U S A* **105**, 17414-17419 (2008).

291. She, Q.B. *et al.* 4E-BP1 is a key effector of the oncogenic activation of the AKT and ERK signaling pathways that integrates their function in tumors. *Cancer Cell* **18**, 39-51 (2010).

292. Tchevkina, E. & Komelkov, A. Protein phosphorylation as a key mechanism of mTORC1/2 signaling pathways, in *Protein Phosphorylation in Human Health* (ed. C. Huang) (IntechOpen, London; 2012).

293. Wolfson, R.L. & Sabatini, D.M. The Dawn of the Age of Amino Acid Sensors for the mTORC1 Pathway. *Cell Metab* **26**, 301-309 (2017).

294. Kim, S.G., Buel, G.R. & Blenis, J. Nutrient regulation of the mTOR complex 1 signaling pathway. *Mol Cells* **35**, 463-473 (2013).

295. Calvo, S.E., Clauser, K.R. & Mootha, V.K. MitoCarta2.0: an updated inventory of mammalian mitochondrial proteins. *Nucleic Acids Res* **44**, D1251-1257 (2016).

296. Cai, W., Wei, Y., Jarnik, M., Reich, J. & Lilly, M.A. The GATOR2 Component Wdr24 Regulates TORC1 Activity and Lysosome Function. *PLoS Genet* **12**, e1006036 (2016).

297. Nijman, S.M. Synthetic lethality: general principles, utility and detection using genetic screens in human cells. *FEBS Lett* **585**, 1-6 (2011).

298. Sidrauski, C., McGeachy, A.M., Ingolia, N.T. & Walter, P. The small molecule ISRIB reverses the effects of eIF2alpha phosphorylation on translation and stress granule assembly. *Elife* **4** (2015).

299. Harding, M.W., Galat, A., Uehling, D.E. & Schreiber, S.L. A receptor for the immunosuppressant FK506 is a cis-trans peptidyl-prolyl isomerase. *Nature* **341**, 758-760 (1989).

300. Smith, E.M., Finn, S.G., Tee, A.R., Browne, G.J. & Proud, C.G. The tuberous sclerosis protein TSC2 is not required for the regulation of the mammalian target of rapamycin by amino acids and certain cellular stresses. *J Biol Chem* **280**, 18717-18727 (2005).

301. Faundez, V., Horng, J.T. & Kelly, R.B. A function for the AP3 coat complex in synaptic vesicle formation from endosomes. *Cell* **93**, 423-432 (1998).

302. Seals, D.F., Eitzen, G., Margolis, N., Wickner, W.T. & Price, A. A Ypt/Rab effector complex containing the Sec1 homolog Vps33p is required for homotypic vacuole fusion. *Proc Natl Acad Sci U S A* **97**, 9402-9407 (2000).

303. Falcon-Perez, J.M., Starcevic, M., Gautam, R. & Dell'Angelica, E.C. BLOC-1, a novel complex containing the pallidin and muted proteins involved in the biogenesis of melanosomes and platelet-dense granules. *J Biol Chem* **277**, 28191-28199 (2002).

304. Puertollano, R. mTOR and lysosome regulation. *F1000Prime Rep* **6**, 52 (2014).

305. Shen, K. *et al.* Cryo-EM Structure of the Human FLCN-FNIP2-Rag-Ragulator Complex. *Cell* **179**, 1319-1329 e1318 (2019).

306. Martina, J.A. *et al.* The nutrient-responsive transcription factor TFE3 promotes autophagy, lysosomal biogenesis, and clearance of cellular debris. *Sci Signal* **7**, ra9 (2014).

307. Woodford, M.R. *et al.* The FNIP co-chaperones decelerate the Hsp90 chaperone cycle and enhance drug binding. *Nat Commun* **7**, 12037 (2016).

308. Davis, E.M. *et al.* Comparative Haploid Genetic Screens Reveal Divergent Pathways in the Biogenesis and Trafficking of Glycophosphatidylinositol-Anchored Proteins. *Cell Rep* **11**, 1727-1736 (2015).

309. Manifava, M. *et al.* Dynamics of mTORC1 activation in response to amino acids. *Elife* **5** (2016).

310. Alekhina, O., Burstein, E. & Billadeau, D.D. Cellular functions of WASP family proteins at a glance. *J Cell Sci* **130**, 2235-2241 (2017).

311. Flinn, R.J., Yan, Y., Goswami, S., Parker, P.J. & Backer, J.M. The late endosome is essential for mTORC1 signaling. *Mol Biol Cell* **21**, 833-841 (2010).

312. Parthibane, V. *et al.* Sptlc1 is essential for myeloid differentiation and hematopoietic homeostasis. *Blood Adv* **3**, 3635-3649 (2019).

313. Filipek, P.A. *et al.* LAMTOR/Ragulator is a negative regulator of Arl8b- and BORC-dependent late endosomal positioning. *J Cell Biol* **216**, 4199-4215 (2017).

314. Hatakeyama, R. *et al.* Spatially Distinct Pools of TORC1 Balance Protein Homeostasis. *Mol Cell* **73**, 325-338 e328 (2019).

315. Wada, S. *et al.* The tumor suppressor FLCN mediates an alternate mTOR pathway to regulate browning of adipose tissue. *Genes Dev* **30**, 2551-2564 (2016).

316. Nagashima, K. *et al.* Nutrient-induced FNIP degradation by SCFbeta-TRCP regulates FLCN complex localization and promotes renal cancer progression. *Oncotarget* **8**, 9947-9960 (2017).

317. Peli-Gulli, M.P., Raucci, S., Hu, Z., Dengjel, J. & De Virgilio, C. Feedback Inhibition of the Rag GTPase GAP Complex Lst4-Lst7 Safeguards TORC1 from Hyperactivation by Amino Acid Signals. *Cell Rep* **20**, 281-288 (2017).

318. Hong, S.B. *et al.* Inactivation of the FLCN tumor suppressor gene induces TFE3 transcriptional activity by increasing its nuclear localization. *PLoS One* **5**, e15793 (2010).

319. Wolfson, R.L. *et al.* Sestrin2 is a leucine sensor for the mTORC1 pathway. *Science* **351**, 43-48 (2016).

320. Chantranupong, L. *et al.* The CASTOR Proteins Are Arginine Sensors for the mTORC1 Pathway. *Cell* **165**, 153-164 (2016).

321. Gu, X. *et al.* SAMTOR is an S-adenosylmethionine sensor for the mTORC1 pathway. *Science* **358**, 813-818 (2017).

322. Wajant, H., Pfizenmaier, K. & Scheurich, P. Tumor necrosis factor signaling. *Cell Death Differ* **10**, 45-65 (2003).

323. Sedger, L.M. & McDermott, M.F. TNF and TNF-receptors: From mediators of cell death and inflammation to therapeutic giants - past, present and future. *Cytokine Growth Factor Rev* **25**, 453-472 (2014).

324. Carswell, E.A. *et al.* An endotoxin-induced serum factor that causes necrosis of tumors. *Proc Natl Acad Sci U S A* **72**, 3666-3670 (1975).

325. Mizrahi, K. & Askenasy, N. Physiological functions of TNF family receptor/ligand interactions in hematopoiesis and transplantation. *Blood* **124**, 176-183 (2014).

326. Mestan, J. *et al.* Antiviral effects of recombinant tumour necrosis factor in vitro. *Nature* **323**, 816-819 (1986).

327. Bradley, J.R. TNF-mediated inflammatory disease. *J Pathol* **214**, 149-160 (2008).

328. Black, R.A. *et al.* A metalloproteinase disintegrin that releases tumour-necrosis factor-alpha from cells. *Nature* **385**, 729-733 (1997).

329. Chen, G. & Goeddel, D.V. TNF-R1 signaling: a beautiful pathway. *Science* **296**, 1634-1635 (2002).

330. Banner, D.W. *et al.* Crystal structure of the soluble human 55 kd TNF receptor-human TNF beta complex: implications for TNF receptor activation. *Cell* **73**, 431-445 (1993).

331. Yang, S., Wang, J., Brand, D.D. & Zheng, S.G. Role of TNF-TNF Receptor 2 Signal in Regulatory T Cells and Its Therapeutic Implications. *Front Immunol* **9**, 784 (2018).

332. Holbrook, J., Lara-Reyna, S., Jarosz-Griffiths, H. & McDermott, M. Tumour necrosis factor signalling in health and disease. *F1000Res* **8** (2019).

333. Mak, T.W. & Yeh, W.C. Signaling for survival and apoptosis in the immune system. *Arthritis Res* **4 Suppl 3**, S243-252 (2002).

334. Hsu, H., Xiong, J. & Goeddel, D.V. The TNF receptor 1-associated protein TRADD signals cell death and NF-kappa B activation. *Cell* **81**, 495-504 (1995).

335. Ashkenazi, A. & Dixit, V.M. Death receptors: signaling and modulation. *Science* **281**, 1305-1308 (1998).

336. Haas, T.L. *et al.* Recruitment of the linear ubiquitin chain assembly complex stabilizes the TNF-R1 signaling complex and is required for TNF-mediated gene induction. *Mol Cell* **36**, 831-844 (2009).

337. Ting, A.T. & Bertrand, M.J.M. More to Life than NF-kappaB in TNFR1 Signaling. *Trends Immunol* **37**, 535-545 (2016).

338. Xanthoulea, S. *et al.* Tumor necrosis factor (TNF) receptor shedding controls thresholds of innate immune activation that balance opposing TNF functions in infectious and inflammatory diseases. *J Exp Med* **200**, 367-376 (2004).

339. Van Hauwermeiren, F. *et al.* Safe TNF-based antitumor therapy following p55TNFR reduction in intestinal epithelium. *J Clin Invest* **123**, 2590-2603 (2013).

340. McDermott, M.F. *et al.* Germline mutations in the extracellular domains of the 55 kDa TNF receptor, TNFR1, define a family of dominantly inherited autoinflammatory syndromes. *Cell* **97**, 133-144 (1999).

341. Sarrauste de Menthiere, C. *et al.* INFEVERS: the Registry for FMF and hereditary inflammatory disorders mutations. *Nucleic Acids Res* **31**, 282-285 (2003).

342. Puimege, L., Libert, C. & Van Hauwermeiren, F. Regulation and dysregulation of tumor necrosis factor receptor-1. *Cytokine Growth Factor Rev* **25**, 285-300 (2014).

343. Cui, X. *et al.* Identification of ARTS-1 as a novel TNFR1-binding protein that promotes TNFR1 ectodomain shedding. *J Clin Invest* **110**, 515-526 (2002).

344. Peschon, J.J. *et al.* An essential role for ectodomain shedding in mammalian development. *Science* **282**, 1281-1284 (1998).

345. Dreymueller, D., Pruessmeyer, J., Groth, E. & Ludwig, A. The role of ADAM-mediated shedding in vascular biology. *Eur J Cell Biol* **91**, 472-485 (2012).

346. Mosselmans, R., Hepburn, A., Dumont, J.E., Fiers, W. & Galand, P. Endocytic pathway of recombinant murine tumor necrosis factor in L-929 cells. *J Immunol* **141**, 3096-3100 (1988).

347. Maminska, A. *et al.* ESCRT proteins restrict constitutive NF-kappaB signaling by trafficking cytokine receptors. *Sci Signal* **9**, ra8 (2016).

348. Kemper, O. & Wallach, D. Cloning and partial characterization of the promoter for the human p55 tumor necrosis factor (TNF) receptor. *Gene* **134**, 209-216 (1993).

349. Bristol, J.A., Morrison, T.E. & Kenney, S.C. CCAAT/enhancer binding proteins alpha and beta regulate the tumor necrosis factor receptor 1 gene promoter. *Mol Immunol* **46**, 2706-2713 (2009).

350. Baxter, F.O. *et al.* IKKbeta/2 induces TWEAK and apoptosis in mammary epithelial cells. *Development* **133**, 3485-3494 (2006).

351. Egusquiaguirre, S.P., Yeh, J.E., Walker, S.R., Liu, S. & Frank, D.A. The STAT3 Target Gene TNFRSF1A Modulates the NF-kappaB Pathway in Breast Cancer Cells. *Neoplasia* **20**, 489-498 (2018).

352. Huang, Y., Tan, M., Gosink, M., Wang, K.K. & Sun, Y. Histone deacetylase 5 is not a p53 target gene, but its overexpression inhibits tumor cell growth and induces apoptosis. *Cancer Res* **62**, 2913-2922 (2002).

353. Winzen, R. *et al.* Interaction between the mRNA of the 55-kDa tumor necrosis factor receptor and cellular proteins. Possible involvement in post-transcriptional regulation of receptor expression. *J Biol Chem* **271**, 13461-13467 (1996).

354. Geer, L.Y. *et al.* The NCBI BioSystems database. *Nucleic Acids Res* **38**, D492-496 (2010).

355. Kim, S.Y. & Solomon, D.H. Tumor necrosis factor blockade and the risk of viral infection. *Nat Rev Rheumatol* **6**, 165-174 (2010).

356. Cleynen, I. & Vermeire, S. Paradoxical inflammation induced by anti-TNF agents in patients with IBD. *Nat Rev Gastroenterol Hepatol* **9**, 496-503 (2012).

357. Wong, A.K., Kerkoutian, S., Said, J., Rashidi, H. & Pullarkat, S.T. Risk of lymphoma in patients receiving antitumor necrosis factor therapy: a meta-analysis of published randomized controlled studies. *Clin Rheumatol* **31**, 631-636 (2012).

358. Mohan, N. *et al.* Demyelination occurring during anti-tumor necrosis factor alpha therapy for inflammatory arthritides. *Arthritis Rheum* **44**, 2862-2869 (2001).

359. Faustman, D. & Davis, M. TNF receptor 2 pathway: drug target for autoimmune diseases. *Nat Rev Drug Discov* **9**, 482-493 (2010).

360. Kollias, G. & Kontoyiannis, D. Role of TNF/TNFR in autoimmunity: specific TNF receptor blockade may be advantageous to anti-TNF treatments. *Cytokine Growth Factor Rev* **13**, 315-321 (2002).

361. Fischer, R. *et al.* Novel strategies to mimic transmembrane tumor necrosis factor-dependent activation of tumor necrosis factor receptor 2. *Sci Rep* **7**, 6607 (2017).

362. Williams, S.K. *et al.* Anti-TNFR1 targeting in humanized mice ameliorates disease in a model of multiple sclerosis. *Sci Rep* **8**, 13628 (2018).

363. Uhlen, M. *et al.* Proteomics. Tissue-based map of the human proteome. *Science* **347**, 1260419 (2015).

364. Lakshmana, M.K., Araki, W. & Tabira, T. Amyloid beta peptide binds a novel death-inducing protein, AB-DIP. *FASEB J* **19**, 1362-1364 (2005).

365. Kao, W.P. *et al.* The versatile roles of CARDs in regulating apoptosis, inflammation, and NF-kappaB signaling. *Apoptosis* **20**, 174-195 (2015).

366. Kersse, K., Verspurten, J., Vanden Berghe, T. & Vandenabeele, P. The death-fold superfamily of homotypic interaction motifs. *Trends Biochem Sci* **36**, 541-552 (2011).

367. Park, H.H. *et al.* The death domain superfamily in intracellular signaling of apoptosis and inflammation. *Annu Rev Immunol* **25**, 561-586 (2007).

368. Ververi, A., Splitt, M., Dean, J.C.S., Study, D.D.D. & Brady, A.F. Phenotypic spectrum associated with de novo mutations in QRICH1 gene. *Clin Genet* **93**, 286-292 (2018).

369. Lui, J.C. *et al.* QRICH1 mutations cause a chondrodysplasia with developmental delay. *Clin Genet* **95**, 160-164 (2019).

370. Gonzalez-Flores, J.N., Shetty, S.P., Dubey, A. & Copeland, P.R. The molecular biology of selenocysteine. *Biomol Concepts* **4**, 349-365 (2013).

371. Na, J. *et al.* Selenophosphate synthetase 1 and its role in redox homeostasis, defense and proliferation. *Free Radic Biol Med* **127**, 190-197 (2018).

372. Itoh, Y. *et al.* Structure of selenophosphate synthetase essential for selenium incorporation into proteins and RNAs. *J Mol Biol* **385**, 1456-1469 (2009).

373. Persson, B.C., Bock, A., Jackle, H. & Vorbruggen, G. SelD homolog from Drosophila lacking selenide-dependent monoselenophosphate synthetase activity. *J Mol Biol* **274**, 174-180 (1997).

374. Xu, X.M. *et al.* Biosynthesis of selenocysteine on its tRNA in eukaryotes. *PLoS Biol* **5**, e4 (2007).

375. Tobe, R. *et al.* Selenophosphate synthetase 1 is an essential protein with roles in regulation of redox homoeostasis in mammals. *Biochem J* **473**, 2141-2154 (2016).

376. Kumar, R. *et al.* ZNF652, a novel zinc finger protein, interacts with the putative breast tumor suppressor CBFA2T3 to repress transcription. *Mol Cancer Res* **4**, 655-665 (2006).

377. Kumar, R. *et al.* CBFA2T3-ZNF652 corepressor complex regulates transcription of the E-box gene HEB. *J Biol Chem* **283**, 19026-19038 (2008).

378. Kumar, R. *et al.* Genome-wide mapping of ZNF652 promoter binding sites in breast cancer cells. *J Cell Biochem* **112**, 2742-2747 (2011).

379. Gewurz, B.E. *et al.* Genome-wide siRNA screen for mediators of NF-kappaB activation. *Proc Natl Acad Sci U S A* **109**, 2467-2472 (2012).

380. Warner, N. *et al.* A genome-wide siRNA screen reveals positive and negative regulators of the NOD2 and NF-kappaB signaling pathways. *Sci Signal* **6**, rs3 (2013).

381. Nickles, D., Falschlehner, C., Metzig, M. & Boutros, M. A genome-wide RNA interference screen identifies caspase 4 as a factor required for tumor necrosis factor alpha signaling. *Mol Cell Biol* **32**, 3372-3381 (2012).

382. Feldman, D. *et al.* Optical Pooled Screens in Human Cells. *Cell* **179**, 787-799 e717 (2019).

383. Lo, C.H. *et al.* Noncompetitive inhibitors of TNFR1 probe conformational activation states. *Sci Signal* **12** (2019).

384. Fauster, A. *et al.* Systematic genetic mapping of necroptosis identifies SLC39A7 as modulator of death receptor trafficking. *Cell Death Differ* **26**, 1138-1155 (2019).

385. Brown, K., Gerstberger, S., Carlson, L., Franzoso, G. & Siebenlist, U. Control of I kappa B-alpha proteolysis by site-specific, signal-induced phosphorylation. *Science* **267**, 1485-1488 (1995).

386. Schmidt, R.L. & Simonovic, M. Synthesis and decoding of selenocysteine and human health. *Croat Med J* **53**, 535-550 (2012).

387. Wertz, I.E. & Dixit, V.M. Signaling to NF-kappaB: regulation by ubiquitination. *Cold Spring Harb Perspect Biol* **2**, a003350 (2010).

388. Kuleshov, M.V. *et al.* Enrichr: a comprehensive gene set enrichment analysis web server 2016 update. *Nucleic Acids Res* **44**, W90-97 (2016).

389. Israel, A. The IKK complex, a central regulator of NF-kappaB activation. *Cold Spring Harb Perspect Biol* **2**, a000158 (2010).

390. Jaattela, M., Mouritzen, H., Elling, F. & Bastholm, L. A20 zinc finger protein inhibits TNF and IL-1 signaling. *J Immunol* **156**, 1166-1173 (1996).

391. Mahoney, D.J. *et al.* Both cIAP1 and cIAP2 regulate TNFalpha-mediated NF-kappaB activation. *Proc Natl Acad Sci U S A* **105**, 11778-11783 (2008).

392. Tada, K. *et al.* Critical roles of TRAF2 and TRAF5 in tumor necrosis factor-induced NF-kappa B activation and protection from cell death. *J Biol Chem* **276**, 36530-36534 (2001).

393. Collins, P.E., Mitxitorena, I. & Carmody, R.J. The Ubiquitination of NF-kappaB Subunits in the Control of Transcription. *Cells* **5** (2016).

394. Chen, Z.J. Ubiquitin signalling in the NF-kappaB pathway. *Nat Cell Biol* **7**, 758-765 (2005).

395. Rolland, T. *et al.* A proteome-scale map of the human interactome network. *Cell* **159**, 1212-1226 (2014).

396. Bruckner, A., Polge, C., Lentze, N., Auerbach, D. & Schlattner, U. Yeast two-hybrid, a powerful tool for systems biology. *Int J Mol Sci* **10**, 2763-2788 (2009).

397. Lakshmana, M.K., Hara, H. & Tabira, T. Amyloid beta protein-related death-inducing protein induces G2/M arrest: Implications for neurodegeneration in Alzheimer's disease. *J Neurosci Res* **85**, 2262-2271 (2007).

398. Sun, L. & Fang, J. Macromolecular crowding effect is critical for maintaining SIRT1's nuclear localization in cancer cells. *Cell Cycle* **15**, 2647-2655 (2016).

399. Lue, N.F. & Kornberg, R.D. Accurate initiation at RNA polymerase II promoters in extracts from Saccharomyces cerevisiae. *Proc Natl Acad Sci U S A* **84**, 8839-8843 (1987).

400. Holden, P. & Horton, W.A. Crude subcellular fractionation of cultured mammalian cell lines. *BMC Res Notes* **2**, 243 (2009).

401. Subramanian, A. *et al.* A Next Generation Connectivity Map: L1000 Platform and the First 1,000,000 Profiles. *Cell* **171**, 1437-1452 e1417 (2017).

402. Hughes, T.R. *et al.* Functional discovery via a compendium of expression profiles. *Cell* **102**, 109-126 (2000).

403. Lamb, J. *et al.* The Connectivity Map: using gene-expression signatures to connect small molecules, genes, and disease. *Science* **313**, 1929-1935 (2006).

404. Subramanian, A. *et al.* Gene set enrichment analysis: a knowledge-based approach for interpreting genome-wide expression profiles. *Proc Natl Acad Sci U S A* **102**, 15545-15550 (2005).

405. Mootha, V.K. *et al.* PGC-1alpha-responsive genes involved in oxidative phosphorylation are coordinately downregulated in human diabetes. *Nat Genet* **34**, 267-273 (2003).

406. Mitchell, A.L. *et al.* InterPro in 2019: improving coverage, classification and access to protein sequence annotations. *Nucleic Acids Res* **47**, D351-D360 (2019).

407. Kosugi, S. *et al.* Six classes of nuclear localization signals specific to different binding grooves of importin alpha. *J Biol Chem* **284**, 478-485 (2009).

408. Wagner, S.A., Satpathy, S., Beli, P. & Choudhary, C. SPATA2 links CYLD to the TNF-alpha receptor signaling complex and modulates the receptor signaling outcomes. *EMBO J* **35**, 1868-1884 (2016).

409. Kuznetsova, I.M., Turoverov, K.K. & Uversky, V.N. What macromolecular crowding can do to a protein. *Int J Mol Sci* **15**, 23090-23140 (2014).

410. Thurmond, J. *et al.* FlyBase 2.0: the next generation. *Nucleic Acids Res* **47**, D759-D765 (2019).

411. Kojima, K.K. & Jurka, J. Crypton transposons: identification of new diverse families and ancient domestication events. *Mob DNA* **2**, 12 (2011).

412. Meissner, T.B. *et al.* NLR family member NLRC5 is a transcriptional regulator of MHC class I genes. *Proc Natl Acad Sci U S A* **107**, 13794-13799 (2010).

413. Neerincx, A., Rodriguez, G.M., Steimle, V. & Kufer, T.A. NLRC5 controls basal MHC class I gene expression in an MHC enhanceosome-dependent manner. *J Immunol* **188**, 4940-4950 (2012).

414. Warner, N., Burberry, A., Pliakas, M., McDonald, C. & Nunez, G. A genome-wide small interfering RNA (siRNA) screen reveals nuclear factor-kappaB (NF-kappaB)-independent regulators of NOD2-induced interleukin-8 (IL-8) secretion. *J Biol Chem* **289**, 28213-28224 (2014).

415. Kearney, C.J. *et al.* Tumor immune evasion arises through loss of TNF sensitivity. *Sci Immunol* **3** (2018).

416. Wang, K.T., Wang, J., Li, L.F. & Su, X.D. Crystal structures of catalytic intermediates of human selenophosphate synthetase 1. *J Mol Biol* **390**, 747-759 (2009).

417. Consortium, E.P. An integrated encyclopedia of DNA elements in the human genome. *Nature* **489**, 57-74 (2012).

418. Tuladhar, R. *et al.* CRISPR-Cas9-based mutagenesis frequently provokes on-target mRNA misregulation. *Nat Commun* **10**, 4056 (2019).

419. Smits, A.H. *et al.* Biological plasticity rescues target activity in CRISPR knock outs. *Nat Methods* **16**, 1087-1093 (2019).

420. Kumar, R., Cheney, K.M., Neilsen, P.M., Schulz, R.B. & Callen, D.F. CBFA2T3-ZNF651, like CBFA2T3-ZNF652, functions as a transcriptional corepressor complex. *FEBS Lett* **584**, 859-864 (2010).

421. Morita, M. *et al.* A novel 4EHP-GIGYF2 translational repressor complex is essential for mammalian development. *Mol Cell Biol* **32**, 3585-3593 (2012).

422. Song, B.C., Joo, N.S., Aldini, G. & Yeum, K.J. Biological functions of histidine-dipeptides and metabolic syndrome. *Nutr Res Pract* **8**, 3-10 (2014).

423. Miceli, V. *et al.* Carnosine protects pancreatic beta cells and islets against oxidative stress damage. *Mol Cell Endocrinol* **474**, 105-118 (2018).

424. Yehia, R., Saleh, S., El Abhar, H., Saad, A.S. & Schaalan, M. L-Carnosine protects against Oxaliplatin-induced peripheral neuropathy in colorectal cancer patients: A perspective on targeting Nrf-2 and NF-kappaB pathways. *Toxicol Appl Pharmacol* **365**, 41-50 (2019).

425. Huang, Z., Rose, A.H. & Hoffmann, P.R. The role of selenium in inflammation and immunity: from molecular mechanisms to therapeutic opportunities. *Antioxid Redox Signal* **16**, 705-743 (2012).

426. Avery, J.C. & Hoffmann, P.R. Selenium, Selenoproteins, and Immunity. *Nutrients* **10** (2018).

427. Matthews, J.R., Wakasugi, N., Virelizier, J.L., Yodoi, J. & Hay, R.T. Thioredoxin regulates the DNA binding activity of NF-kappa B by reduction of a disulphide bond involving cysteine 62. *Nucleic Acids Res* **20**, 3821-3830 (1992).

428. Lobito, A.A. *et al.* Abnormal disulfide-linked oligomerization results in ER retention and altered signaling by TNFR1 mutants in TNFR1-associated periodic fever syndrome (TRAPS). *Blood* **108**, 1320-1327 (2006).

429. Peng, D.F., Hu, T.L., Soutto, M., Belkhiri, A. & El-Rifai, W. Loss of glutathione peroxidase 7 promotes TNF-alpha-induced NF-kappaB activation in Barrett's carcinogenesis. *Carcinogenesis* **35**, 1620-1628 (2014).

430. Hill, K.E., Lyons, P.R. & Burk, R.F. Differential regulation of rat liver selenoprotein mRNAs in selenium deficiency. *Biochem Biophys Res Commun* **185**, 260-263 (1992).

431. Chen, J.J. *et al.* Mislocalization of death receptors correlates with cellular resistance to their cognate ligands in human breast cancer cells. *Oncotarget* **3**, 833-842 (2012).

432. Mutlu, N. & Kumar, A. Mapping paths: new approaches to dissect eukaryotic signaling circuitry. *F1000Res* **5** (2016).

433. Tang, F. *et al.* mRNA-Seq whole-transcriptome analysis of a single cell. *Nat Methods* **6**, 377-382 (2009).

434. Luo, C. *et al.* Single-cell methylomes identify neuronal subtypes and regulatory elements in mammalian cortex. *Science* **357**, 600-604 (2017).

435. Cadwell, C.R. *et al.* Multimodal profiling of single-cell morphology, electrophysiology, and gene expression using Patch-seq. *Nat Protoc* **12**, 2531-2553 (2017).

436. Camacho, D.M., Collins, K.M., Powers, R.K., Costello, J.C. & Collins, J.J. Next-Generation Machine Learning for Biological Networks. *Cell* **173**, 1581-1592 (2018).

437. Marbach, D. *et al.* Wisdom of crowds for robust gene network inference. *Nat Methods* **9**, 796-804 (2012).

438. Langille, M.G. *et al.* Predictive functional profiling of microbial communities using 16S rRNA marker gene sequences. *Nat Biotechnol* **31**, 814-821 (2013).

439. Alipanahi, B., Delong, A., Weirauch, M.T. & Frey, B.J. Predicting the sequence specificities of DNA- and RNA-binding proteins by deep learning. *Nat Biotechnol* **33**, 831-838 (2015).

440. Zou, D., Ma, L., Yu, J. & Zhang, Z. Biological databases for human research. *Genomics Proteomics Bioinformatics* **13**, 55-63 (2015).

441. Mall, R., Cerulo, L., Bensmail, H., Iavarone, A. & Ceccarelli, M. Detection of statistically significant network changes in complex biological networks. *BMC Syst Biol* **11**, 32 (2017).

442. Greene, C.S. *et al.* Understanding multicellular function and disease with human tissue-specific networks. *Nat Genet* **47**, 569-576 (2015).

443. Adamson, B. *et al.* A Multiplexed Single-Cell CRISPR Screening Platform Enables Systematic Dissection of the Unfolded Protein Response. *Cell* **167**, 1867-1882 e1821 (2016).

444. Dixit, A. *et al.* Perturb-Seq: Dissecting Molecular Circuits with Scalable Single-Cell RNA Profiling of Pooled Genetic Screens. *Cell* **167**, 1853-1866 e1817 (2016).

445. Jaitin, D.A. *et al.* Dissecting Immune Circuits by Linking CRISPR-Pooled Screens with Single-Cell RNA-Seq. *Cell* **167**, 1883-1896 e1815 (2016).

446. Datlinger, P. *et al.* Pooled CRISPR screening with single-cell transcriptome readout. *Nat Methods* **14**, 297-301 (2017).

447. Lanning, B.R. & Vakoc, C.R. Single-minded CRISPR screening. *Nat Biotechnol* **35**, 339-340 (2017).

448. McFarland, J.M. *et al.* Improved estimation of cancer dependencies from large-scale RNAi screens using model-based normalization and data integration. *Nat Commun* **9**, 4610 (2018).

449. Mimitou, E.P. *et al.* Multiplexed detection of proteins, transcriptomes, clonotypes and CRISPR perturbations in single cells. *Nat Methods* **16**, 409-412 (2019).

450. Peterson, V.M. *et al.* Multiplexed quantification of proteins and transcripts in single cells. *Nat Biotechnol* **35**, 936-939 (2017).

451. Stoeckius, M. *et al.* Simultaneous epitope and transcriptome measurement in single cells. *Nat Methods* **14**, 865-868 (2017).

452. Emanuel, G., Moffitt, J.R. & Zhuang, X. High-throughput, image-based screening of pooled genetic-variant libraries. *Nat Methods* **14**, 1159-1162 (2017).

453. Lawson, M.J. *et al.* In situ genotyping of a pooled strain library after characterizing complex phenotypes. *Mol Syst Biol* **13**, 947 (2017).

454. Camsund, D. *et al.* Time-resolved imaging-based CRISPRi screening. *Nat Methods* **17**, 86-92 (2020).

455. Ke, R. *et al.* In situ sequencing for RNA analysis in preserved tissue and cells. *Nat Methods* **10**, 857-860 (2013).

Chapter 8: **Appendices**

8.1 QRICH1 cDNA inserts in pLenti GFP

8.1.1 *Relevant genetic elements*

AACATG	Kozac sequence + ATG
TAGTAG	Stop codon
GACTACAAAGACGATGACGACAAG	FLAG tag
CGGTGGTGGTGGTAGT	Glycine-Serine linker
ATGAAT...CAC	QRICH1 protein (Q2TAL8-1)
C > T	synonymous substitution (avoid creation of BamHI cutting site)

8.1.2 *QRICH1 cDNA sequences*

pLenti - QRICH1

AACATGAATAATTCCCTAGAGAACACCATCTCCTTTGAAGAGTACATCCGAGTAAAGGCAC
GGTCTGTCCCGCAACACAGGATGAAGGAATTTCTGGACTCACTGGCCTCTAAGGGGCCAGA
AGCCCTTCAGGAGTTCCAGCAGACAGCCACCACTACCATGGTGTACCAACAGGGTGGGAAC
TGCATATACACAGACAGCACTGAAGTGGCTGGGTCTTTGCTTGAACTTGCCTGTCCAGTCAC
CACCAGTGTTCAGCCACAAACCCAGCAAGAACAGCAGATCCAGGTTCAGCAGCCGCAGCAG
GTTCAGGTCCAGGTGCAGGTACAGCAGTCTCCGCAACAGGTCTCGGCTCAGCTCTCCCCACA
ACTCACCGTTCACCAGCCTACTGAGCAACCCATCCAGGTCCAGGTGCAGATCCAAGGCCAGG
CACCACAGTCAGCAGCCCCCTCCATTCAGACCCCGTCTCTGCAGAGTCCCAGTCCCTCGCAG
CTGCAAGCAGCTCAGATCCAGGTGCAGCACGTGCAAGCAGCCCAGCAGATCCAGGCTGCAG
AAATCCCGGAGGAGCACATCCCACATCAGCAAATCCAGGCTCAGCTGGTGGCTGGCCAGTC
TCTTGCTGGTGGTCAGCAGATCCAAATCCAGACCGTGGGTGCCCTTTCCCCACCACCATCCC
AGCAGGGCTCACCCCGGGAAGGGGAGCGGCGGGTTGGCACGGCCAGTGTCCTCCAACCAGT
GAAGAAGCGCAAAGTGGACATGCCCATCACTGTGTCCTACGCCATCTCAGGGCAGCCGGTG
GCCACCGTGCTGGCCATTCCACAGGGCCAGCAGCAGAGTTATGTGTCTTTGAGGCCAGACTT
ACTGACAGTAGACAGTGCCCACCTGTACAGTGCCACTGGGACCATTACTAGCCCTACAGGAG
AAACCTGGACCATCCCTGTTTATTCTGCCCAGCCCCGGGGGGACCCTCAGCAGCAGAGCATT
ACCCACATTGCCATTCCCCAGGAAGCCTACAACGCAGTTCACGTCAGTGGCTCACCCACAGC
CCTGGCAGCTGTTAAGCTGGAGGATGACAAGGAGAAGATGGTGGGCACCACATCTGTAGTG
AAAAACTCCCATGAAGAGGTAGTGCAGACCCTTGCAAACTCTCTCTTTCCAGCACAGTTCAT
GAATGGCAACATCCACATTCCAGTGGCTGTGCAGGCTGTGGCAGGCACGTACCAGAATACG
GCTCAAACTGTCCATATATGGGACCCCCAACAGCAGCCGCAGCAGCAAACTCCCCAGGAAC
AGACACCACCACCACAGCAGCAGCAGCAGCAACTCCAAGTTACTTGTTCAGCTCAAACTGTC
CAGGTTGCTGAAGTTGAACCACAGTCACAGCCACAGCCTTCCCCAGAACTTCTGCTTCCAAA
TTCTTTGAAGCCAGAAGAAGGGCTTGAAGTATGGAAAAACTGGGCCCAGACCAAGAATGCT
GAACTAGAGAAGGATGCTCAGAACAGATTGGCACCCATTGGGAGGCGCCAACTGCTGCGAT
TCCAGGAAGATCTCATCTCCTCTGCTGTGGCAGAGTTGAATTATGGGCTCTGTCTAATGACA
CGGGAAGCTCGAAATGGAGAAGGTGAACCCTATGACCCAGATGTGCTCTACTATATTTTCCT

GTGTATTCAAAAGTATCTTTTTGAAAATGGAAGGGTAGATGACATTTTCTCCGATCTTTATTA
TGTTCGGTTCACGGAGTGGCTACATGAAGTTCTGAAGGATGTTCAGCCCCGGGTCACTCCAC
TTGGCTATGTCTTGCCCAGCCACGTGACTGAGGAGATGCTATGGGAGTGCAAGCAGCTTGGG
GCTCACTCCCCCTCCACCTTGCTGACCACCCTCATGTTCTTTAATACCAAGTACTTCCTATTG
AAGACAGTGGACCAGCACATGAAGCTGGCCTTCTCCAAGGTCTTGCGACAGACAAAGAAGA
ACCCCTCTAATCCCAAGGATAAAAGCACGAGTATCCGGTACTTGAAGGCCCTTGGAATACAC
CAGACTGGCCAGAAAGTTACAGATGACATGTATGCAGAACAGACGGAAAATCCAGAGAATC
CATTGAGATGTCCCATCAAGCTCTATGATTTCTACCTCTTCAAATGCCCCCAGAGTGTGAAA
GGCCGGAATGACACCTTTTACCTGACACCTGAGCCAGTGGTGGCCCCCAACAGCCCAATCTG
GTACTCAGTCCAGCCTATCAGCAGAGAGCAGATGGGACAAATGCTGACGCGGATCTTGGTG
ATAAGAGAAATTCAGGAGGCCATCGCAGTGGCCAATGCAAGCACTATGCACTGATAG

pLenti - QRICH1 - FLAG

AACATGAATAATTCCCTAGAGAACACCATCTCCTTTGAAGAGTACATCCGAGTAAAGGCACG
GTCTGTCCCGCAACACAGGATGAAGGAATTTCTGGACTCACTGGCCTCTAAGGGGCCAGAA
GCCCTTCAGGAGTTCCAGCAGACAGCCACCACTACCATGGTGTACCAACAGGGTGGGAACT
GCATATACACAGACAGCACTGAAGTGGCTGGGTCTTTGCTTGAACTTGCCTGTCCAGTCACC
ACCAGTGTTCAGCCACAAACCCAGCAAGAACAGCAGATCCAGGTTCAGCAGCCGCAGCAGG
TTCAGGTCCAGGTGCAGGTACAGCAGTCTCCGCAACAGGTCTCGGCTCAGCTCTCCCCACAA
CTCACCGTTCACCAGCCTACTGAGCAACCCATCCAGGTCCAGGTGCAGATCCAAGGCCAGGC
ACCACAGTCAGCAGCCCCCTCCATTCAGACCCCGTCTCTGCAGAGTCCCAGTCCCTCGCAGC
TGCAAGCAGCTCAGATCCAGGTGCAGCACGTGCAAGCAGCCCAGCAGATCCAGGCTGCAGA
AATCCCGGAGGAGCACATCCCACATCAGCAAATCCAGGCTCAGCTGGTGGCTGGCCAGTCTC
TTGCTGGTGGTCAGCAGATCCAAATCCAGACCGTGGGTGCCCTTTCCCCACCACCATCCCAG
CAGGGCTCACCCCGGGAAGGGGAGCGGCGGGTTGGCACGGCCAGTGTCCTCCAACCAGTGA
AGAAGCGCAAAGTGGACATGCCCATCACTGTGTCCTACGCCATCTCAGGGCAGCCGGTGGC
CACCGTGCTGGCCATTCCACAGGGCCAGCAGCAGAGTTATGTGTCTTTGAGGCCAGACTTAC
TGACAGTAGACAGTGCCCACCTGTACAGTGCCACTGGGACCATTACTAGCCCTACAGGAGA
AACCTGGACCATCCCTGTTTATTCTGCCCAGCCCCGGGGGGACCCTCAGCAGCAGAGCATTA
CCCACATTGCCATTCCCCAGGAAGCCTACAACGCAGTTCACGTCAGTGGCTCACCCACAGCC
CTGGCAGCTGTTAAGCTGGAGGATGACAAGGAGAAGATGGTGGGCACCACATCTGTAGTGA
AAAACTCCCATGAAGAGGTAGTGCAGACCCTTGCAAACTCTCTCTTTCCAGCACAGTTCATG
AATGGCAACATCCACATTCCAGTGGCTGTGCAGGCTGTGGCAGGCACGTACCAGAATACGG
CTCAAACTGTCCATATATGGGACCCCCAACAGCAGCCGCAGCAGCAAACTCCCCAGGAACA
GACACCACCACCACAGCAGCAGCAGCAGCAACTCCAAGTTACTTGTTCAGCTCAAACTGTCC
AGGTTGCTGAAGTTGAACCACAGTCACAGCCACAGCCTTCCCCAGAACTTCTGCTTCCAAAT
TCTTTGAAGCCAGAAGAAGGGCTTGAAGTATGGAAAAACTGGGCCCAGACCAAGAATGCTG
AACTAGAGAAGGATGCTCAGAACAGATTGGCACCCATTGGGAGGCGCCAACTGCTGCGATT
CCAGGAAGATCTCATCTCCTCTGCTGTGGCAGAGTTGAATTATGGGCTCTGTCTAATGACAC
GGGAAGCTCGAAATGGAGAAGGTGAACCCTATGACCCAGATGTGCTCTACTATATTTTCCTG
TGTATTCAAAAGTATCTTTTTGAAAATGGAAGGGTAGATGACATTTTCTCCGATCTTTATTAT
GTTCGGTTCACGGAGTGGCTACATGAAGTTCTGAAGGATGTTCAGCCCCGGGTCACTCCACT
TGGCTATGTCTTGCCCAGCCACGTGACTGAGGAGATGCTATGGGAGTGCAAGCAGCTTGGGG
CTCACTCCCCCTCCACCTTGCTGACCACCCTCATGTTCTTTAATACCAAGTACTTCCTATTGA
AGACAGTGGACCAGCACATGAAGCTGGCCTTCTCCAAGGTCTTGCGACAGACAAAGAAGAA
CCCCTCTAATCCCAAGGATAAAAGCACGAGTATCCGGTACTTGAAGGCCCTTGGAATACACC
AGACTGGCCAGAAAGTTACAGATGACATGTATGCAGAACAGACGGAAAATCCAGAGAATCC
ATTGAGATGTCCCATCAAGCTCTATGATTTCTACCTCTTCAAATGCCCCCAGAGTGTGAAAG
GCCGGAATGACACCTTTTACCTGACACCTGAGCCAGTGGTGGCCCCCAACAGCCCAATCTGG
TACTCAGTCCAGCCTATCAGCAGAGAGCAGATGGGACAAATGCTGACGCGGATCTTGGTGA
TAAGAGAAATTCAGGAGGCCATCGCAGTGGCCAATGCAAGCACTATGCACGGTGGTGGTGG
TAGTGACTACAAAGACGATGACGACAAGTGATAG

pLenti - QRICH1 – ΔCARD – FLAG

AACATGAATAATTCCCTAGAGAACACCATCTCCTTTGAAGAGTACATCCGAGTAAAGGCAC
GGTCTGTCCCGCAACACAGGATGAAGGAATTTCTGGACTCACTGGCCTCTAAGGGGCCAGA
AGCCCTTCAGGAGTTCCAGCAGACAGCCACCACTACCATGGTGTACCAACAGGGTGGGAAC
TGCATATACACAGACAGCACTGAAGTGGCTGGGTCTTTGCTTGAACTTGCCTGTCCAGTCAC
CACCAGTGTTCAGCCACAAACCCAGCAAGAACAGCAGATCCAGGTTCAGCAGCCGCAGCAG
GTTCAGGTCCAGGTGCAGGTACAGCAGTCTCCGCAACAGGTCTCGGCTCAGCTCTCCCCACA
ACTCACCGTTCACCAGCCTACTGAGCAACCCATCCAGGTCCAGGTGCAGATCCAAGGCCAGG
CACCACAGTCAGCAGCCCCCTCCATTCAGACCCCGTCTCTGCAGAGTCCCAGTCCCTCGCAG
CTGCAAGCAGCTCAGATCCAGGTGCAGCACGTGCAAGCAGCCCAGCAGATCCAGGCTGCAG
AAATCCCGGAGGAGCACATCCCACATCAGCAAATCCAGGCTCAGCTGGTGGCTGGCCAGTC
TCTTGCTGGTGGTCAGCAGATCCAAATCCAGACCGTGGGTGCCCTTTCCCCACCACCATCCC
AGCAGGGCTCACCCCGGGAAGGGGAGGTTGGCACGGCCAGTGTCCTCCAACCAGTGAAGAA
GCGCAAAGTGGACATGCCCATCACTGTGTCCTACGCCATCTCAGGGCAGCCGGTGGCCACCG
TGCTGGCCATTCCACAGGGCCAGCAGCAGAGTTATGTGTCTTTGAGGCCAGACTTACTGACA
GTAGACAGTGCCCACCTGTACAGTGCCACTGGGACCATTACTAGCCCTACAGGAGAAACCTG
GACCATCCCTGTTTATTCTGCCCAGCCCCGGGGGGACCCTCAGCAGCAGAGCATTACCCACA
TTGCCATTCCCCAGGAAGCCTACAACGCAGTTCACGTCAGTGGCTCACCCACAGCCCTGGCA
GCTGTTAAGCTGGAGGATGACAAGGAGAAGATGGTGGGCACCACATCTGTAGTGAAAAACT
CCCATGAAGAGGTAGTGCAGACCCTTGCAAACTCTCTCTTTCCAGCACAGTTCATGAATGGC
AACATCCACATTCCAGTGGCTGTGCAGGCTGTGGCAGGCACGTACCAGAATACGGCTCAAA
CTGTCCATATATGGGACCCCCAACAGCAGCCGCAGCAGCAAACTCCCCAGGAACAGACACC
ACCACCACAGCAGCAGCAGCAGCAACTCCAAGTTACTTGTTCAGCTCAAACTGTCCAGGTTG
CTGAAGTTGAACCACAGTCACAGCCACAGCCTTCCCCAGAACTTCTGCTTCCAAATTCTTTG
AAGCCAGAAGAAGGGCTTGAAGTATGGAAAAACTGGGCCCAGACCAAGAATGCTGAACTA
GAGAAGGATGCTCAGAACAGATTGGCACCCATTGGGAGGCGCCAACTGCTGCGATTCCAGG
AAGATCTCATCTCCTCTGCTGTGGCAGAGTTGAATTATGGGCTCTGTCTAATGACACGGGAA
GCTCGAAATGGAGAAGGTGAACCCTATGACCCAGATGTGCTCTACTATATTTTCCTGTGTAT
TCAAAAGTATCTTTTTGAAAATGGAAGGGTAGATGACATTTTCTCCGATCTTTATTATGTTCG
GTTCACGGAGTGGCTACATGAAGTTCTGAAGGATGTTCAGCCCCGGGTCACTCCACTTGGCT
ATGTCTTGCCCAGCCACGTGACTGAGGAGATGCTATGGGAGTGCAAGCAGCTTGGGGCTCAC
TCCCCCTCCACCTTGCTGACCACCCTCATGTTCTTTAATACCAAGTACTTCCTATTGAAGACA
GTGGACCAGCACATGAAGCTGGCCTTCTCCAAGGTCTTGCGACAGACAAAGAAGAACCCCT
CTAATCCCAAGGATAAAAGCACGAGTATCCGGTACTTGAAGGCCCTTGGAATACACCAGAC
TGGCCAGAAAGTTACAGATGACATGTATGCAGAACAGACGGAAAATCCAGAGAATCCATTG
AGATGTCCCATCAAGCTCTATGATTTCTACCTCTTCAAATGCCCCCAGAGTGTGAAAGGCCG
GAATGACACCTTTTACCTGACACCTGAGCCAGTGGTGGCCCCCAACAGCCCAATCTGGTACT
CAGTCCAGCCTATCAGCAGAGAGCAGATGGGACAAATGCTGACGCGGATCTTGGTGATAAG
AGAAATTCAGGAGGCCATCGCAGTGGCCAATGCAAGCACTATGCACGGTGGTGGTGGTAGT
GACTACAAAGACGATGACGACAAGTGATAG

pLenti - QRICH1 – ΔNLS – FLAG

AACATGGTGTACCAACAGGGTGGGAACTGCATATACACAGACAGCACTGAAGTGGCTGGGT
CTTTGCTTGAACTTGCCTGTCCAGTCACCACCAGTGTTCAGCCACAAACCCAGCAAGAACAG
CAGATCCAGGTTCAGCAGCCGCAGCAGGTTCAGGTCCAGGTGCAGGTACAGCAGTCTCCGC
AACAGGTCTCGGCTCAGCTCTCCCCACAACTCACCGTTCACCAGCCTACTGAGCAACCCATC
CAGGTCCAGGTGCAGATCCAAGGCCAGGCACCACAGTCAGCAGCCCCCTCCATTCAGACCC
CGTCTCTGCAGAGTCCCAGTCCCTCGCAGCTGCAAGCAGCTCAGATCCAGGTGCAGCACGTG
CAAGCAGCCCAGCAGATCCAGGCTGCAGAAATCCCGGAGGAGCACATCCCACATCAGCAAA
TCCAGGCTCAGCTGGTGGCTGGCCAGTCTCTTGCTGGTGGTCAGCAGATCCAAATCCAGACC
GTGGGTGCCCTTTCCCCACCACCATCCCAGCAGGGCTCACCCCGGGAAGGGGAGGTTGGCAC
GGCCAGTGTCCTCCAACCAGTGAAGAAGCGCAAAGTGGACATGCCCATCACTGTGTCCTACG
CCATCTCAGGGCAGCCGGTGGCCACCGTGCTGGCCATTCCACAGGGCCAGCAGCAGAGTTAT
GTGTCTTTGAGGCCAGACTTACTGACAGTAGACAGTGCCCACCTGTACAGTGCCACTGGGAC
CATTACTAGCCCTACAGGAGAAACCTGGACCATCCCTGTTTATTCTGCCCAGCCCCGGGGGG
ACCCTCAGCAGCAGAGCATTACCCACATTGCCATTCCCCAGGAAGCCTACAACGCAGTTCAC
GTCAGTGGCTCACCCACAGCCCTGGCAGCTGTTAAGCTGGAGGATGACAAGGAGAAGATGG
TGGGCACCACATCTGTAGTGAAAAACTCCCATGAAGAGGTAGTGCAGACCCTTGCAAACTCT
CTCTTTCCAGCACAGTTCATGAATGGCAACATCCACATTCCAGTGGCTGTGCAGGCTGTGGC
AGGCACGTACCAGAATACGGCTCAAACTGTCCATATATGGGACCCCCAACAGCAGCCGCAG
CAGCAAACTCCCCAGGAACAGACACCACCACCACAGCAGCAGCAGCAGCAACTCCAAGTTA
CTTGTTCAGCTCAAACTGTCCAGGTTGCTGAAGTTGAACCACAGTCACAGCCACAGCCTTCC
CCAGAACTTCTGCTTCCAAATTCTTTGAAGCCAGAAGAAGGGCTTGAAGTATGGAAAAACTG
GGCCCAGACCAAGAATGCTGAACTAGAGAAGGATGCTCAGAACAGATTGGCACCCATTGGG
AGGCGCCAACTGCTGCGATTCCAGGAAGATCTCATCTCCTCTGCTGTGGCAGAGTTGAATTA
TGGGCTCTGTCTAATGACACGGGAAGCTCGAAATGGAGAAGGTGAACCCTATGACCCAGAT
GTGCTCTACTATATTTTCCTGTGTATTCAAAAGTATCTTTTTGAAAATGGAAGGGTAGATGAC
ATTTTCTCCGATCTTTATTATGTTCGGTTCACGGAGTGGCTACATGAAGTTCTGAAGGATGTT
CAGCCCCGGGTCACTCCACTTGGCTATGTCTTGCCCAGCCACGTGACTGAGGAGATGCTATG
GGAGTGCAAGCAGCTTGGGGCTCACTCCCCCTCCACCTTGCTGACCACCCTCATGTTCTTTAA
TACCAAGTACTTCCTATTGAAGACAGTGGACCAGCACATGAAGCTGGCCTTCTCCAAGGTCT
TGCGACAGACAAAGAAGAACCCCTCTAATCCCAAGGATAAAAGCACGAGTATCCGGTACTT
GAAGGCCCTTGGAATACACCAGACTGGCCAGAAAGTTACAGATGACATGTATGCAGAACAG
ACGGAAAATCCAGAGAATCCATTGAGATGTCCCATCAAGCTCTATGATTTCTACCTCTTCAA
ATGCCCCCAGAGTGTGAAAGGCCGGAATGACACCTTTTACCTGACACCTGAGCCAGTGGTGG
CCCCCAACAGCCCAATCTGGTACTCAGTCCAGCCTATCAGCAGAGAGCAGATGGGACAAAT
GCTGACGCGGATCTTGGTGATAAGAGAAATTCAGGAGGCCATCGCAGTGGCCAATGCAAGC
ACTATGCACGGTGGTGGTGGTAGTGACTACAAAGACGATGACGACAAGTGATAG

8.2 List of gene hits (FDR < 0.05) for FACS-genetic screens

8.2.1 *p-RPS6 (NKI) screen*

Gene	FDR	MI	Gene	FDR	MI	Gene	FDR	MI
DEPDC5	0.00E+00	51.68	FAM78A	4.57E-08	1.38	YWHAE	6.73E-09	0.50
NPRL2	2.40E-87	43.21	TNRC18	1.87E-03	1.38	COQ2	1.24E-03	0.50
SZT2	2.15E-79	36.25	MPP5	3.31E-02	1.38	CLCF1	4.55E-02	0.50
LOC728485	8.18E-06	29.35	FRMD4A	7.23E-03	1.38	NDUFB10	4.02E-03	0.49
TSC2	8.89E-155	28.11	ARRDC3	1.44E-05	1.37	PXN	2.40E-03	0.49
NPRL3	0.00E+00	27.98	DPYD	1.47E-02	1.37	HK2	4.59E-02	0.49
TSC1	4.08E-251	27.59	UHRF1	1.63E-02	1.37	NDUFS8	7.77E-03	0.49
TTC4	4.03E-03	17.61	FBXO8	2.10E-02	1.37	SREK1	2.27E-04	0.49
RPS25	1.17E-28	13.70	MROH8	2.76E-02	1.37	DDX10	2.99E-04	0.49
KCTD5	3.32E-68	13.06	CDH2	1.86E-08	1.36	VARS2	4.62E-03	0.48
C12orf66	1.36E-65	11.32	KIF15	6.85E-03	1.36	KDM2A	1.55E-36	0.48
TMEM174	1.01E-04	10.27	CTBP2	8.24E-05	1.36	NUDT4	4.07E-02	0.48
DPH5	5.43E-39	9.98	PHF14	2.76E-02	1.35	RTN4IP1	8.86E-03	0.48
CNOT2	1.47E-57	9.39	XIAP	1.66E-03	1.35	PTAR1	1.67E-02	0.48
MEAF6	1.15E-04	8.44	NCOA6	4.88E-03	1.35	PIK3R4	3.15E-02	0.47
DNMT3L	2.40E-03	8.31	PREP	5.32E-04	1.34	UQCC1	2.60E-07	0.47
NAA35	3.55E-35	8.22	GRK5	4.84E-02	1.34	SCAP	5.94E-05	0.47
NAA30	4.93E-18	8.07	DPYSL3	4.78E-02	1.34	NSUN3	2.94E-04	0.47
ZNF793	2.16E-25	7.91	ARHGAP21	7.64E-03	1.34	PMM2	5.67E-04	0.47
SFTPB	2.07E-06	7.83	TBL1X	2.40E-03	1.33	BPTF	1.02E-05	0.47
EPC2	3.08E-101	7.70	SESN3	4.90E-02	1.33	MANBA	4.07E-02	0.47
NF2	5.23E-54	7.11	WNK3	3.25E-02	1.32	XRN2	4.07E-02	0.47
DDX6	7.58E-28	6.91	FAM65B	2.98E-02	1.32	VPS26A	1.15E-04	0.46
ST8SIA1	5.53E-04	6.46	MYO1E	1.63E-02	1.32	NDUFS1	8.28E-04	0.46
INPP4A	4.27E-266	6.33	MEIS2	9.93E-09	1.32	BRD1	4.62E-03	0.46
CUL5	1.74E-51	5.87	TMEFF2	4.29E-03	1.31	SEC63	1.66E-02	0.46
LCMT1	9.01E-07	5.87	SLCO1A2	1.28E-02	1.31	SAP30	1.89E-02	0.46
ZSCAN18	4.42E-02	5.87	C1orf43	9.89E-03	1.31	CRKL	2.78E-02	0.46
UBASH3B	7.68E-16	5.63	PSPH	4.90E-02	1.31	MAU2	1.12E-02	0.46
ZNF578	9.43E-05	5.50	SET	3.15E-02	1.31	SMG7	4.86E-04	0.46
CD44	2.97E-08	5.18	SEC14L1	6.17E-04	1.31	YBEY	5.01E-19	0.45
KPTN	2.61E-14	5.05	UNK	2.32E-05	1.31	TIMMDC1	3.20E-04	0.45
MTBP	1.61E-03	5.03	BCL7C	7.80E-05	1.31	XPNPEP3	1.96E-10	0.45
CNOT3	1.60E-05	4.94	SIPA1L3	4.81E-05	1.31	PDSS1	2.53E-06	0.45
ITFG2	5.07E-24	4.93	PEX14	3.88E-02	1.30	MIOS	1.59E-03	0.45
NAA38	4.52E-13	4.84	FAM222B	2.40E-03	1.30	MRPL1	2.43E-04	0.45
INPPL1	1.48E-25	4.83	SLC43A2	4.42E-02	1.30	NDUFS3	2.03E-03	0.45
CFAP53	2.80E-05	4.80	IGSF11	2.18E-02	1.30	MBIP	1.25E-06	0.45
DPH6	1.22E-185	4.50	RBM6	8.45E-03	1.30	TIMM8B	6.53E-03	0.45
UBE2F	1.31E-08	4.40	NF1	9.16E-13	1.30	SLC25A32	9.73E-03	0.44
GREM1	4.07E-02	4.40	TRPS1	2.12E-09	1.30	GPBP1	1.85E-10	0.44
DPH1	4.24E-06	4.22	SETBP1	1.94E-03	1.29	VMP1	4.99E-25	0.44
TFDP1	6.72E-08	4.19	NKIRAS2	2.38E-02	1.29	FZR1	2.91E-03	0.44
TRPC7	1.19E-06	4.16	FRYL	7.37E-07	1.29	F2R	7.39E-03	0.44
ACTL8	3.70E-02	4.16	UBE2R2	3.78E-03	1.28	SLC16A1	4.00E-04	0.44
GPS2	3.71E-03	4.08	PITPNC1	3.41E-07	1.28	G3BP1	2.08E-02	0.44
TSPAN16	2.62E-15	4.04	CCDC102B	4.78E-02	1.28	NDUFV2	6.13E-16	0.43
CHMP5	3.67E-04	4.04	CSGALNACT1	4.59E-02	1.28	OTUD6B	9.33E-03	0.43
DBF4	9.03E-33	4.00	KIF9	3.90E-04	1.28	ENO1	2.32E-02	0.43
DPH2	5.01E-07	3.98	PBX1	3.69E-05	1.27	TAF5L	2.32E-02	0.43
ANKRD11	7.90E-143	3.95	ACOX1	4.71E-02	1.27	SCD	1.14E-04	0.43

Gene	FDR	MI	Gene	FDR	MI	Gene	FDR	MI
FAAH2	2.78E-07	3.94	SGCZ	5.84E-03	1.27	GCN1	4.97E-05	0.43
RCE1	6.02E-05	3.91	ABCC2	9.69E-03	1.27	CYCS	1.05E-02	0.43
FLVCR2	2.86E-11	3.90	MKL1	3.90E-04	1.26	NMT1	1.05E-02	0.43
RNF7	8.31E-12	3.89	ADAM18	9.40E-03	1.26	MBTPS1	1.80E-08	0.42
ZNF569	3.94E-07	3.83	PRMT2	3.61E-02	1.26	COX19	1.33E-02	0.42
DLEC1	4.60E-20	3.75	RERE	4.31E-06	1.26	MRPS34	3.15E-04	0.42
PARVG	2.90E-03	3.74	MGME1	5.14E-03	1.26	METTL5	2.36E-03	0.42
UBE2L3	1.04E-22	3.60	MATR3	1.70E-02	1.25	TM2D3	2.01E-02	0.42
AGAP5	1.57E-02	3.59	ZFHX4	1.25E-02	1.25	WDR59	9.07E-04	0.41
PPP4R2	2.06E-18	3.56	BIRC6	2.88E-05	1.25	COMMD8	9.79E-06	0.41
DEFB108B	6.37E-04	3.52	LARGE	1.06E-02	1.25	NDUFAF7	5.91E-03	0.41
SIN3B	6.07E-06	3.42	BRD2	7.33E-03	1.25	PIGK	2.39E-03	0.41
ARIH2	1.78E-55	3.37	PRTFDC1	3.20E-02	1.24	MRPS6	7.06E-15	0.41
PDGFRA	2.76E-07	3.30	SREBF2	1.97E-02	1.23	MED23	7.47E-04	0.41
TBC1D7	1.94E-11	3.28	DEPTOR	6.45E-03	1.23	STARD7	4.13E-02	0.41
ADGRE3	3.92E-02	3.26	USP34	2.29E-04	1.23	CDC42	2.11E-05	0.40
MYH14	4.60E-03	3.25	GAS8	9.71E-03	1.23	RNF126	4.92E-03	0.40
OIT3	2.53E-05	3.24	SLC3A2	7.69E-03	1.23	TOE1	9.09E-03	0.39
UBA3	2.55E-03	3.23	TBC1D1	2.90E-02	1.23	PRPF39	2.41E-03	0.39
BDNF	3.17E-02	3.23	MLLT10	2.95E-04	1.23	SDHB	2.66E-03	0.39
NCOR1	5.53E-70	3.22	EFHC2	2.15E-02	1.22	SHMT2	3.30E-04	0.39
CUL3	9.93E-25	3.17	RAI1	1.55E-02	1.21	SEC62	1.40E-02	0.39
USP14	1.06E-117	3.16	RFWD2	6.47E-03	1.21	CCDC22	6.77E-03	0.38
SPEN	3.20E-169	3.14	IGF2BP3	4.20E-02	1.20	COA7	4.46E-03	0.38
CDK13	2.31E-24	3.12	ZFHX3	9.11E-09	1.20	TAF6L	7.95E-06	0.38
TIPRL	1.85E-03	3.11	EXOC6B	3.13E-02	1.20	ATAD3A	2.27E-02	0.38
ARID2	1.54E-40	3.05	MYBPC1	1.17E-04	1.20	ZFAND5	6.84E-03	0.38
RPRD2	1.87E-46	3.05	GNG7	6.29E-03	1.19	SP1	5.45E-10	0.38
DNAJC24	1.36E-05	3.03	ISPD	2.73E-02	1.18	TNFRSF8	1.67E-02	0.37
PPP2R4	2.01E-33	3.03	HP1BP3	4.48E-02	1.18	RQCD1	1.46E-07	0.37
LARP7	1.82E-26	3.02	CDC42BPB	1.05E-03	1.17	IPO9	1.11E-02	0.37
PIK3R1	1.62E-24	3.00	RBPMS	1.08E-03	1.16	CCDC90B	3.30E-03	0.37
RRAGA	2.74E-04	3.00	SPAG9	1.50E-03	1.16	SDHC	6.89E-06	0.37
GATAD1	4.91E-11	2.98	DNMBP	2.54E-02	1.16	COX14	1.84E-02	0.37
MTF2	3.95E-47	2.98	PTPRG	1.87E-03	1.15	CYC1	8.11E-03	0.37
FAM193A	1.04E-19	2.98	ATF7IP	2.87E-02	1.14	SLC25A26	8.11E-03	0.37
CREB1	8.19E-10	2.96	MECOM	7.13E-05	1.13	TSC22D2	2.15E-05	0.36
FGFRL1	2.87E-02	2.93	DIP2B	2.59E-02	1.12	NDUFA10	2.83E-03	0.35
DOT1L	3.38E-50	2.90	MAP1B	1.66E-02	1.11	COQ5	3.81E-07	0.35
UPP2	1.98E-04	2.88	MACROD2	1.72E-02	1.11	GFM2	5.77E-04	0.35
B4GALNT2	5.15E-04	2.87	PAK3	2.90E-02	0.93	MRPS28	3.74E-67	0.35
UBE2M	9.35E-03	2.85	RORA	2.25E-02	0.93	COQ4	2.47E-08	0.35
EIF5B	4.18E-02	2.82	NRXN1	2.03E-02	0.93	WNK1	4.28E-14	0.34
DNTT	6.16E-08	2.82	MAGI2	2.57E-02	0.93	MTX1	5.81E-06	0.34
CDC7	2.00E-04	2.78	TRPM3	4.72E-02	0.93	FARS2	1.76E-13	0.33
ADGRD1	9.45E-04	2.76	ATP8A2	1.77E-02	0.93	ATP5J	1.22E-10	0.33
DEFB123	5.52E-03	2.71	NELL1	3.28E-02	0.93	CSNK1A1	1.46E-04	0.33
SLC1A2	1.16E-04	2.71	IL1RAPL1	5.58E-05	0.92	FECH	7.47E-03	0.33
C4orf19	3.02E-03	2.68	TANC2	3.41E-07	0.91	HTRA2	7.18E-04	0.33
ZMYM2	7.86E-22	2.68	PBX3	4.28E-02	0.91	DNAJC2	3.55E-03	0.33
PDCD10	1.61E-05	2.68	ADGRV1	1.87E-04	0.91	AZIN1	1.09E-03	0.33
ILF3	4.93E-06	2.67	AFF2	3.45E-02	0.91	RNMTL1	3.14E-05	0.33
FBXW7	6.42E-100	2.66	LAMA2	3.80E-02	0.90	TIMM8A	5.15E-04	0.32
PHF12	1.20E-34	2.65	SOX5	1.24E-04	0.90	LAMTOR5	5.91E-08	0.32
CSNK2A1	2.21E-15	2.63	CRADD	1.75E-02	0.90	LIG3	7.08E-11	0.32
RRAGC	1.38E-02	2.63	PARK2	4.14E-04	0.90	MLST8	6.89E-06	0.32
FOXK1	1.41E-08	2.60	FHIT	2.65E-06	0.90	TADA2B	2.63E-09	0.32
PCGF6	6.30E-14	2.60	EPHA6	2.56E-02	0.90	MRRF	2.23E-16	0.31
CHMP3	9.40E-03	2.59	FOXP1	7.96E-03	0.90	COQ6	2.57E-04	0.31
TRIP12	1.35E-46	2.58	CHN1	5.57E-05	0.90	MIPEP	2.66E-03	0.30
PIKFYVE	1.65E-04	2.57	ROBO2	2.12E-03	0.90	CCDC47	9.85E-14	0.30
TRPM6	4.99E-02	2.57	FOXN3	4.60E-02	0.89	MED15	7.31E-13	0.30

Gene	FDR	MI	Gene	FDR	MI	Gene	FDR	MI
KMT2E	4.44E-66	2.54	CACNA2D1	7.11E-03	0.89	MTRF1L	3.73E-02	0.30
CLPSL1	3.42E-02	2.53	ZNF385B	4.82E-03	0.89	PARL	1.63E-06	0.30
GPATCH8	2.43E-25	2.51	ZBTB20	4.22E-14	0.89	SDHA	1.78E-02	0.30
RALGAPB	1.94E-08	2.51	LDB2	6.05E-03	0.89	NCKAP1	1.13E-06	0.30
MYO1F	4.14E-02	2.50	ERC2	3.53E-05	0.89	EMC1	2.63E-02	0.29
RBFOX1	2.86E-02	2.47	ADAMTSL1	1.16E-03	0.89	KMT2B	2.63E-02	0.29
CD48	1.30E-03	2.45	ADGRG4	4.79E-02	0.88	CASC3	5.78E-05	0.29
MIB1	1.56E-50	2.44	EIF4G3	3.57E-02	0.88	MRPL42	1.83E-05	0.29
BRD7	1.61E-03	2.43	FBXL7	1.24E-04	0.88	MRPL13	6.73E-10	0.29
SETD5	5.09E-21	2.43	DACH2	6.49E-04	0.88	MRPL17	4.13E-04	0.29
DPH7	5.19E-06	2.42	DACH1	2.97E-08	0.88	UBE2G2	8.14E-07	0.29
RBM18	7.25E-07	2.42	LRRC1	3.50E-06	0.88	ICT1	2.57E-07	0.29
SCAF8	1.52E-13	2.40	CPQ	4.78E-02	0.87	SLC39A10	1.20E-06	0.28
IWS1	1.87E-03	2.40	MYOM1	4.25E-02	0.87	COX20	2.87E-04	0.28
MAP1LC3A	4.09E-02	2.39	KCNK2	4.86E-03	0.86	MAPKAP1	1.56E-35	0.28
MAOB	1.25E-03	2.39	PTCH1	3.28E-02	0.86	EMC2	4.09E-17	0.28
CSNK2A2	5.80E-03	2.38	LOC339862	1.01E-02	0.86	PGM3	2.73E-02	0.28
LIPC	1.47E-03	2.36	GPR158	9.81E-03	0.86	CREBBP	1.79E-18	0.27
ZCCHC8	9.02E-17	2.36	AGPS	1.06E-05	0.86	NRBP1	4.28E-04	0.27
OTX2	2.60E-04	2.35	SAMD4A	2.46E-02	0.86	MRPL19	5.68E-07	0.27
LINC00649	4.57E-02	2.35	MAML2	3.47E-06	0.86	FAM136A	2.65E-06	0.27
SYK	3.15E-02	2.33	TMC1	7.04E-17	0.85	RAC1	1.91E-02	0.27
GRK6	8.92E-05	2.32	DLG2	2.95E-22	0.85	SLC30A9	6.23E-04	0.27
STK11	3.07E-09	2.31	THSD7A	5.74E-04	0.85	MRPS16	2.06E-11	0.27
TMEM30A	1.58E-12	2.30	CDKAL1	1.80E-10	0.85	ATPAF2	1.86E-06	0.26
TAOK1	6.07E-62	2.23	MVB12B	2.86E-02	0.85	ATP5E	5.83E-06	0.26
EDC4	4.86E-02	2.23	NAV3	1.03E-06	0.85	IFT20	1.97E-02	0.26
RBM7	1.38E-03	2.22	ZNF804B	3.48E-04	0.85	NOA1	1.97E-02	0.26
CNBP	7.74E-09	2.21	PDE11A	1.98E-04	0.84	SUPT20H	1.15E-08	0.26
GIGYF2	5.23E-28	2.20	MAP2K5	1.02E-02	0.84	CYB5B	5.22E-08	0.25
DEAF1	7.20E-09	2.20	NKAIN3	6.13E-05	0.84	MED12	2.80E-02	0.25
PTGES3	7.07E-16	2.20	TMEM135	4.49E-02	0.84	SAMD4B	2.80E-02	0.25
E2F3	1.56E-13	2.20	PPP3CA	1.93E-05	0.84	TOMM70A	2.80E-02	0.25
ATP2C1	6.85E-90	2.17	UBE2D1	2.42E-02	0.84	PTCD1	2.60E-06	0.25
FKBP1A	1.38E-04	2.14	KIZ	4.41E-02	0.83	TMEM208	9.02E-03	0.24
TBL1XR1	1.28E-12	2.14	CTTNBP2	2.02E-02	0.83	SCO1	3.77E-06	0.24
CBL	1.41E-17	2.14	AHCYL2	2.48E-02	0.83	COX15	2.69E-05	0.24
PAK7	2.18E-05	2.11	NEDD9	6.18E-05	0.83	KIAA0391	2.88E-15	0.24
PPP1CA	2.22E-02	2.11	PPFIA2	4.91E-06	0.83	SLC4A7	1.17E-11	0.24
ZNF91	6.97E-04	2.10	EPHA5	1.66E-04	0.82	ACTR3	7.20E-28	0.24
RANBP17	1.68E-02	2.10	UBR2	4.31E-02	0.82	UBE3D	5.96E-10	0.23
EIF4H	1.10E-04	2.08	FOXP2	6.18E-04	0.82	MTX2	6.85E-08	0.23
NFYB	1.17E-06	2.08	UBE2H	1.82E-07	0.82	GFM1	4.22E-04	0.23
PBX4	3.73E-08	2.07	FTO	2.44E-05	0.81	MYO7A	1.29E-02	0.23
MYH9	4.02E-13	2.04	NRG1	4.13E-02	0.81	RICTOR	4.57E-08	0.23
SETD2	6.81E-05	2.04	PTPRM	1.24E-02	0.81	COA5	8.34E-05	0.23
DICER1	8.67E-10	2.04	SYT1	1.10E-22	0.81	MRPS25	2.77E-03	0.23
C11orf30	7.46E-43	2.03	TPK1	2.04E-03	0.81	RPS6KB1	6.29E-09	0.22
BTLA	9.77E-10	2.01	FBXL17	5.39E-04	0.81	C14orf2	8.70E-03	0.22
SPOP	1.21E-17	2.01	MAST2	9.63E-04	0.81	SMAD4	8.65E-23	0.22
PBRM1	1.58E-51	2.01	STK39	1.13E-02	0.80	SRD5A3	2.44E-10	0.22
TEX11	8.52E-08	2.00	BMPR1A	6.43E-06	0.80	COQ3	6.05E-26	0.22
PI4K2A	4.31E-02	2.00	CHD2	9.00E-04	0.80	UQCRC2	4.60E-07	0.22
EPHB1	6.33E-07	2.00	CD200	3.45E-02	0.79	ATIC	7.45E-06	0.22
MTF1	7.30E-03	2.00	TLK2	2.87E-03	0.79	COX11	4.88E-06	0.21
MPHOSPH8	3.28E-02	2.00	MICU1	7.15E-03	0.79	DYRK1A	5.74E-52	0.21
C3	1.44E-02	1.99	ZNF462	6.38E-05	0.79	PDCL	1.26E-03	0.21
PAPD7	4.61E-03	1.99	ELF2	4.13E-02	0.78	PPA2	1.26E-03	0.21
WAC	1.55E-02	1.98	SNTB2	2.58E-02	0.78	ARPC3	2.54E-04	0.21
RELB	3.71E-03	1.97	PARD3	2.33E-05	0.78	IMPDH2	1.63E-05	0.21
UBALD2	2.98E-02	1.97	SLC22A23	3.81E-02	0.78	PET117	6.44E-07	0.21
CCDC39	3.25E-02	1.96	TNMD	8.09E-04	0.78	MTHFD1	5.68E-12	0.21
CDH1	8.14E-07	1.95	PDZD8	4.13E-02	0.77	MBTPS2	1.68E-72	0.21
FBXW11	2.76E-07	1.95	BORCS5	1.24E-02	0.77	MRPL2	4.24E-07	0.21
PRMT7	1.79E-14	1.94	PDZRN3	4.04E-04	0.77	MRPL24	3.99E-11	0.21

Gene	FDR	MI	Gene	FDR	MI	Gene	FDR	MI
HNRNPD	1.76E-12	1.94	TAL1	4.28E-02	0.77	CLPB	2.66E-03	0.20
CUL1	4.82E-03	1.92	OCIAD1	2.55E-02	0.77	WARS2	6.63E-06	0.20
SESN2	6.47E-03	1.92	YTHDF3	4.20E-02	0.76	MRPL28	1.22E-02	0.20
IRX5	8.71E-03	1.92	RASGRF2	3.04E-02	0.76	NARS2	1.32E-257	0.20
SCARA5	6.82E-04	1.91	ENAH	6.16E-05	0.76	MTCH2	4.75E-05	0.19
WDR72	2.87E-02	1.90	ZFAND3	2.30E-03	0.76	HSD17B12	7.38E-26	0.19
NSD1	1.86E-20	1.90	EXT1	4.18E-02	0.76	COX7B	3.83E-07	0.19
CDK8	1.48E-02	1.89	MYCBP2	1.21E-02	0.76	PTDSS1	1.19E-09	0.19
ARL15	3.30E-12	1.88	UVRAG	4.27E-05	0.74	SLIRP	4.76E-05	0.19
CCDC109B	1.07E-10	1.88	PEBP4	1.29E-03	0.74	TRMT61A	2.52E-02	0.18
NOX5	1.34E-04	1.88	NCOR2	4.14E-02	0.74	IMMT	9.82E-05	0.18
SLC4A1AP	8.73E-04	1.87	KIAA1033	1.17E-04	0.74	TCOF1	1.92E-05	0.18
TMEM165	5.55E-03	1.86	RRAS2	7.07E-03	0.74	MRPL51	6.32E-08	0.18
ST6GALNAC1	4.04E-02	1.86	SFTA3	2.07E-03	0.74	TAF1B	5.34E-09	0.18
FOXK2	1.26E-10	1.85	NLK	1.20E-17	0.73	OGDH	1.65E-06	0.18
FXR1	1.71E-04	1.85	TMX4	7.27E-04	0.73	PET100	1.67E-02	0.18
SEC61A2	2.73E-02	1.85	ARID3B	7.46E-03	0.72	UROS	1.67E-02	0.18
HTR7	1.52E-06	1.84	BMPR1B	7.23E-04	0.72	LRPPRC	1.18E-106	0.17
F8	2.00E-04	1.83	L3MBTL3	1.35E-02	0.72	ISCA2	1.49E-03	0.17
NOSIP	6.90E-03	1.82	GSK3B	4.87E-03	0.72	DCAF7	4.37E-11	0.17
SPAST	6.90E-03	1.82	ZCCHC2	7.81E-03	0.72	ATP5O	2.78E-09	0.17
CTNND1	6.86E-07	1.80	EFNA5	1.28E-19	0.72	ACTR2	1.61E-05	0.17
AMOT	2.81E-19	1.80	C12orf65	2.96E-03	0.72	UQCRC1	1.75E-07	0.17
KDM5A	3.88E-07	1.79	ITGB5	1.35E-02	0.72	ATP5J2	2.12E-14	0.16
CWC27	5.25E-06	1.79	KLF7	3.05E-06	0.72	LARS2	4.93E-37	0.16
MARK2	4.69E-02	1.78	PAN2	3.38E-02	0.71	COX5B	1.16E-02	0.16
UBA5	4.69E-02	1.78	RASSF8	1.44E-02	0.71	MTERF4	9.56E-04	0.16
ZEB2	6.80E-28	1.78	PARVB	1.29E-03	0.71	MRPS5	1.28E-04	0.16
CAND1	8.85E-05	1.78	MYO10	1.19E-30	0.71	TMEM41B	1.02E-05	0.16
SMARCA4	3.16E-06	1.77	BBX	1.95E-04	0.71	CARS2	1.26E-16	0.16
PCDH10	3.76E-02	1.76	MTFMT	2.31E-02	0.71	LAYN	6.58E-06	0.16
VAC14	8.23E-03	1.76	REPS1	6.51E-03	0.70	PPAT	3.20E-15	0.16
TULP4	1.83E-05	1.75	WWTR1	1.22E-13	0.70	ARPC2	6.15E-26	0.16
EIF2AK1	2.41E-02	1.75	NADK2	2.97E-03	0.70	MRPS15	6.83E-06	0.16
OAZ1	9.22E-03	1.74	ATXN7	1.39E-06	0.70	PDAP1	4.28E-06	0.15
ACSL1	2.07E-03	1.74	LYPD6B	4.13E-02	0.70	PNPT1	4.70E-03	0.15
UBE2V2	3.10E-03	1.74	ALG8	3.86E-03	0.70	TOP1	2.62E-04	0.15
NRD1	1.72E-06	1.74	NCOA2	8.57E-11	0.70	MTG1	4.06E-13	0.15
GLYR1	3.52E-03	1.73	ACVR2A	3.17E-02	0.69	MRPS33	1.65E-06	0.15
HELZ	5.31E-10	1.73	VCL	2.70E-14	0.69	WDR4	9.98E-16	0.15
SNRK	6.78E-04	1.73	DLX5	4.34E-02	0.69	FTSJ2	5.31E-10	0.15
SUV420H1	4.24E-02	1.72	RAPGEF1	5.10E-04	0.69	RPS27	3.33E-02	0.15
MAP4K4	9.12E-16	1.72	WDR7	3.96E-03	0.69	YME1L1	6.65E-07	0.14
PPHLN1	6.10E-20	1.72	MNT	2.50E-08	0.68	KAT7	1.32E-10	0.14
SMARCC1	2.85E-11	1.72	USP46	4.90E-02	0.67	RPIA	1.92E-03	0.14
WDR45B	1.83E-02	1.72	ERI3	6.17E-04	0.67	GRSF1	8.45E-09	0.14
HTT	3.77E-06	1.71	COX18	3.68E-03	0.67	MRPL36	1.46E-02	0.13
ABHD2	9.11E-04	1.71	ITGA4	5.43E-04	0.66	ARPC4	4.00E-05	0.13
AKR1A1	3.28E-03	1.71	THRA	1.09E-02	0.66	ATP5L	1.25E-06	0.13
SETDB1	8.19E-07	1.71	DIDO1	1.32E-02	0.66	METTL17	5.06E-04	0.13
PIK3R2	2.47E-08	1.71	PSME4	4.05E-02	0.66	UQCRB	5.06E-04	0.13
PPME1	1.82E-02	1.71	EXOC4	8.63E-15	0.66	C1D	1.47E-02	0.13
DGUOK	1.99E-04	1.70	INO80C	1.09E-06	0.66	MRPL52	1.47E-02	0.13
STRADA	4.61E-05	1.70	PHF21A	4.19E-08	0.66	YY1	1.47E-02	0.13
UBE4B	3.04E-09	1.70	NME6	4.14E-02	0.66	RPS6KB2	2.47E-08	0.13
ANKH	1.63E-02	1.70	MAPK14	2.01E-02	0.66	OPA1	5.01E-07	0.13
DNMT1	9.64E-03	1.69	TMEM131	1.50E-05	0.66	MRPS26	5.28E-07	0.12
UFL1	2.07E-03	1.68	RAPH1	3.42E-02	0.66	BAP1	3.15E-04	0.12
SYT11	3.54E-02	1.68	TOMM7	3.42E-02	0.66	MTG2	1.94E-07	0.12
PPP6R3	4.95E-07	1.67	VDAC1	4.78E-02	0.65	RNASEH1	1.94E-07	0.12
PTCH2	2.72E-03	1.67	SLMAP	4.48E-03	0.65	TUFM	5.80E-03	0.12
PDS5A	9.81E-04	1.66	ARHGEF12	5.90E-08	0.65	PCNP	4.03E-11	0.12
ADNP2	9.58E-03	1.66	SALL1	4.62E-03	0.64	TRIT1	3.59E-21	0.12
KIRREL	2.11E-06	1.66	AKT3	2.78E-38	0.64	PARS2	2.28E-06	0.12
DPP9	2.78E-02	1.66	SOS1	1.98E-02	0.64	PLA2G4D	3.63E-03	0.11

Gene	FDR	MI	Gene	FDR	MI	Gene	FDR	MI
RASA2	2.55E-06	1.65	PHF20	1.10E-04	0.64	RPUSD3	3.63E-03	0.11
ZNF326	2.20E-02	1.65	PPP4R1	6.13E-03	0.64	ATP5F1	3.44E-12	0.11
ZNF611	2.20E-02	1.65	MED13L	1.67E-22	0.64	C19orf43	3.44E-12	0.11
VPS45	3.46E-02	1.65	TRPC4AP	4.18E-03	0.64	MAGOHB	2.30E-03	0.11
PPEF1	2.76E-07	1.62	COX17	1.47E-02	0.63	MRPS24	2.30E-03	0.11
SLC44A2	4.14E-02	1.62	WDR20	2.38E-24	0.63	MRPS27	2.39E-109	0.11
FAM208A	8.54E-07	1.62	DOCK1	1.79E-02	0.63	DDX28	1.27E-12	0.11
VEZF1	1.90E-02	1.61	WASL	4.15E-02	0.63	C1QBP	1.02E-20	0.10
SAV1	5.02E-05	1.61	TNRC6A	5.71E-03	0.63	ATP5D	2.63E-11	0.10
ZCCHC14	2.66E-05	1.60	DNAJC3	8.45E-03	0.63	MRPS9	2.96E-78	0.10
BCL2L1	1.53E-02	1.60	MAP2K6	2.96E-03	0.63	MRPL4	2.10E-07	0.10
EDARADD	1.53E-02	1.60	C15orf41	1.06E-04	0.63	SMARCA5	9.06E-04	0.10
ZNF638	1.29E-03	1.60	PTP4A2	2.10E-02	0.63	MRPS23	1.26E-07	0.10
BMPR2	6.23E-11	1.60	PFAS	4.09E-03	0.63	VPS29	1.31E-19	0.10
GFOD2	1.48E-02	1.59	SPTLC1	5.40E-03	0.62	ATP5H	6.47E-06	0.10
FAM46B	4.20E-02	1.59	PRMT3	7.38E-11	0.62	POLG2	1.52E-16	0.10
NFIC	1.83E-17	1.59	SMARCAD1	2.47E-03	0.62	ATP5C1	2.87E-08	0.10
C11orf58	3.94E-02	1.59	METTL4	4.57E-02	0.62	EXOSC1	5.77E-04	0.09
C16orf72	2.85E-03	1.59	SLTM	1.53E-06	0.61	MRPL20	1.09E-15	0.09
CCM2	1.67E-02	1.58	STX18	1.05E-02	0.61	PTCD3	1.06E-22	0.09
HN1	1.04E-04	1.57	MAPK6	6.90E-07	0.61	MRPL30	2.63E-11	0.09
KCTD9	3.35E-03	1.57	RAP1GDS1	4.09E-02	0.61	MRPL45	7.77E-05	0.08
CARM1	6.72E-15	1.57	SERBP1	4.09E-02	0.61	TFB1M	1.21E-12	0.08
AHCY	2.26E-02	1.57	UBE2E3	2.01E-06	0.61	MRPL37	2.76E-02	0.08
UBA6	1.49E-03	1.57	YWHAZ	5.58E-03	0.61	MRPL44	2.76E-02	0.08
PLAA	2.09E-02	1.57	TRIM71	5.01E-12	0.60	MRPS2	4.79E-05	0.08
TTYH1	2.09E-02	1.57	ITGB1	2.72E-03	0.60	EARS2	2.29E-18	0.08
INO80D	4.75E-03	1.57	GMEB2	4.00E-03	0.60	ERAL1	1.09E-10	0.08
KCTD3	1.96E-03	1.56	BAZ1B	7.47E-12	0.60	RARS2	6.31E-22	0.08
RNF40	8.73E-03	1.56	IL23R	5.95E-03	0.60	RBFA	1.56E-13	0.08
ZNF83	1.75E-03	1.56	PHACTR4	8.61E-06	0.60	MRPL49	4.47E-08	0.08
SPTAN1	6.28E-04	1.56	MPP6	3.36E-02	0.60	IBA57	1.69E-02	0.08
PPP4R3A	1.34E-02	1.56	CCDC58	1.47E-02	0.60	MALSU1	3.14E-05	0.08
BTBD9	4.73E-05	1.54	ZFR	4.86E-02	0.59	NGRN	2.75E-08	0.08
DDRGK1	3.66E-02	1.54	NDUFAF6	7.93E-05	0.59	TRUB2	2.75E-08	0.08
UBE3C	2.90E-02	1.54	PYM1	2.75E-06	0.59	TSFM	1.83E-05	0.08
C2CD5	1.73E-03	1.53	ZRANB1	2.72E-03	0.59	AIFM1	1.46E-11	0.08
EIF4EBP1	3.72E-04	1.52	NDUFAF5	1.05E-02	0.59	MRPL48	1.01E-29	0.07
ARID4A	6.32E-03	1.52	SALL3	7.05E-04	0.59	PITRM1	1.03E-02	0.07
KIAA1551	2.37E-02	1.52	YES1	6.72E-04	0.59	SSBP1	1.06E-05	0.07
PPM1G	1.75E-02	1.51	PIGU	1.48E-03	0.59	MRPL11	1.01E-08	0.07
MGA	4.07E-08	1.50	PIK3CA	2.61E-02	0.58	GADD45GIP1	4.19E-15	0.07
WWP1	4.70E-02	1.49	DARS2	4.84E-02	0.58	TADA1	6.31E-06	0.07
ZSWIM3	2.02E-02	1.49	COMMD7	9.80E-04	0.58	MRPL47	3.78E-06	0.07
NUDT5	3.63E-03	1.48	KAT6A	6.98E-04	0.58	SARS2	2.09E-09	0.07
ZNF146	3.66E-02	1.48	GFPT1	9.57E-14	0.58	GATB	8.22E-30	0.07
HERC4	2.44E-04	1.48	COX10	1.13E-05	0.58	MTERF3	3.82E-13	0.07
LAMTOR4	2.03E-02	1.48	AEBP2	6.09E-12	0.58	TARS2	7.50E-10	0.07
CSK	7.63E-05	1.48	PIGP	1.20E-04	0.57	MRPL32	3.86E-03	0.07
AKAP8	1.47E-02	1.48	SP2	1.53E-02	0.57	GATC	4.46E-14	0.06
BCR	1.56E-02	1.48	TEAD1	8.56E-33	0.57	MRPS18B	3.42E-36	0.06
HMCN1	9.02E-03	1.48	INPP5A	1.43E-06	0.57	MRPS14	2.40E-03	0.06
PICALM	1.67E-08	1.48	NDC1	3.70E-02	0.57	MRPS18A	2.40E-03	0.06
PTPN12	5.53E-04	1.47	PLCL2	2.00E-12	0.57	MRPS22	2.40E-03	0.06
TMEM94	3.75E-03	1.47	ASCC3	2.03E-02	0.56	GTPBP10	1.55E-10	0.06
XPO4	3.75E-03	1.47	NFU1	8.79E-03	0.56	MRPS35	4.76E-18	0.06
HYAL1	9.76E-03	1.47	PIGS	9.23E-03	0.56	MRPL18	9.09E-34	0.06
C16orf45	2.80E-02	1.47	HEATR6	1.78E-02	0.56	MRPS7	5.45E-11	0.06
MSI1	3.39E-02	1.47	FERMT2	7.64E-09	0.56	MRPL16	1.48E-03	0.06
CTNNA1	9.83E-20	1.47	EXOC2	1.58E-08	0.56	NUDT14	1.48E-03	0.06
HNRNPR	1.12E-04	1.46	NUBPL	2.00E-18	0.56	POLRMT	3.13E-07	0.06
PAK2	3.86E-03	1.46	RPTOR	1.07E-03	0.56	LAMTOR3	1.84E-07	0.06
SLC25A36	1.83E-02	1.46	PHIP	2.05E-06	0.56	RPUSD4	9.11E-04	0.06
ZMYM1	2.10E-02	1.46	GSK3A	8.46E-03	0.55	SUPV3L1	9.57E-04	0.06
SUFU	3.30E-02	1.46	GAB2	6.24E-08	0.55	MRPL10	2.32E-08	0.06

Gene	FDR	MI	Gene	FDR	MI	Gene	FDR	MI
KLRG2	2.38E-03	1.45	PTK2	8.52E-10	0.55	HSD17B10	5.65E-04	0.05
VPS8	1.06E-02	1.45	MAPKAPK5	6.04E-04	0.55	MRPL33	5.65E-04	0.05
TULP2	1.15E-02	1.45	SMAD5	6.86E-04	0.55	MRPL15	8.32E-09	0.05
KIF3B	2.33E-09	1.45	EIF4B	3.20E-07	0.55	MRPL3	2.00E-18	0.05
RAB5C	2.27E-02	1.45	KL	7.82E-03	0.55	PGLS	1.96E-04	0.05
EPS15	2.08E-04	1.45	MMD	3.04E-02	0.55	MRPL22	1.15E-04	0.05
LATS1	9.88E-04	1.44	MED13	4.10E-05	0.55	MRPL50	9.45E-10	0.05
EPC1	1.76E-13	1.44	USP22	5.80E-05	0.54	ATP5B	4.24E-15	0.05
MAP4K3	1.36E-43	1.44	RNF4	8.45E-03	0.54	DAP3	8.56E-21	0.05
URI1	7.88E-04	1.44	CCDC6	4.94E-03	0.54	TRMT10C	4.22E-05	0.05
ERF	3.74E-04	1.44	AHCYL1	1.87E-02	0.54	ISCA1	1.98E-10	0.05
CDC25A	6.17E-04	1.44	EHMT1	2.63E-06	0.54	LAMTOR2	1.98E-10	0.05
CCDC170	6.31E-03	1.43	GTF3C2	2.77E-02	0.54	QRSL1	1.98E-10	0.05
RFX7	6.27E-03	1.43	OXSR1	1.65E-02	0.54	MTPAP	1.76E-17	0.04
CDKN2A	4.83E-06	1.43	NDUFS7	6.77E-03	0.53	GTPBP8	8.12E-12	0.04
RC3H2	8.40E-03	1.43	ALG9	2.15E-02	0.53	MRPL54	4.93E-12	0.04
CFAP74	9.08E-03	1.42	CBX3	3.15E-04	0.53	AARS2	5.11E-06	0.04
LARP1B	2.86E-02	1.42	TLN1	3.19E-02	0.53	MRPS31	5.11E-06	0.04
DCUN1D3	1.14E-06	1.42	TMEM126B	3.13E-03	0.53	MRPL39	6.45E-07	0.04
PPP2R5C	5.05E-04	1.42	ACACA	1.16E-67	0.53	TEFM	4.05E-07	0.03
TRIM33	2.94E-02	1.42	UQCC2	3.61E-03	0.53	MRPL21	2.32E-07	0.03
E2F2	2.02E-03	1.41	FLVCR1	4.79E-02	0.53	MRPL12	7.69E-25	0.03
ASAP2	4.86E-05	1.41	NDUFA13	3.76E-02	0.52	MCAT	4.34E-08	0.03
USP15	3.13E-03	1.41	PKN2	2.02E-05	0.52	MRPS18C	4.34E-08	0.03
FAM173B	2.39E-02	1.41	LIN28B	5.27E-23	0.52	HARS2	5.62E-09	0.03
ASB3	9.64E-04	1.41	TRMT10A	3.86E-02	0.52	MRPL27	1.21E-10	0.02
MARK3	7.78E-03	1.40	RREB1	5.77E-09	0.52	MRPL38	1.25E-10	0.02
NPAS2	4.25E-02	1.40	YAP1	1.01E-08	0.52	MRPS30	1.25E-10	0.02
PRDM16	9.54E-04	1.40	SRPK1	3.12E-04	0.52	MRPL23	2.65E-22	0.02
TULP3	2.56E-02	1.40	BTBD3	1.25E-02	0.51	WBSCR16	7.26E-28	0.02
UQCR11	2.56E-02	1.40	NDUFA1	3.95E-02	0.51	YARS2	3.13E-14	0.02
BCAR3	3.45E-03	1.40	PDSS2	2.77E-69	0.51	MRPS10	1.03E-14	0.02
STAG2	3.45E-03	1.40	TADA2A	4.43E-05	0.51	MRPL40	7.33E-18	0.02
PATZ1	1.28E-02	1.39	MRPS21	5.81E-03	0.51	MRPL35	2.49E-18	0.02
ZEB1	1.75E-02	1.39	SP3	8.46E-09	0.51			
HNRNPUL1	3.90E-04	1.39	HNRNPA2B1	2.11E-02	0.51			

8.2.2 *p-RPS6 (OX) 1% screen*

Gene	FDR	MI	Gene	FDR	MI	Gene	FDR	MI
TTC4	1.26E-03	19.98	GON4L	1.26E-03	1.36	MAPKAP1	7.34E-29	0.42
DEPDC5	4.38E-114	8.50	TBC1D14	8.64E-04	1.36	COX15	2.38E-02	0.42
TSC2	1.32E-21	7.38	KIF3B	2.87E-06	1.35	WDR4	1.48E-04	0.41
NPRL2	2.90E-18	7.38	LTBP4	2.77E-03	1.35	MED12	2.72E-02	0.41
TSC1	6.07E-54	6.57	HRASLS5	3.68E-02	1.35	OPA1	4.77E-02	0.41
RPS25	1.49E-20	6.38	WDPCP	1.18E-03	1.33	MBTPS1	3.59E-03	0.41
NPRL3	1.79E-112	6.14	BMPR2	3.07E-03	1.32	WDR24	3.06E-02	0.41
KPTN	2.12E-11	5.55	UNC13B	7.93E-03	1.32	DARS2	1.42E-04	0.40
SZT2	2.20E-15	5.24	RAI1	1.69E-02	1.32	GFM2	8.18E-04	0.40
C12orf66	1.17E-22	5.22	WNK3	1.87E-02	1.32	GATC	3.54E-02	0.40
WAC	8.86E-14	3.79	TNPO2	3.60E-02	1.30	PET117	2.30E-02	0.40
LCMT1	7.36E-04	3.67	ARRDC3	1.46E-02	1.29	RHEB	4.07E-02	0.39
TFDP1	7.15E-05	3.33	FRMD4A	1.01E-02	1.29	TRMT10A	7.84E-04	0.39
KCTD5	1.31E-06	3.29	RBL1	1.36E-02	1.29	UBE3D	4.00E-08	0.38
CACNA1H	2.35E-02	3.13	SLC4A8	2.18E-03	1.29	KAT7	7.03E-06	0.38
DPH5	6.81E-08	3.07	PBRM1	4.71E-07	1.28	AZIN1	3.77E-02	0.38
ACTL8	5.15E-04	3.05	C11orf30	3.55E-04	1.28	LAMTOR5	1.42E-05	0.38
INPP4A	1.58E-37	3.05	SLCO1A2	2.16E-02	1.28	ZNF217	8.90E-03	0.38
DPH2	1.78E-02	2.99	DNAJC15	1.51E-02	1.28	PARL	2.00E-03	0.38
SMARCB1	5.74E-06	2.97	GIGYF2	1.37E-02	1.28	KIAA0391	1.99E-08	0.37
DPH1	2.92E-02	2.96	USP14	5.08E-05	1.26	TSEN15	1.80E-02	0.37
ITFG2	1.76E-07	2.94	SIPA1L3	3.61E-03	1.26	GRSF1	1.32E-02	0.36
CD44	1.59E-06	2.92	CCDC102B	4.49E-02	1.25	MTX2	1.32E-02	0.36
MEAF6	4.16E-02	2.87	APBA2	1.07E-02	1.25	SLC25A3	4.77E-02	0.36
STK11	2.08E-07	2.80	ABCC2	2.78E-02	1.24	SEC63	4.68E-05	0.36
MTF2	1.94E-25	2.76	ZFHX3	1.30E-08	1.24	ATG16L1	3.25E-03	0.36
ADGRD1	4.45E-08	2.71	CTNNA1	1.00E-04	1.22	SLC25A26	2.11E-04	0.36
PARVG	2.38E-02	2.71	SPTBN1	3.14E-03	1.22	MRPL17	3.63E-03	0.35
CHMP5	1.81E-02	2.65	REPS2	4.05E-02	1.22	SCD	3.63E-03	0.35
ZNF606	3.31E-02	2.64	CLIP1	3.32E-02	1.21	ACAD9	5.94E-04	0.35
CD48	3.42E-07	2.54	ATF7IP	2.07E-02	1.21	WDR59	1.01E-05	0.35
ZNF91	9.76E-08	2.48	LYST	1.69E-02	1.21	LIG3	1.55E-08	0.34
ZNF793	5.10E-13	2.48	SETBP1	4.12E-02	1.19	ATG14	7.26E-03	0.34
ODF3L2	4.70E-02	2.47	PITPNC1	7.45E-03	1.18	ATPAF2	2.88E-04	0.34
DOT1L	9.34E-15	2.46	NCOA3	2.68E-02	1.17	MRPL19	1.97E-05	0.34
DHX29	3.63E-06	2.46	ATP2C1	3.10E-02	1.16	SHMT2	2.19E-05	0.33
ZNF569	1.31E-04	2.45	MEGF9	4.40E-02	1.14	ATP5E	7.93E-03	0.33
UBASH3B	3.36E-12	2.42	DLG2	3.99E-03	0.94	DYRK1A	4.71E-60	0.33
TIPRL	1.45E-03	2.39	HDAC9	4.11E-03	0.93	PTCD1	9.53E-04	0.32
FANCB	3.46E-02	2.39	DACH1	3.66E-02	0.93	WARS2	9.53E-04	0.32
NAA35	1.05E-03	2.38	NELL1	1.54E-02	0.92	ATP5J	9.23E-09	0.32
PPP2R4	8.79E-19	2.38	PAK3	2.74E-02	0.92	LAMTOR3	3.82E-03	0.31
FAAH2	2.19E-05	2.38	TRPM3	7.23E-03	0.91	CLPB	1.37E-02	0.31
DLEC1	2.20E-15	2.37	NAV3	2.98E-02	0.90	MRPS28	2.48E-66	0.31
DNMT3L	8.47E-03	2.34	ST18	4.40E-02	0.90	MTHFD1	2.89E-09	0.31
TTYH3	4.94E-05	2.33	GPC3	3.08E-04	0.90	MRPS6	1.67E-13	0.30
DDX6	3.38E-04	2.30	CAMKMT	4.31E-02	0.90	HAX1	1.65E-03	0.30
ILF3	5.12E-03	2.29	CHN1	7.01E-04	0.90	CARS2	8.01E-09	0.30
TRPC7	7.65E-04	2.28	AGPS	2.26E-02	0.89	AIFM1	5.41E-05	0.30
CFAP53	3.32E-02	2.27	FRMD6	2.38E-02	0.89	MRPL2	1.15E-03	0.30
INPPL1	1.34E-02	2.26	MAML2	2.27E-03	0.88	MRPL39	3.60E-02	0.30
SLC1A2	1.29E-06	2.24	FOXP1	6.93E-04	0.87	NDUFB7	3.60E-02	0.30
UBE2L3	4.46E-09	2.20	LRRC4C	1.37E-02	0.87	COA7	2.14E-04	0.30
MYH14	1.32E-03	2.19	CSMD3	4.06E-05	0.86	C19orf43	6.31E-05	0.29
TSSC1	2.18E-04	2.18	TCF12	1.17E-03	0.86	LRPPRC	8.68E-62	0.29
CCDC39	5.08E-04	2.17	KCND2	4.85E-03	0.85	MRPL51	8.56E-04	0.28
FLVCR2	3.09E-06	2.16	GRIA3	3.74E-03	0.85	TRIT1	9.02E-11	0.27
SETDB1	2.50E-06	2.15	FTO	2.35E-02	0.85	RBFA	1.62E-04	0.27
C17orf99	2.88E-03	2.14	ADGRG4	5.51E-03	0.85	QRSL1	6.09E-04	0.27
DPH6	9.73E-34	2.13	EPHA5	7.28E-03	0.85	PPAT	1.43E-10	0.27
DPH7	1.61E-02	2.12	EFNA5	5.62E-05	0.84	RICTOR	1.06E-11	0.27

Gene	FDR	MI	Gene	FDR	MI	Gene	FDR	MI
ZNF517	4.12E-02	2.10	EXOC4	7.01E-03	0.84	NARS2	8.10E-170	0.27
PEX5	2.18E-03	2.10	CDKAL1	7.08E-11	0.84	LARS2	8.79E-19	0.27
NCOR1	1.89E-18	2.08	CTTNBP2	2.74E-02	0.83	MTX1	4.02E-04	0.27
SYK	9.25E-03	2.08	SYT1	4.31E-20	0.82	MRPS25	2.13E-03	0.26
DNTT	3.61E-04	2.04	VTI1A	1.33E-02	0.81	ATIC	5.74E-09	0.26
FIBP	4.31E-02	2.04	GFPT1	2.24E-02	0.81	DAP3	4.84E-05	0.26
MAP1LC3A	1.69E-02	2.04	STK39	2.41E-02	0.81	MRPL48	6.93E-11	0.26
CREB1	4.24E-03	2.03	RTKN2	2.10E-02	0.81	EMC2	3.29E-12	0.26
RPRD2	5.31E-16	2.00	MAST2	3.36E-04	0.80	PDAP1	3.99E-02	0.26
EED	2.26E-02	1.97	SNX3	4.31E-02	0.80	MRPL42	7.41E-05	0.25
CHMP3	1.33E-03	1.95	MED13L	9.02E-06	0.80	MRPL11	2.20E-03	0.25
DBF4	3.64E-03	1.94	MBNL1	2.72E-04	0.79	RPS6KB2	5.30E-03	0.25
PDGFRA	1.55E-02	1.94	NCOA2	1.43E-05	0.79	SARS2	6.31E-04	0.25
VEZF1	1.46E-03	1.94	MYO10	4.12E-15	0.78	LAMTOR1	3.75E-09	0.24
TBL1XR1	9.47E-07	1.94	ELF2	2.44E-02	0.77	FAM136A	5.81E-06	0.24
GLYR1	3.77E-04	1.93	ANKRD30A	7.13E-04	0.77	MTCH2	1.81E-02	0.24
CDC42EP2	3.98E-02	1.93	MYCBP2	4.88E-02	0.77	IMPDH2	5.30E-03	0.24
CDH1	3.07E-12	1.93	VMP1	6.23E-03	0.76	MRPL35	8.90E-06	0.23
NF2	7.55E-06	1.92	KDM3B	1.42E-03	0.75	MRPS35	8.90E-06	0.23
TSPAN16	6.38E-07	1.92	IGF1R	4.01E-03	0.75	MRPS18B	1.15E-15	0.23
TRIP12	5.72E-12	1.92	EIF2A	9.55E-03	0.75	DCAF7	3.84E-10	0.23
PPP4R2	6.48E-05	1.90	AKT3	7.72E-17	0.74	MRPL45	2.74E-02	0.22
PIK3R2	1.19E-06	1.89	FRYL	2.88E-10	0.73	MRPS26	2.74E-02	0.22
TULP4	1.39E-07	1.86	GPBP1	4.80E-02	0.72	GTPBP10	4.90E-05	0.22
TMPRSS9	4.73E-02	1.86	C15orf41	4.42E-03	0.71	MRPS9	2.46E-36	0.22
SPTLC2	2.30E-07	1.85	MAPK6	4.85E-03	0.71	ERAL1	9.93E-07	0.22
PRRC2A	4.30E-04	1.83	AP2B1	8.48E-04	0.71	MRPL22	1.81E-02	0.21
NSD1	5.45E-13	1.83	WDR7	1.21E-02	0.69	LAMTOR2	3.15E-05	0.21
GPATCH8	1.51E-08	1.82	EXOC2	1.33E-03	0.69	RARS2	3.62E-10	0.21
CNOT2	3.63E-04	1.81	WDR20	4.69E-22	0.67	MRPL50	1.13E-04	0.21
PCMTD2	1.51E-03	1.81	ACACA	5.41E-27	0.66	POLG2	1.47E-09	0.21
NDRG3	7.17E-03	1.81	TRIM71	9.40E-06	0.66	MRPS27	4.83E-61	0.21
EPC2	3.40E-07	1.80	C12orf65	7.36E-04	0.66	MRPS24	4.12E-02	0.20
ZNF611	2.18E-04	1.79	CDC42	3.89E-02	0.65	ICT1	5.72E-12	0.20
MGA	6.09E-11	1.79	UQCC1	4.79E-02	0.65	MRPS15	6.28E-04	0.20
E2F3	1.09E-03	1.78	RSRC1	6.24E-04	0.64	RPUSD3	7.67E-03	0.20
ARID1A	2.26E-09	1.77	PYM1	5.98E-04	0.64	RNMTL1	6.45E-08	0.20
TRPV3	8.56E-04	1.77	SMARCAD1	1.17E-03	0.64	MRPL38	1.37E-03	0.20
RORC	1.14E-02	1.77	TAL1	1.31E-02	0.63	ISCA1	1.87E-05	0.20
PTGES3	2.33E-05	1.77	ACTR3	2.27E-03	0.63	GATB	6.45E-14	0.20
RANBP17	8.83E-03	1.76	PTP4A2	3.22E-02	0.63	ATP5D	2.72E-02	0.19
FBXW7	3.36E-18	1.75	PDSS2	2.74E-29	0.63	WBSCR16	2.49E-08	0.19
MIB1	3.14E-11	1.75	APAF1	3.00E-02	0.62	PNPT1	2.51E-04	0.19
CCL26	2.57E-02	1.73	PAN3	3.23E-03	0.61	MIPEP	4.78E-12	0.19
FOXK1	9.03E-03	1.72	AEBP2	5.94E-09	0.61	MRPL12	3.40E-07	0.19
UFL1	6.86E-03	1.71	KDM2A	1.11E-16	0.60	MRPL27	1.76E-02	0.19
ZCCHC8	2.63E-03	1.69	INTS6	2.78E-02	0.60	REXO2	1.76E-02	0.19
PCGF6	6.67E-03	1.69	PIK3CA	2.13E-02	0.60	MRPS23	1.58E-04	0.19
PPEF1	2.80E-09	1.67	XPNPEP3	3.09E-05	0.60	MRPL30	1.31E-06	0.19
CSNK2A1	6.97E-03	1.65	MBIP	2.89E-02	0.59	HTRA2	1.34E-07	0.18
EPHB1	3.65E-06	1.65	FASTKD2	1.02E-02	0.59	MRPL20	1.00E-04	0.18
NGEF	8.17E-03	1.63	PIGU	1.53E-03	0.58	EARS2	1.40E-11	0.17
DEAF1	2.68E-02	1.62	NUBPL	4.66E-14	0.58	MTPAP	1.93E-08	0.17
IL6R	3.04E-02	1.62	ARPC2	5.38E-03	0.57	TRUB2	1.46E-04	0.17
HTR7	2.85E-06	1.62	YTHDF2	2.83E-03	0.57	TFB1M	1.23E-08	0.17
SCARA5	3.75E-03	1.61	ZRANB1	2.09E-04	0.57	MTERF3	6.01E-07	0.16
SLC44A2	1.61E-02	1.61	RPTOR	8.82E-04	0.57	MRPL18	4.15E-17	0.16
BTLA	1.94E-06	1.61	HECTD1	3.09E-06	0.57	GTPBP8	3.60E-07	0.16
ZEB2	2.96E-18	1.60	NSUN3	2.62E-02	0.57	YME1L1	1.70E-03	0.15
CUL5	1.90E-02	1.58	NFU1	2.79E-02	0.57	ATP5J2	2.25E-08	0.15
ANKRD11	8.65E-07	1.57	TNRC6A	1.65E-03	0.56	MRPL24	1.37E-10	0.15
PBX4	1.26E-03	1.57	COX10	3.94E-04	0.56	MTRF1L	1.07E-03	0.15
PIK3R1	2.10E-02	1.57	MTIF2	6.20E-03	0.55	NGRN	5.09E-08	0.15
ARHGAP39	1.49E-02	1.55	WNK1	5.33E-05	0.55	MRPL10	1.03E-02	0.14

Gene	FDR	MI	Gene	FDR	MI	Gene	FDR	MI
SCAF8	1.39E-02	1.55	UNC5D	2.75E-02	0.55	TOMM70A	1.03E-02	0.14
PLEC	1.05E-03	1.55	PDSS1	1.19E-02	0.54	C1QBP	1.73E-13	0.14
ARL15	2.50E-05	1.54	NCKAP1	2.72E-02	0.54	TEFM	4.65E-05	0.14
PARVB	3.12E-07	1.54	GART	5.41E-05	0.54	MRPL40	1.90E-08	0.14
PPHLN1	1.23E-05	1.53	TIMMDC1	1.77E-02	0.54	PITRM1	3.86E-03	0.13
ARIH2	2.51E-03	1.53	MBTPS2	4.65E-05	0.53	MRPS5	1.03E-05	0.13
TRPM8	4.76E-02	1.52	NDUFV2	1.97E-05	0.53	ATP5H	3.45E-02	0.13
PHF12	5.32E-03	1.51	ACO2	3.69E-02	0.53	MRPL15	1.54E-04	0.13
TOM1L2	1.65E-04	1.51	PIGB	1.31E-02	0.53	RNASEH1	2.27E-06	0.12
MARCH8	4.12E-02	1.50	MIOS	1.50E-02	0.53	TARS2	2.27E-06	0.12
NOX5	1.68E-03	1.50	BPTF	1.04E-04	0.53	MRPL47	3.43E-05	0.12
HMCN1	3.97E-04	1.49	PFAS	3.92E-06	0.52	ABHD11	1.37E-02	0.12
ZMYM2	2.55E-02	1.49	PIGK	2.92E-02	0.52	MRPS18A	1.37E-02	0.12
RANBP3L	3.68E-02	1.49	SMAD4	8.18E-04	0.52	PTCD3	7.19E-13	0.12
SMARCA4	1.27E-03	1.49	COQ3	4.81E-06	0.52	MTG2	1.23E-05	0.11
FAM193A	2.96E-02	1.48	LIN28B	1.53E-21	0.51	TFB2M	8.37E-03	0.11
LPIN1	6.79E-03	1.48	SDK1	3.04E-02	0.51	TRMT10C	8.37E-03	0.11
CCDC109B	2.06E-05	1.47	MRPL13	4.07E-02	0.51	MRPL54	7.47E-06	0.11
URI1	3.12E-04	1.47	HINT1	1.81E-02	0.51	GFM1	1.91E-04	0.11
PNPLA1	1.10E-02	1.47	NDUFB8	4.91E-02	0.50	MRPL3	3.15E-14	0.11
CSPP1	1.55E-02	1.47	MRRF	2.02E-07	0.50	MRPS10	9.45E-08	0.11
SETD5	1.55E-02	1.47	PRMT9	2.88E-02	0.49	METTL1	5.09E-03	0.11
CDK13	3.15E-05	1.46	RMND1	1.94E-02	0.49	MRPS30	2.66E-06	0.11
PPTC7	4.34E-03	1.45	YWHAE	8.46E-11	0.48	ATP5B	1.13E-04	0.10
HOMER2	5.83E-03	1.45	HSD17B12	4.74E-04	0.48	ATP5O	1.58E-06	0.10
SPOP	2.19E-04	1.45	MRPS16	4.20E-03	0.47	TSFM	6.68E-05	0.10
TRPC6	1.69E-02	1.45	NDUFAF6	1.25E-08	0.47	GADD45GIP1	4.53E-12	0.10
KMT2E	2.39E-07	1.45	YBEY	2.25E-18	0.47	MTG1	2.80E-12	0.10
MLLT10	4.49E-12	1.44	GIF	1.23E-02	0.46	YARS2	6.51E-09	0.10
MBD3	1.14E-02	1.44	MLST8	5.06E-03	0.46	MALSU1	3.13E-03	0.10
SPEN	1.97E-08	1.43	ASCC3	1.58E-04	0.46	MRPL23	1.71E-13	0.09
SMARCC1	6.62E-08	1.43	MTHFD1L	1.81E-05	0.46	DDX28	1.26E-09	0.09
PPP6R3	1.02E-02	1.42	CSNK1A1	2.48E-04	0.46	ATP5F1	8.17E-06	0.09
HTT	2.65E-03	1.42	IPO9	3.19E-02	0.45	MRPL37	3.77E-04	0.08
TEX11	1.53E-03	1.41	NRBP1	4.81E-02	0.45	MRPS7	9.68E-07	0.08
COX5A	4.12E-02	1.40	SLC30A9	2.11E-02	0.45	HSD17B10	1.29E-04	0.08
ABCC1	8.37E-04	1.39	CHP1	1.39E-07	0.45	MRPL52	2.55E-02	0.07
PAK7	4.07E-02	1.39	SRD5A3	3.54E-06	0.45	MRPL4	1.42E-05	0.07
HERC4	1.42E-03	1.39	COQ4	3.29E-03	0.44	HARS2	4.69E-06	0.06
TULP2	1.71E-02	1.39	COQ2	5.11E-04	0.44	FAM98B	3.20E-03	0.06
NRD1	3.47E-02	1.39	NDUFAF5	1.04E-04	0.44	MRPS18C	2.18E-04	0.05
NFIC	2.55E-04	1.38	MAGOHB	1.82E-02	0.44	RPUSD4	1.27E-04	0.04
C6orf99	1.05E-03	1.38	UBR4	4.16E-02	0.44	AARS2	7.34E-05	0.04
LY96	3.77E-02	1.37	CHCHD3	8.87E-04	0.43	MRPL33	7.34E-05	0.04
RAD54L2	2.13E-02	1.37	PIGX	5.03E-03	0.43	SSBP1	1.26E-06	0.03
FGD3	1.69E-02	1.36	FARS2	6.92E-10	0.43			

8.2.3 *p-RPS6 3% screen*

Gene	FDR	MI	Gene	FDR	MI	Gene	FDR	MI
C19orf81	3.49E-04	21.47	TET2	9.41E-04	1.41	MTHFD1	2.31E-03	0.49
MS4A5	2.31E-02	14.00	UNC13B	9.41E-04	1.41	MTHFD1L	1.37E-04	0.49
TSC2	2.62E-18	12.14	HELZ	7.47E-03	1.41	BPTF	1.38E-05	0.49
NPRL2	4.24E-16	11.09	ZNF83	2.88E-02	1.41	TIMMDC1	4.69E-03	0.48
RPS25	1.31E-20	8.05	MPRIP	4.41E-02	1.40	RTN4IP1	3.29E-02	0.47
DEPDC5	3.88E-87	7.59	BAIAP2	4.25E-02	1.39	YBEY	1.06E-15	0.47
SZT2	2.26E-13	7.04	TBC1D14	6.97E-04	1.39	MRPS16	1.17E-02	0.47
PI4KA	2.83E-03	6.30	APBA2	4.04E-05	1.39	PRPF39	4.29E-03	0.47
NPRL3	3.62E-84	6.14	PRDM16	2.89E-02	1.39	CHP1	6.68E-07	0.46
TSC1	4.21E-37	6.00	ZEB2	3.25E-07	1.38	YWHAE	1.06E-11	0.46
RCE1	6.94E-03	5.83	FGD3	1.82E-02	1.38	UBE2G2	9.24E-03	0.46
NLRP12	7.55E-03	5.04	IGSF11	1.59E-02	1.37	NDUFB4	2.61E-02	0.46
CHMP5	1.75E-04	4.67	BMPR2	1.34E-03	1.37	SLC25A32	1.36E-03	0.46
KCTD5	6.63E-07	4.60	TMEM116	3.04E-02	1.36	HSD17B12	4.63E-04	0.45
TDRD12	5.01E-03	4.40	ARL15	1.88E-02	1.35	CHORDC1	4.96E-02	0.45
TMEM206	1.72E-02	4.36	RTN4RL1	3.47E-02	1.35	KIAA0391	4.97E-06	0.44
ODF3L2	9.78E-04	4.25	PPFIA3	2.41E-02	1.34	MAPKAP1	5.26E-24	0.44
PARVG	3.12E-03	3.73	CCDC102B	3.90E-03	1.34	FAM136A	2.00E-02	0.44
KPTN	3.89E-07	3.69	UBR1	3.18E-02	1.33	PIGK	3.47E-03	0.44
ADGRD1	2.77E-10	3.67	ADD1	4.54E-02	1.32	NDUFS1	9.73E-03	0.44
SFTPB	2.01E-03	3.65	RAI1	2.63E-02	1.32	DYRK1A	1.44E-29	0.43
C12orf66	1.45E-11	3.51	DENND2A	2.61E-02	1.31	MBTPS1	1.33E-02	0.42
ITFG2	4.22E-07	3.32	ZNRF1	4.14E-02	1.31	NDUFB9	1.33E-02	0.42
NAA35	1.20E-05	3.25	CUX1	1.12E-02	1.31	CARS2	1.16E-04	0.42
AGAP5	1.76E-02	3.14	WDPCP	8.08E-03	1.31	RNMTL1	1.76E-02	0.41
NAA30	3.15E-03	3.11	GON4L	1.25E-02	1.30	NDUFA1	8.37E-03	0.41
DNMT3L	1.99E-03	3.09	RAP1GAP2	3.60E-02	1.30	LAMTOR5	3.84E-05	0.41
WAC	1.60E-08	2.98	IQGAP2	4.62E-02	1.28	EMC2	4.09E-06	0.40
CTDNEP1	2.35E-04	2.92	KIF3B	1.36E-03	1.27	OPA1	4.97E-02	0.39
DOT1L	2.47E-17	2.79	ATF7IP	9.13E-03	1.24	TRIT1	8.34E-06	0.38
ZNF793	8.91E-14	2.75	CARM1	2.57E-02	1.22	PGM3	4.16E-02	0.38
UBE2L3	5.83E-12	2.72	PBRM1	1.20E-03	1.20	SLC25A3	4.77E-02	0.37
ACTL8	3.52E-03	2.71	GNG7	8.41E-03	1.20	COX7B	1.68E-02	0.37
ILF3	1.18E-03	2.68	ZFHX3	6.27E-05	1.18	AIFM1	2.27E-03	0.37
C5orf38	2.00E-02	2.68	CTNNA1	5.25E-03	1.18	ATIC	2.67E-05	0.36
TBC1D7	3.52E-04	2.63	USP14	3.68E-02	1.17	MRPL13	7.83E-04	0.36
CAD	2.00E-02	2.63	CDC42BPB	3.67E-02	1.15	C19orf43	1.89E-02	0.36
FOXK1	4.15E-07	2.62	PTPRG	2.42E-02	1.13	ACLY	2.59E-03	0.36
STK11	7.41E-06	2.59	LRP1B	1.79E-02	0.94	ICT1	5.62E-05	0.36
MTF2	2.62E-18	2.55	ROBO1	8.90E-03	0.94	MTX1	2.16E-02	0.36
DLEC1	1.56E-15	2.55	FHIT	1.95E-02	0.93	MRPL19	5.48E-04	0.36
UBE2J2	4.21E-02	2.55	TANC2	4.68E-03	0.93	KAT7	2.95E-06	0.36
DPH7	4.55E-03	2.52	TMC1	5.51E-03	0.93	UQCRC1	2.47E-02	0.35
INPPL1	9.24E-03	2.46	DLG2	9.07E-06	0.92	MRPS6	4.76E-11	0.35
ATAD3C	3.64E-03	2.42	MAGI2	2.90E-02	0.92	PCNP	7.14E-04	0.35
TFDP1	6.32E-03	2.39	ZBTB20	4.09E-06	0.92	GRSF1	1.57E-02	0.35
UBOX5	2.88E-02	2.38	CTNNA3	1.57E-02	0.91	LIG3	3.12E-08	0.35
TIPRL	3.68E-03	2.35	GPC3	4.55E-03	0.91	PDE12	2.71E-03	0.34
TRPC7	3.19E-03	2.33	EYS	2.68E-02	0.91	RBFA	1.68E-03	0.34
UBASH3B	3.75E-10	2.31	TRPM3	9.24E-03	0.91	SEC62	1.68E-03	0.34
INPP4A	3.78E-18	2.27	ATP8A2	2.18E-03	0.90	MTG1	2.11E-04	0.34
FLVCR2	6.33E-06	2.26	IL1RAPL1	1.48E-07	0.90	DBX2	1.96E-02	0.34
EED	1.49E-02	2.25	ROBO2	2.33E-02	0.90	WDR59	1.15E-05	0.33
NF2	1.63E-07	2.23	SEMA3E	1.63E-02	0.90	FARS2	5.58E-15	0.33
PPP2R4	2.26E-13	2.22	NRXN1	6.79E-05	0.90	DCAF7	4.18E-05	0.33
TRA2A	1.12E-02	2.22	TOX	7.64E-03	0.90	HTRA2	1.49E-03	0.32
UPP2	8.37E-03	2.20	THSD7A	4.76E-02	0.90	WDR4	1.68E-05	0.32
DPH5	1.37E-03	2.19	PCDH9	2.94E-04	0.89	MRPS28	6.40E-61	0.32
DHX29	4.43E-04	2.19	LRBA	2.21E-02	0.89	MRPL30	3.90E-03	0.32
BFSP2	4.41E-02	2.19	NAV3	9.38E-03	0.89	WARS2	2.44E-03	0.32
MSN	2.22E-02	2.19	CAMKMT	3.11E-02	0.89	ATP5J	1.04E-06	0.31

Gene	FDR	MI	Gene	FDR	MI	Gene	FDR	MI
CREB1	5.49E-03	2.17	PAK3	3.51E-04	0.89	LARS2	1.09E-14	0.31
SMARCB1	1.10E-02	2.17	CACNA2D1	8.08E-03	0.88	LRPPRC	1.59E-51	0.31
CHMP3	3.18E-04	2.15	NLK	3.47E-02	0.88	MRPL15	4.55E-02	0.31
MAP1LC3A	2.83E-02	2.13	FBXL7	2.71E-03	0.88	ERAL1	4.33E-03	0.31
WDR72	2.30E-03	2.11	RBMS3	8.91E-03	0.88	COX15	2.70E-03	0.31
IL6R	9.08E-05	2.10	CHN1	7.06E-05	0.88	COA7	4.68E-03	0.30
ZNF91	2.25E-04	2.10	MAML2	4.97E-03	0.88	STARD7	1.21E-02	0.30
NCOR1	7.50E-17	2.09	PRR16	2.47E-02	0.88	EARS2	2.66E-05	0.30
TRIP12	5.13E-14	2.06	ADGRV1	9.61E-07	0.88	MTG2	1.92E-02	0.30
SLC44A2	5.41E-05	2.04	DACH2	1.06E-03	0.87	HAX1	5.14E-03	0.29
PBX4	1.35E-07	2.02	GRIK2	1.09E-02	0.87	RICTOR	1.14E-09	0.29
VAC14	5.49E-03	2.02	FOXP1	1.26E-03	0.87	MRPL23	5.19E-05	0.29
MYH14	2.55E-02	2.00	ST18	1.85E-03	0.87	GATC	1.38E-03	0.29
B4GALNT2	1.90E-02	2.00	DACH1	1.92E-07	0.87	SHMT2	8.03E-07	0.29
CDH1	1.34E-11	1.99	PTPRD	8.69E-04	0.87	ATPAF2	5.91E-04	0.29
CD44	1.39E-02	1.98	UBE2H	1.76E-03	0.87	ENO1	1.47E-02	0.28
FANCD2	4.34E-02	1.98	ANGPT1	6.06E-03	0.87	SLIRP	2.40E-03	0.28
PIK3R2	4.58E-06	1.94	HDAC9	2.32E-12	0.87	NARS2	2.08E-160	0.27
PRTN3	5.32E-03	1.94	COLGALT2	4.11E-02	0.87	MIPEP	1.59E-06	0.27
CCDC180	2.35E-02	1.94	AGPS	7.83E-04	0.87	MRPL22	3.80E-02	0.26
SPTLC2	4.22E-07	1.93	LRRC4C	1.43E-02	0.87	MRPL54	4.50E-03	0.25
C4orf19	3.92E-02	1.92	TCF12	4.57E-03	0.86	LAMTOR1	2.79E-08	0.25
TTYH3	1.12E-02	1.89	FRMD6	2.28E-03	0.86	ATP5J2	1.83E-03	0.25
SLC1A2	2.28E-03	1.87	GRIA3	7.32E-03	0.86	MRPS18B	1.80E-11	0.25
STARD3	4.10E-03	1.87	CYP7B1	8.36E-03	0.85	CYCS	1.71E-02	0.25
TTYH1	1.42E-02	1.87	NCOA2	3.14E-02	0.85	RARS2	1.95E-07	0.25
DPH6	4.94E-20	1.85	ERC1	1.29E-02	0.85	MRPS30	1.23E-03	0.25
SETDB1	2.63E-04	1.85	NELL1	2.24E-09	0.85	POLG2	4.93E-08	0.25
COL4A3BP	4.69E-03	1.84	CDKAL1	6.51E-09	0.85	MTPAP	4.99E-04	0.24
ANKRD11	2.50E-10	1.83	CSMD3	4.97E-06	0.84	TOP1	4.02E-02	0.24
GLYR1	2.53E-03	1.83	MAST2	2.61E-02	0.84	MRPL51	1.99E-04	0.24
PCMTD2	4.50E-03	1.82	MAP2	4.41E-02	0.84	ATP5F1	4.68E-03	0.24
PTGES3	4.18E-05	1.82	ERBB4	1.83E-02	0.84	FTSJ2	4.68E-03	0.24
MIB1	2.32E-12	1.82	PARD3	1.59E-02	0.84	MTX2	4.68E-03	0.24
PCGF6	2.71E-03	1.81	LOC339862	2.71E-03	0.83	MRPS23	2.64E-02	0.23
TGFB1	1.80E-03	1.80	TRDN	1.39E-03	0.83	MTERF3	7.97E-05	0.23
PLEC	6.89E-06	1.78	CDH9	3.25E-02	0.83	MRPL35	3.33E-05	0.23
CSDE1	1.12E-02	1.78	FGF13	3.67E-02	0.83	CLPB	1.99E-03	0.23
DNTT	1.04E-02	1.78	SAMD4A	1.61E-02	0.83	HSD17B10	4.14E-02	0.22
NSD1	3.83E-11	1.77	AGR3	3.14E-02	0.82	MRPL2	5.21E-04	0.22
GPATCH8	1.16E-06	1.77	SYT1	1.52E-19	0.82	YARS2	1.30E-03	0.22
CD48	7.86E-03	1.77	FAM13A	1.48E-03	0.82	GADD45GIP1	2.13E-05	0.22
SPEN	3.78E-18	1.74	EFNA5	8.04E-07	0.81	IMMT	3.18E-03	0.22
PHF12	6.22E-05	1.74	ANKRD30A	2.67E-02	0.81	LAMTOR2	1.27E-05	0.21
PPP6R3	7.36E-06	1.73	KDM3B	4.49E-02	0.80	MRPL18	4.86E-12	0.20
FLT3LG	1.78E-02	1.73	MYO10	6.04E-11	0.80	C1QBP	1.57E-09	0.20
GNA15	3.57E-02	1.73	KCND2	4.23E-06	0.80	PPAT	2.57E-13	0.20
RPRD2	3.91E-09	1.72	WDFY3	8.35E-03	0.79	NOA1	4.14E-02	0.20
MREG	3.53E-02	1.71	EXOC4	6.70E-05	0.79	MRPL48	5.54E-15	0.19
PPP4R2	7.61E-03	1.70	ANO3	1.10E-03	0.79	MRPS25	5.16E-04	0.19
EPHB1	6.36E-06	1.69	IGF1R	4.82E-02	0.78	HARS2	2.63E-02	0.19
TEX11	8.47E-07	1.69	FRYL	9.07E-06	0.78	MRPS26	2.63E-02	0.19
NGEF	6.06E-03	1.68	MED13L	3.40E-07	0.78	YME1L1	7.47E-03	0.19
EYA2	1.71E-02	1.67	CHD2	1.72E-03	0.77	MRPS5	1.29E-03	0.19
EIF4H	3.14E-02	1.67	ADAMTS5	1.57E-02	0.75	TARS2	1.29E-03	0.19
ARID1A	1.29E-06	1.67	INO80C	1.81E-03	0.74	DDX28	2.95E-06	0.18
AKAP8	1.59E-02	1.67	MBNL1	1.20E-06	0.74	SARS2	1.94E-04	0.18
TRPV3	9.51E-03	1.66	TRIM71	6.17E-03	0.74	MRPS27	2.36E-63	0.18
TSPAN16	6.80E-04	1.66	EIF2A	5.57E-03	0.73	MRPL24	2.03E-09	0.18
TULP4	7.34E-05	1.65	C15orf41	2.95E-02	0.73	POLRMT	1.70E-02	0.18
ZNF611	8.37E-03	1.64	SLTM	1.25E-02	0.72	GATB	3.96E-14	0.17
CSNK2A1	2.62E-02	1.64	KDM2A	1.48E-06	0.72	GTPBP8	1.04E-05	0.17
FAM208A	2.44E-02	1.63	ATG7	3.63E-03	0.71	MRPS33	1.04E-05	0.17
PDS5A	1.37E-02	1.63	C12orf65	1.49E-02	0.70	MRPS35	3.71E-08	0.17

Gene	FDR	MI	Gene	FDR	MI	Gene	FDR	MI
CHID1	2.48E-02	1.62	AKT3	1.00E-23	0.69	TEFM	1.88E-03	0.17
PRRC2A	2.41E-02	1.61	ACTR3	4.39E-02	0.69	MRPS9	2.78E-47	0.17
URI1	3.14E-05	1.60	HECTD1	9.73E-03	0.69	MRPS18C	3.95E-02	0.16
NOX5	3.18E-04	1.60	PYM1	7.55E-03	0.68	TOMM70A	3.95E-02	0.16
ARIH2	9.78E-04	1.60	ZRANB1	4.97E-02	0.68	ISCA1	1.82E-04	0.16
FBXW7	1.07E-11	1.59	COX18	3.34E-02	0.68	RPUSD4	6.87E-03	0.16
MGA	1.33E-06	1.59	GPBP1	8.91E-03	0.67	TRUB2	6.87E-03	0.16
STRADA	6.10E-03	1.58	NUBPL	2.02E-07	0.67	MRPL20	1.20E-03	0.16
LDLRAD3	3.55E-02	1.57	MYCBP2	1.89E-04	0.67	MRPL3	3.12E-08	0.16
CNOT2	1.37E-02	1.56	WDR20	9.21E-22	0.67	TFB1M	3.67E-12	0.15
ZSWIM3	7.06E-03	1.56	RB1CC1	1.56E-02	0.66	GTPBP10	8.47E-07	0.15
PARVB	2.82E-06	1.56	XPNPEP3	1.09E-03	0.64	MRPS7	5.68E-06	0.15
ZMYM2	1.12E-02	1.56	PDSS2	4.37E-26	0.64	ATP5B	2.67E-04	0.15
SCARA5	1.75E-02	1.56	YTHDF2	2.56E-02	0.62	MRPL4	2.67E-04	0.15
KIAA1324	5.75E-04	1.55	ACACA	3.18E-35	0.62	MRPL40	3.09E-07	0.15
CDK13	4.06E-06	1.54	ACVR2A	3.87E-03	0.61	MRPL11	1.62E-04	0.15
PIK3CD	2.56E-02	1.54	ARPC2	4.77E-02	0.61	WBSCR16	6.99E-10	0.14
AGO4	9.63E-03	1.53	SREK1	2.84E-02	0.61	MRPL39	6.07E-04	0.13
EDARADD	1.74E-02	1.53	ATG13	2.62E-03	0.61	MRPL49	3.47E-02	0.12
CCDC109B	9.06E-06	1.53	PTP4A2	1.76E-02	0.60	MRPS22	3.47E-02	0.12
DICER1	1.15E-02	1.52	FASTKD2	7.47E-03	0.59	MRPS24	3.47E-02	0.12
FAM193A	1.59E-02	1.52	PFAS	1.57E-03	0.58	PITRM1	3.47E-02	0.12
HTR7	2.17E-04	1.51	WDR7	3.94E-05	0.58	PTCD3	7.99E-13	0.12
BTLA	2.16E-04	1.51	AEBP2	1.82E-09	0.58	DAP3	5.83E-12	0.12
CADM1	5.97E-03	1.50	NSUN3	1.71E-02	0.57	MTERF4	7.91E-04	0.11
EPC2	4.09E-03	1.50	SMAD4	7.64E-03	0.57	QRSL1	2.60E-05	0.11
MAP4K4	6.79E-05	1.49	PIK3CA	4.59E-03	0.57	MRPL12	2.35E-08	0.10
ESYT2	1.34E-02	1.49	NDUFAF6	7.97E-05	0.56	MRPS10	9.10E-07	0.10
MLLT10	4.64E-13	1.48	PIGU	3.71E-03	0.56	TFB2M	5.19E-05	0.09
HOXC11	2.90E-02	1.48	MTIF2	4.96E-03	0.56	ATP5O	1.67E-05	0.09
PPP2R5E	4.41E-02	1.47	NDUFV2	5.14E-04	0.56	MRPS15	9.25E-08	0.09
C6orf99	1.29E-04	1.47	COQ5	2.41E-02	0.55	MALSU1	9.58E-04	0.08
TMEM30A	2.06E-02	1.46	WNK1	4.07E-04	0.55	MRPL10	5.43E-04	0.08
BAHCC1	4.71E-02	1.46	CSNK1A1	1.24E-02	0.55	NGRN	7.83E-09	0.08
PPEF1	3.79E-04	1.45	MBTPS2	1.82E-04	0.53	MRPL16	2.64E-02	0.07
NRXN2	1.43E-02	1.44	COX10	5.63E-05	0.52	MRPL52	2.64E-02	0.07
MBD3	1.36E-02	1.44	SRD5A3	7.72E-04	0.51	RNASEH1	9.46E-05	0.07
DIAPH1	7.55E-03	1.44	NDUFS3	4.91E-02	0.51	MRPL38	5.44E-05	0.07
NFIC	2.86E-05	1.44	SLC20A1	1.83E-02	0.51	MRPL21	1.57E-02	0.07
LTBP4	2.19E-04	1.43	LIN28B	1.40E-21	0.51	MRPL37	1.57E-02	0.07
GIGYF2	7.59E-05	1.42	COQ3	3.04E-05	0.51	SSBP1	3.06E-05	0.07
CNOT4	9.57E-03	1.42	SEH1L	4.68E-03	0.51	AARS2	9.11E-03	0.06
SPOP	9.67E-04	1.41	VPS29	1.37E-03	0.51	MRPL47	9.38E-06	0.06
KMT2E	9.78E-06	1.41	PDSS1	1.98E-03	0.50	METTL1	3.04E-03	0.05
PPHLN1	1.22E-03	1.41	MRRF	2.14E-06	0.50	MRPL50	9.08E-07	0.05
TFAP2C	3.64E-03	1.41	GCN1	1.47E-03	0.49	MRPL27	8.64E-05	0.04

8.2.4 *HIF-1α screen*

Gene	FDR	MI	Gene	FDR	MI	Gene	FDR	MI
VHL	7.01E-16	16.59	PBX4	1.30E-02	1.43	DARS2	4.97E-02	0.57
CNOT3	5.56E-24	14.28	CDH1	3.72E-04	1.42	MRRF	2.49E-05	0.56
TYMS	8.41E-07	10.81	PRMT7	1.06E-02	1.42	UBR5	1.83E-03	0.56
SNF8	3.72E-04	9.74	KMT2E	3.11E-08	1.42	AIFM1	4.96E-02	0.53
RNF20	3.14E-05	9.06	PHF12	3.29E-02	1.40	ACTR3	4.52E-06	0.52
CNOT2	1.83E-200	8.84	DPH6	1.72E-07	1.40	WDR4	2.62E-02	0.52
WAC	5.98E-77	8.36	SETD5	2.61E-02	1.40	MRPS28	6.35E-30	0.51
TCEB2	8.35E-04	7.60	CWC27	1.83E-02	1.39	PARL	2.51E-02	0.51
PSMD4	7.36E-07	7.34	ZFAT	5.36E-04	1.39	ICT1	4.29E-03	0.50
HNRNPM	3.87E-06	7.01	ARID4B	2.33E-02	1.38	MRPS6	5.27E-06	0.50
NAA30	2.66E-19	6.40	FBXW7	2.01E-07	1.37	FARS2	7.38E-07	0.50
TFDP1	4.51E-23	6.12	SPIDR	2.29E-03	1.36	GFM2	4.65E-02	0.49
SMARCB1	5.55E-20	5.64	BTLA	6.33E-03	1.35	MRPL13	1.60E-02	0.49
RPS25	2.05E-29	5.50	EPHB1	1.73E-02	1.35	MTHFD1	1.06E-03	0.48
DDX6	4.26E-29	5.31	POU2F1	2.16E-02	1.34	CARS2	2.03E-05	0.48
CCNC	2.84E-03	5.26	NCOR1	1.21E-03	1.34	MRPL17	3.71E-02	0.47
UBE2M	3.70E-12	4.58	TBC1D14	8.48E-04	1.33	MRPS21	9.68E-03	0.47
NAA35	1.80E-15	3.72	PPEF1	2.28E-03	1.33	MTG1	7.19E-03	0.47
PPP2R4	1.29E-52	3.22	BRIP1	2.31E-02	1.33	KIAA0391	4.37E-06	0.47
PCBP2	2.22E-04	3.13	CARM1	4.74E-06	1.33	PSIP1	1.24E-03	0.46
SMARCA4	4.07E-35	3.04	CELF1	4.61E-02	1.31	LARS2	3.09E-10	0.45
PPP4R2	1.42E-22	3.03	GON4L	6.31E-03	1.31	ZNF217	4.97E-02	0.45
CUL1	5.78E-10	3.02	UBE4B	2.52E-02	1.30	RBFA	1.95E-02	0.45
TIPRL	5.61E-12	2.97	NFIC	4.87E-03	1.29	MRPS35	2.54E-02	0.45
YBX1	2.63E-02	2.92	MAP4K4	1.59E-02	1.29	NARS2	1.95E-85	0.45
TSC1	5.48E-19	2.81	CCDC109B	1.37E-02	1.28	MRPL19	2.50E-03	0.44
CKS1B	1.23E-09	2.79	UBE2R2	2.52E-02	1.28	OPA1	1.48E-02	0.44
VPS28	1.53E-03	2.78	TRIP12	4.32E-02	1.27	PPAT	1.60E-04	0.44
BRD7	2.01E-05	2.76	VPS41	5.65E-03	1.27	SLC30A9	4.94E-03	0.43
CUL2	4.03E-02	2.70	CNBD1	3.38E-02	1.26	RNMTL1	1.11E-02	0.43
PIKFYVE	2.29E-03	2.61	CTNNA1	1.26E-06	1.25	LRPPRC	8.37E-38	0.43
NPRL2	5.43E-04	2.60	MBNL1	1.22E-03	1.24	WDR59	2.11E-03	0.43
TSC2	2.66E-05	2.59	SIPA1L3	5.65E-03	1.23	MRPL24	7.96E-04	0.42
IPO11	4.70E-04	2.59	REPS2	2.43E-02	1.22	TRIT1	5.10E-06	0.42
CUL3	5.33E-28	2.59	ABCC2	4.03E-02	1.22	FZR1	1.06E-02	0.41
EDC4	6.91E-03	2.59	APBA2	3.20E-02	1.21	MIPEP	1.03E-04	0.41
ARID2	3.68E-40	2.57	SPEN	9.66E-03	1.20	WARS2	1.89E-02	0.41
SMARCE1	1.62E-11	2.55	MSI2	3.60E-02	1.15	KAT7	3.85E-07	0.40
EPC2	4.44E-22	2.53	MAP4K3	8.35E-04	1.13	POLG2	3.00E-05	0.40
CXXC1	2.28E-02	2.44	ROBO1	4.43E-02	0.95	C1QBP	4.40E-05	0.40
DEPDC5	1.83E-23	2.34	TANC2	1.83E-02	0.94	MBTPS1	1.86E-05	0.39
CYB5R4	1.54E-02	2.26	TMC1	2.56E-02	0.94	MRPL35	7.38E-03	0.39
RBM33	4.12E-03	2.21	DLG2	4.98E-04	0.94	SCAP	7.02E-04	0.39
USP14	8.95E-89	2.18	NRXN1	1.90E-02	0.93	SMAD4	3.24E-10	0.39
GIGYF2	2.40E-35	2.12	NLGN1	1.41E-02	0.92	MRPS27	8.00E-32	0.39
CACYBP	1.09E-03	2.09	LRRC1	4.18E-02	0.92	GATB	7.63E-07	0.39
NPRL3	2.07E-21	2.09	IL1RAPL1	3.87E-06	0.91	ATPAF2	3.30E-04	0.39
GLMN	1.66E-04	2.09	ATP8A2	5.47E-03	0.91	ATP5J	2.34E-06	0.37
RANBP3	2.67E-07	2.09	ROBO2	4.96E-02	0.91	MRPL12	1.89E-03	0.37
SZT2	1.04E-02	2.08	PCDH9	2.99E-03	0.91	HARS2	4.89E-02	0.37
POT1	2.74E-02	2.07	CCDC91	1.85E-02	0.91	MRPL2	2.07E-02	0.37
CTNNBL1	3.05E-03	2.06	EPHA6	2.38E-02	0.90	FAM136A	3.25E-03	0.37
E2F3	2.61E-06	2.05	DACH1	7.66E-05	0.90	MRPL48	1.05E-08	0.37
CDK4	3.63E-02	2.04	EFNA5	1.29E-02	0.88	MRPS18B	7.58E-10	0.36
ACTL8	2.70E-02	1.99	CAMKMT	6.52E-03	0.88	GATC	1.91E-03	0.35
MYLIP	6.31E-03	1.98	RIMS2	2.31E-02	0.88	DAP3	3.35E-04	0.35
SUV420H1	1.26E-03	1.96	AGPS	3.94E-03	0.88	MRPL23	9.53E-05	0.35
FAM193A	2.38E-08	1.92	AKT3	2.63E-03	0.87	HAX1	7.55E-03	0.34
DBF4	2.66E-04	1.89	GRIA3	1.20E-02	0.87	GTPBP8	5.03E-03	0.34
CDK13	2.21E-17	1.87	TRDN	2.16E-02	0.87	SARS2	2.05E-02	0.33
FOXK1	1.22E-03	1.86	EIF4G3	1.73E-02	0.86	DDX28	4.48E-04	0.33

Gene	FDR	MI	Gene	FDR	MI	Gene	FDR	MI
TMED10	8.36E-03	1.84	ASCC1	1.20E-02	0.86	ATP5F1	4.69E-02	0.32
UBE2L3	7.75E-07	1.84	MED13L	1.83E-02	0.86	PNPT1	2.20E-02	0.32
PBRM1	2.17E-50	1.83	DNAH14	3.63E-02	0.86	TARS2	6.33E-03	0.32
RNF40	7.08E-04	1.83	NAALADL2	7.86E-03	0.85	MRPL39	1.56E-02	0.31
ARID1A	1.71E-10	1.79	ERBB4	1.30E-02	0.85	ATP5J2	1.33E-03	0.31
RPRD2	3.34E-16	1.79	XPO6	3.51E-02	0.85	ERAL1	6.16E-04	0.31
NF2	9.67E-06	1.78	MAST2	1.15E-02	0.84	MTPAP	9.10E-06	0.30
CNBP	6.15E-04	1.78	CSMD3	3.48E-07	0.84	METTL17	3.67E-02	0.30
CHMP3	1.24E-03	1.77	EPHA5	2.04E-03	0.84	MBTPS2	2.11E-34	0.30
ANKRD17	1.22E-09	1.76	CCDC141	4.23E-03	0.83	MRPL54	2.23E-03	0.30
DLEC1	4.00E-08	1.76	SYT1	1.09E-20	0.83	TFB1M	4.37E-06	0.30
ZNF793	4.40E-06	1.76	MCTP1	2.92E-03	0.82	MRPL10	3.91E-02	0.29
DPH5	3.45E-03	1.76	WWTR1	2.66E-04	0.82	GADD45GIP1	9.00E-05	0.29
ZC3H11A	2.63E-02	1.75	MME	5.44E-03	0.81	MRPL50	7.20E-04	0.29
ADGRD1	3.96E-03	1.75	PAWR	3.06E-02	0.81	MRPS33	3.67E-03	0.29
ANKRD11	2.07E-14	1.75	ANO3	8.80E-04	0.80	MRPL30	2.53E-05	0.28
INPP4A	3.00E-10	1.72	SNX3	2.73E-02	0.80	POLRMT	2.72E-02	0.28
TTYH1	1.50E-02	1.72	ARHGEF12	3.51E-02	0.79	TRUB2	7.36E-04	0.28
CDK6	6.23E-14	1.72	SESN1	4.08E-02	0.79	MRPL40	7.46E-06	0.28
VAC14	1.83E-02	1.71	ACACA	7.54E-10	0.79	MRPS9	3.96E-38	0.28
IL6R	3.22E-03	1.68	TLK1	4.96E-02	0.78	TFB2M	1.23E-02	0.28
UBASH3B	2.96E-05	1.68	INO80C	9.00E-03	0.78	YARS2	5.12E-04	0.28
UHRF1	4.91E-05	1.68	LIN28B	3.31E-03	0.78	MRPL15	2.53E-03	0.27
CCND2	3.83E-02	1.67	EYA3	5.31E-03	0.78	RARS2	2.99E-08	0.27
SMARCC1	1.07E-17	1.66	EXOC4	6.85E-07	0.77	MRPL45	4.06E-02	0.27
PRTN3	2.09E-02	1.66	TRPC1	1.41E-02	0.77	MRPL38	8.29E-03	0.27
ADSS	4.89E-02	1.66	ANKRD30A	1.86E-04	0.77	EARS2	3.07E-08	0.27
UBAP1	1.35E-03	1.65	GLRB	4.59E-02	0.76	MRPS15	2.36E-04	0.27
LARP7	8.90E-05	1.64	ADAMTS5	1.06E-02	0.76	MTERF3	2.36E-04	0.27
PLAA	5.18E-03	1.64	ALG8	3.83E-02	0.76	TEFM	5.24E-04	0.26
DICER1	8.81E-04	1.61	PARN	2.67E-07	0.75	NGRN	1.00E-04	0.26
LMNB1	4.91E-04	1.61	SREBF2	8.52E-04	0.72	MTRF1L	5.65E-03	0.26
KLF16	2.84E-03	1.60	PDSS2	1.58E-17	0.72	MRPL11	1.60E-04	0.26
PCNT	3.85E-02	1.60	XPNPEP3	6.31E-03	0.71	MRPL20	2.83E-05	0.26
RFX7	6.82E-04	1.59	YWHAE	6.45E-03	0.69	MRPL27	3.87E-03	0.26
GNPTAB	5.33E-03	1.59	WNK1	2.53E-02	0.69	PTCD3	1.01E-06	0.26
PPP6R3	9.22E-06	1.58	MLLT10	3.00E-15	0.69	RPUSD4	1.95E-02	0.26
HELZ	7.68E-06	1.55	REC114	2.75E-02	0.68	DCAF7	2.29E-09	0.24
CD48	4.03E-02	1.55	TLK2	4.31E-05	0.67	DYRK1A	4.11E-100	0.24
SETD1B	2.08E-04	1.53	YBEY	2.19E-05	0.67	MRPL3	7.05E-11	0.23
CUL5	2.52E-02	1.52	NUBPL	1.71E-09	0.66	MRPS30	2.40E-04	0.23
ZEB2	1.50E-13	1.51	GPBP1	1.33E-03	0.66	MRPS7	4.28E-05	0.23
FLVCR2	3.71E-02	1.51	COX10	9.10E-03	0.66	MRPL18	7.53E-18	0.22
KIRREL	1.07E-03	1.48	BPTF	4.34E-02	0.66	MRPS31	2.88E-02	0.22
TSPAN16	5.29E-03	1.48	RHOJ	1.73E-02	0.65	ATP5B	5.65E-03	0.21
ZNF148	2.72E-03	1.48	UQCC1	3.15E-02	0.65	WBSCR16	7.64E-09	0.21
ARIH2	1.18E-03	1.48	MAPKAP1	7.23E-07	0.65	ATP5O	7.51E-04	0.20
CDC25A	8.35E-04	1.45	NDUFAF6	1.76E-03	0.65	MRPL9	2.81E-02	0.19
TMPO	3.42E-02	1.45	MTIF2	4.68E-02	0.64	MRPL47	3.56E-05	0.19
FAM53B	1.11E-08	1.44	COQ3	2.43E-03	0.63	AARS2	2.28E-03	0.18
ATP2C1	3.55E-16	1.44	PPP4R1	1.34E-04	0.62	TOMM70A	2.65E-03	0.13
HTR7	3.50E-04	1.44	KDM2A	1.65E-18	0.61	TRMT10C	2.65E-03	0.13
RAD51B	5.10E-06	1.44	PYM1	3.37E-06	0.60	MRPL22	1.60E-05	0.11
AKT1S1	5.41E-03	1.43	TAF3	8.30E-04	0.60	HSD17B10	7.20E-04	0.09
PLEC	5.92E-03	1.43	NDUFV2	1.89E-04	0.59	MRPL49	4.47E-04	0.08

8.2.5 *HIF-1α +DFOM screen*

Gene	FDR	MI	Gene	FDR	MI	Gene	FDR	MI
CNOT3	3.41E-23	21.30	DOT1L	1.90E-06	1.65	CPQ	7.35E-03	0.84
HNRNPM	2.82E-11	17.01	LMNB1	9.73E-04	1.65	NKAIN3	5.36E-04	0.84
PRAMEF18 @chr1-	3.56E-03	11.62	IL34	2.05E-03	1.64	AFF1	1.03E-02	0.84
CNOT2	1.68E-270	11.17	PMM2	1.84E-02	1.63	AFF2	1.65E-04	0.84
WAC	2.11E-73	9.08	ABLIM2	1.12E-04	1.63	KCND2	7.01E-04	0.83
SMARCB1	8.99E-18	7.51	UHRF1	1.32E-04	1.63	RALGAPA2	4.76E-02	0.83
DDX6	2.85E-45	7.05	TSSC1	3.54E-02	1.62	EXOC4	3.56E-03	0.83
IPO11	3.44E-14	6.39	FXYD5	9.44E-03	1.62	PPP3CA	6.25E-04	0.83
RNF20	1.95E-03	5.81	EDARADD	7.55E-04	1.61	PLD5	5.53E-03	0.82
PSMD4	4.85E-05	4.84	NGEF	3.78E-03	1.60	SYNE2	2.82E-03	0.82
TFDP1	1.60E-13	4.63	RNF40	2.64E-02	1.60	MAP2	4.46E-03	0.82
TSC1	2.56E-44	4.53	ANKRD11	1.59E-09	1.60	USP48	3.07E-02	0.82
NAA30	2.70E-08	4.18	ZNF83	1.50E-05	1.59	CTTNBP2	1.10E-02	0.81
VHL	6.76E-03	3.98	PLEC	3.40E-05	1.59	MBNL1	7.67E-03	0.81
NAA35	2.96E-15	3.89	ZCCHC8	4.59E-03	1.58	PDSS2	1.96E-07	0.79
CUL3	9.84E-73	3.80	PDS5A	3.83E-04	1.58	EPB41L4B	1.09E-02	0.79
TSC2	8.13E-11	3.78	WDR37	4.66E-03	1.58	FSIP1	1.49E-02	0.79
EDC4	1.47E-05	3.70	DMRT1	1.18E-02	1.57	CUX2	3.21E-02	0.79
ART1	4.86E-02	3.50	CD200R1	1.18E-05	1.57	MAST2	8.91E-05	0.78
TYMS	1.09E-02	3.45	TFAP4	7.32E-06	1.56	CCDC33	1.63E-02	0.78
PPP2R4	7.63E-59	3.43	ZC3HC1	3.01E-02	1.56	TLK2	3.75E-02	0.78
HNRNPA1	5.52E-10	3.39	LHFPL3	1.87E-03	1.56	PPP2R2B	1.06E-02	0.78
ZNF329	2.88E-03	3.23	PLAA	3.18E-02	1.55	NCOA2	6.53E-05	0.78
CACNA1H	1.22E-02	3.03	MARCH8	5.35E-03	1.55	ASH1L	4.85E-02	0.77
EED	5.34E-13	3.02	ERF	1.60E-03	1.55	WDR44	1.58E-02	0.77
UBE2M	1.13E-05	3.00	ARID1A	1.85E-05	1.54	NUBPL	1.43E-03	0.77
ADGRD1	1.27E-14	2.98	PTGES3	5.24E-04	1.53	NHSL2	3.27E-02	0.77
PVRL4	2.29E-02	2.90	MROH8	9.05E-05	1.53	GFPT1	1.43E-03	0.77
TIPRL	1.39E-08	2.85	CSPP1	6.68E-04	1.53	HS2ST1	1.38E-02	0.76
PARVG	1.13E-03	2.83	TRPM8	3.54E-02	1.52	PARN	1.82E-05	0.76
DCP2	2.83E-04	2.80	PIK3R1	4.78E-02	1.51	WDFY2	3.29E-02	0.76
ZNF793	1.24E-23	2.78	DPH6	1.14E-10	1.51	COL11A1	2.45E-02	0.76
OTX2	5.78E-03	2.74	FUBP3	3.76E-02	1.51	MORF4L1	1.11E-03	0.76
ILF3	1.99E-08	2.72	FAM193A	8.98E-03	1.51	PRMT3	1.54E-04	0.75
DEPDC5	2.82E-31	2.70	TMPO	1.45E-02	1.51	PREX1	2.08E-02	0.74
DLEC1	5.79E-28	2.67	BRD9	3.27E-02	1.51	AKT3	8.20E-16	0.73
EPC2	6.05E-27	2.67	CRAMP1	2.94E-02	1.50	ASXL1	2.89E-02	0.72
INPP4A	2.85E-39	2.65	KIF3B	9.93E-13	1.49	GAB2	3.14E-02	0.72
TRIP12	3.16E-46	2.65	CUL5	2.64E-02	1.49	FAM168A	1.07E-03	0.71
ODF3L2	6.55E-03	2.62	KMT2E	9.87E-10	1.48	TTBK1	2.91E-02	0.71
DBF4	1.36E-10	2.61	ACTN1	1.53E-02	1.48	KDM2A	1.47E-08	0.70
B4GALNT2	8.75E-07	2.60	NSD1	1.27E-06	1.48	RXFP2	3.14E-02	0.68
SMARCE1	8.47E-11	2.57	PACSIN2	3.26E-02	1.47	WNK1	3.73E-02	0.68
ZNF569	8.20E-07	2.54	RANBP3L	3.17E-02	1.46	COQ3	1.84E-02	0.67
UBASH3B	5.12E-20	2.54	HMCN1	4.20E-04	1.46	PPP4R1	1.45E-03	0.65
DNMT3L	5.23E-05	2.52	KEAP1	4.66E-03	1.46	MRRF	3.25E-03	0.64
CD44	5.15E-07	2.51	ANKRD13C	1.04E-03	1.46	MEMO1	1.34E-02	0.63
ZNF823	4.08E-02	2.49	ZMYM2	2.25E-02	1.46	YWHAE	1.78E-04	0.62
KCTD5	5.69E-05	2.47	CNTNAP5	1.30E-06	1.45	LCOR	9.74E-04	0.62
SNRPA	1.71E-06	2.46	TNRC18	1.85E-04	1.45	MNT	1.52E-08	0.62
AGAP5	3.33E-03	2.46	CDC25A	2.02E-03	1.45	MAPKAP1	2.95E-08	0.61
SMARCA4	2.72E-19	2.45	C6orf99	3.76E-05	1.43	FARS2	7.55E-04	0.60
CHMP3	1.19E-09	2.45	SPOP	3.24E-05	1.43	DARS2	4.45E-02	0.58
USP14	1.55E-107	2.44	MED15	4.12E-02	1.43	MRPS28	4.44E-18	0.58
NAA38	8.67E-03	2.43	TMEM218	1.01E-02	1.43	MDH2	4.15E-02	0.57
ZNF91	5.18E-10	2.43	HOXC11	3.50E-02	1.43	LARS2	8.91E-05	0.57
RPS25	7.55E-04	2.41	TMEM62	3.42E-02	1.43	LIG3	4.03E-03	0.55
PPP4R2	7.19E-14	2.40	GCH1	1.42E-02	1.43	KIAA0391	4.33E-04	0.55
CNOT10	3.83E-04	2.40	EDA	4.78E-02	1.42	SDHC	9.25E-04	0.52
TAF13	3.25E-02	2.39	SETD5	1.52E-02	1.42	SUPT20H	4.39E-02	0.51

Gene	FDR	MI	Gene	FDR	MI	Gene	FDR	MI
EIF4ENIF1	4.83E-05	2.39	SLCO1A2	1.34E-05	1.42	MBTPS1	3.92E-02	0.51
MAP1LC3A	1.11E-04	2.38	SPEN	1.49E-10	1.42	LRPPRC	6.66E-23	0.50
TMEM209	1.87E-08	2.38	CLIC2	1.71E-02	1.41	VPS13D	1.85E-02	0.49
ATAD3C	8.48E-05	2.37	PAK7	1.63E-02	1.41	UCHL5	4.58E-04	0.49
NUP210	3.29E-09	2.37	HNRNPD	2.59E-02	1.41	MTHFD1	7.23E-03	0.49
SFTPB	9.39E-03	2.36	AGO4	3.06E-02	1.41	SCAP	4.90E-02	0.48
EZH2	3.80E-09	2.36	NCOR1	1.16E-04	1.40	SSR1	4.90E-02	0.48
TMED10	2.83E-04	2.36	PPHLN1	4.78E-05	1.40	MTG1	2.09E-02	0.48
TRPC7	6.40E-06	2.35	KDM1A	3.92E-02	1.39	MRPS6	3.07E-06	0.47
GREM1	3.09E-02	2.34	TBC1D14	9.37E-05	1.39	POLG2	2.42E-03	0.47
ACTL8	4.10E-04	2.32	CDK6	5.39E-04	1.39	COX15	4.90E-02	0.46
RPRD2	4.48E-34	2.30	UNC13B	1.80E-04	1.39	SCD	3.50E-02	0.46
RBM33	5.70E-04	2.29	WNK3	9.01E-04	1.38	NARS2	8.27E-73	0.46
CLPSL1	1.19E-02	2.28	CAPRIN1	2.78E-02	1.38	PPAT	2.92E-03	0.46
CKS1B	1.38E-04	2.27	MGA	2.76E-03	1.38	RICTOR	4.66E-03	0.45
NPRL3	1.97E-23	2.26	RFWD2	1.29E-08	1.37	GCN1	4.53E-04	0.45
CD48	1.12E-07	2.26	RAD54L2	9.39E-03	1.36	MBTPS2	5.77E-13	0.43
DNTT	1.59E-07	2.24	FBXW7	5.99E-07	1.36	MRPS16	5.34E-04	0.43
SZT2	6.05E-03	2.24	SCN8A	3.78E-03	1.36	TADA2B	1.62E-02	0.43
LCMT1	3.01E-02	2.23	HOMER2	1.53E-02	1.35	CARS2	4.99E-06	0.42
THEG	6.76E-03	2.23	C16orf45	1.97E-02	1.35	WARS2	2.63E-02	0.42
TSPAN16	3.61E-14	2.22	FBXL20	1.10E-02	1.35	GFM2	1.22E-02	0.42
S100Z	4.15E-02	2.21	FGD3	1.05E-02	1.35	MRPS27	1.51E-23	0.41
MYH14	1.12E-04	2.19	NRXN2	3.92E-02	1.34	MRPL35	2.30E-03	0.41
ZNF578	3.27E-02	2.16	TULP2	3.27E-02	1.34	MRPS34	3.36E-02	0.40
LARP7	8.52E-12	2.15	LY96	3.89E-02	1.34	MRPS18B	3.34E-06	0.40
CDC7	7.10E-03	2.15	APBA2	3.02E-05	1.34	COA3	3.65E-02	0.39
FLVCR2	8.40E-09	2.14	EIF4B	1.10E-02	1.34	MRPS10	3.92E-02	0.39
MTF2	3.01E-21	2.09	HERC4	2.67E-03	1.34	MRPS7	3.92E-02	0.39
SLC1A2	8.96E-08	2.08	KIF4A	3.22E-03	1.33	GATB	1.18E-05	0.38
ACLY	9.51E-03	2.08	STAG2	1.02E-02	1.33	RBFA	2.28E-03	0.38
KPTN	6.38E-03	2.07	PPTC7	3.53E-02	1.33	MRPL19	1.27E-04	0.38
EPHB1	2.38E-15	2.06	REPS2	9.55E-05	1.33	MTG2	4.62E-02	0.37
SUZ12	2.67E-03	2.06	LTBP4	5.52E-03	1.33	C1QBP	7.49E-05	0.36
SPTLC2	1.09E-11	2.06	VPS41	5.39E-04	1.32	GTPBP8	1.77E-02	0.36
CST8	2.13E-02	2.05	MYO1E	6.34E-03	1.32	MRPS9	1.66E-21	0.36
XPO7	1.89E-05	2.05	RAPGEF1	2.85E-02	1.32	MIPEP	4.23E-06	0.36
TIGD7	2.29E-02	2.04	TIA1	4.43E-02	1.30	SDHB	6.27E-03	0.36
BTAF1	3.54E-02	2.03	WDPCP	2.67E-03	1.30	MRPL17	1.06E-03	0.36
FBRS	3.84E-02	2.02	RSBN1L	3.44E-02	1.30	MTERF3	1.06E-03	0.36
CCL26	4.73E-05	2.02	PITPNC1	1.16E-07	1.30	TRIT1	1.51E-08	0.35
OIT3	1.05E-03	2.02	EPC1	1.34E-06	1.29	MTPAP	5.31E-04	0.35
FANCB	2.04E-02	2.00	PVRL2	3.94E-03	1.29	MRPL48	2.33E-08	0.35
METAP1	4.62E-02	1.99	EGLN3	5.34E-03	1.28	MRPL40	1.67E-03	0.34
CDH1	2.17E-18	1.98	NFIC	7.55E-03	1.28	MRPL24	4.15E-04	0.34
CNBP	3.33E-05	1.98	FN3K	2.08E-02	1.28	EARS2	2.37E-05	0.34
PBX4	4.92E-10	1.96	RAD51B	2.85E-02	1.27	GATC	3.52E-03	0.34
E2F3	1.12E-06	1.96	LRRTM4	3.20E-03	1.26	MRPL23	1.02E-04	0.34
ST6GALNAC 1	4.73E-04	1.95	CUX1	1.52E-02	1.26	PNPT1	2.97E-02	0.33
PPP6R3	6.89E-13	1.94	KIF9	9.35E-04	1.26	TAF6L	1.84E-03	0.33
C4orf19	4.66E-03	1.93	ABCC1	3.06E-02	1.26	MRPL54	3.70E-03	0.33
MTF1	2.91E-02	1.92	ZFX	1.64E-02	1.25	RHEB	1.08E-02	0.33
GIGYF2	8.29E-25	1.92	DET1	8.52E-04	1.25	SDHD	3.10E-02	0.32
CUL1	1.42E-02	1.92	CCDC102B	3.01E-02	1.25	DDX28	2.02E-03	0.31
FAAH2	2.87E-04	1.91	SLC4A8	1.55E-02	1.24	MRPS30	2.27E-02	0.31
ING3	3.75E-03	1.91	C11orf30	2.19E-03	1.24	MRPL51	6.88E-04	0.31
CCDC39	9.79E-04	1.91	ATF7IP	7.01E-04	1.24	MRPL11	3.20E-02	0.30
TSPAN14	4.74E-04	1.91	MYBPC1	6.55E-05	1.24	NGRN	2.07E-03	0.30
DPH5	1.64E-03	1.90	LYST	3.16E-03	1.23	MRPL4	4.31E-02	0.30
SETDB1	6.39E-07	1.89	TBC1D23	1.08E-02	1.23	PTCD3	1.51E-05	0.30
FANCA	2.88E-03	1.89	ABCC2	3.41E-02	1.23	GFM1	4.41E-02	0.28
ST8SIA1	2.13E-02	1.88	NCOA3	8.19E-04	1.22	MRPS15	8.57E-03	0.28
TULP4	1.14E-10	1.88	UNK	4.82E-02	1.22	DYRK1A	1.39E-69	0.27
HHLA2	1.23E-02	1.86	KREMEN1	5.98E-03	1.21	MRPS35	2.23E-05	0.27

Gene	FDR	MI	Gene	FDR	MI	Gene	FDR	MI
TEX11	1.78E-13	1.86	NINJ2	3.53E-02	1.20	TEFM	2.97E-03	0.27
KLF16	1.02E-05	1.85	C9orf85	3.83E-02	1.20	WDR24	8.67E-03	0.27
HTR7	8.74E-13	1.85	EIF2AK2	3.73E-02	1.20	TFB1M	5.18E-06	0.27
BTLA	2.57E-13	1.84	ADAM18	3.27E-02	1.19	WBSCR16	5.18E-06	0.27
CREB1	4.26E-03	1.84	ACACA	1.12E-04	1.19	ATPAF2	3.11E-05	0.27
CHST6	3.53E-02	1.83	UGP2	2.80E-02	1.19	DCAF7	8.20E-07	0.27
SLC44A2	2.37E-05	1.83	UVRAG	3.36E-02	1.19	MRPL21	3.28E-02	0.26
SUV420H1	3.02E-03	1.83	PBRM1	5.35E-03	1.19	DAP3	1.51E-05	0.26
IL6R	1.96E-04	1.82	EFHC2	4.91E-02	1.19	YARS2	1.73E-04	0.26
PXMP4	3.95E-04	1.82	ISPD	4.44E-02	1.17	HIF1A	2.92E-11	0.26
UPP2	1.02E-02	1.81	PXDNL	4.43E-02	1.16	RARS2	3.67E-08	0.26
RHOA	1.88E-04	1.81	ZFHX3	4.46E-04	1.14	IMPDH2	2.41E-02	0.26
CARM1	9.94E-27	1.80	ITPR2	4.48E-03	1.14	MRPL12	8.78E-05	0.25
SEH1L	4.14E-02	1.80	RYR2	3.92E-02	1.12	GADD45GIP1	2.05E-05	0.25
PCGF6	1.88E-04	1.78	UNC79	3.70E-02	1.12	TFB2M	1.16E-02	0.24
SEPSECS	3.23E-02	1.78	ARID5B	1.47E-02	1.10	MTCH2	1.44E-03	0.24
UBE2L3	1.85E-05	1.78	IL1RAPL1	2.30E-03	0.93	MRPL10	3.27E-02	0.24
CCPG1	1.32E-04	1.78	NELL1	2.98E-02	0.92	MTERF4	3.27E-02	0.24
SCAF8	8.48E-05	1.77	NRXN1	4.30E-03	0.92	MRPL18	5.17E-15	0.23
SNX8	1.22E-02	1.76	DLG2	1.79E-06	0.92	MRPL47	1.38E-03	0.22
POU2F1	7.55E-10	1.76	CHN1	1.09E-02	0.91	MRPL2	5.23E-05	0.22
SETD2	5.78E-05	1.75	PARK2	3.94E-03	0.91	MRPL49	3.14E-02	0.21
FANCD2	3.12E-02	1.75	MYO10	4.78E-02	0.91	MRPS31	3.14E-02	0.21
ZNF718	2.15E-03	1.75	FHIT	2.03E-04	0.91	PITRM1	2.21E-02	0.20
ZNF611	3.20E-05	1.75	NAV3	2.50E-02	0.90	MRPS26	3.56E-03	0.20
CDK13	6.80E-14	1.75	CACNA2D1	2.64E-02	0.90	MRPS25	1.32E-04	0.20
GLYR1	8.18E-04	1.74	CSMD3	8.56E-03	0.89	ERAL1	2.73E-06	0.18
TRPV3	1.57E-04	1.74	GPC6	3.75E-02	0.89	TRUB2	5.23E-05	0.17
SCARA5	2.31E-05	1.73	GLIS3	4.83E-02	0.89	MRPL3	2.25E-12	0.17
SYK	4.08E-02	1.73	TOX	2.53E-03	0.89	MRPL22	1.97E-02	0.17
SP1	3.01E-04	1.73	CCSER1	4.45E-02	0.89	MRPL39	2.62E-04	0.14
C12orf66	4.88E-03	1.72	MAML2	9.14E-03	0.89	HSD17B10	3.92E-03	0.14
ZEB2	3.70E-24	1.71	NEDD4L	3.87E-02	0.88	C14orf166	2.44E-02	0.13
WDR72	8.27E-03	1.71	LRRC4C	3.66E-02	0.88	SAMD4B	2.44E-02	0.13
C17orf99	4.01E-02	1.70	PLCB1	1.64E-02	0.88	TUFM	2.44E-02	0.13
PPEF1	1.55E-12	1.70	ADGRL3	2.85E-02	0.88	HARS2	1.91E-04	0.12
ZNF814	2.12E-02	1.70	PDE11A	2.60E-02	0.87	MRPL33	1.97E-04	0.09
ATP2C1	9.19E-35	1.69	FOXN3	2.51E-02	0.87	POLRMT	1.97E-04	0.09
TTYH3	7.22E-03	1.69	SH3KBP1	3.13E-02	0.87	MRPS24	1.14E-02	0.07
CCDC109B	1.26E-12	1.69	FRYL	2.78E-02	0.86	MRPL38	8.38E-06	0.07
RAPGEF2	4.93E-02	1.68	FAM13A	4.04E-02	0.86	MRPL27	5.51E-06	0.07
NOX5	7.79E-07	1.68	ARID1B	3.26E-02	0.86	MRPL37	1.88E-03	0.06
DICER1	1.61E-04	1.68	CACNB2	3.92E-02	0.85	MRPS22	2.02E-03	0.06
PARVB	2.89E-12	1.68	ASCC1	7.33E-03	0.85			
CAND1	2.05E-03	1.67	SYT1	4.01E-13	0.85			
IGSF11	1.39E-08	1.66	SNCAIP	1.97E-02	0.85			

8.2.6 *MR1 screen*

Gene	FDR	MI	Gene	FDR	MI	Gene	FDR	MI
HLA-A	4.86E-03	18.06	MECOM	4.53E-02	0.88	CCDC6	7.62E-05	0.37
EIF4G2	1.45E-02	15.94	MYO10	1.13E-02	0.86	ASCC3	6.06E-06	0.37
TIPRL	4.28E-28	9.39	ADK	1.39E-03	0.83	ZNF236	6.17E-05	0.37
METTL17	2.07E-02	9.03	WDR20	2.82E-02	0.83	YWHAE	1.34E-08	0.36
LAMTOR2	1.39E-04	7.22	EXOC4	3.84E-03	0.78	YTHDF2	1.59E-04	0.35
NAA30	2.73E-07	5.15	NFAT5	1.78E-02	0.75	SPPL3	4.86E-03	0.35
TFDP1	3.82E-09	4.78	USP14	5.24E-08	0.74	VPS26A	3.16E-02	0.35
RALGAPB	4.05E-24	4.60	ENAH	4.22E-02	0.73	ECE1	4.99E-02	0.34
FANCL	4.74E-07	4.60	USP34	1.94E-02	0.72	PSIP1	3.84E-03	0.34
PPP4R2	6.67E-20	4.60	CTNNA1	3.71E-04	0.72	RAB10	1.90E-06	0.34
RQCD1	2.50E-09	4.45	UBE2G1	1.53E-03	0.72	HTT	6.28E-13	0.34
CUL3	2.94E-41	4.35	DPH6	1.39E-03	0.72	PCYT1A	2.23E-02	0.34
DBF4	9.59E-11	4.33	UBE2H	1.23E-08	0.70	FBXO42	3.81E-05	0.33
VAC14	7.39E-06	4.25	GNG7	1.83E-03	0.69	PARN	1.83E-27	0.32
PPP2R4	1.12E-32	3.95	SEC14L1	1.07E-02	0.67	HSD17B12	1.33E-05	0.32
FLCN	2.91E-03	3.93	SMURF1	7.28E-03	0.64	ZC3H13	2.80E-02	0.32
FIG4	1.05E-03	3.68	HUWE1	1.11E-02	0.64	BPTF	3.46E-06	0.32
TAP2	1.39E-03	3.49	NFE2L1	6.91E-03	0.63	GTF3C2	1.39E-03	0.31
RNF146	1.18E-02	3.28	TNRC18	2.93E-02	0.63	TADA2B	1.93E-02	0.31
TAP1	3.57E-04	3.13	ERC1	9.43E-10	0.63	UGGT1	1.30E-02	0.30
TMEM131	4.77E-25	3.10	RFWD2	3.48E-06	0.62	HVCN1	4.82E-02	0.30
LAMTOR5	1.64E-04	2.90	HNRNPD	4.15E-02	0.61	AHCY	4.88E-07	0.30
DROSHA	2.84E-02	2.88	AIMP2	3.82E-02	0.61	KAT7	6.72E-04	0.30
LAMTOR4	8.42E-04	2.76	ZFX	1.82E-04	0.61	REPS1	4.70E-14	0.29
PDCD10	6.79E-03	2.71	XPO6	5.23E-07	0.61	SRF	6.48E-03	0.29
TAPBP	9.12E-06	2.70	WHSC1	2.99E-03	0.60	UBE2G2	3.28E-04	0.28
NFYC	2.20E-05	2.66	KDM2A	2.68E-05	0.60	FAM136A	2.26E-02	0.28
YBX1	1.78E-02	2.60	GGNBP2	3.11E-03	0.59	EP300	2.08E-12	0.28
GLMN	4.49E-02	2.54	PFKFB3	1.19E-02	0.59	NOSIP	3.85E-02	0.27
TSC1	5.97E-05	2.41	NFIC	3.62E-04	0.59	SNX18	1.66E-02	0.26
UBE2M	2.10E-02	2.28	BIRC6	4.38E-07	0.59	WDR59	1.66E-02	0.26
ZCCHC11	7.65E-13	2.24	ANKRD11	5.88E-03	0.58	SND1	7.38E-15	0.26
SUCO	1.11E-02	2.22	SYNRG	6.34E-03	0.58	HNRNPM	2.62E-02	0.26
CYLD	7.31E-03	2.22	EIF2A	2.26E-03	0.57	PMVK	1.07E-05	0.25
DHX29	2.02E-02	2.19	ASXL2	8.20E-03	0.57	CSNK2A1	2.14E-07	0.25
CDC25A	5.39E-09	2.19	GPATCH8	3.23E-02	0.57	CHMP3	4.86E-03	0.25
PPP6R3	8.04E-10	2.13	TFAP4	1.96E-03	0.56	ARPC2	1.90E-06	0.25
VPS33A	2.11E-02	2.07	TLK2	2.20E-06	0.56	NUP188	1.37E-03	0.25
ADNP	6.27E-06	2.05	SLTM	1.06E-04	0.56	NHLRC2	1.10E-05	0.25
PICALM	1.29E-10	2.04	CDYL	6.79E-03	0.56	OTUD5	1.76E-02	0.24
ANKRD17	9.42E-12	2.02	MERTK	4.64E-02	0.55	RBM15	4.31E-05	0.23
NDUFAF6	1.37E-04	2.02	BMPR2	9.30E-04	0.54	WAC	1.82E-18	0.23
FCHO2	2.00E-03	2.01	CUX1	5.11E-06	0.54	SEC63	9.24E-04	0.23
LIN28B	6.35E-12	2.01	STT3B	4.30E-03	0.54	DPH5	8.39E-08	0.23
KDM6A	1.02E-04	2.00	HECTD1	4.80E-02	0.53	SPATA5	7.53E-03	0.23
ARHGEF38	3.32E-06	1.96	PFAS	2.84E-02	0.53	EIF3L	5.91E-04	0.22
UBE2L3	6.11E-04	1.96	TRAPPC13	3.25E-02	0.52	BOD1	3.98E-02	0.22
RANBP3	5.53E-03	1.84	ACACA	1.31E-23	0.52	ADSS	2.44E-09	0.22
BAZ1B	3.66E-08	1.82	GART	3.57E-04	0.52	DYRK1A	5.74E-62	0.22
RAD51B	7.69E-05	1.78	TTC37	3.45E-02	0.52	MR1	2.90E-14	0.22
BRIP1	5.00E-04	1.74	INSR	3.98E-02	0.52	EIF3K	7.51E-03	0.21
ATF7IP	6.40E-12	1.73	CARM1	1.25E-09	0.52	PDAP1	5.03E-03	0.21
CDK6	7.47E-07	1.66	PHF12	6.07E-03	0.52	TAF1B	7.28E-03	0.19
EIF2AK4	1.98E-02	1.63	KIAA1033	4.52E-06	0.52	DCPS	3.82E-06	0.19
NKTR	3.45E-02	1.63	APAF1	8.24E-03	0.51	IMMT	3.82E-06	0.19
WDR7	1.01E-02	1.58	DNAJC7	2.35E-03	0.51	RFXAP	6.55E-07	0.19
KMT2E	8.83E-07	1.57	LSM14A	6.70E-03	0.50	PIN1	2.49E-02	0.18
MED15	3.78E-02	1.52	MTF2	1.55E-04	0.50	SGF29	1.32E-03	0.18
NADK2	1.11E-02	1.52	KDM3B	3.93E-08	0.50	TAF11	1.32E-03	0.18
TASP1	4.52E-03	1.52	MGA	6.27E-09	0.50	VPS29	7.04E-18	0.18
VPS41	9.56E-05	1.52	MLLT10	4.44E-16	0.49	IRF2	2.39E-10	0.17

Gene	FDR	MI	Gene	FDR	MI	Gene	FDR	MI
TRIM71	1.27E-02	1.51	CDCA4	4.82E-02	0.49	DOT1L	3.19E-22	0.16
AP2B1	2.34E-02	1.50	XPOT	7.37E-03	0.49	MEAF6	3.52E-02	0.16
NCOA2	6.84E-10	1.50	MNT	5.85E-09	0.48	SP7	3.52E-02	0.16
SMARCC1	1.93E-02	1.48	ALG8	3.29E-05	0.47	VPS53	4.55E-04	0.16
FBXL5	3.16E-02	1.44	RANBP1	1.07E-03	0.47	TTC4	2.22E-02	0.15
MAP4K4	2.90E-02	1.42	CNOT2	3.28E-04	0.47	RHEB	6.08E-04	0.14
RALGAPA2	7.37E-03	1.41	EIF4B	1.43E-08	0.47	NPM1	2.17E-04	0.13
PBRM1	6.74E-05	1.35	SUV39H1	4.53E-02	0.46	DCAF7	7.20E-07	0.13
PRSS12	9.05E-03	1.33	SRD5A3	6.55E-05	0.46	MED16	4.82E-02	0.12
MRPS28	4.16E-02	1.32	DDX10	1.11E-02	0.45	SSR3	4.41E-07	0.12
FAM198B	8.88E-03	1.28	VPS50	3.09E-03	0.45	FAM98B	2.96E-02	0.12
FTO	1.19E-02	1.28	VPS52	1.11E-02	0.45	EIF3J	1.82E-02	0.11
HDAC9	4.29E-21	1.26	EZH2	4.20E-03	0.45	DOLK	1.11E-02	0.11
IMMP2L	4.96E-03	1.25	SHMT2	7.32E-03	0.44	SRP9	1.11E-02	0.11
TBCK	9.37E-03	1.25	COMMD7	7.31E-03	0.43	MOGS	3.23E-05	0.09
TRDN	3.85E-02	1.25	C16orf62	1.12E-03	0.43	TIMM50	3.23E-05	0.09
MED13L	1.31E-02	1.23	RPTOR	1.37E-04	0.43	SETD1B	1.49E-58	0.09
FOXN3	2.80E-02	1.23	PPAT	8.57E-05	0.42	VHL	2.09E-06	0.08
GRIK2	8.88E-03	1.22	BMP2K	4.77E-03	0.42	TTI1	1.66E-04	0.08
NLGN1	9.84E-05	1.19	ZNF292	3.84E-28	0.42	TIMM17B	2.12E-02	0.07
DACH1	2.48E-07	1.19	PUM1	1.35E-06	0.41	GANAB	7.46E-23	0.06
CSMD3	4.65E-03	1.19	CFDP1	2.91E-02	0.40	SEPHS2	1.23E-02	0.06
TRPM3	3.91E-04	1.18	CREBBP	1.87E-12	0.40	TRIM28	1.23E-02	0.06
ROBO1	1.48E-09	1.17	UBR5	2.40E-03	0.39	ATP13A1	2.28E-09	0.06
GPC3	1.39E-03	1.17	NONO	1.50E-03	0.39	SPEN	4.41E-218	0.06
SLIT2	8.91E-04	1.17	GPBP1	5.35E-08	0.39	SRRD	7.37E-03	0.06
POU6F2	1.28E-03	1.17	MTHFD1	2.75E-03	0.39	KMT2A	2.23E-27	0.04
ZBTB20	1.47E-10	1.16	PDS5A	1.28E-03	0.38	ZCCHC14	3.10E-65	0.04
MAGI2	1.10E-03	1.16	VPS13D	3.60E-03	0.38	B2M	1.47E-34	0.03
CADM2	7.03E-03	1.12	ZFR	2.56E-03	0.38			
DLG2	1.50E-03	1.10	ACTR3	4.31E-08	0.38			

8.2.7 *p-RPS6$_{combined}$ screen*

Gene	FDR	MI	Gene	FDR	MI	Gene	FDR	MI
TSC2	1.73E-19	8.64	TOM1L2	1.82E-02	1.36	CHP1	4.03E-07	0.46
NPRL2	4.44E-17	8.49	TULP2	4.71E-02	1.35	ATG16L1	3.77E-02	0.45
DEPDC5	3.98E-100	8.04	RAD54L2	4.84E-02	1.35	NDUFA1	2.39E-02	0.45
RPS25	1.19E-20	7.04	GIGYF2	1.36E-03	1.35	TRMT10A	8.98E-03	0.44
TSC1	6.47E-45	6.26	BMPR2	2.49E-03	1.34	MRPL13	5.78E-03	0.44
NPRL3	3.76E-97	6.09	GON4L	3.83E-03	1.34	MAPKAP1	9.21E-27	0.43
SZT2	3.27E-14	5.80	MAP4K4	1.34E-02	1.33	MED12	2.68E-02	0.41
KPTN	7.64E-09	4.50	TFAP2C	3.55E-02	1.32	MBTPS1	5.63E-03	0.41
C12orf66	2.12E-16	4.31	WDPCP	3.96E-03	1.32	KIAA0391	3.95E-07	0.41
PI4KA	3.02E-02	3.86	SMARCC1	2.31E-04	1.32	OPA1	3.56E-02	0.40
RCE1	3.21E-02	3.85	RAI1	2.26E-02	1.32	LAMTOR5	2.99E-05	0.39
KCTD5	1.57E-06	3.71	KIF3B	8.63E-05	1.31	MRPL17	1.99E-02	0.39
WAC	3.94E-11	3.37	APBA2	9.76E-04	1.31	MTHFD1	3.79E-06	0.39
CHMP5	3.58E-03	3.33	TET2	2.69E-02	1.30	COX7B	4.07E-02	0.39
PARVG	8.42E-03	3.10	ABCC1	2.30E-02	1.30	FARS2	2.52E-12	0.38
ITFG2	4.18E-07	3.08	CCDC102B	1.39E-02	1.29	DYRK1A	1.56E-44	0.37
ADGRD1	1.14E-08	3.06	FRMD4A	4.96E-02	1.25	PTCD1	7.53E-03	0.37
ODF3L2	1.53E-02	3.06	PBRM1	2.64E-05	1.25	WDR4	8.18E-05	0.37
MEAF6	4.93E-02	2.92	SIPA1L3	1.82E-02	1.23	KAT7	6.59E-06	0.37
ACTL8	1.76E-03	2.88	SLC4A8	3.91E-02	1.23	TSEN15	4.28E-02	0.36
LCMT1	2.15E-02	2.84	ATF7IP	1.53E-02	1.22	COX15	1.05E-02	0.36
SFTPB	1.36E-02	2.82	USP14	2.04E-03	1.22	GRSF1	1.53E-02	0.36
TFDP1	6.90E-04	2.81	ZFHX3	1.26E-06	1.21	CARS2	1.62E-06	0.36
NAA35	1.54E-04	2.74	C11orf30	2.68E-02	1.21	LAMTOR3	2.35E-02	0.35
STK11	1.42E-06	2.70	CTNNA1	9.24E-04	1.20	LIG3	1.92E-08	0.35
MTF2	1.36E-21	2.65	ZBTB20	2.09E-03	0.94	MRPL19	8.63E-05	0.34
INPP4A	4.19E-27	2.64	FHIT	4.15E-02	0.94	GATC	9.63E-03	0.34
DNMT3L	7.42E-03	2.61	DLG2	2.84E-04	0.93	MRPL42	3.37E-03	0.34
DOT1L	4.86E-16	2.61	IL1RAPL1	5.10E-04	0.93	FAM136A	7.26E-04	0.34
DPH5	1.22E-05	2.60	NRXN1	1.89E-02	0.93	WDR59	1.43E-05	0.34
ZNF793	2.70E-13	2.59	ADGRV1	1.23E-02	0.92	AIFM1	2.42E-04	0.33
SMARCB1	2.84E-04	2.55	ATP8A2	3.23E-02	0.92	MRPS6	4.88E-12	0.33
ILF3	2.27E-03	2.46	TRPM3	8.65E-03	0.91	TRIT1	4.27E-08	0.33
DLEC1	3.43E-15	2.45	GPC3	1.46E-03	0.90	EMC2	1.43E-08	0.32
AGAP5	4.43E-02	2.44	PAK3	4.60E-03	0.90	C19orf43	7.50E-04	0.32
CD44	3.62E-04	2.41	DACH1	2.81E-04	0.90	WARS2	1.07E-03	0.32
UBE2L3	2.43E-10	2.41	HDAC9	9.81E-07	0.90	MRPS28	1.67E-63	0.32
TIPRL	2.32E-03	2.38	FBXL7	2.10E-02	0.90	ATP5J	6.47E-08	0.31
UBASH3B	2.75E-11	2.37	PTPRD	2.70E-02	0.90	ATIC	9.43E-07	0.31
INPPL1	1.23E-02	2.35	NAV3	2.04E-02	0.90	ATPAF2	2.88E-04	0.31
CTDNEP1	4.28E-03	2.35	CAMKMT	4.05E-02	0.89	MTX1	5.98E-03	0.31
DHX29	4.30E-05	2.33	UBE2H	2.17E-02	0.89	SHMT2	4.93E-06	0.31
NAA30	3.93E-02	2.31	CHN1	2.69E-04	0.89	RBFA	5.10E-04	0.31
PPP2R4	6.40E-16	2.30	ST18	1.36E-02	0.89	MTX2	1.52E-02	0.30
ZNF91	6.91E-06	2.29	NELL1	3.23E-05	0.88	LRPPRC	9.21E-57	0.30
TRPC7	1.99E-03	2.29	AGPS	5.63E-03	0.88	HAX1	3.14E-03	0.30
DPH7	7.87E-03	2.27	MAML2	3.60E-03	0.88	COA7	6.06E-04	0.30
THEG	4.58E-02	2.27	FRMD6	9.01E-03	0.88	LARS2	1.17E-16	0.29
FLVCR2	5.71E-06	2.20	FOXP1	1.07E-03	0.87	RNMTL1	9.82E-05	0.29
CD48	7.26E-05	2.12	ADGRG4	3.77E-02	0.87	RICTOR	7.00E-11	0.28
TTYH3	8.20E-04	2.10	LRRC4C	1.63E-02	0.87	ICT1	7.66E-08	0.27
MYH14	6.99E-03	2.09	EPHA5	2.61E-02	0.86	NARS2	2.01E-165	0.27
NCOR1	1.36E-17	2.08	LOC339862	2.43E-02	0.86	DCAF7	1.40E-07	0.27
CREB1	5.15E-03	2.08	TCF12	2.62E-03	0.86	CLPB	8.68E-03	0.27
MAP1LC3A	2.26E-02	2.07	GRIA3	6.09E-03	0.86	MRPL51	2.92E-04	0.26
EED	2.18E-02	2.07	CSMD3	1.51E-05	0.85	MRPL2	9.95E-04	0.26
FOXK1	1.58E-04	2.07	CDKAL1	8.44E-10	0.84	ERAL1	1.19E-04	0.25
SLC1A2	4.76E-05	2.05	FAM13A	1.27E-02	0.84	LAMTOR1	1.14E-08	0.25
NF2	1.77E-06	2.05	ANO3	3.70E-02	0.83	HTRA2	2.22E-05	0.25
CHMP3	7.15E-04	2.04	EFNA5	9.11E-06	0.83	MRPL30	5.46E-05	0.25

Gene	FDR	MI	Gene	FDR	MI	Gene	FDR	MI
ZNF569	1.08E-02	2.02	KCND2	2.10E-04	0.83	MRPL22	2.33E-02	0.24
SETDB1	2.52E-05	2.00	SYT1	1.08E-19	0.82	MRPS33	1.76E-03	0.24
DPH6	1.39E-26	1.99	MAST2	3.67E-03	0.82	MRPS18B	1.21E-13	0.24
TRIP12	4.84E-13	1.99	GFPT1	3.77E-02	0.82	PPAT	6.73E-12	0.23
ATAD3C	3.14E-02	1.98	NCOA2	8.68E-04	0.81	MRPL35	1.44E-05	0.23
C17orf99	1.99E-02	1.96	EXOC4	8.29E-04	0.81	RARS2	7.59E-09	0.23
CDH1	7.74E-12	1.95	CHD2	2.68E-02	0.81	EARS2	1.72E-08	0.23
DDX6	8.33E-03	1.94	ANKRD30A	4.90E-03	0.79	POLG2	1.14E-08	0.23
SYK	4.44E-02	1.94	MED13L	2.44E-06	0.79	MRPS25	7.48E-04	0.23
TBC1D7	1.89E-02	1.94	MYO10	4.46E-13	0.78	MRPL48	1.18E-12	0.22
PIK3R2	2.23E-06	1.91	VMP1	2.26E-02	0.78	MTRF1L	1.03E-02	0.22
DNTT	2.76E-03	1.91	INO80C	1.92E-02	0.78	MIPEP	2.90E-09	0.22
FAAH2	5.58E-03	1.90	KDM3B	9.06E-03	0.77	MTG1	2.59E-07	0.22
TSSC1	1.02E-02	1.89	AP2B1	3.86E-02	0.77	MRPL15	4.28E-03	0.22
GLYR1	9.95E-04	1.88	MBNL1	2.24E-05	0.77	SARS2	2.98E-04	0.21
SPTLC2	3.89E-07	1.88	IGF1R	1.47E-02	0.76	MRPL39	6.69E-03	0.21
PEX5	1.99E-02	1.87	FRYL	6.10E-08	0.75	LAMTOR2	1.37E-05	0.21
PDGFRA	3.90E-02	1.86	MAPK6	3.02E-02	0.74	MRPS26	2.32E-02	0.20
RPRD2	1.67E-12	1.86	EIF2A	7.42E-03	0.74	RPUSD3	2.32E-02	0.20
B4GALNT2	4.27E-02	1.83	EXOC2	1.90E-02	0.73	PNPT1	4.28E-03	0.20
IL6R	2.65E-03	1.83	AKT3	4.75E-20	0.72	MTG2	1.10E-03	0.20
VAC14	2.50E-02	1.81	MYCBP2	4.08E-03	0.72	MRPS23	1.06E-03	0.20
PCMTD2	3.15E-03	1.81	C15orf41	1.20E-02	0.72	MRPS35	5.64E-07	0.20
CCDC39	2.17E-02	1.81	TRIM71	3.03E-04	0.70	MTPAP	3.52E-06	0.20
NSD1	3.38E-12	1.80	GPBP1	1.99E-02	0.70	MRPL11	7.26E-04	0.20
SLC44A2	1.31E-03	1.80	SMARCAD1	1.89E-02	0.69	QRSL1	1.20E-04	0.20
PPP4R2	1.10E-03	1.80	RSRC1	8.33E-03	0.68	MTERF3	8.44E-06	0.20
GPATCH8	1.82E-07	1.79	C12orf65	4.65E-03	0.68	MRPS27	2.93E-62	0.19
PTGES3	2.57E-05	1.79	WDR20	7.35E-22	0.67	GFM1	9.63E-03	0.19
TSPAN16	2.24E-05	1.79	ACVR2A	3.36E-02	0.67	MRPS9	8.20E-42	0.19
DBF4	2.17E-02	1.79	PYM1	2.39E-03	0.66	ATP5J2	8.44E-06	0.19
MIB1	6.73E-12	1.78	ACTR3	1.35E-02	0.66	MRPL23	1.30E-08	0.18
WDR72	3.35E-02	1.77	KDM2A	3.94E-11	0.66	GTPBP10	7.94E-06	0.18
PBX4	2.34E-05	1.76	ATG13	1.86E-02	0.65	GATB	4.29E-14	0.18
TULP4	2.32E-06	1.76	ACACA	8.91E-31	0.64	MRPL54	2.63E-04	0.18
PCGF6	5.98E-03	1.74	GART	1.52E-02	0.64	TSFM	3.73E-03	0.18
ARID1A	7.28E-08	1.72	WDR7	7.23E-04	0.64	ISCA1	1.20E-04	0.18
PRRC2A	4.27E-03	1.72	PDSS2	2.06E-27	0.63	MRPL18	9.28E-15	0.18
TRPV3	3.67E-03	1.72	NUBPL	2.00E-10	0.63	MRPS30	1.12E-04	0.18
ZNF611	1.64E-03	1.71	HECTD1	3.19E-04	0.63	DAP3	8.03E-08	0.18
CNOT2	2.04E-03	1.69	ZRANB1	4.70E-03	0.62	MTERF4	9.63E-03	0.17
MGA	1.14E-08	1.69	XPNPEP3	2.59E-04	0.62	YME1L1	2.29E-03	0.17
ANKRD11	2.36E-08	1.68	PTP4A2	2.68E-02	0.61	MRPL20	2.63E-04	0.17
FBXW7	8.40E-15	1.67	TNRC6A	1.17E-02	0.60	C1QBP	1.43E-11	0.17
E2F3	9.63E-03	1.67	YTHDF2	1.07E-02	0.60	WBSCR16	1.16E-08	0.17
EPHB1	5.96E-06	1.66	FASTKD2	9.56E-03	0.59	MRPL24	3.10E-10	0.17
VEZF1	4.45E-02	1.66	VPS29	3.30E-02	0.59	ATP5F1	6.92E-04	0.17
RANBP17	4.09E-02	1.66	AEBP2	2.31E-09	0.59	TRMT10C	4.93E-02	0.16
EIF4H	4.96E-02	1.65	ARPC2	1.43E-02	0.59	TRUB2	9.70E-04	0.16
PLEC	1.37E-04	1.65	PIK3CA	1.23E-02	0.59	TFB1M	1.89E-10	0.16
TBL1XR1	9.46E-04	1.65	NSUN3	2.24E-02	0.57	GTPBP8	2.59E-06	0.16
NGEF	6.06E-03	1.65	PIGU	1.98E-03	0.57	MRPS5	2.63E-04	0.16
EPC2	5.94E-05	1.65	MTIF2	6.09E-03	0.56	TOMM70A	2.17E-02	0.15
CSNK2A1	1.89E-02	1.64	SEH1L	2.11E-02	0.56	TEFM	2.31E-04	0.15
PHF12	7.03E-04	1.62	GCN1	1.36E-02	0.55	GADD45GIP1	2.31E-08	0.15
STARD3	4.26E-02	1.61	ASCC3	1.47E-02	0.55	ABHD11	3.02E-02	0.15
DEAF1	4.71E-02	1.61	WNK1	1.39E-04	0.55	POLRMT	3.02E-02	0.15
ZCCHC8	1.35E-02	1.61	PFAS	8.31E-05	0.55	MRPL33	2.17E-02	0.15
SCARA5	1.03E-02	1.58	SMAD4	3.37E-03	0.54	TARS2	9.91E-05	0.15
SPEN	1.14E-12	1.57	MIOS	4.71E-02	0.54	YARS2	1.77E-06	0.15
HTR7	2.58E-05	1.57	NDUFV2	9.47E-05	0.54	MRPL12	1.20E-07	0.14
ARIH2	1.46E-03	1.56	COX10	1.45E-04	0.54	MRPL40	7.28E-08	0.14
PPEF1	2.59E-06	1.56	PRPF39	2.98E-02	0.53	HSD17B10	6.01E-03	0.14
BTLA	2.22E-05	1.56	RMND1	4.59E-02	0.53	MRPL50	3.70E-05	0.14
PPP6R3	3.63E-04	1.55	MBTPS2	6.58E-05	0.53	DDX28	1.20E-07	0.14

Gene	FDR	MI	Gene	FDR	MI	Gene	FDR	MI
NOX5	9.02E-04	1.54	PDSS1	5.36E-03	0.52	MRPS15	2.26E-05	0.14
PARVB	1.37E-06	1.54	COQ4	4.89E-02	0.52	MRPL38	5.14E-04	0.13
URI1	1.25E-04	1.53	NDUFAF5	5.67E-03	0.52	ATP5B	1.87E-04	0.13
ZMYM2	1.56E-02	1.52	NDUFAF6	1.85E-06	0.51	PITRM1	6.82E-03	0.13
TEX11	8.27E-05	1.52	LIN28B	1.39E-21	0.51	MRPL3	3.94E-11	0.13
FAM193A	1.99E-02	1.50	COQ3	1.19E-05	0.51	MRPS7	3.84E-06	0.12
CCDC109B	1.39E-05	1.50	TIMMDC1	1.17E-02	0.51	PTCD3	1.69E-12	0.12
CDK13	1.41E-05	1.50	BPTF	5.92E-05	0.51	NGRN	2.37E-08	0.11
ZEB2	3.88E-12	1.49	SLC25A32	1.56E-02	0.50	MRPL4	1.87E-04	0.11
PPHLN1	1.24E-04	1.47	CSNK1A1	3.44E-03	0.50	HARS2	3.96E-04	0.11
DICER1	3.77E-02	1.46	NDUFS1	3.14E-02	0.50	MRPL10	1.38E-03	0.11
MLLT10	1.37E-12	1.46	MRRF	4.93E-07	0.50	MRPL27	8.12E-04	0.11
STRADA	4.24E-02	1.45	CHCHD3	1.75E-02	0.50	TFB2M	4.75E-04	0.10
ARL15	9.64E-04	1.45	COQ2	5.67E-03	0.50	MRPS10	9.61E-08	0.10
MBD3	1.15E-02	1.44	DARS2	9.00E-03	0.48	MRPS18C	6.82E-03	0.10
SPOP	4.47E-04	1.44	PIGK	1.42E-02	0.48	RNASEH1	2.33E-05	0.10
KMT2E	1.77E-06	1.43	SRD5A3	6.58E-05	0.48	ATP5O	8.24E-06	0.10
C6orf99	3.53E-04	1.42	GFM2	1.99E-02	0.48	MRPL47	1.62E-05	0.09
NFIC	8.63E-05	1.41	MTHFD1L	6.72E-05	0.47	MALSU1	2.39E-03	0.09
LTBP4	7.99E-04	1.39	YWHAE	3.34E-11	0.47	RPUSD4	8.12E-04	0.09
KIAA1324	2.55E-02	1.39	MRPS16	6.27E-03	0.47	MRPL52	3.86E-02	0.07
TBC1D14	7.62E-04	1.37	YBEY	4.29E-17	0.47	MRPL21	2.26E-02	0.07
FGD3	1.67E-02	1.37	HSD17B12	3.62E-04	0.47	METTL1	2.62E-03	0.05
HTT	1.67E-02	1.37	SLC25A26	2.07E-02	0.46	MRPL37	1.46E-03	0.05
UNC13B	3.31E-03	1.36	PCNP	1.82E-02	0.46	SSBP1	1.70E-05	0.05
DIAPH1	3.82E-02	1.36	UBE3D	9.69E-05	0.46	AARS2	8.34E-04	0.05

8.2.8 *p-RPS6$_{rapamycin}$ screen*

Gene	FDR	MI	Gene	FDR	MI	Gene	FDR	MI
TTC4	5.09E-07	13.96	BCR	6.45E-03	1.42	SREK1	5.25E-04	0.52
RPS25	1.92E-47	11.17	MARK3	9.68E-03	1.42	NSUN3	1.52E-03	0.52
PRAMEF18@chr1-	5.01E-03	10.11	CCDC102B	7.58E-06	1.42	TRNAU1AP	1.02E-02	0.52
TSC2	6.09E-28	8.73	C16orf45	1.28E-03	1.42	RPTOR	1.25E-05	0.52
GPX6	9.61E-03	7.22	NPAS2	7.56E-03	1.42	YWHAE	2.54E-09	0.52
NPRL2	2.73E-20	6.39	MARK1	4.28E-02	1.42	PTAR1	9.32E-03	0.51
TSC1	2.99E-67	6.38	ITGAV	4.77E-02	1.42	COMMD3	1.37E-02	0.51
DEPDC5	1.80E-104	5.62	TRPC6	1.46E-02	1.42	SLC4A7	2.36E-03	0.50
NPRL3	1.49E-113	5.27	KIF3B	1.02E-08	1.41	PSPC1	3.59E-04	0.50
SMARCB1	2.52E-09	4.40	ABCC1	9.76E-05	1.40	SUPT20H	8.46E-03	0.50
TMEM174	1.78E-03	4.33	GON4L	1.24E-04	1.40	BRD1	3.05E-02	0.50
TBX22	2.76E-02	4.33	RTN4RL1	1.69E-03	1.40	NDUFAF7	3.05E-02	0.50
ADGRD1	2.64E-19	4.14	LARP1B	2.82E-02	1.40	CDC42	9.73E-04	0.50
NLRP12	4.30E-03	3.90	MBD3	1.56E-02	1.40	UNC5D	5.91E-04	0.50
TFDP1	7.59E-07	3.87	AGO4	3.35E-02	1.40	DARS2	4.60E-03	0.49
FKBP1A	2.44E-13	3.83	LY96	7.95E-03	1.40	UBE3D	3.50E-05	0.49
PARVG	4.22E-05	3.82	BAIAP2	1.73E-02	1.40	OTUB1	3.50E-02	0.49
GREM1	2.67E-04	3.82	UBA6	2.12E-02	1.39	PDSS1	3.24E-04	0.49
BIN3	1.20E-02	3.69	ARL15	7.02E-04	1.39	NCKAP1	3.56E-03	0.49
ZNF329	1.82E-03	3.55	TAOK1	2.53E-09	1.39	DNAAF2	5.25E-04	0.48
STK11	1.68E-18	3.52	SPTLC2	1.91E-02	1.39	ACAD9	2.40E-02	0.48
SZT2	7.60E-11	3.45	HNRNPR	6.49E-03	1.39	MTO1	3.58E-03	0.48
DHX29	3.00E-16	3.38	TNPO2	2.23E-03	1.38	LAMTOR4	2.18E-04	0.48
KCTD5	1.65E-07	3.33	IER2	1.56E-02	1.38	YTHDF2	6.43E-06	0.48
CHMP5	3.26E-04	3.27	RNF135	2.84E-02	1.38	WNK1	5.87E-07	0.48
SFTPB	2.70E-04	3.25	ATF7IP	1.61E-08	1.38	NUBPL	1.60E-25	0.48
DLEC1	3.42E-32	3.25	HTT	8.16E-03	1.37	COX10	1.33E-07	0.47
CHMP3	2.37E-13	3.21	APBA2	2.69E-06	1.37	CSNK1A1	4.04E-04	0.47
ZNF793	4.67E-23	3.19	FRMD4A	4.87E-05	1.37	DDX5	1.61E-02	0.46
UBE2L3	6.27E-27	3.18	E2F2	2.16E-02	1.37	TRPM7	3.09E-02	0.46
NAA30	1.10E-04	3.14	PPHLN1	2.14E-04	1.37	NDUFA13	1.40E-02	0.46
TMEM196	1.81E-02	3.13	FGD3	5.72E-03	1.37	NDUFAF5	9.41E-05	0.45
DNMT3L	2.53E-05	3.10	PFKFB3	3.55E-02	1.36	SEH1L	6.45E-05	0.45
PPP1R2	8.65E-03	3.09	CCDC7	6.66E-03	1.36	SMAD4	4.61E-06	0.45
ZNF578	2.99E-04	3.09	LPIN1	3.70E-02	1.36	PIK3CA	6.00E-06	0.45
ZNF569	4.27E-09	3.07	CSPP1	4.13E-02	1.36	NDUFA1	1.35E-02	0.44
UBASH3B	2.59E-22	3.05	PNKD	8.05E-04	1.36	CTSH	3.84E-02	0.44
KPTN	6.40E-07	3.00	BRD2	5.47E-04	1.35	NDUFB2	2.60E-02	0.43
NF2	4.64E-20	2.99	KIF9	1.22E-06	1.35	PDSS2	5.34E-89	0.43
MAP1LC3A	1.03E-05	2.98	PRRX2	1.47E-03	1.35	PARL	3.76E-03	0.43
UBOX5	3.29E-04	2.95	C11orf30	4.25E-07	1.35	NDUFS3	7.00E-03	0.43
CNOT2	4.07E-14	2.94	PLCE1	1.09E-04	1.35	TIMMDC1	3.73E-04	0.43
FLVCR2	1.28E-13	2.93	WNK3	1.82E-03	1.34	FZR1	1.72E-02	0.43
CFAP53	1.02E-03	2.89	MIPOL1	8.18E-03	1.34	NDUFV2	6.83E-10	0.42
C17orf99	1.08E-06	2.85	RGS6	3.49E-02	1.34	UQCC1	2.78E-07	0.42
TSPAN16	1.22E-19	2.83	BMPR2	8.16E-04	1.33	NDUFB8	3.56E-03	0.42
CD44	4.99E-08	2.81	PPCDC	4.92E-02	1.33	ARPC2	3.57E-05	0.42
C12orf66	1.59E-12	2.80	PPFIA3	1.27E-02	1.32	COQ7	8.72E-03	0.42
CDC16	2.40E-02	2.79	ZFAT	6.92E-03	1.32	HNRNPA2B1	5.39E-03	0.42
MEAF6	2.40E-02	2.79	MATR3	7.46E-03	1.32	ACTR3	3.07E-10	0.42
MISP	7.93E-03	2.74	ALDH2	2.79E-03	1.32	CTR9	9.73E-03	0.42
MYH14	1.42E-06	2.70	KIAA1324	3.76E-02	1.32	NDUFB4	7.16E-04	0.41
CACNA1H	3.49E-02	2.70	PHKA1	1.91E-02	1.32	ATIC	1.35E-03	0.41
STRAP	4.61E-03	2.69	ISPD	1.03E-06	1.31	PET117	1.82E-02	0.41
AMBN	5.65E-03	2.68	FAR2	4.28E-02	1.31	MTHFD2	1.36E-03	0.40
ST6GALNAC1	4.48E-08	2.67	ELAVL2	4.95E-02	1.30	YBEY	1.44E-22	0.40
LCMT1	3.18E-03	2.65	NFIX	1.94E-02	1.30	BPTF	2.58E-08	0.40
PI4KA	2.45E-02	2.63	PI4K2B	1.72E-02	1.30	HSD17B12	1.04E-06	0.40
SLC1A2	8.61E-12	2.63	CDA	3.52E-02	1.30	MTHFD1	3.76E-05	0.39
DBF4	8.01E-08	2.62	CNBD1	2.70E-03	1.30	SCD	6.15E-03	0.39
ACTL8	4.17E-04	2.58	UNC13B	4.22E-03	1.30	UQCRC2	2.54E-02	0.38

Gene	FDR	MI	Gene	FDR	MI	Gene	FDR	MI
CYB5R4	7.96E-03	2.57	SLC4A8	1.05E-03	1.29	NSUN4	9.07E-04	0.38
ODF3L2	9.46E-03	2.56	SIPA1L3	8.11E-05	1.29	C19orf43	1.10E-02	0.38
DPH5	6.41E-09	2.55	HMOX2	3.76E-02	1.29	SEC62	1.10E-02	0.38
NAA35	4.69E-06	2.55	CDC14A	1.83E-02	1.29	NDUFB9	9.90E-04	0.38
S100Z	5.53E-03	2.54	PITPNC1	6.40E-07	1.28	MRPS34	7.46E-03	0.38
ATAD3C	7.61E-05	2.51	LYST	1.23E-04	1.28	NDUFA10	3.83E-02	0.38
INPP4A	1.76E-29	2.48	DNAJC15	7.62E-03	1.27	COQ4	2.19E-04	0.38
CCL26	4.43E-07	2.48	RALGPS1	1.67E-02	1.27	MINOS1	1.65E-03	0.38
INPPL1	5.91E-04	2.48	CUX1	1.09E-02	1.27	PTCD1	3.68E-03	0.37
SIN3B	6.60E-03	2.44	NFIC	9.70E-03	1.27	MRPL19	6.83E-05	0.37
DPH7	8.77E-05	2.44	SLCO1A2	1.21E-02	1.27	NDUFAF6	3.63E-14	0.37
CD48	6.53E-09	2.40	CNTNAP5	1.66E-02	1.26	NDUFA9	3.61E-04	0.37
DOT1L	9.37E-17	2.37	DCST1	2.76E-02	1.26	NDUFS1	3.61E-04	0.37
CLPSL1	1.03E-02	2.35	PVRL2	8.88E-03	1.26	COX19	2.82E-02	0.37
TSKS	1.58E-03	2.34	ZFHX3	6.38E-12	1.26	WDR59	1.04E-04	0.37
HHLA2	1.14E-04	2.33	DENND2A	2.82E-02	1.26	GRSF1	4.01E-03	0.37
CDH1	6.31E-24	2.31	ADD3	4.57E-02	1.26	SAP30	2.73E-03	0.37
TRPC7	2.53E-05	2.26	ABCC2	7.26E-03	1.26	PDE12	8.14E-04	0.37
TIPRL	2.06E-03	2.26	BBC3	4.60E-02	1.26	MAPKAP1	4.72E-33	0.37
PPP4R2	8.81E-09	2.25	EML2	9.68E-03	1.26	SLC25A26	3.94E-04	0.37
WDR72	7.36E-06	2.25	EFHC2	1.04E-03	1.25	WDR4	1.03E-05	0.36
DDX6	1.63E-04	2.25	ADAM18	4.63E-04	1.25	ATP5E	3.06E-02	0.36
DPH6	1.58E-46	2.24	RAP1GAP2	4.58E-02	1.25	NRBP1	1.35E-02	0.36
PBX4	1.29E-12	2.23	RBL1	2.98E-02	1.24	MRPL42	4.46E-03	0.36
ST8SIA1	1.96E-03	2.22	UNK	9.69E-03	1.24	COQ2	2.48E-06	0.36
PPP2R4	5.59E-14	2.21	FAM78A	3.71E-03	1.24	CAB39	6.66E-03	0.35
ZNF611	3.11E-10	2.21	STAT3	1.76E-03	1.24	KIAA0391	6.43E-13	0.35
PLEKHA6	3.76E-02	2.19	SETBP1	1.95E-03	1.24	WDFY4	3.35E-02	0.35
MAPK15	3.83E-04	2.18	MLLT10	3.04E-05	1.23	IMPDH2	4.98E-02	0.35
AGAP5	3.12E-02	2.17	GAS8	2.71E-02	1.23	COA7	6.88E-04	0.35
ZNF606	4.51E-02	2.17	NINJ2	9.68E-03	1.23	GFM2	6.51E-05	0.35
TCERG1	5.95E-03	2.13	SGCZ	9.03E-03	1.22	FARS2	7.75E-16	0.35
GATAD1	4.04E-04	2.11	FMN2	2.67E-02	1.22	PIK3R4	4.83E-03	0.35
PPP6R3	8.91E-14	2.10	EPC1	6.26E-04	1.21	RPRD1B	5.08E-04	0.34
CST8	4.63E-02	2.09	FADS2	3.79E-02	1.21	MRPS21	7.48E-05	0.34
MTF2	1.23E-17	2.09	BIRC6	2.94E-03	1.21	TAF1B	1.15E-02	0.34
ZNF91	2.36E-06	2.08	NCOA3	8.96E-04	1.21	COMMD8	7.36E-06	0.34
TULP4	8.08E-13	2.08	ITPR2	1.02E-06	1.21	FOXRED1	2.47E-02	0.34
ITFG2	9.92E-05	2.07	MMP24	2.32E-03	1.20	VARS2	1.72E-04	0.33
FOXK1	2.02E-05	2.06	KREMEN1	6.66E-03	1.20	NDUFB5	1.19E-03	0.33
AIP	4.29E-02	2.05	ABCA1	2.09E-02	1.19	SLC30A9	3.85E-05	0.33
CCDC180	1.54E-03	2.05	RNF157	1.92E-02	1.19	ATG14	1.80E-03	0.33
FAAH2	5.22E-05	2.05	RFWD2	2.49E-02	1.18	BTAF1	1.16E-02	0.33
B4GALNT2	1.43E-03	2.03	CAMTA1	1.11E-02	1.16	PCNP	4.09E-04	0.33
CCDC39	3.90E-04	2.03	BCOR	7.70E-03	1.15	SHMT2	4.09E-04	0.33
PIK3R2	1.56E-08	2.03	PXDNL	2.82E-02	1.15	MBTPS2	4.24E-19	0.32
PHF12	1.87E-09	2.00	ATP2C1	3.38E-02	1.15	FBRS	6.00E-03	0.32
SYK	2.96E-03	1.99	BNC2	2.57E-02	1.14	MBTPS1	6.33E-06	0.32
ADGRL4	2.49E-02	1.99	MYBPC1	3.97E-02	1.14	ATPAF2	1.42E-05	0.31
B3GALT6	4.67E-02	1.98	MAP4K3	2.88E-04	1.13	IPO9	1.37E-03	0.31
BRD7	4.67E-02	1.98	RYR2	1.82E-02	1.13	XRN2	1.37E-03	0.31
THEG	4.67E-02	1.98	ZBTB20	1.63E-02	0.95	MRPS25	4.23E-03	0.31
ZCCHC8	7.72E-07	1.98	PARK2	3.10E-02	0.93	MRRF	2.73E-20	0.31
SETDB1	5.87E-07	1.98	NRXN1	2.30E-03	0.92	LAMTOR3	6.35E-03	0.31
IL6R	6.51E-05	1.98	MAGI2	5.65E-03	0.91	COQ3	1.57E-17	0.31
EPC2	9.60E-10	1.97	CHN1	2.81E-03	0.91	COX20	3.01E-03	0.31
EPHB1	1.07E-13	1.97	SLIT3	2.43E-02	0.91	COX7B	6.76E-04	0.30
ZNF260	2.04E-03	1.97	DLG2	4.24E-09	0.91	COX6B1	6.69E-03	0.30
XPO7	3.37E-05	1.96	ATP8A2	9.39E-04	0.91	MRPL13	4.72E-07	0.29
BTLA	1.63E-14	1.95	FOXP1	2.90E-02	0.91	KAT7	1.70E-11	0.29
PCGF6	3.13E-05	1.95	IL1RAPL1	1.18E-08	0.90	HAX1	7.19E-04	0.29
ABAT	3.24E-02	1.95	MECOM	5.72E-03	0.90	MTX1	2.40E-04	0.28
DNTT	6.42E-05	1.94	DACH1	4.18E-05	0.90	EMC2	7.84E-13	0.28
HTR7	1.04E-13	1.94	TRPM3	1.17E-03	0.90	COQ5	1.98E-10	0.28
ILF3	3.82E-03	1.93	TOX	3.04E-03	0.90	LAMTOR5	1.35E-10	0.28

Gene	FDR	MI	Gene	FDR	MI	Gene	FDR	MI
GPATCH8	7.28E-13	1.93	ADGRV1	1.83E-05	0.89	FTSJ2	3.23E-03	0.28
OIT3	3.18E-03	1.93	DACH2	3.68E-03	0.89	RICTOR	3.04E-09	0.28
HGS	3.92E-02	1.93	CAMKMT	7.57E-03	0.89	PPA2	5.02E-04	0.27
TNNT1	3.92E-02	1.93	IMMP2L	3.75E-02	0.88	SLIRP	5.02E-04	0.27
SYTL5	4.22E-02	1.91	GPC3	1.28E-05	0.88	MCAT	3.05E-02	0.27
URI1	4.14E-15	1.91	FRMD6	8.72E-03	0.88	FAF2	2.26E-03	0.27
CCDC109B	1.32E-16	1.91	PDE11A	2.82E-02	0.88	MRPS16	2.01E-10	0.27
C4orf19	5.48E-03	1.90	BICD1	4.98E-02	0.88	PPAT	9.65E-10	0.27
PPEF1	2.15E-16	1.90	GPC6	2.79E-03	0.88	DYRK1A	1.36E-84	0.27
PRTN3	8.60E-04	1.90	EPHA5	2.80E-02	0.87	TOMM70A	9.75E-03	0.27
ANKRD11	5.84E-16	1.89	EPHA6	2.06E-04	0.87	LIG3	7.76E-14	0.26
CASQ2	4.76E-04	1.89	CCSER1	5.53E-03	0.87	ICT1	7.05E-08	0.26
RPRD2	3.55E-15	1.88	PPP3CA	1.62E-02	0.87	MLST8	7.82E-06	0.26
DMRT1	1.05E-04	1.88	MET	2.83E-02	0.87	NDUFV1	1.43E-02	0.25
PEX5	3.60E-03	1.87	AFF2	2.20E-03	0.87	MRPL17	1.67E-05	0.25
DPPA2	2.10E-02	1.87	GRIK2	1.81E-03	0.87	RNMTL1	3.58E-05	0.25
ZNF718	2.98E-04	1.87	TEAD1	4.10E-02	0.86	MRPS6	7.56E-20	0.25
TTYH3	1.57E-03	1.86	BTRC	7.23E-03	0.86	BAP1	9.84E-03	0.25
UPP2	9.01E-03	1.85	NEDD9	2.88E-03	0.86	MRPS28	2.53E-95	0.25
VEZF1	3.87E-04	1.85	CACNA2D1	6.16E-05	0.86	SLC25A3	3.31E-03	0.25
TRIP12	5.41E-15	1.84	COLGALT2	9.77E-03	0.85	VPS29	4.08E-10	0.25
SMARCA4	2.08E-07	1.84	MAP2K5	3.56E-03	0.85	RHEB	1.63E-04	0.24
EIF4EBP2	4.76E-02	1.83	THSD7A	8.93E-05	0.85	NDUFB1	1.08E-04	0.24
ZNF791	3.86E-02	1.83	STAU2	2.96E-03	0.85	SEPSECS	1.08E-04	0.24
SCARA5	6.38E-06	1.83	NELL1	2.11E-10	0.85	MRPL2	2.38E-05	0.24
NCOR1	6.56E-14	1.83	UBE2H	1.58E-05	0.84	CARS2	6.65E-14	0.24
SLC44A2	9.03E-05	1.82	VTI1A	4.98E-02	0.84	MRPL14	2.26E-03	0.24
CD38	1.76E-02	1.81	MED13L	1.01E-03	0.84	DCAF7	1.99E-12	0.23
PXMP4	7.67E-04	1.81	LHFP	6.78E-03	0.84	MTG2	4.87E-04	0.23
FBXW7	2.54E-25	1.78	ARHGEF6	2.33E-02	0.84	COA5	1.52E-03	0.23
WAC	1.62E-02	1.78	SYNE2	5.98E-03	0.84	TRIT1	5.53E-14	0.22
TEX11	9.26E-11	1.77	FTO	3.06E-03	0.83	LRPPRC	4.95E-92	0.22
PCMTD2	8.96E-04	1.77	CSMD3	5.16E-08	0.83	MRPL45	3.16E-03	0.22
PIK3R1	1.65E-04	1.77	MAST2	4.92E-03	0.83	AIFM1	2.70E-08	0.22
DEAF1	7.50E-04	1.77	ANO3	8.06E-03	0.83	FAM136A	9.17E-07	0.22
GLYR1	1.01E-03	1.77	AGPS	1.74E-06	0.83	ATP5J	2.37E-13	0.22
LRRC4B	1.54E-02	1.76	MORF4L1	4.75E-02	0.83	C1QBP	4.21E-11	0.22
LIPC	4.48E-02	1.76	WDFY3	4.81E-02	0.83	MTX2	9.87E-06	0.22
TP53	5.34E-05	1.76	MAML2	1.97E-07	0.82	METTL1	3.09E-02	0.21
TRPV3	9.03E-05	1.74	KCND2	7.37E-05	0.82	MRPL51	4.11E-07	0.21
PWWP2B	1.30E-02	1.74	MARCH10	4.58E-02	0.82	RBFA	4.11E-07	0.21
TTYH1	8.89E-03	1.74	NRG1	4.39E-02	0.82	ATP5L	6.60E-03	0.21
MSN	1.65E-02	1.74	TEX2	3.31E-03	0.81	TSFM	6.60E-03	0.21
WSB2	1.16E-02	1.73	PIAS1	4.33E-02	0.81	MRPL30	2.74E-07	0.21
FANCD2	2.60E-02	1.73	CCDC141	7.08E-04	0.81	NARS2	1.55E-242	0.21
ADAMTS6	1.21E-03	1.73	ASCC1	7.41E-05	0.81	GFM1	4.41E-03	0.21
ZBED4	4.98E-02	1.72	LMBR1	4.67E-02	0.81	MRPS33	6.57E-05	0.21
NGEF	3.84E-04	1.72	INO80C	4.25E-02	0.81	SCO1	1.36E-05	0.21
ARRDC3	1.30E-12	1.72	LAMA3	1.15E-02	0.81	GATC	3.75E-07	0.20
CD200R1	7.48E-09	1.72	STK39	9.68E-03	0.80	TOP1	2.96E-03	0.20
TSPAN14	4.66E-03	1.72	MYO10	5.15E-12	0.80	MRPL50	1.86E-06	0.20
STARD3	2.26E-03	1.72	WWTR1	2.55E-05	0.80	LARS2	1.90E-30	0.20
RAPGEF2	4.74E-02	1.71	CDKAL1	7.30E-19	0.80	DAP3	2.38E-10	0.20
NOX5	9.71E-07	1.71	PPARG	4.87E-02	0.80	MRPL21	8.97E-03	0.19
FAM193A	2.55E-05	1.71	CBLB	3.95E-02	0.80	MTCH2	5.86E-05	0.19
RPL29	6.80E-03	1.70	PLEKHA5	6.87E-03	0.79	GMPS	4.23E-02	0.19
CMIP	1.82E-04	1.70	SLC44A1	4.81E-02	0.79	COX15	2.08E-07	0.19
RORC	9.42E-03	1.69	ZNF462	5.30E-04	0.79	MRPS24	2.82E-02	0.18
SPON2	5.22E-03	1.68	BORCS5	3.12E-02	0.79	NOA1	2.82E-02	0.18
TIAL1	1.10E-02	1.68	ANKRD30A	9.62E-04	0.78	TUFM	2.82E-02	0.18
PRRC2A	3.47E-03	1.68	ERBB4	7.82E-06	0.78	GATB	1.25E-17	0.18
CCPG1	1.59E-03	1.67	CTTNBP2	2.88E-04	0.78	MRPS35	2.15E-12	0.17
CSNK2A1	4.01E-04	1.67	SSBP2	3.39E-02	0.78	MRPL24	1.41E-12	0.17
RANBP3L	4.01E-04	1.67	PARN	4.04E-05	0.78	HTRA2	3.76E-07	0.17
LHFPL3	1.79E-04	1.67	METTL15	1.31E-02	0.78	ATP5F1	3.48E-05	0.17

Gene	FDR	MI	Gene	FDR	MI	Gene	FDR	MI
C3	1.82E-02	1.67	MAP3K13	3.86E-02	0.78	ISCA1	4.48E-08	0.17
ADAMTS10	7.90E-03	1.67	EYA3	3.72E-03	0.78	MIPEP	3.21E-14	0.16
PPP2R2A	3.76E-02	1.66	HS2ST1	7.06E-03	0.77	WARS2	1.80E-08	0.16
CNBD2	4.53E-03	1.66	SYT1	2.00E-36	0.77	TFB1M	2.35E-11	0.16
CP	2.49E-03	1.66	OSBPL3	1.83E-02	0.76	ATP5C1	7.30E-04	0.16
NRD1	3.86E-06	1.66	WDR20	3.42E-09	0.76	MRPS5	7.41E-07	0.16
PRMT7	1.59E-05	1.66	ECHDC2	4.98E-02	0.76	QRSL1	7.41E-07	0.16
PLEC	8.56E-06	1.65	RTKN2	3.45E-04	0.76	MRPS18B	9.87E-23	0.15
ZDHHC15	4.87E-02	1.65	METAP1D	3.38E-03	0.76	HARS2	5.66E-06	0.15
CDKN2A	8.48E-11	1.65	HUWE1	1.41E-02	0.75	COX11	4.62E-07	0.15
NPFFR2	3.12E-02	1.64	COL24A1	1.61E-03	0.75	METTL17	4.76E-04	0.15
CDK13	1.63E-09	1.64	TNFRSF19	6.69E-04	0.75	GTPBP10	2.30E-08	0.15
CLIC5	4.32E-02	1.64	SESTD1	3.69E-02	0.75	MTERF3	1.83E-09	0.15
EDARADD	3.20E-04	1.63	DAAM1	4.86E-02	0.75	TEFM	4.24E-05	0.15
CFAP74	3.58E-05	1.63	ELF2	3.78E-03	0.75	MRPL52	5.53E-03	0.15
MROH8	6.38E-06	1.63	SNX3	6.88E-04	0.75	CLPB	1.42E-06	0.15
UHRF1	2.61E-04	1.62	EML1	4.44E-02	0.74	COX5B	3.70E-02	0.14
MAP4K4	5.32E-10	1.62	ARHGEF12	1.79E-03	0.74	HCCS	3.70E-02	0.14
TP73	3.38E-02	1.62	FERMT2	3.94E-03	0.74	MRPL39	1.08E-05	0.14
STRADA	5.52E-04	1.62	RSRC1	4.67E-02	0.74	UQCRC1	1.08E-05	0.14
UBE2Q1	4.73E-02	1.61	GTF2I	7.84E-04	0.74	GTPBP8	2.19E-09	0.14
PARVB	1.38E-09	1.61	NTN4	1.02E-02	0.74	MRPS27	3.16E-86	0.14
SETD5	1.49E-04	1.61	AKT3	1.06E-16	0.74	DDX28	1.40E-09	0.14
UFL1	1.86E-03	1.61	PPP4R1	3.16E-02	0.74	MRPS23	3.57E-07	0.14
CUL5	1.01E-03	1.61	HERC1	1.64E-04	0.73	OPA1	5.63E-10	0.14
ZMYM2	3.90E-04	1.61	RCOR1	2.79E-03	0.73	MRPS15	1.07E-08	0.13
SPEN	2.18E-19	1.60	PROM1	1.00E-02	0.73	YME1L1	8.28E-05	0.13
WDR37	8.90E-03	1.60	TFDP2	1.41E-03	0.72	TARS2	1.37E-07	0.13
ZCCHC14	3.06E-03	1.60	NCOA2	5.38E-09	0.72	EARS2	3.08E-16	0.13
ARIH2	4.49E-05	1.59	ADAMTS5	6.76E-04	0.72	MRPL37	5.81E-04	0.13
ARID2	1.70E-06	1.59	TLK2	1.17E-03	0.72	PARS2	5.81E-04	0.13
CNBP	1.25E-02	1.59	TRIM71	4.82E-04	0.72	MRPS7	1.04E-06	0.13
PTEN	4.06E-05	1.59	TSC22D1	4.95E-02	0.72	TRUB2	3.33E-08	0.13
NSD1	2.07E-08	1.59	ITSN2	6.27E-03	0.72	MRPL44	3.83E-04	0.12
COLEC11	3.35E-02	1.59	GPBP1	1.06E-02	0.71	MRPL35	5.57E-16	0.12
MGA	8.49E-07	1.58	MAP2K6	4.92E-03	0.71	MRPS18C	1.28E-05	0.12
GLYATL2	3.02E-02	1.58	ATG13	4.87E-02	0.71	TFB2M	1.28E-05	0.12
KMT2E	1.21E-12	1.58	IL23R	4.74E-02	0.71	MRPS9	6.47E-76	0.12
ANKRD13C	4.00E-05	1.57	PYM1	7.46E-03	0.70	LAMTOR1	1.62E-15	0.12
TRPM8	7.56E-03	1.57	BANK1	4.51E-03	0.70	MRPL23	3.31E-14	0.12
RPP25	4.22E-02	1.57	TRPC4AP	2.35E-02	0.70	MRPL9	6.66E-03	0.12
C6orf99	5.92E-08	1.57	RAB10	5.00E-02	0.70	MRPL15	1.02E-07	0.11
SMARCC1	3.08E-11	1.56	ARID4B	1.15E-02	0.70	MRPL18	1.76E-29	0.11
HNRNPD	1.06E-03	1.56	TMEM47	4.59E-02	0.69	MRPS10	4.50E-12	0.11
PTGES3	8.53E-04	1.56	VMP1	6.79E-06	0.69	MRPL11	8.21E-09	0.11
ZEB2	5.06E-16	1.56	WDR64	2.35E-02	0.69	POLG2	8.39E-20	0.11
MAF	2.73E-02	1.55	LRRC7	1.71E-02	0.69	HSD17B10	3.62E-05	0.11
NRXN2	1.61E-04	1.55	MARCH6	5.31E-03	0.68	MALSU1	4.44E-07	0.11
RAD54L2	4.32E-05	1.55	HECTD1	2.76E-03	0.68	MRPL48	7.75E-32	0.10
PBRM1	1.61E-19	1.54	LCOR	5.95E-03	0.68	RARS2	2.75E-21	0.10
TULP2	8.66E-05	1.54	C12orf65	8.57E-04	0.68	WBSCR16	1.99E-17	0.10
PAK7	6.09E-04	1.54	SPTLC1	3.10E-02	0.68	IBA57	1.04E-03	0.10
FRAS1	7.33E-03	1.54	GAB2	1.13E-03	0.67	UQCRB	6.64E-04	0.10
SEPT10	2.51E-03	1.53	CHD1	1.41E-03	0.66	MRPL10	9.48E-06	0.10
TMEM209	1.97E-02	1.53	PUM1	3.02E-03	0.66	POLRMT	9.48E-06	0.10
TMEM163	5.02E-04	1.53	ALB	1.39E-02	0.66	MRPS22	4.20E-04	0.09
ABCC8	3.25E-02	1.52	SLC39A10	3.98E-02	0.66	PDAP1	4.44E-04	0.09
ARID1A	9.03E-05	1.52	ACVR2A	1.10E-02	0.66	PNPT1	5.17E-09	0.09
TMEM30A	2.48E-03	1.52	OGFOD1	3.32E-03	0.66	MRPS14	2.90E-02	0.08
IGSF11	3.28E-05	1.51	EXOC2	1.02E-04	0.66	ZBTB11	2.90E-02	0.08
MARCH8	9.69E-03	1.51	ZFPM2	1.78E-03	0.65	PITRM1	1.63E-04	0.08
PARP14	1.96E-02	1.51	NME6	4.23E-02	0.65	MRPS30	1.91E-09	0.08
TMEM116	9.24E-05	1.51	KDM2A	1.64E-13	0.65	MRPL54	1.64E-12	0.08
IL34	1.93E-02	1.51	INTS6	4.14E-02	0.64	NGRN	1.64E-12	0.08
HOXC11	6.20E-03	1.51	PHF20	3.15E-05	0.64	SARS2	6.83E-10	0.08

Gene	FDR	MI	Gene	FDR	MI	Gene	FDR	MI
SPTAN1	1.32E-02	1.50	RHOJ	9.50E-03	0.63	MRPL12	2.65E-15	0.08
TBC1D14	3.84E-07	1.50	EXOC4	6.19E-20	0.63	MRPL28	1.83E-02	0.08
KIAA1551	3.09E-02	1.50	ACACA	3.51E-29	0.63	MRPL36	1.92E-02	0.08
NKTR	4.90E-03	1.50	FGF1	4.91E-03	0.63	RNASEH1	3.54E-08	0.08
FHL2	1.76E-02	1.50	PAN3	4.09E-03	0.63	STARD7	3.54E-08	0.08
ACTN1	1.24E-02	1.49	LIN28B	2.84E-11	0.62	MRPL22	1.42E-05	0.07
CUL3	4.04E-04	1.49	STX18	3.20E-02	0.62	MRPL20	1.10E-11	0.07
MTA2	9.77E-03	1.49	WDR7	2.85E-05	0.62	MTPAP	5.13E-21	0.07
HERC4	7.45E-06	1.49	APC	1.56E-04	0.62	SUPV3L1	7.18E-03	0.07
TMEM62	8.65E-03	1.49	ZRANB1	1.94E-03	0.62	AARS2	5.42E-06	0.07
PNPLA1	2.80E-03	1.49	RFX4	2.37E-03	0.61	ATP5B	1.72E-09	0.07
LTBP4	4.90E-06	1.48	EEFSEC	1.41E-02	0.61	MRPL49	3.14E-06	0.07
DICER1	1.47E-02	1.48	RLF	1.09E-02	0.60	TFAP2D	2.75E-03	0.06
MIB1	3.69E-06	1.48	ZC3H12C	7.06E-03	0.60	MRPL38	4.11E-07	0.06
REST	1.04E-02	1.48	VPS45	4.80E-02	0.60	ATP5H	1.69E-03	0.06
KDM5A	7.12E-03	1.48	PAG1	4.52E-02	0.60	MRPS18A	1.04E-03	0.06
CARM1	1.87E-10	1.47	PTP4A2	1.83E-02	0.60	SSBP1	1.53E-07	0.06
CAND1	3.93E-02	1.47	COX18	6.66E-04	0.60	ERAL1	1.21E-12	0.05
SPOP	3.44E-05	1.46	FASTKD2	1.09E-02	0.60	MRPL40	2.62E-17	0.05
FBXL20	2.58E-04	1.46	PFAS	1.17E-03	0.59	C14orf166	4.09E-04	0.05
EIF2AK4	1.78E-03	1.46	YWHAZ	2.25E-02	0.59	MRPL16	4.09E-04	0.05
PDE3B	3.48E-02	1.45	TAL1	6.20E-04	0.59	ATP5D	2.54E-04	0.05
WDPCP	6.06E-07	1.45	EHMT1	2.73E-03	0.59	TRMT10C	2.54E-04	0.05
RAP1A	1.91E-02	1.45	COX17	1.51E-02	0.59	MRPL3	2.80E-24	0.05
HYAL1	1.38E-02	1.45	NFU1	3.27E-02	0.59	GADD45GIP1	1.07E-14	0.05
CBL	1.00E-02	1.45	PRPF39	3.27E-02	0.59	MRPL32	3.24E-05	0.04
SCN8A	9.03E-05	1.45	CCDC47	1.48E-02	0.58	MRPS2	3.24E-05	0.04
SHC1	1.52E-03	1.44	AEBP2	1.89E-09	0.58	MTERF4	3.24E-05	0.04
ZNF83	1.86E-03	1.44	C10orf2	3.25E-02	0.58	MRPS31	1.96E-05	0.04
UNC5B	3.61E-03	1.44	MTIF2	6.49E-03	0.57	MRPL47	3.24E-11	0.04
ABCA3	9.75E-03	1.44	SRD5A3	2.88E-03	0.56	RPUSD4	1.20E-05	0.04
ABLIM2	2.09E-02	1.44	TBX4	4.87E-02	0.56	PTCD3	4.93E-24	0.04
CNOT4	3.93E-04	1.44	MRPL1	1.32E-02	0.56	MRPS26	2.42E-06	0.04
GCNT1	3.60E-03	1.44	RHOA	2.57E-03	0.55	YARS2	1.13E-14	0.03
BAHCC1	3.20E-02	1.43	KIAA1033	1.81E-13	0.55	MRPL27	1.79E-07	0.03
STMN1	4.50E-02	1.43	KDM1A	1.48E-05	0.55	MRPL33	8.26E-10	0.03
PPTC7	1.95E-03	1.43	SEC63	3.25E-02	0.55	MTG1	4.81E-21	0.03
CTDSPL2	8.57E-03	1.43	XPNPEP3	1.56E-08	0.54	MRPL4	1.57E-10	0.02
REPS2	8.20E-08	1.43	MIOS	1.21E-02	0.54	ATP5O	1.86E-12	0.02
HMCN1	8.09E-04	1.43	ASCC3	6.44E-03	0.54	LAMTOR2	7.76E-14	0.02
TBL1XR1	1.37E-02	1.43	RTN4IP1	4.00E-02	0.53	ATP5J2	3.15E-15	0.02
ZSWIM3	1.90E-02	1.43	VPS13D	4.00E-02	0.53			
FN3K	4.02E-05	1.43	CHP1	2.70E-04	0.53			

8.2.9 *ΔMI p-RPS6$_{combined}$ - p-RPS6$_{rapamycin}$*

Gene	FDR	ΔMI
FKBP1A	2.83E-02	2.57
ARRDC3	2.83E-02	1.44
TAOK1	1.55E-02	1.34
FRYL	2.83E-02	1.26
EXOC4	2.48E-02	0.77
NARS2	4.30E-02	0.76
PDSS2	8.40E-08	0.68
KIAA1033	1.57E-04	0.59
SPTLC1	2.48E-02	0.52
LAMTOR4	4.92E-03	0.38

8.2.10 *p-RPS6$_{\Delta LAMTOR4}$ screen*

Gene	FDR	MI	Gene	FDR	MI	Gene	FDR	MI
TTC4	2.34E-12	27.71	TLK2	1.24E-03	0.71	UQCRC2	1.70E-04	0.30
TSC2	2.49E-20	9.87	SREBF2	1.29E-03	0.71	MRPS6	1.70E-12	0.30
TSC1	4.73E-62	9.13	ZSWIM6	2.75E-09	0.69	AASDHPPT	4.23E-05	0.30
PIKFYVE	4.20E-17	7.53	PHACTR4	4.19E-03	0.69	NDUFB9	4.23E-05	0.30
PSMD4	1.71E-03	5.65	SRPK1	4.01E-06	0.69	ACTR2	4.40E-04	0.29
PI4KA	8.42E-05	5.59	TRIM71	3.89E-06	0.68	MRPS2	2.93E-03	0.29
DHX29	7.26E-30	5.14	TFAP4	2.20E-02	0.68	PGM3	2.93E-03	0.29
NAA30	3.92E-04	5.12	MAPK14	1.98E-02	0.67	PTCD1	3.03E-07	0.29
SMARCB1	1.11E-09	4.92	LIAS	2.44E-03	0.67	XPNPEP3	5.93E-30	0.28
STK11	4.61E-20	4.63	PYM1	1.41E-03	0.66	LARS2	1.69E-38	0.28
TFDP1	1.25E-05	4.11	BAZ1B	1.05E-07	0.66	COA7	3.48E-07	0.28
UBE2L3	6.91E-29	4.07	RANBP9	1.07E-02	0.65	RMND1	8.62E-08	0.28
LCMT1	6.42E-03	3.74	TRAPPC13	2.05E-02	0.65	BLOC1S1	3.28E-06	0.28
TMEM251	4.50E-02	3.57	UBE2H	1.58E-22	0.65	TMEM41B	1.94E-03	0.28
CHMP5	1.77E-04	3.55	EXOC4	6.67E-20	0.65	NARS2	0.00E+00	0.28
CREBBP	7.16E-99	3.48	PHF20	3.26E-05	0.63	ATP5J	1.02E-10	0.27
USP8	2.30E-07	3.43	RAB10	1.57E-04	0.63	FBRS	4.87E-03	0.27
INPP4A	1.55E-37	3.36	KIAA1033	7.96E-06	0.63	SLC25A3	4.87E-03	0.27
NF2	5.26E-25	3.23	PIK3CA	1.51E-02	0.62	FAM136A	2.04E-04	0.27
UBE2M	2.10E-05	3.17	DNAAF2	3.32E-02	0.62	RNASEH1	2.04E-04	0.27
HGS	1.05E-07	3.16	PAN3	4.32E-04	0.62	NSUN4	3.72E-07	0.27
CREB1	3.26E-08	3.01	ATG13	2.33E-03	0.62	WARS2	1.70E-10	0.27
TIPRL	9.98E-10	2.98	ARNT	1.25E-03	0.62	METTL1	8.36E-04	0.27
CCNC	2.83E-05	2.94	CEP350	6.69E-03	0.62	TMEM261	8.36E-04	0.27
UBR5	6.75E-19	2.92	EMC2	3.20E-10	0.61	FARS2	1.17E-30	0.26
RNF7	5.49E-03	2.81	LIG3	1.26E-02	0.61	NOA1	1.92E-02	0.26
DPH5	3.46E-08	2.77	YBEY	1.53E-08	0.61	NAF1	5.41E-04	0.26
CSNK2A1	1.54E-17	2.77	LARP4	5.34E-03	0.61	MRPS16	3.59E-15	0.26
SEPHS2	8.05E-03	2.75	CCDC58	2.19E-02	0.60	RHOA	4.26E-25	0.25
PPP1CA	4.13E-03	2.75	MTIF2	1.28E-02	0.60	TFB1M	9.46E-15	0.25
INPPL1	1.92E-04	2.74	RREB1	6.62E-04	0.59	SLC25A26	7.28E-19	0.25
KCTD5	1.00E-04	2.74	RRAGD	5.21E-04	0.59	PITRM1	3.31E-03	0.25
USP14	9.09E-159	2.70	NSUN3	1.96E-03	0.59	AP3D1	1.95E-11	0.25
TIAL1	1.56E-07	2.68	SRD5A3	3.57E-07	0.58	MRPL19	2.09E-12	0.25
MTF2	3.15E-24	2.67	PFAS	4.33E-03	0.58	MAPKAP1	3.13E-69	0.25
NFYC	7.33E-07	2.67	MAP3K4	2.04E-02	0.58	MTCH2	1.62E-06	0.24
CAD	1.39E-05	2.64	SNTB2	4.09E-11	0.58	COX16	2.14E-03	0.24
CSNK2A2	4.39E-03	2.64	GNA13	1.60E-03	0.58	STARD7	3.97E-06	0.24
WAC	1.22E-07	2.62	C16orf62	1.00E-03	0.58	TKT	5.22E-03	0.24
PQLC2	1.00E-03	2.52	NDUFAF1	3.23E-02	0.58	COQ5	3.71E-14	0.23
OTUD5	4.84E-06	2.45	TADA2A	2.88E-05	0.57	ZC3H13	3.21E-22	0.23
GATAD1	4.23E-05	2.44	WNK1	2.15E-04	0.57	NDUFA3	3.23E-02	0.23
GPATCH8	1.43E-18	2.44	BLOC1S6	3.25E-02	0.57	MTERF4	9.55E-05	0.23
IWS1	6.00E-05	2.41	MBIP	1.63E-02	0.57	PARS2	2.14E-03	0.22
TRIP12	8.14E-33	2.41	RBM12B	1.62E-03	0.57	CYCS	5.92E-05	0.22
RPS25	6.52E-03	2.39	CCDC51	2.05E-02	0.56	VPS35	1.35E-03	0.22
DNAJC13	4.07E-14	2.37	GAB2	3.10E-05	0.56	CLPP	1.06E-08	0.21
AIP	4.75E-02	2.34	PMVK	1.91E-02	0.55	MRPL2	1.10E-10	0.21
PIK3R1	3.48E-25	2.34	CHP1	2.11E-04	0.55	RPUSD3	3.33E-03	0.21
IRF7	4.63E-03	2.32	BPTF	2.05E-05	0.55	GATC	6.48E-10	0.21
ITPK1	3.39E-07	2.32	NUBPL	5.21E-24	0.55	UQCRFS1	3.22E-02	0.21
PDGFRA	2.07E-02	2.31	RAB18	4.75E-02	0.55	VPS33A	1.19E-17	0.20
TFG	3.91E-07	2.30	MICU1	1.12E-19	0.55	COQ3	6.95E-34	0.20
PPP2R4	5.81E-16	2.26	SMAD4	1.44E-04	0.55	EIF3J	3.36E-04	0.20
IPMK	1.04E-02	2.25	AEBP2	2.12E-15	0.55	GATB	1.44E-12	0.19
TMEM30A	1.54E-07	2.20	ACACA	1.84E-43	0.55	ISCA1	3.39E-07	0.19
PPP4R2	2.98E-10	2.19	NDUFAF6	2.39E-06	0.54	ATIC	8.96E-13	0.19
NPC1	3.64E-03	2.17	AP3B1	4.96E-15	0.54	MTRF1L	2.10E-05	0.19
UBE2A	2.76E-02	2.17	KDM2A	1.50E-23	0.54	ICMT	8.74E-12	0.19
CACYBP	1.72E-04	2.15	ZFR	5.30E-03	0.54	COX7B	2.13E-08	0.19

Gene	FDR	MI	Gene	FDR	MI	Gene	FDR	MI
MOSPD2	2.10E-03	2.15	CDC42	4.84E-03	0.53	MRPS5	3.08E-07	0.18
PCGF6	3.28E-07	2.10	CHCHD1	2.66E-02	0.53	MRPL13	1.61E-17	0.18
CNOT2	6.84E-04	2.09	GPBP1	5.74E-10	0.53	MAX	4.89E-06	0.18
NAA35	2.82E-02	2.07	LDLR	2.16E-04	0.52	GTPBP8	6.52E-14	0.18
PIK3R2	8.58E-08	2.07	NDUFB6	3.84E-02	0.52	ATP5L	1.22E-03	0.18
DEAF1	3.40E-05	2.05	COMMD10	3.41E-05	0.52	ERAL1	1.04E-11	0.18
PSME4	4.55E-08	2.04	KAT7	2.16E-02	0.52	MRPL16	8.02E-03	0.17
CTDNEP1	3.00E-02	2.01	PPP5C	2.54E-02	0.51	C14orf2	3.00E-02	0.17
MYO9B	3.60E-04	1.98	UBE3D	1.46E-06	0.51	WTAP	3.00E-02	0.17
DOT1L	2.55E-08	1.98	MAP2K6	4.26E-10	0.51	MIPEP	4.99E-22	0.17
VAC14	2.84E-03	1.98	INPP5A	6.53E-18	0.51	LRPPRC	1.31E-201	0.17
MTMR9	2.67E-03	1.97	SEL1L	1.98E-04	0.51	TARS2	4.02E-09	0.17
PRKAA1	3.62E-07	1.97	VPS41	4.77E-17	0.51	VPS16	4.02E-09	0.17
CARNMT1	7.97E-03	1.96	FNIP2	4.06E-08	0.51	PGLS	6.83E-06	0.17
FBXW7	7.68E-20	1.93	TIMMDC1	5.39E-04	0.50	RICTOR	7.00E-30	0.16
SEPSECS	1.14E-02	1.91	TAF3	2.00E-05	0.50	OPA1	1.46E-09	0.16
FAM193A	6.66E-08	1.89	NDUFA9	8.02E-03	0.50	MRPS23	6.02E-08	0.16
ZEB2	6.80E-43	1.89	MTO1	3.25E-03	0.50	RRAGA	2.57E-05	0.16
EIF2AK1	4.43E-02	1.89	ECSIT	1.33E-02	0.49	RNMTL1	1.94E-10	0.16
DBF4	3.59E-03	1.88	NDUFAF5	4.32E-04	0.49	CYB5B	1.89E-18	0.15
RPRD2	3.88E-14	1.87	NDUFB11	7.17E-03	0.49	DAP3	1.18E-16	0.15
URI1	1.39E-14	1.87	CSNK1A1	4.45E-04	0.49	MRPL24	1.33E-15	0.15
PLAA	5.21E-04	1.87	RTN4IP1	3.94E-03	0.49	MRPS27	3.85E-120	0.15
CNOT4	3.44E-12	1.87	COX17	2.90E-04	0.49	MRPL30	1.46E-14	0.15
GIGYF2	3.95E-14	1.86	COX19	2.54E-02	0.49	RPS6KB1	7.13E-10	0.15
CUL5	9.84E-05	1.86	COQ2	3.38E-04	0.49	MRPS26	8.41E-08	0.15
DPH6	4.12E-24	1.86	FDX1	5.41E-03	0.49	MRPL42	4.26E-10	0.15
CUL3	5.15E-07	1.85	NDUFA11	2.23E-02	0.49	DYRK1A	1.87E-173	0.15
SCAF8	2.49E-07	1.84	VMP1	7.46E-26	0.49	PARL	3.41E-13	0.15
DICER1	7.81E-07	1.84	CHORDC1	3.04E-02	0.48	PPA2	2.69E-16	0.15
MGA	1.45E-17	1.83	NETO2	7.66E-03	0.48	MRPL51	1.02E-23	0.15
CAND1	1.37E-04	1.82	COX18	3.62E-09	0.48	YARS2	1.30E-12	0.14
DHX35	6.46E-03	1.81	MTX1	1.97E-02	0.48	MRPS9	9.23E-115	0.14
UBA6	7.38E-11	1.80	EMC1	1.23E-02	0.48	TSFM	3.48E-05	0.14
MBD3	2.34E-08	1.80	PDZD8	1.27E-19	0.47	SPCS2	4.19E-03	0.14
MTA2	1.26E-04	1.78	SNAP23	3.03E-05	0.47	ZBTB11	3.87E-04	0.14
CDK10	1.33E-02	1.76	SFSWAP	3.66E-02	0.47	TOP1	2.91E-12	0.14
SLC17A5	3.26E-03	1.76	DARS2	5.78E-05	0.47	DLST	4.22E-02	0.14
PHF12	1.47E-05	1.74	MERTK	1.32E-12	0.47	PGGT1B	1.25E-05	0.14
RNF40	1.11E-02	1.74	NFU1	1.26E-05	0.46	PTDSS1	1.02E-12	0.14
COX7A2L	4.53E-02	1.73	MLST8	3.78E-04	0.46	MTG2	2.05E-09	0.13
ARID2	1.35E-09	1.71	INTS6	5.71E-07	0.46	KIAA0391	6.40E-46	0.13
AGK	3.99E-13	1.71	GFM2	1.28E-02	0.46	MRPS25	6.77E-11	0.13
DGUOK	5.18E-03	1.70	UBE2G2	6.97E-04	0.46	TEFM	6.77E-11	0.13
GNPTAB	6.68E-03	1.70	NDUFS3	9.50E-03	0.46	MRPS18B	8.00E-36	0.13
PRRC2A	1.26E-03	1.69	MTHFD1	3.69E-05	0.46	MRPS10	7.86E-13	0.13
FOXK1	5.87E-03	1.69	LIN28B	9.05E-28	0.46	PET117	7.33E-17	0.13
AGO2	2.23E-04	1.69	NDUFS1	5.13E-03	0.46	ATP5H	9.05E-04	0.13
NSD1	9.06E-12	1.67	UQCC1	2.74E-08	0.46	QRSL1	2.60E-13	0.12
PBRM1	1.66E-30	1.66	NDUFB2	5.18E-04	0.45	MTERF3	1.45E-17	0.12
BIRC6	2.34E-20	1.64	POLDIP2	3.28E-03	0.45	LAMTOR5	1.52E-20	0.12
ARIH2	2.50E-08	1.63	C12orf65	1.17E-14	0.45	MRPS33	8.30E-11	0.12
FBXW11	8.02E-03	1.63	PIH1D1	3.81E-02	0.45	RFT1	1.51E-02	0.12
UVRAG	1.63E-21	1.63	COMMD7	5.83E-07	0.45	MRPS22	9.17E-04	0.12
C11orf30	5.06E-17	1.62	UQCC2	1.06E-06	0.44	LONP1	8.51E-07	0.12
FOXK2	2.15E-05	1.62	NDUFS8	3.30E-03	0.44	MRPS35	8.44E-24	0.12
VPS45	4.93E-02	1.61	HIRA	2.82E-02	0.44	ATP5J2	9.34E-12	0.12
STRADA	3.61E-03	1.61	YTHDF2	3.04E-10	0.44	PGD	9.00E-03	0.11
KMT2E	9.07E-14	1.60	MRRF	4.88E-24	0.44	MRPL17	3.26E-15	0.11
EPC2	1.66E-04	1.60	WDR4	1.71E-06	0.44	MRPS15	3.18E-12	0.11

Gene	FDR	MI	Gene	FDR	MI	Gene	FDR	MI
DEPDC5	3.71E-04	1.59	ENO1	3.84E-03	0.43	LAMTOR3	1.85E-12	0.11
QRICH1	4.19E-03	1.59	CCDC6	4.94E-07	0.43	ATP5F1	1.88E-11	0.11
MARK3	2.20E-04	1.58	MTX2	4.99E-06	0.43	AARS2	3.46E-08	0.11
ZCCHC14	1.12E-03	1.57	PDSS2	1.42E-107	0.43	EARS2	4.65E-27	0.11
ZFAT	8.79E-12	1.56	EIF3L	2.83E-03	0.43	GFM1	3.56E-12	0.10
PITPNB	1.58E-02	1.55	MRPL1	2.25E-06	0.43	RARS2	5.27E-25	0.10
CDK13	9.90E-07	1.55	NDUFA10	9.48E-03	0.43	ATP5C1	5.83E-07	0.10
ARID4A	1.24E-02	1.55	CFDP1	8.73E-08	0.42	MRPS31	5.83E-07	0.10
ZNF507	1.91E-02	1.54	PDSS1	9.01E-06	0.42	DCAF7	4.17E-18	0.10
RFX7	2.50E-02	1.54	SCAP	1.68E-05	0.42	MRPS14	1.83E-03	0.10
MAP4K4	1.00E-06	1.53	PTAR1	2.35E-03	0.42	VHL	3.43E-07	0.10
PPP6R3	1.10E-04	1.52	ACAD9	1.08E-03	0.42	C1QBP	1.46E-22	0.10
CCDC50	1.40E-02	1.51	NDUFA1	1.08E-03	0.42	HARS2	1.26E-13	0.10
BZW2	4.93E-02	1.51	FOXRED1	3.17E-02	0.42	DDX28	1.43E-15	0.09
REST	9.22E-03	1.50	ARPC2	4.66E-06	0.42	ATP5D	7.15E-10	0.09
TBCK	3.06E-18	1.49	PDE12	1.26E-03	0.41	ATP5O	4.16E-10	0.09
KEAP1	1.26E-02	1.49	PPAT	5.78E-09	0.41	MRPL11	7.70E-15	0.09
C16orf72	4.54E-02	1.48	SCO1	1.24E-04	0.41	SUPV3L1	3.63E-06	0.09
CMIP	2.08E-02	1.48	BLOC1S2	1.89E-04	0.41	PTCD3	1.60E-23	0.08
CTDSPL2	1.16E-03	1.48	DNAJC2	6.79E-07	0.41	GTPBP10	4.07E-14	0.08
WHSC1	5.52E-04	1.47	NDUFV2	1.70E-19	0.40	VPS29	1.96E-34	0.08
GATAD2A	8.62E-04	1.47	GLRX5	4.28E-02	0.40	MALSU1	4.11E-12	0.08
CDKN2A	2.27E-06	1.47	OGT	1.95E-06	0.40	PDCD2	3.17E-02	0.08
NCOR1	1.64E-04	1.45	CRKL	1.30E-05	0.40	MRPL37	2.12E-07	0.08
CWC27	3.22E-02	1.44	COX10	1.14E-19	0.40	GRSF1	1.45E-18	0.08
MIB1	9.01E-06	1.44	NDUFB10	1.00E-03	0.40	MRPL21	6.67E-08	0.07
SLC25A33	2.38E-02	1.44	MRPS34	3.01E-03	0.40	MRPL36	1.84E-02	0.07
SNRK	1.47E-02	1.44	NMT1	1.06E-05	0.40	TOMM40	1.84E-02	0.07
CAPRIN1	8.89E-03	1.43	COX11	3.34E-04	0.39	MRPL22	4.08E-11	0.07
SPTAN1	2.82E-02	1.41	KIAA0196	7.14E-04	0.39	MRPL54	4.11E-17	0.07
SLC16A10	1.92E-02	1.41	NCKAP1	7.14E-04	0.39	SARS2	6.80E-15	0.07
ANKRD17	1.10E-06	1.41	DDX5	2.33E-04	0.39	IMMT	1.08E-58	0.07
PPP1R21	1.14E-02	1.40	FAM60A	1.20E-07	0.39	OXA1L	1.05E-02	0.07
ARID4B	8.82E-03	1.40	SEC62	1.35E-02	0.38	RCL1	1.05E-02	0.07
ARHGAP12	5.53E-03	1.40	MBTPS1	1.24E-08	0.38	MRPL15	3.80E-15	0.07
FAM20B	2.87E-02	1.39	HSPA14	1.07E-03	0.38	ATP5B	1.30E-12	0.06
HNRNPR	4.73E-03	1.39	COQ6	9.58E-03	0.38	MRPL38	7.22E-13	0.06
USP15	9.50E-04	1.38	RPTOR	2.51E-17	0.38	GADD45GIP1	1.11E-24	0.06
HELZ	3.93E-02	1.38	SP2	1.99E-03	0.37	PTPMT1	1.16E-06	0.06
PIGL	6.20E-03	1.36	YWHAE	6.16E-30	0.37	MRPL4	1.94E-10	0.06
NPRL3	3.15E-02	1.34	MRPS21	1.57E-04	0.37	MRPL3	4.73E-62	0.06
ITM2A	8.26E-03	1.31	NDUFAF7	3.51E-05	0.37	MRPS18C	1.08E-10	0.06
DMXL1	1.52E-03	1.30	VARS2	2.18E-05	0.37	SSBP1	1.06E-14	0.06
RABGAP1	6.50E-06	1.29	PCBP2	1.60E-03	0.36	ADSL	1.94E-03	0.06
NCOA6	3.40E-02	1.29	FZR1	9.82E-04	0.36	MRPL20	5.13E-23	0.06
ITPR2	1.22E-08	1.29	ATPAF2	1.26E-04	0.36	MRPL10	1.85E-11	0.06
FBXL5	1.35E-02	1.27	COX15	1.26E-04	0.36	TFB2M	9.74E-16	0.06
SNX3	5.63E-03	1.26	VPS18	1.26E-04	0.36	MTG1	1.49E-24	0.05
CARM1	4.22E-02	1.23	AGPAT5	5.21E-05	0.36	SLC30A9	7.87E-26	0.05
UNK	2.04E-02	1.23	ATP5E	6.83E-04	0.36	MRPL23	1.28E-30	0.05
MGME1	4.48E-02	1.22	HTRA2	6.83E-04	0.36	REXO2	1.88E-08	0.05
PTPRG	2.13E-07	1.19	YME1L1	3.31E-03	0.36	MRPL40	3.89E-31	0.05
RFWD2	1.81E-02	1.19	MRPS28	5.52E-90	0.36	PDAP1	3.43E-04	0.05
MPPED2	1.75E-05	1.19	YEATS4	8.74E-03	0.35	TRMT10C	1.03E-08	0.05
TAOK1	3.08E-02	1.19	COQ4	7.89E-07	0.35	MRPS30	3.99E-23	0.05
ZFHX3	1.42E-05	1.18	TAF1B	1.99E-04	0.35	MRPL18	1.27E-91	0.05
TNS3	3.24E-02	1.18	ACTR3	2.24E-19	0.35	MRPL45	8.92E-10	0.05
CTNNA1	3.46E-02	1.17	TAF6	1.63E-02	0.34	TTI1	4.74E-15	0.04
ARID5B	1.32E-05	1.14	NDUFS7	2.83E-05	0.34	MRPL44	5.92E-05	0.04
MAP4K3	1.79E-02	1.10	NDUFB4	4.66E-05	0.34	MRPL50	1.01E-17	0.04
SOX5	4.75E-02	1.09	COX20	9.88E-04	0.34	TPI1	1.02E-05	0.04
TRPM3	4.75E-02	1.09	HAX1	4.75E-02	0.34	MRPL49	7.15E-12	0.04
MYO10	1.40E-02	0.90	SURF1	4.19E-03	0.34	MRPL47	2.95E-18	0.04
EIF4G3	3.03E-02	0.88	ATG14	6.08E-04	0.34	MRPL39	1.88E-13	0.04
CDKAL1	1.54E-08	0.87	TIMM50	1.27E-02	0.33	PGAM1	1.01E-13	0.03

Gene	FDR	MI	Gene	FDR	MI	Gene	FDR	MI
EYA3	8.32E-03	0.86	RBFA	8.52E-07	0.33	PNPT1	6.26E-29	0.03
MBNL1	3.14E-02	0.86	CARS2	1.02E-09	0.33	HSD17B10	5.11E-07	0.03
AUTS2	6.55E-08	0.82	VPS39	4.71E-03	0.33	RHEB	5.11E-07	0.03
SAMHD1	2.51E-02	0.81	DNAJC3	4.87E-25	0.33	TUFM	5.11E-07	0.03
PLEKHA5	2.65E-02	0.81	ICT1	2.69E-05	0.33	METTL17	2.89E-07	0.03
WDR20	9.57E-06	0.81	TRIT1	1.11E-11	0.32	MRPL9	2.89E-07	0.03
EBF3	2.46E-03	0.81	MBTPS2	4.21E-46	0.32	MRPS24	1.58E-07	0.03
NLK	3.81E-08	0.80	MRPL14	8.29E-04	0.32	MRPL48	3.16E-67	0.03
USP48	3.82E-02	0.80	SHQ1	3.20E-04	0.32	MRPL52	4.80E-08	0.03
UBE2G1	2.01E-02	0.79	WRB	2.01E-05	0.32	MRPL32	2.05E-09	0.03
FOXP1	4.24E-14	0.79	AIFM1	2.87E-08	0.32	RPUSD4	2.05E-09	0.03
FBXL17	7.98E-07	0.78	RQCD1	2.70E-09	0.32	TFAM	5.90E-10	0.02
HUWE1	4.75E-02	0.78	OGDH	8.44E-06	0.32	TRUB2	3.22E-21	0.02
ZFX	8.24E-03	0.78	SLIRP	2.14E-04	0.32	MRPL33	1.69E-10	0.02
ERC1	7.32E-10	0.77	POLG2	7.30E-12	0.31	MRPS18A	8.99E-11	0.02
PARN	7.59E-05	0.75	COA5	1.47E-03	0.31	MRPL35	2.17E-46	0.02
EXOC2	3.30E-03	0.74	HSD17B12	1.91E-11	0.31	MRPL12	3.85E-30	0.02
FASTKD1	1.35E-02	0.74	VPS13D	1.49E-07	0.31	MTPAP	1.23E-51	0.02
ATRX	1.33E-02	0.73	NDUFA13	6.11E-06	0.31	LAMTOR2	1.45E-17	0.01
UBE2E3	4.27E-02	0.72	FLCN	2.38E-05	0.31	POLRMT	1.45E-17	0.01
ZMYND8	4.51E-06	0.72	ZNF407	1.26E-16	0.30	WBSCR16	3.12E-38	0.01
LUC7L2	6.73E-05	0.72	ISCA2	1.04E-02	0.30	MRPL27	6.75E-19	0.01
TFE3	4.49E-02	0.72	NDUFB8	6.67E-08	0.30	MRPS7	3.61E-19	0.01
TRPC4AP	2.76E-02	0.72	AP2M1	4.01E-02	0.30	NGRN	1.35E-26	0.01
AKT3	5.23E-22	0.72	TSEN15	1.70E-04	0.30			

8.2.11 *TNFR1 screen*

Gene	FDR	MI	Gene	FDR	MI	Gene	FDR	MI
GPX4	5.03E-10	24.86	BRIP1	9.07E-03	1.41	LMBR1	4.91E-03	0.78
SEPHS2	2.40E-19	19.21	CDA	4.55E-02	1.41	GALNTL6	2.11E-08	0.77
CNOT3	2.92E-03	19.21	TLE6	2.11E-02	1.41	ADGRA3	8.91E-03	0.77
CD80	2.42E-02	14.69	PRMT7	1.30E-02	1.41	PROM1	2.53E-02	0.76
NAA20	4.04E-02	13.56	ANKRD13C	3.28E-03	1.40	RARB	9.68E-03	0.76
CNOT2	4.58E-57	11.03	KEAP1	1.52E-02	1.40	SATB2	1.92E-02	0.76
CHMP5	9.30E-12	10.33	GIPR	3.34E-02	1.40	NR2F2	2.99E-02	0.76
SNF8	1.27E-02	9.60	MYO1E	1.32E-02	1.37	TRIP12	6.84E-03	0.76
EEFSEC	2.88E-58	8.76	ARID2	1.32E-03	1.37	C2CD5	4.80E-02	0.75
HNRNPM	1.10E-04	8.47	ZFAT	1.61E-05	1.37	C12orf40	4.80E-02	0.75
TFDP1	3.19E-11	7.40	TAOK1	1.50E-08	1.36	MAPRE2	4.81E-04	0.75
TYMS	8.71E-04	7.34	KIF3B	3.88E-08	1.36	MAP2K6	1.44E-02	0.74
SEPSECS	3.60E-25	7.25	CLPX	1.31E-02	1.36	SMAD1	4.80E-02	0.73
PSTK	9.90E-08	6.21	ZEB2	5.86E-08	1.35	BRWD3	2.54E-02	0.73
PSMD4	6.41E-03	6.21	ZNF143	1.05E-04	1.35	GSK3B	1.89E-02	0.72
ZNF141	2.49E-02	5.37	MYH7B	7.51E-04	1.35	CCDC6	4.80E-02	0.72
UBE2L3	5.46E-43	5.34	FN3K	1.25E-02	1.35	PDSS2	5.63E-13	0.72
TIMM22	3.86E-02	5.08	PARP16	4.92E-02	1.34	ETV1	6.61E-03	0.72
HSD17B12	1.71E-44	4.99	PPCDC	3.77E-02	1.34	ZADH2	3.66E-02	0.72
UBE2N	1.06E-02	4.36	KLRB1	4.05E-02	1.33	KDM2A	1.82E-06	0.71
TIPRL	2.05E-07	3.98	KIF9	8.26E-04	1.33	MYCBP2	2.52E-03	0.71
PPP4R2	5.46E-19	3.92	DAG1	4.92E-02	1.33	TSHZ1	9.94E-04	0.70
GIGYF2	1.38E-79	3.74	DAPK2	6.18E-03	1.32	RREB1	3.77E-02	0.70
PTPN23	3.77E-03	3.70	TEN1	6.31E-07	1.32	ADAMTS3	8.21E-06	0.70
UBAP1	1.40E-33	3.61	SPOP	1.44E-02	1.31	USP6NL	1.98E-02	0.69
XPO5	2.78E-05	3.50	WDR20	6.10E-11	1.31	NRN1	6.61E-03	0.69
NF2	5.63E-13	3.49	KMT2E	8.76E-06	1.31	BRINP3	2.16E-04	0.69
PPP2R4	4.32E-37	3.44	MGA	2.01E-02	1.31	TAF3	4.04E-02	0.68
NAA30	6.02E-06	3.44	HERC4	4.56E-03	1.30	TTLL7	6.18E-03	0.68
DDX6	7.68E-10	3.36	SPEN	1.23E-02	1.30	C3orf58	1.48E-02	0.68
UBE2M	3.74E-07	3.35	MAP4K3	2.56E-15	1.29	CNOT4	2.43E-03	0.67
B4GALNT2	2.92E-03	3.31	RNF157	9.20E-05	1.29	EMC2	4.18E-03	0.67
FANCM	1.45E-02	3.20	CUX1	3.66E-02	1.29	YBEY	9.40E-06	0.66
ZNF569	9.03E-07	3.14	ANKRD6	4.59E-02	1.29	PCDH15	8.31E-04	0.65
NPRL2	4.61E-04	3.11	C6orf106	5.48E-03	1.29	PTPRN2	1.01E-02	0.65
SMARCB1	1.07E-03	3.09	TET1	6.31E-07	1.29	MBIP	2.23E-02	0.65
NASP	2.80E-05	3.05	MBNL1	4.39E-06	1.29	ACADSB	2.16E-04	0.65
VPS45	7.20E-15	3.03	SPATS2	4.80E-02	1.29	RAPGEF6	5.68E-03	0.63
C9orf84	1.65E-02	2.99	GTF2I	2.17E-02	1.28	KIAA0391	3.27E-02	0.63
CHMP3	2.49E-07	2.98	TCF7L1	3.77E-02	1.28	MRRF	7.47E-04	0.63
KNG1	4.57E-02	2.98	ADAM10	4.30E-02	1.28	ADRA1A	1.42E-02	0.63
TSPAN16	5.56E-10	2.98	UBE2R2	1.34E-02	1.27	DPH5	3.25E-02	0.62
TRPC7	3.46E-06	2.96	NF1	7.90E-07	1.27	SLC10A7	2.17E-02	0.61
MAP1LC3A	2.56E-02	2.95	STAT3	1.82E-03	1.27	IGF1R	1.57E-06	0.61
ZNF793	1.43E-10	2.82	ARMC9	8.74E-03	1.27	LEMD3	3.26E-02	0.61
PARVG	4.30E-02	2.74	DDB2	4.76E-02	1.26	ALB	8.26E-04	0.60
ZNF578	5.30E-04	2.72	CLIP1	8.28E-03	1.26	MRPS18B	4.01E-02	0.60
UBASH3B	3.55E-10	2.62	KREMEN1	2.02E-04	1.26	MSR1	9.97E-03	0.60
EWSR1	3.85E-03	2.58	MEGF9	9.68E-08	1.26	NUBPL	1.13E-16	0.60
POT1	1.08E-02	2.52	SPIDR	4.84E-02	1.26	RHOJ	7.10E-03	0.59
CUL3	2.04E-36	2.48	PIK3R3	3.82E-03	1.26	QRICH1	1.69E-02	0.59
HGS	1.50E-07	2.45	CHIC2	3.76E-03	1.25	PTPN18	3.72E-02	0.59
ST6GALNAC1	1.08E-02	2.45	TMEM33	4.62E-02	1.25	SMAD4	2.62E-03	0.57
UBA3	4.51E-02	2.45	CLTCL1	1.92E-02	1.25	CARNMT1	4.72E-02	0.57
OIT3	8.54E-05	2.44	IFT81	3.38E-02	1.25	EXT1	3.81E-09	0.57
WAC	2.47E-04	2.43	IGDCC3	5.99E-03	1.25	ZBTB10	3.95E-02	0.56
RPS25	1.79E-06	2.39	TRERF1	3.87E-03	1.24	TRIT1	4.89E-04	0.56
DEPDC5	2.64E-11	2.34	CTNNA1	2.70E-04	1.23	COX10	1.71E-06	0.56
NAA38	2.17E-02	2.30	UNK	1.62E-02	1.23	RAVER2	2.34E-02	0.55
FANCB	6.77E-03	2.30	KIF1B	4.18E-02	1.23	DARS2	1.01E-02	0.55

Gene	FDR	MI	Gene	FDR	MI	Gene	FDR	MI
USP8	3.81E-04	2.26	PITPNC1	7.49E-04	1.23	NSUN3	9.94E-04	0.55
MED27	1.85E-02	2.26	RASSF3	2.97E-02	1.23	HMBS	6.27E-03	0.55
TMED10	1.86E-07	2.23	DIP2B	3.03E-04	1.23	MTX2	1.13E-02	0.54
EIF4E2	4.38E-03	2.23	RALGPS1	6.49E-03	1.22	PAG1	4.05E-02	0.54
FANCD2	1.38E-02	2.22	CDK6	3.79E-02	1.22	FASTKD2	1.64E-04	0.54
SLC44A2	1.03E-04	2.22	DCAKD	4.43E-02	1.22	SDC1	1.62E-02	0.54
DBF4	1.63E-04	2.20	CSNK1G1	1.36E-04	1.22	NARS2	4.24E-57	0.53
CDK2	4.80E-02	2.17	HP1BP3	3.36E-02	1.22	WBSCR16	4.67E-02	0.52
TTYH1	1.72E-02	2.15	ADCY9	6.61E-03	1.21	UBR5	3.52E-04	0.52
DLEC1	8.57E-09	2.15	CENPT	4.05E-02	1.21	TAL1	1.45E-05	0.52
VPS53	4.04E-02	2.14	LRRC8D	1.62E-02	1.21	NHLRC2	5.30E-03	0.51
EPC2	6.71E-13	2.13	FAM78A	1.90E-02	1.20	VMA21	4.86E-02	0.51
NFYC	5.67E-04	2.11	VPS37B	1.15E-02	1.20	TM9SF2	3.05E-02	0.51
USP14	2.35E-86	2.07	ANKS1A	2.94E-02	1.19	MRPL48	3.37E-03	0.50
FANCA	1.72E-03	2.05	UBE2H	6.28E-04	1.19	LARS2	5.23E-08	0.50
NAA35	1.00E-03	2.04	MSI2	5.03E-03	1.18	MRPL24	1.48E-02	0.50
DOCK6	4.25E-02	2.04	CDC42BPB	6.18E-03	1.18	POLG2	2.92E-04	0.50
NSD1	6.29E-17	2.02	TUBA1C	4.94E-02	1.18	MRPL18	2.06E-03	0.49
CD48	1.92E-02	2.02	FRYL	4.21E-02	1.18	TMEM126B	3.88E-04	0.49
CUL1	7.32E-03	2.01	LYST	4.62E-02	1.17	MAGOHB	4.14E-03	0.49
RPRD2	1.09E-17	2.01	C11orf49	2.84E-02	1.17	MRPL1	5.11E-04	0.49
FOSB	2.66E-02	1.97	PRR11	3.42E-02	1.17	GATB	3.74E-02	0.49
UPP2	3.38E-02	1.94	RERE	2.54E-02	1.16	PDSS1	2.08E-04	0.49
KDSR	1.63E-02	1.92	MTMR3	1.33E-02	1.15	ERAL1	4.20E-02	0.49
FLVCR2	3.37E-03	1.89	GRAP2	3.42E-02	1.15	SDK1	4.76E-02	0.48
DNAJC9	2.77E-02	1.88	NCOA3	4.61E-02	1.15	MYO16	1.72E-02	0.48
PXMP4	1.97E-03	1.87	DYM	6.30E-10	1.15	MRPS35	1.97E-02	0.48
VPS28	1.54E-02	1.85	ARID1B	1.45E-02	1.15	UNC5D	2.91E-03	0.48
NPRL3	6.30E-10	1.85	ATL1	2.61E-02	1.15	MRPS28	1.41E-27	0.48
CD44	2.99E-02	1.84	MYBPC1	7.17E-03	1.15	RNMTL1	4.30E-02	0.47
PAICS	3.74E-02	1.84	MTA3	6.09E-03	1.14	COX11	4.30E-02	0.47
STK11	2.41E-02	1.83	ASCC1	3.95E-02	1.14	HK2	4.45E-03	0.47
CCPG1	2.56E-02	1.81	NRG4	4.21E-02	1.11	SNX18	2.04E-02	0.47
ARID1A	2.87E-07	1.77	TCF12	4.62E-02	1.11	NDUFB11	2.63E-03	0.47
PAIP2	3.80E-03	1.77	TANC2	8.67E-08	1.11	ZNF652	8.63E-08	0.47
PFKFB4	1.98E-02	1.77	PLEKHG1	4.72E-02	1.09	NDUFAF6	6.91E-11	0.47
CNOT6	2.11E-02	1.76	ARID5B	4.01E-02	1.09	PSIP1	2.34E-03	0.46
FDPS	2.54E-02	1.73	TMC1	3.09E-03	1.08	DCAF7	3.95E-02	0.46
ACLY	4.80E-02	1.72	TRPM3	2.49E-02	1.08	SRD5A1	2.34E-02	0.46
CKS1B	4.41E-04	1.72	ZBTB20	1.96E-06	1.08	ATP5J	4.41E-04	0.46
RANBP3	2.16E-04	1.72	TTC28	2.21E-03	1.07	NDUFAF5	1.66E-05	0.46
FBXL5	2.48E-10	1.71	DMD	3.38E-02	0.93	HNRNPA2B1	5.02E-04	0.46
TULP2	5.30E-04	1.71	NELL1	6.01E-03	0.92	LRPPRC	2.72E-24	0.46
SECISBP2	4.18E-04	1.70	CDKAL1	5.83E-03	0.92	MRPL19	1.25E-02	0.46
HELZ	2.57E-04	1.70	CTNNA3	7.21E-03	0.91	COQ3	3.87E-09	0.46
SMARCA4	1.72E-06	1.69	CSMD1	1.05E-03	0.91	EXT2	1.83E-02	0.46
KLF16	8.83E-04	1.69	RBMS3	2.99E-02	0.91	NDUFS8	4.43E-02	0.45
PBX4	1.30E-02	1.68	NRXN1	1.25E-03	0.90	TAF4	1.25E-02	0.45
RAB5C	9.86E-03	1.66	KCNH5	2.46E-02	0.90	NDUFB10	1.25E-02	0.45
SMARCAL1	1.95E-03	1.66	ZFHX3	1.70E-02	0.90	SEC62	4.93E-02	0.45
MARK3	1.08E-04	1.66	CCDC91	9.93E-03	0.90	TBR1	9.87E-03	0.45
PDS5A	1.11E-02	1.66	ABCA13	1.23E-03	0.90	FARS2	6.03E-06	0.44
TTYH3	3.95E-02	1.65	DACH2	2.16E-02	0.90	NDUFS1	5.83E-03	0.44
AS3MT	4.14E-03	1.64	ESRRG	3.95E-02	0.89	NDUFAF7	1.25E-02	0.44
FOXM1	3.24E-02	1.64	MACROD2	7.01E-03	0.89	TIMMDC1	2.52E-04	0.43
ZNF91	1.45E-02	1.63	MGAT4C	2.43E-03	0.89	NDUFA1	5.13E-03	0.43
FANCC	8.26E-04	1.63	AFF2	3.38E-02	0.89	DNER	1.62E-02	0.43
SAV1	1.52E-04	1.63	HS6ST3	1.07E-02	0.88	NDUFV2	9.63E-13	0.43
SMARCC1	5.71E-14	1.62	PTPRD	2.92E-04	0.88	GRSF1	2.33E-02	0.42
ANKRD11	4.56E-06	1.61	LUZP2	4.92E-02	0.88	NDUFB5	3.38E-02	0.42
PPEF1	2.49E-07	1.61	GPR158	1.07E-02	0.88	GATC	3.38E-02	0.42
LIPH	3.09E-02	1.61	CDH12	1.86E-02	0.88	ICT1	2.22E-03	0.41
CDC25A	9.39E-05	1.60	KCNK2	1.10E-02	0.87	MRPL23	1.22E-02	0.41
CCDC40	2.47E-02	1.60	PCDH11X	1.95E-02	0.87	SEPHS1	1.52E-13	0.41
RABGEF1	1.83E-02	1.60	TEAD1	1.16E-02	0.87	NDUFB2	7.09E-03	0.41

Gene	FDR	MI	Gene	FDR	MI	Gene	FDR	MI
FBXL20	7.29E-04	1.59	B4GALT6	3.54E-02	0.87	RBFA	6.08E-04	0.41
TEX11	3.11E-04	1.59	GPC5	7.01E-03	0.87	TNFRSF1A	8.93E-20	0.41
PPP6R3	2.45E-10	1.58	EYS	3.76E-07	0.86	MRPL3	3.52E-04	0.41
CELF1	2.38E-06	1.58	AKT3	7.91E-05	0.86	C1QBP	1.45E-05	0.41
CDH1	1.49E-02	1.58	SNTG1	7.20E-05	0.86	EARS2	2.16E-03	0.41
ZNF410	1.23E-02	1.57	NAALADL2	1.29E-02	0.86	TFB1M	1.36E-04	0.41
SPTAN1	7.01E-03	1.56	RIMS2	1.63E-04	0.86	GTPBP8	2.27E-02	0.41
GON4L	1.50E-11	1.56	ZNF827	1.72E-02	0.86	MTG1	2.41E-03	0.40
UBE4B	1.64E-06	1.56	GPC6	2.08E-04	0.86	NDUFA9	4.61E-04	0.40
GNPTAB	2.99E-02	1.55	CNTNAP2	1.04E-08	0.85	EXOC1	2.58E-02	0.40
FAM193A	5.59E-03	1.55	RALYL	1.13E-02	0.85	PET117	4.15E-03	0.40
DDRGK1	4.16E-02	1.55	ATF7IP	3.34E-02	0.85	PDE12	9.88E-04	0.40
ARHGAP35	5.13E-03	1.55	AGPS	1.93E-05	0.85	NDUFB9	4.70E-03	0.39
FXYD5	1.72E-02	1.55	CSMD3	6.31E-08	0.84	MTERF3	7.42E-04	0.39
IP6K2	1.45E-02	1.54	PCDH7	4.92E-02	0.84	SLC16A7	2.42E-02	0.38
HNRNPR	5.20E-04	1.54	EPHA5	1.35E-03	0.84	CARS2	3.39E-09	0.38
VPS54	5.50E-03	1.52	SLX4IP	1.42E-02	0.84	MRPS27	3.60E-25	0.38
BTLA	9.42E-05	1.52	FBXL7	7.14E-08	0.84	MRPS6	4.53E-11	0.37
AGK	2.11E-08	1.52	CCDC178	2.65E-02	0.84	DYRK1A	2.83E-46	0.37
NOX5	5.04E-03	1.51	EPHA3	9.12E-05	0.84	TOP1	4.92E-02	0.37
NCOR1	2.62E-05	1.51	GPM6A	3.85E-03	0.84	MRPL11	3.77E-02	0.36
PAK2	3.26E-02	1.51	PLCB1	2.90E-04	0.84	RHEB	4.09E-02	0.35
UBE2K	4.50E-03	1.50	UNC5C	2.74E-02	0.84	NDUFB4	8.43E-06	0.34
RAD51B	2.28E-04	1.50	ANKRD30A	9.07E-03	0.84	MRPL50	8.97E-03	0.34
FGD3	5.32E-03	1.50	LRRC16A	7.99E-03	0.83	MRPS9	1.70E-20	0.33
PBRM1	8.83E-17	1.50	LRRC4C	4.61E-04	0.83	GTPBP10	8.83E-04	0.32
MND1	2.95E-03	1.49	MAP2	2.22E-02	0.83	IGLON5	1.08E-02	0.32
UBAP2	3.29E-02	1.49	ERBB4	1.08E-02	0.83	GPRASP2	2.08E-04	0.31
PIK3CD	4.45E-02	1.48	SPOCK3	2.56E-02	0.83	MRPL30	1.79E-03	0.29
TMEM105	5.83E-03	1.48	ANO3	6.23E-04	0.83	ADAT2	4.15E-02	0.28
GSS	5.83E-03	1.48	BCOR	5.67E-05	0.83	NDUFS3	4.91E-05	0.28
CARM1	6.66E-09	1.48	TRIO	3.79E-02	0.82	ATP5J2	2.95E-03	0.28
PARN	1.06E-12	1.48	EXOC4	6.16E-06	0.82	PITRM1	2.21E-05	0.27
SMARCE1	4.92E-02	1.48	XPO6	4.45E-02	0.82	MRPL15	4.67E-03	0.24
JUP	1.08E-02	1.47	CAMK2D	1.88E-02	0.81	GFM1	2.09E-02	0.24
TECPR2	1.00E-02	1.47	CDH9	3.60E-03	0.81	ATP5B	2.09E-02	0.24
ALG8	1.70E-03	1.47	FGF13	5.07E-03	0.81	DLD	8.76E-05	0.24
HMCN1	8.28E-03	1.46	GRID2	3.92E-07	0.81	MTRF1L	1.00E-02	0.24
HTR7	3.68E-02	1.46	MALRD1	5.13E-03	0.81	REXO2	4.41E-04	0.24
CCDC109B	4.73E-05	1.46	ARHGEF12	3.31E-02	0.81	PDAP1	1.45E-02	0.23
SPG21	1.45E-02	1.45	CDH10	8.26E-04	0.81	NDUFV1	3.02E-02	0.23
ACOX1	2.40E-03	1.44	RFX3	1.63E-05	0.81	FLT4	3.02E-02	0.23
CDK13	1.68E-04	1.44	MSRA	1.68E-04	0.80	NDUFB7	4.71E-03	0.23
MERTK	4.56E-03	1.43	NET1	5.59E-03	0.80	ATP5O	8.71E-04	0.20
DYNLL1	2.68E-02	1.43	MAML3	1.84E-02	0.80	ATP5D	2.92E-03	0.18
FBXW7	8.71E-04	1.42	KLF7	2.37E-03	0.80	ATP5F1	5.34E-04	0.18
CEP83	8.25E-03	1.42	ZSWIM6	6.61E-03	0.80	NOA1	1.83E-02	0.15
DICER1	2.06E-03	1.42	PDZD8	4.21E-02	0.79			
AGO4	1.34E-02	1.41	TNR	5.13E-03	0.79			

8.2.12 *TNFα-dependent NF-κB activation screen*

Gene	FDR	MI	Gene	FDR	MI	Gene	FDR	MI
IKBKG	1.04E-25	53.90	PPEF1	1.27E-06	1.50	RICTOR	4.68E-05	0.49
MAP3K7	5.86E-45	19.60	RALGAPB	3.26E-02	1.49	NDUFB4	2.82E-02	0.49
TNFRSF1A	2.51E-183	15.90	TEX11	1.38E-04	1.49	NFKB1	5.89E-14	0.48
PCBP2	6.67E-19	13.18	ZFAT	1.01E-06	1.49	ACAD9	2.87E-02	0.48
CUL1	7.59E-52	11.53	GPATCH8	5.06E-04	1.48	NDUFB9	1.95E-02	0.47
QRICH1	2.38E-71	10.67	NCOR1	8.55E-05	1.48	METTL5	2.25E-02	0.47
SEPHS1	3.43E-72	10.58	SLTM	7.77E-05	1.47	PPAT	2.84E-06	0.47
INTS10	2.09E-04	9.76	CUL3	6.68E-03	1.47	MBTPS2	1.80E-15	0.47
FBXW11	8.77E-37	9.63	PRMT7	3.47E-03	1.47	PTAR1	1.73E-02	0.46
MED26	1.89E-02	8.79	EPC2	1.38E-02	1.47	MRPS28	2.08E-33	0.46
ZNF652	4.48E-79	7.58	RSBN1L	8.19E-05	1.47	RBFA	2.28E-02	0.45
ZNF578	4.40E-07	6.74	SPTLC2	2.74E-02	1.46	FAM136A	4.51E-02	0.45
DPY30	7.31E-08	6.33	IGSF11	1.49E-03	1.45	SLC30A9	5.35E-03	0.44
SFTPB	1.11E-03	6.09	HECTD1	8.85E-03	1.45	IPO9	1.73E-02	0.44
SHARPIN	1.21E-05	5.86	RSF1	1.01E-09	1.45	DDX5	8.20E-03	0.44
TRAF2	2.35E-22	5.78	ARIH2	2.56E-03	1.45	ATP5J	7.70E-05	0.44
CHUK	5.16E-16	5.71	ZEB2	4.53E-11	1.44	SMG7	1.23E-03	0.44
DCPS	6.54E-04	5.66	MKRN1	2.67E-02	1.43	GTPBP8	1.11E-02	0.44
DHX36	5.65E-05	5.57	BCR	3.97E-02	1.43	MRPL50	1.95E-02	0.43
PARVG	1.23E-05	5.47	RAD54L2	2.83E-02	1.42	MTX2	1.95E-02	0.43
BRD7	1.24E-14	5.40	RAD51B	2.33E-03	1.42	NDUFA11	1.95E-02	0.42
ZNF793	3.57E-19	5.03	UBA6	3.23E-03	1.42	EIF4E2	3.30E-03	0.42
CNOT2	1.31E-17	4.98	NOX5	4.69E-03	1.42	KDM1A	1.97E-11	0.42
SMARCB1	1.86E-11	4.97	NRXN2	1.04E-02	1.41	MRPL11	1.23E-02	0.42
BIRC2	2.33E-12	4.94	TNRC18	2.37E-03	1.40	GRSF1	4.37E-02	0.41
SMARCA4	2.18E-66	4.49	ABCC1	1.46E-03	1.40	ATPAF2	1.66E-04	0.41
ARID2	1.70E-80	4.41	ARHGAP17	2.48E-02	1.40	MRPS16	1.89E-05	0.41
RNF31	2.24E-10	4.31	GSTA4	3.02E-02	1.40	SLIRP	2.80E-02	0.41
TFDP1	6.63E-04	4.22	BIRC6	6.70E-08	1.39	SLC25A26	1.28E-03	0.41
PBRM1	1.42E-203	3.82	ATF7IP	6.11E-08	1.38	TRIT1	2.11E-10	0.39
UBASH3B	2.97E-17	3.79	C6orf99	1.74E-02	1.38	KIAA0391	3.73E-10	0.39
WDR82	2.46E-03	3.73	MROH8	4.18E-02	1.36	PDE12	9.16E-05	0.39
BAP1	3.15E-04	3.68	DPH6	3.39E-06	1.36	WDR59	1.21E-05	0.39
ZFP14	4.93E-02	3.68	CTNNA1	6.88E-08	1.36	VPS45	9.72E-07	0.39
TRADD	2.77E-04	3.59	SPEN	4.35E-05	1.35	RBM33	1.09E-02	0.38
DLEC1	1.37E-16	3.48	SRPK1	2.77E-02	1.35	MRPS5	1.76E-02	0.38
SERBP1	8.13E-08	3.36	SUPT3H	1.26E-06	1.33	EZH2	2.11E-04	0.38
MAP1LC3A	8.10E-03	3.32	PPHLN1	1.66E-02	1.31	MTHFD1	2.82E-06	0.38
TRPC7	1.02E-04	3.28	TBC1D14	2.67E-02	1.31	DCAF7	4.09E-07	0.38
UBR4	3.49E-02	3.28	EIF4B	4.10E-02	1.30	WARS2	2.76E-04	0.38
WAC	4.05E-08	3.27	TAOK1	9.60E-06	1.30	NARS2	3.82E-152	0.37
TSC2	8.11E-04	3.24	TRAF3	8.17E-03	1.30	LRPPRC	2.03E-49	0.36
NAA30	3.12E-02	3.20	MLLT10	4.15E-07	1.29	MTERF3	3.04E-05	0.35
NFKBIA	2.52E-13	3.19	KMT2E	1.72E-03	1.29	LARS2	2.44E-20	0.35
THEG	1.87E-02	3.12	RABGAP1L	3.94E-02	1.27	EED	2.46E-06	0.35
SLC1A2	4.95E-08	3.06	UNC13B	2.70E-02	1.27	C1QBP	4.40E-07	0.34
CXXC1	5.45E-04	3.05	JAZF1	4.92E-04	1.27	YME1L1	2.25E-02	0.33
IKBKB	4.79E-05	3.02	GON4L	2.67E-02	1.26	RANBP3	1.02E-17	0.33
DDX6	1.06E-07	3.00	VPS41	3.97E-02	1.26	MRPL17	1.69E-03	0.33
ZNF569	8.02E-05	3.00	SIPA1L3	4.65E-02	1.20	ZC3H15	3.71E-02	0.33
RBCK1	1.53E-09	2.99	TEN1	4.72E-02	1.17	GTPBP10	7.98E-04	0.32
CFAP53	1.14E-03	2.80	ZFHX3	4.79E-03	1.13	ERAL1	3.85E-05	0.32
SMARCE1	2.08E-15	2.79	UBE2H	3.86E-02	1.11	MRPL24	3.60E-07	0.31
TSC1	1.35E-09	2.79	MECOM	1.23E-02	1.10	FTSJ2	4.10E-02	0.31
DNTT	4.61E-06	2.79	IL1RAPL1	2.09E-02	0.95	DDX28	2.84E-05	0.31
DNMT1	2.20E-07	2.74	LRP1B	2.68E-03	0.93	MRPS27	3.36E-48	0.31
YBX1	1.11E-02	2.73	CHN1	1.76E-02	0.92	CYLD	2.17E-13	0.30
GLMN	1.49E-08	2.73	DACH1	5.34E-03	0.92	MRPS33	9.59E-04	0.30
CLPSL1	9.50E-03	2.71	SYT1	2.83E-05	0.92	GFM1	4.43E-02	0.30
ST6GAL	2.10E-04	2.71	GRID2	3.16E-02	0.89	HARS2	2.82E-02	0.30

Gene	FDR	MI	Gene	FDR	MI	Gene	FDR	MI
NAC1								
NPRL2	1.23E-03	2.67	CSMD3	3.00E-03	0.89	CLPB	1.48E-03	0.30
ACTL8	1.04E-03	2.66	EPHA5	9.78E-03	0.87	GATB	1.07E-06	0.29
NFKBIE	2.28E-02	2.60	ANO3	1.87E-02	0.85	AIFM1	2.07E-07	0.29
NAA35	4.91E-03	2.60	TEAD1	7.92E-03	0.85	OPA1	1.15E-06	0.29
MYH14	1.12E-05	2.56	AKT3	2.24E-05	0.85	ATP5F1	1.06E-03	0.28
ZZZ3	7.10E-05	2.56	ASCC1	2.18E-03	0.85	MTG1	5.13E-07	0.28
TRA2A	1.93E-04	2.51	ANKRD30A	2.17E-02	0.84	GATC	1.20E-06	0.28
FLVCR2	2.38E-07	2.50	RERE	3.96E-03	0.83	ISCA1	1.69E-03	0.27
CDK13	9.02E-31	2.47	TET1	1.69E-03	0.83	MRPS35	1.71E-10	0.27
SNRPA	2.30E-04	2.47	PRMT3	8.91E-03	0.83	GIGYF2	2.79E-41	0.26
ADGRD1	7.13E-05	2.46	MAP2	3.57E-02	0.82	ISCA2	4.86E-02	0.26
TIPRL	2.74E-02	2.46	NCOA2	1.72E-05	0.80	MTCH2	9.66E-03	0.26
LARP7	9.88E-05	2.43	EFNA5	5.35E-09	0.80	MRPL23	3.84E-07	0.26
METAP1	5.96E-03	2.39	GFPT1	1.54E-02	0.79	YARS2	1.13E-05	0.26
NF2	4.49E-07	2.34	PARN	2.56E-04	0.79	OGDH	8.89E-05	0.26
CARNMT1	2.14E-03	2.34	FBXL17	8.92E-06	0.78	TFB2M	4.90E-04	0.26
ASH2L	2.42E-10	2.32	ARHGEF12	4.86E-03	0.78	MRPS9	8.41E-42	0.25
CREB1	1.07E-03	2.31	MYO10	2.85E-15	0.78	MRPL18	1.81E-13	0.25
ATAD3C	8.20E-03	2.30	ZMYND8	2.71E-03	0.77	RARS2	5.64E-09	0.25
USP14	3.19E-94	2.29	TMEM131	1.42E-02	0.77	MRPL48	6.05E-18	0.25
TOE1	4.08E-03	2.27	CHIC2	4.89E-05	0.74	MRPL49	1.16E-03	0.25
TSPAN16	3.74E-09	2.27	EXOC4	1.18E-09	0.74	NGRN	1.67E-07	0.25
RPRD2	3.57E-19	2.23	MTF2	3.85E-02	0.73	MIPEP	3.56E-12	0.24
TADA2A	3.74E-09	2.21	GPBP1	1.76E-02	0.72	MRPL39	2.25E-02	0.24
CREBBP	4.14E-17	2.21	WDR20	7.35E-14	0.72	TSFM	2.25E-02	0.24
ZNF611	4.94E-07	2.18	EXOC2	8.85E-03	0.72	DAP3	7.22E-08	0.24
POU2F1	9.79E-14	2.16	PDSS2	2.21E-15	0.72	MRPS15	2.64E-05	0.24
FANCD2	2.76E-02	2.15	C11orf73	8.86E-05	0.72	METTL17	1.51E-02	0.23
SP1	2.19E-15	2.15	YES1	4.52E-02	0.71	MRPL51	8.88E-07	0.23
DEPDC5	2.42E-10	2.14	YBEY	1.07E-04	0.70	POLG2	6.79E-16	0.23
E2F3	6.73E-06	2.13	EIF2A	1.54E-04	0.69	MTG2	1.36E-04	0.23
OIT3	2.28E-04	2.11	ACVR2A	3.53E-02	0.69	PTDSS1	8.88E-07	0.23
SMARCC1	5.20E-34	2.10	AEBP2	4.23E-05	0.69	MRPL27	9.69E-03	0.23
NPRL3	1.62E-14	2.09	TANK	3.73E-02	0.69	PARS2	9.69E-03	0.23
HTR7	1.50E-07	2.09	COX10	1.76E-03	0.68	TRUB2	1.65E-05	0.22
ZNF91	2.70E-05	2.09	RNF19A	4.79E-02	0.68	RPUSD4	2.79E-03	0.22
PCMTD2	2.86E-05	2.07	GAB2	2.48E-02	0.68	MALSU1	4.84E-04	0.22
SETDB1	1.64E-05	2.05	TLK2	4.77E-05	0.67	TFB1M	8.32E-13	0.22
LIPC	2.36E-02	2.05	NDUFAF6	3.69E-03	0.67	MRPL54	8.36E-07	0.22
ZNF808	4.57E-02	2.05	WDR44	1.60E-07	0.67	MRPL19	1.39E-09	0.22
CD44	2.30E-03	2.04	VMP1	9.45E-10	0.66	TOMM70A	2.27E-02	0.22
NFKBIB	8.95E-22	2.03	COL13A1	4.40E-02	0.66	WDR4	1.24E-15	0.21
SGF29	2.57E-03	2.03	TMEM47	2.09E-02	0.65	ATP5J2	1.19E-06	0.21
CSNK2A1	6.45E-06	1.99	ADNP	5.79E-03	0.65	MRPL3	4.72E-13	0.21
SUV420H1	4.46E-03	1.98	NUBPL	5.37E-11	0.64	MRPS18B	4.81E-16	0.21
CAND1	5.03E-05	1.97	USP7	4.01E-02	0.62	TEFM	6.44E-06	0.20
CDH1	6.32E-08	1.96	NDUFV2	5.06E-04	0.62	PITRM1	1.69E-03	0.20
PPP2R4	1.92E-06	1.92	RQCD1	4.47E-02	0.61	MRPL38	8.02E-05	0.20
PXMP4	4.19E-04	1.91	MAPKAP1	2.17E-10	0.61	SARS2	2.30E-05	0.20
CD48	2.54E-02	1.88	KEAP1	4.02E-04	0.61	MRPS10	1.15E-06	0.20
INPP4A	1.04E-07	1.88	TBK1	3.16E-04	0.61	QRSL1	9.30E-06	0.19
PPP4R2	5.57E-03	1.87	NDUFAF5	3.29E-02	0.60	TSEN15	6.86E-04	0.19
DOT1L	8.03E-08	1.87	MEF2A	7.05E-03	0.59	MRPL30	5.40E-08	0.19
PBX4	6.47E-04	1.85	UBR5	1.84E-02	0.59	MRPS7	5.89E-06	0.19
DBF4	2.17E-02	1.83	UNC5D	1.19E-02	0.59	EARS2	2.64E-15	0.19
SLC44A2	5.40E-04	1.83	COQ2	2.95E-02	0.58	MTPAP	1.07E-12	0.18
CNOT4	1.01E-10	1.81	CHP1	5.08E-04	0.57	ATP5D	4.63E-05	0.18
ARID1A	2.05E-09	1.81	KDM2A	2.32E-22	0.57	MTERF4	9.59E-04	0.17
TSPAN14	2.48E-02	1.79	PYM1	4.98E-09	0.57	MRPL15	1.83E-05	0.17
MIB1	2.11E-12	1.79	ARPC2	2.62E-02	0.57	TUFM	3.02E-02	0.17
DPH5	1.37E-02	1.78	RCOR1	8.91E-10	0.56	MRPL32	5.57E-03	0.17
MAZ	5.50E-06	1.77	ICT1	4.19E-02	0.56	MRPL37	5.57E-03	0.17
FAAH2	3.35E-03	1.77	SUPT20H	4.84E-02	0.56	MRPS25	2.00E-06	0.17
RNF40	3.96E-03	1.76	MIOS	1.60E-02	0.56	TARS2	3.56E-08	0.16

Gene	FDR	MI	Gene	FDR	MI	Gene	FDR	MI
ABLIM2	1.08E-04	1.75	PUM1	1.15E-06	0.55	MRPS23	2.49E-05	0.16
YEATS2	3.53E-02	1.75	PDSS1	2.10E-03	0.55	MRPL35	4.18E-14	0.16
UHRF1	7.05E-06	1.73	NFU1	1.78E-03	0.55	SRD5A3	7.26E-33	0.15
FAM208A	1.15E-03	1.72	REL	5.01E-08	0.54	MRPL33	1.55E-05	0.15
HSD17B12	7.94E-03	1.72	SEC63	3.73E-02	0.54	MRPL4	1.55E-05	0.15
BTLA	2.53E-07	1.71	LIG3	4.10E-04	0.53	PNPT1	2.22E-08	0.15
KHDRBS1	7.36E-03	1.70	YTHDF2	6.79E-05	0.53	MRPL40	5.55E-14	0.15
FBXW7	1.63E-08	1.70	PFAS	6.44E-06	0.53	MRPS26	5.89E-06	0.15
NSD1	6.63E-09	1.68	MRPS6	1.73E-04	0.53	PTCD3	1.24E-14	0.15
SCARA5	4.27E-03	1.68	MRPL13	4.53E-02	0.53	MRPL47	4.09E-07	0.14
NOSIP	2.68E-02	1.67	FAM60A	1.50E-04	0.53	GADD45GIP1	6.77E-11	0.14
TULP4	9.25E-04	1.66	MRRF	3.01E-07	0.53	MRPS24	4.76E-03	0.14
RANBP17	4.62E-02	1.65	ACTR3	2.15E-08	0.52	MRPL22	1.79E-04	0.13
CCDC39	4.85E-02	1.64	DYRK1A	2.33E-26	0.52	MRPL12	1.02E-12	0.13
PLAA	2.48E-02	1.64	PARL	1.61E-02	0.52	MRPL20	1.19E-11	0.12
ANKRD17	3.93E-07	1.64	ALG8	9.89E-11	0.52	ATP5B	7.83E-08	0.11
CTDSPL2	4.14E-03	1.62	ZFR	3.09E-03	0.52	ATP5C1	1.35E-04	0.11
FBXO11	5.92E-03	1.60	SPAG7	5.22E-04	0.52	CHMP5	2.01E-06	0.11
PLEC	1.03E-04	1.60	RHOA	6.50E-05	0.51	WBSCR16	1.12E-18	0.10
WDR72	2.36E-02	1.60	RNF19B	3.35E-03	0.51	POLRMT	1.20E-06	0.10
ACTN1	2.67E-02	1.59	HTRA2	4.10E-02	0.50	ATP5H	4.80E-05	0.10
PIK3R2	3.12E-03	1.55	WNK1	2.99E-08	0.50	MRPS30	3.52E-06	0.09
PTGES3	4.45E-03	1.55	YLPM1	3.55E-02	0.50	SSBP1	1.54E-07	0.08
ANKRD13C	2.70E-05	1.55	MBTPS1	1.14E-03	0.50	MRPL52	3.30E-02	0.07
HMCN1	1.89E-03	1.54	NCKAP1	1.58E-02	0.50	MRPS18C	5.59E-05	0.07
ASXL1	2.23E-05	1.54	GFM2	2.40E-02	0.50	ATP5O	3.29E-08	0.07
WDR37	7.19E-03	1.53	CARS2	6.98E-05	0.49	MRPL21	1.87E-05	0.07
CCDC109B	1.40E-05	1.52	COQ3	3.39E-08	0.49	METTL1	2.00E-06	0.06
EPHB1	1.79E-04	1.51	FARS2	8.21E-07	0.49	MRPL10	2.61E-05	0.04
METTL18	2.15E-02	1.50	ALG5	4.85E-02	0.49	HSD17B10	8.79E-06	0.04

8.2.13 *TNFR1$_{\Delta QRICH1}$ screen*

Gene	FDR	MI	Gene	FDR	MI	Gene	FDR	MI
GPX4	3.00E-15	15.13	SSH2	2.21E-02	1.28	WNK1	1.43E-04	0.62
CNOT3	5.68E-03	6.16	CLASP1	1.67E-02	1.27	NSUN3	3.02E-02	0.62
TIPRL	1.60E-12	5.85	FRYL	4.70E-05	1.27	SLC25A32	2.16E-02	0.62
CNOT2	2.46E-28	5.81	SPIDR	1.68E-02	1.27	PIGU	2.70E-03	0.62
HNRNPM	2.30E-04	5.34	SREBF2	2.86E-02	1.27	UBE3D	9.00E-03	0.61
PSMD4	1.48E-02	4.93	MCM8	3.05E-02	1.26	LIG3	3.85E-03	0.61
UROD	5.34E-05	4.41	ATP2C1	5.30E-05	1.23	ITGAV	4.26E-02	0.60
SEPHS2	6.57E-06	4.19	MBNL1	1.10E-03	1.22	KDM6A	6.18E-04	0.59
SEPSECS	2.81E-06	3.71	NF1	1.43E-05	1.22	MAPKAP1	3.90E-10	0.58
EEFSEC	4.90E-18	3.55	CDK6	4.73E-02	1.21	PPAT	9.56E-03	0.58
TFDP1	4.16E-06	3.17	ANKS1A	3.26E-02	1.18	PECR	4.64E-02	0.58
NAA30	1.38E-05	3.15	GNG7	4.46E-02	1.17	COX18	5.39E-06	0.58
XPO5	1.09E-03	2.95	MECOM	1.28E-09	1.16	NME6	4.95E-03	0.58
BRD7	5.47E-08	2.91	C11orf30	2.55E-02	1.16	PIGK	2.31E-02	0.57
RPS25	1.10E-11	2.90	RNF220	4.18E-03	1.15	PCNP	3.62E-02	0.57
FUS	2.85E-02	2.88	SH3KBP1	2.08E-02	1.15	KDM2A	7.41E-23	0.57
DPY30	1.92E-03	2.81	MAP4K3	1.54E-04	1.14	NDUFAF5	1.70E-03	0.56
SMARCB1	1.13E-03	2.78	PDE11A	3.92E-02	1.11	AIFM1	2.20E-02	0.54
NASP	1.65E-08	2.76	TRPM3	5.01E-03	1.08	CHCHD1	2.20E-02	0.54
FANCE	3.15E-02	2.66	ZBTB20	5.17E-06	1.07	ZNF407	2.06E-02	0.54
NF2	8.00E-08	2.65	FHIT	3.05E-02	1.06	MTO1	1.11E-02	0.54
NFYC	1.22E-08	2.65	LRP1B	4.60E-02	0.94	LAMTOR5	1.98E-03	0.54
TANGO6	3.80E-02	2.60	DMD	2.23E-02	0.93	WDR59	1.03E-02	0.54
PPP4R2	5.19E-08	2.60	CDKAL1	1.78E-02	0.93	MAP3K4	1.79E-02	0.53
CDK2	4.11E-03	2.59	DACH1	6.33E-04	0.92	NDUFAF6	4.82E-09	0.53
UBE2M	1.37E-03	2.58	CTNNA3	1.25E-02	0.92	PDE12	3.53E-02	0.52
PPP2R4	1.59E-23	2.50	CSMD1	3.06E-03	0.91	HNRNPA2B1	1.03E-02	0.52
DDX6	1.31E-05	2.39	CADM2	8.24E-04	0.91	VPS29	1.04E-07	0.52
ZBTB14	7.39E-05	2.34	CCDC91	2.78E-02	0.91	NARS2	6.19E-75	0.52
WAC	1.84E-03	2.32	EXOC4	4.05E-02	0.91	FARS2	9.33E-05	0.51
FANCL	1.15E-02	2.28	EPHA6	3.48E-02	0.90	DNAJC2	1.92E-03	0.51
KCTD5	8.77E-03	2.24	ABCA13	1.42E-03	0.90	COQ3	9.87E-06	0.50
FANCB	3.25E-02	2.23	EYS	1.70E-03	0.90	MRPS18B	2.20E-03	0.50
UBE2A	3.25E-02	2.19	KCNH5	1.97E-03	0.90	MLST8	4.18E-03	0.50
ARID2	6.02E-24	2.16	MARCH1	7.67E-03	0.90	TFB1M	2.85E-02	0.48
EPC2	1.32E-13	2.15	RIMS2	9.51E-03	0.89	MRPS27	3.00E-15	0.48
CUL1	1.66E-03	2.13	NFIB	4.05E-02	0.89	NDUFV2	4.10E-11	0.48
HSD17B12	3.04E-10	2.09	RBMS3	2.54E-03	0.89	MRPL18	1.09E-04	0.47
DBF4	6.16E-04	2.08	MED13L	1.53E-02	0.89	LRPPRC	9.41E-22	0.47
DEPDC5	1.28E-08	2.07	RYR2	3.98E-02	0.88	PTCD3	3.29E-02	0.46
UBE2L3	4.31E-06	2.06	AGPS	1.08E-03	0.88	MRPS35	2.16E-02	0.46
PBRM1	1.06E-64	2.03	TNS3	3.69E-02	0.88	WBSCR16	5.81E-03	0.46
EWSR1	1.35E-02	2.00	MACROD2	1.50E-02	0.88	NCKAP1	1.35E-03	0.46
NPRL2	4.27E-02	1.98	SNTG1	1.35E-03	0.88	CARS2	2.85E-07	0.46
ARID1A	3.68E-12	1.92	DACH2	2.56E-03	0.88	ATP5J	2.15E-06	0.45
RPRD2	4.02E-16	1.88	AFF2	2.06E-02	0.88	NDUFB9	1.02E-02	0.45
USP14	2.19E-71	1.82	TTC6	3.87E-04	0.87	LARS2	5.82E-12	0.45
TSC1	3.32E-03	1.81	PTPRM	4.60E-04	0.87	MRPL35	3.05E-02	0.45
NPRL3	1.26E-09	1.80	GPR158	1.84E-03	0.87	ARPC2	4.97E-08	0.45
SLC38A10	1.39E-02	1.77	MYO10	2.37E-06	0.87	NDUFA1	2.61E-02	0.45
FAM193A	2.83E-04	1.76	FOXP1	4.39E-05	0.87	WDR4	9.35E-08	0.45
C17orf53	3.67E-02	1.75	WWTR1	1.04E-03	0.86	TIMMDC1	2.11E-04	0.44
SMARCC1	6.09E-19	1.74	SGCZ	2.08E-02	0.86	PET117	1.09E-02	0.44
TRA2A	2.31E-02	1.73	FBXL7	8.49E-04	0.86	MRPS28	1.03E-36	0.44
CDK13	1.79E-10	1.70	TNKS	3.83E-02	0.86	TRIT1	1.46E-09	0.44
LARP7	3.62E-02	1.69	PXDNL	3.69E-02	0.85	LAMTOR3	4.26E-02	0.43
SMAD7	2.42E-04	1.67	GRM8	4.50E-02	0.85	C7orf73	1.72E-02	0.43
GIGYF2	3.71E-10	1.67	CDH10	1.89E-02	0.85	TMEM261	8.03E-03	0.43
NSF	2.30E-03	1.65	VRK2	7.98E-03	0.85	GADD45GIP1	4.37E-02	0.43
ANKRD11	3.90E-10	1.65	DPH6	1.43E-02	0.84	MRPL17	2.78E-02	0.43
SCAF8	7.95E-04	1.64	CNTNAP2	4.82E-09	0.84	DDX28	1.53E-02	0.43

Gene	FDR	MI	Gene	FDR	MI	Gene	FDR	MI
C12orf66	2.85E-02	1.63	VMP1	3.41E-02	0.84	SMAD4	1.05E-07	0.43
FBXL5	1.46E-08	1.60	CDH12	4.31E-06	0.82	NDUFS3	9.50E-03	0.42
FBXW7	5.68E-07	1.60	PRMT3	1.62E-03	0.82	E2F7	3.27E-02	0.42
NSD1	7.76E-09	1.59	SETBP1	9.43E-03	0.82	RICTOR	3.68E-04	0.41
SETD5	5.16E-04	1.56	SGIP1	3.69E-02	0.82	POLG2	7.67E-07	0.41
EP300	3.40E-03	1.55	GALNTL6	1.03E-04	0.82	MTERF3	1.00E-04	0.41
VPS54	3.27E-04	1.55	AKT3	1.05E-10	0.81	GATC	5.81E-03	0.41
PPP6R3	2.67E-09	1.55	TEAD1	6.57E-08	0.81	MRPS9	1.49E-15	0.41
STX18	3.88E-03	1.54	INO80C	1.88E-02	0.81	ICT1	4.31E-06	0.41
SMARCA4	2.50E-04	1.54	LRRTM4	8.76E-05	0.81	C1QBP	5.74E-06	0.40
INPP4A	2.36E-03	1.53	ACACA	5.11E-08	0.80	LAMTOR2	3.06E-03	0.40
SECISBP2	1.50E-02	1.52	ZSWIM6	3.62E-03	0.80	RBFA	7.03E-05	0.39
ZFAT	2.64E-10	1.51	ATF7IP	3.07E-04	0.79	MTG1	1.44E-05	0.38
DOT1L	3.03E-03	1.50	L3MBTL3	4.73E-02	0.78	MRPS6	1.67E-12	0.38
E2F3	2.97E-02	1.50	PIGL	4.09E-02	0.78	COX19	9.29E-03	0.38
RAD51B	3.10E-05	1.49	METTL15	9.92E-04	0.77	YARS2	2.27E-02	0.37
HELZ	6.83E-03	1.49	PPP4R1	3.75E-02	0.76	RNMTL1	2.04E-04	0.37
NCOR1	1.34E-05	1.48	MAP2K6	1.80E-02	0.75	EARS2	6.20E-05	0.37
TAOK1	6.56E-15	1.48	EXT1	2.53E-02	0.74	MRPL3	7.27E-05	0.36
DICER1	6.12E-04	1.47	CHRM3	1.19E-02	0.74	GRSF1	2.71E-04	0.36
PAQR5	4.36E-02	1.47	PARVB	1.15E-02	0.73	WARS2	6.27E-03	0.36
ARIH2	5.51E-04	1.47	PYM1	3.85E-03	0.72	NDUFA9	3.68E-04	0.35
ARHGAP35	7.43E-03	1.46	IGF1R	1.03E-02	0.72	OPA1	2.88E-04	0.35
SPTAN1	4.70E-02	1.46	LRFN5	7.46E-06	0.72	DYRK1A	1.03E-39	0.34
CDC25A	3.14E-03	1.45	UBE2E3	6.29E-03	0.72	FTSJ2	2.40E-03	0.34
UBE4B	4.86E-06	1.44	USP22	3.61E-02	0.72	MRPS30	1.80E-02	0.34
CUL3	3.19E-06	1.44	SP3	5.54E-03	0.70	TOMM70A	2.03E-02	0.33
CARM1	1.83E-10	1.43	MAN1A2	3.29E-02	0.70	HSD17B10	3.72E-02	0.33
RANBP3	1.65E-02	1.43	CNOT4	1.68E-02	0.69	MRPS5	5.08E-03	0.32
RAB6A	1.65E-02	1.42	PFAS	1.30E-02	0.68	MMS22L	4.31E-02	0.32
POU2F1	7.19E-04	1.42	PDSS2	1.65E-19	0.67	TOP1	2.61E-02	0.32
MND1	4.59E-02	1.41	CREBBP	2.02E-02	0.67	METTL17	1.62E-02	0.32
ZEB2	2.26E-11	1.40	CLUH	4.98E-02	0.66	TSFM	1.80E-02	0.31
SPEN	4.67E-05	1.40	PIGP	1.26E-03	0.66	MIPEP	1.83E-14	0.29
AGK	5.87E-08	1.39	YES1	8.76E-05	0.65	PITRM1	1.09E-04	0.28
CTNNA1	8.94E-11	1.39	LIN28B	3.02E-11	0.65	RAG2	1.67E-02	0.26
CELF1	9.92E-04	1.36	SNTB2	2.08E-04	0.65	RPUSD3	1.67E-02	0.26
HARBI1	4.73E-02	1.35	YBEY	5.21E-08	0.65	ATP5B	4.38E-03	0.26
MIB1	1.33E-04	1.33	DPH5	4.39E-02	0.65	ATP5J2	5.90E-05	0.25
KMT2E	8.09E-07	1.33	DOCK1	1.03E-03	0.65	DCAF7	4.21E-04	0.24
UBE2R2	1.90E-04	1.32	SRD5A3	4.68E-03	0.64	METTL1	2.71E-04	0.24
MSI2	4.55E-11	1.29	GPBP1	1.42E-05	0.64	NDUFB7	7.29E-04	0.23
MGA	1.65E-02	1.29	ACTR3	5.51E-06	0.62	ATP5O	4.57E-04	0.22
CDH6	4.31E-03	1.28	NUBPL	6.56E-15	0.62	DLD	5.96E-05	0.16
SIK3	1.10E-02	1.28	MRRF	1.08E-03	0.62	AARS2	3.52E-05	0.11

8.2.14 *(TNFα-dependent NF-κB activation $_{\Delta QRICH1}$) screen*

Gene	FDR	MI	Gene	FDR	MI	Gene	FDR	MI
C7orf26	3.07E-02	13.13	KIAA0391	8.40E-03	1.52	PTAR1	9.68E-04	0.60
ELOF1	2.54E-02	8.11	ZCCHC14	3.19E-03	1.51	RPTOR	8.00E-04	0.60
RBBP5	1.32E-03	7.98	SS18	1.52E-02	1.51	USP7	4.27E-04	0.60
UBR4	2.12E-03	7.72	HNRNPD	6.01E-03	1.50	ATF7IP	1.64E-22	0.59
NELFE	3.14E-02	5.92	RBM26	1.15E-06	1.50	BAZ1B	1.49E-19	0.58
CREBBP	2.25E-96	4.94	DNAJA2	1.55E-06	1.49	TLK2	5.83E-13	0.58
DHX36	1.51E-05	4.49	CKS1B	7.50E-03	1.48	TSEN15	1.52E-02	0.58
NFKBIE	2.91E-08	4.49	MTHFD1L	4.96E-02	1.48	PDS5A	1.13E-02	0.58
MYL5	1.11E-02	4.38	ATP2C1	2.22E-20	1.48	SCD	7.43E-03	0.58
TFDP1	1.47E-16	4.25	GPATCH8	7.43E-03	1.47	CCNT1	1.57E-02	0.58
DDX6	6.00E-35	4.07	SKP2	1.37E-02	1.47	UCHL5	2.96E-03	0.57
NAA30	1.48E-14	4.05	SLTM	2.79E-06	1.46	FAR1	1.61E-02	0.57
MRPL37	3.52E-02	3.99	TADA2B	3.94E-02	1.46	C16orf72	1.13E-05	0.57
CUL1	1.97E-19	3.95	CSNK2A1	4.99E-02	1.44	VPS29	4.91E-07	0.57
PGD	5.91E-07	3.74	SETD1B	1.49E-04	1.44	PAICS	1.31E-02	0.56
ANKRD17	2.51E-70	3.68	ZMYM4	1.59E-02	1.41	EHMT1	3.90E-11	0.56
ACLY	5.65E-20	3.68	RAB10	1.37E-02	1.41	MNT	2.25E-18	0.56
TIPRL	8.80E-14	3.32	CCDC33	3.34E-03	1.41	SRD5A3	7.62E-08	0.56
NFKBIB	3.01E-72	3.23	BMPR2	5.20E-05	1.41	SRM	2.50E-02	0.56
EIF4A1	6.47E-03	3.22	CDK13	1.98E-03	1.40	RCOR1	6.18E-09	0.56
CNOT3	1.06E-05	3.09	KLF9	7.40E-05	1.39	FAM208A	2.09E-03	0.56
NAA35	7.75E-16	3.00	PATZ1	2.12E-02	1.37	CCDC6	3.64E-04	0.55
SDHB	2.69E-07	2.97	UBE2R2	3.15E-05	1.36	IPO9	3.46E-02	0.55
CNOT2	1.34E-45	2.93	CHD2	1.63E-06	1.35	PPHLN1	4.89E-11	0.54
UQCRC1	9.01E-04	2.89	TAOK1	1.92E-07	1.35	CDYL	1.14E-04	0.54
ARID2	1.34E-45	2.86	APC	3.77E-02	1.35	MTX2	8.19E-03	0.54
SDHC	6.09E-16	2.82	ZNF280C	5.73E-04	1.33	ZC3H4	2.30E-15	0.54
SDHAF4	3.02E-07	2.75	NCOA6	8.57E-03	1.33	L3MBTL3	2.00E-12	0.54
BRD7	1.81E-07	2.73	PDSS2	1.07E-11	1.31	RREB1	1.39E-07	0.54
DNAJC8	2.77E-02	2.70	WDR7	3.78E-03	1.30	GIGYF2	1.72E-22	0.54
TMED2	4.94E-07	2.66	MRPS27	2.96E-03	1.30	PAXIP1	2.92E-02	0.53
TADA3	6.64E-03	2.64	TRIM71	2.43E-03	1.30	PEX13	4.54E-03	0.53
CCNC	7.32E-03	2.54	RPRD2	2.50E-02	1.28	USP9X	6.01E-03	0.53
ZC3H14	2.74E-02	2.50	ATXN7	4.95E-03	1.26	VPS28	1.10E-03	0.52
SGF29	1.40E-07	2.50	PHF21A	1.44E-02	1.25	MARCH5	4.51E-02	0.52
HECTD1	4.00E-15	2.49	LIN28B	8.79E-03	1.25	ZNF628	1.44E-03	0.52
PBRM1	4.18E-110	2.49	MYH7B	4.46E-03	1.25	PSIP1	3.80E-03	0.52
FBXW11	5.83E-13	2.47	NARS2	1.71E-11	1.25	INPP5K	1.37E-02	0.51
STRAP	4.35E-02	2.40	MRPS28	7.43E-03	1.23	SEH1L	1.26E-02	0.50
SDHA	2.27E-03	2.40	ABCC4	3.52E-02	1.23	DPH6	1.28E-42	0.50
KLF16	4.58E-15	2.38	CTNNA1	8.52E-04	1.22	TADA2A	7.03E-06	0.50
HYPK	4.85E-03	2.29	RERE	8.98E-04	1.21	SMC6	2.86E-05	0.50
PDCD10	1.37E-02	2.29	PARD3	7.68E-04	1.21	SAP30	4.41E-02	0.49
PPP2R4	2.14E-35	2.28	MED13L	4.49E-06	1.20	PUM1	1.87E-10	0.49
TRAF3	1.92E-40	2.24	FAM53B	3.61E-02	1.19	EP300	2.59E-10	0.48
DNAJC9	6.48E-05	2.24	RSF1	3.09E-02	1.19	NRD1	4.68E-09	0.48
ALKBH8	2.48E-07	2.21	ARID1B	1.09E-02	1.17	KDM2A	5.81E-37	0.48
CXXC1	2.17E-03	2.21	ALPK1	1.30E-02	1.16	WDR4	4.39E-06	0.47
COX20	2.06E-02	2.20	EPC1	8.36E-03	1.16	MBD3	6.72E-15	0.47
XPO5	7.52E-04	2.19	TRPM3	1.36E-09	1.15	MTCH2	1.30E-05	0.47
PPP4R2	4.17E-09	2.15	TCF12	7.21E-04	1.14	BPTF	1.87E-10	0.46
HNRNPM	2.88E-03	2.15	MSI2	4.66E-02	1.12	SMG6	3.49E-03	0.46
PLAA	3.34E-06	2.13	MAP4K3	4.90E-03	1.12	UBAP1	1.25E-14	0.46
E2F4	1.95E-03	2.12	TNRC6B	4.37E-02	1.11	GNPAT	2.12E-03	0.45
STIP1	3.07E-02	2.12	HDAC9	2.95E-06	1.09	ARPC2	2.49E-10	0.45
FAM65B	2.06E-02	2.09	TMC1	2.27E-03	1.08	DOT1L	4.58E-15	0.45
TXLNG	1.11E-08	2.08	TTC28	4.66E-02	1.05	DPH2	3.18E-02	0.44
ZC3H13	1.51E-05	2.06	ZBTB20	2.41E-02	1.05	USP8	3.54E-05	0.44
COX15	2.82E-03	2.05	DMD	3.85E-02	0.93	BRD1	3.50E-03	0.43
ZEB2	5.31E-72	2.04	CSMD1	6.74E-03	0.91	RNF4	4.59E-08	0.43
KCMF1	8.25E-10	2.04	CCDC91	1.37E-02	0.90	COG7	4.28E-03	0.43

Gene	FDR	MI	Gene	FDR	MI	Gene	FDR	MI
TMED10	2.09E-07	2.01	CTNNA3	2.58E-03	0.90	TAF3	3.79E-09	0.43
YLPM1	1.20E-03	2.00	ARID5B	1.78E-04	0.89	RAB18	1.66E-02	0.43
FBXO11	2.58E-07	1.99	PTPRM	1.59E-02	0.89	ADNP	3.09E-17	0.42
COX19	2.49E-02	1.95	PHKB	6.08E-03	0.89	NSMCE2	2.09E-04	0.42
ASH2L	1.47E-13	1.95	CNTNAP2	1.18E-03	0.89	ZZZ3	1.24E-02	0.42
E2F3	3.01E-06	1.95	AGBL1	1.46E-03	0.88	FBRS	6.48E-03	0.41
CHUK	3.59E-02	1.94	CDH12	1.60E-02	0.87	VPS13D	1.63E-09	0.41
UBA6	6.02E-12	1.94	SNTG1	8.75E-04	0.87	FAF2	4.55E-03	0.39
BIRC2	4.11E-02	1.93	PARN	2.12E-02	0.86	UBE2M	6.61E-08	0.39
MIB1	2.93E-29	1.93	EFNA5	1.23E-04	0.86	ATXN2L	4.08E-02	0.39
SMARCA4	2.99E-14	1.93	AUTS2	2.07E-05	0.86	TAF1	8.83E-03	0.39
SP3	1.73E-10	1.92	MACROD2	1.26E-03	0.85	PEX7	1.11E-05	0.38
ZBTB2	2.29E-02	1.91	GPC5	3.53E-02	0.85	CSRP2BP	1.58E-03	0.37
PCNP	1.13E-02	1.89	XPO6	4.66E-02	0.84	RHEB	2.03E-02	0.37
SUPT20H	7.50E-03	1.88	USP34	2.97E-02	0.83	CRAMP1	4.88E-11	0.36
NOSIP	2.52E-02	1.88	CDK2AP1	1.57E-02	0.82	CUL3	2.43E-109	0.36
UQCRC2	1.66E-02	1.88	MAN2A1	8.59E-03	0.82	ATP5O	3.85E-02	0.35
ASUN	9.78E-04	1.86	TASP1	4.28E-02	0.82	NCAPH	3.85E-02	0.35
EPC2	1.11E-09	1.85	MAD1L1	1.11E-02	0.81	CHMP3	9.63E-07	0.35
CDK8	5.54E-03	1.82	MLLT10	2.83E-04	0.80	VPS36	1.68E-03	0.35
DHX29	8.36E-03	1.79	ACACA	1.93E-09	0.78	UBR5	1.75E-11	0.33
ACO2	1.89E-02	1.77	TNS3	2.74E-08	0.78	TTI1	8.98E-04	0.33
SMARCC1	1.97E-19	1.75	C15orf41	1.51E-05	0.78	N4BP1	3.01E-06	0.33
SHMT2	1.48E-02	1.75	TNKS	9.44E-06	0.78	HGS	1.26E-14	0.33
ATIC	1.30E-02	1.74	BRE	1.04E-02	0.76	VPS35	7.50E-03	0.32
KHDRBS1	1.13E-02	1.74	UNK	1.12E-04	0.76	COG4	2.42E-04	0.31
EIF4B	5.17E-12	1.73	KIAA1033	1.84E-02	0.76	ACTR2	2.30E-06	0.31
BIRC6	6.89E-20	1.73	FAF1	4.17E-02	0.74	DPH5	2.02E-15	0.30
KAT2A	4.52E-02	1.73	STT3B	4.99E-02	0.74	VPS45	3.99E-26	0.30
SDHAF2	2.87E-02	1.72	GTF2I	6.84E-05	0.73	EIF3L	6.48E-05	0.29
COX11	3.77E-02	1.72	ZMIZ1	2.06E-02	0.73	MTF2	4.01E-31	0.29
TP53BP2	2.89E-02	1.71	SND1	1.86E-02	0.72	NFKB1	7.02E-71	0.28
NFKB2	1.71E-04	1.71	DDX31	1.09E-02	0.72	SMARCA5	8.16E-03	0.27
PPP4R1	6.33E-11	1.71	NSD1	4.25E-06	0.72	ABHD11	3.99E-02	0.27
USP14	8.02E-73	1.71	ATRX	3.26E-04	0.71	IMMT	3.15E-08	0.26
SIRT1	9.60E-05	1.70	MBTPS1	6.21E-03	0.71	SMAD4	1.89E-21	0.26
SMARCE1	2.27E-04	1.70	PEX14	8.47E-04	0.70	SUMO2	5.83E-03	0.26
PPP4R3A	2.04E-03	1.69	UBE2L3	6.77E-03	0.69	EIF3K	9.64E-06	0.25
ADSS	1.66E-02	1.68	TFAP4	2.84E-03	0.69	TAF4	4.77E-09	0.24
ZFR	2.84E-02	1.66	PYM1	1.87E-04	0.69	DYRK1A	1.49E-71	0.24
UBE2H	2.61E-67	1.66	TMX1	2.31E-07	0.68	MAX	8.57E-04	0.24
RBCK1	2.16E-02	1.65	PRKDC	1.82E-02	0.67	CYB5B	2.00E-17	0.23
NF2	2.63E-02	1.64	GPBP1	1.31E-03	0.67	KDM1A	6.14E-43	0.22
UBE3D	7.11E-03	1.64	COG5	1.59E-02	0.67	SPAG7	3.49E-23	0.21
KDM3B	1.63E-06	1.63	AHCY	1.09E-02	0.66	PTPMT1	4.41E-10	0.19
FOXM1	2.76E-02	1.63	AP3D1	4.66E-02	0.66	PTPN23	4.37E-06	0.19
CWC27	3.50E-05	1.63	AGPS	1.65E-47	0.66	SUZ12	1.48E-10	0.19
POU2F1	2.26E-09	1.63	APAF1	3.80E-02	0.65	HEATR3	3.27E-02	0.18
ZFAT	2.41E-13	1.62	MBTPS2	5.34E-13	0.65	DCAF7	4.91E-07	0.18
GMEB2	1.96E-02	1.62	CARM1	6.84E-14	0.65	RELA	3.86E-23	0.18
UBP1	2.27E-03	1.62	ZFX	2.22E-08	0.64	TIMM50	1.19E-13	0.17
PFDN1	2.37E-02	1.61	LIAS	8.79E-03	0.64	ADAT2	9.01E-04	0.17
EEFSEC	2.96E-03	1.61	NFAT5	1.25E-18	0.64	EZH2	8.40E-21	0.17
TCEA1	1.29E-02	1.60	PCGF6	4.85E-02	0.64	SNF8	2.46E-07	0.16
TAF6L	4.14E-02	1.60	NUFIP2	2.10E-03	0.63	CNOT10	1.85E-22	0.13
RABIF	4.93E-02	1.58	TRIP12	7.25E-09	0.63	HNRNPA1	8.20E-11	0.12
PRKRIR	1.52E-02	1.57	PHF8	3.23E-04	0.62	CNOT11	1.59E-08	0.11
SYNCRIP	1.12E-02	1.56	GATAD2B	8.47E-10	0.62	CYLD	3.78E-67	0.10
CDK6	1.40E-11	1.56	LSM12	7.16E-05	0.62	RANBP3	1.00E-76	0.10
HNRNPR	1.06E-05	1.56	SLC16A1	8.36E-03	0.61	EED	6.57E-46	0.10
ARID1A	3.59E-05	1.55	KDM5A	7.42E-05	0.61	TTC4	1.30E-11	0.07

8.2.15 *ΔMI TNFR1 – TNFR1$_{\Delta QRICH1}$*

Gene	FDR	ΔMI	Gene	FDR	ΔMI	Gene	FDR	ΔMI
MYO16	1.61E-02	3.29	MAP4K3	1.97E-02	0.88	BTLA	2.33E-03	0.59
EXOC1	2.32E-02	2.90	ACACA	4.82E-02	0.87	PFAS	6.08E-03	0.59
TAL1	1.05E-02	2.86	PRR11	3.21E-02	0.83	TEX11	4.08E-03	0.59
GPRASP2	3.38E-02	2.56	TEN1	1.97E-02	0.82	WDR4	3.21E-02	0.58
SEPHS1	3.31E-06	2.42	MEGF9	1.12E-03	0.82	CUL3	3.31E-06	0.58
BRD7	3.12E-02	2.28	LRRC8D	3.21E-02	0.81	MERTK	1.74E-03	0.58
RAVER2	8.83E-03	2.23	TET1	2.04E-03	0.80	SRD5A3	3.59E-03	0.57
TNFRSF1A	4.69E-04	2.23	WDR20	1.41E-04	0.80	CREBBP	2.58E-03	0.56
ZNF652	2.25E-04	2.16	KDM2A	3.23E-02	0.79	ALG8	3.50E-05	0.54
QRICH1	5.02E-03	2.01	KIF3B	3.59E-03	0.78	ITGAV	1.61E-02	0.53
ZBTB10	2.98E-02	1.99	ZNF143	2.71E-02	0.78	RICTOR	4.48E-02	0.49
ADRA1A	2.01E-02	1.70	UBE2H	1.33E-05	0.77	ARPC2	1.74E-03	0.48
ALB	7.57E-03	1.69	CHIC2	5.02E-03	0.77	DOCK6	4.22E-02	0.45
SETD5	8.29E-03	1.65	VMP1	3.59E-03	0.76	MIPEP	3.42E-03	0.45
STX18	4.76E-02	1.64	GON4L	5.80E-03	0.75	GIGYF2	3.09E-12	0.45
ARID2	4.69E-04	1.58	LIN28B	7.00E-03	0.75	TSPAN16	1.25E-02	0.43
TTLL7	1.78E-02	1.54	DDB2	3.21E-02	0.75	HGS	7.45E-04	0.42
NRN1	3.21E-02	1.44	CCDC109B	3.21E-02	0.73	HSD17B12	1.33E-05	0.42
PBRM1	5.07E-05	1.36	GTF2I	6.50E-03	0.72	VPS45	1.52E-04	0.42
ADAMTS3	2.36E-02	1.35	PARN	1.22E-05	0.71	USP8	1.03E-02	0.42
MAML3	5.80E-03	1.34	ANKRD13C	4.93E-02	0.70	EEFSEC	1.74E-03	0.41
CDH6	3.77E-02	1.28	MAPKAP1	5.80E-03	0.69	CHMP3	2.30E-02	0.39
TNR	3.82E-02	1.25	KEAP1	1.78E-02	0.68	UBE2L3	3.88E-05	0.39
ATP2C1	4.08E-03	1.24	FBXL20	4.34E-02	0.68	OIT3	2.32E-02	0.36
BCOR	7.00E-03	1.19	PARVB	4.08E-03	0.67	UBASH3B	1.63E-02	0.33
RFX3	1.61E-02	1.19	YES1	8.29E-03	0.65	ST6GALNAC 1	3.75E-02	0.31
GPC6	4.69E-03	1.17	KDM6A	4.82E-02	0.65	RAG2	4.93E-02	0.27
ZFHX3	2.45E-02	1.13	PPEF1	3.59E-03	0.64	UBAP1	1.47E-13	0.27
MECOM	1.56E-02	1.11	SNTB2	3.66E-03	0.64	MMS22L	3.01E-02	0.24
NELL1	8.83E-03	1.10	AS3MT	2.36E-02	0.62	SEPHS2	3.92E-02	0.22
TMC1	1.63E-02	0.92	VPS29	3.01E-02	0.62	CHMP5	3.31E-03	0.12
DYM	7.57E-03	0.91	NOX5	2.07E-02	0.60			
TANC2	2.02E-04	0.90	HMCN1	4.99E-03	0.60			

8.2.16 *ΔMI TNFα-dependent NF-κB activation – (TNFα-dependent NF-κB activation)* $_{\Delta QRICH1}$

Gene	FDR	ΔMI	Gene	FDR	ΔMI	Gene	FDR	ΔMI
MRPL10	9.45E-04	44.21	NDUFV2	1.36E-05	1.94	WDR37	1.81E-03	0.59
HSD17B10	1.46E-03	37.15	ACO2	8.34E-03	1.92	CNOT2	2.01E-02	0.59
MRPL21	1.00E-04	25.61	PPP4R1	1.11E-07	1.91	TRIP12	6.16E-06	0.59
MRPL37	2.30E-05	23.84	LIG3	1.32E-03	1.91	C16orf72	3.21E-03	0.58
MRPS18C	2.39E-04	23.20	FAM65B	1.86E-02	1.90	BPTF	9.11E-04	0.58
SSBP1	1.10E-05	20.55	RBM26	6.26E-08	1.90	TRA2A	4.41E-02	0.58
MRPS30	2.88E-05	17.10	COX10	7.13E-06	1.89	YEATS2	2.13E-02	0.58
MRPL52	1.68E-02	16.17	MTHFD1	1.01E-02	1.87	TEX11	1.93E-04	0.58
WBSCR16	4.96E-12	13.09	MRRF	1.46E-04	1.87	ZC3H4	1.21E-06	0.58
MRPL20	1.92E-08	12.40	UBE3D	2.22E-03	1.86	NFKB1	1.61E-05	0.58
GADD45GIP1	1.36E-09	11.81	RHOA	7.63E-04	1.84	RPRD2	4.82E-06	0.58
MRPS26	4.67E-06	11.30	PDSS2	0.00E+00	1.83	CDYL	3.49E-03	0.58
POLRMT	1.07E-04	11.10	TANK	4.52E-04	1.81	PLEC	8.00E-04	0.58
MRPL12	9.32E-10	10.95	MRPS6	2.05E-03	1.81	UBAP1	4.09E-03	0.57
MRPS24	1.08E-03	10.49	COX11	3.69E-02	1.81	SEH1L	3.66E-02	0.57
MRPS25	8.38E-07	10.38	SS18	1.09E-03	1.80	HMCN1	7.01E-04	0.57
ATP5H	7.65E-03	10.25	KLF16	6.88E-04	1.80	UBR5	1.54E-02	0.57
MRPL33	8.51E-05	9.77	RAB10	9.08E-05	1.80	LSM12	1.67E-04	0.57
MRPL15	7.10E-06	9.74	MEF2A	4.17E-03	1.79	CTDSPL2	1.41E-03	0.57
MRPL22	3.14E-04	9.61	SP3	5.30E-05	1.78	PTGES3	3.43E-04	0.57
MRPL4	2.05E-05	9.57	ICT1	1.93E-02	1.78	CDK13	2.44E-06	0.57
PTCD3	8.41E-11	9.39	TBK1	8.99E-04	1.77	TULP4	1.88E-03	0.56
MRPL47	3.80E-06	9.30	ALG8	2.40E-05	1.76	UCHL5	6.42E-03	0.56
MRPL38	5.18E-06	9.09	NDUFAF5	7.77E-03	1.75	EPHB1	7.07E-06	0.56
MTG2	3.44E-06	9.02	NUBPL	1.06E-10	1.74	TOE1	3.06E-02	0.56
MRPL40	7.57E-10	8.67	TRAF3	2.85E-08	1.73	PEX14	3.57E-06	0.55
NELFE	9.62E-03	8.66	HECTD1	8.72E-04	1.72	NPRL3	5.18E-06	0.55
PARS2	3.10E-04	8.65	RQCD1	9.15E-03	1.71	RBCK1	1.32E-02	0.55
MRPS23	4.48E-05	8.43	ATP5J	2.57E-02	1.71	TSPAN16	3.90E-02	0.55
PNPT1	1.12E-05	8.42	GMEB2	8.25E-03	1.70	RANBP17	4.46E-02	0.55
MRPS10	3.60E-07	8.38	VMP1	2.53E-10	1.69	BCR	2.24E-03	0.55
TUFM	4.39E-03	8.36	CDK6	4.85E-07	1.65	L3MBTL3	7.27E-07	0.54
TARS2	1.77E-06	8.14	RNF19A	9.47E-03	1.64	INPP5K	2.73E-02	0.54
MRPL35	1.46E-09	8.07	PFAS	5.19E-03	1.61	CD48	4.06E-02	0.54
MTERF4	6.54E-04	7.97	KCMF1	2.72E-03	1.61	KDM1A	6.33E-04	0.53
SARS2	4.82E-06	7.57	MAPKAP1	1.97E-05	1.61	CCDC6	8.00E-04	0.53
MRPL49	3.01E-05	7.50	AEBP2	4.90E-06	1.60	TFAP4	2.02E-06	0.53
QRSL1	1.63E-05	6.99	ZNF280C	5.56E-05	1.60	PCGF6	2.84E-03	0.53
EARS2	2.93E-11	6.77	NFKBIB	1.63E-05	1.59	KDM5A	2.43E-05	0.52
MRPL19	7.97E-09	6.70	WDR7	1.72E-04	1.58	CARNMT1	3.75E-02	0.52
TFB2M	1.56E-05	6.68	SETD1B	1.03E-03	1.56	TSC1	2.72E-03	0.51
ATP5B	2.89E-03	6.67	GAB2	1.12E-02	1.56	CAND1	7.63E-04	0.51
MRPL3	1.21E-10	6.59	SKP2	2.03E-02	1.54	CD44	2.66E-02	0.51
MRPL27	9.04E-04	6.49	ATXN7	1.11E-05	1.52	FAR1	3.00E-03	0.51
GATC	2.37E-08	6.40	ACTR3	3.90E-03	1.51	BRD7	2.91E-02	0.51
MRPS7	2.54E-05	6.34	WDR20	5.04E-14	1.51	MNT	2.25E-12	0.51
MRPL32	5.27E-03	6.31	FOXM1	4.55E-02	1.51	USP8	3.40E-02	0.50
RARS2	5.59E-10	6.26	KDM3B	5.28E-04	1.51	FBXW7	4.52E-09	0.50
TEFM	2.83E-05	6.26	LIN28B	9.60E-06	1.50	PEX13	4.65E-03	0.50
MRPL51	2.44E-06	6.18	WDR44	2.75E-05	1.49	FBRS	4.34E-02	0.50
NGRN	6.44E-08	6.11	UBE2H	0.00E+00	1.49	SPTLC2	3.63E-05	0.50
TRUB2	1.27E-05	6.04	WNK1	1.49E-02	1.49	SP1	8.03E-08	0.50
MYL5	3.29E-03	6.03	TMEM47	1.14E-02	1.47	VPS13D	1.37E-02	0.50
MALSU1	2.37E-04	5.99	PHF21A	5.56E-05	1.46	SLC44A2	3.74E-03	0.49
METTL17	2.59E-03	5.82	RERE	3.53E-08	1.45	HSD17B12	1.17E-04	0.47
METTL1	4.12E-02	5.81	NDUFAF6	1.08E-02	1.44	ACTR2	4.76E-02	0.47
MTPAP	4.42E-08	5.77	DNAJA2	2.11E-03	1.43	DNMT1	1.58E-03	0.47
MRPS15	1.53E-05	5.73	NCOA6	3.72E-03	1.41	CYB5B	2.75E-02	0.47
MIPEP	7.61E-12	5.68	ZEB2	5.93E-07	1.41	DYRK1A	7.56E-12	0.47

Gene	FDR	ΔMI	Gene	FDR	ΔMI	Gene	FDR	ΔMI
DAP3	7.98E-08	5.66	APC	1.86E-02	1.41	ZNF628	7.88E-03	0.47
MRPS18B	1.69E-11	5.53	EXOC4	5.53E-10	1.41	EP300	6.41E-07	0.47
MRPL48	0.00E+00	5.52	UBE2R2	1.16E-03	1.41	ZNF91	2.88E-03	0.46
TFB1M	2.03E-08	5.38	MBTPS2	4.65E-03	1.39	CDH1	4.87E-03	0.46
CHMP5	7.77E-03	5.29	UBA6	1.93E-02	1.37	ABLIM2	1.34E-03	0.46
MRPL30	1.42E-05	5.28	TRIM71	1.77E-03	1.37	CLPSL1	4.28E-02	0.46
POLG2	6.76E-12	5.28	NCOA2	1.68E-07	1.36	PDS5A	1.52E-04	0.45
WARS2	4.13E-06	5.09	REL	4.28E-02	1.36	INPP4A	2.31E-07	0.45
ATP5C1	2.83E-02	5.04	ARHGEF12	3.13E-03	1.34	ZNF808	2.43E-02	0.45
HARS2	7.41E-04	5.03	CCDC33	1.12E-02	1.34	TSPAN14	3.27E-03	0.45
MRPL54	4.01E-05	4.95	MED13L	6.44E-08	1.34	PEX7	5.09E-03	0.45
YARS2	1.42E-05	4.94	ATP2C1	2.75E-05	1.33	MARCH5	7.48E-03	0.45
MRPL39	3.10E-03	4.92	EIF4B	1.42E-02	1.33	EZH2	1.15E-02	0.44
ATP5O	2.98E-02	4.86	ABCC4	1.04E-02	1.32	LIPC	2.82E-02	0.44
MRPS9	0.00E+00	4.81	C11orf73	5.89E-03	1.32	FANCD2	5.09E-03	0.43
GATB	7.08E-07	4.79	HNRNPR	3.73E-02	1.32	SMARCA4	2.85E-10	0.43
MRPL24	3.27E-08	4.75	YBEY	1.15E-02	1.31	NSD1	0.00E+00	0.43
ISCA2	9.86E-03	4.63	ASCC1	2.80E-06	1.31	DNTT	4.74E-03	0.43
MRPL18	7.50E-11	4.61	KLF9	8.25E-03	1.30	ATF7IP	0.00E+00	0.42
TSFM	6.38E-03	4.46	PRMT3	5.47E-04	1.30	IKBKB	4.38E-03	0.42
UQCRC1	1.96E-04	4.31	ANKRD30A	4.36E-03	1.29	GLMN	2.72E-04	0.42
MRPS35	2.03E-07	4.28	TET1	8.20E-05	1.29	SERBP1	5.11E-03	0.42
COX20	1.80E-04	4.25	TCF12	4.13E-06	1.27	PPHLN1	2.05E-13	0.41
MRPS27	0.00E+00	4.25	EIF2A	3.48E-02	1.27	SPAG7	2.30E-04	0.41
ERAL1	1.21E-05	4.18	GFPT1	8.33E-03	1.27	NPRL2	4.97E-03	0.40
COX19	7.82E-05	4.08	MYH7B	1.20E-02	1.25	MTF2	3.75E-09	0.39
MRPL23	1.52E-05	4.07	TMEM131	3.25E-02	1.25	BIRC2	4.68E-03	0.39
YLPM1	1.66E-06	4.00	ALPK1	1.04E-03	1.25	SMC6	6.97E-03	0.39
RPUSD4	1.12E-02	3.96	BIRC6	9.47E-03	1.24	GNPAT	8.98E-04	0.39
DDX28	2.54E-05	3.93	FBXL17	2.74E-03	1.23	METAP1	1.17E-02	0.39
PGD	4.81E-03	3.93	CHIC2	1.32E-02	1.22	TAF3	6.44E-08	0.38
SDHA	3.45E-04	3.89	MYO10	2.33E-06	1.22	N4BP1	2.24E-03	0.38
MTG1	7.07E-06	3.89	CHD2	2.57E-02	1.21	TSC2	8.33E-03	0.37
KIAA0391	8.12E-13	3.87	TRPM3	9.98E-06	1.17	DPH6	0.00E+00	0.37
MRPL17	2.72E-04	3.73	DACH1	8.20E-06	1.15	PCMTD2	4.31E-06	0.36
SDHB	7.13E-05	3.72	CHN1	1.07E-04	1.14	ZNF611	1.20E-05	0.36
PDE12	1.35E-05	3.72	HDAC9	2.85E-05	1.11	ATAD3C	1.31E-02	0.35
GTPBP10	4.63E-04	3.67	TMC1	1.73E-03	1.10	DLEC1	8.93E-04	0.35
MTERF3	8.02E-06	3.66	SYT1	1.62E-03	1.08	HTR7	1.01E-07	0.35
SRD5A3	7.00E-09	3.63	ZBTB20	3.06E-03	1.07	EIF3L	3.26E-03	0.35
FTSJ2	8.22E-03	3.50	DMD	3.52E-02	0.94	CYLD	1.49E-05	0.34
LARS2	0.00E+00	3.49	CTNNA3	2.83E-02	0.92	CUL1	1.76E-04	0.34
MRPL11	4.38E-04	3.49	CNTNAP2	2.65E-02	0.92	FAAH2	3.92E-03	0.34
MRPS33	1.97E-03	3.49	AUTS2	2.62E-02	0.90	CHUK	1.04E-03	0.34
SLIRP	8.31E-04	3.48	AGBL1	2.81E-02	0.90	WAC	1.77E-05	0.33
ATP5J2	4.74E-03	3.44	CDH12	4.30E-02	0.90	CREB1	1.90E-04	0.33
MRPS16	5.79E-07	3.42	SNTG1	1.16E-02	0.89	CRAMP1	1.68E-07	0.33
NARS2	0.00E+00	3.37	MECOM	1.06E-03	0.88	RNF31	1.30E-03	0.33
OPA1	2.41E-04	3.36	MACROD2	9.15E-03	0.88	EIF3K	4.78E-03	0.33
SUPT20H	5.04E-06	3.36	ARID5B	1.74E-05	0.85	FAM208A	2.57E-08	0.32
ZC3H15	6.88E-03	3.35	KDM2A	3.41E-02	0.83	CNOT10	4.35E-03	0.31
SDHC	1.42E-08	3.33	RSF1	1.32E-02	0.82	RANBP3	3.53E-08	0.30
TRIT1	4.20E-11	3.26	TNS3	2.89E-03	0.82	ATXN2L	4.08E-03	0.30
PITRM1	3.17E-02	3.26	ZFHX3	4.08E-06	0.81	ADGRD1	9.23E-03	0.29
ZFR	1.09E-06	3.21	ACACA	7.37E-05	0.81	EED	5.53E-05	0.29
LRPPRC	0.00E+00	3.19	SIPA1L3	2.46E-03	0.78	SUV420H1	1.59E-05	0.29
COX15	1.31E-04	3.11	JAZF1	7.62E-04	0.77	CFAP53	4.08E-03	0.28
TSEN15	2.57E-02	3.06	GATAD2B	9.47E-03	0.76	CHMP3	2.01E-04	0.27
ISCA1	7.84E-03	3.04	POU2F1	2.85E-02	0.75	SMARCB1	1.94E-05	0.27
RBFA	3.87E-04	3.00	USP14	6.44E-08	0.75	SLC1A2	7.62E-04	0.26
STRAP	4.68E-03	2.98	VPS41	3.54E-03	0.74	SMAD4	5.86E-11	0.26
MRPL50	2.05E-03	2.90	TMX1	8.39E-03	0.74	FBXW11	5.55E-07	0.26
RNF19B	2.72E-04	2.88	CARM1	5.56E-04	0.74	NFKBIA	2.05E-13	0.25
SDHAF4	4.76E-04	2.88	NFAT5	2.30E-05	0.74	CUL3	0.00E+00	0.24
FARS2	1.92E-08	2.85	KMT2E	1.80E-04	0.73	DOT1L	0.00E+00	0.24

Gene	FDR	ΔMI	Gene	FDR	ΔMI	Gene	FDR	ΔMI
SLC30A9	3.21E-04	2.85	PPEF1	1.07E-02	0.72	TRADD	1.88E-03	0.24
PTDSS1	3.37E-03	2.84	CCDC109B	9.86E-03	0.72	SUZ12	3.14E-04	0.23
GTPBP8	1.88E-03	2.83	ANKRD13C	2.31E-02	0.71	UBASH3B	6.49E-05	0.23
UQCRC2	8.72E-04	2.77	USP34	1.52E-05	0.71	PTPMT1	3.41E-02	0.23
NDUFA11	3.87E-03	2.75	IGSF11	2.68E-02	0.71	TADA2A	0.00E+00	0.22
C1QBP	8.92E-05	2.74	TNRC18	2.32E-03	0.70	CSRP2BP	8.59E-06	0.22
MRPS28	0.00E+00	2.68	SUPT3H	1.11E-05	0.70	SUMO2	1.45E-02	0.22
TADA2B	1.60E-04	2.68	BAZ1B	1.17E-04	0.69	TAF1	6.84E-05	0.22
GRSF1	7.69E-03	2.61	ASXL1	8.39E-03	0.69	ZNF569	8.86E-04	0.21
AIFM1	1.81E-03	2.56	CNOT4	7.77E-03	0.68	VPS36	8.37E-03	0.21
MRPL13	1.88E-03	2.54	UNK	8.59E-06	0.67	TRAF2	7.13E-09	0.20
YTHDF2	1.55E-06	2.47	SPEN	1.68E-05	0.67	THEG	4.55E-02	0.20
TXLNG	3.87E-07	2.42	NOX5	1.80E-02	0.67	SHARPIN	5.94E-04	0.19
MRPS5	2.32E-02	2.40	UHRF1	5.02E-03	0.67	WDR82	1.18E-03	0.19
ATIC	7.23E-04	2.36	NRXN2	6.94E-03	0.66	ZNF793	1.31E-02	0.18
NFU1	8.92E-05	2.36	PBRM1	3.54E-10	0.65	TAF4	6.42E-08	0.18
NDUFB9	8.17E-03	2.34	ADNP	7.88E-03	0.65	UBE2M	1.52E-05	0.17
SLC25A26	4.32E-03	2.32	ARID2	5.38E-04	0.65	DPH5	7.55E-15	0.17
SDHAF2	1.77E-03	2.28	BTLA	3.61E-03	0.64	ZZZ3	4.42E-08	0.16
ANKRD17	7.47E-11	2.24	ZMIZ1	1.41E-03	0.64	DPY30	1.55E-05	0.15
ACLY	1.75E-03	2.24	RSBN1L	3.66E-04	0.64	TIMM50	9.05E-04	0.15
CREBBP	2.64E-09	2.24	DDX31	1.53E-03	0.64	PCBP2	4.50E-05	0.14
METTL5	1.11E-02	2.22	NRD1	4.04E-03	0.64	HEATR3	8.33E-03	0.14
WDR4	2.89E-03	2.22	RNF40	2.43E-02	0.63	CNOT11	1.89E-03	0.13
ADSS	2.47E-03	2.20	SETDB1	1.69E-02	0.63	SFTPB	4.41E-02	0.13
PDSS1	1.90E-04	2.18	MAZ	1.98E-03	0.63	TRPC7	3.65E-04	0.13
PPAT	2.41E-04	2.15	AGPS	0.00E+00	0.63	ZNF652	0.00E+00	0.12
COQ2	1.10E-03	2.15	DEPDC5	3.48E-03	0.62	DCPS	1.36E-05	0.11
ACAD9	1.66E-02	2.14	NCOR1	5.91E-05	0.62	HNRNPA1	2.54E-05	0.10
PARL	8.84E-03	2.11	WDR72	2.75E-02	0.62	MED26	8.33E-03	0.10
CARS2	3.27E-04	2.07	MLLT10	2.25E-12	0.62	QRICH1	0.00E+00	0.10
GIGYF2	8.03E-08	2.04	ABCC1	1.64E-05	0.62	MAP3K7	3.19E-10	0.09
ZC3H13	8.22E-03	2.03	AHCY	1.07E-02	0.62	RELA	5.49E-09	0.08
TAF6L	7.77E-03	2.03	MBD3	6.67E-04	0.61	ZNF578	1.31E-04	0.08
EIF4E2	1.98E-02	2.03	ZFX	2.94E-07	0.61	SEPHS1	0.00E+00	0.07
EEFSEC	1.83E-03	2.00	PRMT7	6.10E-04	0.61	TNFRSF1A	0.00E+00	0.07
NDUFB4	2.92E-02	1.99	SMARCE1	6.42E-03	0.61	IKBKG	1.92E-05	0.03
SHMT2	8.17E-03	1.98	PRKDC	4.83E-03	0.60	WDR37	1.81E-03	0.59
COQ3	2.75E-05	1.96	RREB1	2.38E-03	0.60	CNOT2	2.01E-02	0.59
ALKBH8	1.89E-03	1.94	RALGAPB	7.77E-03	0.60	TRIP12	6.16E-06	0.59